HOKKAIDO UNIVERSITY

Title	Chemical Studies on β-Glucuronidase Inhibition of Compounds Derived from Marine Algae
Author(s)	張, 鐸
Degree Grantor	北海道大学
Degree Name	博士(水産科学)
Dissertation Number	甲第13100号
Issue Date	2018-03-22
DOI	https://doi.org/10.14943/doctoral.k13100
Doc URL	https://hdl.handle.net/2115/73150
Type	doctoral thesis
File Information	Duo_ZHANG.pdf



Hokkaido University Collection of Scholarly and Academic Papers : HUSCAP

Chemical Studies on β-Glucuronidase Inhibition of Compounds Derived from Marine Algae

（海藻由来化合物のβ - グルクロニダーゼ阻害に関する化学的研究）

北海道大学大学院水産科学院
海洋応用生命科学専攻

Graduate School of Fisheries Sciences
Division of Marine Life Science

張　鐸
Duo Zhang

2018（平成30年）

Contents

List of abbreviations and acronyms 1
Introduction 2
Chapter 1 Screening of β-Glucuronidase Inhibitors 16
1.1 Collection and organic solvent extraction of marine algae 17
1.1.1 Chemicals and instruments 17
1.1.2 Collection of marine algae 18
1.1.3 Organic solvent extraction of marine algae 19
1.2 β-Glucuronidase inhibitory activity assay 31
1.2.1 β-Glucuronidase enzymatic activity test 31
1.2.2 Screening of β-glucuronidase inhibitors from marine algae 34
1.3 Discussion 46
Chapter 2 β-Glucuronidase Inhibitors Derived from Marine Red Algae 48
2.1 Chromatography and chemical analysis instrument 49
2.1.1 Chromatography 49
2.1.2 Analysis instruments 50
2.2 β-Glucuronidase inhibitors derived from the marine red alga *Neorhodomela aculeata* 51
2.2.1 Isolation and purification of β-glucuronidase inhibitors from *N. aculeata* 51
2.2.1.1 Silica gel column chromatography 51
2.2.1.2 Purification of β-glucuronidase inhibitor F1 57
2.2.1.3 Purification of β-glucuronidase inhibitor F2 57
2.2.1.4 Purification of β-glucuronidase inhibitor F3 57
2.2.2 Structural elucidation of β-glucuronidase inhibitors from *N. aculeate* 66
2.2.2.1 Structural elucidation of β-glucuronidase inhibitor F1 66
2.2.2.2 Structural elucidation of β-glucuronidase inhibitor F2 75
2.2.2.3 Structural elucidation of β-glucuronidase inhibitor F3 85
2.3 β-Glucuronidase inhibitors derived from the marine red alga *Neodilsea yendoana* 95
2.3.1 Isolation and purification of β-glucuronidase inhibitors from *N. yendoana* 95
2.3.1.1 Purification of β-glucuronidase inhibitor A1 100
2.3.1.2 Purification of β-glucuronidase inhibitors A2-A5 100
2.3.1.3 Purification of β-glucuronidase inhibitor A6 100
2.3.2 Structural elucidation of β-glucuronidase inhibitors from *N. yendoana* 113
2.3.2.1 Structural elucidation of β-glucuronidase inhibitor A1 113

2.3.2.2 Structural elucidation of β-glucuronidase inhibitory compounds A2 & A3 127
2.3.2.3 Structural elucidation of β-glucuronidase inhibitor A4 161
2.3.2.4 Structural elucidation of β-glucuronidase inhibitor A5 185
2.3.2.5 Structural elucidation of β-glucuronidase inhibitor A6 206
2.4 Discussion 220
Chapter 3 β-Glucuronidase Inhibitors Derived from Marine Brown Algae 224
3.1 Chromatography and chemical analysis instruments 225
3.2 β-Glucuronidase inhibitors derived from the marine brown alga *Sargassum confusum* 225
3.2.1 Isolation of β-glucuronidase inhibitor J1 from *S. confusum* 225
3.2.2 Structural elucidation of β-glucuronidase inhibitor J1 232
3.3 β-Glucuronidase inhibitors derived from the marine brown alga *Sargassum thunbergii* 242
3.3.1 Isolation and purification of β-glucuronidase inhibitors from *S. thunbergii* 242
3.3.1.1 Silica gel column chromatography of *n*-hexane-soluble fraction 242
3.3.1.2 Silica gel column chromatography of fraction H-4 243
3.3.1.3 MS and NMR data of compound J1 obtained from *S. thunbergii* 249
3.3.1.4 Structural elucidation of β-glucuronidase inhibitor U2 253
3.4 β-Glucuronidase inhibitors derived from the marine brown alga *Agarum clathratum* 259
3.4.1 Isolation and purification of β-glucuronidase inhibitors from *A. clathratum* 259
3.4.1.1 β-Glucuronidase inhibitors isolated from *n*-hexane-soluble fraction of *A. clathratum* 262
3.4.1.2 β-Glucuronidase inhibitors isolated from ethyl acetate-soluble fraction of *A. clathratum* 267
3.4.2 Structural elucidation of β-glucuronidase inhibitors from *A. clathratum* 274
3.4.2.1 Structural elucidation of β-glucuronidase inhibitor C3 274
3.4.2.2 Structure elucidation of inhibitor G2 283
3.5 Discussion 289
Chapter 4 Molecular Modeling Base SAR Analysis of the Purified β-Glucuronidase Inhibitors 293
4.1 *In vitro* β-glucuronidase inhibitory activities 294
4.1.1 Chemicals and instruments 294
4.1.2 Kinetic study of the purified β-glucuronidase inhibitors 294
4.2 *In silico* β-glucuronidase inhibitory activities analysis 308

4.2.1 Molecular docking protocols 308
4.2.2 The structures of β-glucuronidase from *E. coli* (PDB code: 3LPG)..... 309
4.2.3.1 Molecular modeling based SAR analysis of bromophenol monomer (F1) 311
4.2.3.2 Molecular modeling based SAR analysis of bromophenol dimer (F2) ..311
4.2.3.3 Molecular modeling based SAR analysis of bromophenol dimer (F3) . 312
4.2.3.4 Molecular modeling based SAR analysis of compound phytal (A1)..... 313
4.2.3.5 Molecular modeling based SAR analysis of phytol (A2) and cholesta-4,22-diene-3,6-dione (A3)..... 313
4.2.3.6 Molecular modeling based SAR analysis of compound cholesterol (A4) 314
4.2.3.7 Molecular modeling based SAR analysis of 22-dehydrocholesterol (A5) 314
4.2.3.8 Molecular modeling based SAR analysis of isogloiosiphone B (A6) ... 314
4.2.4 Molecular modeling based SAR analysis of inhibitors purified from brown algae *S. confusum*, *S. thunbergii* and *A. clathratum* 333
4.2.4.1 Molecular modeling based SAR analysis of henicosapentaene (J1)..... 333
4.2.4.2 Molecular modeling based SAR analysis of henicosahexaene (U2) 333
4.2.4.3 Molecular modeling based SAR analysis of squalene (C3)..... 333
4.2.4.4 Molecular modeling based SAR analysis of phloroglucinol (G2)..... 334
4.3 Discussion..... 346
Conclusion 350
References..... 352
Acknowledgements 369

List of abbreviations and acronyms

COSY	Correlation spectroscopy
DFQ COSY	Double quantum filtered correlation spectroscopy
DMBA	2,4-Dimethoxybenzaldehyde
DMSO	Dimethyl sulfoxide
E. coli	*Escherichia coli*
FD-HR-MS	Field desorption-high resolutional-mass spectrometry
FD-MS	Field desorption-mass spectrometry
FI-HR-MS	Field ionization-high resolutional-mass spectrometry
FI-MS	Field ionization-mass spectrometry
HMBC	Heteronuclear multiple bond correlation
HPLC	High performance liquid chromatography
HSQC	Heteronuclear single quantum coherence spectroscopy
IC_{50}	Half maximal inhibitory concentration
MS	Mass spectrometry
NMR	Nuclear magnetic resonance
NOESY	Nuclear Overhauser effect spectroscopy
PLC	Preparative thin layer chromatography
p-NPG	*p*-Nitrophenyl β-D-glucuronide
ROESY	Rotating frame nuclear Overhauser effect spectroscopy
SAR	Structure-activity relationship
TLC	Thin layer chromatography
UV	Ultraviolet

Introduction

β-Glucuronidase (EC 3.2.1.31) is an inducible enzyme commonly found in anaerobic *Escherichia*, *Bacteroides*, *Clostridia*, *Peptostreptococcus* genera (Khan et al., 2014c) and responsible for catalyzing the cleavage of β-glucuronosyl-*O*-bond (Sperker, Backman, & Kroemer, 1997). The enzyme extensively presents in all mammalian organs and human body fluids with, especially in liver, kidney, spleen, bile, gastrointestinal tract, epididymis, serum and urine (Oleson & Court, 2008). The enzyme is possessing the capable of eliminating and excreting large number of xenobiotics from body as glucuronides via glucuronidation reaction (Taha et al., 2015).

All organisms are constantly exposed to the numerous compounds which are extrinsic and cannot be used as energy sources for human beings, such as drugs, pesticides, food additives, environmental and industrial chemicals as well as other foreign chemicals from other organisms lack metabolic function and potentially harmful compounds are defined as xenobiotics or xenobiotic compounds (Spanogiannopoulos, Bess, Carmody, & Turnbaugh, 2016). Generally, the xenobiotic clearance metabolism can be divided into three major phases: phase I—modification: oxidize the xenobiotics into more hydrophilic and provide suitable sites for phase II; phase II—conjugation: conjugate the hydrophilic compounds with glucuronic acid and other molecules; phase III—excretion: transport the conjugated compounds out of body by bile and urine and feces (Croom, 2012).

Glucuronidation is known as a one of the most classic detoxification processes which occurs in almost all mammalian species (Tukey & Strassburg, 2000). It is one of the major conjugation reactions belonging to phase II xenobiotic metabolism (Xu, Li, &

Kong, 2005). This conjugation reaction involves the covalent linkage of the phase I modified xenobiotics to uridine 5'-diphospho (UDP)-glucuronic acid cofactor derived glucuronic acid mediated with UDP-glucuronosyltransferases (UGTs) by bimolecular nucleophilic substitution (S_N2) mechanism (Tukey & Strassburg, 2000) to form β-D-glucuronide conjugates (Caldwell, Gardner, & Swales, 1995) (Figure 1). Numerous nucleophiles can serve as the receptor group for glucuronidation, including aliphatic alcohols, phenols, carboxylic acids, aromatic and aliphatic amines, thiols and acidic carbon atoms. After glucuronidation, the conjugated glucuronides possess hydrophilic properties which allow the easier excretion into bile and intestine (Rowland, Miners, & Mackenzie, 2013).

Glucuronidation proceeds as an essential elimination pathway and clearance mechanism for numerous structurally diverse endogenous and exogenous compounds. However, a considerable amount of β-glucuronidase produced by intestinal bacteria would hydrolyze the glucuronide conjugates to liberate the xenobiotics which can in turn be reabsorbed and finally enter in to the enterohepatic circulation (Graaf, Boven, Scheeren, Haisma, & Pinedo, 2002) (Figure 2).

Likewise, during the chemotherapeutic treatment of common colon cancer by CPT-11 (irinotecan), the active anticancer metabolites SN-38, having side effects, is converted in liver to inactive SN-38 glucuronide (SN-38G). It is excreted via the biliary ducts into the gastrointestinal tract. However, once transported into intestines, the non-toxic SN-38G is hydrolyzed by microbial β-glucuronidase to form the toxic SN-38 in situ which finally causes severe diarrhea (Wallace et al., 2010). Additionally, the excessive expression of β-glucuronidase may be related with diverse pathological symptoms. Many researches showed in breast, lung and gastrointestinal tract

carcinomas and melanomas, high concentration of the enzymatically active β-glucuronidase were examined in the necrotic areas of human tumor tissue biopsies (Schumacher, Adam, Zangemeister-Wittkel, & Gossrau, 1996). Bank & Bailine found that β-glucuronidase concentration significantly elevated in the urine of urinary-tract infected patients (Bank & Bailine, 1965). Same observations were also found in patients with rheumatoid arthritis (Jacox & Feldmahn, 1955) and hepatic related disorders (Ohta, Ono, Sekiya, & Namiki, 1992). Therefore, development of specific inhibitors of β-glucuronidase should be effective in promoting the excretion of xenobiotics and preventing various diseases which may provide useful insights in pharmacology.

The foremost β-glucuronidase inhibitor used for *in vitro* assays is D-glucaro-1,4-lactone (saccharolactone) (**1**) found by Levvy in 1952, which has been widely used as the positive control of β-glucuronidase inhibitors by a competitive mechanism (Levvy, 1952). So far, several secondary metabolites derived from terrestrial and marine sources have been isolated as β-glucuronidase inhibitors. Bello et al. isolated 2(*S*)-carboxy-3*R*,4*R*,5*S*-trihydroxypiperidine (**2**) from the seeds of *Baphia racemosa*, shrub of family Fabaceae which showed intense inhibitory activity against β-glucuronidase as well as α-L-iduronide inhibitory activity (Bello, Dorling, Fellows, & Winchester, 1984). Also, researches showed isovitexina (**3**), 5,7,8,3',4',5'-hexahydroxyflavone7-*O*-β-D-glucuronide (**4**) and scoparic acid A (**5**) derived from perennial herbal plant *Scoparia dulcis* (Scrophulariaceae) (Kawasaki, Hayashi, Arisawa, Morita, & Berganza, 1988) (Hayashi et al., 1992); ganoderenic acid A (**6**) derived from oriental fungus *Ganoderma lucidum* (Ganodermataceae) (D. H. Kim, Shim, Kim, & Jang, 1999); 1β,3β,5α,23,24-pentahydroxy-30-norolean-12,20(29)-dien-28-oic acid (**7**) derived from the herbal plant *Paeonia emodi* (Paeniaceae) (Nawaz, Malik, Khan,

Shujaat, & Rahman, 2000); trehalose (**8**) derived from macrofungus *Leninus edodes* (Marasmiaceae) (Han, Bae, & Kim, 2001) and glycyrrhizin (**9**) and 18β-glycyrrhetinic acid (**10**) derived from the rhizomes of *Glycyrrhiza uralensis* (Leguminosae) (Shim, Kim, & Kim, 2000) might be good candidates for β-glucuronidase inhibitors. Moreover, Rhee et al and Han & Kim also found the extracts of some traditional herbal medicines and root vegetables also showed strong inhibitory activity against β-glucuornidase, such as *Glycyrrhiziae radix* (Fabaceae), *Zizyphi fructus* (Rhamnaceae), *Solanum tuberosum* (Solanaceae), *Codonopsis lanceolata* (Campanulaceae), *Dioscorea japonica* (Dioscoreaceae) and *colocisia antiquorum* (Araceae) (Rhee, Kim, & Han, 1998) (Han & Kim, 1999). Furthermore, some marine source derived β-glucuronidase inhibitors also have been found, such as glycyrrhizin (**9**), baicalin (**11**), wogonoside (**12**) and luteolin-3′-glucuronide (**13**) derived from a kampo (Japanese herb) medicine (Narita et al., 1993); and two bromophenols, 2,4,6-tribromophenol (**14**) and 2,4-dibromophenol (**15**) derived from the red alga, *Grateloupia elliptica* (Halymeniaceae) (K. Y. Kim, Chi, Kurihara, & Kim, 2008) (Figure 3).

Besides, some purine nucleotides especially inosine 5'-monophosphate (IMP) (**16**), adenosine 5'-monophosphate (AMP) (**17**) and adenosine 5'-triphosphate (ATP) (**18**) also showed potential inhibitory activity (Parish, 1977) (Tohda, Kurihara, Hosokawa, & Takahashi, 1999). Furthermore, according to fluorescent high-throughput screening assay, a set of chemically similar compounds have been screened for potent inhibition against β-glucuronidase involving thioamide, carbamide, pyrimidine, thiophene and acetamide derivatives (**19-34**) (Ahmad et al., 2011) (Roberts, Wallace, Venkatesh, Mani, & Redinbo, 2013) (Figure 3).

Recently, many researchers are focusing on the synthesis of β-glucuronidase

inhibitors from lead compounds including benzaldehydes (**35**) (Khan et al., 2014b); benzothiazoles (**36**) (Khan et al., 2011) (Taha, Ismail, Imran, Selvajar, & Rhim, 2016); bisindolylmethanes (**37**) (Khalid Mohammed Khan, Rahim, et al., 2014); N-arylidenequinoline-3-carbohydrazides (**38**) (Taha et al., 2016a); hydrazones (**39**) (Taha et al., 2016b); benzimidazoles (**40**) (Taha et al., 2015a); 3,4,5-trihydroxybenzohydrazones (**41**) (Taha et al., 2015b); indole hydrazones (**42**) (Baharudin et al., 2017); oxadiazole benzohydrazones (**43**) (Taha et al., 2015c); Dihydropyrimidones (**44**) (Ali et al., 2016); hydrazide derivatives (**45**) (Khan et al., 2002); thiadiazols (**46**) (Salar et al., 2016); 5-nitroimidazoles (**47**) (Salar et al., 2016); Disulfide and sulfone hybrid analogs (**48**) (Taha, Ismail, Imran, Wadood, et al., 2016); coumarins (**49**) (Khan et al., 2014c) and thienothiophenes (**50**) (Mabkhot et al., 2014). All of these kinds of synthesized compounds showed potent inhibitory activity (Figure 3).

As the vast chemical and biological diversity of natural products, discovery of the bioactive natural products has been historically considered as a promising source of drug discovery (Nautiyal, 2013). Over the last decades, there has been a surge of focus globally on marine derived natural products, as their distinct environments of marine life and unique biological diversities of marine organisms (Monaco & Quinlan, 2014). Marine algae, which have been traditionally consumed as food or food ingredient and medical treatments in many countries, are of the particular interest as they contain natural occurring bioactive primary and secondary metabolites, such as pigments, lipids, fatty acids, sterols, polysaccharides, proteins, peptides, mycosporine-like amino acids, phenolic compounds, and terpenes (Blunt, Copp, Munro, Northcote, & Prinsep, 2006). Indeed, bioactivities of these compounds have been described to date ranging from

antioxidant, anti-inflammatory, anti-diabetic, anticancer, antiviral, antimicrobial, anti-tumor, anti-obesity, anti-malarial, anti-fungal, anti-flouring to various enzymatically inhibitory activities (Blunt, Copp, Keyzers, Munro, & Prinsep, 2017). Therefore the metabolites from marine algae provide the large potentials in nutraceutical, cosmeceutical, pharmaceutical and biomedical industries. Thus, the exploration of β-glucuronidase inhibitors from marine algae has been strong expected.

Enzyme inhibition is one of the most significant tools which has been extensively used assays in pharmaceutical research as well as in the field of drug discoveries (Khan et al., 2011). And molecular recognition is one of the basic features of all the biological phenomena (Barakat et al., 2016). Binding action of the inhibitors to the enzyme can prevent the substrate from entering the enzyme's active site. Ideal inhibitors are often judged by the potency of the binding affinity with the enzyme. High binding capability always leads to the high enzymatic inhibitory activity. Generally, non-covalent interactions between the inhibitors (ligands) and enzyme macromolecule (receptor), including hydrogen bonds, van der Waals forces, electrostatic forces and hydrophobic interactions are the basic criteria for successful docking (Bissantz, Kuhn, & Stahl, 2010). In order to yield deep insights into the molecular interactions of compounds with the active sites of enzyme and subsequently predict the optimum structure of the inhibitors, molecular docking study has been conducted to establish the structure-activity relationship (SAR) which tries to demonstrate the mechanism of inhibitory potential (Ali et al., 2016). Molecular docking is a computational technique that has been validated as a means of exploring the possible binding mode of the ligand to the receptor and or another binding site. It can predict the binding affinity and give the appropriate conformation of the ligands within the target binding site of the enzyme,

together with the interacting residues and their intermolecular distances, which is also a prerequisite for the rational drugs design (Guido, Oliva, & Andricopulo, 2008).

The overall aim of this study is to isolate β-glucuronidase inhibitors from marine algae collected from the coastline of Hokkaido, Japan and try to evaluate their inhibition mechanism by analyzing enzyme inhibition kinetics *in vitro* and molecular docking studies *in silico*.

The specific objectives of the each chapter are as follows:

1. Screening of the potential *E. coli* β-glucuronidase containing marine algae which collected along the coastline of Hokkaido, Japan

2. Isolation and purification of *E. coli* β-glucuronidase inhibitory compounds derived from marine red algae—*Neorhodomela aculeata* (Rhodomelaceae, Ceramiales) and *Neodilsea yendoana* (Dumontiaceae, Gigartinales)

3. Isolation and purification of *E. coli* β-glucuronidase inhibitory compounds derived from brown algae—*Sargassum confusum* (Sargassaceae, Fucales), *Sargassum thunbergii* (Sargassaceae, Fucales) and *Agarum clathratum* (Agaraceae, Laminariales)

4. *In vitro* enzymatic analysis and *in silico* molecular modeling based SAR analysis between the obtained β-glucuronidase inhibitory compounds and *E. coli* β-glucuronidase

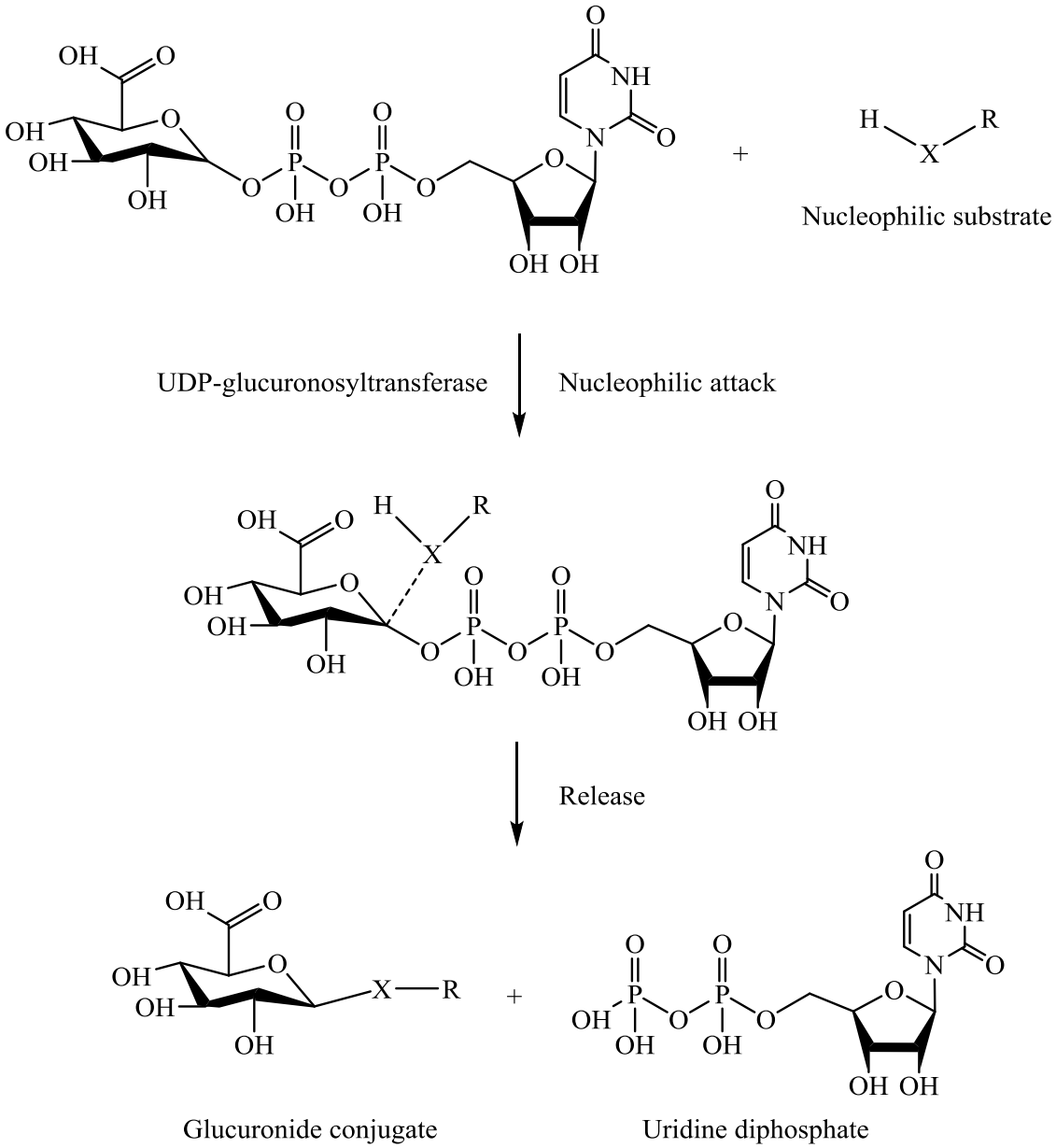


Figure 1. Glucuronidation reaction scheme.

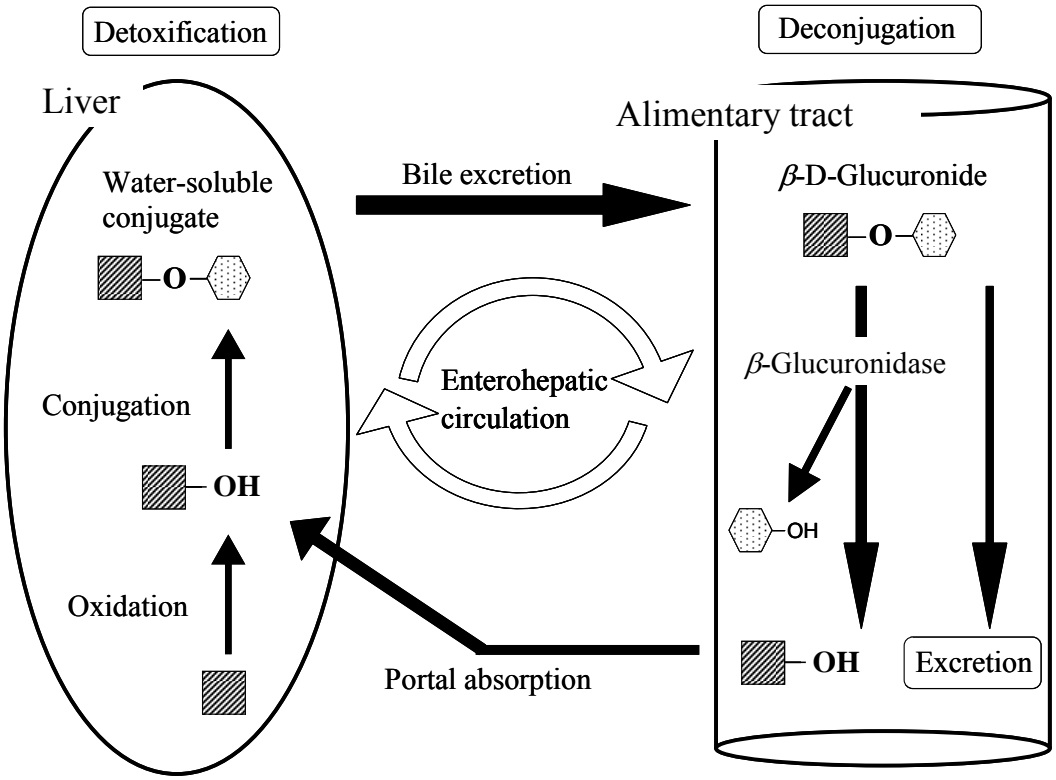
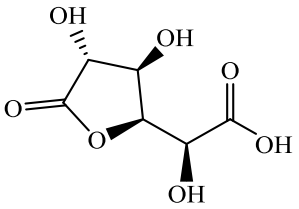
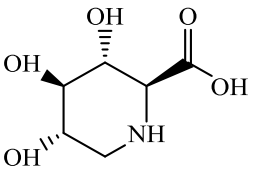


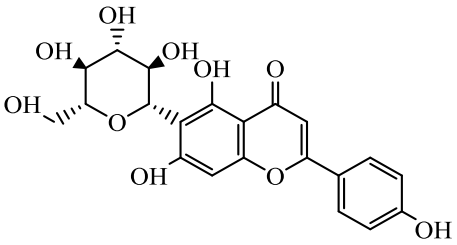
Figure 2. Biotransformation pathway and β-glucuronidase reaction.



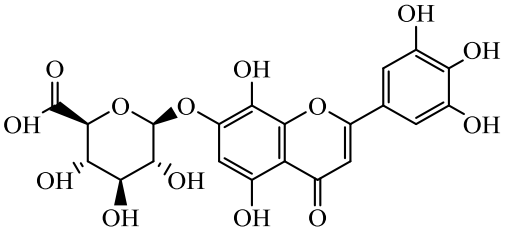
D-Glucaro-1,4-lactone
(**1**)



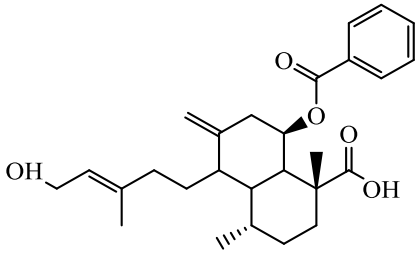
2(*S*)-Carboxy-3(*R*),4(*R*),5(*S*)-trihydroxypiperidine
(**2**)



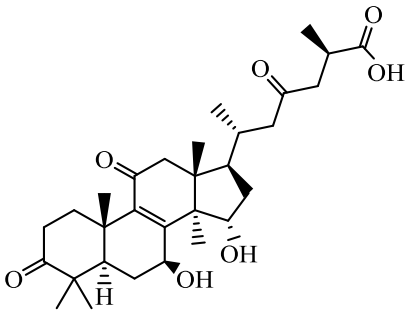
Isovitexin
(**3**)



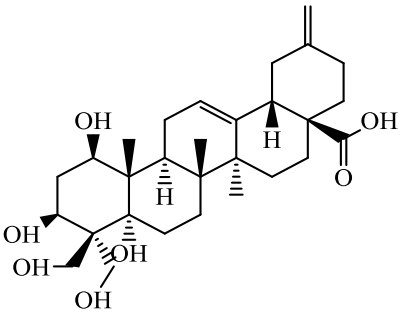
5,7,8,3',4',5'-Hexahydroxyflavone 7-*O*-β-D-glucuronide
(**4**)



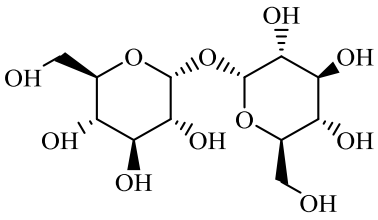
Scoparic acid A
(**5**)



Ganoderenic acid A
(**6**)

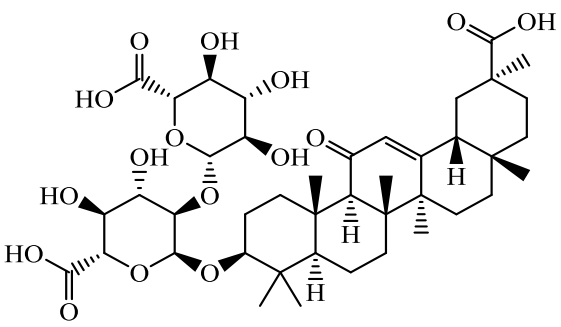


1,3,5,23,24-Pentahydroxy-30-norolean-12,20(29)-dien-28-oic acid
(**7**)

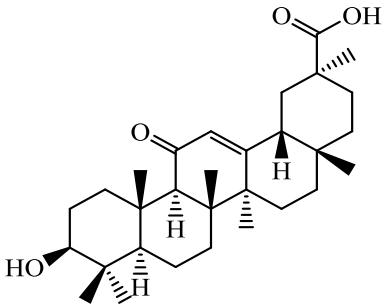


Trehalose
(**8**)

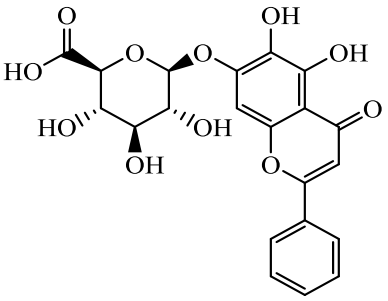
Figure 3. Known β-glucuronidase inhibitors (a).



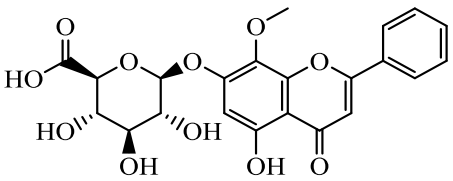
Glycyrrhizin
(**9**)



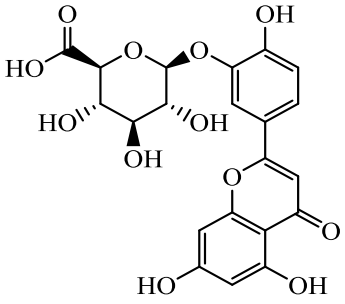
18β-Glycyrrhetinic acid
(**10**)



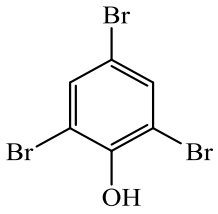
Baicalin
(**11**)



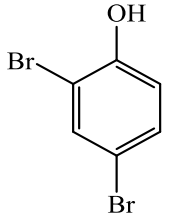
Wogonoside
(**12**)



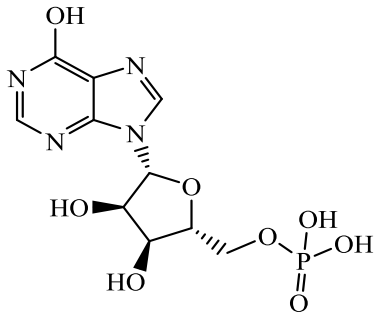
Luteolin-3'-glucuronide
(**13**)



2,4,6-Tribromophenol
(**14**)



2,4-Dibromophenol
(**15**)



IMP (**16**)

Figure 3. Known β-glucuronidase inhibitors (b).

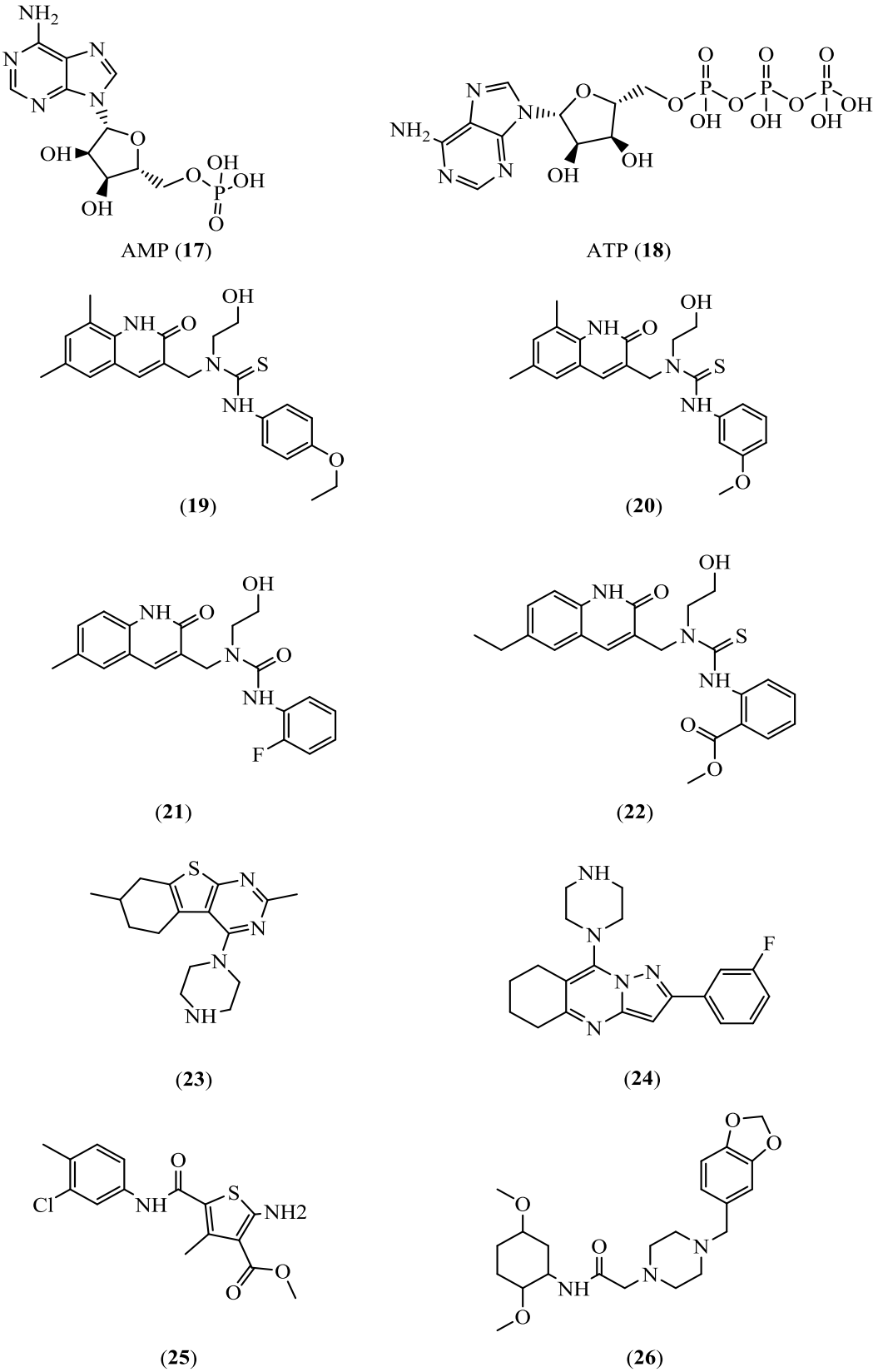
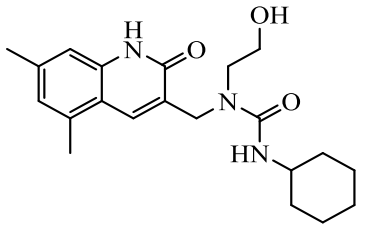
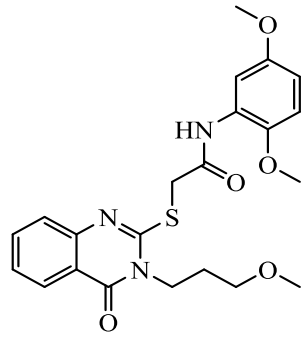


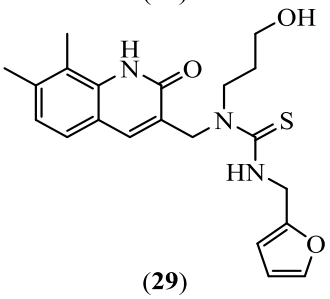
Figure 3. Known β-glucuronidase inhibitors (c).



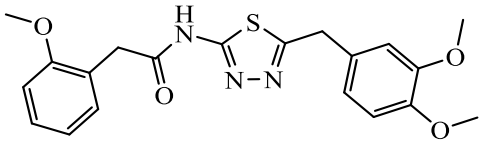
(**27**)



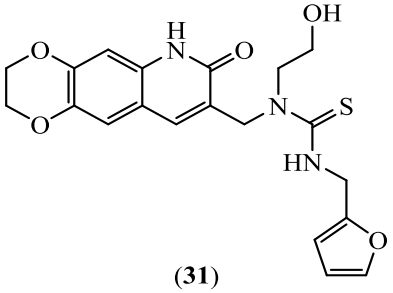
(**28**)



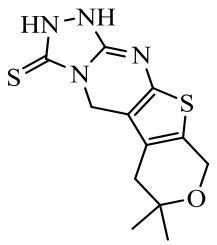
(**29**)



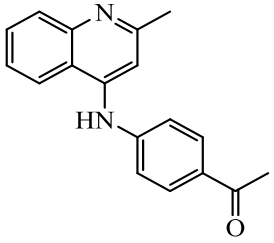
(**30**)



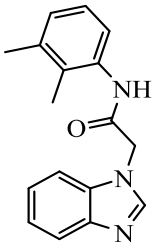
(**31**)



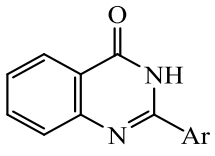
(**32**)



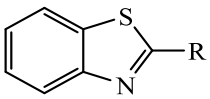
(**33**)



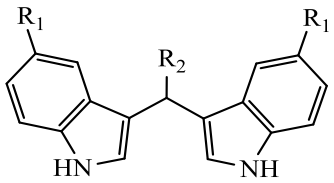
(**34**)



Benzaldehydes
(**35**)

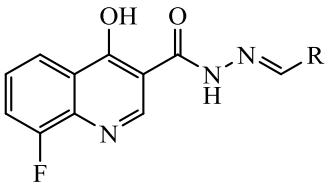


Benzothiazoles
(**36**)

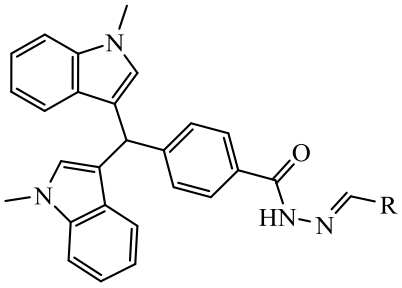


Bisindolylmethanes
(**37**)

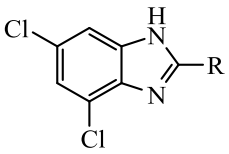
Figure 3. Known β-glucuronidase inhibitors (d).



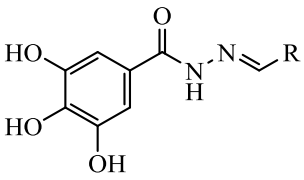
N-Arylidenequinoline-3-carbohydrazides
(**38**)



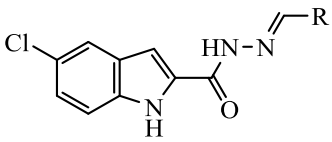
Hydrazoneas
(**39**)



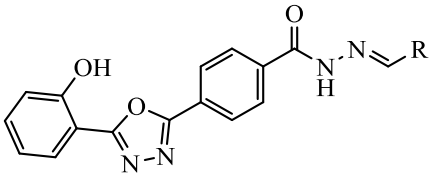
Benzimidazoles
(**40**)



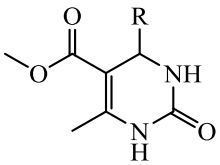
3,4,5-Trihydroxybenzohydrazones
(**41**)



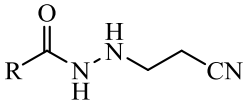
Indole hydrazones
(**42**)



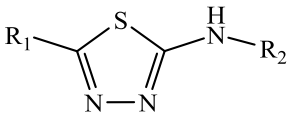
Oxadiazole benzohydrazones
(**43**)



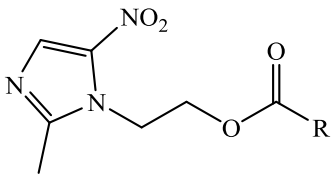
Dihydropyrimidones
(**44**)



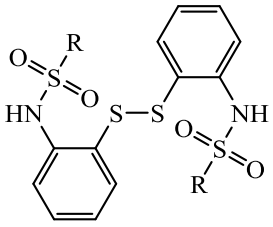
Hydrazideas
(**45**)



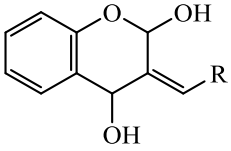
Thiadiazoleas
(**46**)



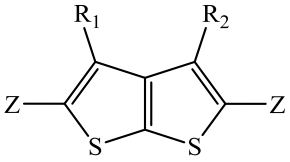
5-Nitroimidazoles
(**47**)



Disulfide and sulfone hybrid analogs
(**48**)



Coumarins
(**49**)



Thienothiophenes
(**50**)

R, R_1, R_2 = Alkyl, Aryl;
Z = Functionnalised group

Figure 3. Known β-glucuronidase inhibitors (e).

Chapter 1

Screening of β-Glucuronidase Inhibitors

In this chapter, marine algae collected along Hokkaido coast were extracted with methanol and the extracts were screened for the potential β-glucuronidase inhibitors.

1.1 Collection and organic solvent extraction of marine algae

1.1.1 Chemicals and instruments

(1) Chemicals

- *Escherichia coli* β-glucuronidase (type IX-A)

  Sigma-Aldrich (St. Louis, Mo, USA)

- *p*-Nitrophenyl β-D-glucuronide

  Sigma-Aldrich (St. Louis, Mo, USA)

- Sodium dihydrogenphosphate dihydrate ($NaH_2PO_4 \cdot 2H_2O$)

  Wako Pure Chemical Industries, Ltd. (Osaka, Japan)

- Disodium hydrogenphosphate (Na_2HPO_4)

  Wako Pure Chemical Industries, Ltd. (Osaka, Japan)

- Sodium carbonate (Na_2CO_3)

  Kanto Chemical Co., Inc. (Tokyo, Japan)

- D-Saccharic acid 1,4-lactone

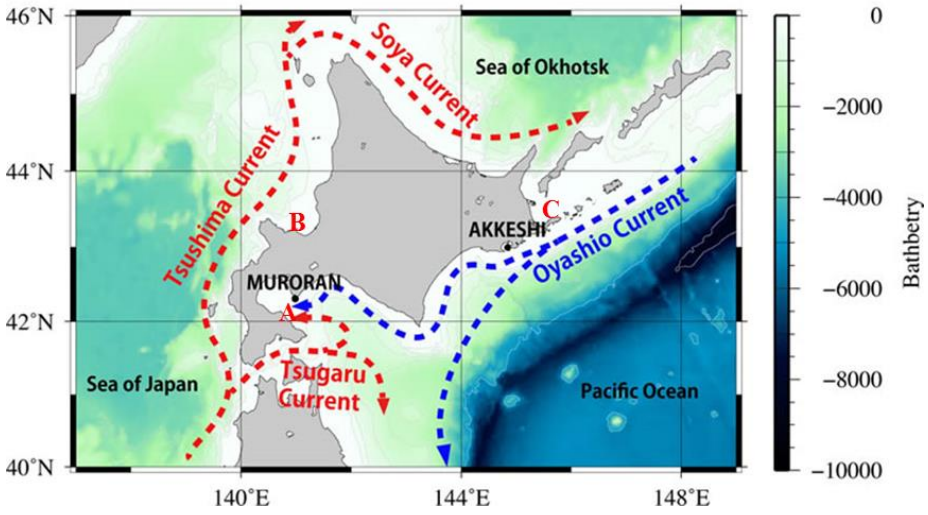
  Sigma-Aldrich (St. Louis, Mo, USA)

(2) Instruments

- Spectrophotometer SP-808 Technical & Try Co., Ltd. (Kanagawa, Japan)
- Filter paper Toyo Roshi Kaisha, Ltd. (Tokyo, Japan)

1.1.2 Collection of marine algae

Algal samples were collected at three typical coastal sites of Hokkaido, Japan during the year 2015~2017 (Figure 1-1). First site was Usujiri Fisheries Station (site A) of Field Science Center for Northern Biosphere (FSC) of Hokkaido University in Hakodate where the cold Oyashio and warm Tsushima current influenced area. Second site was Oshoro Marine Station (site B) of FSC in Otaru where the warm Tsushima current influenced area. Third site was Habomai area (site C) in Nemuro where the cold Oyashio current influenced area. Samples were identified according to the illustrated seaweeds catalogues (Chihara, 2002) and by Prof. Hiroyuki Mizuta, Faculty of Fisheries Sciences, Hokkaido University. The voucher specimens of algae were deposited at the laboratory of Laboratory of Marine Chemical Resource Development of Hokkaido University.



(http://www.fsc.hokudai.ac.jp/KANRYU/english/field.html)

Figure 1- 1. The path of the Oyashio and Tsushima Current around Hokkaido, Japan.

1.1.3 Organic solvent extraction of marine algae

Collected algal samples were brought to the laboratory immediately and washed thoroughly by the tap water to remove the epiphytes, sands and other pollution off. After air drying overnight, the seaweed samples were weighted, cut into small pieces and finally extracted twice with methanol or acetone for 3 or 4 days under room temperature in dark. The solvent was decanted, filtered and evaporated under reduced pressure with rotary evaporator (<40 °C). The primary and secondary extracts (Tables 1-1 to 1-11) of all the algal samples were dissolved in methanol and/or water and/or *n*-hexane and stocked at 4 °C in dark.

Table 1-1. Specimens collected in Usujiri, Hakodate on April 21st, 2015

Specimen	Scientific name	Weight (kg) of specimen	Weight (g) of Primary extract	Weight (g) of secondary extract
Phaeophyceae				
Matsumo	*Analipus japonicus*	0.147	3.569	0.863
Watamo	*Colpomenia bullosa*	0.166	1.739	1.520
Kayamonori	*Scytosiphon lomentaria*	0.013	0.538	0.083
Fushisujimoku	*Sargassum confusum*	0.390	14.459	4.452
Umitoranoo	*Sargassum thunbergii*	285.7	9.821	2.428
Akamoku	*Sargassum horneri*	0.034	2.766	0.100
Rhodophylaceae				
Akaba	*Neodilsea yendoana*	0.007	0.428	0.246
Hirakotoji	*Chondrus pinnulatus*	0.011	0.806	0.197
Fukurofunori	*Gloiopeltis furcata*	0.451	14.296	2.166
Akabaginnansou	*Mazzaella japonica*	0.004	0.028	0.026
Kurohaginnansou	*Chondrus yendoi*	1.391	42.822	8.401
Kushibenihiba	*Ptilota filicina*	0.045	2.791	0.330
Moroitogusa	*Polysiphonia morrowii*	0.007	0.411	0.072
Fujimatsumo	*Neorhodomela aculeata*	0.112	4.969	0.851
Hakesakinokogirihiba	*Odonthalia corymbifera*	0.092	6.400	0.800
Hosobafujimatsumo	*Rhodomela teres*	0.069	3.490	0.502

Table 1-2. Specimens collected in Usujiri, Hakodate on June 3rd, 2015

Specimen	Scientific name	Weight (kg) of specimen	Weight (g) of Primary extract	Weight (g) of secondary extract
Chlorophyceae				
Anaaosa	*Ulva pertusa*	0.103	3.105	0.596
Phaeophyceae				
Matsumo	*Analipus japonicus*	1.700	43.800	17.100
Nebarimo	*Leathesia difformis*	0.052	1.321	0.156
Kayamonori	*Scytosiphon lomentaria*	0.047	1.453	0.032
Chigaiso	*Alaria crassifolia*	0.164	12.529	1.814
Makonbu	*Saccharina japonica*	0.107	7.618	0.524
Fushisujimoku	*Sargassum confusum*	4.800	143.400	28.600
Umitoranoo	*Sargassum thunbergii*	3.500	111.500	35.600
Rhodophylaceae				
Makusa	*Gelidium elegans*	0.093	4.746	0.743
Hirakotoji	*Chondrus pinnulatus*	1.340	35.718	17.316
Kurohaginnansou	*Chondrus yendoi*	1.970	16.877	8.563
Akabaginnansou	*Mazzaella japonica*	0.610	13.476	2.749
Kushibenihiba	*Ptilota filicina*	0.025	0.983	0.225
Fujimatsumo	*Neorhodomela aculeata*	3.000	71.800	16.500
Hakesakinokogirihiba	*Odonthalia corymbifera*	0.664	28.247	4.932

Table 1-3. Specimens collected in Habomai, Nemuro on July 2nd, 2015

Specimen	Scientific name	Weight (kg) of specimen	Weight (g) of Primary extract	Weight (g) of secondary extract
Chlorophyceae				
Anaaosa	*Ulva pertusa*	0.048	1.822	0.552
Ezomiru	*Codium yezoense*	0.900	14.505	7.194
Phaeophyceae				
Matsumo	*Analipus japonicus*	0.360	8.989	2.842
Nagamatsumo	*Chordaria flagelliformis*	1.800	32.261	17.683
Ezofukuro	*Coilodesme japonica*	0.250	5.785	1.220
Aname	*Agarum clathratum*	1.380	26.700	14.000
Tororokonbu	*Saccharina gyrata*	0.530	15.547	2.463
Hibamata	*Fucus distichus* subsp. *evanescens*	0.970	36.500	17.600
Nebutomoku	*Stephanocystis crassipes*	2.300	74.300	31.800
Rhodophylaceae				
Darusu	*Palmaria palmata*	0.020	1.858	0.538
Hirakotoji	*Chondrus pinnulatus*	0.064	2.412	0.734
Kurohaginnansou	*Chondrus yndoi*	0.530	13.792	2.961
Akabaginnansou	*Mazzaella japonica*	0.035	1.208	0.085
Egonori	*Campylaephora hypnaeoides*	0.950	2.246	2.858
Igisu	*Ceramium kondoi*	0.089	0.529	0.183
Fujimatsumo	*Neorhodomela aculeata*	0.160	33.293	4.880
Hakesakinokogirihiba	*Odonthalia corymbifera*	0.330	4.423	0.338

Table 1-4. Specimens collected in Oshoro, Otaru on July 7th, 2015

Specimen	Scientific name	Weight (kg) of specimen	Weight (g) of Primary extract	Weight (g) of secondary extract
Chlorophyceae				
Bouaonori	*Ulva intestinalis*	0.035	0.442	0.098
Anaaosa	*Ulva pertusa*	0.026	0.689	0.241
Sujiaonori	*Ulva prolifera*	0.011	0.118	0.042
Tsuyanashishiogusa	*Cladophora opaca*	0.127	1.580	0.073
Phaeophyceae				
Ezoyahazu	*Dictyopteris divaricata*	0.065	4.976	1.132
Umitoranoo	*Sargassum thunbergii*	1.300	40.617	15.001
Azumanejimoku	*Sargussum yamadae*	0.240	38.359	6.505
Rhodophylaceae				
Makusa	*Gelidium elegans*	0.163	9.225	1.921
Marubatsunomata	*Chondrus nipponicus*	0.232	7.000	1.540
Hirakotoji	*Chondrus pinnulatus*	0.022	1.182	0.249
Haneigisu	*Ceramium japonicum*	0.183	6.826	0.657
Fujimatsumo	*Neorhodomela aculeata*	0.790	37.799	11.351

Table 1-5. Specimens collected in Usujiri, Hakodate on May 10th, 2016

Specimen	Scientific name	Weight (kg) of specimen	Weight (g) of Primary extract	Weight (g) of secondary extract
Phaeophyceae				
Matsumo	*Analipus japonicus*	0.119	4.010	0.410
Kayamonori	*Scytosiphon lomentaria*	0.582	10.040	1.820
Chigaiso	*Alaria crassifolia*	0.575	14.219	4.638
Fushisujimoku	*Sargassum confusum*	2.052	73.529	18.129
Uminoranoo	*Sargassum thunbergii*	1.099	40.139	10.519
Rhodophylaceae				
Sangomo	*Corallina officinalis*	0.008	0.080	0.015
Makusa	*Gelidium elegans*	1.350	45.799	12.633
Akaba	*Neodilsea yendoana*	0.264	12.520	2.770
Hirakotoji	*Chondrus pinnulatus*	0.182	12.330	2.520
Kurohaginnansou	*Chondrus yndoi*	0.161	4.600	0.880
Akabaginnansou	*Mazzaella japonica*	0.148	3.923	0.627
Matsunori	*Polyopes affinis*	0.006	0.125	0.024
Kushibenihiba	*Ptilota filicina*	0.141	4.029	0.603
Fujimatsumo	*Neorhodomela aculeata*	2.430	51.039	15.109
Hakesakinogirihiba	*Odonthalia corymbifera*	1.140	69.629	16.220
Hosobafujimatsumo	*Rhodomela teres*	0.419	19.489	4.749

Table 1-6. Specimens collected in Usujiri, Hakodate on May 25th, 2016

Specimen	Scientific name	Weight (kg) of specimen	Weight (g) of Primary extract	Weight (g) of secondary extract
Phaeophyceae				
Matsumo	*Analipus japonicus*	0.239	7.462	1.579
Ezoyahazu	*Dictyopteris divaricata*	0.232	7.340	1.541
Kayamonori	*Scytosiphon lomentaria*	0.063	1.262	0.481
Chigaiso	*Alaria crassifolia*	0.274	7.459	2.810
Umitoranoo	*Sargassum thunbergii*	0.188	8.147	1.364
Nebarimo	*Leathesia difformis*	0.007	0.233	0.025
Makonbu	*Saccharina japonica*	0.069	4.281	0.738
Rhodophylaceae				
Makusa	*Gelidium elegans*	0.315	11.057	2.651
Akaba	*Neodilsea yendoana*	1.470	49.080	14.351
Fukurofunori	*Gloiopeltis furcata*	0.383	9.338	1.350
Togetsunomata	*Chondrus armatus*	0.037	1.336	0.357
Tsunomata	*Chondrus ocellatus*	0.007	0.439	0.113
Hirahitoji	*Chondrus pinnulatus*	0.213	12.36	2.42
Kurohaginnansou	*Chondrus yndoi*	0.008	0.185	0.028
Akabaginnansou	*Mazzaella japonica*	0.041	1.178	0.192
Karekigusa	*Tichocarpus crinitus*	0.625	32.700	7.540
Kushibenihiba	*Ptilota filicina*	0.006	0.517	0.040
Fujimatsumo	*Neorhodomela aculeata*	1.400	36.598	13.420
Hakesakinogirihiba	*Odonthalia corymbifera*	0.692	30.960	10.430

Table 1-7. Specimens collected in Oshoro, Otaru on June 28th, 2016

Specimen	Scientific name	Weight (kg) of specimen	Weight (g) of Primary extract	Weight (g) of secondary extract
Chlorophyceae				
Anaaosa	*Ulva pertusa*	0.009	0.328	0.075
Fujiaonori	*Ulva prolifera*	0.503	5.280	2.276
Tamajuzumo	*Chaetomorpha moniligera*	0.007	0.502	0.102
Phaeophyceae				
Ezoyahazu	*Dictyopteris divaricata*	0.730	31.546	7.119
Tsurumo	*Chorda asiatica*	0.599	18.220	3.480
Uganomoku	*Stephanocystis hakodatensis*	0.180	7.019	2.175
Hondawara	*Sargassum fulvellum*	1.250	39.920	11.790
Fushisujimoku	*Sargassum confusum*	1.040	38.470	7.680
Rhodophylaceae				
Makusa	*Gelidium elegans*	0.293	8.430	1.505
Akaba	*Neodilsea yendoana*	1.060	35.680	6.975
Marubatsunomata	*Chondrus nipponicus*	0.564	16.630	3.418
Hirakotoji	*Chondrus pinnulatus*	0.017	0.569	0.080
Haneigisu	*Ceramium japonicum*	0.007	9.391	2.640
Yuna	*Chondria crassicaulis*	0.049	6.128	1.112
Urasozo	*Laurencia nipponica*	0.840	18.910	3.190
Mitsudesozo	*Laurencia okamurae*	0.385	0.988	0.072
Fujimatsumo	*Neorhodomela aculeata*	0.122	1.114	0.253
Isomurasaki	*Symphyocladia latiuscula*	0.028	9.980	1.567

Table 1-8. Specimens collected in Habomai, Nemuro on July 5th, 2016

Specimen	Scientific name	Weight (g) of specimen	Weight (g) of Primary extract	Weight (g) of secondary extract
Chlorophyceae				
Anaaosa	*Ulva pertusa*	0.039	2.400	0.520
Tsuyanashishiogusa	*Cladophora opaca*	0.721	7.932	3.341
Phaeophyceae				
Nagamatsumo	*Chordaria flagelliformis*	0.208	3.501	0.401
Ezofukuro	*Coilodesme japonica*	0.660	8.282	2.831
Aname	*Agarum clathratum*	1.152	35.834	5.244
Hibamata	*Fucus distichus* subsp. *evanescens*	2.172	109.958	29.404
Nebutomoku	*Stephanocystis crassipes*	3.653	1.000	0.252
Rhodophylaceae				
Darusu	*Palmaria palmata*	0.241	6.671	1.276
Umizoumen	*Nemalion vermiculare*	0.124	2.368	0.716
Akabaginnansou	*Mazzaella japonica*	0.085	1.724	0.204
Karekigusa	*Tichocarpus crinitus*	1.832	55.421	28.153
Katababenihiba	*Neoptilota asplenioides*	0.005	0.221	0.036
Kushibenihiba	*Ptilota filicina*	0.792	13.044	4.789
Isomurasaki	*Symphyocladia latiuscula*	0.023	1.171	0.241

Table 1-9. Specimens collected in Usujiri, Hakodate on April 27th, 2017

Specimen	Scientific name	Weight (kg) of specimen	Weight (g) of Primary extract	Weight (g) of secondary extract
Chlorophyceae				
Anaaosa	*Ulva pertusa*	0.022	0.674	0.096
Phaeophyceae				
Matsumo	*Analipus japonicus*	0.092	1.914	1.868
Watamo	*Colpomenia bullosa*	1.512	27.907	7.817
Kayamonori	*Scytosiphon lomentaria*	1.526	41.588	11.778
Chigaiso	*Alaria crassifolia*	0.667	13.705	6.190
Fushisujimoku	*Sargassum confusum*	1.491	3.298	0.637
Umitoranoo	*Sargassum thunbergii*	0.989	36.571	9.290
Rhodophylaceae				
Akaba	*Neodilsea yendoana*	0.229	4.314	3.308
Matsunori	*Polyopes affinis*	0.025	2.338	0.635
Egonori	*Campylaephora hypnaeoides*	0.127	3.386	0.613
Kushibenihiba	*Ptilota filicina*	0.005	0.207	0.042
Fujimatsumo	*Neorhodomela aculeata*	1.948	39.340	32.170
Hakesakinogirihiba	*Odonthalia corymbifera*	0.108	5.140	0.500
Hosobafujimatsumo	*Rhodomela teres*	0.272	14.930	3.441

Table 1-10. Specimens collected in Habomai, Nemuro on May 26th, 2017

Specimen	Scientific name	Weight (kg) of specimen	Weight (g) of Primary extract	Weight (g) of secondary extract
Chlorophyceae				
Ezomiru	*Codium yezoense*	0.211	0.253	0.134
Phaeophyceae				
Kesorushigusa	*Desmarestia viridis*	0.397	0.193	0.034
Aname	*Agarum clathratum*	1.054	16.970	3.772
Sujime	*Costaria costata*	0.112	0.324	0.102
Hibamata	*Fucus distichus* subsp. *evanescens*	4.708	0.995	0.288
Nebutomoku	*Stephanocystis crassipes*	1.700	0.396	0.194
Rhodophylaceae				
Benifukuronori	*Halosaccion yendoi*	0.489	8.286	1.361
Darusu	*Palmaria palmata*	0.302	5.805	0.963
Akabaginnansou	*Mazzaella japonica*	0.487	4.778	0.909
Kushibenihiba	*Ptilota filicina*	0.106	1.580	0.271
Fujimatsumo	*Neorhodomela aculeata*	0.334	6.449	1.246
Hakesakinogirihiba	*Odonthalia corymbifera*	0.100	2.727	0.388

Table 1-11. Specimens collected in Usujiri, Hakodate on June 9th, 2017

Specimen	Scientific name	Weight (kg) of specimen	Weight (g) of Primary extract	Weight (g) of secondary extract
Phaeophceae				
Kayamonori	*Scytosiphon lomentaria*	0.152	0.779	0.080
Fushisujimoku	*Sargassum confusum*	0.038	1.086	0.262
Umitoranoo	*Sargassum thunbergii*	0.042	1.866	0.326
Rhodophylaceae				
Makusa	*Gelidium elegans*	6.213	0.543	0.213
Akaba	*Neodilsea yendonna*	0.128	7.075	1.824
Igisu	*Ceramium kondoi*	6.678	0.751	0.104
Urasozo	*Laurencia nipponica*	0.056	16.740	1.690
Fujimatsumo	*Neorhodomela aculeata*	0.156	31.132	11.036
Hakesakinogirihiba	*Odonthalia corymbifera*	0.091	5.602	1.522
Isomurasaki	*Symphyocladia latiuscula*	5.850	0.510	0.189

1.2 β-Glucuronidase inhibitory activity assay

1.2.1 β-Glucuronidase enzymatic activity test

Inhibitory activity of β-glucuronidase was determined spectrophotometrically by the hydrolysis reaction from *p*-nitrophenyl β-D-glucuronide to *p*-nitrophenol (Figure 1-2). Experimental assay was carried out according to the method of Kim et al. (2008) with some modification.

Reaction mixture contained 10 mM phosphate buffer (pH 7.0, 440 μL), 10 mM *p*-nitrophenyl β-D-glucuronide in the buffer (20 μL) and test substance (final concentration of 10 μg/mL, 20 μL). After pre-incubated at 37 ºC for 5 min, reaction was initiated by adding *Escherichia coli* β-glucuronidase (80 units/mL, 20 μL) and kept at 37 ºC for 7 min. The reaction was terminated by adding 1 M sodium carbonate (300 μL). The released *p*-nitrophenol was measured at 400 nm. D-Saccharic acid 1,4-lactone was used as the positive control (Diez & Cabezas, 1979) and all assays were conducted in triplicate (Figure 1-3).

Inhibitory activity was calculated as following equation (1):

$$\textit{Inhibition activity}\ (\%) = [(C - C_0) - (T - T_0)] / (C - C_0) \times 100 \qquad (1)$$

C: Absorbance of control

C_0: Absorbance of control's blank

T: Absorbance of test experiment

T_0: Absorbance of test experiment's blank

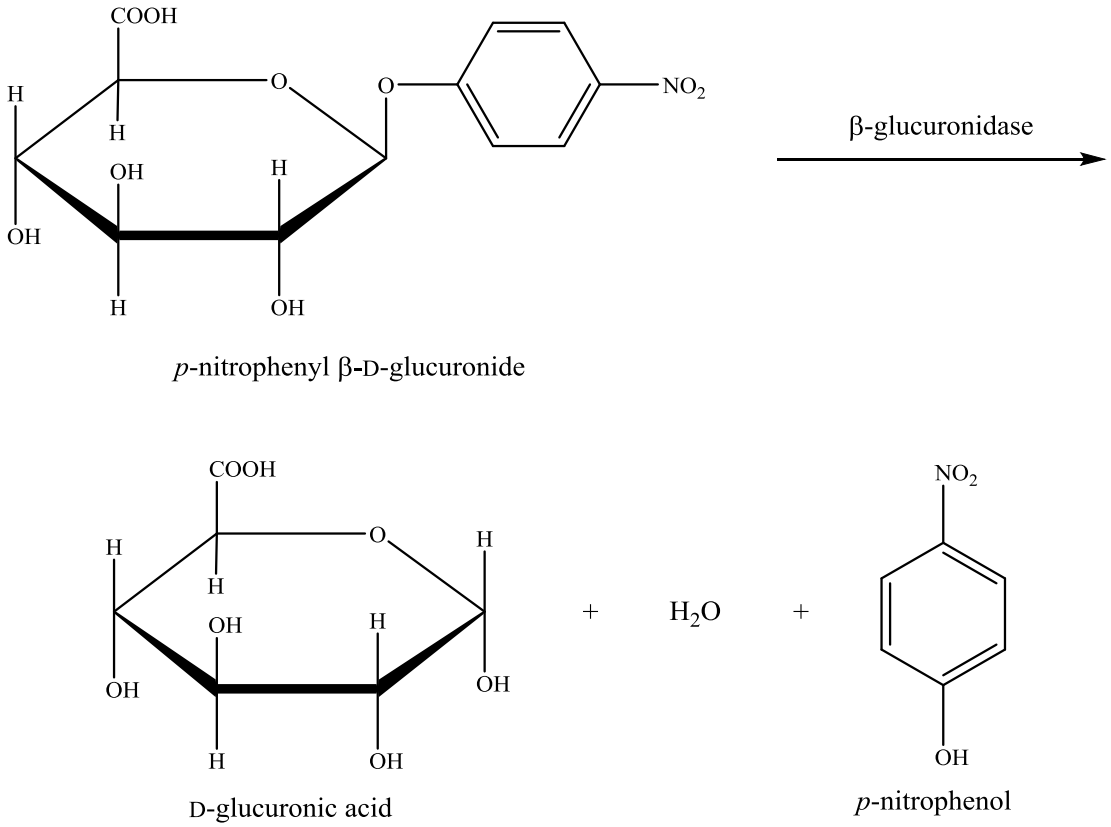


Figure 1-2. Hydrolytic reaction catalyzed by β-glucuronidase.

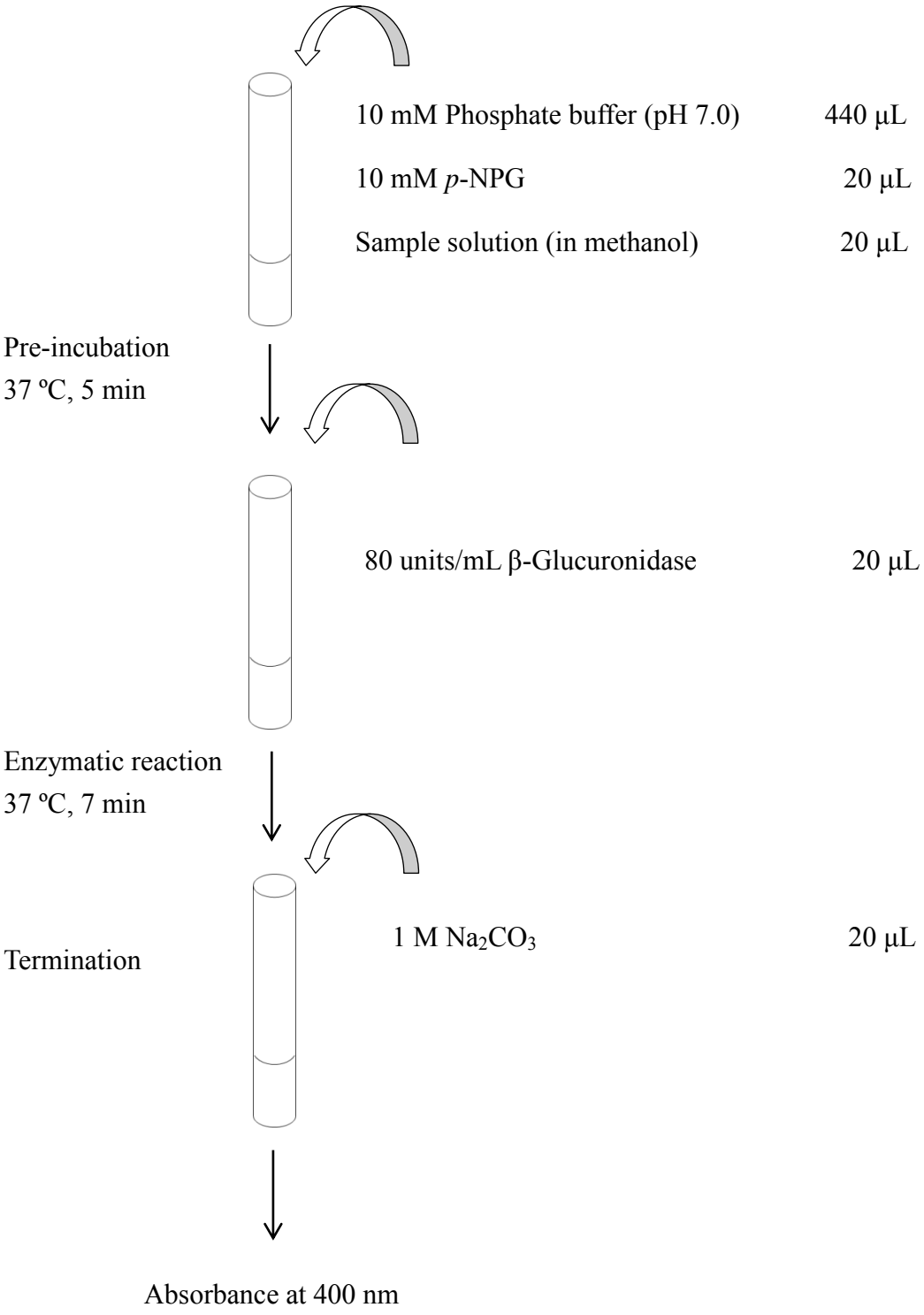


Figure 1-3. β-Glucuronidase inhibitory enzymatic activity test.

1.2.2 Screening of β-glucuronidase inhibitors from marine algae

Primary extracts of all the algae collected during 2015 to 2017 were conducted for the β-glucuronidase inhibitory assay with final sample concentration of 10 μg/mL. Results were shown in Tables 1-12 to 1-22. Inhibitory activity of the extracts of green marine algae showed moderate or no inhibitory activity, except genus *Codium yezoense* (Codiaceae, Bryopsidales) collected at Usujiri, Hakodate (site A) in 2017 that showed about 67% β-glucuronidase inhibition. The primary methanol extracts of brown and red algae showed relatively strong inhibitory activity, especially brown marine algae of families Sargassaceae, Agaraceae, Alariaceae, Scytosiphonaceae, Desmarestiaceae and red marine algae of families Rhodomelaceae, Dumontiaceae, Ceramiaceae, Palmariaceae showed potent inhibitory activity.

Table 1-12. β-Glucuronidase inhibition of methanol extracts of algae collected in Usujiri, Hakodate on April 21st, 2015

Specimen	Scientific name	Inhibition[a] (%)
Phaeophyceae		
Matsumo	*Analipus japonicus*	NI
Watamo	*Colpomenia bullosa*	NI
Fushisujimoku	*Sargassum confusum*	NI[b]
Umitoranoo	*Sargassum thunbergii*	NI
Akamoku	*Sargassum horneri*	NI
Rhodophylaceae		
Akaba	*Neodilsea yendoana*	24.28 ± 1.70
Hirakotoji	*Chondrus pinnulatus*	NI
Fukurofunori	*Gloiopeltis furcata*	NI
Kurohaginnansou	*Chondrus yendoi*	7.81 ± 2.76
Kushibenihiba	*Ptilota filicina*	NI
Moroitogusa	*Polysiphonia morrowii*	19.04 ±2.36
Fujimatsumo	*Neorhodomela aculeata*	NI
Hakesakinokogirihiba	*Odonthalia corymbifera*	11.96 ± 1.13

[a]Assay concentration was 10 μg/mL. Data represent means ± SE (n=3).

[b]NI, no inhibition.

Table 1-13. β-Glucuronidase inhibition of methanol extracts of algae collected in Usujiri, Hakodate on June 3rd, 2015

Specimen	Scientific name	Inhibition[a] (%)
Chlorophyceae		
Anaaosa	*Ulva pertusa*	NI[b]
Phaeophyceae		
Matsumo	*Analipus japonicus*	19.72 ± 1.40
Nebarimo	*Leathesia difformis*	NI
Kayamonori	*Scytosiphon lomentaria*	NI
Chigaiso	*Alaria crassifolia*	18.56 ± 0.16
Makonbu	*Saccharina japonica*	NI
Fushisujimoku	*Sargassum confusum*	25.13 ± 1.45
Umitoranoo	*Sargassum thunbergii*	32.36 ± 1.73
Rhodophylaceae		
Makusa	*Gelidium elegans*	NI
Hirakotoji	*Chondrus pinnulatus*	0.78 ± 1.25
Kurohaginnansou	*Chondrus yendoi*	NI
Akabaginnansou	*Mazzaella japonica*	8.56 ± 1.53
Kushibenihiba	*Ptilota filicina*	NI
Fujimatsumo	*Neorhodomela aculeata*	49.62 ± 1.79
Hakesakinokogirihiba	*Odonthalia corymbifera*	6.12 ± 1.85

[a]Assay concentration was 10 μg/mL. Data represent means ± SE (n=3).

[b]NI, no inhibition.

Table 1-14. β-Glucuronidase inhibition of methanol extracts of algae collected in Habomai, Nemuro on July 2nd, 2015

Specimen	Scientific name	Inhibition[a] (%)
Chlorophyceae		
Anaaosa	*Ulva pertusa*	1.34 ± 1.24
Ezomiru	*Codium yezoense*	NI [b]
Phaeophceae		
Matsumo	*Analipus japonicus*	NI
Nagamatsumo	*Chordaria flagelliformis*	NI
Ezofukuro	*Coilodesme japonica*	NI
Aname	*Agarum clathratum*	98.06 ± 0.27
Tororokonbu	*Saccharina gyrata*	NI
Hibamata	*Fucus distichus* subsp. *evanescens*	98.85 ±0.05
Nebutomoku	*Stephanocystis crassipes*	1.90 ± 1.02
Rhodophylaceae		
Darusu	*Palmaria palmata*	NI
Hirakotoji	*Chondrus pinnulatus*	NI
Akabaginnansou	*Mazzaella japonica*	NI
Igisu	*Ceramium kondoi*	0.69 ± 0.64
Fujimatsumo	*Neorhodomela aculeata*	NI
Hakesakinokogirihiba	*Odonthalia corymbifera*	NI

[a]Assay concentration was 10 μg/mL. Data represent means ± SE (n=3).

[b]NI, no inhibition.

Table 1-15. β-Glucuronidase inhibition of methanol extracts of algae collected in Oshoro, Otaru on July 7th, 2015

Specimen	Scientific name	Inhibition[a] (%)
Chlorophyceae		
Bouaonori	*Ulva intestinalis*	NI[b]
Sujiaonori	*Ulva prolifera*	NI
Phaeophyceae		
Ezoyahazu	*Dictyopteris divaricata*	3.12 ± 1.54
Umitoranoo	*Sargassum thunbergii*	8.70 ± 1.36
Azumanejimoku	*Sargussum yamadae*	NI
Rhodophylaceae		
Makusa	*Gelidium elegans*	NI
Marubatsunomata	*Chondrus nipponicus*	NI
Hirakotoji	*Chondrus pinnulatus*	NI
Haneigisu	*Ceramium japonicum*	NI
Fujimatsumo	*Neorhodomela aculeata*	5.08 ± 1.37

[a]Assay concentration was 10 μg/mL. Data represent means ± SE (n=3).

[b]NI, no inhibition.

Table 1-16. β-Glucuronidase inhibition of methanol extracts of algae collected in Usujiri, Hakodate on May 10th, 2016

Specimen	Scientific name	Inhibition[a] (%)
Phaeophyceae		
Matsumo	*Analipus japonicus*	16.69 ± 0.28
Kayamonori	*Scytosiphon lomentaria*	17.46 ± 3.99
Chigaiso	*Alaria crassifolia*	76.75 ± 2.16
Fushisujimoku	*Sargassum confusum*	71.29 ± 1.59
Uminoranoo	*Sargassum thunbergii*	75.46 ± 2.20
Rhodophylaceae		
Sangomo	*Corallina officinalis*	6.98 ± 2.66
Makusa	*Gelidium elegans*	13.50 ± 2.40
Akaba	*Neodilsea yendoana*	40.33 ± 0.53
Hirakotoji	*Chondrus pinnulatus*	14.92 ± 4.06
Kurohaginnansou	*Chondrus yndoi*	7.98 ± 1.93
Akabaginnansou	*Mazzaella japonica*	13.72 ± 0.37
Matsunori	*Polyopes affinis*	5.89 ± 2.42
Kushibenihiba	*Ptilota filicina*	65.39 ± 3.81
Fujimatsumo	*Neorhodomela aculeata*	57.68 ± 1.07
Hakesakinogirihiba	*Odonthalia corymbifera*	67.17 ± 3.86
Hosobafujimatsumo	*Rhodomela teres*	32.37 ± 2.22

[a]Assay concentration was 10 μg/mL. Data represent means ± SE (n=3).

Table 1-17. β-Glucuronidase inhibition of methanol extracts of algae collected in Usujiri, Hakodate on May 25th, 2016

Specimen	Scientific name	Inhibition[a] (%)
Phaeophyceae		
Matsumo	*Analipus japonicus*	26.94 ± 1.58
Ezoyahazu	*Dictyopteris divaricata*	17.11 ± 2.20
Kayamonori	*Scytosiphon lomentaria*	14.77 ± 2.26
Chigaiso	*Alaria crassifolia*	98.70 ± 0.35
Umitoranoo	*Sargassum thunbergii*	53.44 ± 7.33
Nebarimo	*Leathesia difformis*	16.68 ± 4.51
Makonbu	*Saccharina japonica*	13.71 ± 1.95
Rhodophylaceae		
Makusa	*Gelidium elegans*	11.93 ± 2.79
Akaba	*Neodilsea yendoana*	21.59 ± 0.39
Fukurofunori	*Gloiopeltis furcata*	11.75 ± 0.53
Togetsunomata	*Chondrus armatus*	10.05 ± 1.17
Tsunomata	*Chondrus ocellatus*	12.04 ± 2.39
Hirahitoji	*Chondrus pinnulatus*	7.97±1.41
Kurohaginnansou	*Chondrus yndoi*	18.73 ± 4.18
Akabaginnansou	*Mazzaella japonica*	86.07 ± 2.00
Karekigusa	*Tichocarpus crinitus*	13.57 ± 2.28
Kushibenihiba	*Ptilota filicina*	35.58 ± 3.81
Fujimatsumo	*Neorhodomela aculeata*	30.65 ± 1.02
Hakesakinogirihiba	*Odonthalia corymbifera*	68.17 ± 2.11

[a]Assay concentration was 10 μg/mL. Data represent means ± SE (n=3).

Table 1-18. β-Glucuronidase inhibition of methanol extracts of algae collected in Oshoro, Otaru on June 28th, 2016

Specimen	Scientific name	Inhibition[a] (%)
Chlorophyceae		
Anaaosa	*Ulva pertusa*	NI[b]
Fujiaonori	*Ulva prolifera*	NI
Tamajuzumo	*Chaetomorpha moniligera*	NI
Phaeophyceae		
Ezoyahazu	*Dictyopteris divaricata*	12.85 ± 3.58
Tsurumo	*Chorda asiatica*	NI
Uganomoku	*Stephanocystis hakodatensis*	NI
Hondawara	*Sargassum fulvellum*	62.65 ± 4.48
Fushisujimoku	*Sargassum confusum*	32.73 ± 0.83
Rhodophylaceae		
Makusa	*Gelidium elegans*	NI
Akaba	*Neodilsea yendoana*	NI
Marubatsunomata	*Chondrus nipponicus*	NI
Hirakotoji	*Chondrus pinnulatus*	NI
Haneigisu	*Ceramium japonicum*	NI
Yuna	*Chondria crassicaulis*	NI
Urasozo	*Laurencia nipponica*	NI
Mitsudesozo	*Laurencia okamurae*	NI
Fujimatsumo	*Neorhodomela aculeata*	NI
Isomurasaki	*Symphyocladia latiuscula*	96.04 ± 4.60

[a]Assay concentration was 10 μg/mL. Data represent means ± SE (n=3).

[b]NI, no inhibition.

Table 1-19. β-Glucuronidase inhibition of methanol extracts of algae collected in Habomai, Nemuro on July 5th, 2016

Specimen	Scientific name	Inhibition[a] (%)
Chlorophyceae		
Anaaosa	*Ulva pertusa*	5.79 ± 3.60
Tsuyanashishiogusa	*Cladophora opaca*	NI [b]
Phaeophyceae		
Ezofukuro	*Coilodesme japonica*	NI
Aname	*Agarum clathratum*	88.63 ± 0.42
Hibamata	*Fucus distichus* subsp. *evanescens*	91.63 ± 0.51
Nebutomoku	*Stephanocystis crassipes*	12.42 ± 4.76
Rhodophylaceae		
Darusu	*Palmaria palmata*	76.03 ± 1.17
Umizoumen	*Nemalion vermiculare*	16.98 ± 5.28
Katababenihiba	*Neoptilota asplenioides*	NI
Isomurasaki	*Symphyocladia latiuscula*	38.46 ± 6.24

[a]Assay concentration was 10 μg/mL. Data represent means ± SE (n=3).

[b]NI, no inhibition.

Table 1-20. β-Glucuronidase inhibition of methanol extracts of algae collected in Usujiri, Hakodate on April 27th, 2017

Specimen	Scientific name	Inhibition[a] (%)
Chlorophyceae		
Anaaosa	*Ulva pertusa*	NI [b]
Phaeophyceae		
Matsumo	*Analipus japonicus*	NI
Kayamonori	*Scytosiphon lomentaria*	90.55 ± 0.01
Chigaiso	*Alaria crassifolia*	39.60 ± 0.03
Fushisujimoku	*Sargassum confusum*	85.23 ± 0.04
Umitoranoo	*Sargassum thunbergii*	32.92 ± 0.01
Rhodophylaceae		
Akaba	*Neodilsea yendoana*	97.21 ± 0.01
Matsunori	*Polyopes affinis*	NI
Egonori	*Campylaephora hypnaeoides*	NI
Kushibenihiba	*Ptilota filicina*	NI
Fujimatsumo	*Neorhodomela aculeata*	75.90 ± 0.02
Hakesakinogirihiba	*Odonthalia corymbifera*	93.65 ± 0.02
Hosobafujimatsumo	*Rhodomela teres*	78.65 ± 0.07

[a]Assay concentration was 10 μg/mL. Data represent means ± SE (n=3).

[b]NI, no inhibition.

Table 1-21. β-Glucuronidase inhibition of methanol extracts of algae collected in Usujiri, Hakodate on May 26th, 2017

Specimen	Scientific name	Inhibition[a] (%)
Chlorophyceae		
Ezomiru	*Codium yezoense*	67.83 ± 0.02
Phaeophyceae		
Kesorushigusa	*Desmarestia viridis*	87.44 ± 0.00
Aname	*Agarum clathratum*	98.26 ± 0.01
Sujime	*Costaria costata*	72.92 ± 0.06
Hibamata	*Fucus distichus* subsp. *evanescens*	99.88 ± 0.00
Nebutomoku	*Stephanocystis crassipes*	99.30 ± 0.01
Rhodophylaceae		
Benifukuronori	*Halosaccion yendoi*	54.45 ± 0.01
Darusu	*Palmaria palmata*	58.85 ± 0.01
Akabaginnansou	*Mazzaella japonica*	58.92 ± 0.00
Kushibenihiba	*Ptilota filicina*	62.45 ± 0.00
Fujimatsumo	*Neorhodomela aculeata*	69.39 ± 0.01
Hakesakinogirihiba	*Odonthalia corymbifera*	98.47 ± 0.00

[a]Assay concentration was 10 μg/mL. Data represent means ± SE (n=3).

Table 1-22. β-Glucuronidase inhibition of methanol extracts of algae collected in Usujiri, Hakodate on June 9th, 2017

Specimen	Scientific name	Inhibition[a] (%)
Phaeophyceae		
Kayamonori	*Scytosiphon lomentaria*	7.21 ± 0.49
Fushisujimoku	*Sargassum confusum*	18.33 ± 1.82
Umitoranoo	*Sargassum thunbergii*	31.26 ± 2.10
Rhodophylaceae		
Makusa	*Gelidium elegans*	51.14 ± 0.85
Akaba	*Neodilsea yendonna*	17.17 ± 0.41
Igisu	*Ceramium kondoi*	NI[b]
Urasozo	*Laurencia nipponica*	NI
Fujimatsumo	*Neorhodomela aculeata*	NI
Hakesakinogirihiba	*Odonthalia corymbifera*	49.35 ± 2.21
Isomurasaki	*Symphyocladia latiuscula*	79.99 ± 0.95

[a]Assay concentration was 10 μg/mL. Data represent means ± SE (n=3).

[b]NI, no inhibition.

1.3 Discussion

151 algal samples consisting of 7 species of green algae, 22 species of brown algae, and 30 species of red algae were extracted and tested for β-glucuronidase inhibitory activity assay. Inhibitory screening assay data showed that green algae had no or weak inhibitory activity but most of the collected brown and red algae showed moderate or strong inhibitory activity.

Marine algae are well known for the diversity of bioactive secondary metabolites. Brown and red algae, which contain a broad range of bioactive metabolites, have been attracted considerable research interest, while just fewer secondary metabolites from green algae have been reported (Blunt et al., 2017). Generally, brown and red algae contain terpenes and polyphenolic compounds as dominant secondary metabolites (Blunt et al., 2006). Researches have revealed brown algae of order Fucales (Ferreres et al., 2012) (Raddatz, Guy-Haim, Rilov, & Wahl, 2017), family Laminariaceae (Jung, Roy, Jung, & Choi, 2017) (Y. X. Li, Li, Je, & Kim, 2015), order Ectocarpales (Mori et al., 2004) and order Desmarestiales (Gambato et al., 2014) and red algae of order Ceramiales (Fujii, Cassano, Stein, & Carvalho, 2011) and order Gigartinales (Nylund & Pavia, 2005) (Yokoya, Ávila, Piel, Villanueva, & Alcapan, 2014) might have superior bioactivities such as anti-oxidation, anti-inflammation, anti-diabetes, anti-angiogenesis, anti-fouling, anti-herbivory and anti-retroviral. Also, a series of bromophenols have been purified from Rhodomelaceae species (Ceramiales, Rhodophylaceae) as α-glucuronidase (Kurihara, Mitani, Kawabata, & Hatano, 1997), glucose 6-phosphate dehydrogenase (Mikami, Kurihara, Kim, & Takahashi, 2013), lipoxygenase (Morimoto, 2016) and xanthine oxidase inhibitors (Uemoto, 2011). Brown algae *Sargassum*

confusum (Sargassaceae, Fucales) and *Colpomenia bullosa* (Scytosiphonaceae, Ectocarpales) included alkapolyenes, (6*Z*,9*Z*,12*Z*,15*Z*)-1,6,9,12,15-henicosa-pentaene (HEP) and (6*Z*,9*Z*,12*Z*,15*Z*,18*Z*)-1,6,9,12,15,18-henicosahexaene (HEH) (Kurihara, Kagawa, Konno, Kim, & Takahashi, 2014), and a phlorotannin fucophlorethol C (Kurihara, Konno, & Takahashi, 2015) have been previously purified as potent lipoxygenase inhibitors.

Collecting location and period might also affect the β-glucuronidase inhibitory activity of algae. *Neorhodomela aculeata* (Rhodomelaceae, Ceramiales), *Neodilsea yendoana* (Dumontiaceae, Gigartinales), *Chondrus pinnulatus* (Gigartinaceae, Gigartinales), *and Sargassum thunbergii* (Sargassaceae, Fucales) collected at Oshoro exhibited less inhibitory activity compared to the same algae which collected at Usujiri and Habomai. Different current regimes and oceanographic conditions might have influenced on the variation of β-glucuronidase inhibitory activity.

According to the screening results, extracts showing strong inhibition were selected for the further isolation and purification experiments of β-glucuronidase inhibitory compounds, as follow: the red marine algae *Neorhodomela aculeata* (49.62% inhibition at 10 μg/mL) collected at Usujiri on June 3rd, 2015; *Neodilsea yendoana* (40.33% inhibition at 10 μg/mL) collected from Usujiri on May 10th and May 25th, 2016, and the brown algae *Sargassum confusum* (25.13% inhibition at 10 μg/mL) collected at Usujiri on June 3rd, 2015; *S. thunbergii* (53.44% inhibition at 10 μg/mL) collected at Usujiri, Hakodate on May 25th, 2016; *Agarum clathratum* (98.26% inhibition at 10 μg/mL) collected at Habomai on May 26th, 2017.

Chapter 2

β-Glucuronidase Inhibitors Derived from Marine Red Algae

In this chapter, two red algae *Neorhodomela aculeata* (Rhodomelaceae, Ceramiales) and *Neodilsea yendoana* (Dumontiaceae, Gigartinales) were used for the isolation and purification of β-glucuronidase inhibitory compounds.

2.1 Chromatography and chemical analysis instrument

2.1.1 Chromatography

(1) Silica gel chromatography

- Wakogel C-100 Wako Pure Chemical Industries, Ltd. (Osaka, Japan)
- Cosmosil 140 C_{18}-OPN Nacalai Tesque, Inc. (Kyoto, Japan)
- Sep-Pak Silica Cartridges Vac 12cc (2g) Waters (Dublin, Ireland)
- Sephadex LH-20 GE Healthcare Bio-Sciences AB (Uppsala, Sweden)

(2) Thin layer chromatography (TLC)

- TLC Silica gel 60 F_{254} Merch KGaA (Darmstadt, Germany)
- TLC Silica gel 60 RP-18 F_{254}s Merch KGaA (Darmstadt, Germany)
- HPTLC Silica gel F_{254} Merch KGaA (Darmstadt, Germany)

(3) Preparative thin layer chromatography (PLC)

- PLC Silica gel 60 F_{254}, 0.5 mm Merch KGaA (Darmstadt, Germany)

(4) High performance liquid chromatography (HPLC)

Pump:

- SHIMADZU LC-10ATvp liquid chromatograph

  Shimadzu Corporation (Kyoto, Japan)

Detector:

- SHIMADZU SPD-10AVvp UV-VIS detector

  Shimadzu Corporation (Kyoto, Japan)
- SHIMADZU SPD-M10Avp diode array detector

  Shimadzu Corporation (Kyoto, Japan)

Column:

- ULTRON VX-ODS 250 × 4.6 (5 μm)

  Shinwa Chemical industries, Ltd. (Kyoto, Japan)

- Mightysil RP-18 250 × 4.6 (5 μm)

  Kanto Chemical Co., Inc. (Tokyo, Japan)

- Mightysil RP-18 250 × 10 (5 μm)

  Kanto Chemical Co., Inc. (Tokyo, Japan)

2.1.2 Analysis instruments

(1) Mass spectrometer (MS)

- Field desorption mass spectrum (FD-MS)
- Field ionization mass spectrum (FI-MS)
- Field desorption high resolution mass spectrometry (FD-HR-MS)
- Field ionization high resolution mass spectrometry (FI-HR-MS)

JMS-T100GCV JEOL Ltd. (Tokyo, Japan)

(2) Nuclear magnetic resonance spectroscopy (NMR)

Bruker AMX500 NMR spectrometer Bruker (Karlsruhe, Germany)

JEOL ECZ400S NMR spectrometer JEOL(Akishima, Japan)

2.2 β-Glucuronidase inhibitors derived from the marine red alga *Neorhodomela aculeata*

In this section, high inhibitory activity alga, *N*. *aculeata* (Rhodomelaceae, Ceramiales), collected from Usujiri, Hakodate on June 3rd, 2015 (Table 1-2), was used to perform the isolation and purification of β-glucuronidase inhibitors (Figure 2-1).

2.2.1 Isolation and purification of β-glucuronidase inhibitors from *N. aculeata*

Methanol extract (26.8 g) of *N*. *aculeata* was separated by a series of organic solvent partitioning (Figure 2-2) to obtained *n*-hexane-soluble fraction (1.29 g), ethyl acetate-soluble fraction (2.18 g) and *n*-butanol-soluble fraction (2.54 g), respectively (Table 2-1). Thin layer chromatography (TLC) of each soluble fraction was detected by 5% sulfuric acid as well as potassium ferricyanide-ferric chloride reagent (Figure 2-3). The positive response for the potassium ferricyanide-ferric chloride reagent of ethyl acetate-soluble fraction suggested the presence of bromophenols. The ethyl acetate-soluble fraction was chosen for the further purification.

2.2.1.1 Silica gel column chromatography

The ethyl acetate-soluble fraction (1.02 g) was chromatographed on Cosmosil 140 C_{18}-OPN and eluted with methanol/water to yield 11 fractions (Table 2-2, Figure 2-4). Fractions C2 (33.8 mg), C3 (32.5 mg), C5 (220.2 mg) and C6 (46.2 mg) which showed higher inhibitory activity were chosen for the further purification.

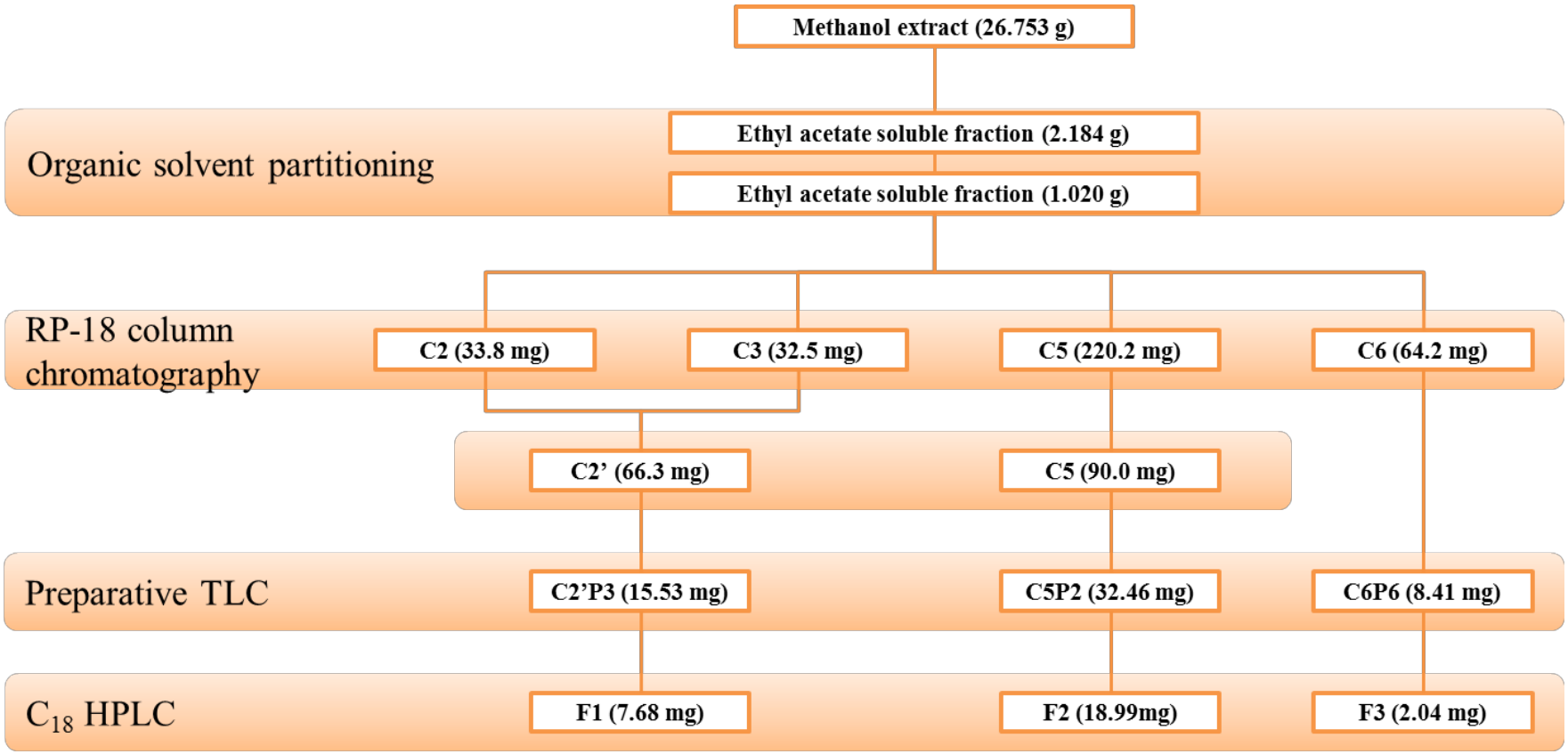


Figure 2-1. Separation scheme of the extract of *Neorhodomela aculeata* collected from Usujiri, Hakodate.

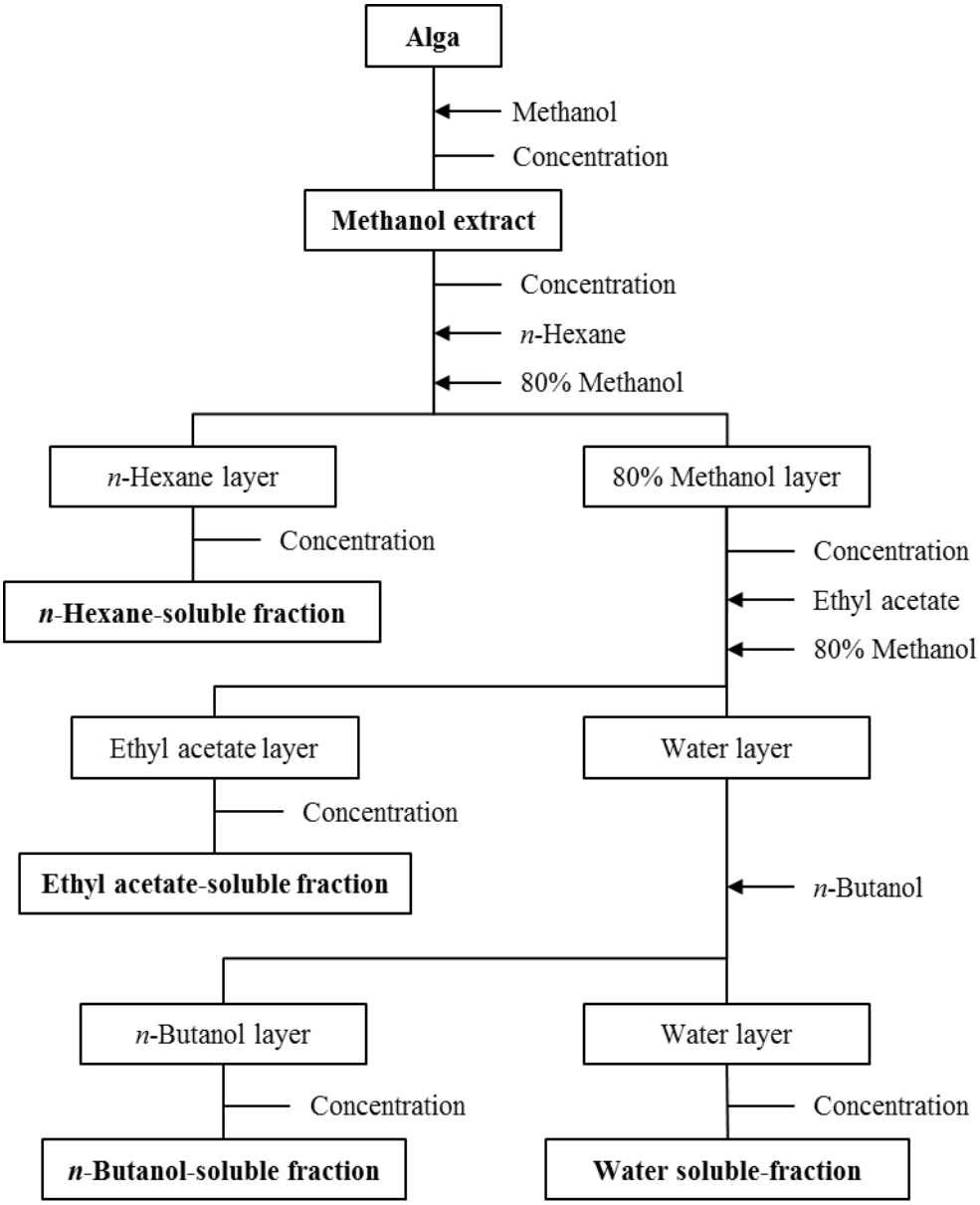


Figure 2-2. Procedure of organic solvent partitioning of algal extracts.

Table 2-1. Amount and β-glucuronidase inhibitory activity of the fractions[a] obtained by organic solvent partitioning

Fraction	Amount (g)	Inhibition[b] (%)
n-Hexane	1.286	NI[c]
Ethyl acetate	2.184	65.19 ± 0.16
n-Butanol	2.543	33.99 ± 1.23

[a]Sample, 26.753 g methanol extracts of *N. aculeata*.

[b]Assay concentration was 10 μg/mL. Data represent means ± SE (n=3).

[c]NI, no inhibition.

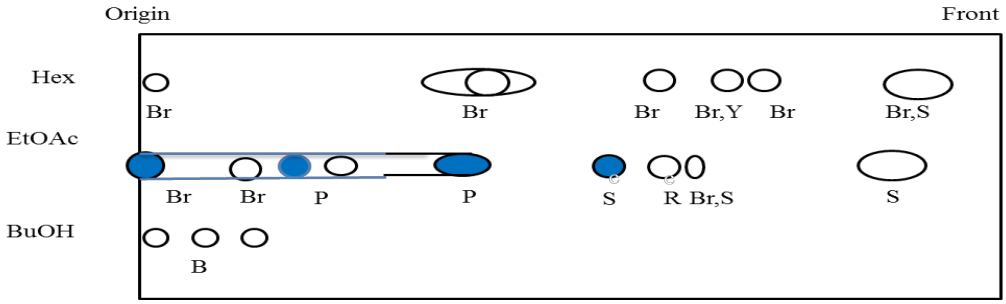


Figure 2-3. Silica gel thin layer chromatogram of the organic solvent extracts of *N. aculeata*.

Developing solvent, chloroform: methanol = 4: 1 (v/v).

⬭ , Visualized with 5% sulfuric acid reagent.

⬬ , Positive response for potassium ferricyanide-ferric chloride reagent.

Abbreviations designate color of the spots: Br, brown; Y, yellow; P, purple; S, quenching spot under short wave UV lamp.

Table 2-2. Amount and β-glucuronidase inhibitory activity of the fractions obtained from ethyl acetate-soluble fraction[a] separated by Cosmosil 140 C_{18}-OPN column chromatography

Fraction	Eluent (v/v)	Amount (mg)	Inhibition[b] (%)
C1	Methanol : water = 1 : 2	78.3	17.89 ± 1.24
C2	Methanol : water = 1 : 1	33.8	61.68 ± 1.66
C3	Methanol : water = 1 : 1	32.5	75.76 ± 0.76
C4	Methanol : water = 2 : 1	188.6	67.55 ± 1.02
C5	Methanol : water = 2 : 1	220.2	85.41 ± 1.01
C6	Methanol : water = 4 : 1	46.2	97.70 ± 0.26
C7	Methanol : water = 4 : 1	49.6	95.05 ± 2.68
C8	Methanol	112.6	67.17 ± 2.45
C9	Methanol	140.8	33.62 ± 0.05
C10	Acetone	80.2	13.67 ± 1.12
C11	Acetone	8.4	10.17 ± 1.21

[a]Sample, ethyl acetate soluble fraction, 1.020 g; stationary phase, Cosmosil 140 C_{18}-OPN; elution volume, 105 mL/fraction.

[b]Assay concentration was 10 μg/mL. Data represent means ± SE (n=3).

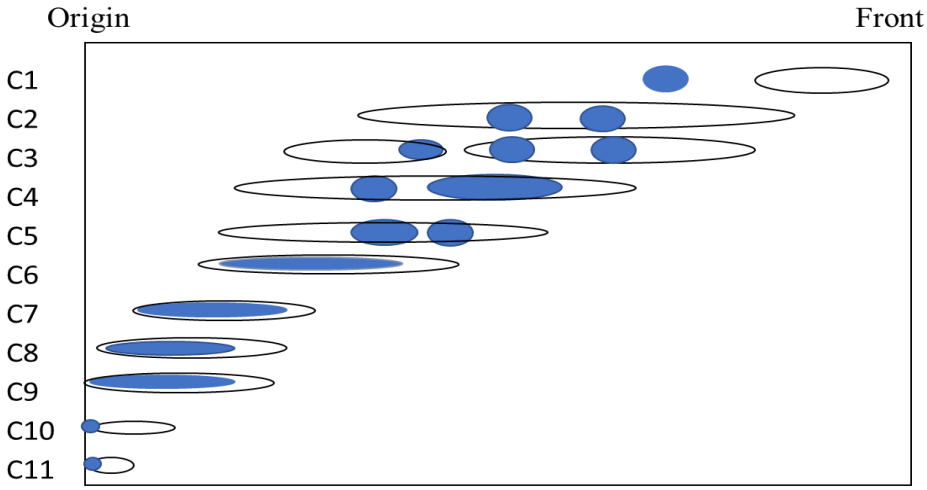


Figure 2-4. RP-18 silica gel thin layer chromatogram of fractions obtained from ethyl acetate-soluble fraction separated by silica gel column chromatography.

Developing solvent, methanol: water = 7: 3 (v/v).

⬭ , Visualized with 5% sulfuric acid reagent.

⬬ , Positive response for potassium ferricyanide-ferric chloride reagent.

2.2.1.2 Purification of β-glucuronidase inhibitor F1

According the TLC profile, fractions C2 (33.8 mg) and C3 (32.5 mg) were combined and renamed as C2'. After separated by preparative TLC developed with toluene/ethyl acetate/acetic acid (7/2/1, v/v/v) (Figure 2-5), fractions C2'P1 to C2'P6 were obtained (Table 2-3). Among them, fraction C2'P3 (15.51 mg) was separated by HPLC (Table 2-4) to yield compound **F1** (7.68 mg, 18 ppm based on air-dried alga) (Table 2-5, Figure 2-7) at retention time of 21.8 min (Figure 2-6).

2.2.1.3 Purification of β-glucuronidase inhibitor F2

An aliquot of fraction C5 (90.0 mg) was charged on preparative TLC developed with toluene/ethyl acetate/acetic acid (7/2/1, v/v/v) (Figure 2-8) to obtain fractions C5P1~C5P3 (Table 2-6). Fraction C5P2 (32.46 mg) was separated by HPLC (Table 2-7) to afford compound **F2** (19.0 mg, 109 ppm on the basis of air-dried alga) (Table 2-8, Figure 2-10) at retention time of 18.0 min (Figure 2-9).

2.2.1.4 Purification of β-glucuronidase inhibitor F3

Fraction C6 (46.2 mg) was loaded on preparative TLC developed with toluene/ ethyl acetate/acetic acid (7/3/2, v/v/v) (Figure 2-11) to give seven fractions (Table 2-9). Fraction C6P6 (8.41 mg) was separated by HPLC (Table 2-10) to afford compound **F3** (2.04 mg, 4.8 ppm on the basis of air dried alga) (Table 2-11, Figure 2-13) at retention time of 8.7 min (Figure 2-12).

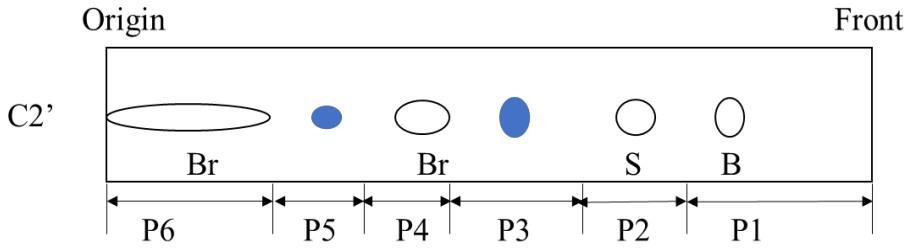


Figure 2-5. Profile of the preparative TLC of fraction C2'.

Developing solvent, toluene: ethyl acetate: acetic acid = 7: 2: 1 (v/v/v).

⬭, Visualized with 5% sulfuric acid reagent.

⬬, Positive response for potassium ferricyanide-ferric chloride reagent.

Abbreviations designate color of the spots: Br, brown; S, quenching spot under short wave UV lamp; B, blue under long wave UV lamp.

Table 2-3. Amount and β-glucuronidase inhibitory activity of the fractions obtained from fraction C2'[a] by preparative thin layer chromatography

Fraction	Amount (mg)	Inhibition[b] (%)
C2'P1	4.39	3.21 ± 1.94
C2'P2	2.41	8.08 ± 1.33
C2'P3	15.53	30.69 ± 1.35
C2'P4	11.33	16.31 ± 1.37
C2'P5	10.71	35.54 ± 1.61
C2'P6	50.23	65.84 ± 1.39

[a]Sample, fraction C2', 66.3 mg.

[b]Assay concentration was 10 μg/mL. Data represent means ± SE (n=3).

Table 2-4. HPLC condition for separating fraction C2'P3

Sample:	C2'P3 15.53 mg
Column:	Mightysil RP-18 (5 μm; 250 × 4.6 mm) (KANTO CHEMICAL CO., Inc.)
Eluting solvent:	Methanol : water = 7 : 3
Flow rate:	0.5 mL/min
Detection:	UV (210 nm, 254 nm)

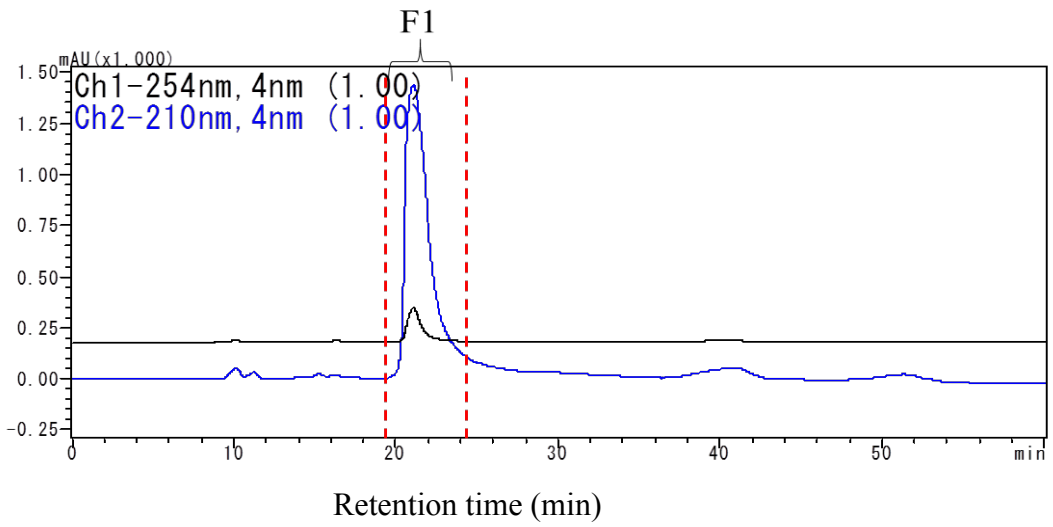


Figure 2-6. HPLC chromatogram of fraction C2'P3 monitored at 210 nm and 254 nm.

Table 2-5. Amount and β-glucuronidase inhibitory activity of compound **F1** obtained by HPLC

Fraction	Amount (mg)	Inhibition[a] (%)
F1	7.68	34.91 ± 0.86

[a]Assay concentration was 10 μg/mL. Data represent means ± SE (n=3).

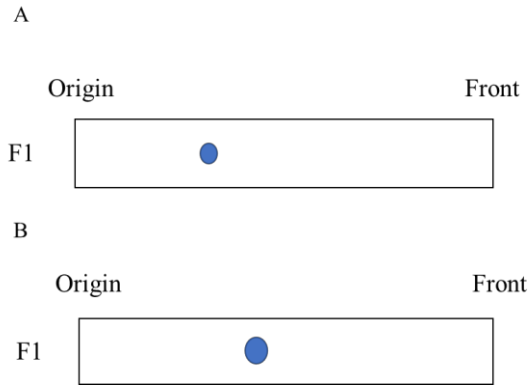


Figure 2-7. Analytical RP-18 thin layer chromatogram (A) and high performance silica gel thin layer chromatogram (B) of compound **F1**.

Developing solvent: (A) methanol: water = 7: 3 (v/v);

(B) toluene: ethyl acetate: acetic acid = 7: 2: 1 (v/v/v).

, Positive response for potassium ferricyanide-ferric chloride.

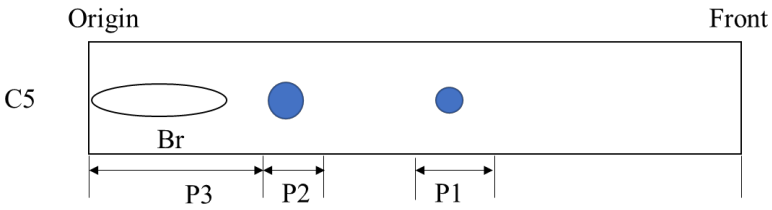


Figure 2-8. Profile of the preparative TLC of fraction C5.

Developing solvent, toluene: ethyl acetate: acetic acid = 7: 2: 1 (v/v/v).

, Visualized with 5% sulfuric acid reagent.

, Positive response for potassium ferricyanide-ferric chloride reagent.

Abbreviations designate color of the spots: Br, brown.

Table 2-6. Amount and β-glucuronidase inhibitory activity of the fractions obtained from fraction C5[a] by preparative thin layer chromatography

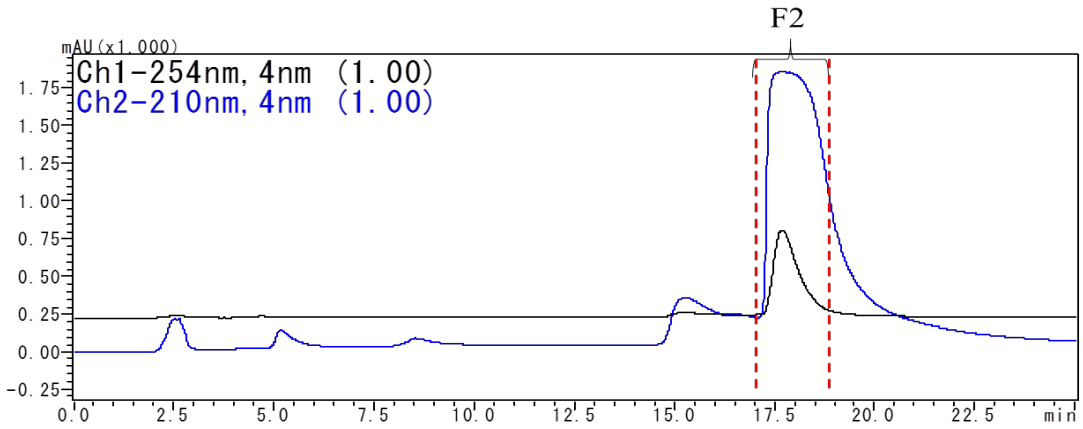
Fraction	Amount (mg)	Inhibition[b] (%)
C5P1	4.29	20.86 ± 1.94
C5P2	32.46	86.03 ± 2.12
C5P3	40.91	42.02 ± 2.59

[a]Sample, fraction C5, 90.0 mg.

[b]Assay concentration was 10 μg/mL. Data represent means ± SE (n=3).

Table 2-7. HPLC condition for separating fraction C5P2

Sample:	C5P2 32.46 mg
Column:	Mightysil RP-18 (5 μm; 250 × 4.6 mm) (KANTO CHEMICAL CO., Inc.)
Eluting solvent:	Acetonitrile : water = 4 : 6
Flow rate:	1 mL/min
Detection:	UV (210 nm, 254 nm)



Retention time (min)

Figure 2-9. HPLC chromatogram of fraction C5P2 monitored at 210 nm and 254 nm.

Table 2-8. Amount and β-glucuronidase inhibitory activity of compound **F2** obtained by HPLC

Fraction	Amount (mg)	Inhibition[a] (%)
F2	18.99	96.33±0.46

[a]Assay concentration was 10 μg/mL. Data represent means ± SE (n=3).

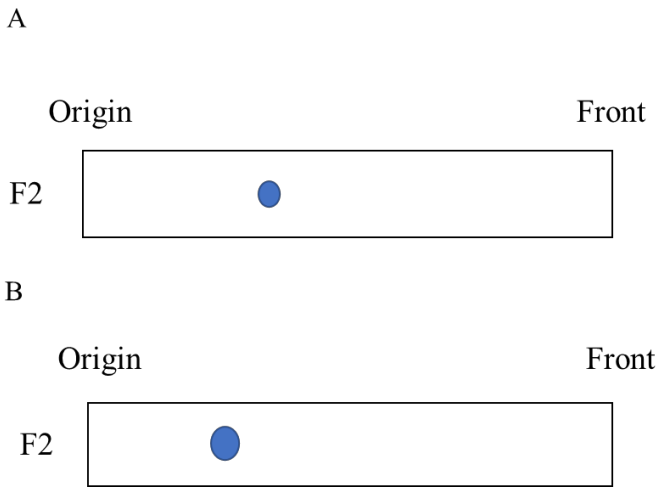


Figure 2-10. Analytical RP-18 thin layer chromatogram (A) and high performance silica gel thin layer chromatogram (B) of compound **F2**.

Developing solvent: (A) methanol: water = 7: 3 (v/v);

(B) toluene: ethyl acetate: acetic acid = 7: 2: 1 (v/v/v).

, Positive response for potassium ferricyanide-ferric chloride reagent.

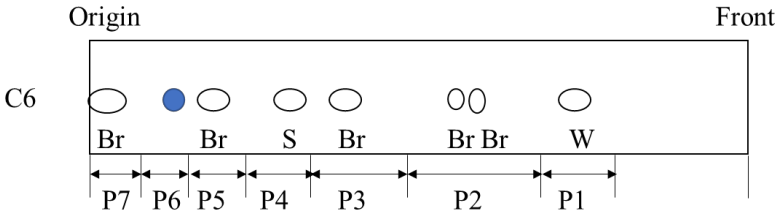


Figure 2-11. Profile of the preparative TLC of fraction C6.

Developing solvent, toluene: ethyl acetate: acetic acid = 7: 3: 2 (v/v/v).

, Visualized with 5% sulfuric acid reagent.

, Positive response for potassium ferricyanide-ferric chloride reagent.

Abbreviations designate color of the spots: Br, brown; S, quenching spot under short wave UV lamp; W, white under long wave UV lamp.

Table 2-9. Amount and β-glucuronidase inhibitory activity of the fractions obtained from fraction C6[a] by preparative thin layer chromatography

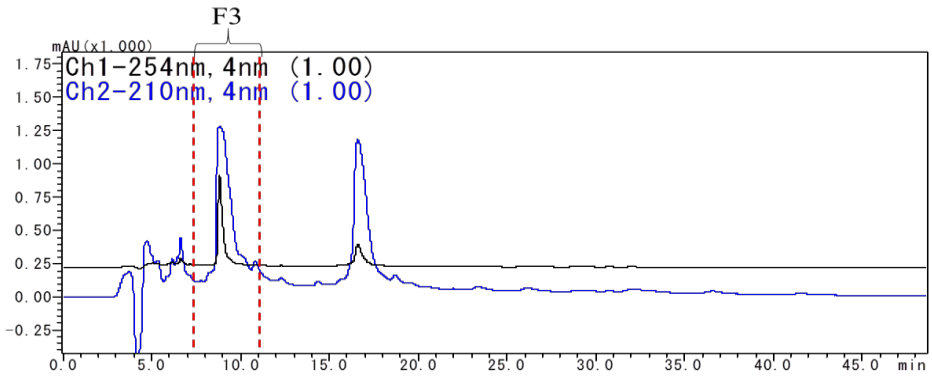
Fraction	Amount (mg)	Inhibition[b] (%)
C6P1	1.80	31.26 ± 1.40
C6P2	4.39	78.62 ± 5.61
C6P3	2.44	42.38 ± 1.79
C6P4	9.15	65.43 ± 1.44
C6P5	1.61	84.33 ± 1.19
C6P6	8.41	91.21 ± 1.75
C6P7	11.8	88.27 ± 1.12

[a]Sample, fraction C6, 46.2 mg.

[b]Assay concentration was 10 μg/mL. Data represent means ± SE (n=3).

Table 2-10. HPLC condition for separating fraction C6P6

Sample:	C6P6 8.41 mg
Column:	Mightysil RP-18 (5 μm; 250 × 4.6 mm) (KANTO CHEMICAL CO., Inc.)
Eluting solvent:	Methanol : 0.1% formic acid = 45 : 55
Flow rate:	1 mL/min
Detection:	UV (210 nm, 254 nm)



Retention time (min)

Figure 2-12. HPLC chromatogram of fraction C6P6 monitored at 210 nm and 254 nm.

Table 2-11. Amount and β-glucuronidase inhibitory activity of compound **F3** obtained by HPLC

Fraction	Amount (mg)	Inhibition[a] (%)
F3	2.04	99.63±0.21

[a]Assay concentration was 10 μg/mL. Data represent means ± SE (n=3).



Figure 2-13. Analytical RP-18 thin layer chromatogram (A) and high performance silica gel thin layer chromatogram (B) of compound **F3**.

Developing solvent: (A) methanol: 0.1% formic acid = 1: 1 (v/v);

(B) toluene: ethyl acetate: Acetic acid = 7: 3: 2 (v/v/v).

, Positive response for potassium ferricyanide-ferric chloride reagent.

2.2.2 Structural elucidation of β-glucuronidase inhibitors from *N. aculeate*

2.2.2.1 Structural elucidation of β-glucuronidase inhibitor F1

Compound **F1** was isolated as brown amorphous solid. In the FD-MS spectrum of compound **F1**, characteristic molecular ion peak cluster at *m/z* 310/312/314 (intensity ratio of 1:2:1) suggested the presence of two bromine atoms (Figure 2-14). Molecular formula of compound **F1** was determined as $C_8H_8{}^{79}Br_2O_3$ from observed peak at *m/z* 309.88452 (calculated 309.88404) in FD-HR-MS.

^{1}H NMR spectrum showed two phenolic hydroxy protons at δ_H 8.65 (OH-4 and OH-5), an aromatic singlet at δ_H 7.04 (H-6), a methoxy signal at δ_H 3.37 (H-8) and two methylene protons at δ_H 4.39 (H-7) (Figure 2-15). ^{13}C NMR spectrum of **F1** displayed six aromatic (113.5 to 145.6 ppm, C-1 to C-6), a methyl (75.1 ppm, C-8) and a methylene (58.4 ppm, C-7) carbon signals (Figure 2-16). Therefore, the structure of compound **F1** was confirmed as 2,3-dibromo-4,5-dihydroxybenzyl ether (Table 2-12, Figure 2-20) by the assistance of 2D NMR spectra (Figures 2-17 to 2-19) and comparison with literature data (Park et al., 2012).

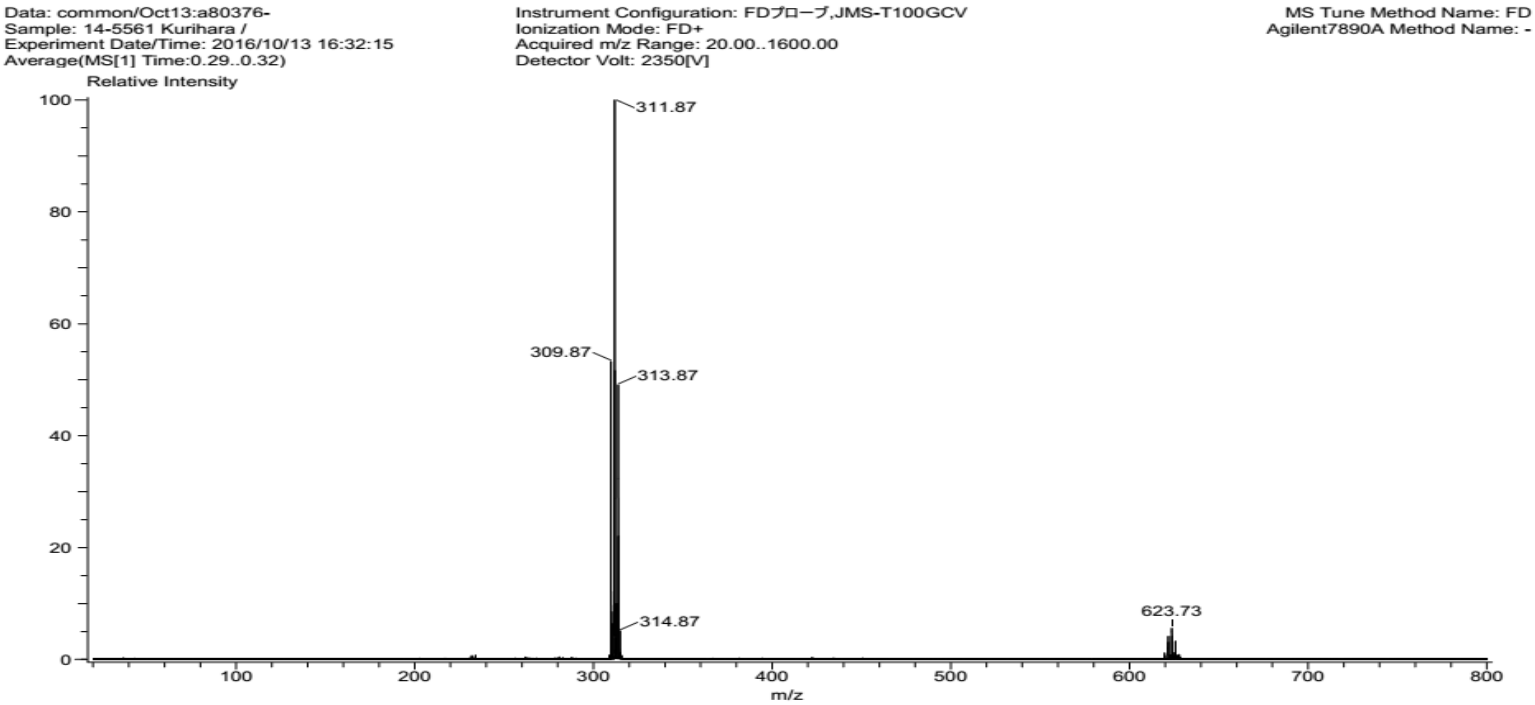


Figure 2-14. FD-MS spectrum of compound **F1**.

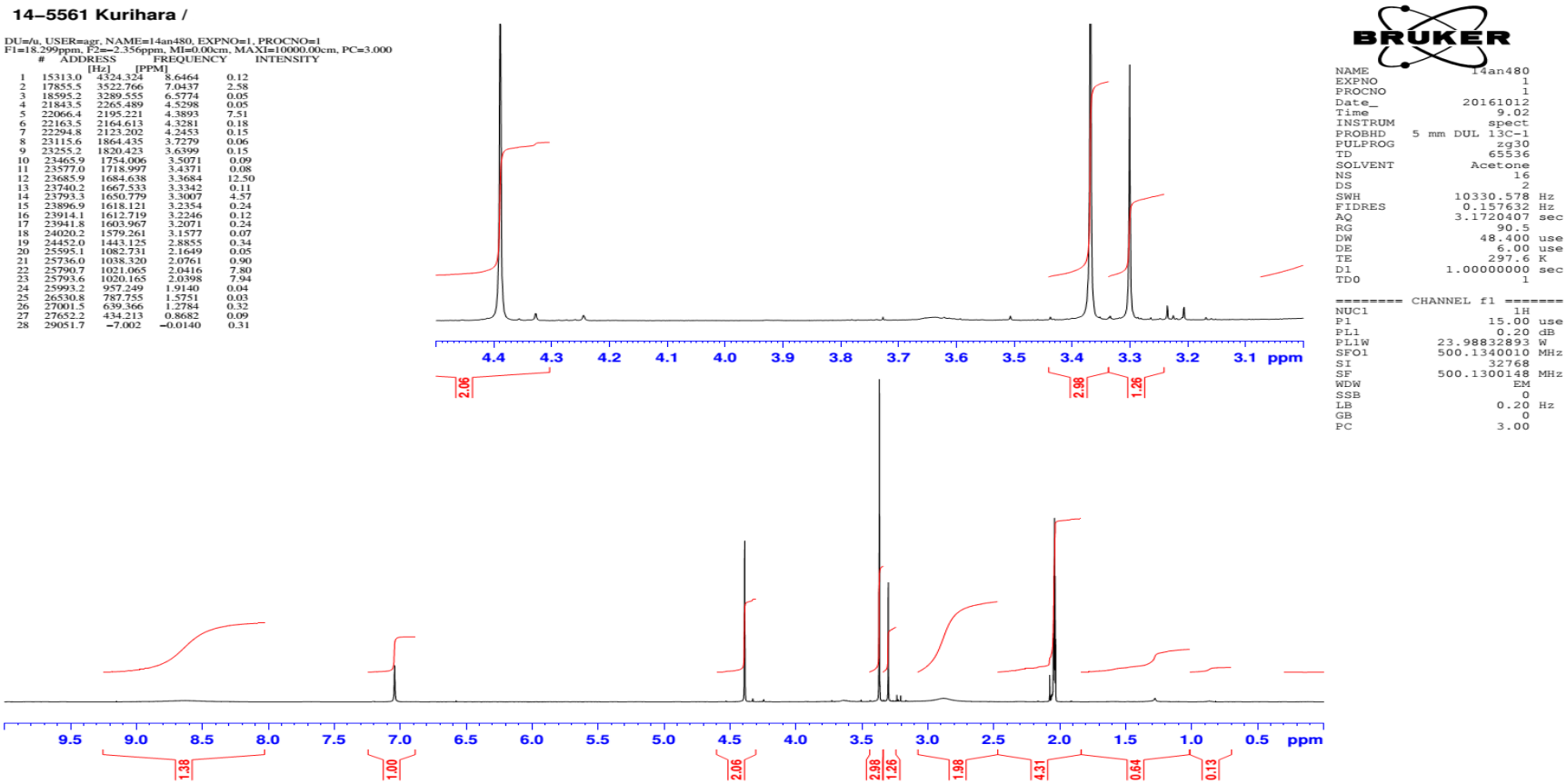


Figure 2-15. ^{1}H-NMR spectrum of compound **F1**.

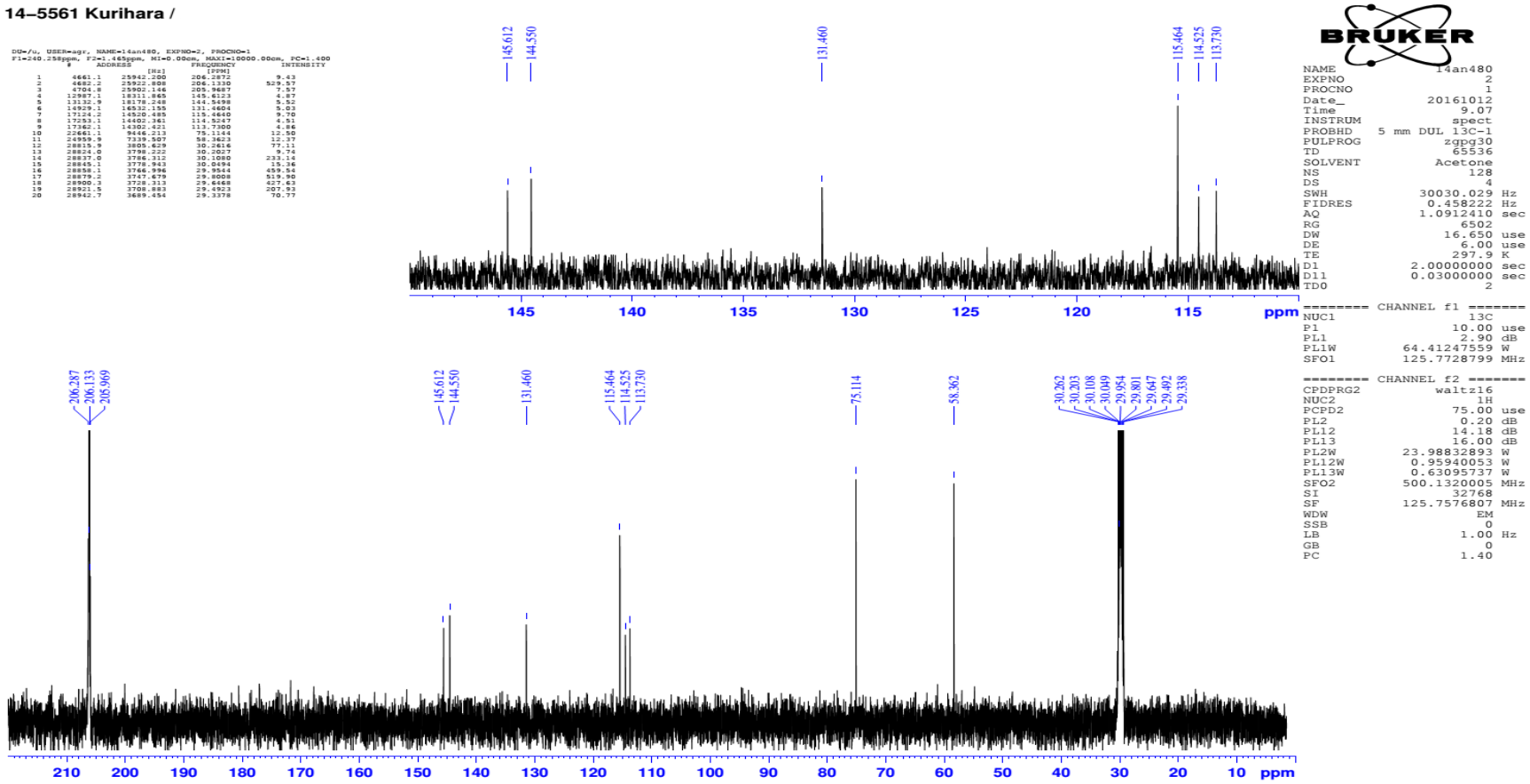


Figure 2-16. ^{13}C-NMR spectrum of compound **F1**.

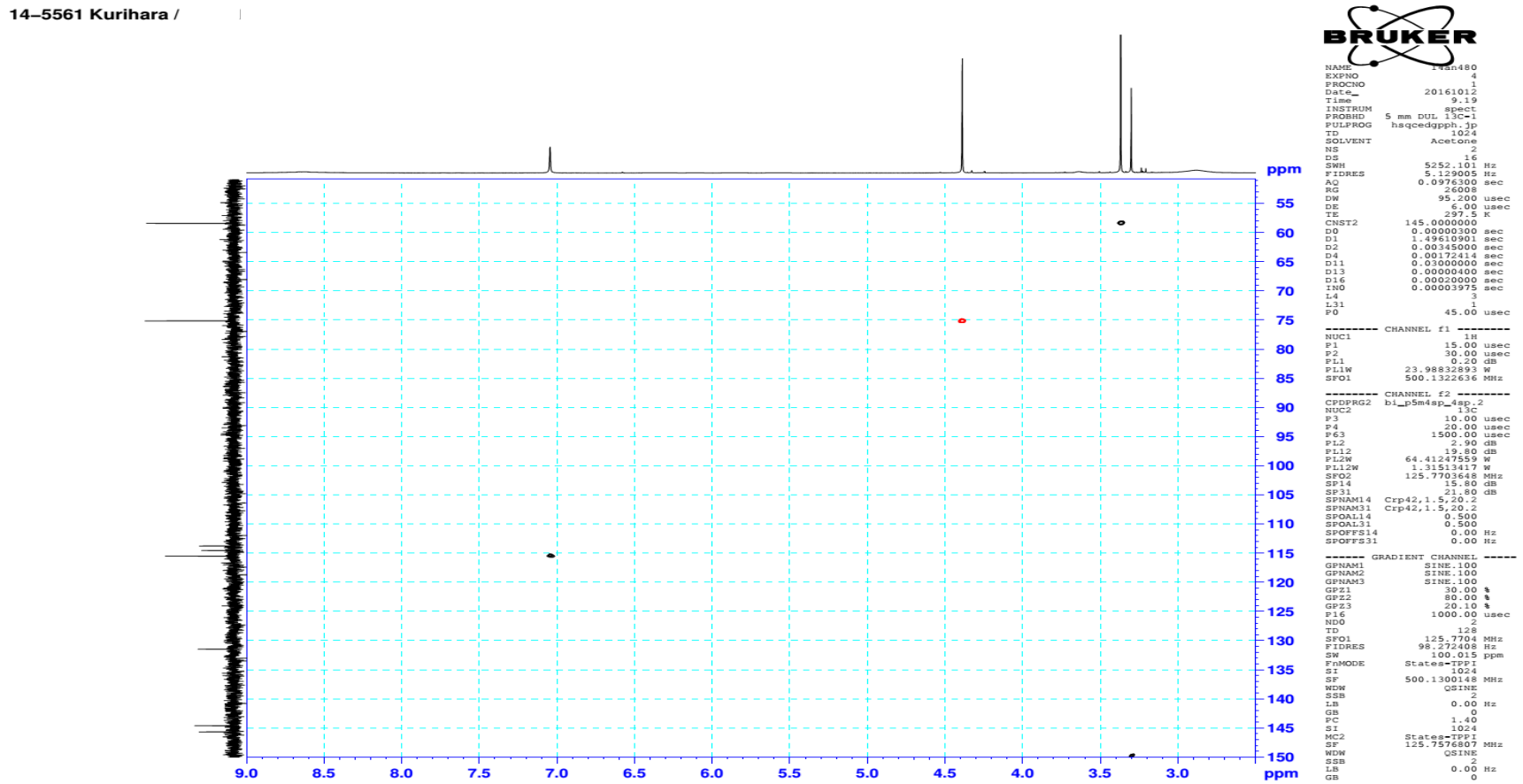


Figure 2-17. HSQC spectrum of compound **F1**.

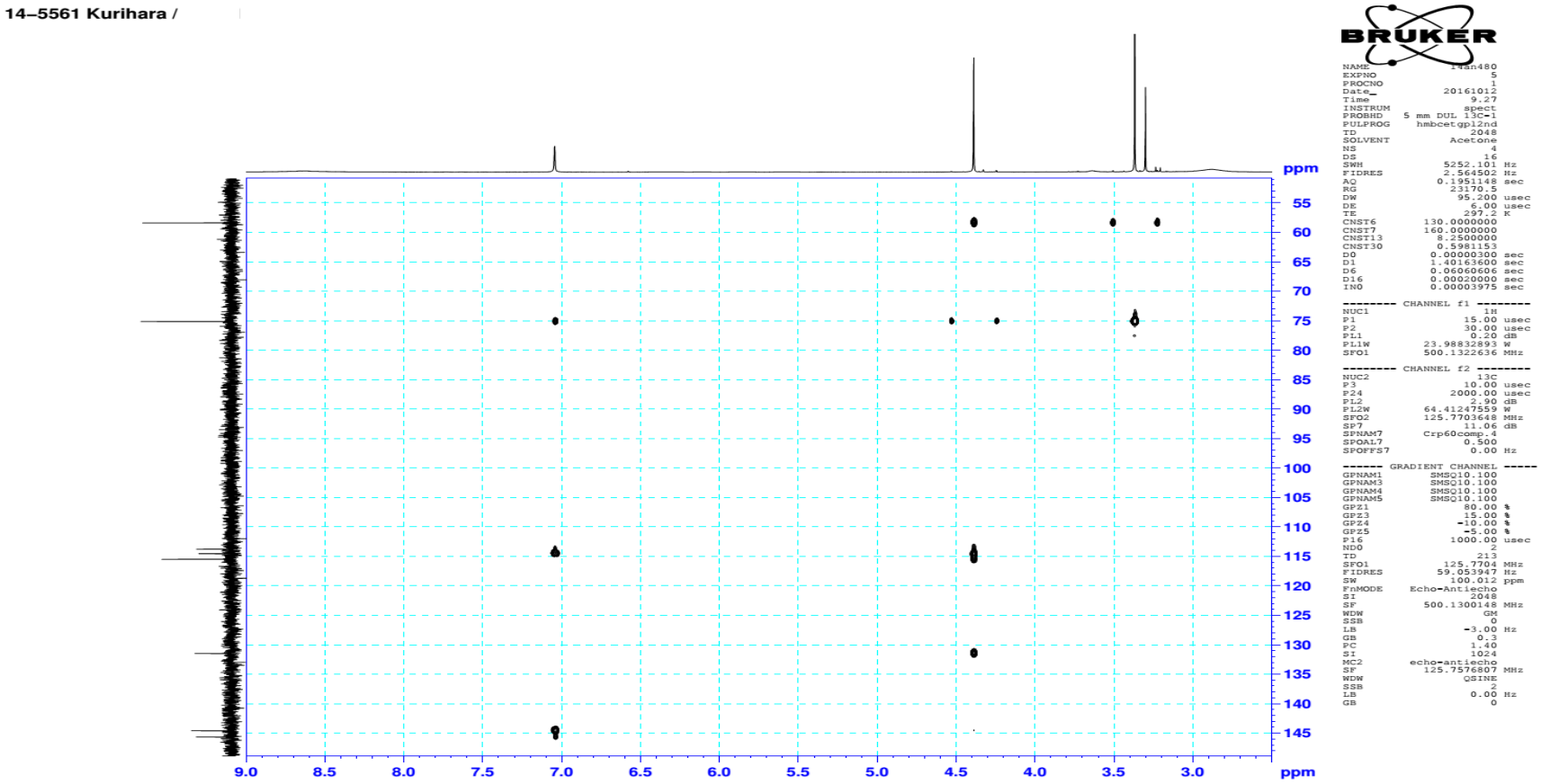


Figure 2-18. HMBC spectrum of compound **F1**.

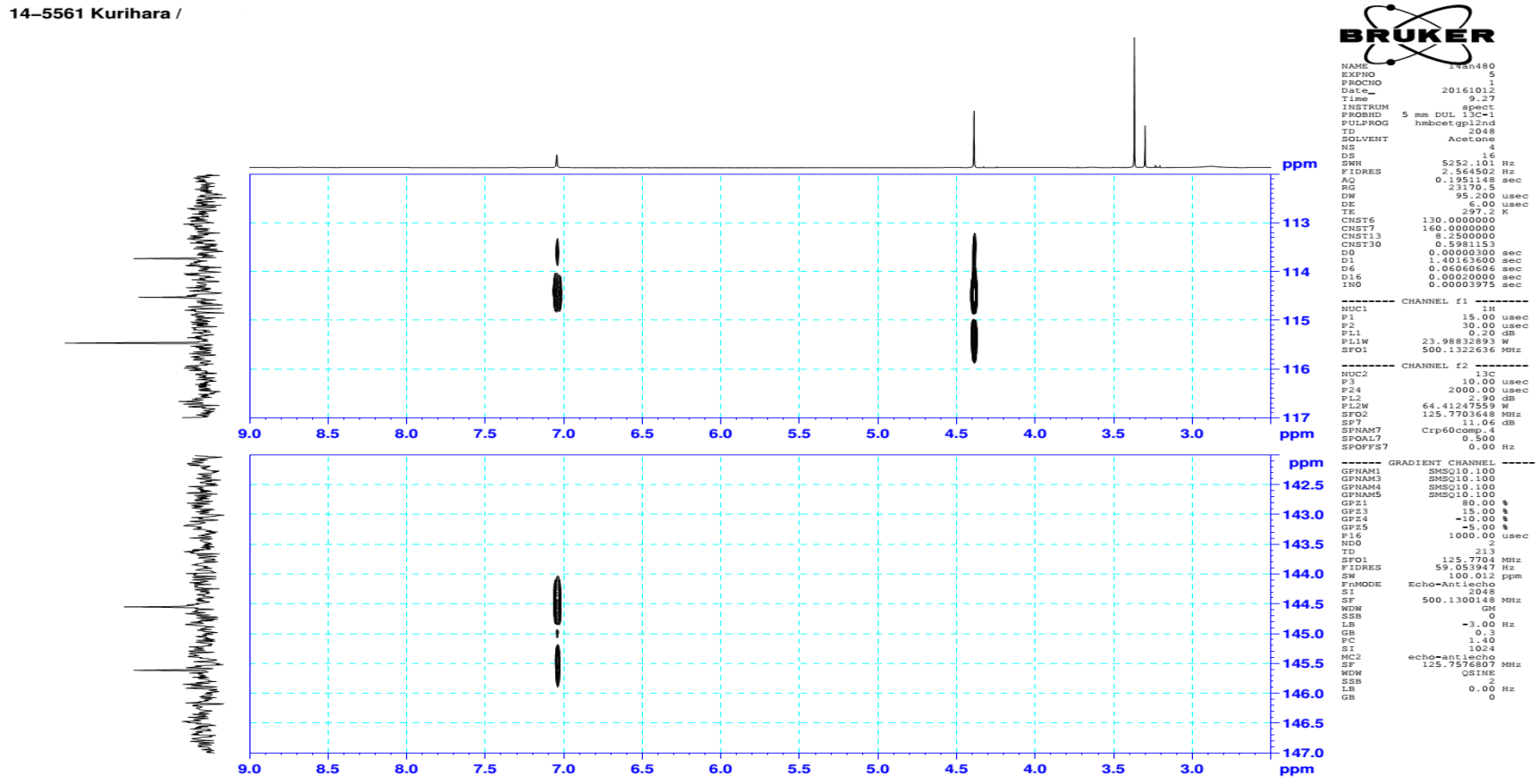


Figure 2-19. Expanded HMBC spectrum of compound **F1**.

Table 2-12. Comparison of NMR data between compound **F1**[a] and literature[b]

	^{1}H NMR		^{13}C NMR	
Position	**F1**	Literature data	**F1**	Literature data
1			131.5	131.6
2			114.5	114.8
3			113.7	114.4
4			145.6 or 144.5	143.7
5			144.5or 145.6	144.9
6	7.04 (s, 1H)	7.20 (s, 1H)	115.5	114.8
7	4.39 (s, 2H)	4.41 (s, 2H)	75.1	75.0
8	3.37 (s, 3H)	3.39 (s, 3H)	58.4	58.4

[a]The NMR data were measured in acetone-d_6 (δ_H 2.04 ppm; δ_C CO 206.3, CH_3 30.3 ppm) at 500 MHz for ^{1}H and at 125 MHz for ^{13}C.

[b]Park et al., 2012.

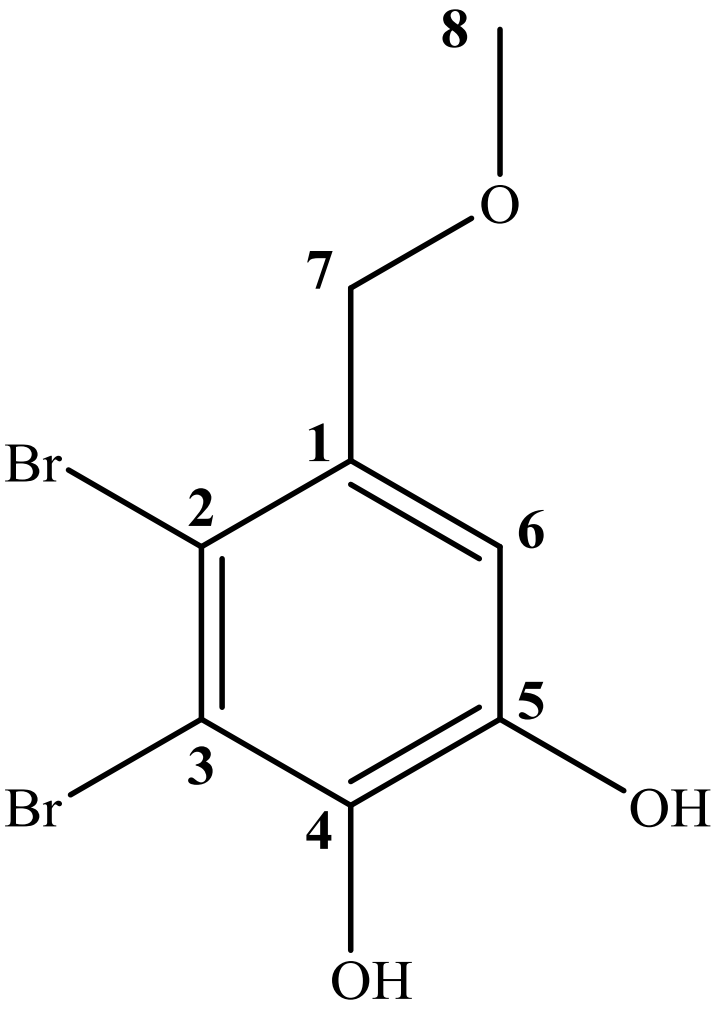


Figure 2-20. Structure of compound **F1**.

2.2.2.2 Structural elucidation of β-glucuronidase inhibitor F2

Compound **F2** was obtained as violet purple color needles. In the FD-MS spectrum, molecular ion peak cluster at *m/z* 510/512/514/516 (intensity ratio 1:3:3:1) suggested the presence of three bromine atoms (Figure 2-21). Molecular formula of compound **F2** was determined as $C_{15}H_{13}{}^{79}Br_3O_5$ by FD-HR-MS at *m/z* 509.83094 (calcultaed 509.83131).

^{1}H NMR spectrum of compound **F2** showed four hydroxy protons at δ_H 8.68-8.06, two singlet aromatic protons at δ_H 6.98 and 6.06, two singlet methylene groups at δ_H 4.20 and 4.11 and a methoxy group at δ_H 3.30 (Figure 2-22). The ^{13}C NMR spectrum of compound **F2** consisted of four oxygenated aromatic carbons at δ_C 145.4-143.5, eight aromatic carbons at δ_C 113.7-132.4, two methylenes at δ_C 72.3 and 39.3, and a methoxy carbon at δ_C 58.1 (Figure 2-23). Above all, the spectral data indicated that compound **F2** possessed a tribrominated diphenylmethane structure with four hydroxy groups and one methoxy group. With the consideration of HSQC, HMBC spectra (Figures 2-24 to 2-27) and literature data (Park et al., 2012), compound **F2** was identified as 3-bromo-2-(2,3-dibromo-4,5-dihydroxybenzyl)-4,5-dihydroxybenzyl methyl ether (Table 2-13, Figure 2-28).

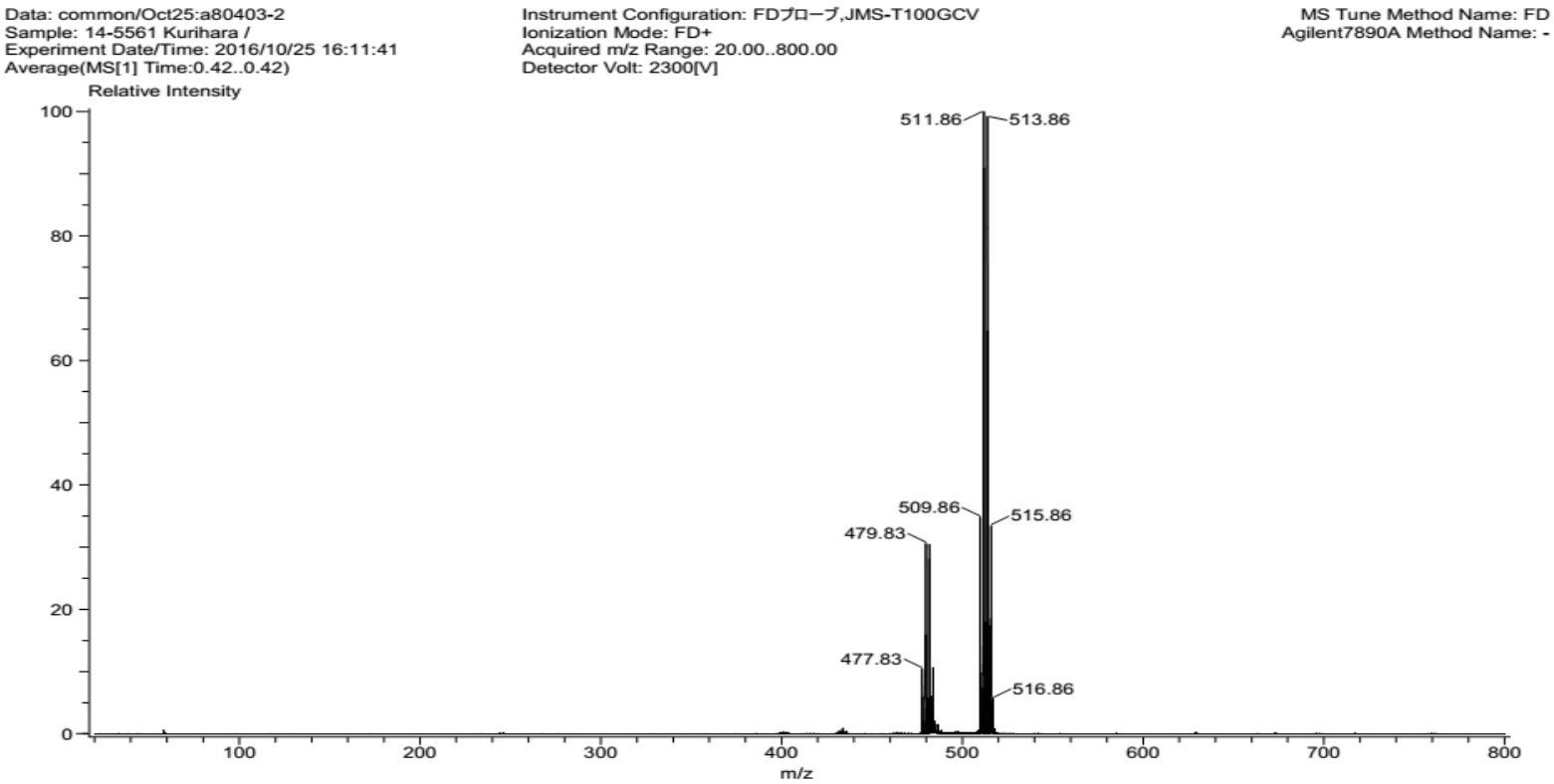


Figure 2-21. FD-MS spectrum of compound **F2**.

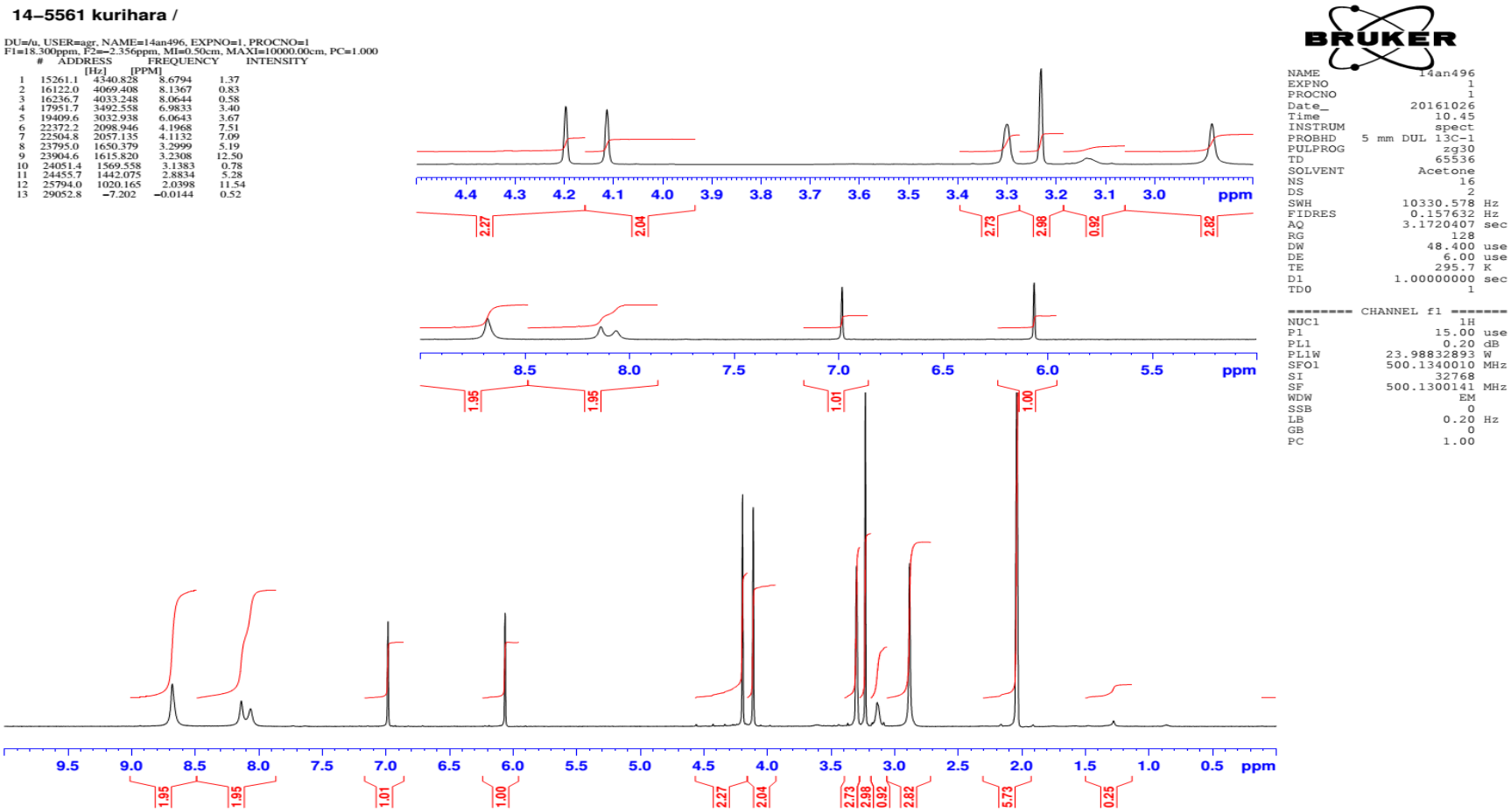


Figure 2-22. ^{1}H-NMR spectrum of compound **F2**.

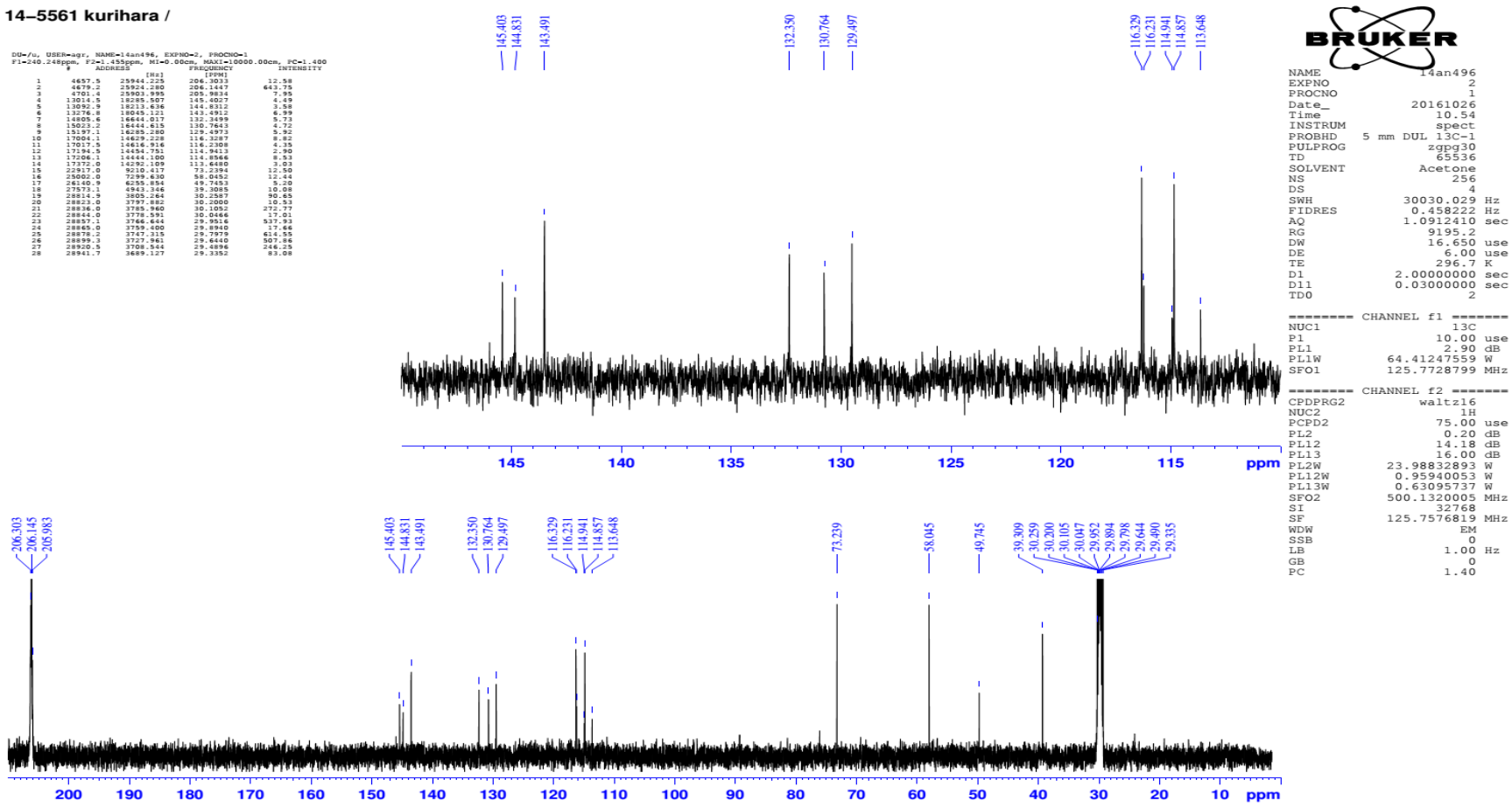


Figure 2-23. ^{13}C-NMR spectrum of compound **F2**.

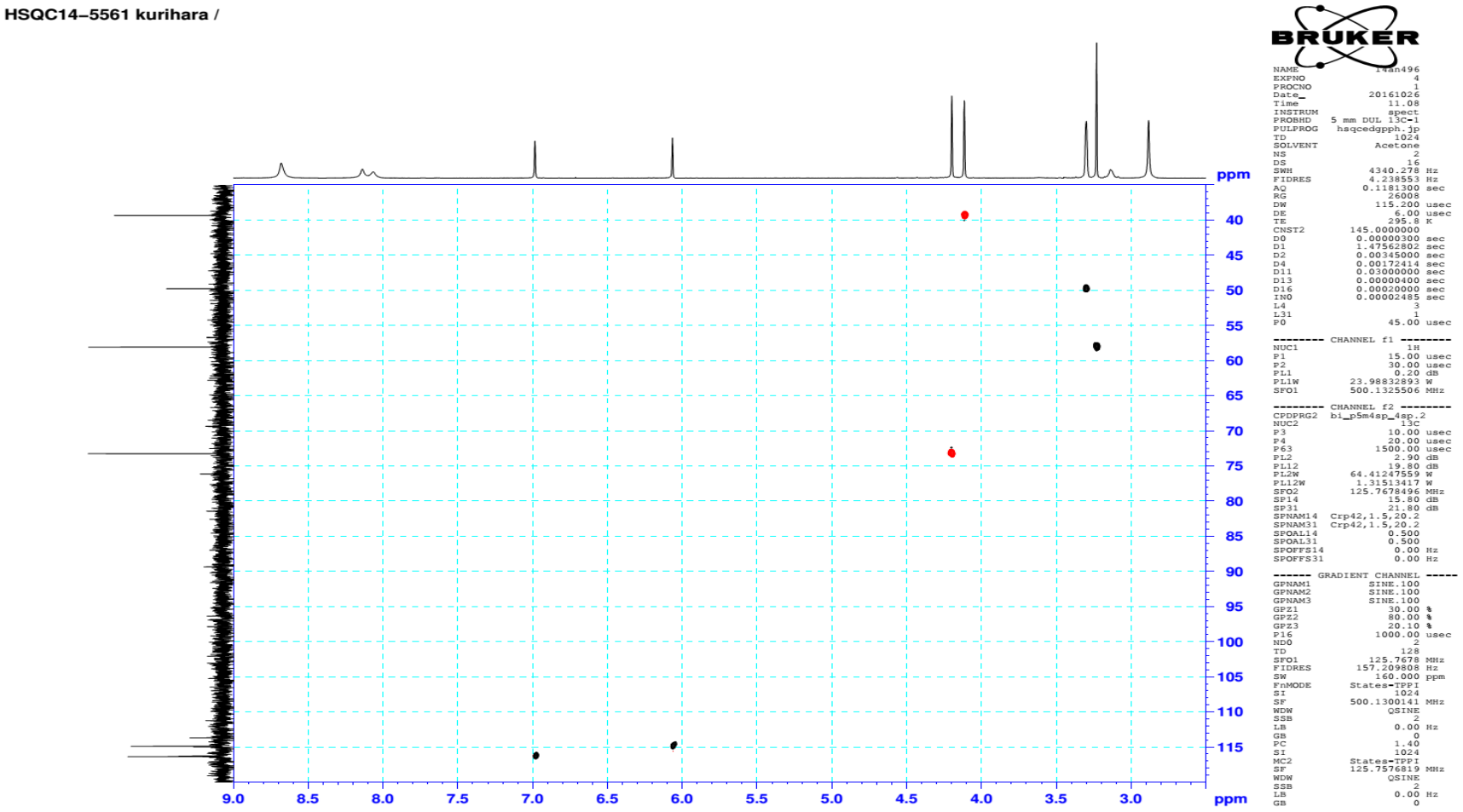


Figure 2-24. HSQC spectrum of compound **F2**.

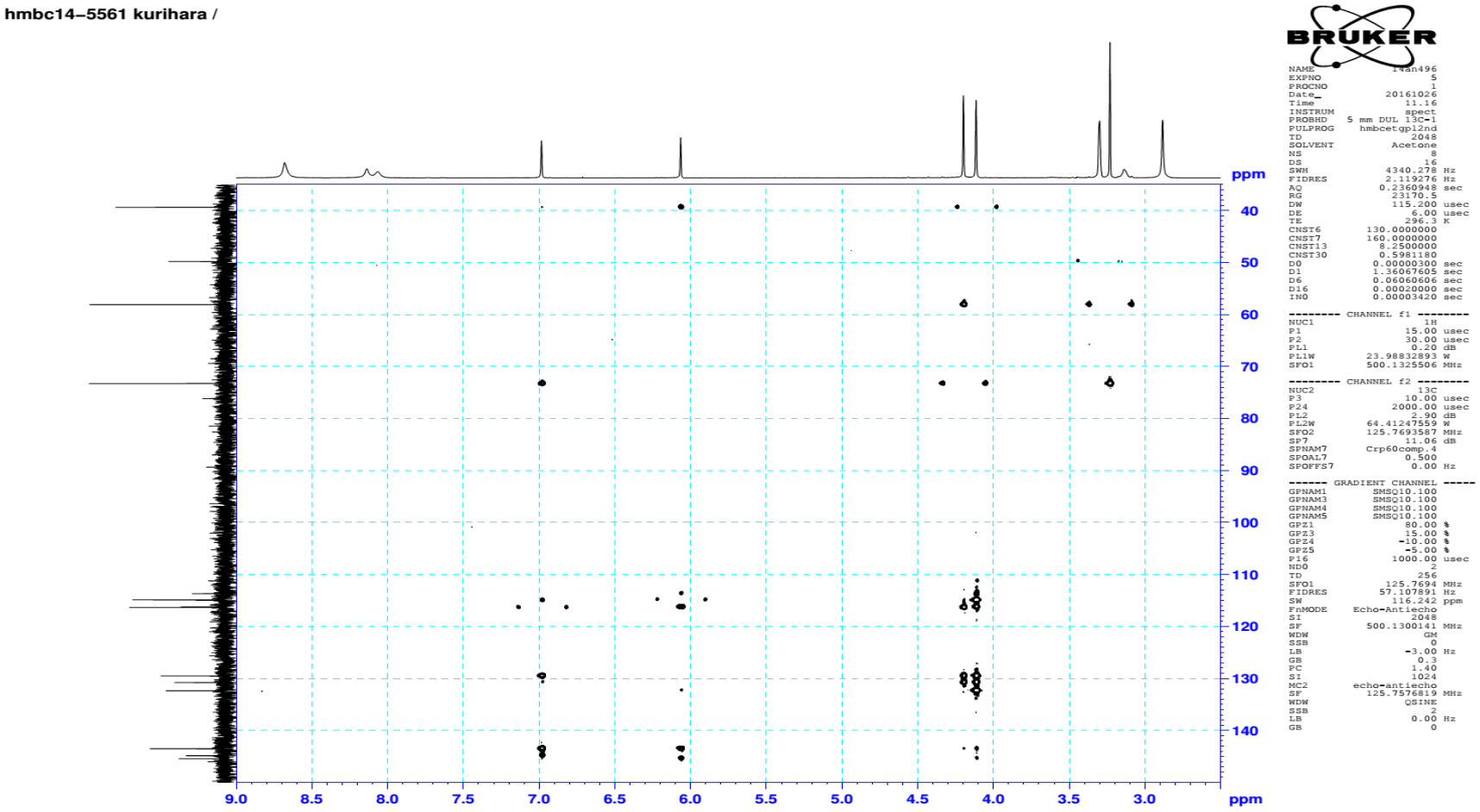


Figure 2-25. HMBC spectrum of compound **F2**.

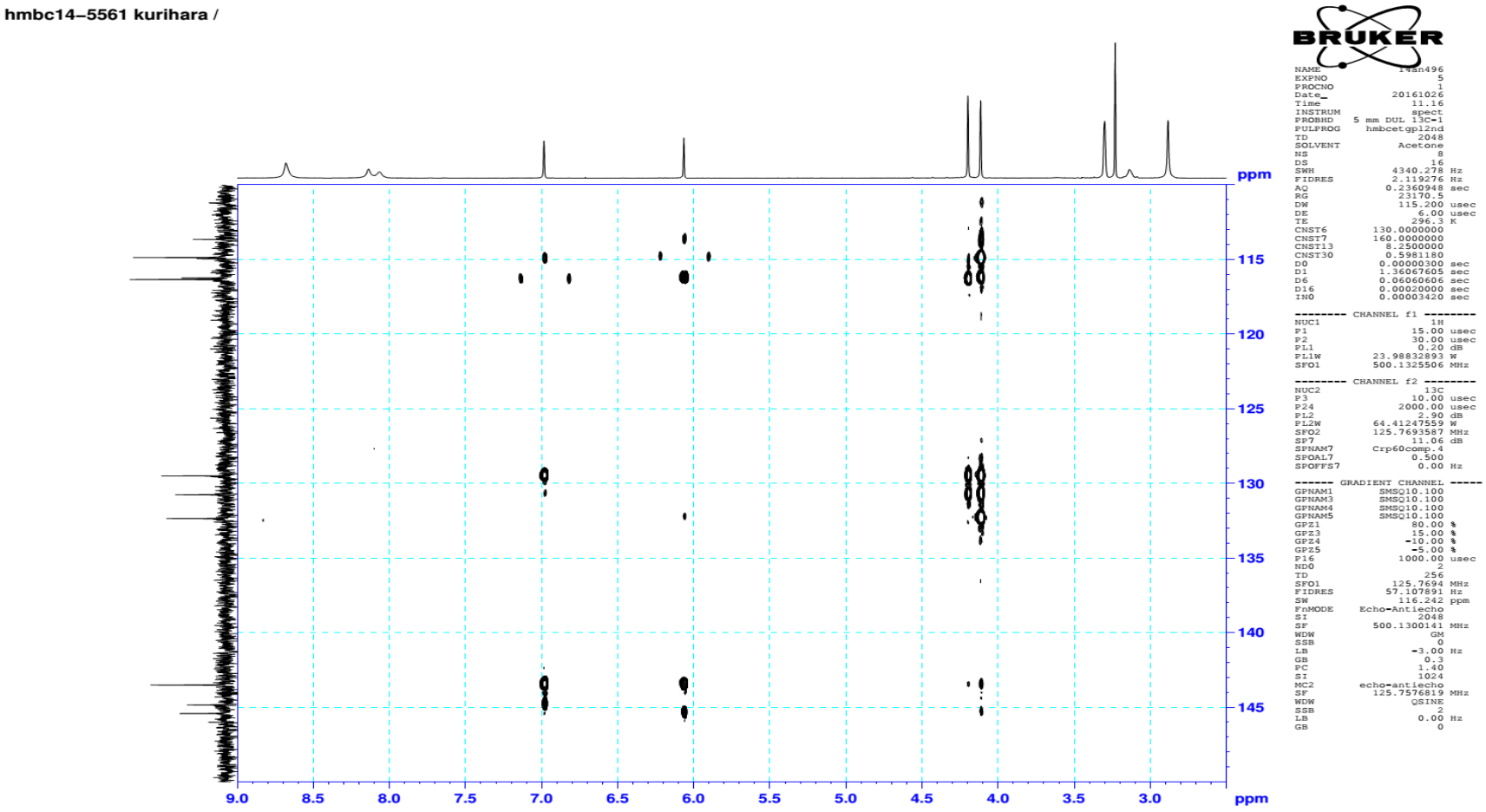


Figure 2-26. Expanded HMBC spectrum (1) of compound **F2**.

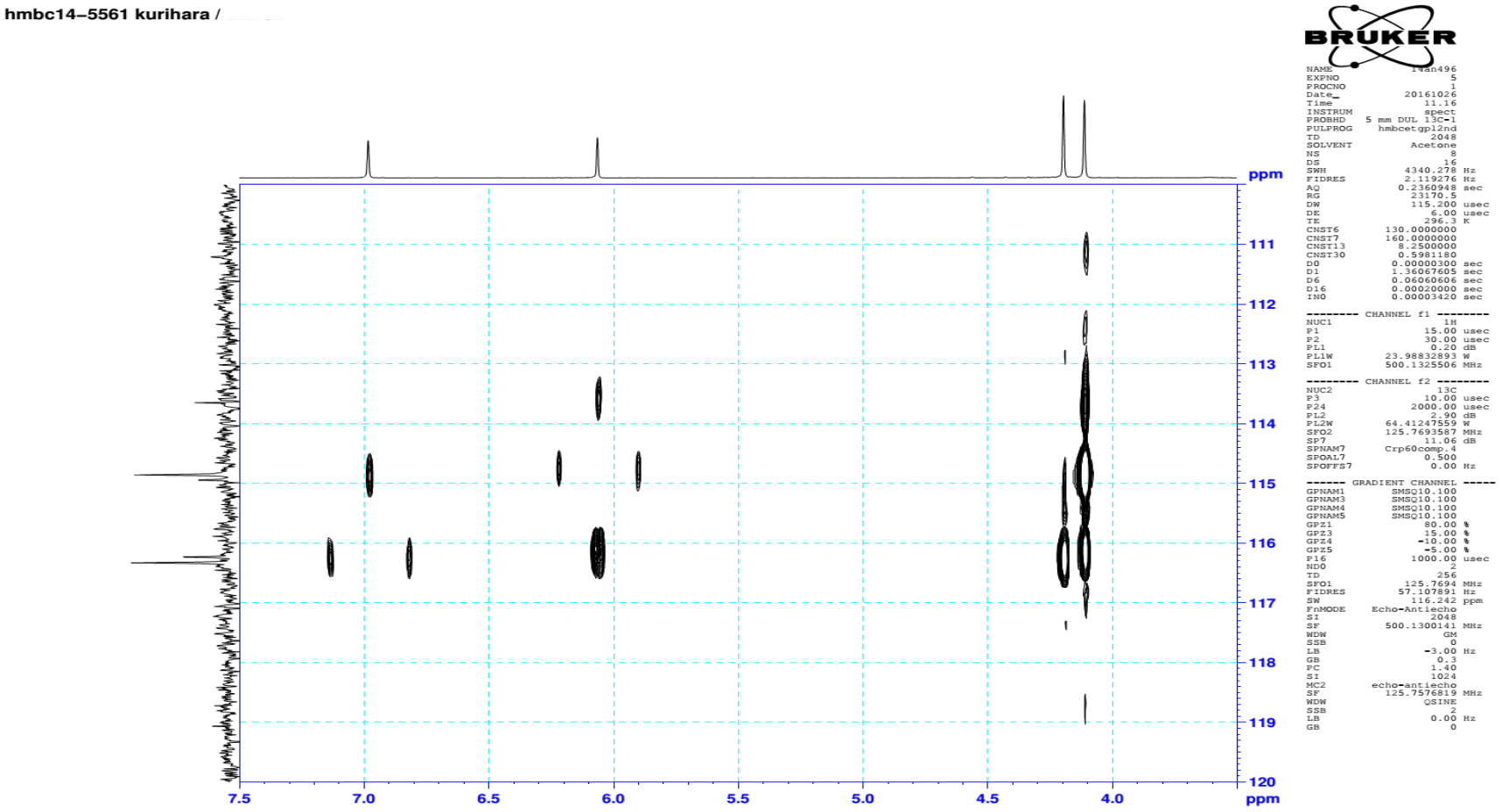


Figure 2-27. Expanded HMBC spectrum (2) of compound **F2**.

Table 2-13. Comparison of NMR data between compound **F2**[a] and literature[b]

	^{1}H NMR		^{13}C NMR	
Position	**F2**	Literature data	**F2**	Literature data
1			132.4	131.5
2			113.7 or 114.9 or 115.0	115.4
3			113.7 or 115.0	112.8
4			145.4 or 144.8 or 143.5	142.6
5			145.4 or 144.8 or 143.5	144.0
6	6.06 (s, 1H)	6.08 (s, 1H)	114.9	114.0
7	4.11 (s, 2H)	4.12 (s, 2H)	39.3	38.4
8	4.20 (s, 2H)	4.21 (s, 2H)	73.2	72.3
9	3.30 (s, 3H)	3.24 (s, 3H)	58.1	57.9
1’			113.7 or 114.9 or 115.0	114.0
2’			145.4 or 144.8 or 143.5	142.6
3’			145.4 or 144.8 or 143.5	144.5
4’	6.98 (s, 1H)	7.00 (s, 1H)	116.3	115.4
5’			129.5 or 130.8	129.8
6’			130.8 or 129.5	128.6

[a]The NMR data were measured in acetone-d_6 (δ_H 2.04 ppm; δ_C CO 206.3, CH_3 30.3 ppm) at 500 MHz for ^{1}H and at 125 MHz for ^{13}C.

[b]Park et al., 2012.

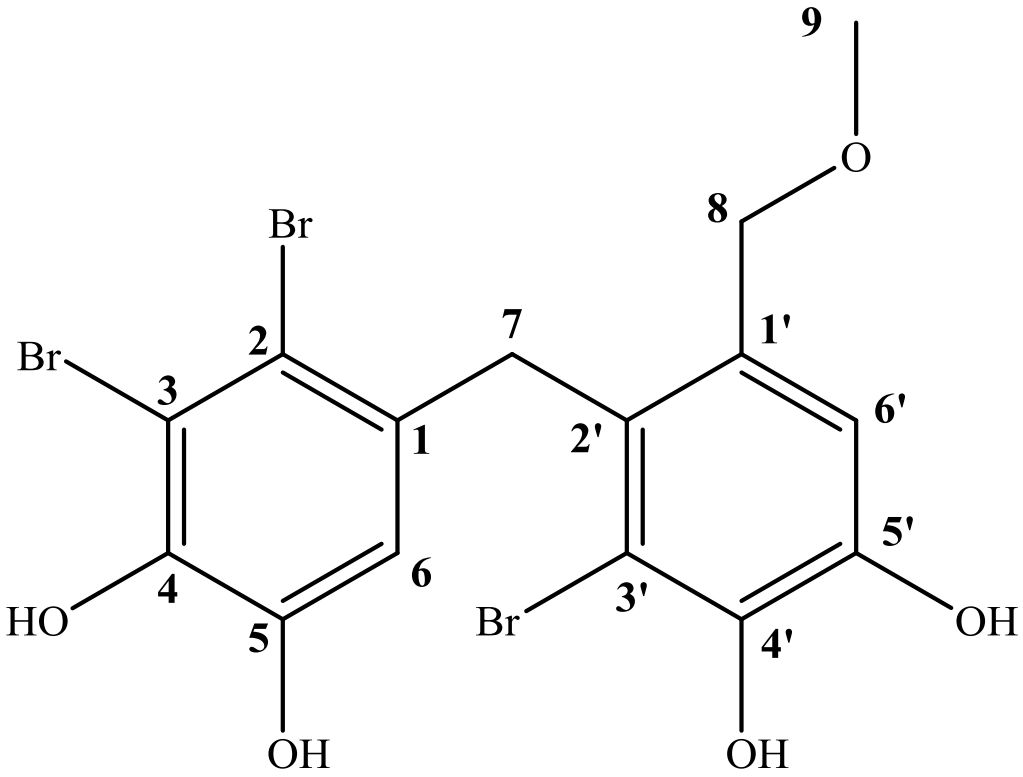


Figure 2-28. Structure of compound **F2**.

2.2.2.3 Structural elucidation of β-glucuronidase inhibitor F3

Compound **F3** was isolated as yellowish amorphous solid. In the FD-MS spectrum, characteristic molecular ion peak cluster at *m/z* 496/498/500/502 (intensity ratio of 1:3:3:1) suggested the presence of three bromine atoms (Figure 2-29). Molecular formula of compound **F3** was determined as $C_{14}H_{11}{}^{79}Br_3O_5$ by FD-HR-MS at *m/z* 495.81542 (calculated 495.81566), which less of CH_2 from the formula of compound **F2**.

^{1}H NMR spectrum showed two singlet aromatic protons at δ_H 6.95 and 6.06, and two methylenes at δ_H 4.35 and 4.12 (Figure 2-30). The ^{13}C NMR spectrum displayed two penta-substituted benzene rings at δc 115.0-146.2 and two methylenes at δc 63.2 and 39.7 (Figure 2-31). These NMR data were similar to those of compound **F2** despite of deletion of methoxy signals. According to the results of 2D NMR spectra (Figures 2-31 to 2-35) and with comparison of literature data (Fan, Xu, & Shi, 2003), compound **F3** was identified as 3-bromo-2-(2,3-dibromo-4.5-dihydroxybenzyl)-4,5-dihyroxybenzyl alcohol (Table 2-14, Figure 2-36).

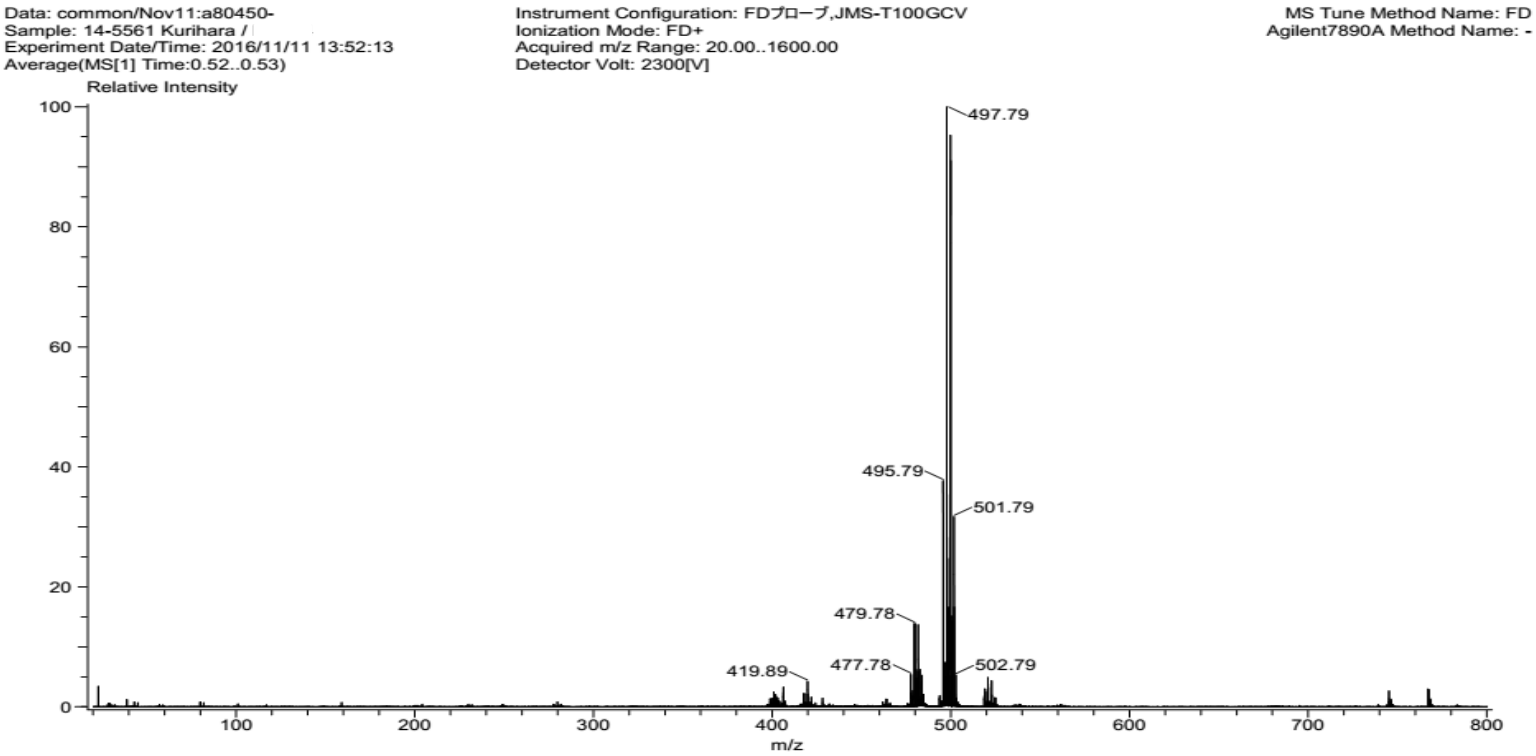


Figure 2-29. FD-MS spectrum of compound **F3**.

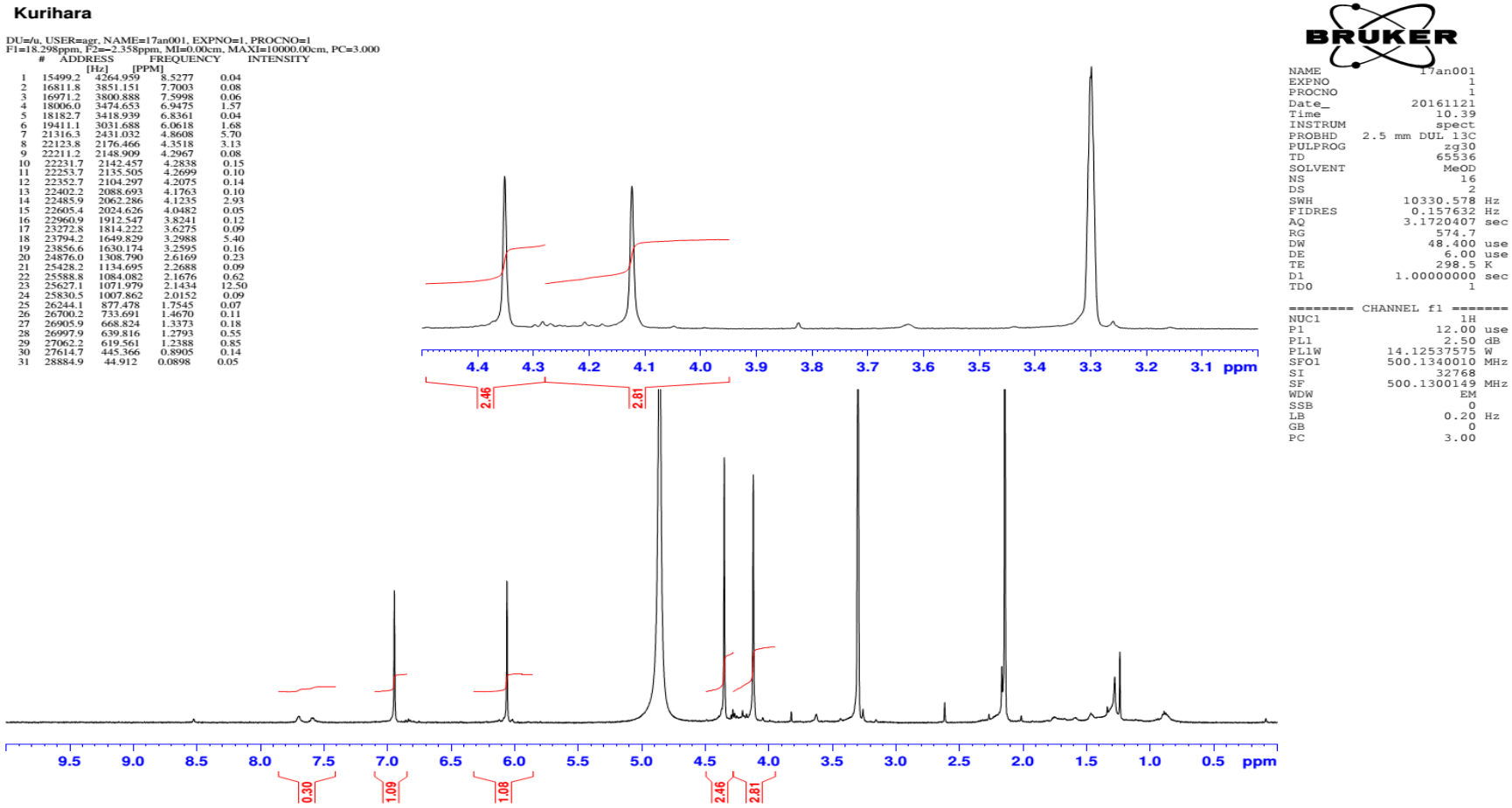


Figure 2-30. ^{1}H-NMR spectrum of compound **F3**.

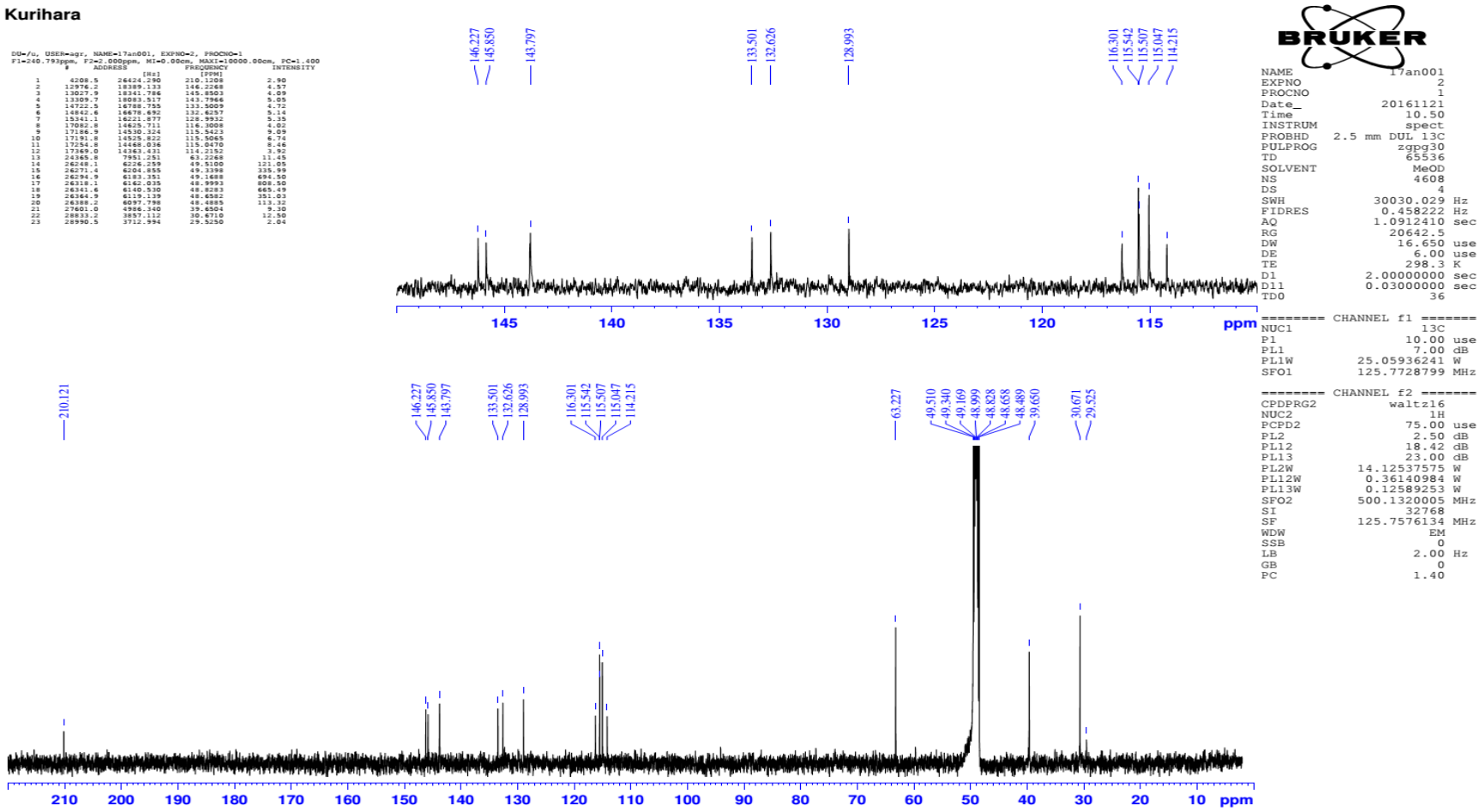


Figure 2-31. ^{13}C-NMR spectrum of compound **F3**.

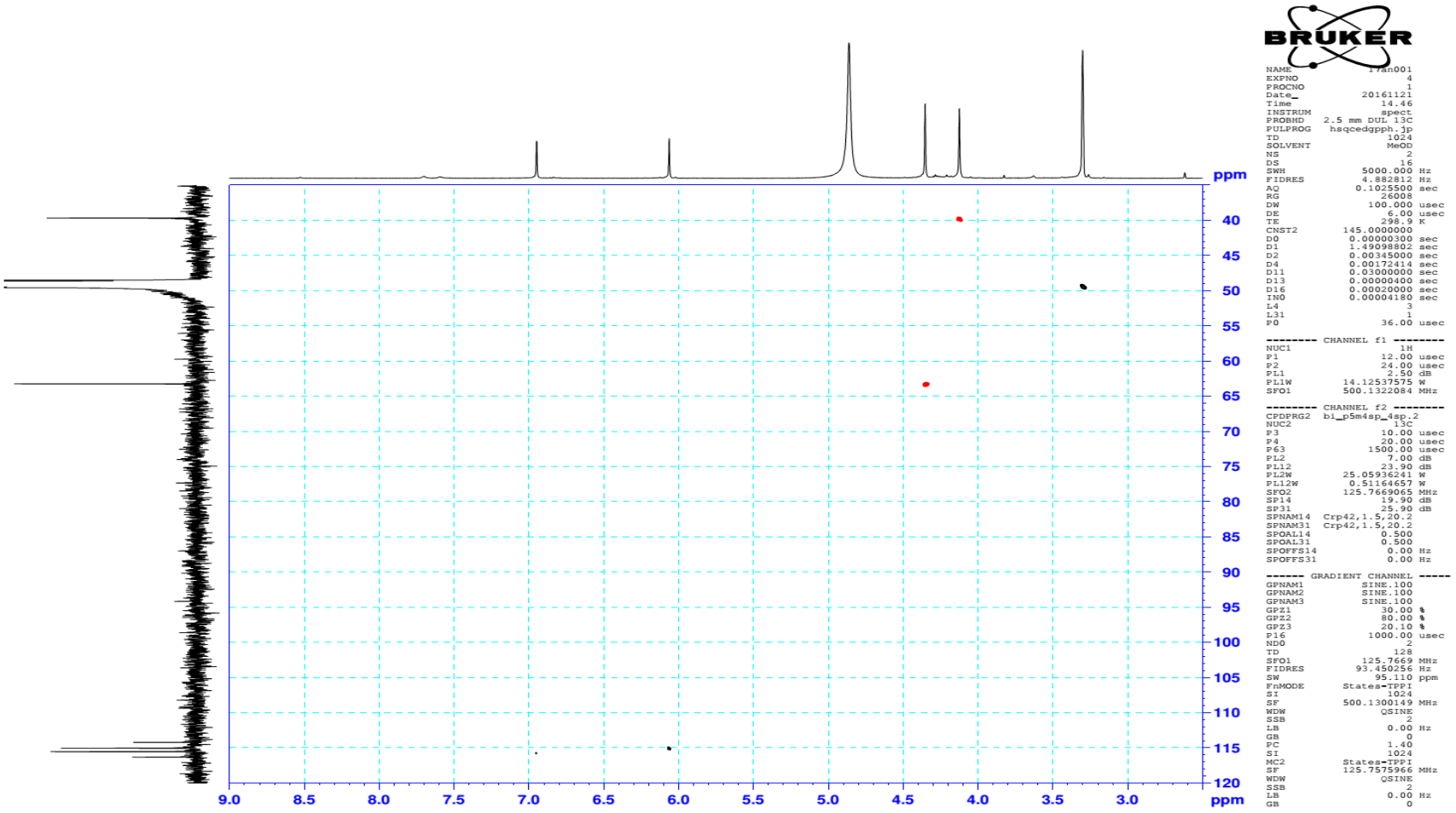


Figure 2-32. HSQC spectrum of compound **F3**.

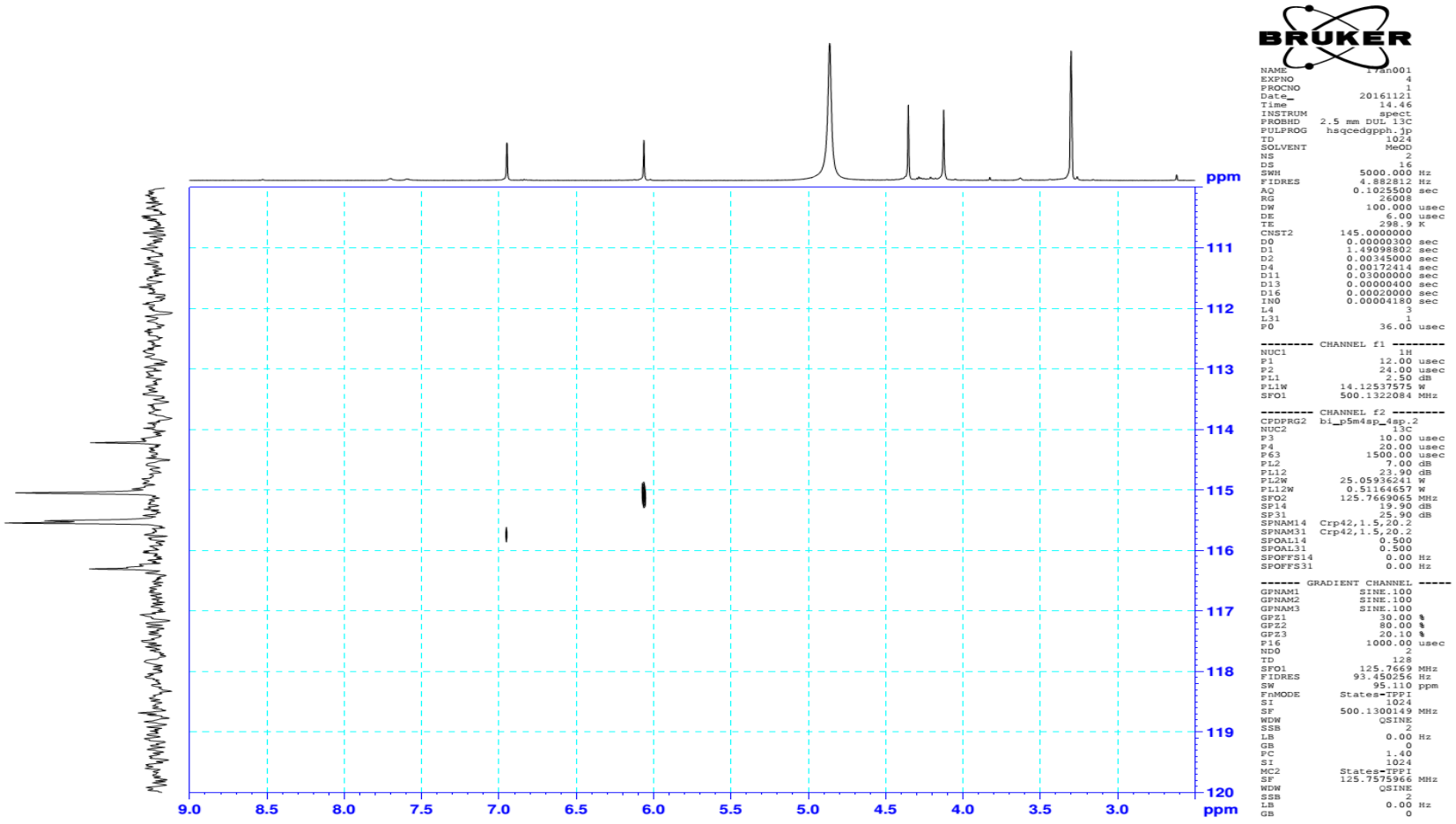


Figure 2-33. Expanded HSQC spectrum of compound **F3**.

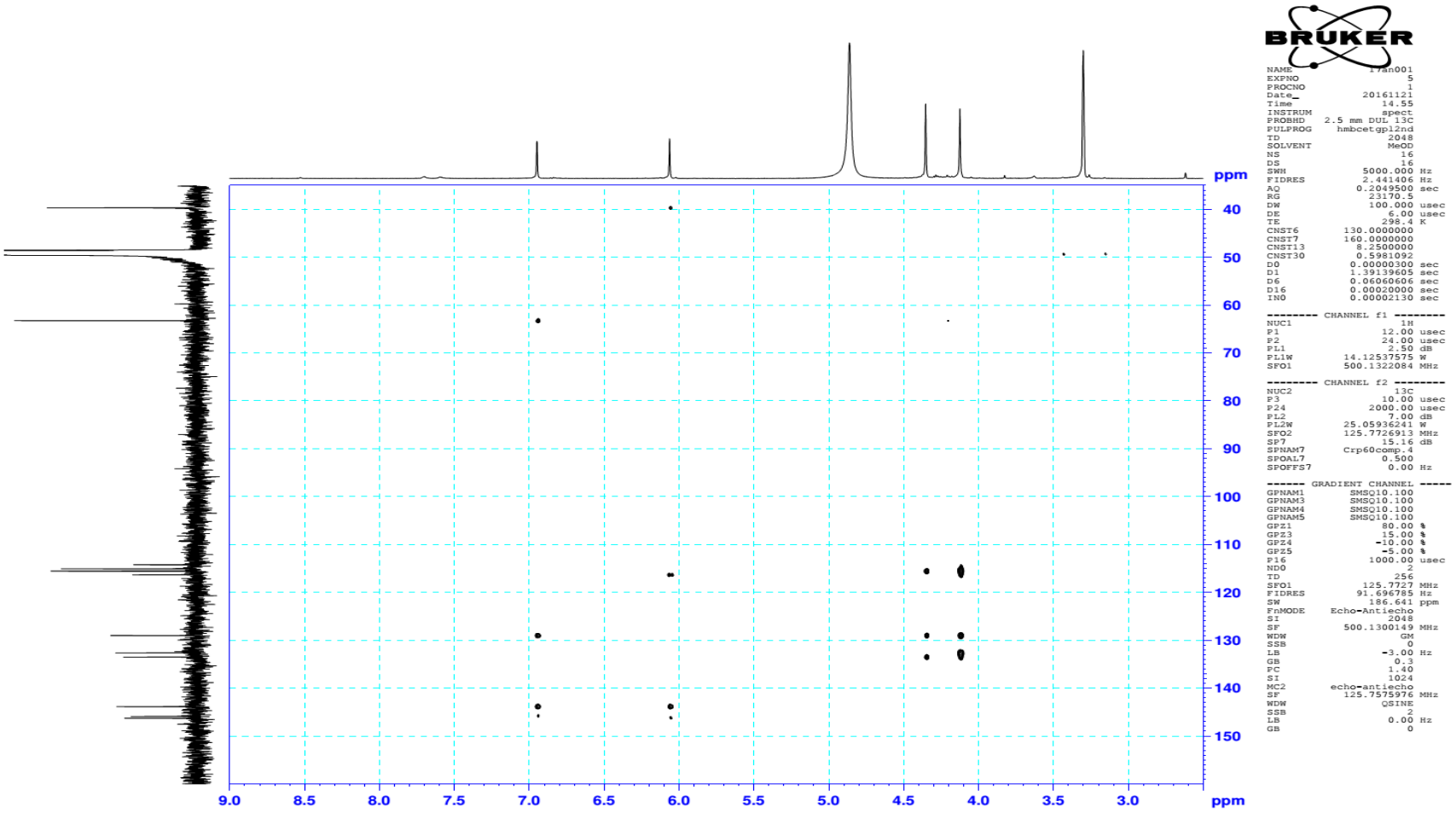


Figure 2-34. HMBC spectrum of compound **F3**.

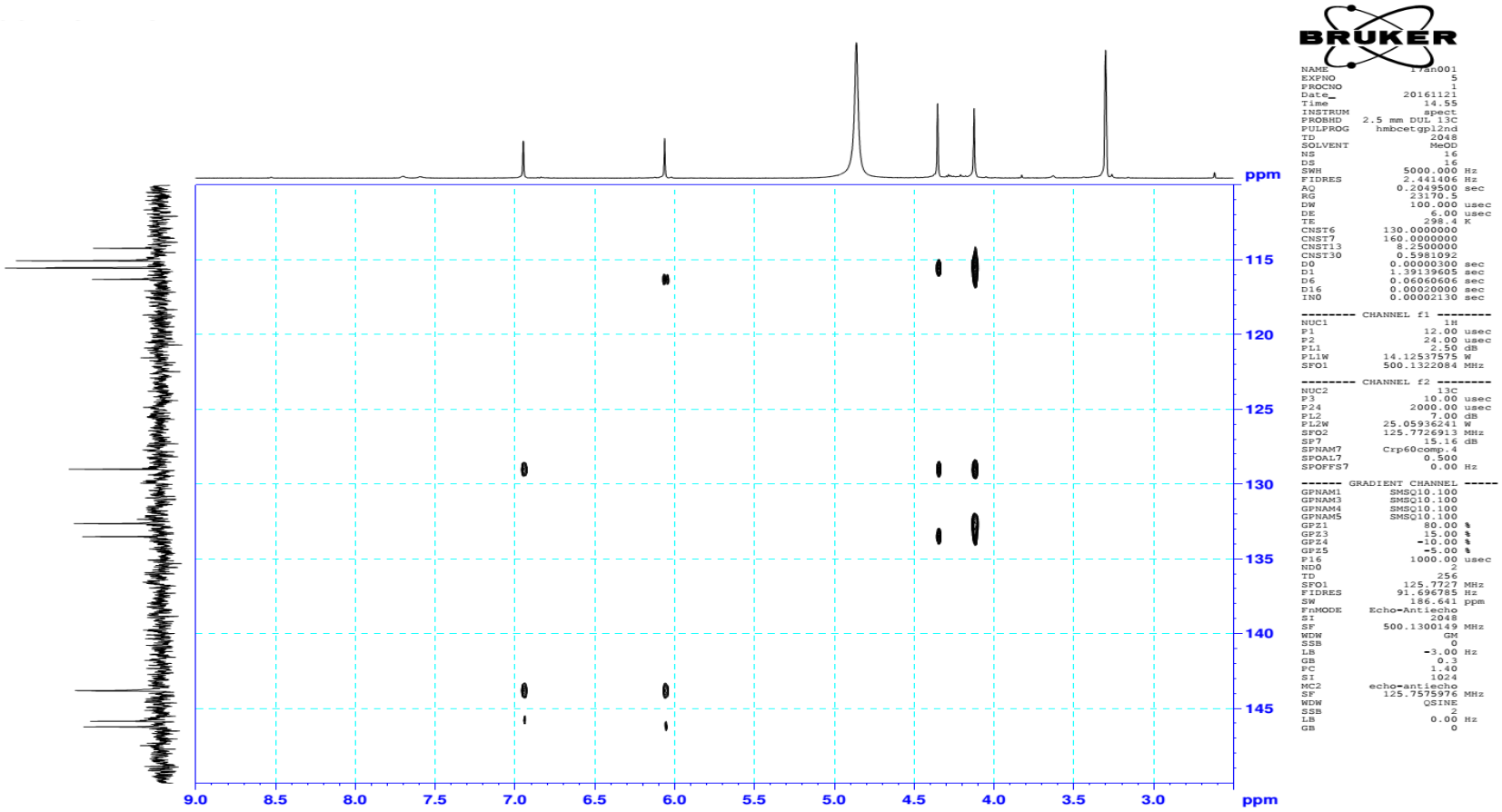


Figure 2-35. Expanded HMBC spectrum of compound **F3**.

Table 2-14. Comparison of NMR data between compound **F3**[a] and literature[b]

	^{1}H NMR		^{13}C NMR	
Position	**F3**	Literature data	**F3**	Literature data
1			129.0	131.7
2			115.0	115.7
3			114.2	113.1
4			143.8	142.9
5			146.2	144.8
6	6.06 (s, 1H)	6.08 (s, 1H)	115.5	114.1
7	4.12 (s, 2H)	4.12 (s, 2H)	39.7	38.6
8	4.35 (s, 2H)	4.42 (s, 2H)	63.2	62.1
1’			116.3	114.2
2’			143.8	142.3
3’			145.9	144.4
4’	6.95 (s, 1H)	7.09 (s, 1H)	115.5	114.4
5’			132.6	133.5
6’			133.5	127.7

[a]The NMR data were measured in acetone-d_6 (δ_H 2.14 ppm; δ_C CO 210.1, CH_3 30.7 ppm) at 500 MHz for ^{1}H and at 125 MHz for ^{13}C.

[b]Fan et al., 2003.

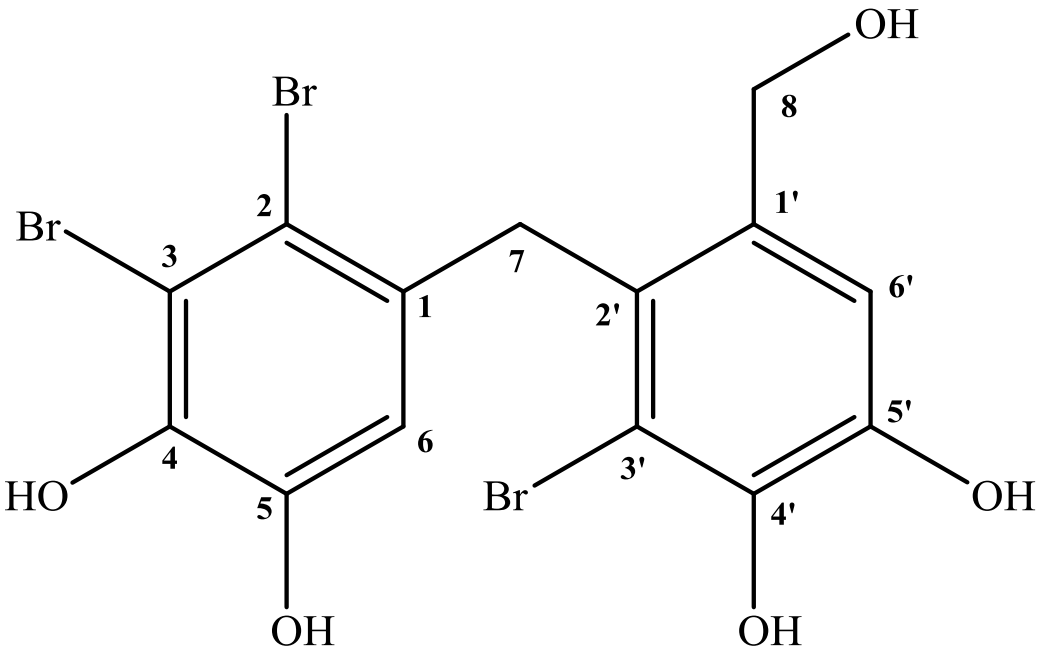


Figure 2-36. Structure of compound **F3**.

2.3 β-Glucuronidase inhibitors derived from the marine red alga *Neodilsea yendoana*

In this section, *N*. *yendoana* collected from Usujiri, Hakodate on May 10th and May 25th in 2016 (total methanol extracts, 78.731 g) (Table 1-5 and Table 1-6) were combined for the isolation and purification of β-glucuronidase inhibitors (Figure 2-37).

2.3.1 Isolation and purification of β-glucuronidase inhibitors from *N. yendoana*

Methanol extracts (total amount 78.7 g) of *N*. *yendoana* were separated by organic solvent partitioning (Figure 2-2) to give *n*-hexane-soluble fraction (0.20 g), ethyl acetate-soluble fraction (2.91 g), *n*-butanol-soluble fraction (10.56 g) (Table 2-15, Figure 2-38). Ethyl acetate-soluble fraction was loaded over silica gel column chromatography and eluted with a combination of chloroform and methanol to afford fractions E1-E14 (Table 2-16, Figure 2-39). Among them, three fractions E2 (34.7 mg), E3 (66.4 mg) and E4 (253.3 mg) were chosen for the further isolation.

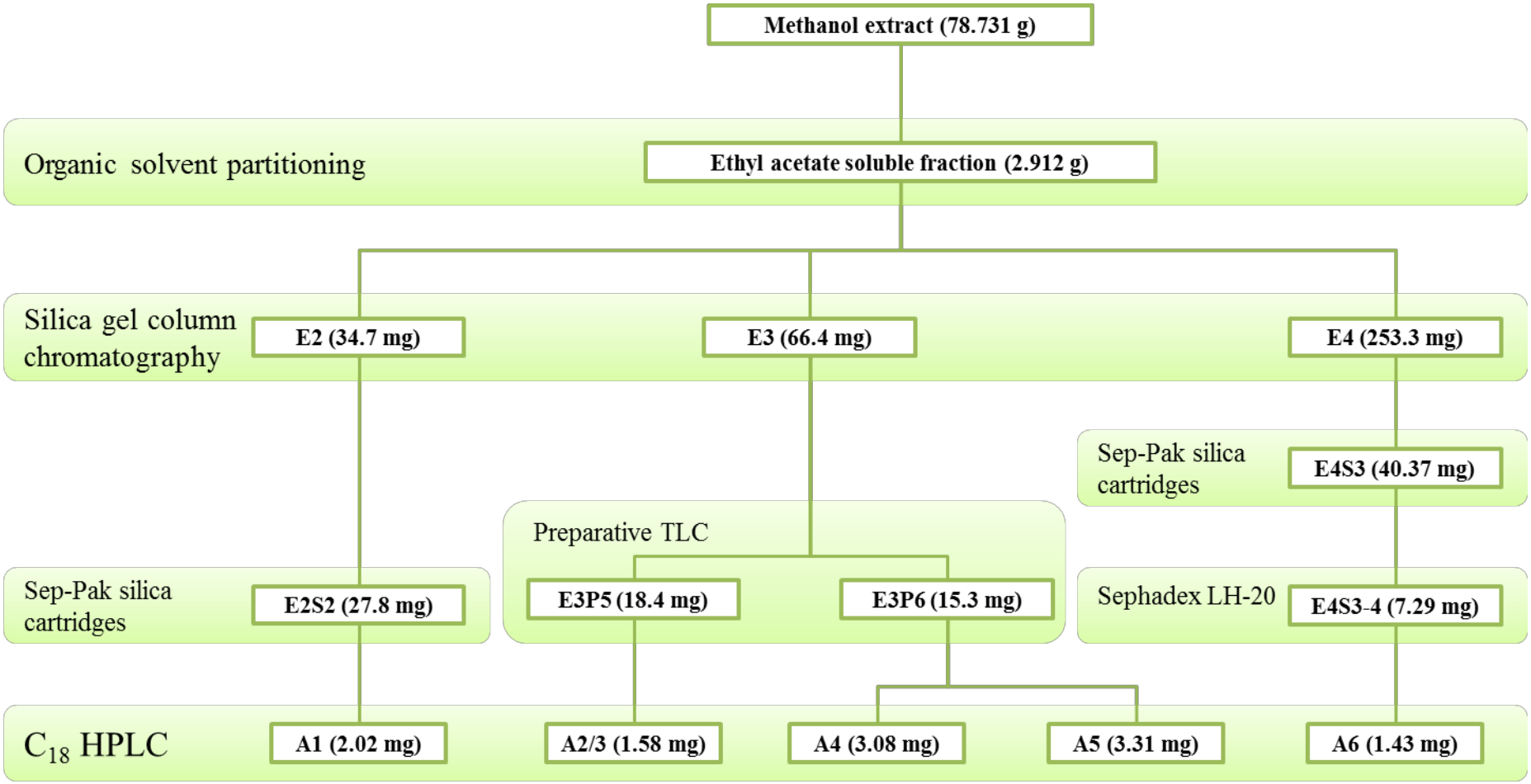


Figure 2-37. Separation scheme of the extract of *N. yendoana*.

Table 2-15. Amount and β-glucuronidase inhibitory activity of the fractions[a] obtained by organic solvent partitioning

Fraction	Amount (g)	Inhibition[b] (%)
n-Hexane	0.1979	23.70 ± 0.31
Ethyl acetate	2.9123	32.23 ± 0.28
n-Butanol	10.5561	25.86 ± 0.30

[a]Sample, 78.731 g methanol extracts of *N. yendoana*.

[b]Assay concentration was 10 μg/mL. Data represent means ± SE (n=3).

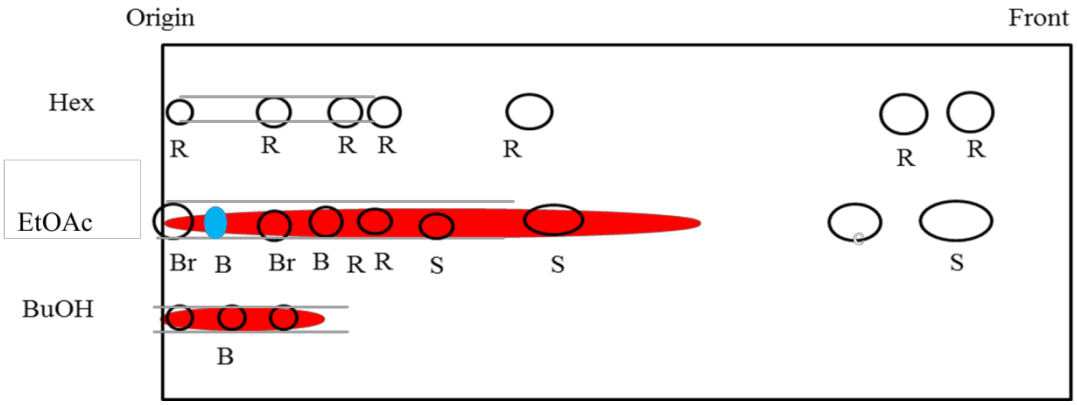


Figure 2-38. Silica gel thin layer chromatogram of the organic solvent extracts of *N. yendoana*.

Developing solvent, chloroform: methanol = 9: 1 (v/v).

⬭, Visualized with 5% sulfuric acid reagent.

🔵, Blue color after detection of 5% sulfuric acid reagent

🔴, Positive response for 0.2% ninhydrin reagent.

Abbreviations designate color of the spots: Br, brown; R, red color under long wave UV lamp; B, blue color under long wave UV lamp.

Table 2-16. Amount and β-glucuronidase inhibitory activity of the fractions obtained from ethyl acetate-soluble fraction[a] separated by silica gel column chromatography

Fraction	Eluent (v/v)	Amount (mg)	Inhibition[b] (%)
E1	Chloroform	33.5	NI[c]
E2	Chloroform	34.7	19.44 ± 2.74
E3	Chloroform : methanol = 29 : 1	66.4	16.64 ± 1.17
E4	Chloroform : methanol = 29 : 1	253.3	13.35 ± 0.67
E5	Chloroform : methanol = 19 : 1	105.3	42.89 ± 0.32
E6	Chloroform : methanol = 19 : 1	104.7	31.51 ± 1.29
E7	Chloroform : methanol = 9 : 1	305.7	28.26 ± 2.82
E8	Chloroform : methanol = 9 : 1	363.3	36.78 ± 3.57
E9	Chloroform : methanol = 4 : 1	229.8	29.82 ± 2.08
E10	Chloroform : methanol = 4 : 1	254.4	20.98 ± 1.99
E11	Chloroform : methanol = 1 : 1	285.2	18.69 ± 1.35
E12	Chloroform : methanol = 1 : 1	207.3	28.51 ± 1.18
E13	Methanol	171.9	22.93 ± 1.72
E14	Methanol	258.0	29.00 ± 1.81

[a]Sample, ethyl acetate-soluble fraction, 2.913 g; stationary phase, Wakogel C-100; elution volume, 525 mL/fraction.

[b]Assay concentration was 10 μg/mL. Data represent means ± SE (n=3).

[c]NI, no inhibition.

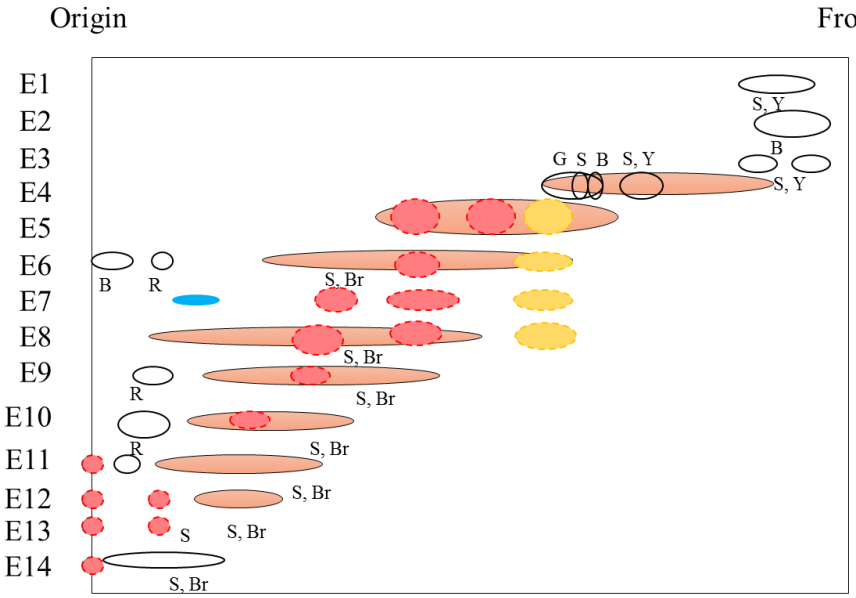


Figure 2-39. Silica gel thin layer chromatogram of fractions obtained from ethyl acetate-soluble fraction separated by silica gel column chromatography.

Developing solvent, chloroform: methanol = 5: 1 (v/v).

⬭, Visualized with 5% sulfuric acid reagent.

⬬, Blue color after detection of 5% sulfuric acid reagent

⬬, Positive response for 0.2% ninhydrin reagent.

⬬, Yellow color after detection of 0.2% ninhydrin reagent.

Abbreviations designate color of the spots: Br, brown; Y, yellow; G, green; R, red color under long wave UV lamp; B, blue color under long wave UV lamp; S, quenching spot under short wave UV lamp.

2.3.1.1 Purification of β-glucuronidase inhibitor A1

Fraction E2 (34.7 mg) was loaded on a Sep-Pak silica cartridge and eluted with *n*-hexane/ethyl acetate to give six fractions (Table 2-17, Figure 2-40). Among them, fraction E2S2 (27.76 mg) obtained from *n*-hexane/ethyl acetate (19/1, v/v) was further purified by RP-18 HPLC (Table 2-18, Figure 2-41) to give compound **A1** (2.02 mg, 1.4 ppm based on air-dried alga) (Table 2-19, Figure 2-42).

2.3.1.2 Purification of β-glucuronidase inhibitors A2-A5

Fraction E3 (66.4 mg) was charged on preparative TLC (Figure 2-43) to afford eight fractions E3P1-E3P8 (Table 2-20). Among them, fractions E3P5 (18.39 mg) and E3P6 (15.28 mg) were conducted for the further separation by RP-18 HPLC.

Peak of fraction E3P5 at retention time of 33.8 min (Figure 2-44) was collected as fraction E3P5-1 (1.58 mg) (Table 2-22). TLC analysis of this fraction showed single spot on both silica gel and RP-18 TLC plates (Figure 2-45), while according to the MS and NMR of fraction E3P5-1 demonstrated it should be a mixture of two compounds, named as compounds **A2** and **A3**.

Fraction E3P6 was separated by RP-18 HPLC (Table 2-23) to afford compounds **A4** (3.08 mg, 2.1 ppm based on air-dried alga) and **A5** (3.31 mg, 2.5 ppm based on air-dried alga) (Table 2-24, Figure 2-47).

2.3.1.3 Purification of β-glucuronidase inhibitor A6

Fraction E4 (253.3 mg) was re-chromatographed over silica gel and eluted with gradient *n*-hexane/ethyl acetate/methanol from 1/0/0 (v/v/v) to 0/0/1 (v/v/v) to afford 100 fractions. Each fraction was collected every 8 mL by test tube. Fractions that showed similar TLC profiles were combined as fractions E4S1 to E4S4 (Table 2-25,

Figure 2-48). Fraction E4S3 which showed an orange color spot after detection by 0.2% ninhydrin reagent was further separated on Sephadex LH-20 (Table 2-26) and eluted with 100% methanol to afford fractions E4S3-1 to E4S3-9 (Table 2-27, Figure 2-49). Among them, fraction E4S3-4 (7.29 mg) was performed for the finally separation by RP-18 HPLC (Table 2-28, Figure 2-50) to give compound **A6** (1.43 mg, 1.0 ppm based on air-dried alga) (Table 2-29, Figure 2-51).

Table 2-17. Amount and β-glucuronidase inhibitory activity of the fractions obtained from fraction E2[a] by Sep-Pak silica cartridge

Fraction	Eluent (v/v)	Amount (mg)	Inhibition[b] (%)
E2S1	*n*-Hexane	1.26	7.18 ± 1.66
E2S2	*n*-Hexane : ethyl acetate = 19 : 1	27.76	27.76 ± 1.73
E2S3	*n*-Hexane : ethyl acetate = 9 : 1	0.99	17.19 ± 0.92
E2S4	*n*-Hexane : ethyl acetate = 4 : 1	0.52	18.59 ± 0.32
E2S5	*n*-Hexane : ethyl acetate = 1 : 1	0.26	19.48 ± 1.44
E2S6	Ethyl acetate	3.69	13.48 ± 1.82

[a]Sample, fraction E2, 34.7 mg; stationary phase, Sep-Pak silica cartridge 12cc, (2g); elution volume, 12 mL/fraction.

[b]Assay concentration was 10 μg/mL. Data represent means ± SE (n=3).

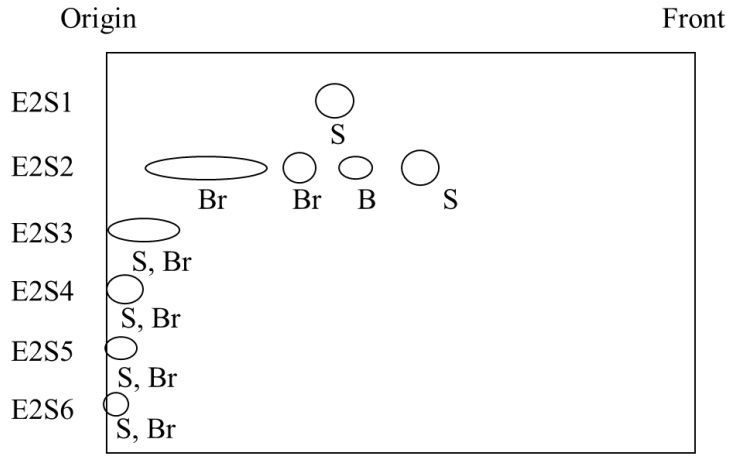


Figure 2-40. Silica gel thin layer chromatogram of fractions obtained from fraction E2 separated by Sep-Pak silica cartridge.

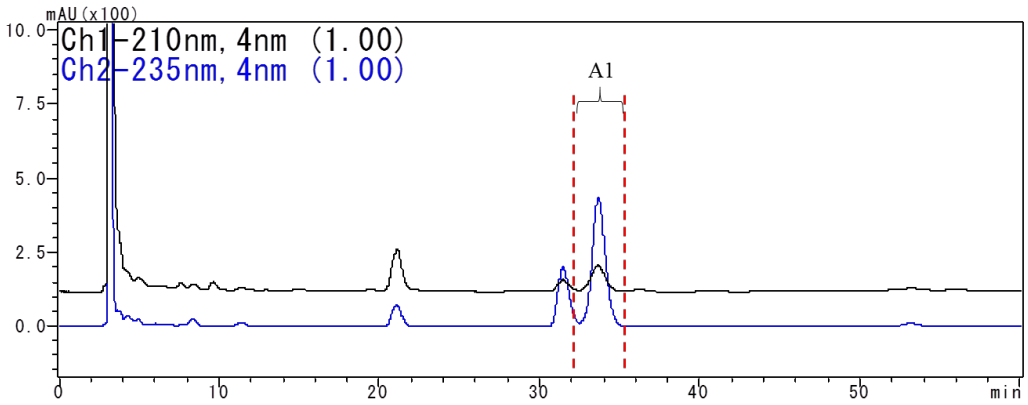
Developing solvent, *n*-hexane: ethyl acetate = 9: 1 (v/v).

⬭, Visualized with 5% sulfuric acid reagent.

Abbreviations designate color of the spots: Br, brown; B, blue color under long wave UV lamp; S, quenching spot under short wave UV lamp.

Table 2-18. HPLC condition for separating fraction E2S2

Sample:	E2S2 27.76 mg
Column:	ULTRON VX-ODS (5 μm; 250 × 4.6 mm) (Shinwa Chemical Industries, Ltd.)
Eluting solvent:	Acetonitrile : water = 9 : 1
Flow rate:	1 mL/min
Detection:	UV (210 nm, 235 nm)



Retention time (min)

Figure 2-41. HPLC chromatogram of fraction E2S2 monitored at 210 nm and 235 nm.

Table 2-19. Amount and β-glucuronidase inhibitory activity of fraction obtained by HPLC

Fraction	Amount (mg)	Inhibition[a] (%)
A1	2.02	30.55 ± 2.30

[a]Assay concentration was 10 μg/mL. Data represent means ± SE (n=3).

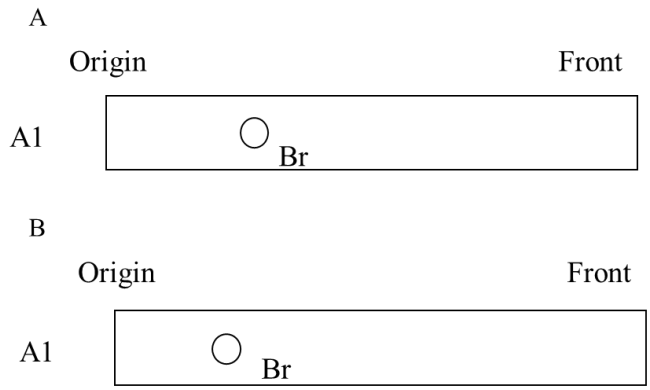


Figure 2-42. Analytical RP-18 thin layer chromatogram (A) and high performance silica gel thin layer chromatogram (B) of fraction **A1**.

Developing solvent: (A) acetonitrile: water = 9: 1 (v/v);

(B) *n*-hexane: ethyl acetate = 19: 1 (v/v).

⬭ , Visualized with 5% sulfuric acid reagent.

Abbreviation designates color of the spots: Br, brown.

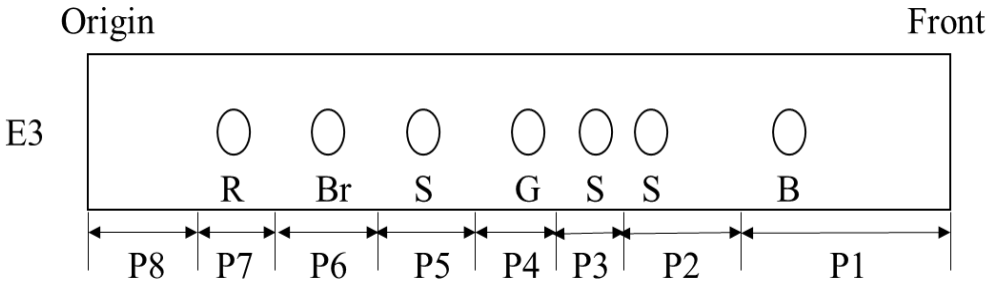


Figure 2-43. Profile of the preparative TLC of fraction E3.

Developing solvent, *n*-hexane: acetone = 6: 1 (v/v).

⬭, Visualized with 5% sulfuric acid reagent.

Abbreviations designate color of the spots: Br, brown; G, green; S, quenching spot under short wave UV lamp; R, red under long wave UV lamp; B, blue under long wave UV lamp.

Table 2-20. Amount and β-glucuronidase inhibitory activity of the fractions obtained from fraction E3[a] by preparative thin layer chromatography

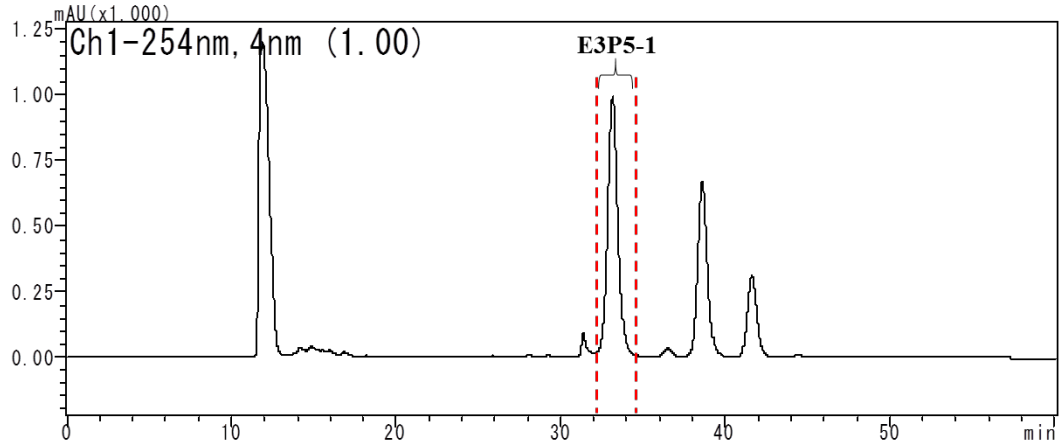
Fraction	Amount (mg)	Inhibition[b] (%)
E3P1	2.22	15.08 ± 1.67
E3P2	3.21	13.37 ± 1.65
E3P3	6.17	10.41 ± 3.08
E3P4	4.97	13.33 ± 0.56
E3P5	18.39	19.13 ± 0.95
E3P6	15.28	26.50 ± 0.30
E3P7	5.46	39.48 ± 1.93
E3P8	9.91	65.17 ± 0.93

[a]Sample, fraction E3, 66.4 mg.

[b]Assay concentration was 10 μg/mL. Data represent means ± SE (n=3).

Table 2-21. HPLC condition for separating fraction E3P5

Sample:	E3P5 18.39 mg
Column:	ULTRON VX-ODS (5 μm; 250 × 4.6 mm) (Shinwa Chemical Industries, Ltd.)
Eluting solvent:	Methanol : water = 95 : 5
Flow rate:	0.5 mL/min
Detection:	UV (254 nm)



Retention time (min)

Figure 2-44. HPLC chromatogram of fraction E3P5 monitored at 254 nm.

Table 2-22. Amount and β-glucuronidase inhibitory activity of fractions obtained by HPLC

Fraction	Amount (mg)	Inhibition[a] (%)
E3P5-1	1.58	36.21±0.48

[a]Assay concentration was 10 μg/mL. Data represent means ± SE (n=3).

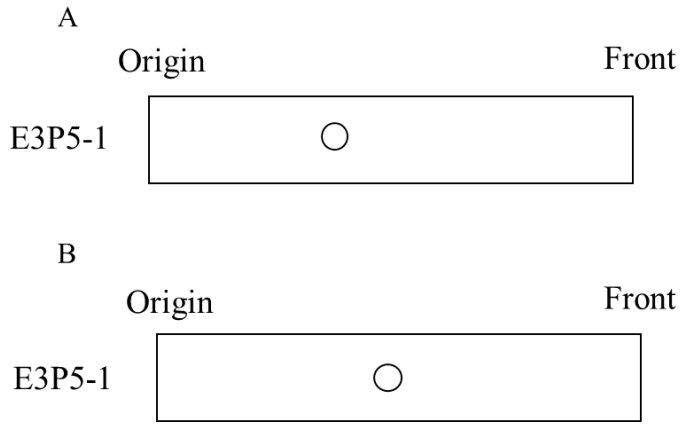


Figure 2-45. Analytical RP-18 thin layer chromatogram (A) and high performance silica gel thin layer chromatogram (B) of fraction E3P5-1.

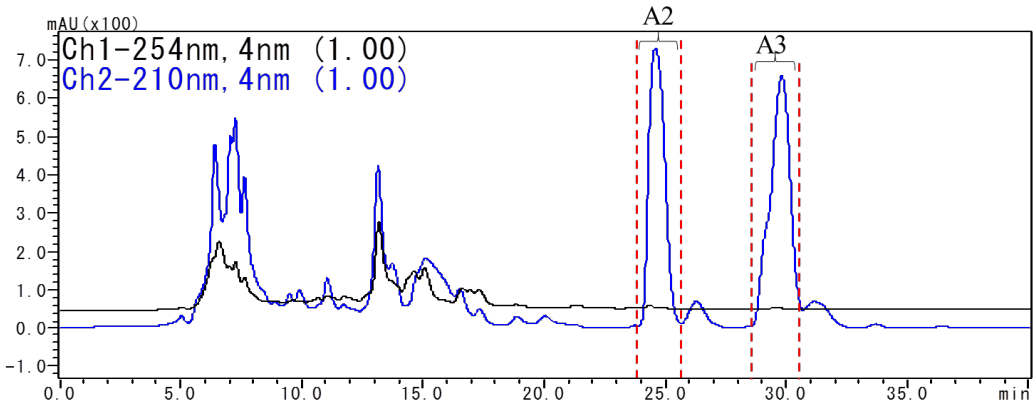
Developing solvent: (A) methanol: water = 9: 1 (v/v);

(B) *n*-hexane: acetone = 6: 1 (v/v).

⬭, Visualized with 5% sulfuric acid reagent.

Table 2-23. HPLC condition for separating fraction E3P6

Sample:	E3P6 15.28 mg
Column:	ULTRON VX-ODS (5 μm; 250 × 4.6 mm) (Shinwa Chemical Industries, Ltd.)
Eluting solvent:	Methanol : water = 9 : 1
Flow rate:	0.5 mL/min
Detection:	UV (210 nm, 254 nm)



Retention time (min)

Figure 2-46. HPLC chromatogram of fraction E3P6 monitored at 210 nm and 254 nm.

Table 2-24. Amount and β-glucuronidase inhibitory activity of compounds **A4** and **A5** obtained by HPLC

Fraction	Amount (mg)	Inhibition[a] (%)
A4	3.08	6.73 ± 2.29
A5	3.31	26.34 ± 0.45

[a]Assay concentration was 10 μg/mL. Data represent means ± SE (n=3).

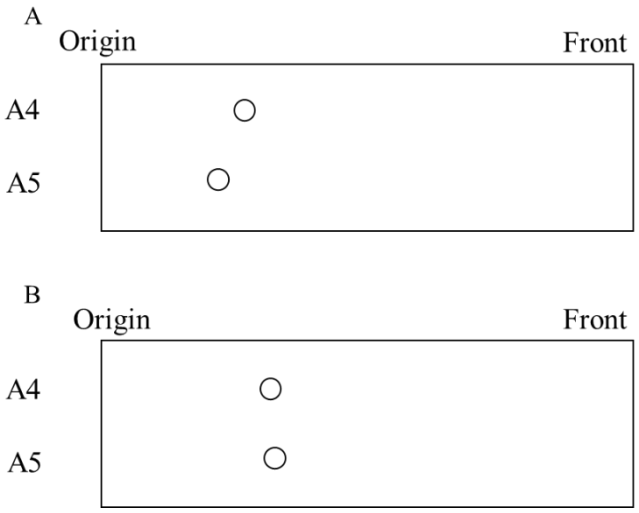


Figure 2-47. Analytical RP-18 thin layer chromatogram (A) and high performance silica gel thin layer chromatogram (B) of compounds **A4** and **A5**.

Developing solvent: (A) methanol: water = 9: 1 (v/v);

(B) *n*-hexane: acetone = 6: 1 (v/v).

⬭, Visualized with 5% sulfuric acid reagent.

Table 2-25. Amount and β-glucuronidase inhibitory activity of the fractions obtained from fraction E4[a] separated by silica gel column chromatography

Fraction	Amount (mg)	Inhibition[b] (%)
E4S1(1~37)	32.89	NI[c]
E4S2(38~63)	73.46	17.17 ± 0.94
E4S3(64~72)	40.37	27.35 ± 2.40
E4S4(73~100)	123.28	39.01 ± 0.70

[a]Sample, fraction E4, 253.3 mg; stationary phase, Wakogel C-100; elution, *n*-hexane/ethyl acetate/methanol (1/0/0 to 0/0/1, v/v/v); elution volume, 80 mL/fraction.

[b]Assay concentration was 10 μg/mL. Data represent means ± SE (n=3).

[c]NI, no inhibition.

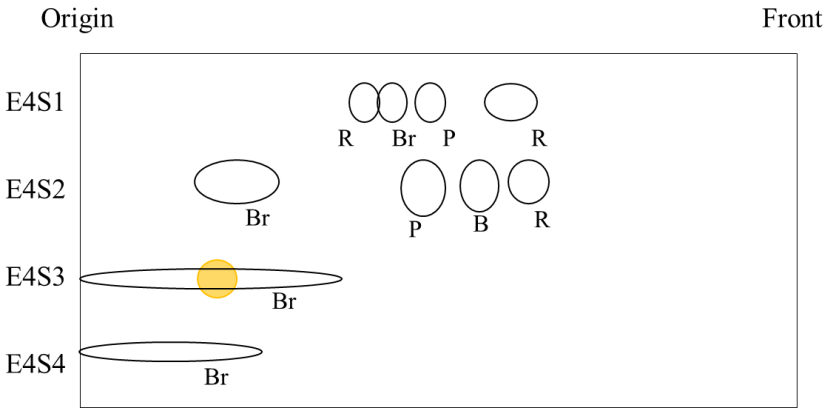


Figure 2-48. Silica gel thin layer chromatogram of fractions obtained from fraction E4 separated by silica gel column chromatography.

Developing solvent, *n*-hexane: ethyl acetate = 1: 1 (v/v).

⬭, Visualized with 5% sulfuric acid reagent.

●, Orange color after detection of 0.2% ninhydrin reagent.

Abbreviations designate color of the spots: Br, brown; P, purple; S, quenching spot under short wave UV lamp; R, red color under long wave UV lamp; B, blue color under long wave UV lamp.

Table 2-26. Sephadex LH-20 column chromatography conditions for separating fraction E4S3

Sample:	E4S3 40.37 mg
Column size:	Diameter 1.0 cm × length 20 cm
Elution solvent:	Methanol
Fraction volume:	8 mL
Flow rate:	0.6 mL/min

Table 2-27. Amount and β-glucuronidase inhibitory activity of the fractions obtained from fraction E4S3 separated by Sephadex LH-20 column chromatography

Fraction	Amount (mg)	Inhibition[a] (%)
E4S3-1	0.54	NI[b]
E4S3-2	5.40	7.60 ± 3.40
E4S3-3	4.30	10.09 ± 0.53
E4S3-4	7.29	32.15 ± 1.30
E4S3-5	10.31	23.62 ± 1.59
E4S3-6	2.57	13.16 ± 1.53
E4S3-7	8.44	12.61 ± 1.56
E4S3-8	0.69	NI
E4S3-9	0.23	NI

[a]Assay concentration was 10 μg/mL. Data represent means ± SE (n=3).

[b]NI, no inhibition.

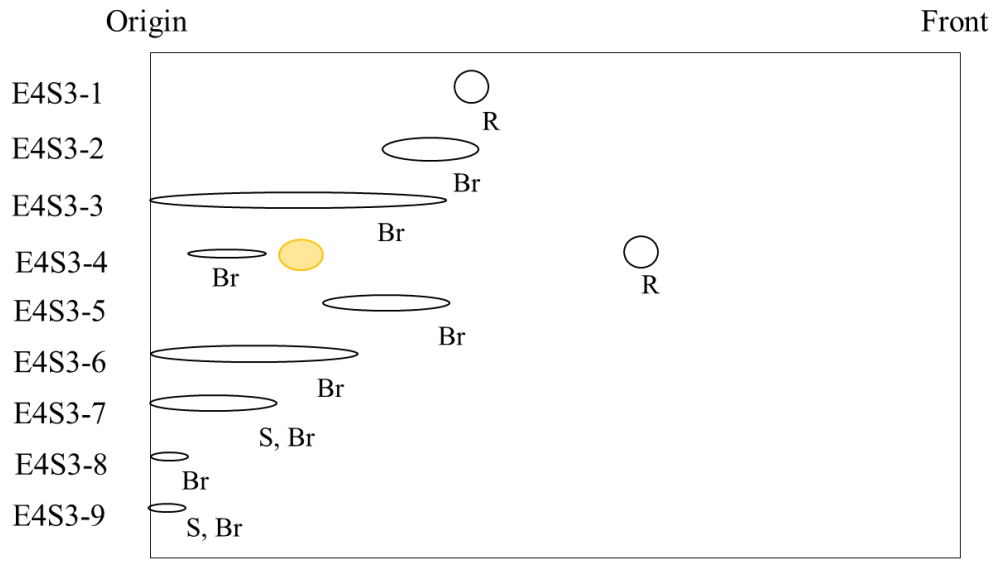


Figure 2-49. Silica gel thin layer chromatogram of fractions obtained from fraction E4S3 separated by Sephadex LH-20 column chromatography.

Developing solvent, *n*-hexane: ethyl acetate = 1: 1 (v/v).

⬭, Visualized with 5% sulfuric acid reagent.

●, Orange color after detection of 0.2% ninhydrin reagent.

Abbreviations designate color of the spots: Br, brown; S, quenching spot under short wave UV lamp; R, red color under long wave UV lamp.

Table 2-28. HPLC condition for separating fraction E4S3-4

Sample:	E4S3-4 7.29 mg
Column:	Mightysil RP-18 (5 μm; 250 × 4.6 mm) (KANTO CHEMICAL CO., Inc.)
Eluting solvent:	Acetonitrile : water = 15 : 85
Flow rate:	0.5 mL/min
Detection:	UV (210 nm, 254 nm)

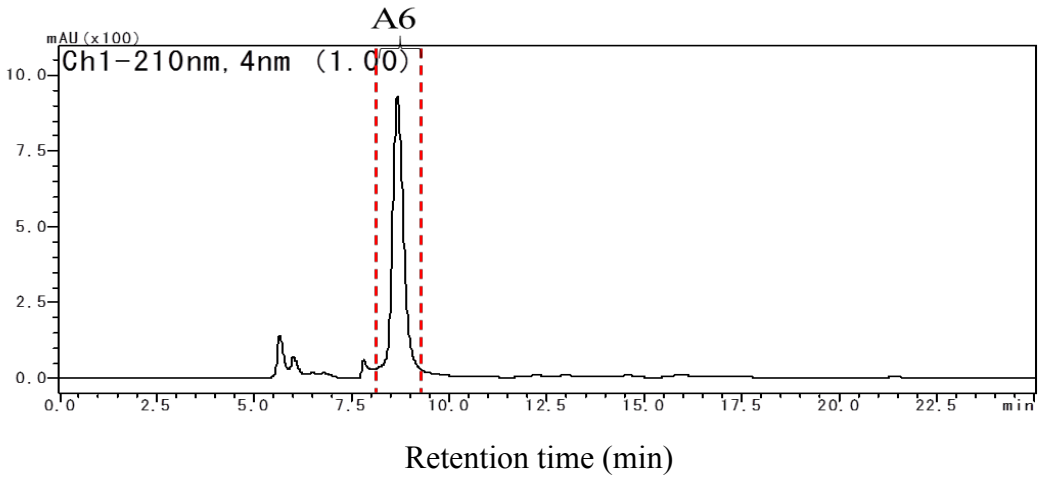


Figure 2-50. HPLC chromatogram of fraction E4S3-4 monitored at 210 nm.

Table 2-29. Amount and β-glucuronidase inhibitory activity of compound **A6** obtained by HPLC

Fraction	Amount (mg)	Inhibition[a] (%)
A6	1.43	46.77 ± 0.14

[a]Assay concentration was 10 μg/mL. Data represent means ± SE (n=3).

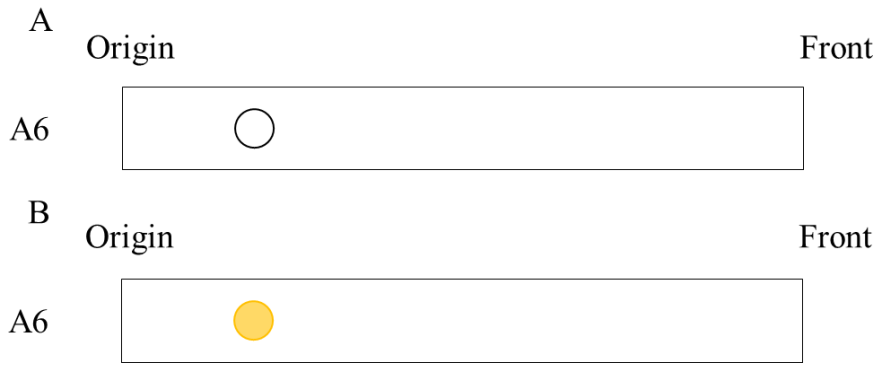


Figure 2-51. High performance silica gel thin layer chromatogram of compound **A6**. Developing solvent, *n*-hexane: ethyl acetate = 1: 1 (v/v).

(A) Detected by 5% sulfuric acid reagent; (B) detected by 0.2% ninhydrin reagent.

⬭, Visualized with 5% sulfuric acid reagent.

⬭, Orange color after detection of 0.2% ninhydrin reagent.

2.3.2 Structural elucidation of β-glucuronidase inhibitors from *N. yendoana*

2.3.2.1 Structural elucidation of β-glucuronidase inhibitor A1

Compound **A1** was obtained as colorless oil. FI-MS showed a molecular ion peak at *m/z* 294 (Figure 2-52). Molecular formula was determined as $C_{20}H_{38}O$ by FI-HR-MS spectrum at 294.29144 (calculated 294.29266) with unsaturation index of 2. The ^{1}H NMR spectrum of compound **A1** exhibited an aldehyde proton signal at δ_H 10.00 (H-1), an doublet olefinic proton signal at δ_H 5.79 (H-2), a methylene at δ_H 2.23 (H-4), a singlet methyl protons at δ_H 2.19 (H-17), three methine protons at δ_H 1.53, 1.43 and 1.37 (H-15, 11, 7), nine methylenes at δ_H 1.08-1.57 (H-5, 6, 8 to 10, 12 to 14) and three methyl protons at δ_H 0.87 (H18 to 20) (Figure 2-53). ^{13}C NMR spectrum revealed 20 carbons, including one aldehyde carbon at δc 191.3 (C-1), two alkene carbons at δc 164.4 and 127.9 (C-2 and 3), and 17 aliphatic carbons at δc 19.9-41.3 (C4 to 20) (Figure 2-54).

According to the HSQC (Figures 2-55 and 2-56), HMBC (Figures 2-57 to 2-60), COSY (Figures 2-61 and 2-62) spectra and literature data (Fürstenau et al., 2013), (Bar et al., 2015), compound **A1** was identified as (*E*)-3,7,11,15-tetramethylhexadec-2-enal, known as phytal (Table 2-30, Figure 2-63). Though compound **A1** possessed asymmetric centers in its structure, optical rotation was measured as $[\alpha]_D^{27}$= 0° (*c*1.32, $CHCl_3$). Stereochemistries including absolute configuration of compound **A1** has not determined yet.

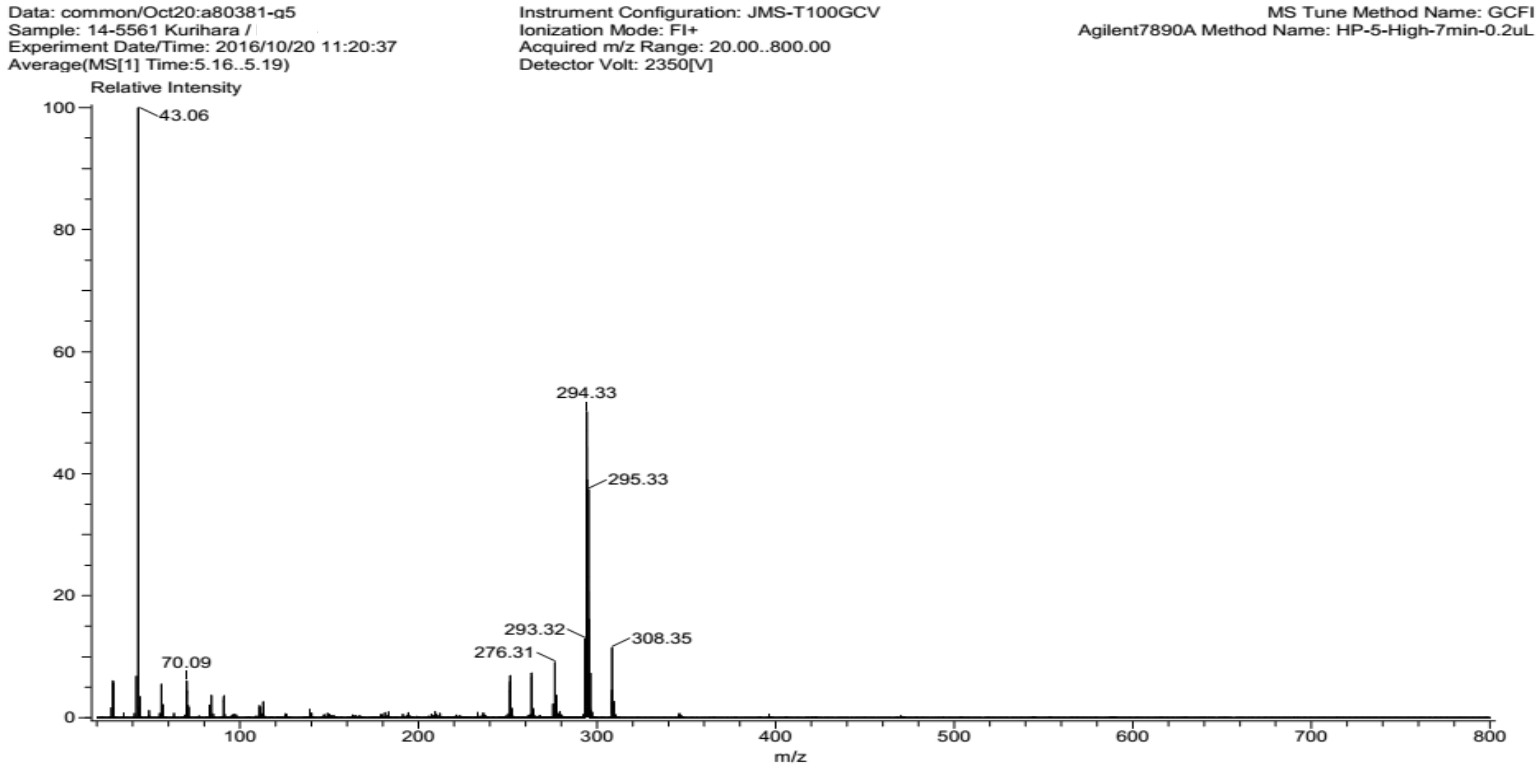


Figure 2-52. FI-MS spectrum of compound **A1**.

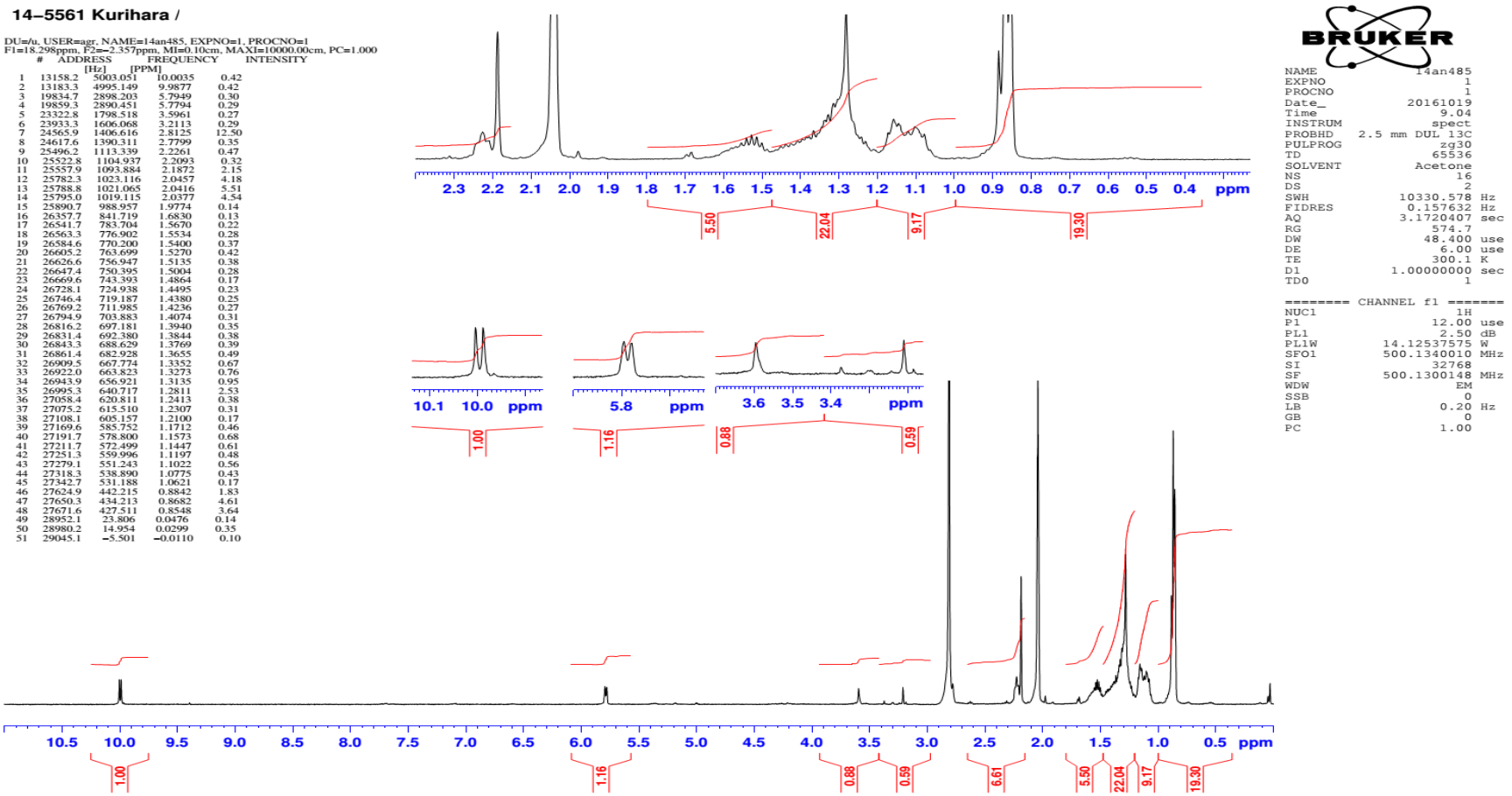


Figure 2-53. ^{1}H-NMR spectrum of compound **A1**.

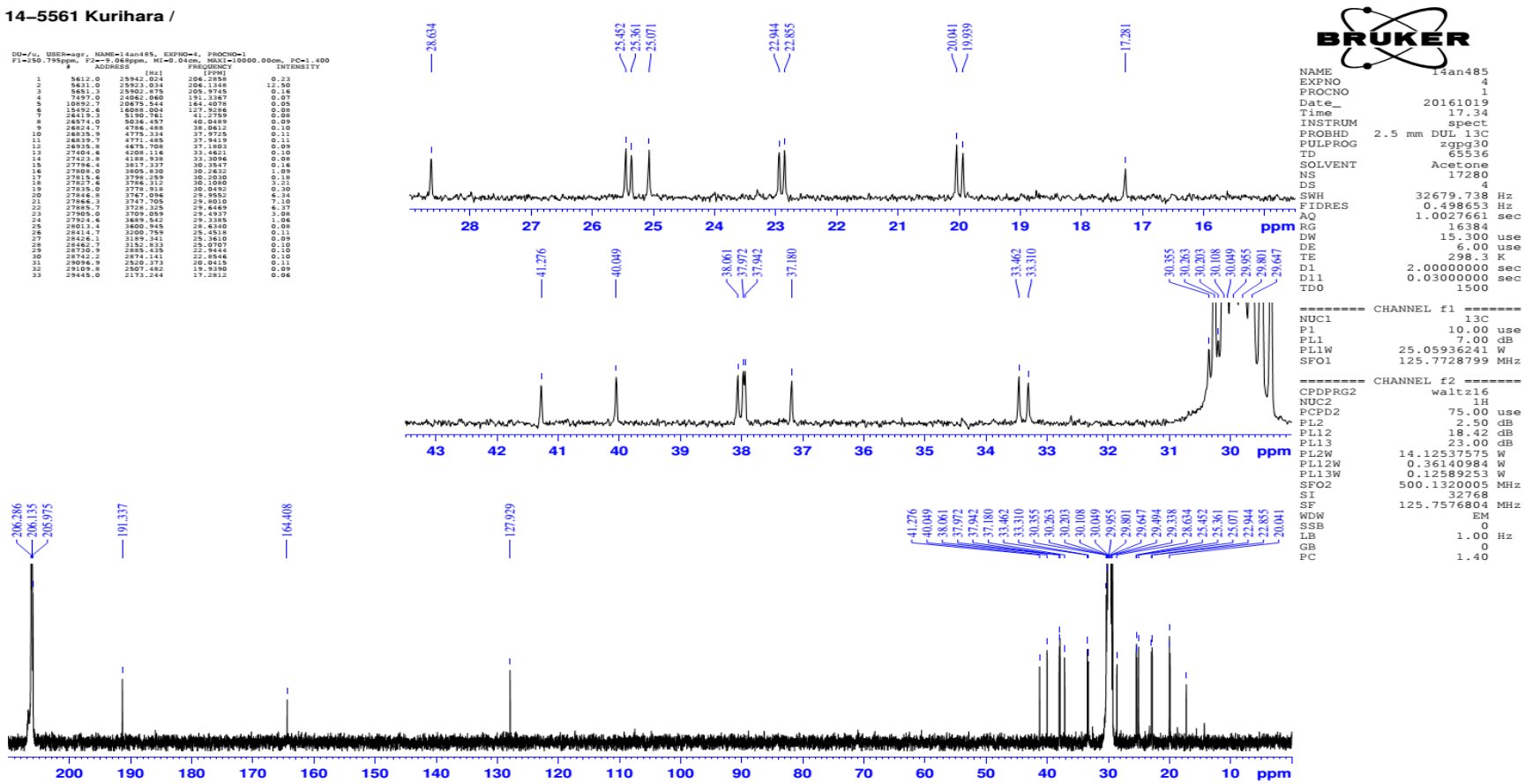


Figure 2-54. ^{13}C-NMR spectrum of compound **A1**.

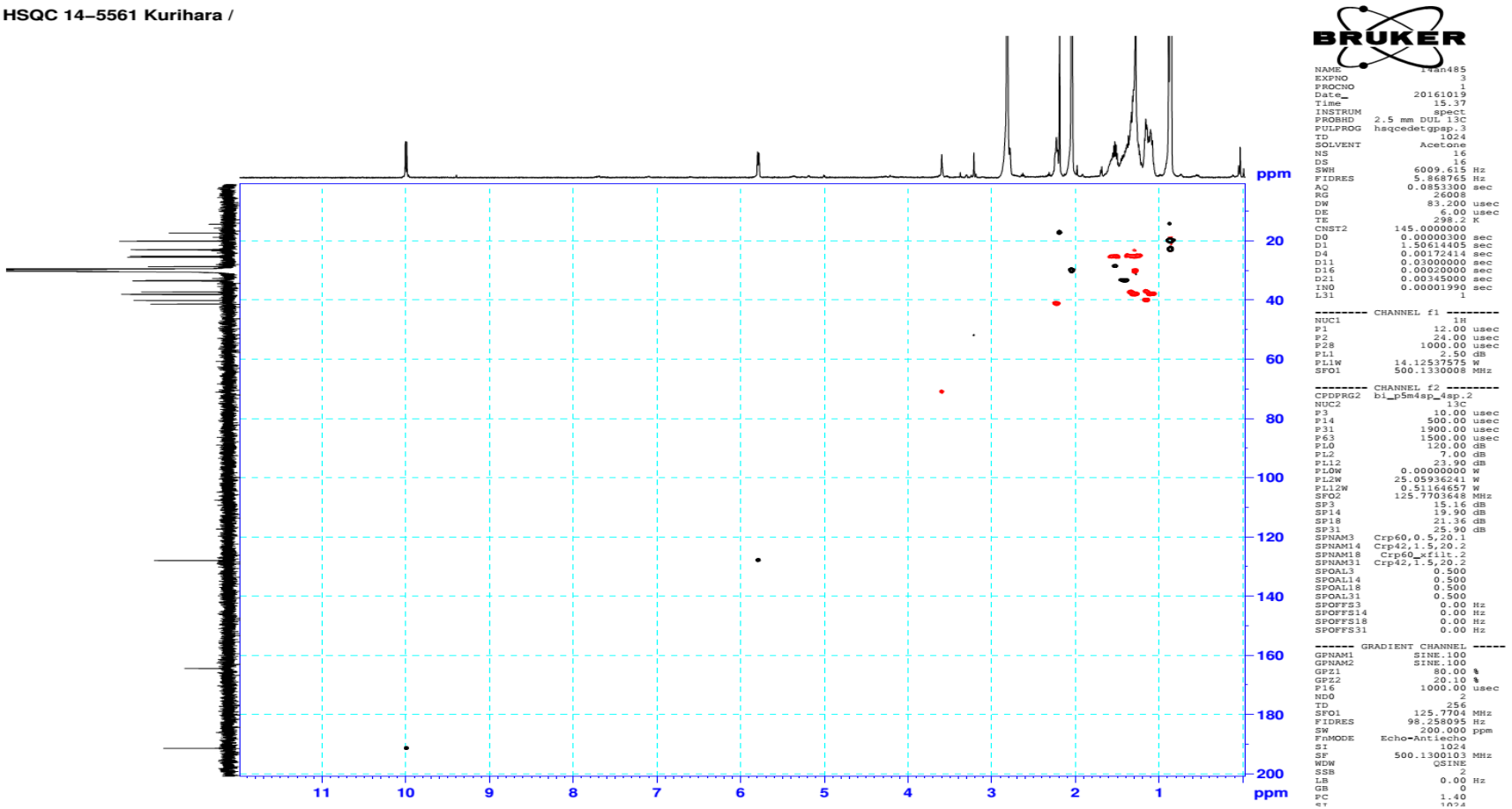


Figure 2-55. HSQC spectrum of compound **A1**.

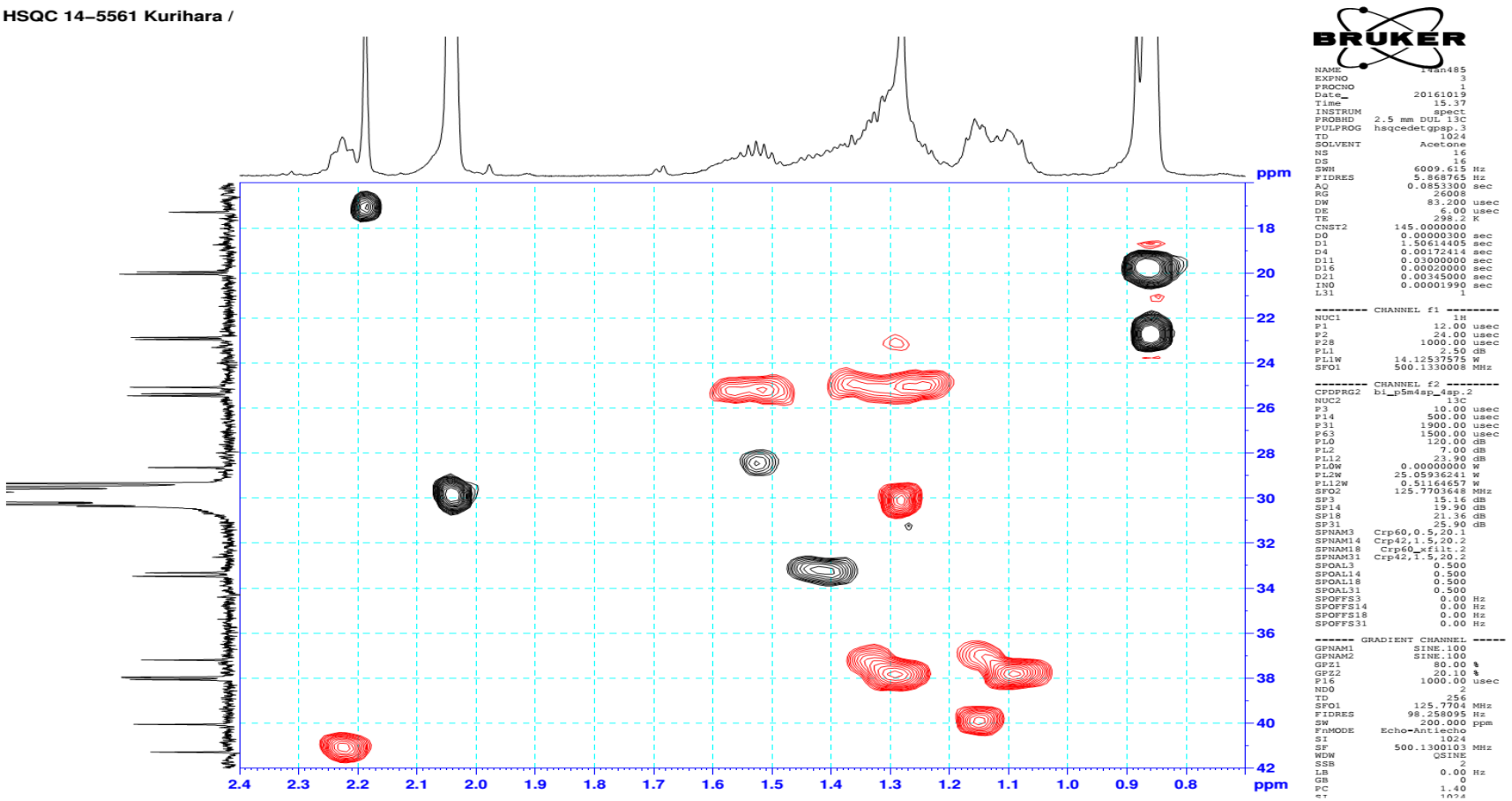


Figure 2-56. Expanded HSQC spectrum of compound **A1**.

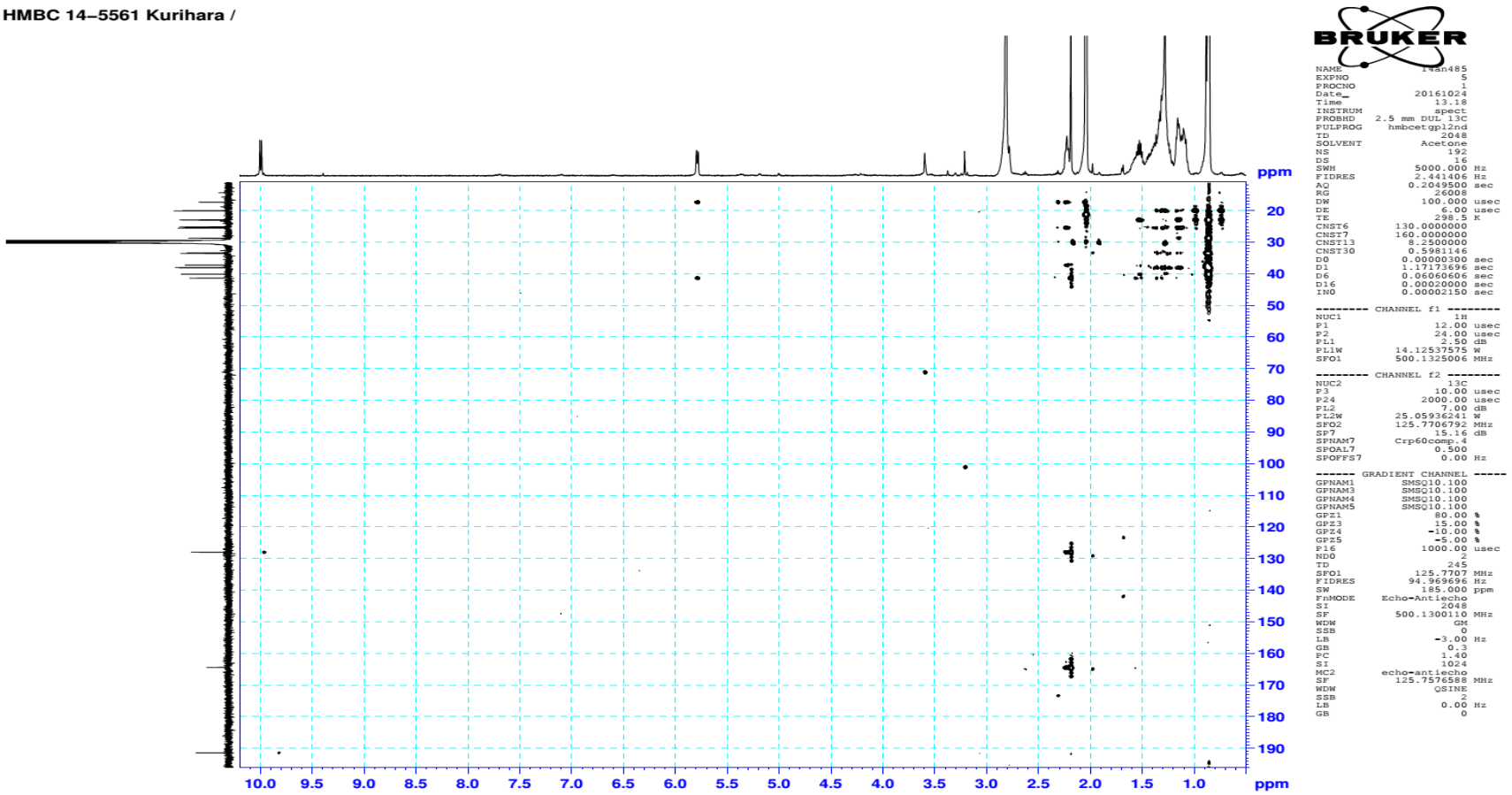


Figure 2-57. HMBC spectrum of compound **A1**.

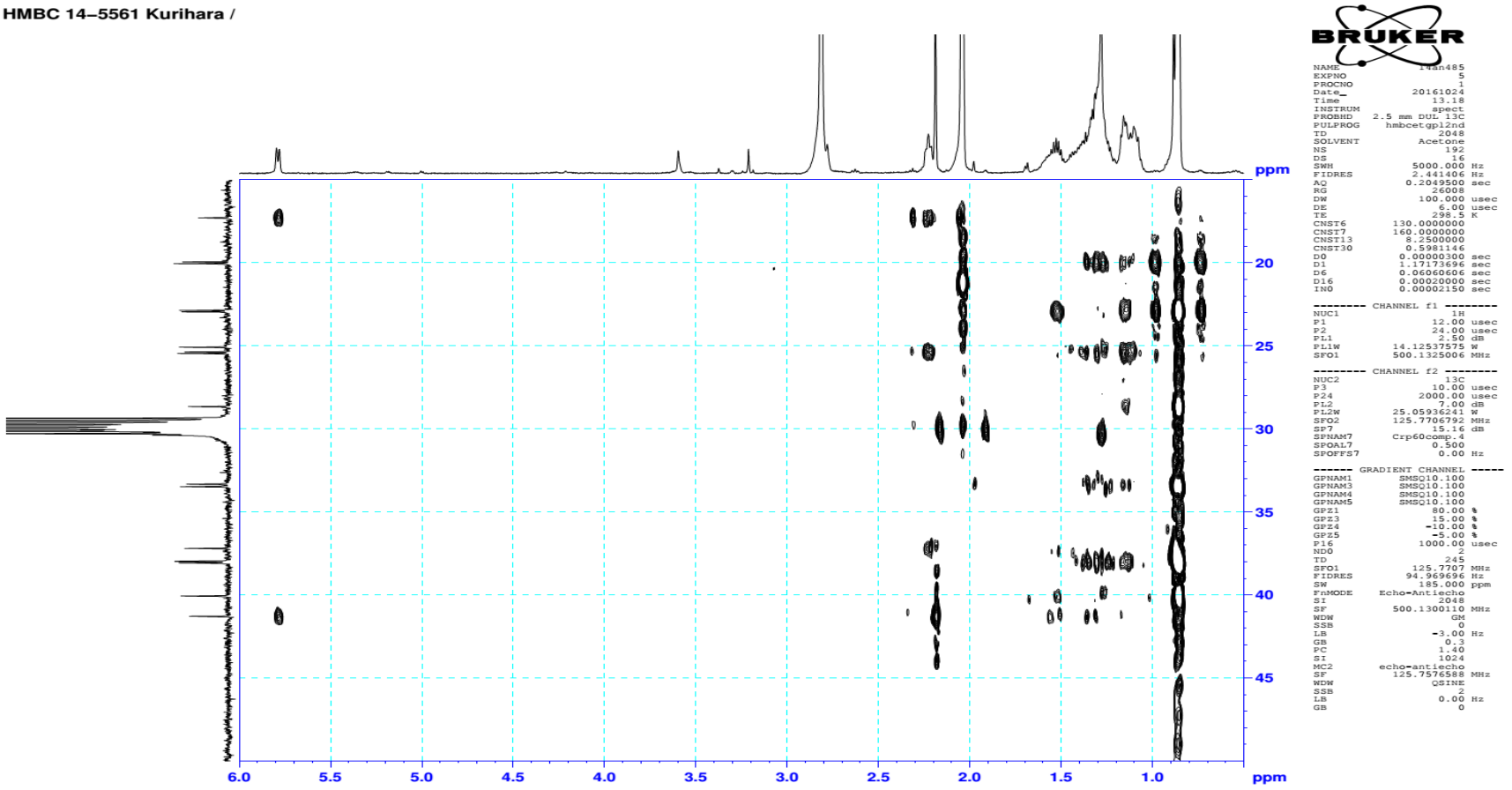


Figure 2-58. Expanded HMBC spectrum (1) of compound **A1**.

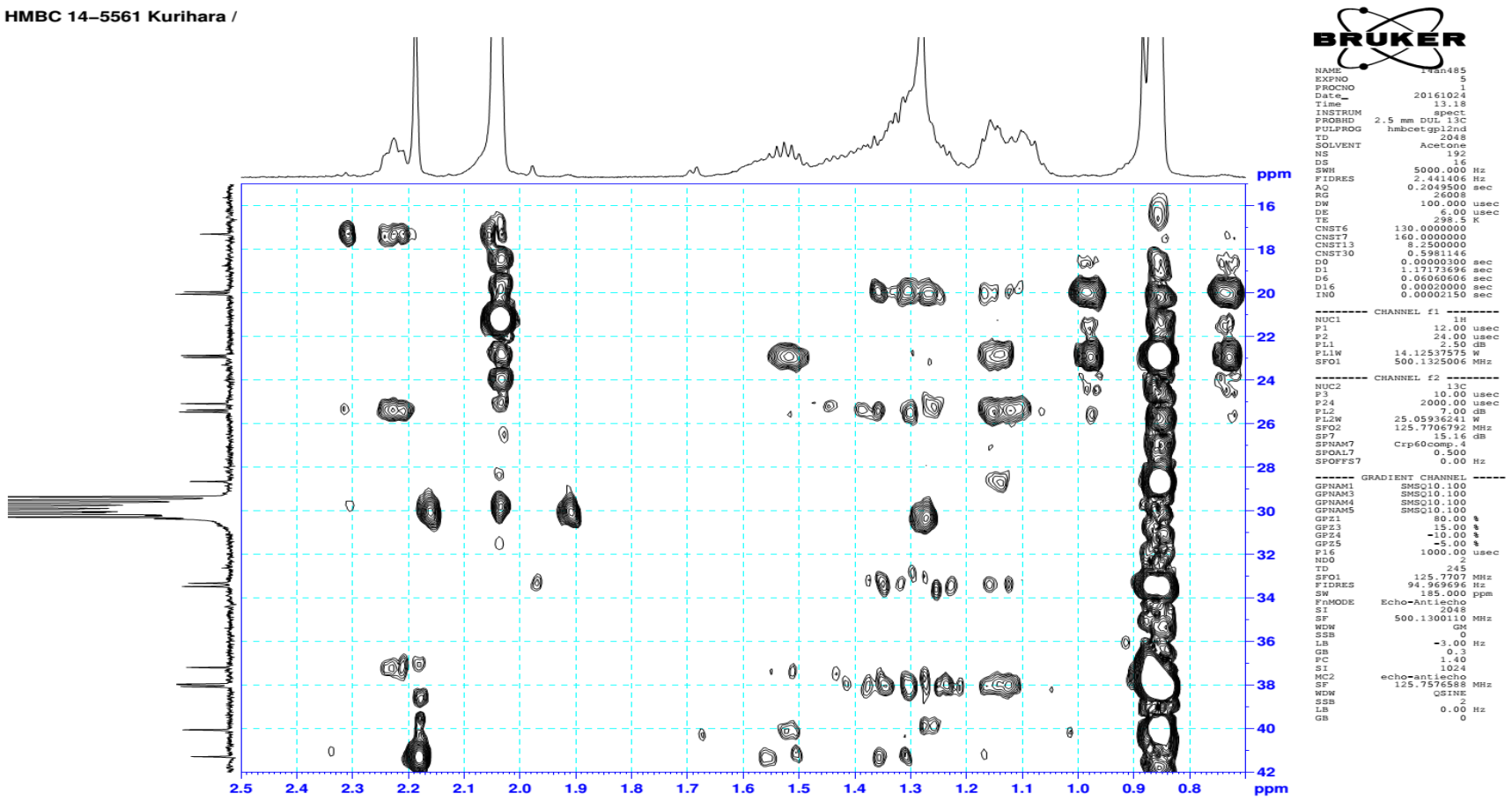


Figure 2-59. Expanded HMBC spectrum (2) of compound **A1**.

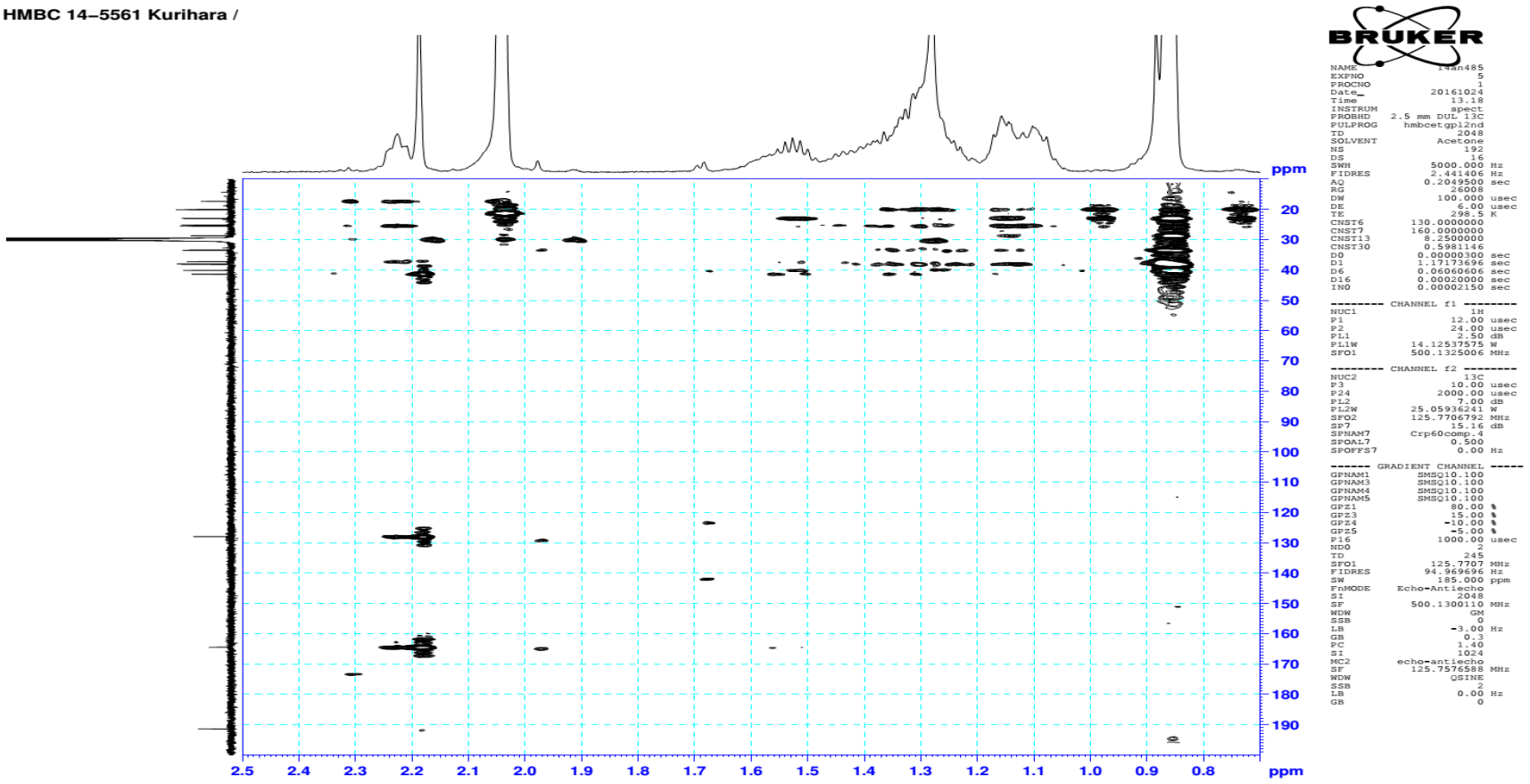


Figure 2-60. Expanded HMBC spectrum (3) of compound **A1**.

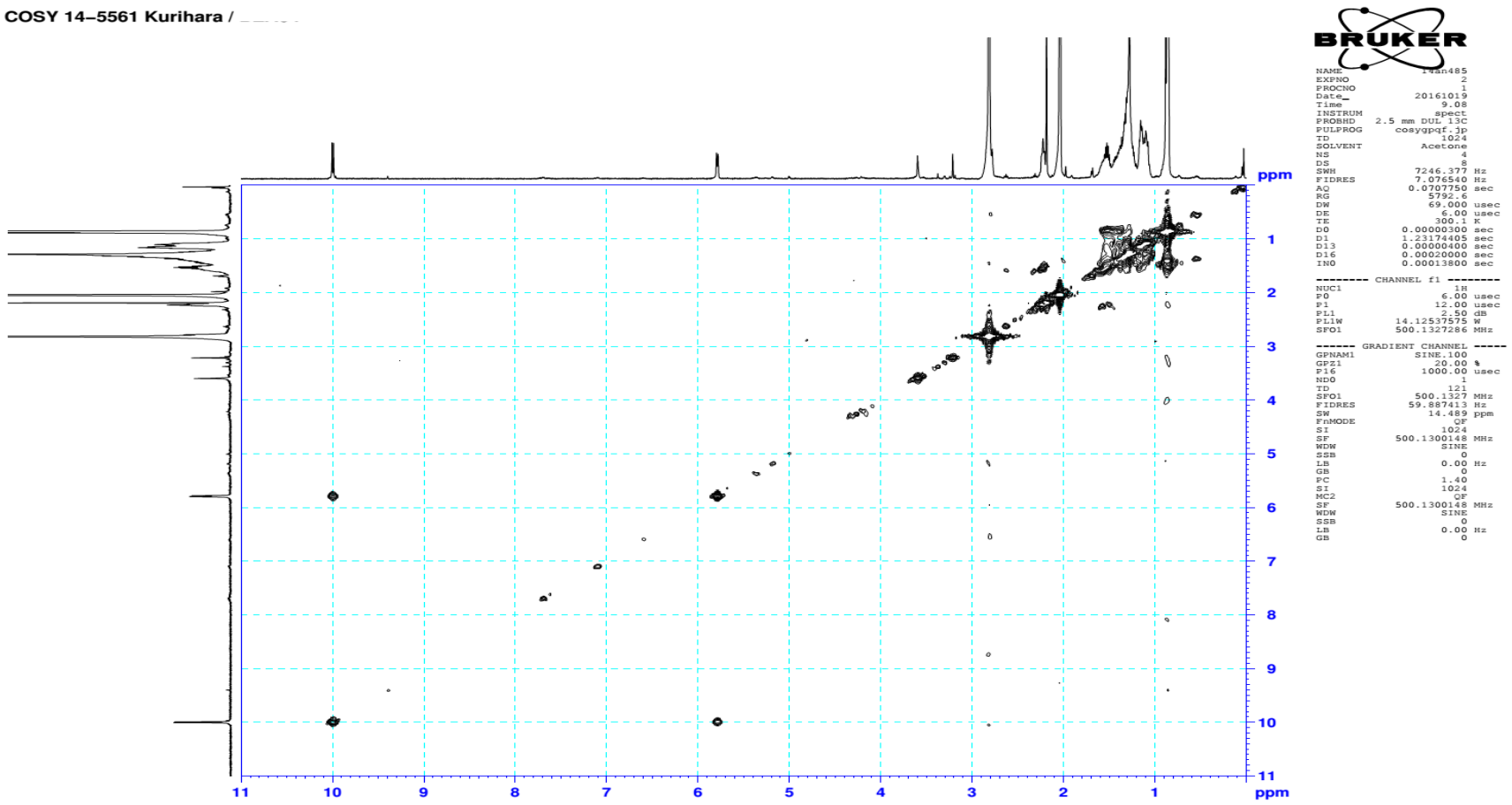


Figure 2-61. COSY spectrum of compound **A1**.

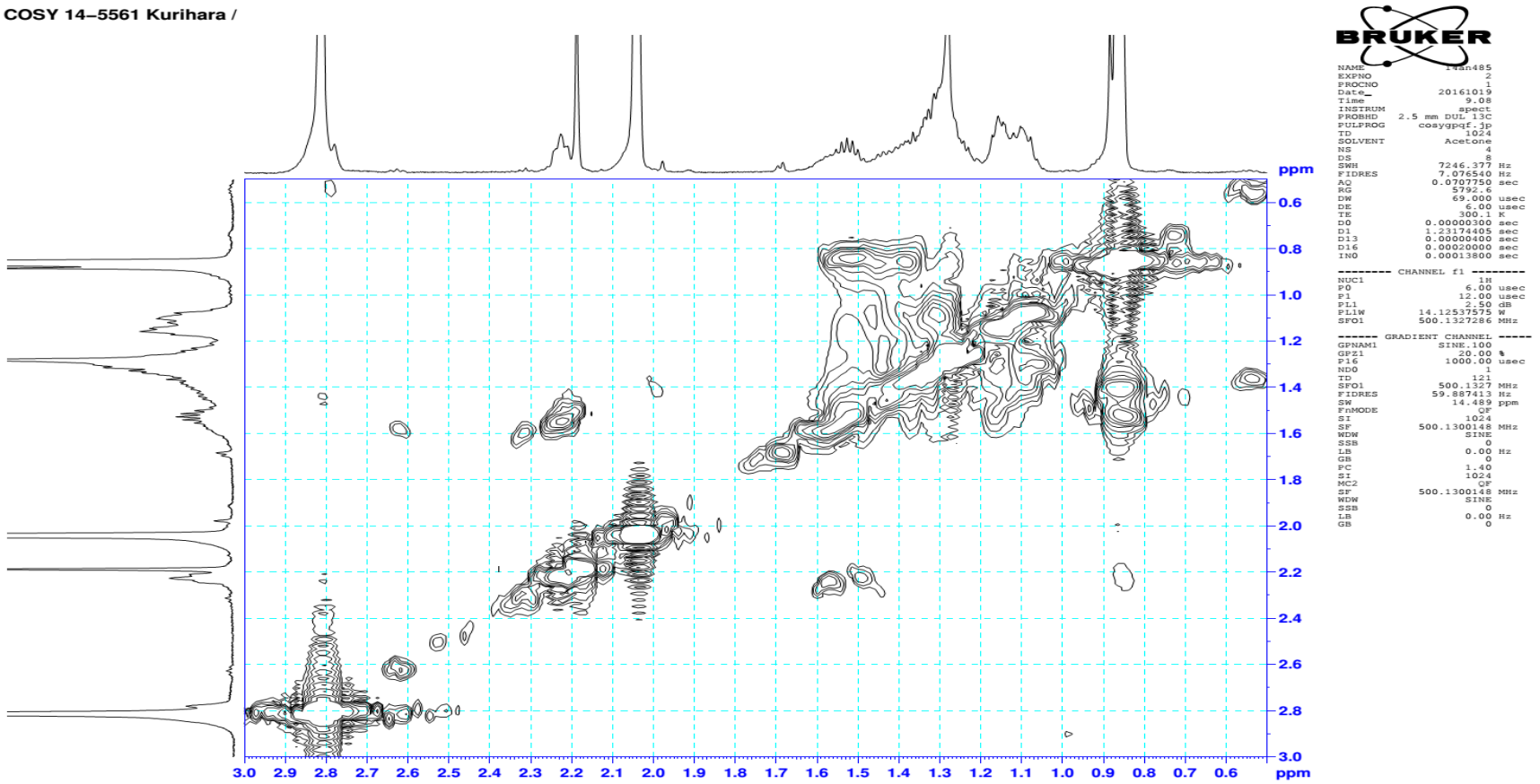


Figure 2-62. Expanded COSY spectrum of compound **A1**.

Table 2-30. Comparison of NMR data between compound **A1**[a] and literature[b]

	^{1}H NMR		^{13}C NMR	
Position	**A1**	Literature data	**A1**	Literature data
1	10.00 (d, 7.9, 1H)	9.98 (d, 12.0, 1H)	191.3	191.3
2	5.79 (d, 7.8, 1H)	5.88 (d, 12.0, 1H)	127.9	127.3
3			164.4	164.4
4	2.23 (t-like, 2H)	2.17 (m, 2H)	41.3	40.9
5	1.57 (m, 1H); 1.30 (m, 1H)	1.04-1.53 (br, 19H)	25.4, 25.1 or 25.5	24.8
6	1.16 (m, 1H);1.34 (m, 1H)	1.04-1.53 (br, 19H)	37.2	37.2
7	1.37 (m, 1H) or 1.43 (m, 1H)	1.04-1.53 (br, 19H)	33.5 or 33.3	32.7
8	1.29 (m, 1H); 1.08 (m, 1H)	1.04-1.53 (br, 19H)	37.9, 38.0 or 38.1	37.3
9	1.57 (m, 1H); 1.30 (m, 1H)	1.04-1.53 (br, 19H)	25.4, 25.1 or 25.5	24.6
10	1.29 (m, 1H); 1.08 (m, 1H)	1.04-1.53 (br, 19H)	37.9, 38.0 or 38.1	36.5
11	1.37 (m, 1H) or 1.43 (m, 1H)	1.04-1.53 (br, 19H)	33.5 or 33.3	32.6
12	1.29 (m, 1H); 1.08 (m, 1H)	1.04-1.53 (br, 19H)	37.9, 38.0 or 38.1	37.2
13	1.57 (m, 1H); 1.30 (m, 1H)	1.04-1.53 (br, 19H)	25.4, 25.1 or 25.5	24.4
14	1.16 (m, 2H)	1.04-1.53 (br, 19H)	40.1	39.3
15	1.53 (m, 1H)	1.04-1.53 (br, 19H)	28.6	27.9
16	0.87 (m, 3H)	0.86 (m, 12H)	23.0 or 22.9	22.6
17	2.19 (s, 3H)	2.15 (s, 3H)	17.3	17.5
18	0.88 (m, 3H)	0.86 (m, 12H)	20.0 or 19.9	19.7
19	0.88 (m, 3H)	0.86 (m, 12H)	20.0 or 19.0	19.6
20	0.87 (m, 3H)	0.86 (m, 12H)	23.0 or 22.9	22.6

[a]The NMR data were measured in acetone-d_6 (δ_H 2.04 ppm; δ_C CO 206.3, CH_3 30.4 ppm) at 500 MHz for ^{1}H and at 125 MHz for ^{13}C.

[b]Fürstenau et al., 2013.

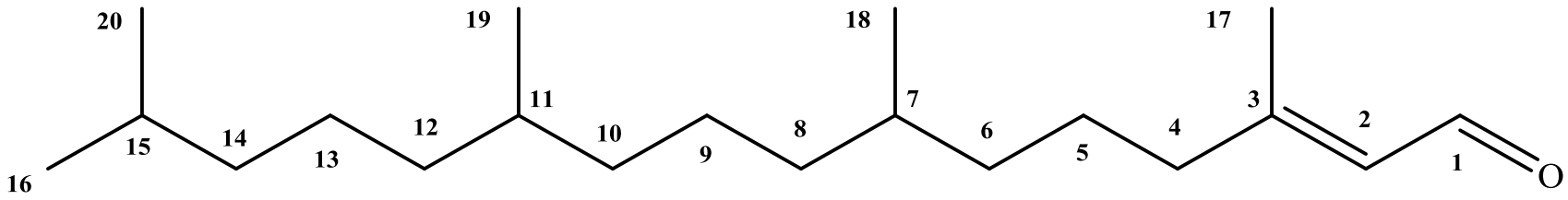


Figure 2-63. Structure of compound **A1**.

2.3.2.2 Structural elucidation of β-glucuronidase inhibitory compounds A2 & A3

After separation by HPLC, fraction E3P5-1 was obtained as colorless oil. FI-MS total ion chromatogram disclosed two ion peaks (Figure 2-64). The mass spectrum of the former peak, named as compound **A2**, included a molecular ion peak at *m/z* 296 (Figure 2-65). Molecular formula of **A2** was given by FI-HR-MS spectrum as 296.70813 for $C_{20}H_{40}O$ (calculated 296.30891). FI-MS of the latter peak, named compound **A3**, showed a molecular ion peak at *m/z* 396 (Figure 2-66). Molecular formula of **A3** was determined by FI-HR-MS for $C_{27}H_{40}O_2$ at *m/z* 396.30177 (calculated 396.30283). Structures of compounds **A2** and **A3** were determined by ^{1}H and ^{13}C NMR spectra (Figures 2-67 and 68), HSQC (Figures 2-69 to 74), HMBC (Figures 2-75 to 85), COSY (Figures 2-86 to 88) and NOESY (Figures 2-89 to 91). ^{1}H and ^{13}C NMR signals were divided into two groups related to compounds **A2** and **A3** in 2D NMR spectra. ^{1}H NMR spectrum showed a group of signals for **A2**: one olefinic proton at δ_H 5.34 (H-2), oxygenated methylene protons at δ_H 4.05 (H-1), thirty-three methine and methylene protons at δ_H 1.08 to 2.55, four methyl protons at δ_H 0.86 (H-16 to 19). The spectrum also showed the other group: three olefinic protons at δ_H 5.95 (H-4), 5.34 (H-23) and 5.25 (H-22), six methyl groups at 0.71 to 1.00 and aliphatic protons for **A3**. ^{13}C NMR spectrum displayed twenty carbons for **A2** and twenty-seven carbons including two ketonic carbons for **A3**. With the assistance of 2D NMR spectra, these signals suggested that compounds **A2** and **A3** should be (*E*)-3,7,11,15-tetramethylhexadec-2-en-1-ol, known as phytol (Tables 2-31, Figure 2-92), and cholesta-4,22-diene-3,6-dione (Table 2-32, Figure 2-93), respectively. Identifications were also supported by literature data (Song et al., 2003) (Kontiza, Abatis, Malakate, Vagias, & Roussis, 2006) (Iorizzi, Minale, Riccio, Debray, & Menou, 1986) (Mansoor et al., 2006).

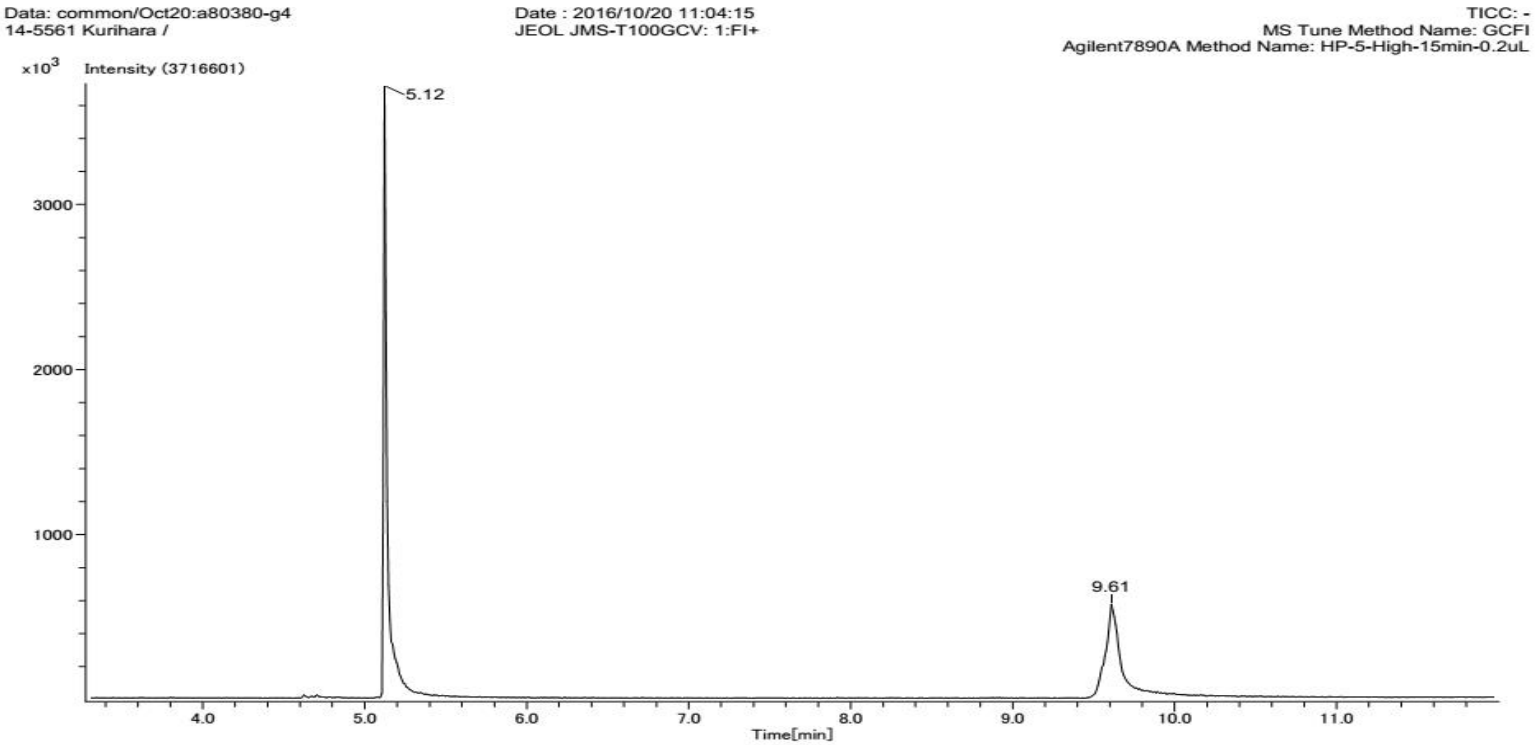


Figure 2-64. FI-MS total ion chromatogram of E3P5-1.

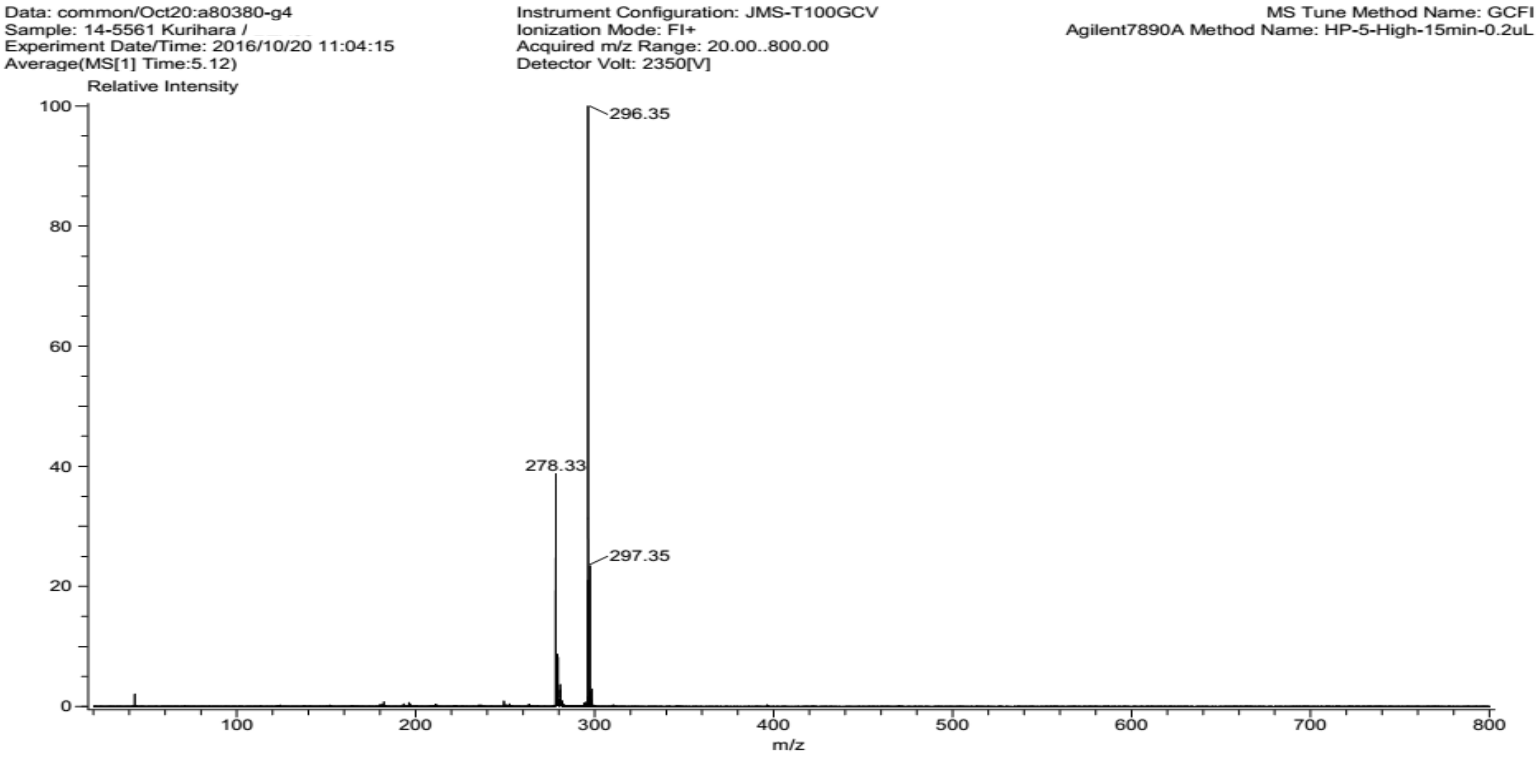


Figure 2-65. FI-MS spectrum of compound **A2**.

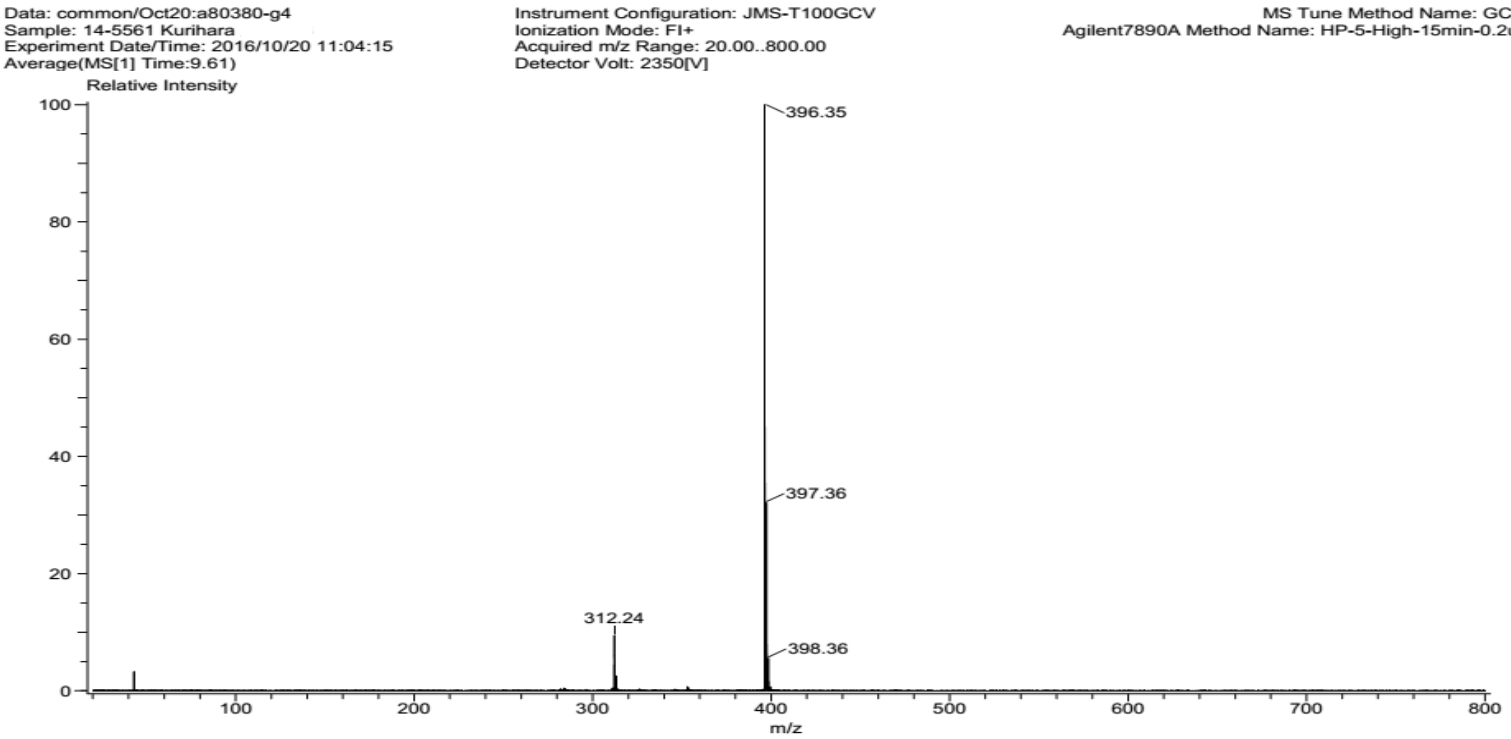


Figure 2-66. FI-MS spectrum of compound **A3**.

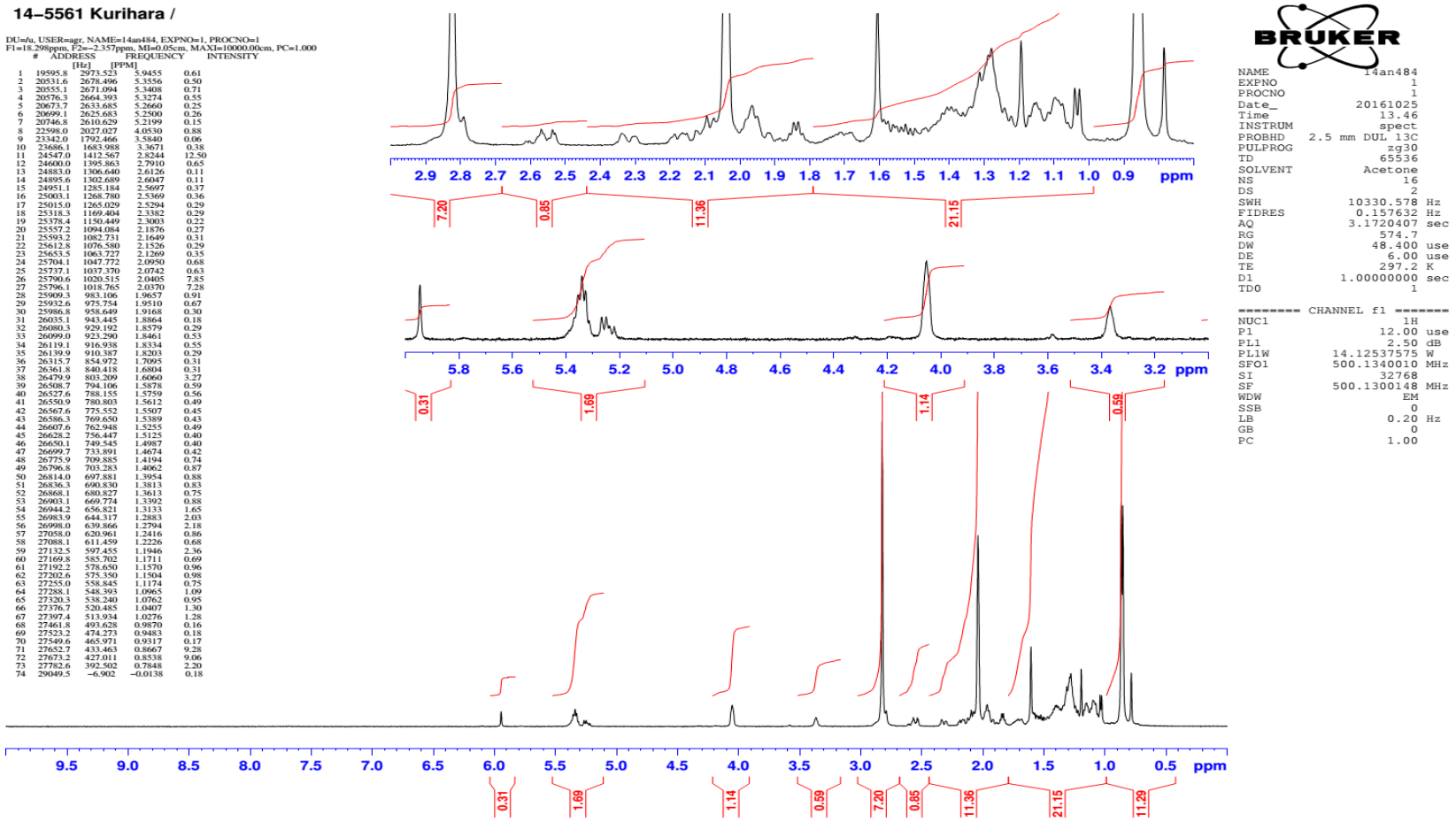


Figure 2-67. ^{1}H-NMR spectrum of compounds **A2** and **A3**.

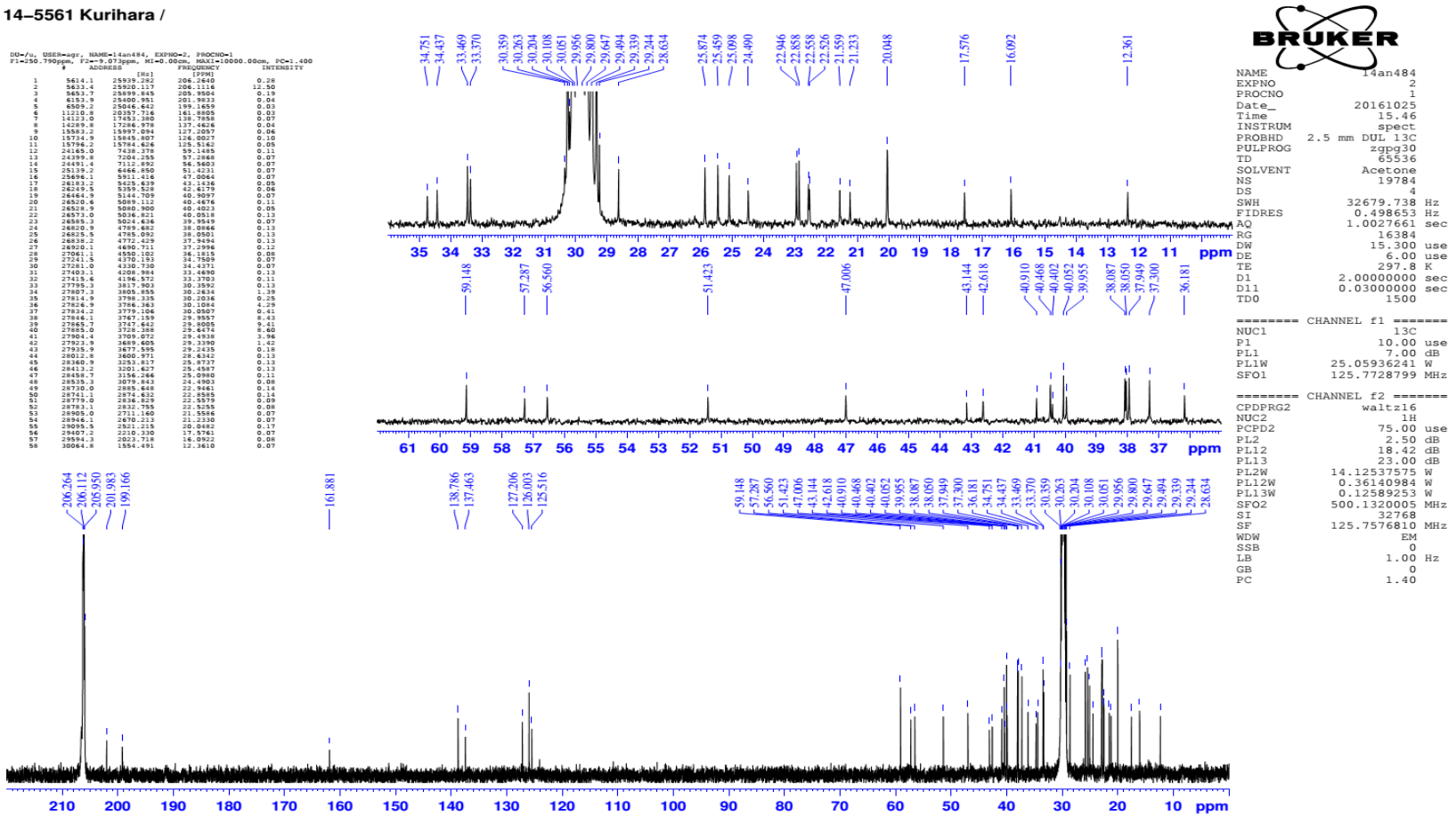


Figure 2-68. ^{13}C-NMR spectrum of compounds **A2** and **A3**.

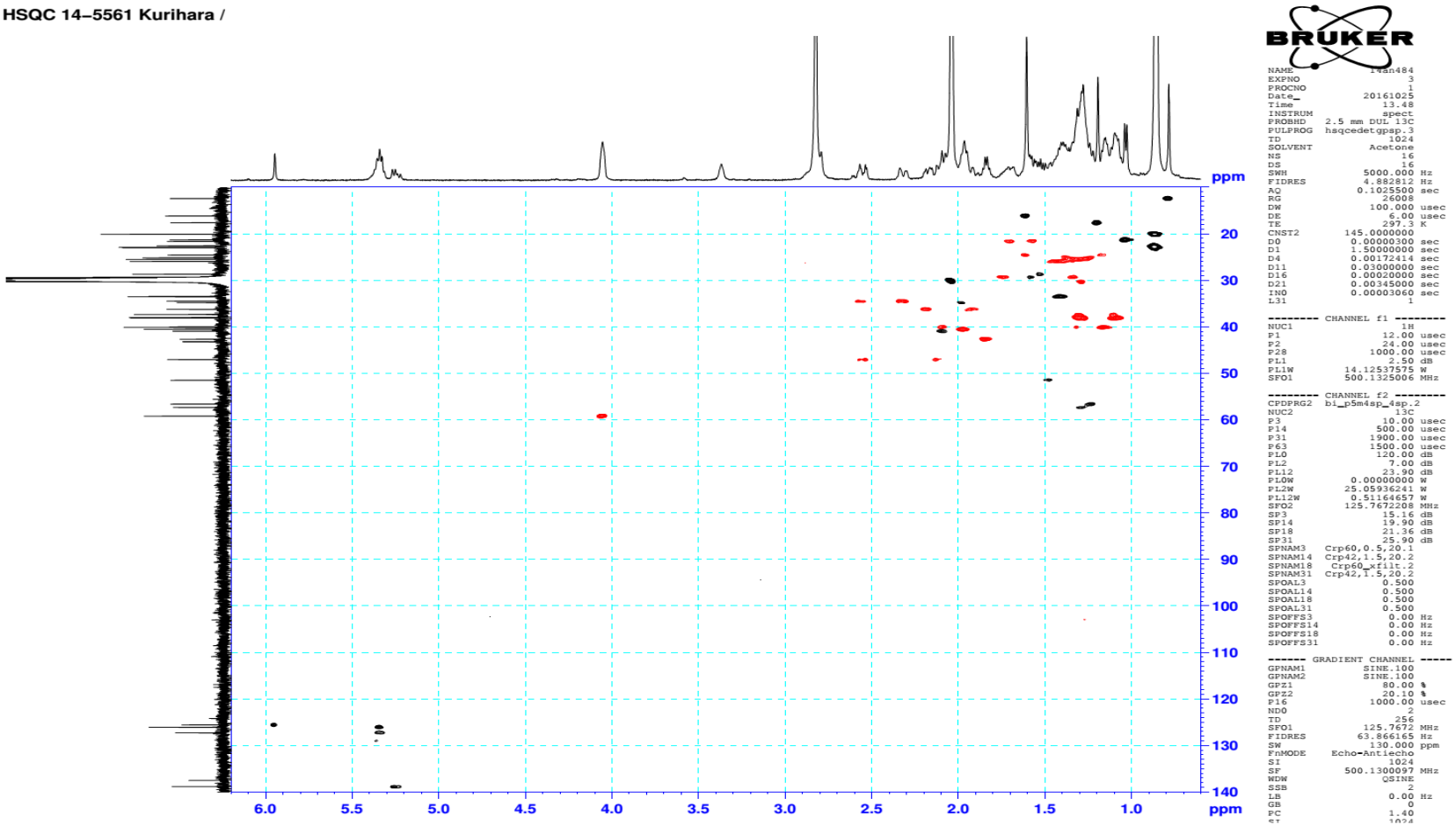


Figure 2-69. HSQC spectrum of compounds **A2** and **A3**.

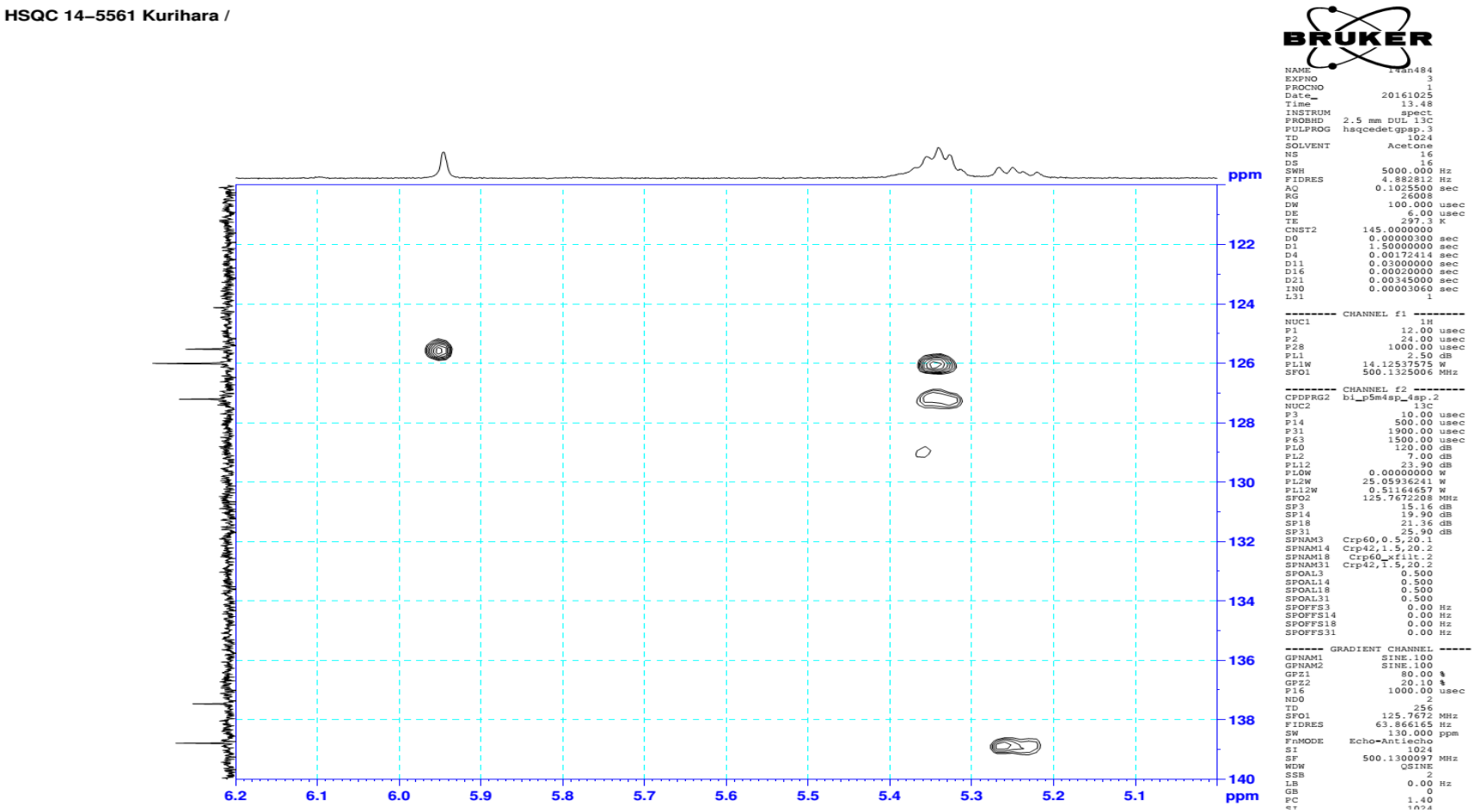


Figure 2-70. Expanded HSQC spectrum (1) of compounds **A2** and **A3**.

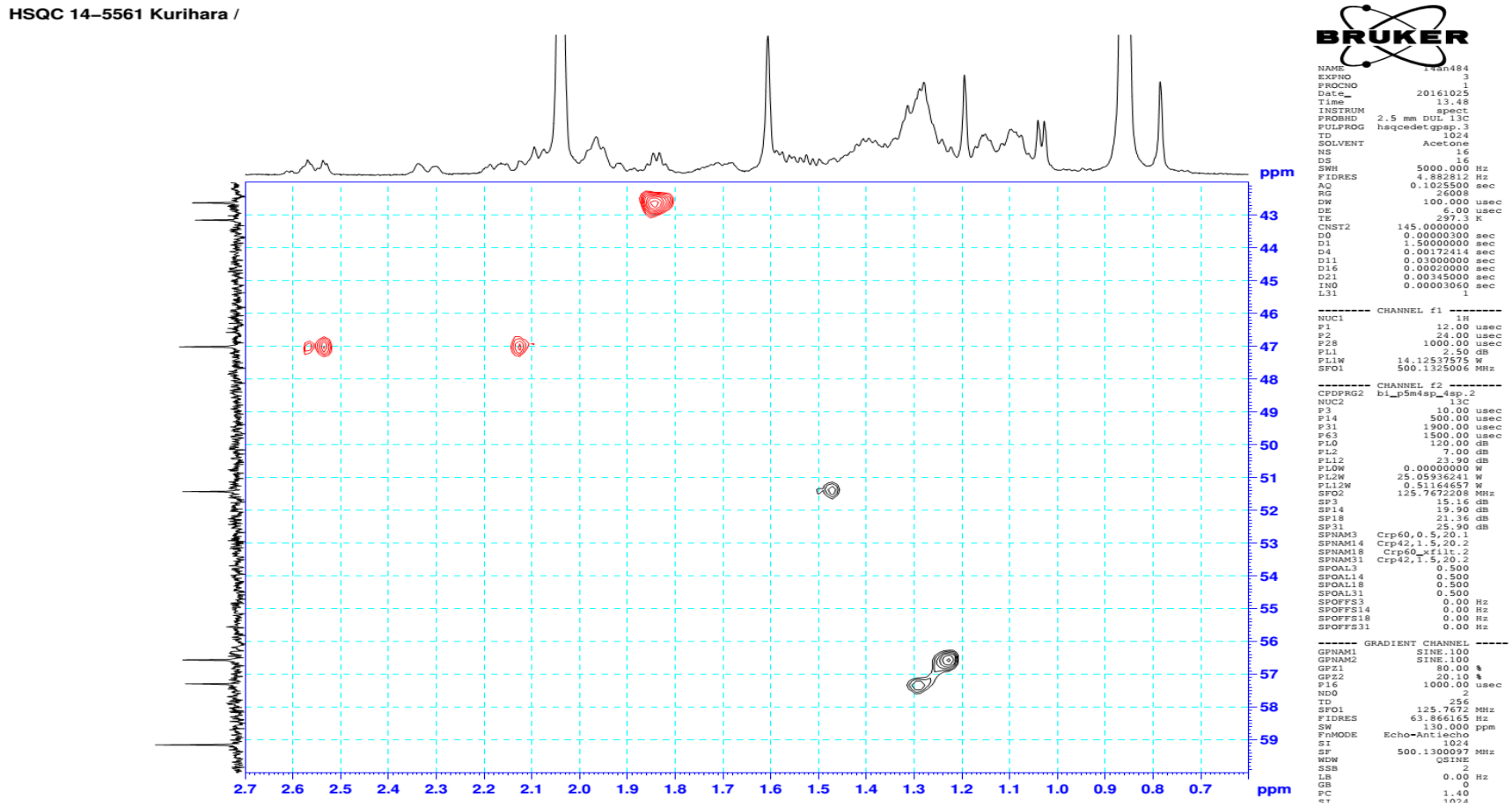


Figure 2-71. Expanded HSQC spectrum (2) of compounds **A2** and **A3**.

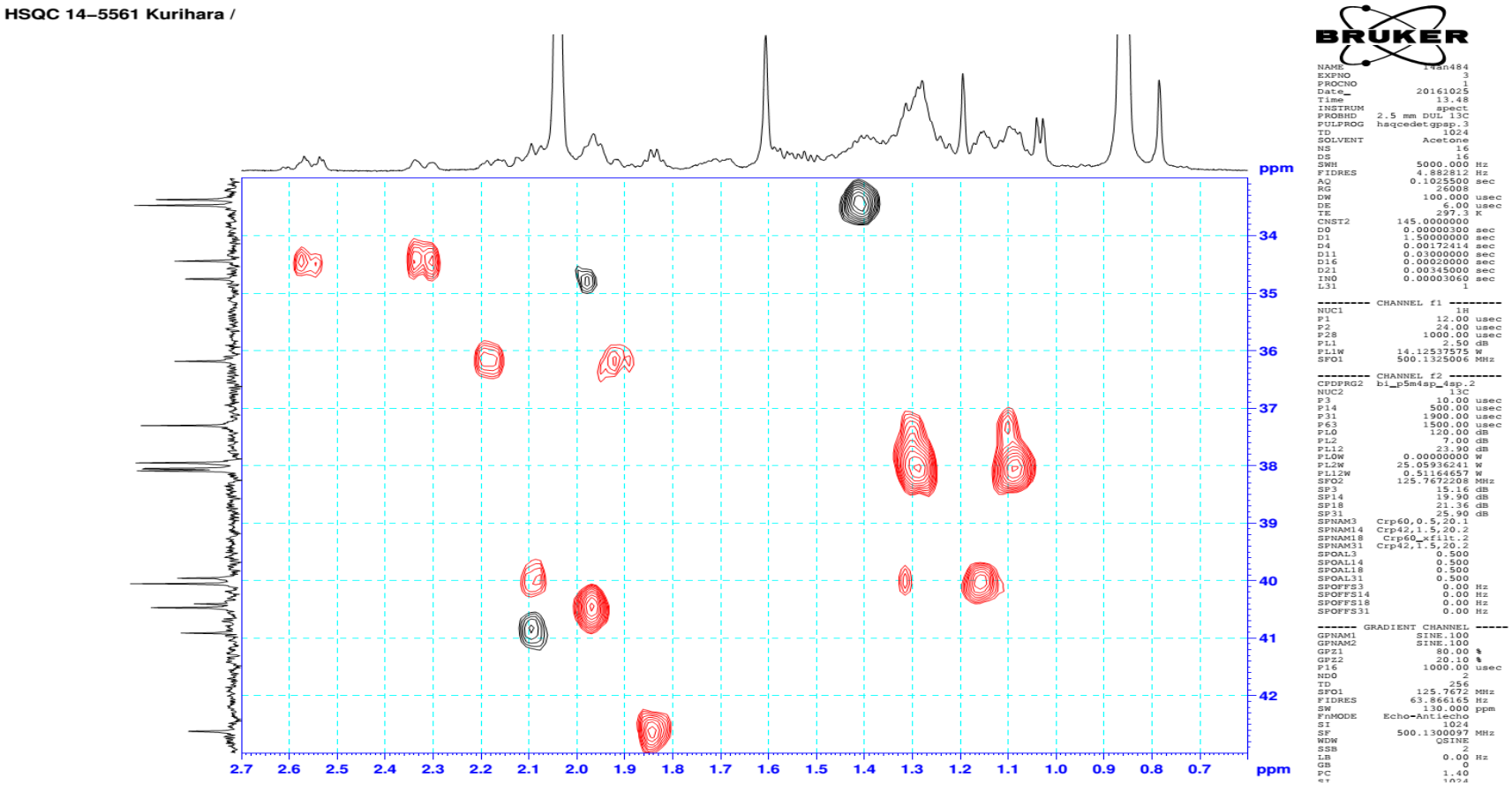


Figure 2-72. Expanded HSQC spectrum (3) of compounds **A2** and **A3**.

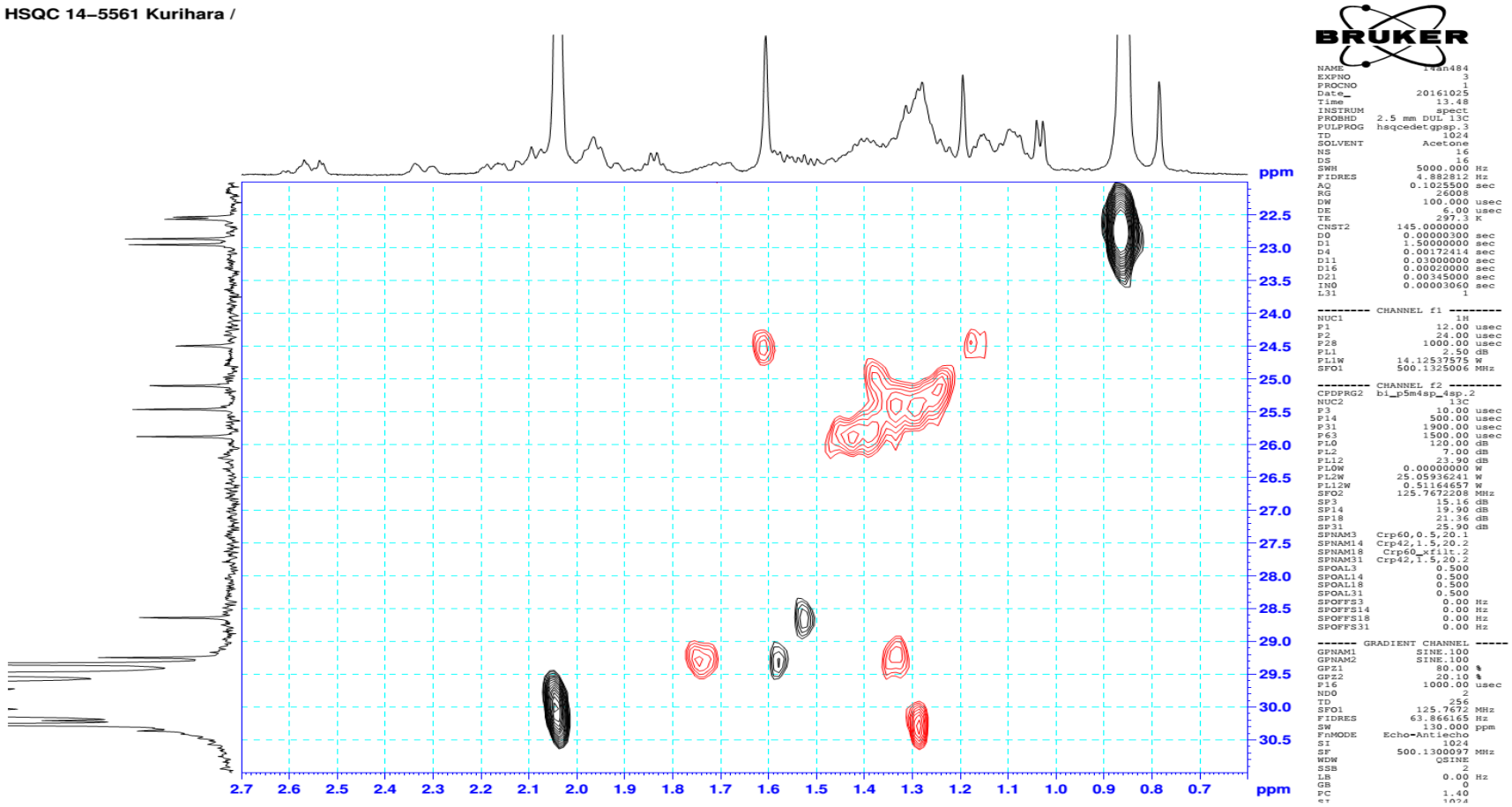


Figure 2-73. Expanded HSQC spectrum (4) of compounds **A2** and **A3**.

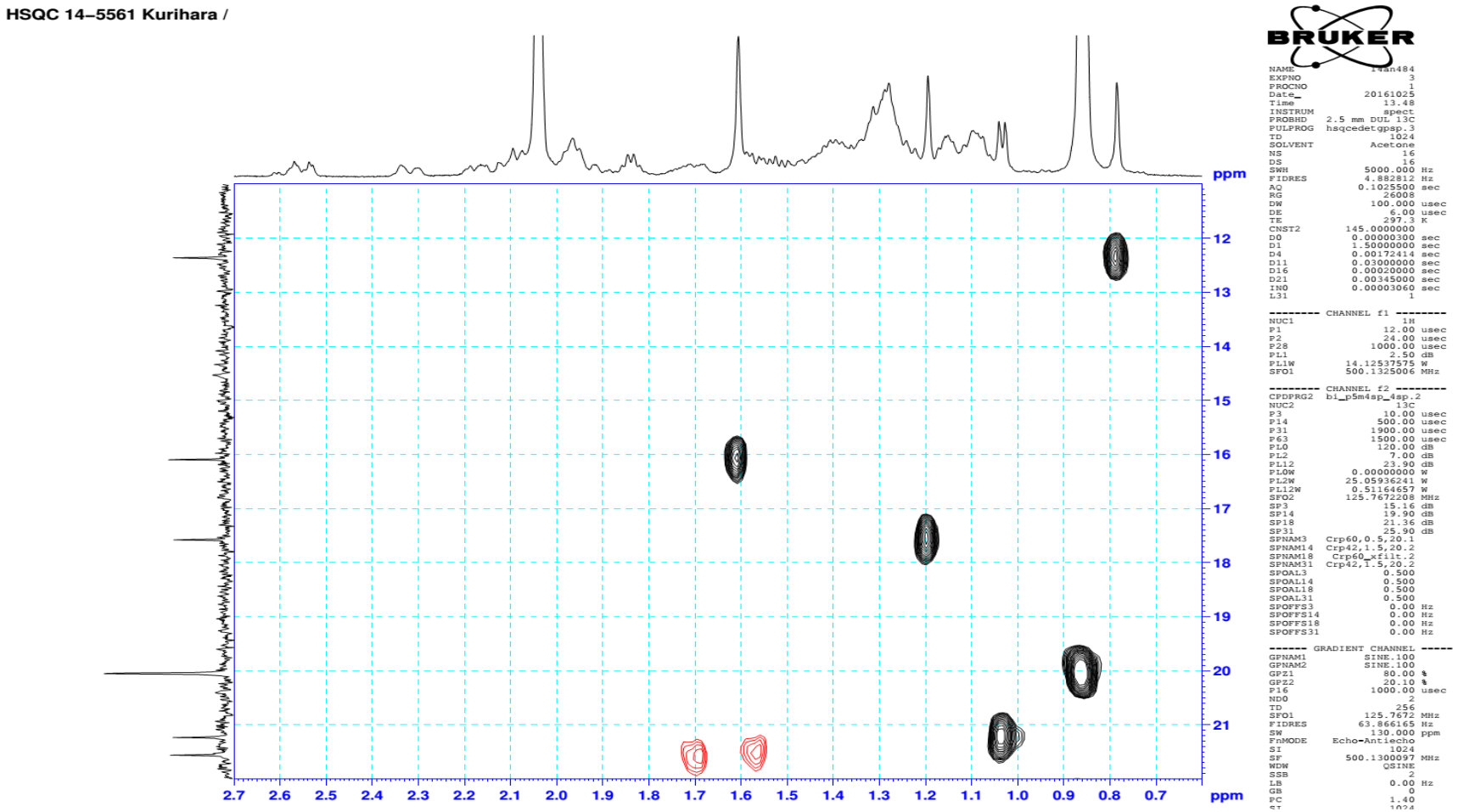


Figure 2-74. Expanded HSQC spectrum (5) of compounds **A2** and **A3**.

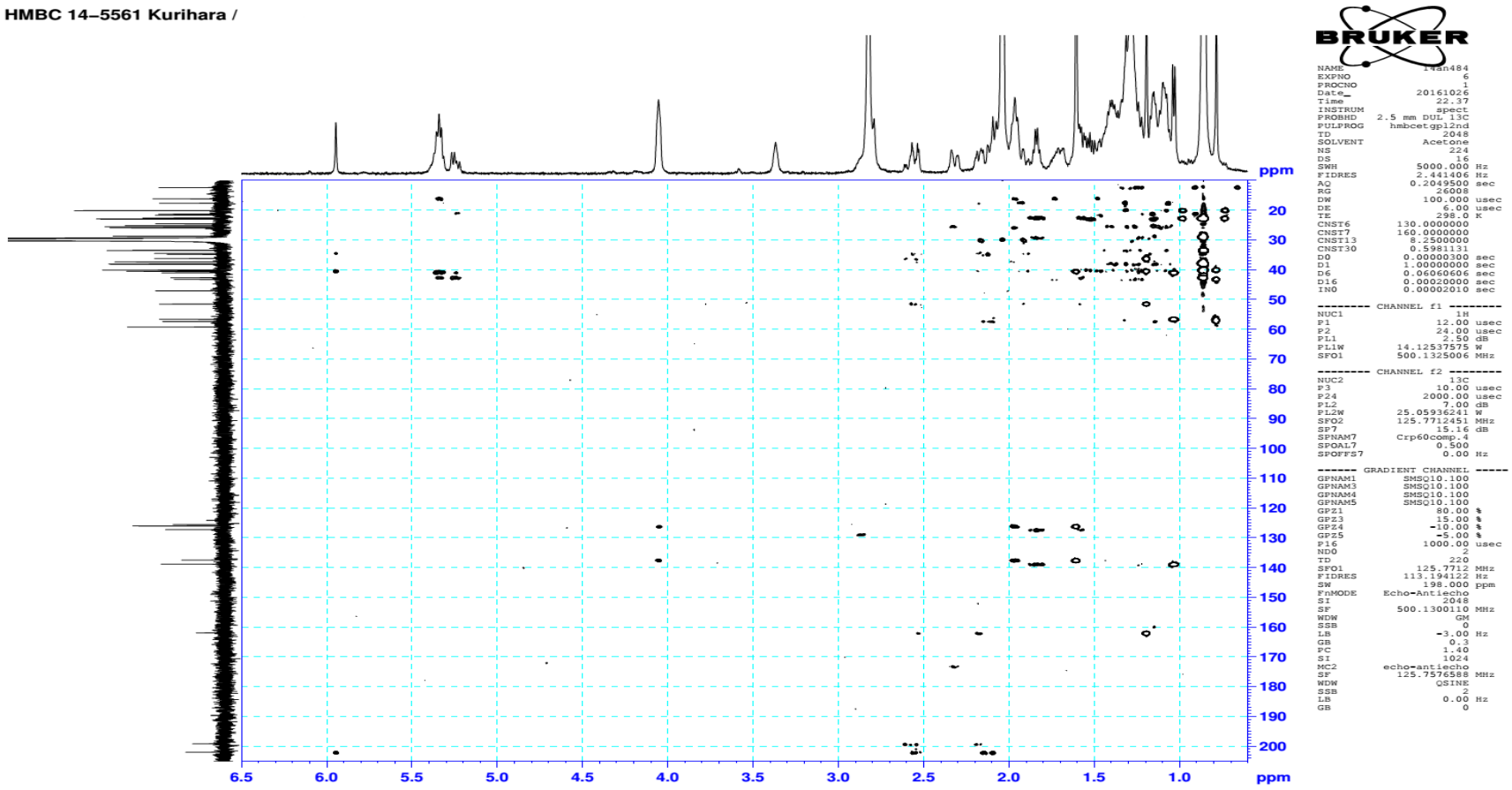


Figure 2-75. HMBC spectrum of compounds **A2** and **A3**.

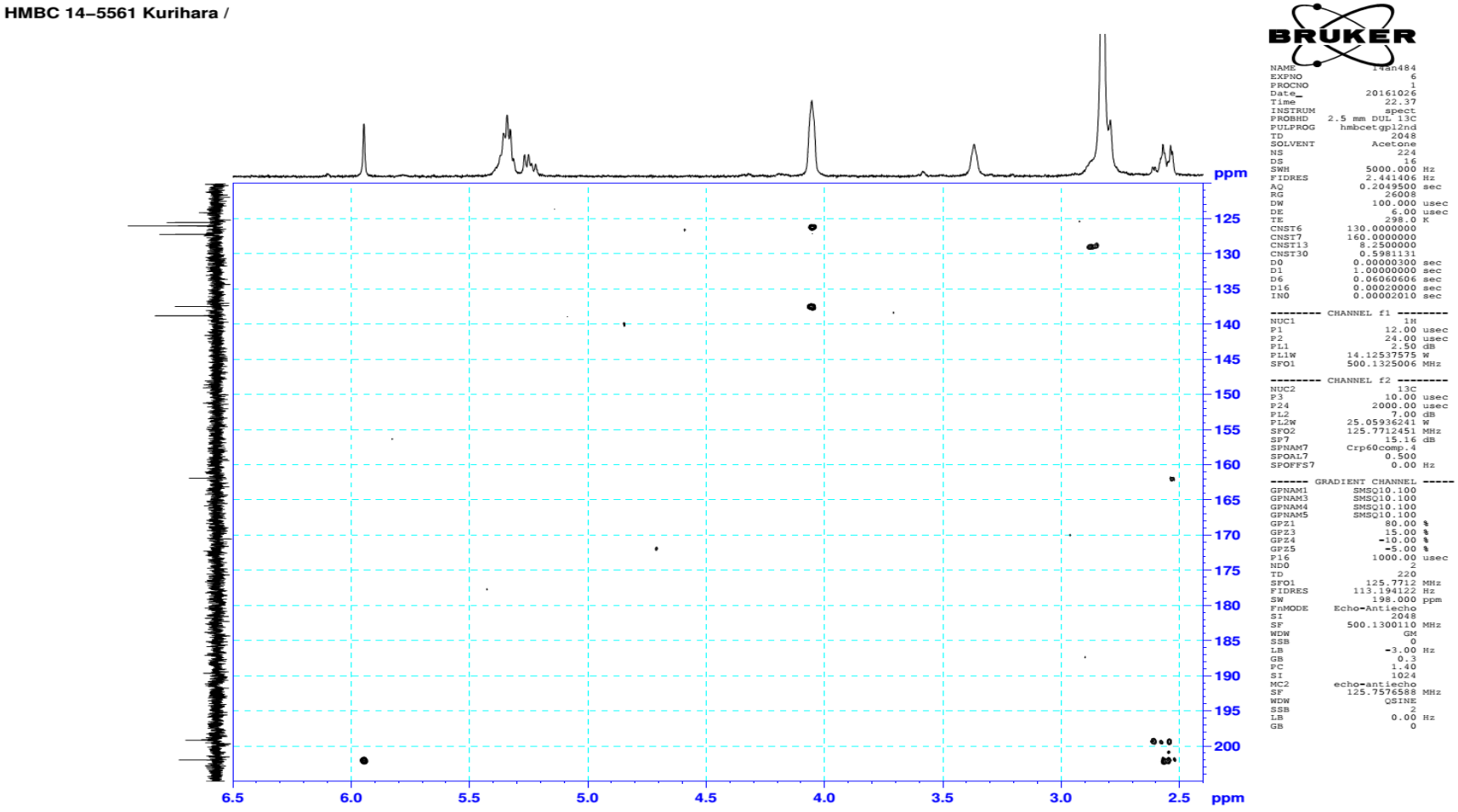


Figure 2-76. Expanded HMBC spectrum (1) of compounds **A2** and **A3**.

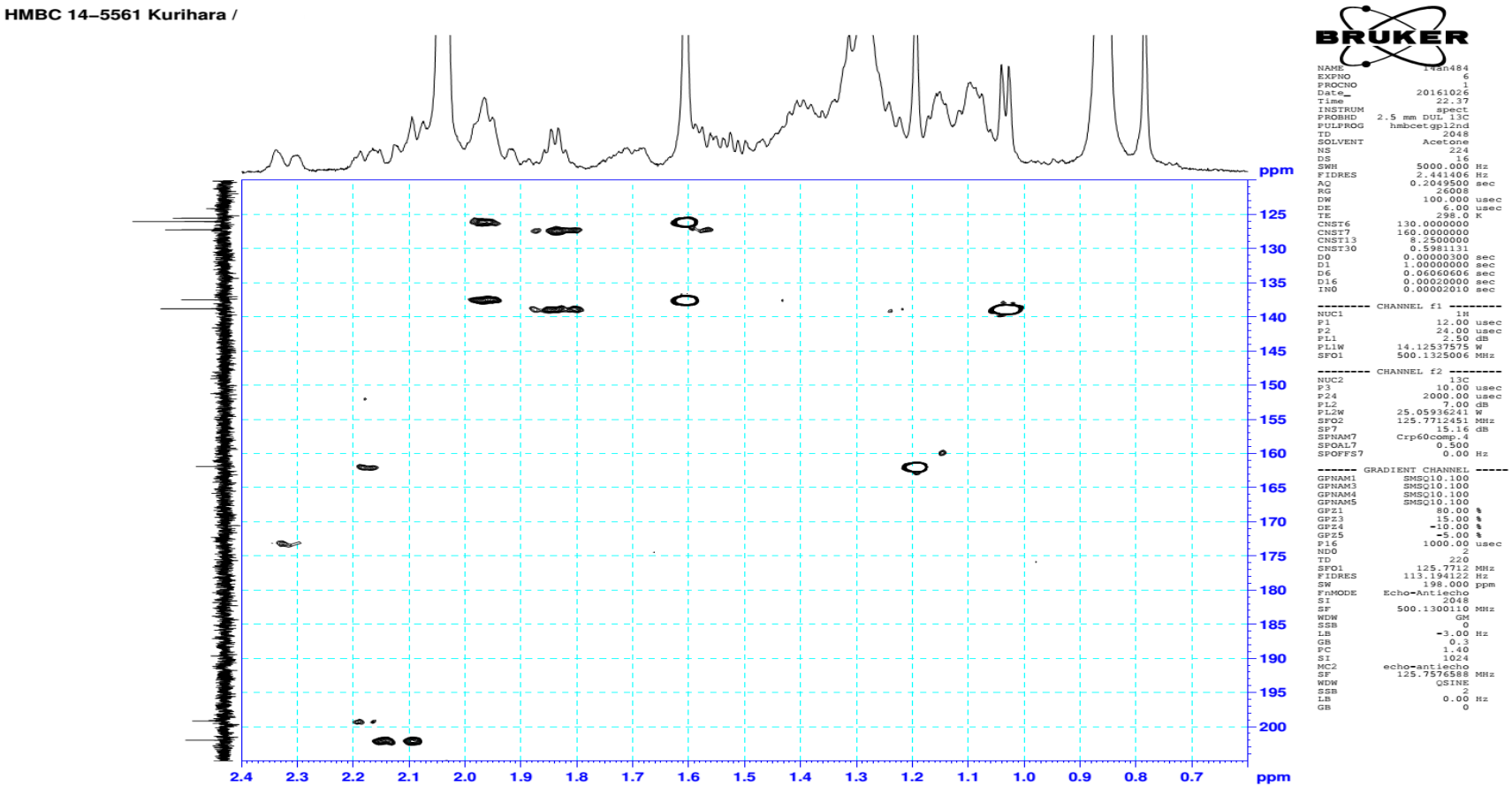


Figure 2-77. Expanded HMBC spectrum (2) of compounds **A2** and **A3**.

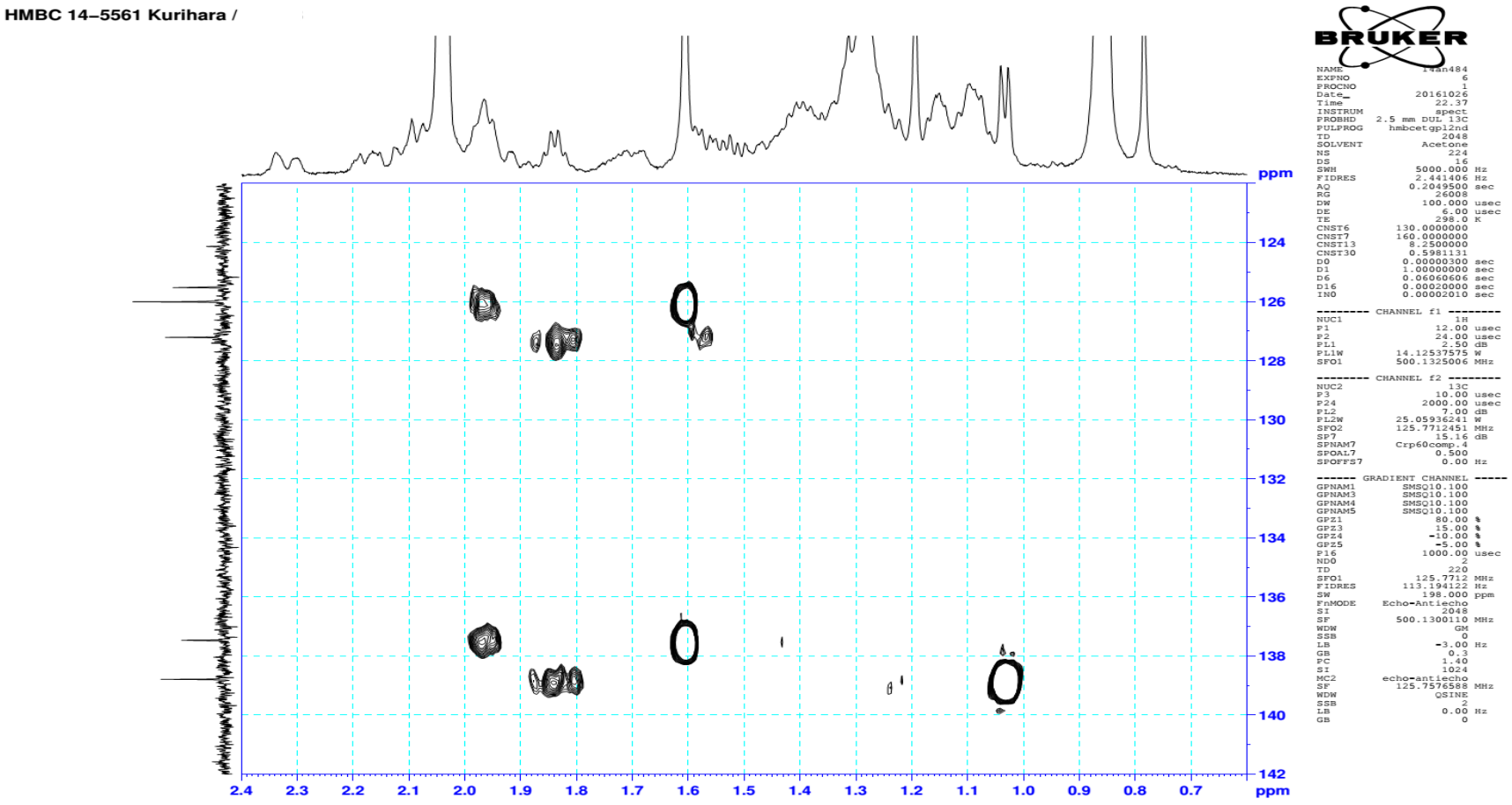


Figure 2-78. Expanded HMBC spectrum (3) of compounds **A2** and **A3**.

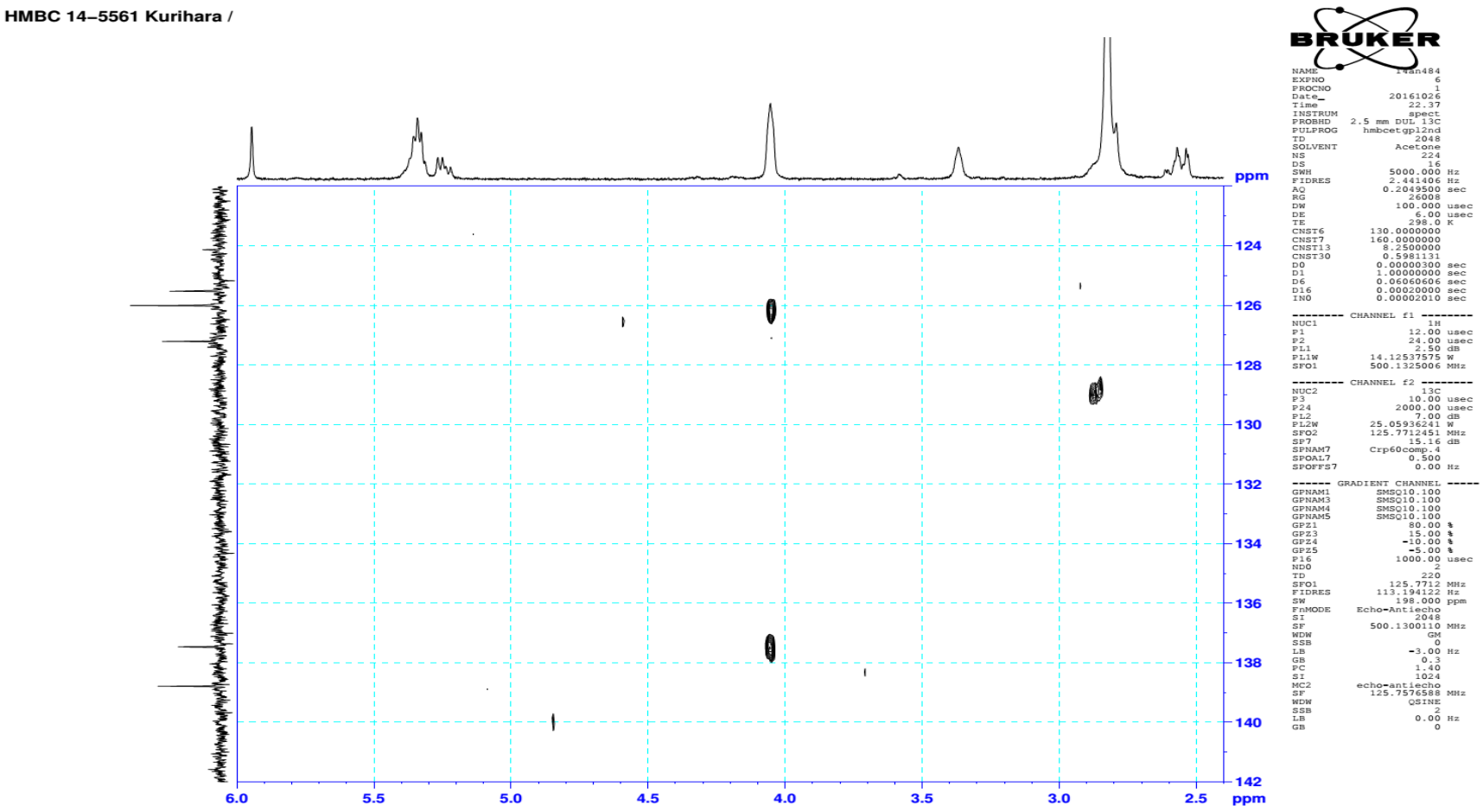


Figure 2-79. Expanded HMBC spectrum (4) of compounds **A2** and **A3**.

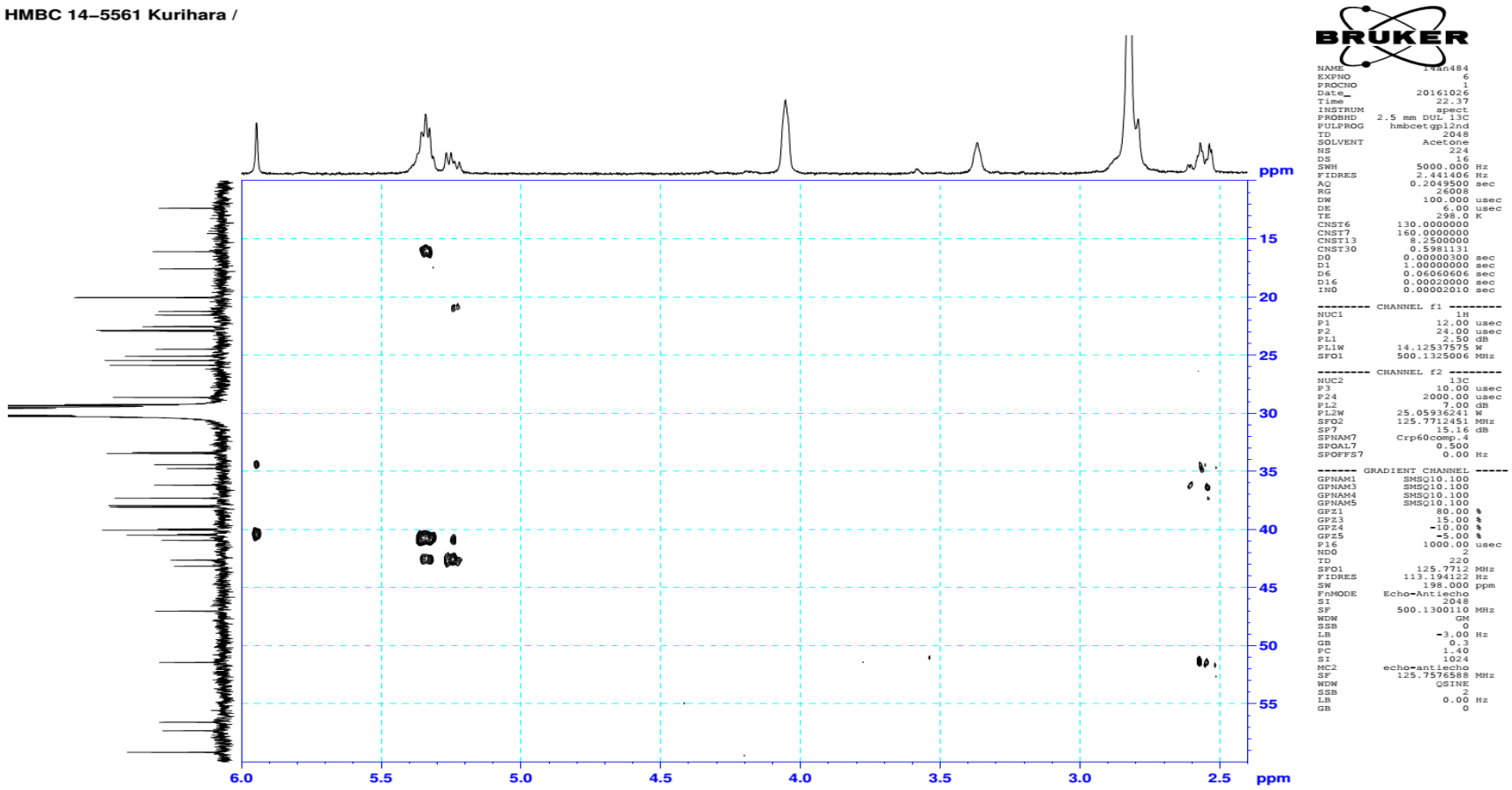


Figure 2-80. Expanded HMBC spectrum (5) of compounds **A2** and **A3**.

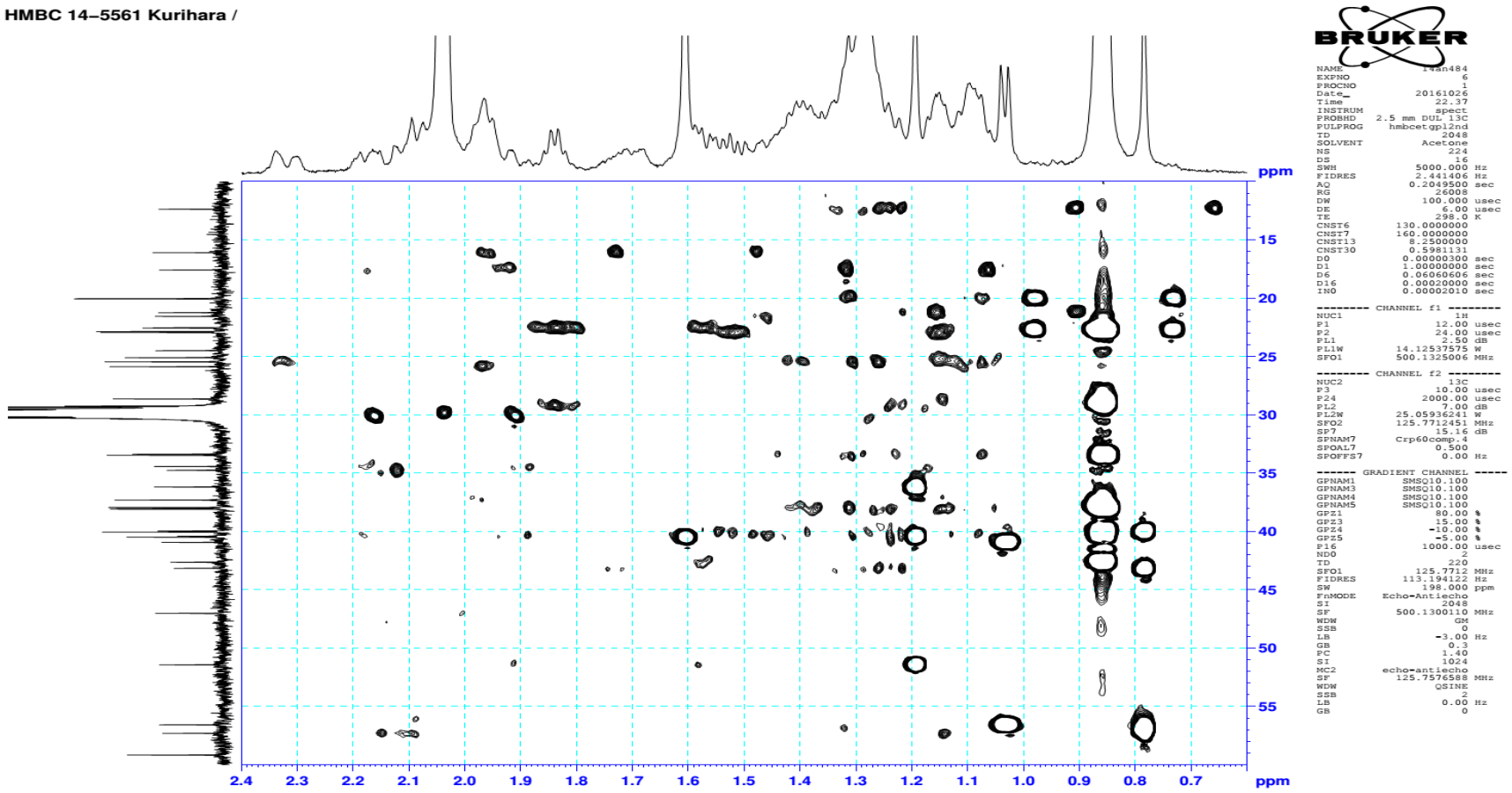


Figure 2-81. Expanded HMBC spectrum (6) of compounds **A2** and **A3**.

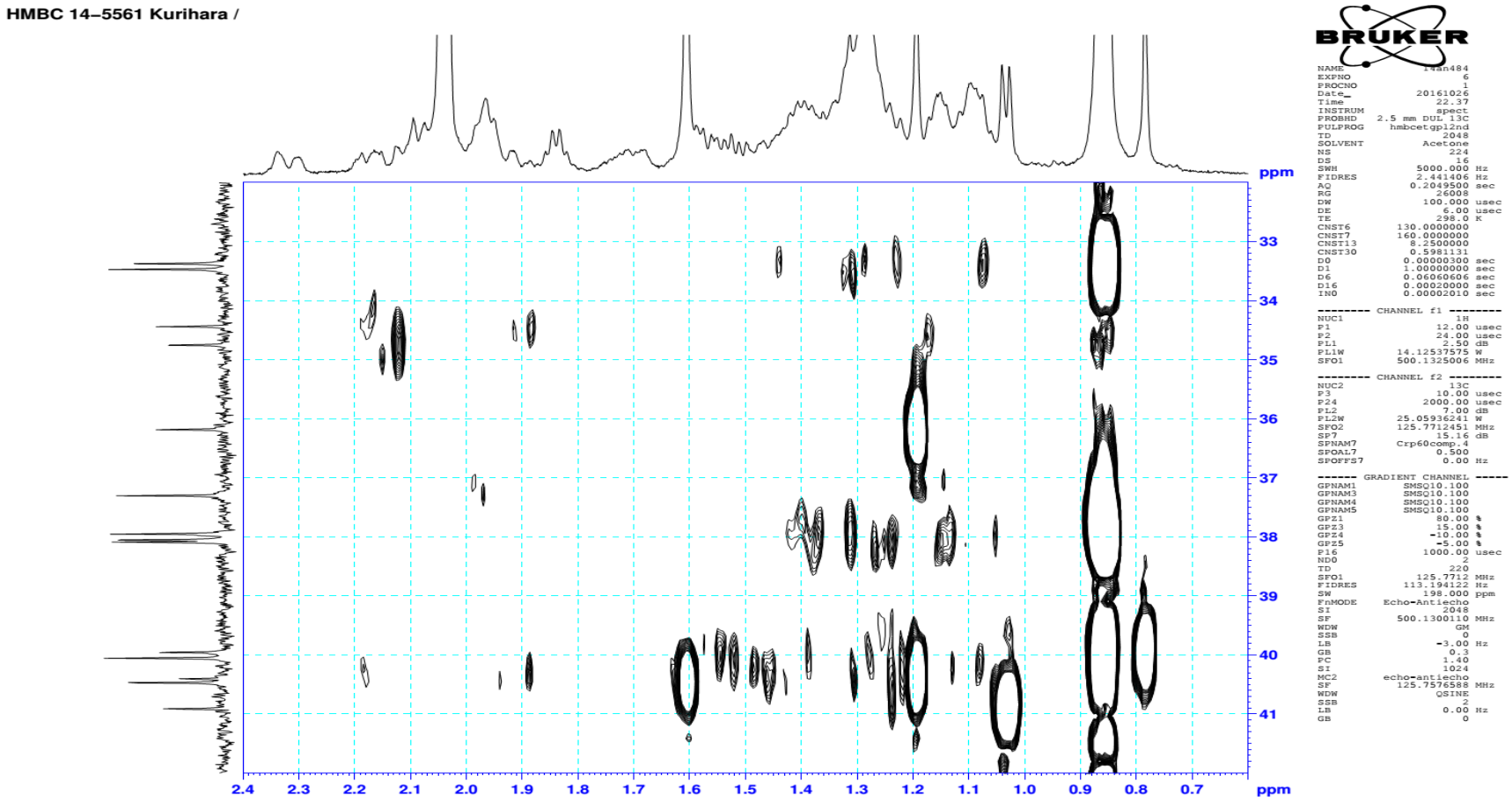


Figure 2-82. Expanded HMBC spectrum (7) of compounds **A2** and **A3**.

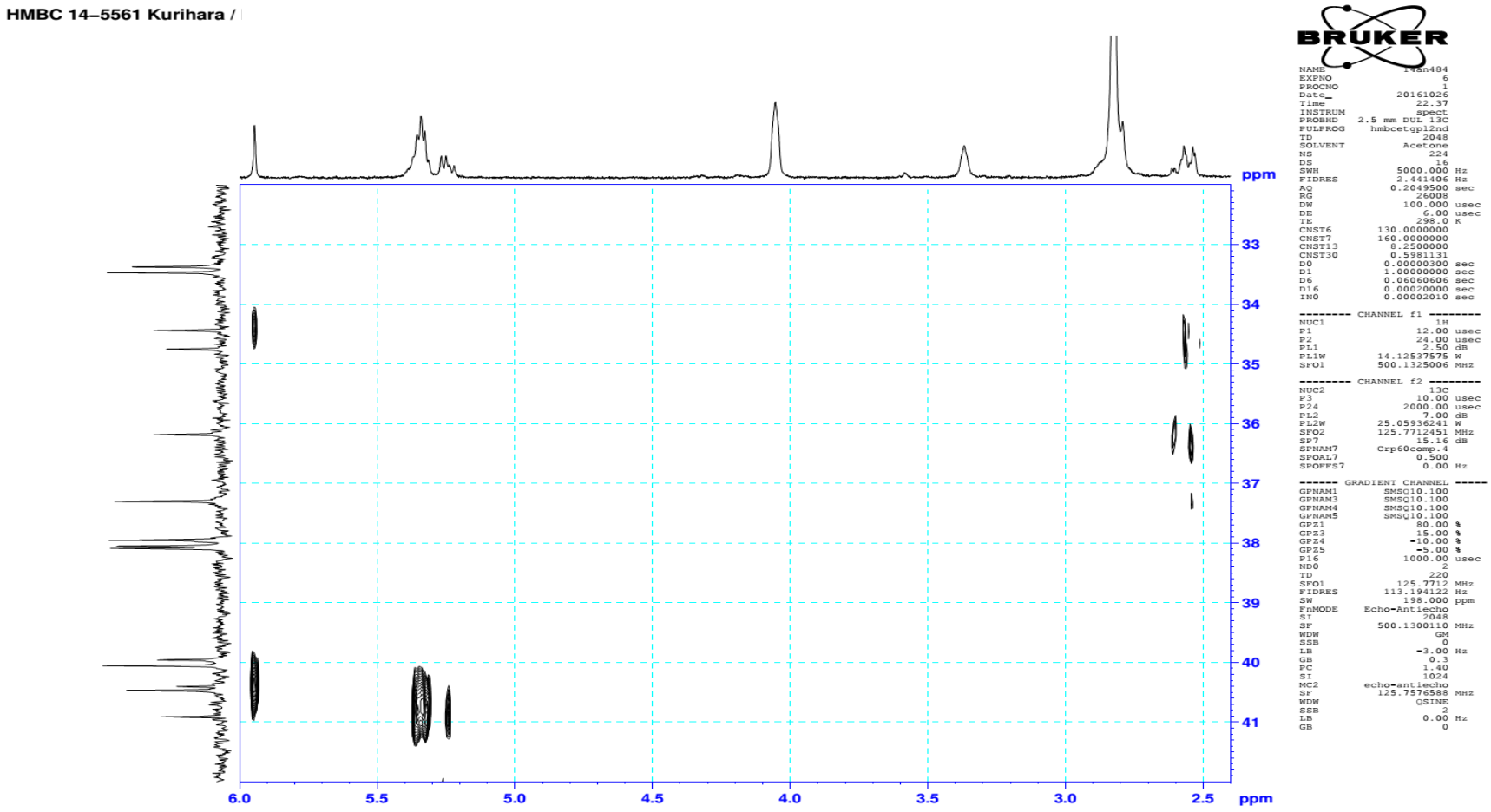


Figure 2-83. Expanded HMBC spectrum (8) of compounds **A2** and **A3**.

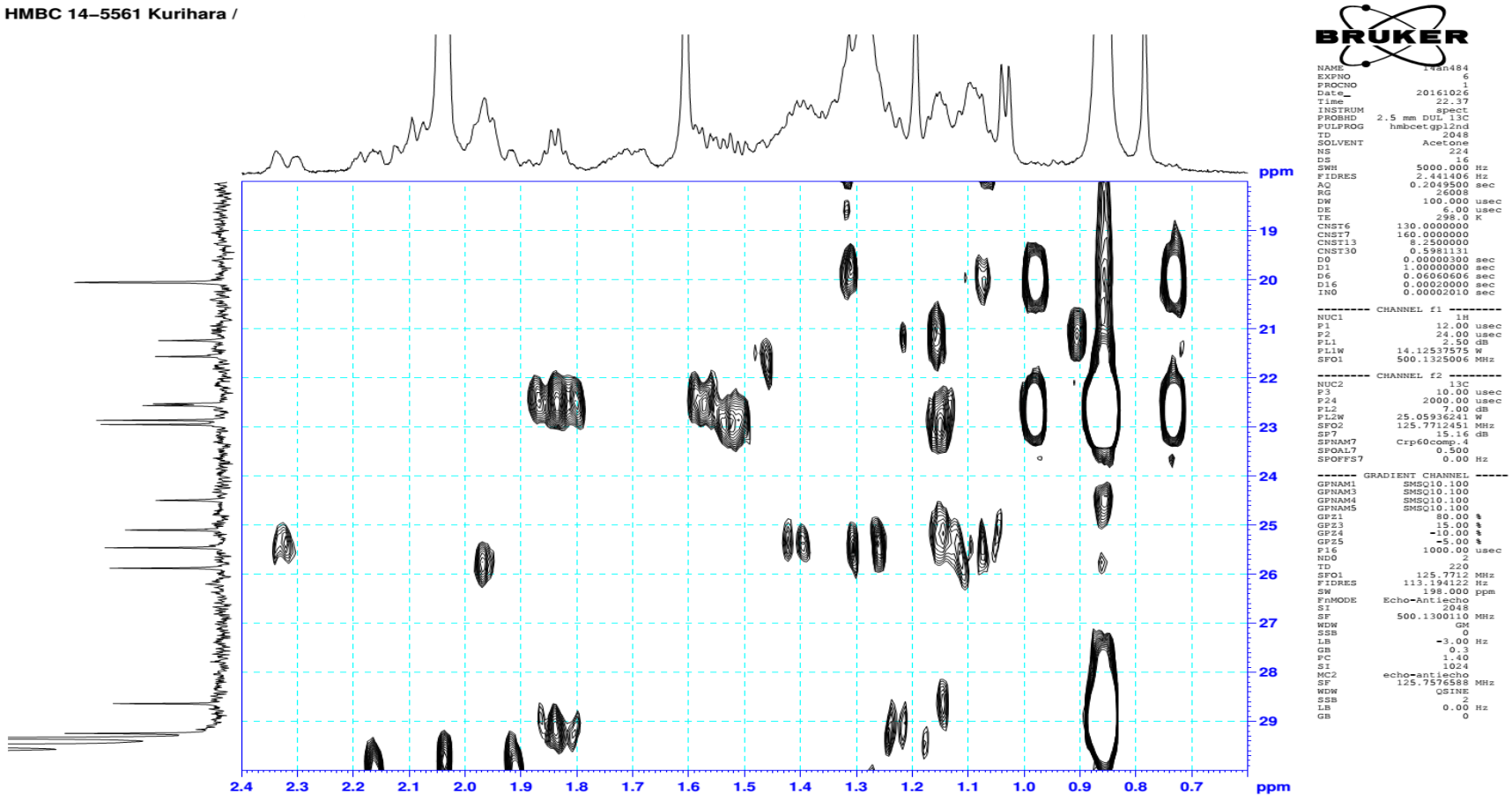


Figure 2-84. Expanded HMBC spectrum (9) of compounds **A2** and **A3**.

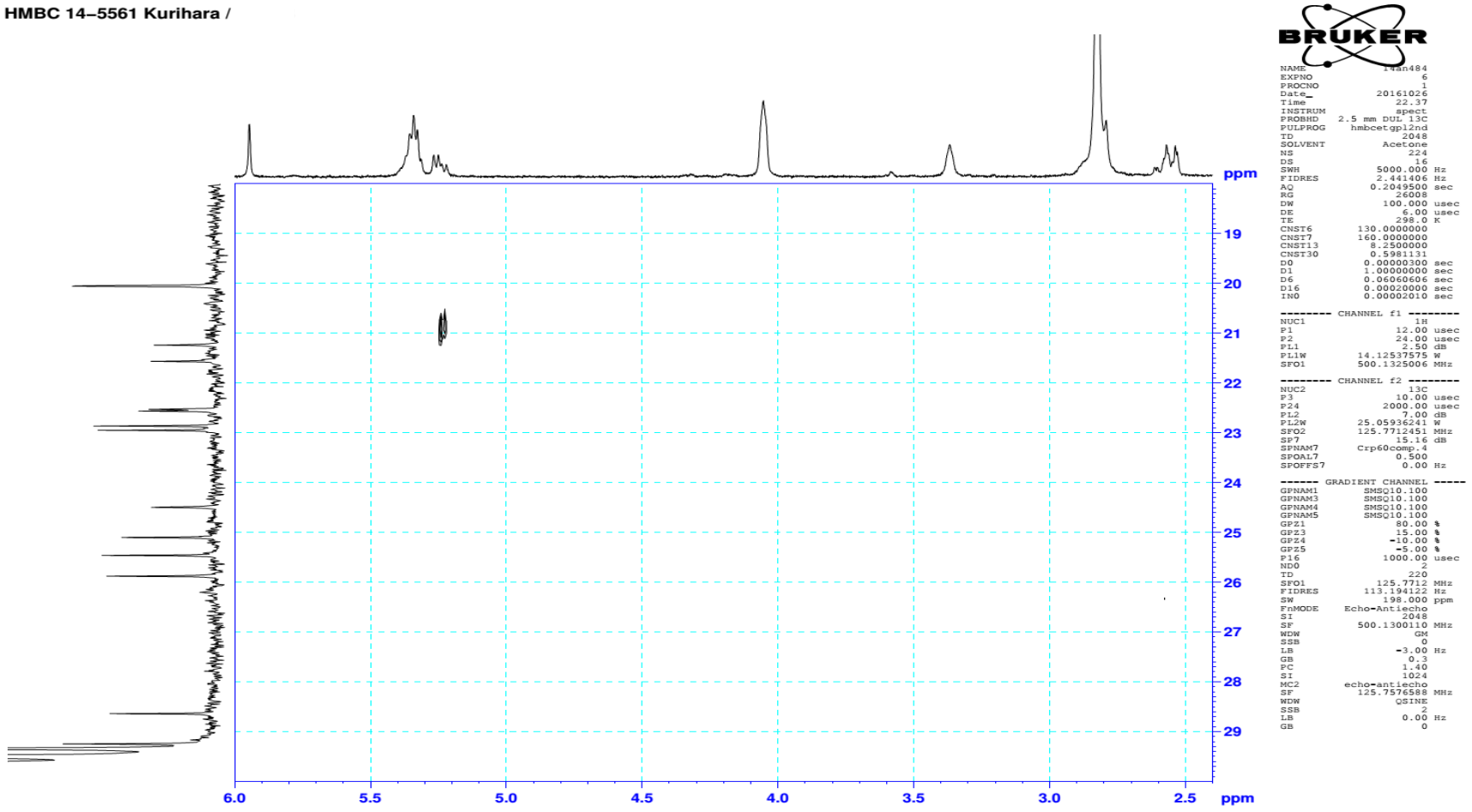


Figure 2-85. Expanded HMBC spectrum (10) of compounds **A2** and **A3**.

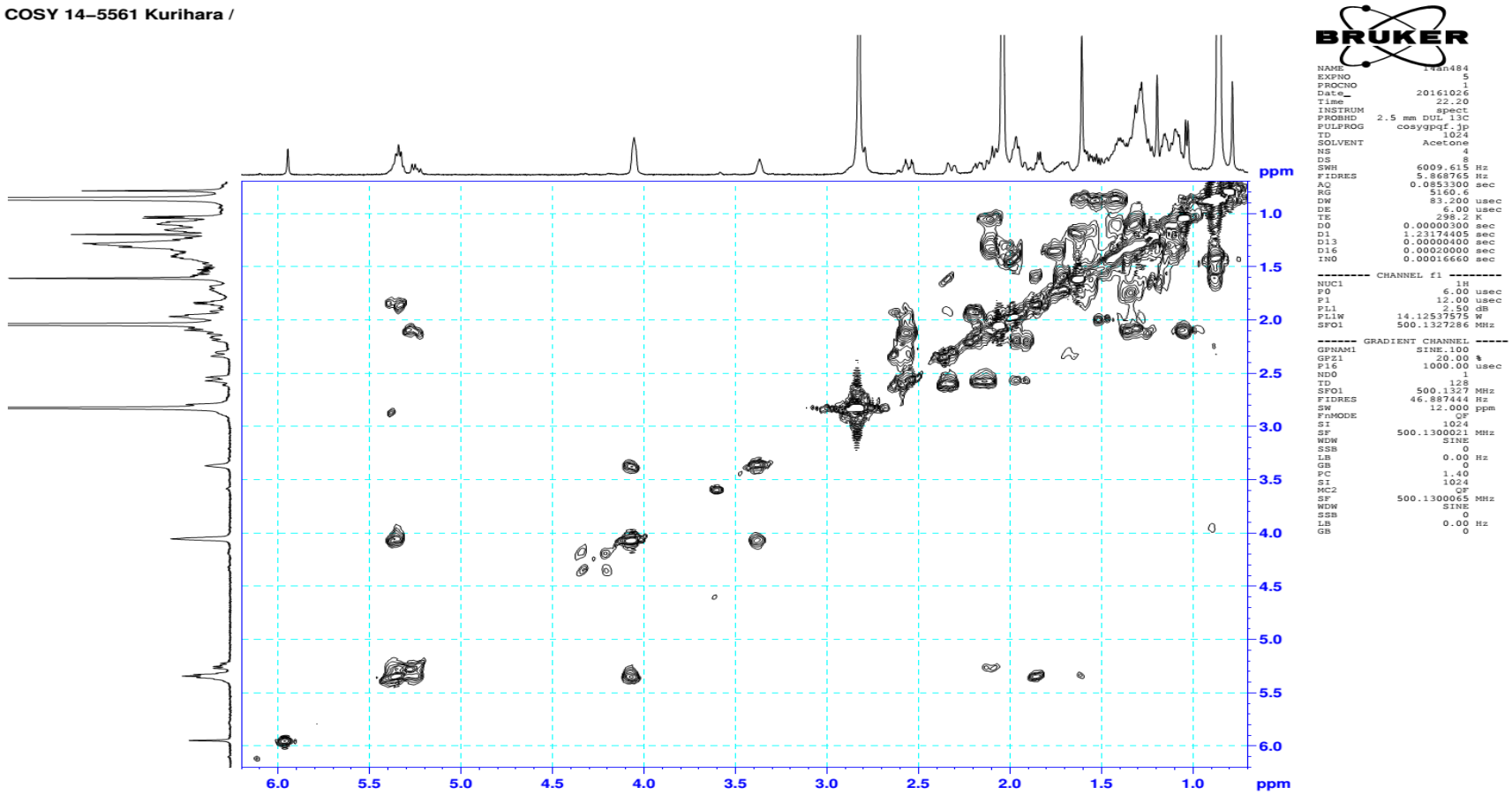


Figure 2-86. COSY spectrum of compounds **A2** and **A3**.

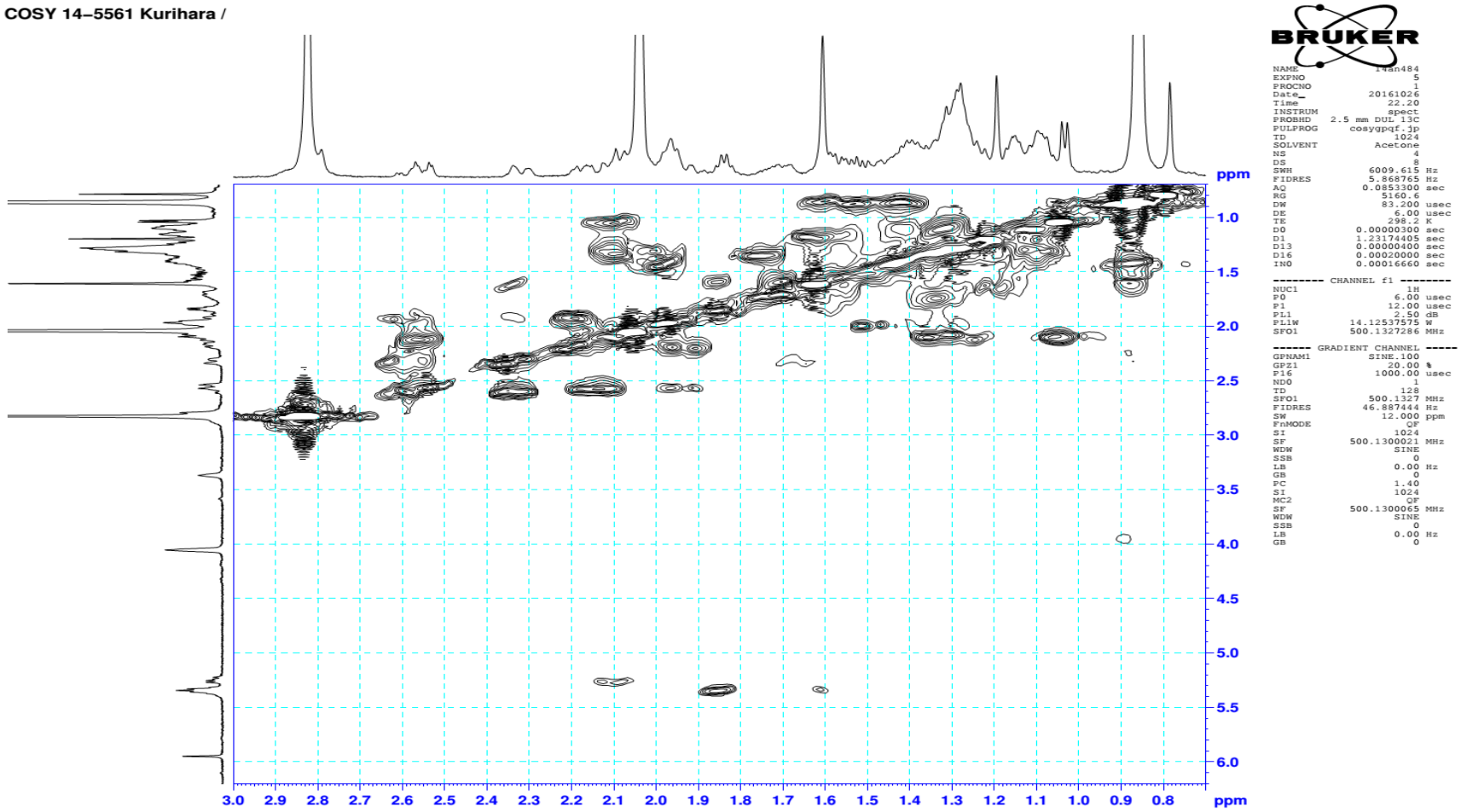


Figure 2-87. Expanded COSY spectrum (1) of compounds **A2** and **A3**.

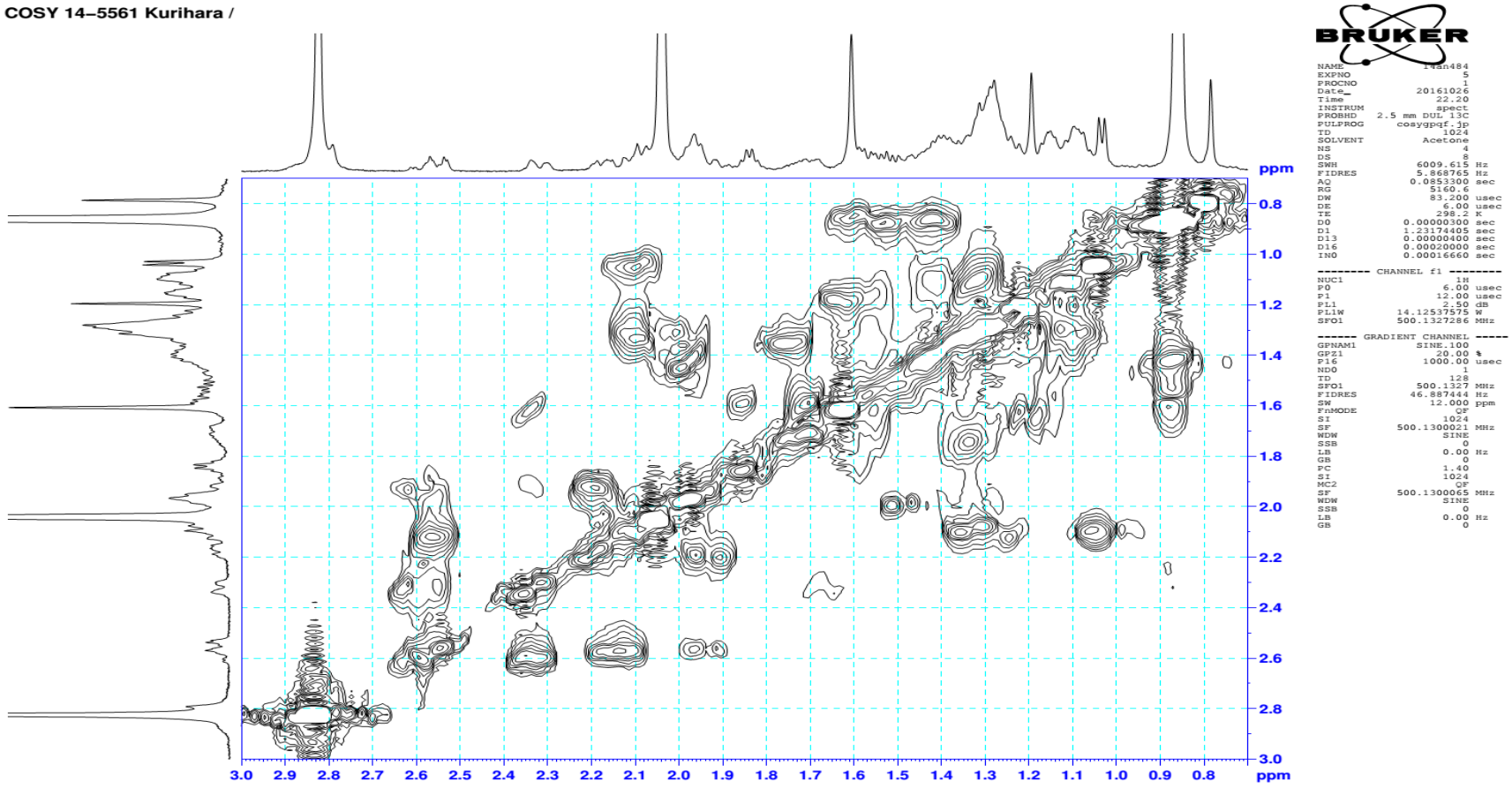


Figure 2-88. Expanded COSY spectrum (2) of compounds **A2** and **A3**.

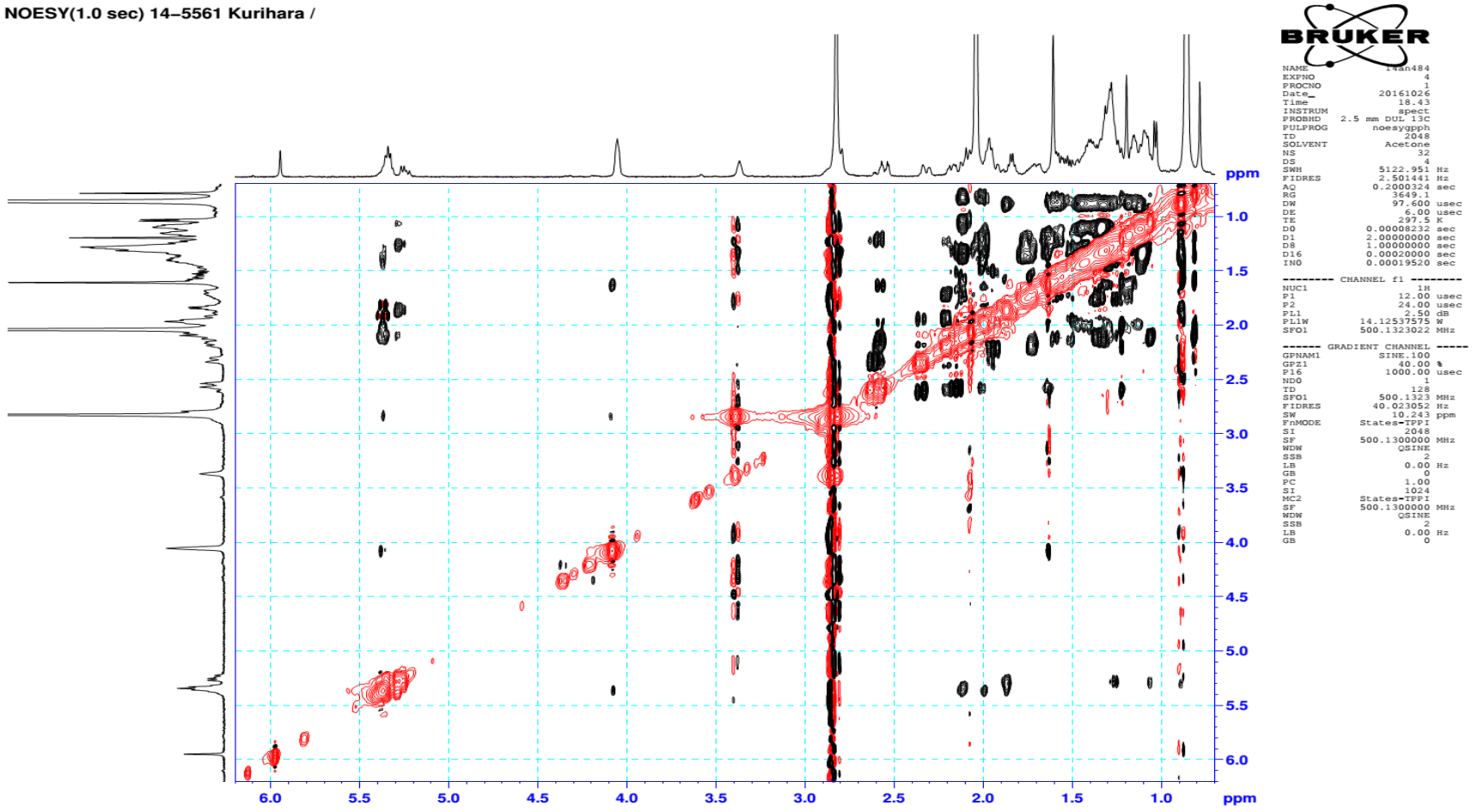


Figure 2-89. NOESY spectrum of compounds **A2** and **A3**.

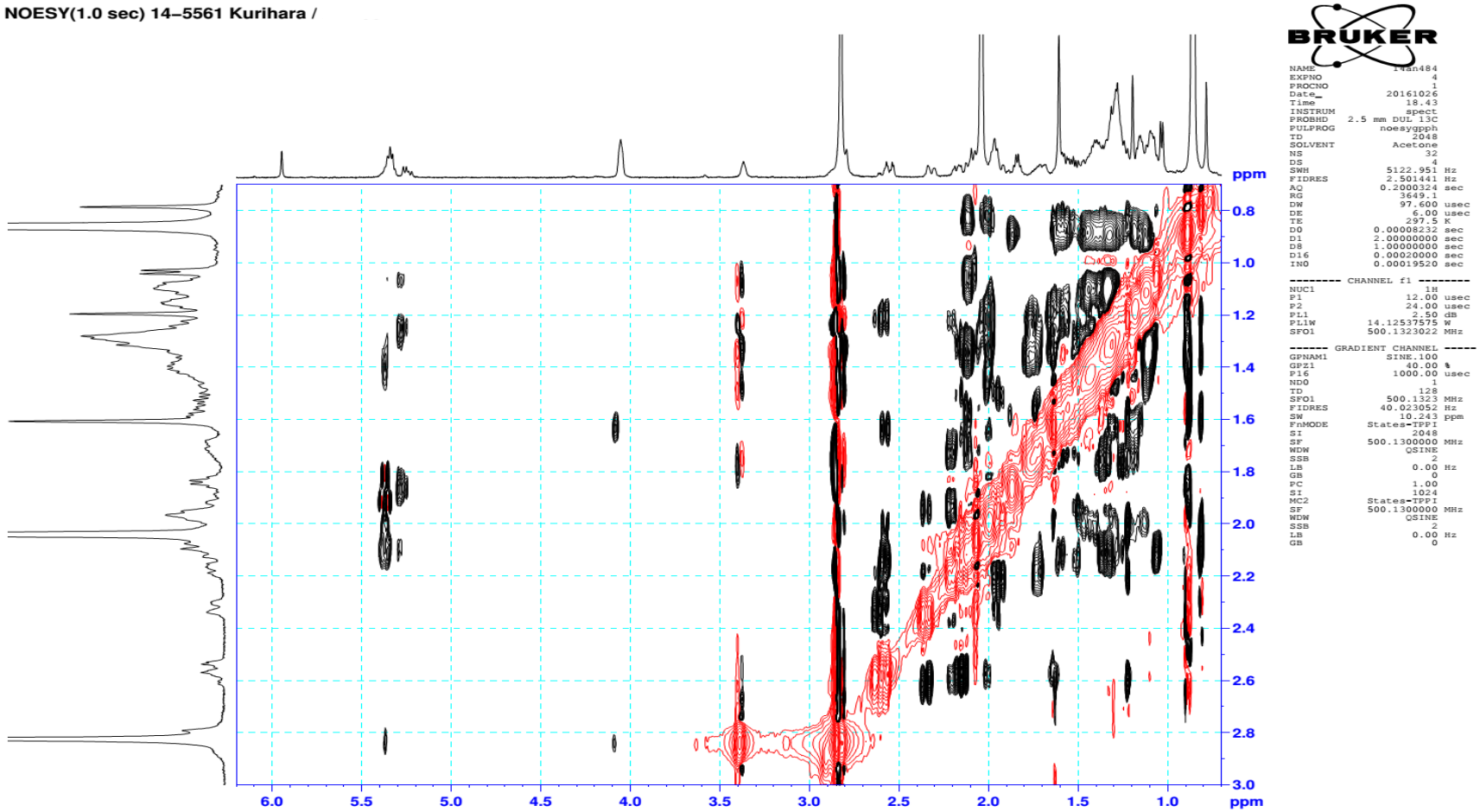


Figure 2-90. Expanded NOESY spectrum (1) of compounds **A2** and **A3**.

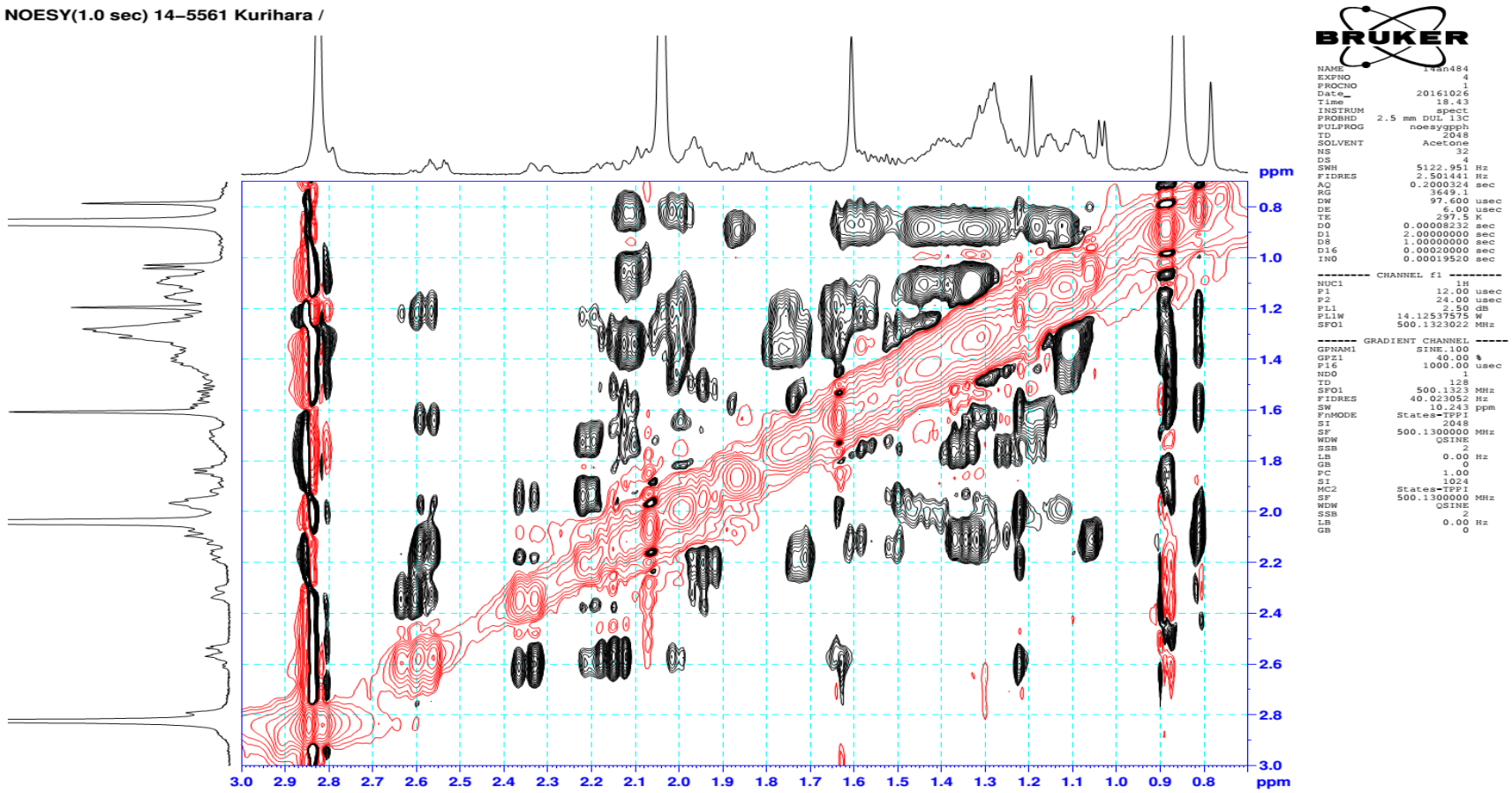


Figure 2-91. Expanded NOESY spectrum (2) of compounds **A2** and **A3**.

Table 2-31. Comparison of NMR data between compound **A2**[a] and literature[b]

	^{1}H NMR		^{13}C NMR	
Position	**A2**	Literature data	**A2**	Literature data
1	4.05(d, 6.6, 2H)	4.14 (d, 6.8, 2H)	59.2	59.2
2	5.34 (m, 1H)	5.40 (m, 1H)	126.0	123.0
3			137.5	139.8
4	1.97 (t, 2H)	1.99 (t, 2H)	40.5	39.9
5	1.38 (m, 1H); 1.25 (m, 1H)	1.00-1.66 (br, 19H)	25.1	25.2
6	1.30 (m, 1H), 1.10 (m, 1H)	1.00-1.66 (br, 19H)	37.3	36.7
7	1.42 (m, 1H)	1.00-1.66 (br, 19H)	33.4	32.8
8	1.28 (m, 1H); 1.08 (m, 1H)	1.00-1.66 (br, 19H)	38.1	37.4
9	1.38 (m, 1H); 1.25 (m, 1H)	1.00-1.66 (br, 19H)	25.5	24.5
10	1.28(m, 1H); 1.08 (m, 1H)	1.00-1.66 (br, 19H)	38.0 or 38.1	37.3 or 37.4
11	1.42 (m, 1H)	1.00-1.66 (br, 19H)	33.5	32.7
12	1.28(m, 1H); 1.08 (m, 1H)	1.00-1.66 (br, 19H)	38.1 or 38.0	37.4 or 37.3
13	1.38 (m, 1H); 1.25 (m, 1H)	1.00-1.66 (br, 19H)	25.9	24.8
14	1.15 (m, 2H)	1.00-1.66 (br, 19H)	40.1	39.4
15	1.12 (m, 1H)	1.00-1.66 (br, 19H)	28.0	28.0
16	0.86 (m, 6.6, 3H)	0.87 (m, 6.6, 3H)	23.0	22.6
17	0.86 (m, 6.6, 3H)	0.87 (m, 6.6, 3H)	22.9	22.7
18	0.86 (d, 6.6, 3H)	0.87 (d, 6.6, 3H)	20.1	19.3 or 19.7
19	0.86 (d, 6.6, 3H)	0.87 (d, 6.6, 3H)	20.1	19.7 or 19.3
20	1.61 (s, 3H)	1.66 (s, 3H)	16.1	16.2

[a]The NMR data were measured in acetone-d_6 (δ_H 2.04 ppm; δ_C CO 206.3, CH_3 30.4 ppm) at 500 MHz for ^{1}H and at 125 MHz for ^{13}C.

[b]Song et al., 2003.

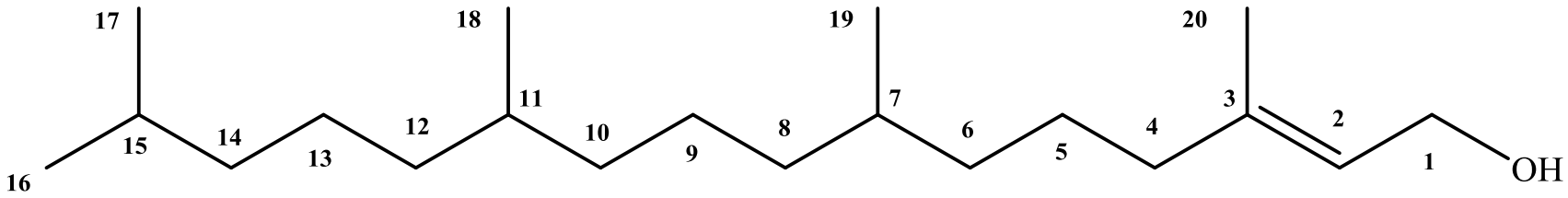


Figure 2-92. Structure of compound **A2**.

Table 2-32. Comparison of NMR data between compound **A3**[a] and literature[b]

	^{1}H NMR		^{13}C NMR	
Position	**A3**	Literature data	**A3**	Literature data
1	2.19 (m, 1H); 1.93 (m, 1H)	2.14(m, 1H); 1.90 (m, 1H)	36.2	35.5
2	2.32 (m, 1H); 2.55 (m, 1H)	2.46 (m, 1H); 2.55 (m, 1H)	34.4	34.0
3			199.2	199.5
4	5.95 (d, 1H)	6.15 (d, 1H)	125.5	125.5
5			161.9	162.8
6			202.0	202.3
7	2.55 (m, 1H); 2.13 (m, 1H)	2.66 (m, 1H); 2.02 (m, 1H)	47.0	46.8
8	1.98 (m, 1H)	2.02 (m, 1H)	34.8	34.2
9	1.29 (m, 1H)	1.37 (m, 1H)	51.4	50.9
10			40.4	39.0
11	1.69 (m, 1H); 1.57 (m, 1H)	1.64 (m, 1H); 1.68 (m, 1H)	21.6	20.8
12	1.74 (m, 1H); 1.34 (m, 1H)	2.11 (m, 1H); 1.23 (m, 1H)	29.3	29.7
13			43.1	41.9
14	1.29 (m, 1H)	1.12 (m, 1H)	57.3	56.6
15	1.62 (m, 1H); 1.19 (m, 1H)	1.14 (m, 1H); 1.59 (m, 1H)	24.5	23.9
16	2.08 (m, 1H); 1.32 (m, 1H)	1.88 (m, 1H); 1.35 (m, 1H)	40.0	39.8
17	1.23 (m, 1H)	1.14 (m, 1H)	56.6	55.8
18	0.78 (s, 3H)	0.70 (s, 3H)	12.4	12.0
19	1.20 (s, 3H)	1.18 (s, 3H)	17.6	17.0
20	2.10 (m, 1H)	1.37 (m, 1H)	40.9	39.0
21	1.03 (d, 6.6, 2H)	0.91 (d, 6.5, 3H)	21.2	20.8
22	5.25 (d, 1H)	5.17 (d, 1H)	138.8	137.6

(To be continued)

(Continued)

	^{1}H NMR		^{13}C NMR	
Position	**A3**	Literature data	**A3**	Literature data
23	5.34 (d, 1H)	5.28 (d, 1H)	127.2	127.9
24	1.85 (m, 2H)	1.14 (m, 2H)	42.6	40.0
25	1.53 (m, 1H)	1.50 (m, 1H)	28.6	28.5
26	0.86 (d, 6.4, 3H)	0.84 (d, 6.5, 3H)	22.6	22.9
27	0.86 (d, 6.4, 3H)	0.84 (d, 6.5, 3H)	22.5	22.3

[a]The NMR data were measured in acetone-d_6 (δ_H 2.04 ppm; δ_C CO 206.3, CH_3 30.4 ppm) at 500 MHz for ^{1}H and at 125 MHz for ^{13}C.

[b]Kontiza et al., 2006.

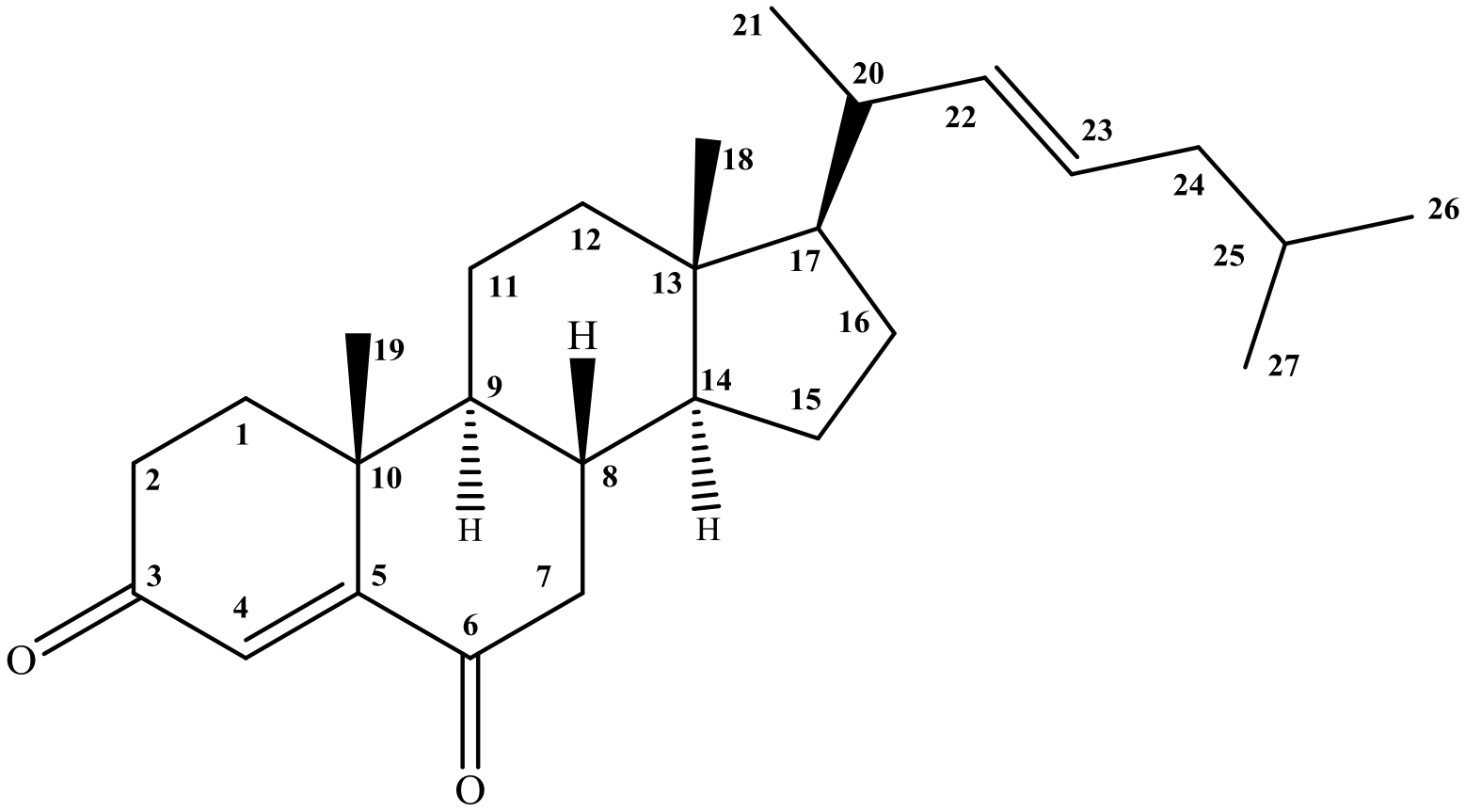


Figure 2-93. Structure of compound **A3**.

2.3.2.3 Structural elucidation of β-glucuronidase inhibitor A4

FD-MS spectrum of compound **A4** displayed a molecular ion peak at *m/z* 386 (Figure 2-94). Molecular formula was determined as $C_{27}H_{46}O$ by FD-HR-MS at *m/z* 386.35400 (calculated 386.35486). The ^{1}H NMR spectrum showed an olefinic proton at δ_H 5.30 (H-6), an oxygenated methine proton at δ_H 3.38 (H-3) and twenty-eight methylene and methine protons at δ_H 0.92 to 2.17, fifteen methyl protons (Figure 2-95). ^{13}C NMR spectrum displayed 27 carbons including two olefinic carbons at δ_c 142.3 (C-5) and 121.5 (C-6), and an oxygenated carbon at δ_c 71.7 (C-3) (Figure 2-96). Compound **A4** was confirmed as cholesterol (Table 2-33, Figure 2-114) with assistance of HSQC (Figures 2-97 to 2-101), HMBC (Figures 2-102 to 2-107), COSY (Figures 2-108 to 2-110), and NOESY (Figures 2-111 to 113) results as well as the comparison with literature data (Nasir, Saeidnia, Mashinchian-moradi, & Gohari, 2011).

Optical rotation of compound **A4** was measured as $[\alpha]_D^{27}$= -31.7° (*c*1.32, $CHCl_3$). The levorotatory character is similar to naturally occurring cholesterol. In addition, cross-peaks in NOESY spectrum showed two typical correlation groups: H-20/H-18, H-18/H-8; H-14/H-9, H-9/H-1a and H-1a/H-3 which supported same stereochemistry as the natural product.

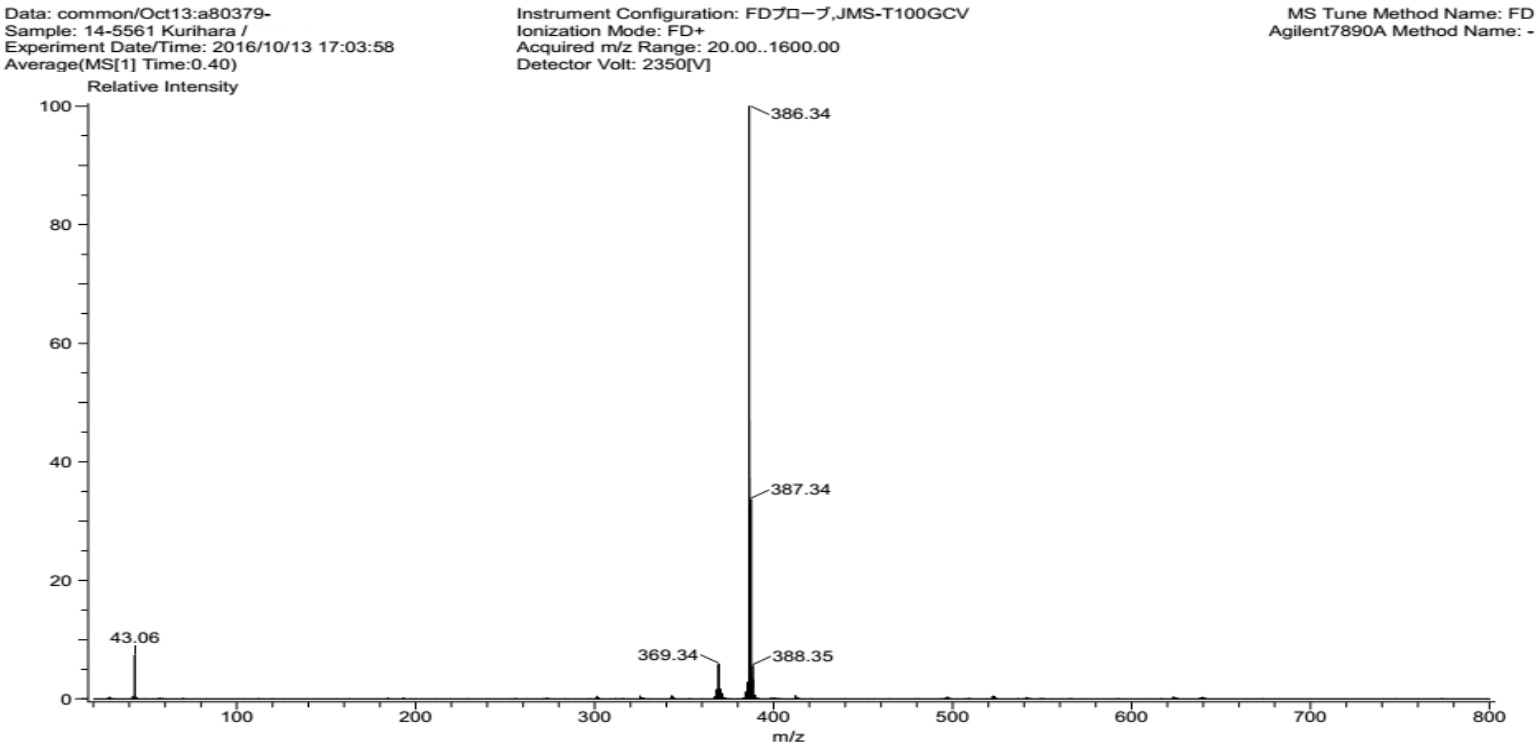


Figure 2-94. FD-MS spectrum of compound **A4**.

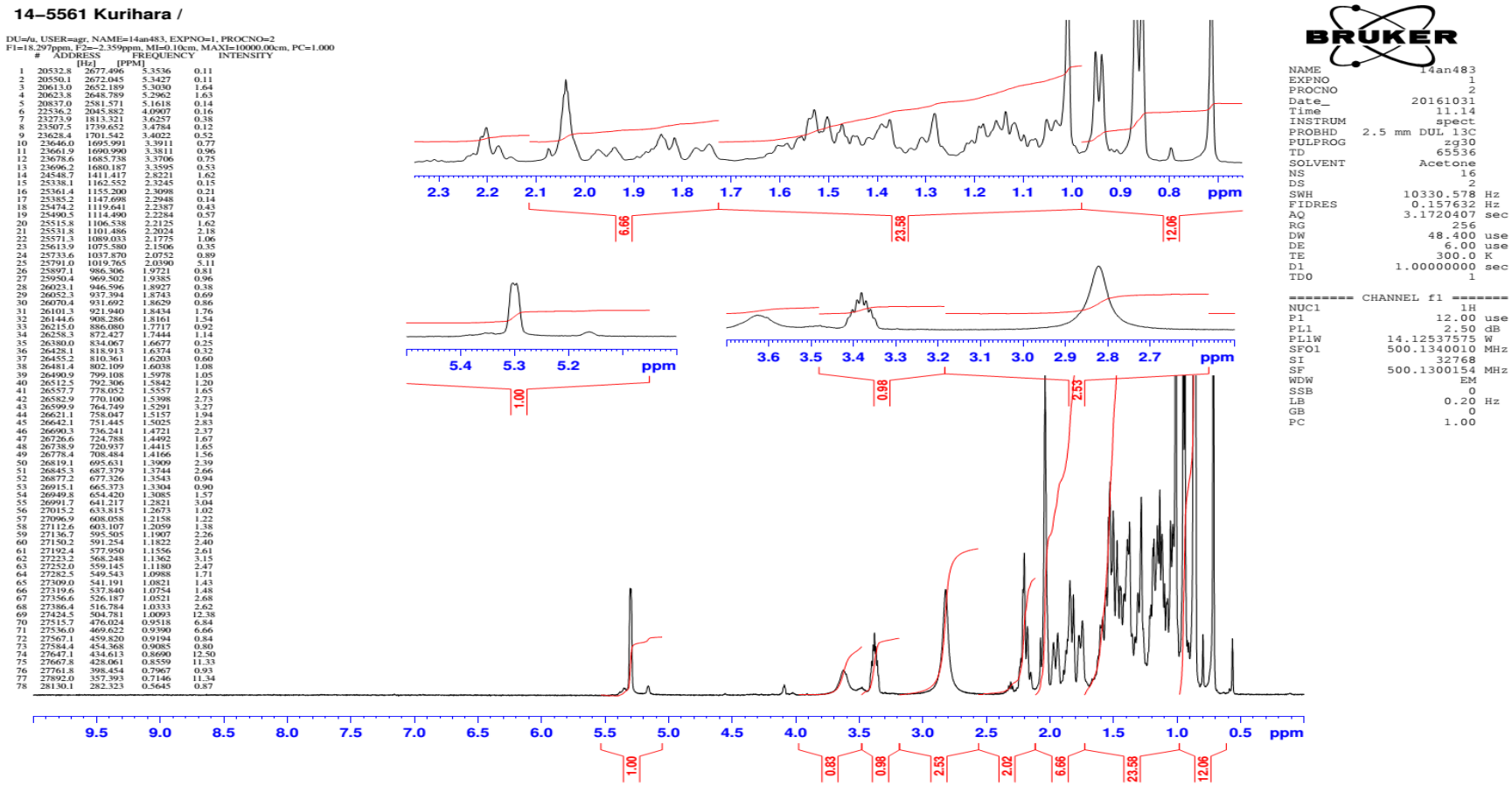


Figure 2-95. ^{1}H-NMR spectrum of compound **A4**.

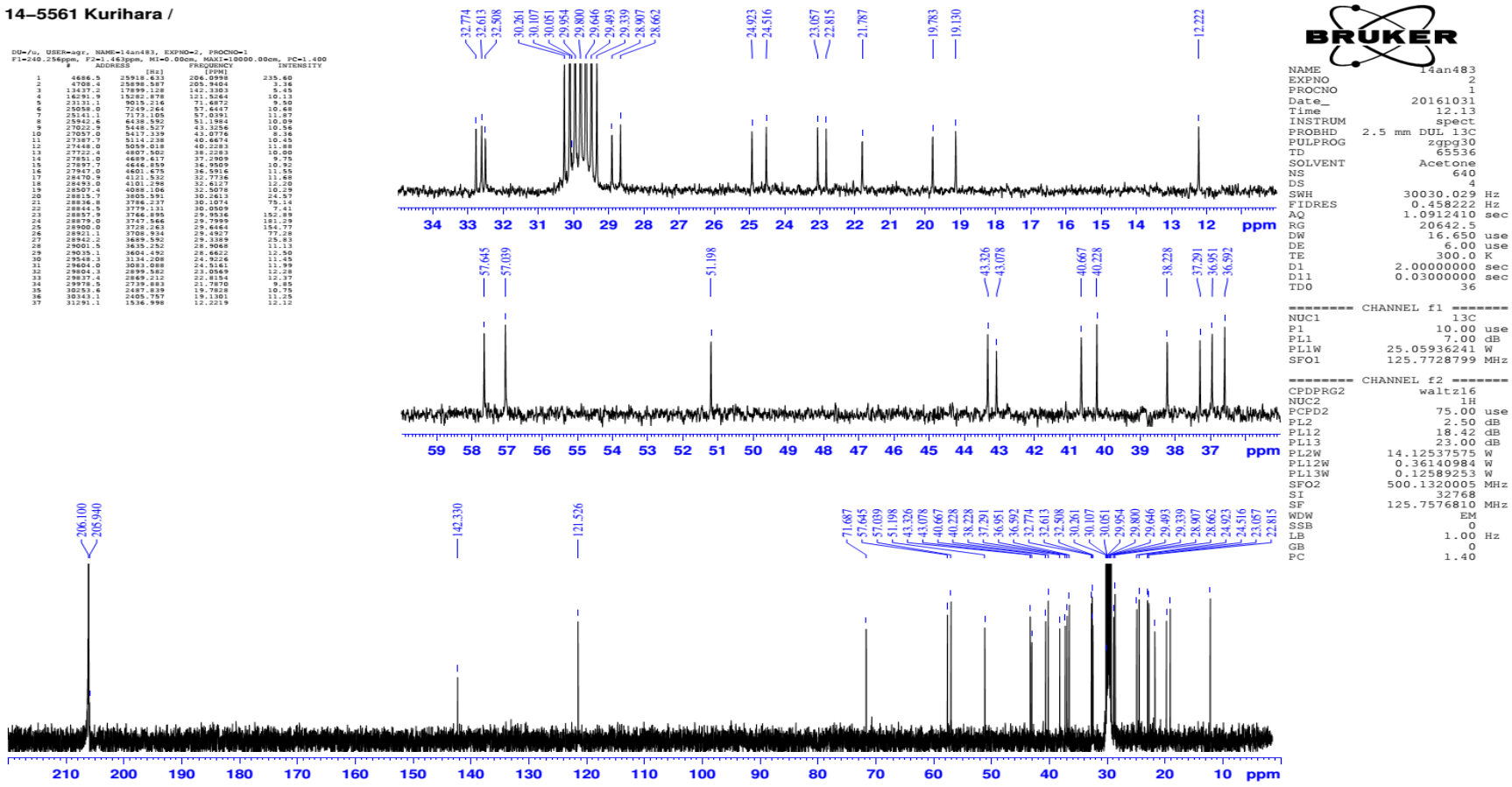


Figure 2-96. ^{13}C-NMR spectrum of compound **A4**.

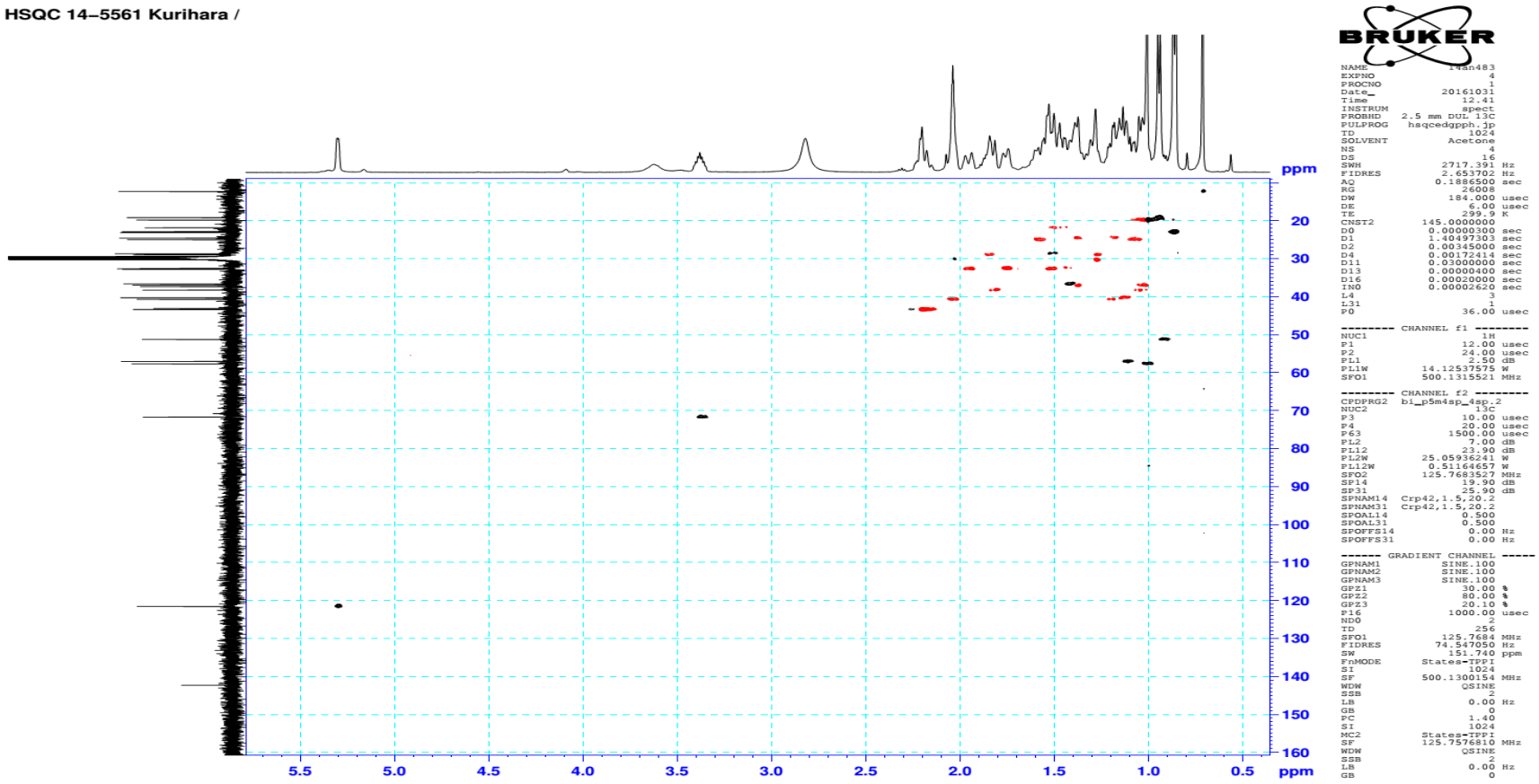


Figure 2-97. HSQC spectrum of compound **A4**.

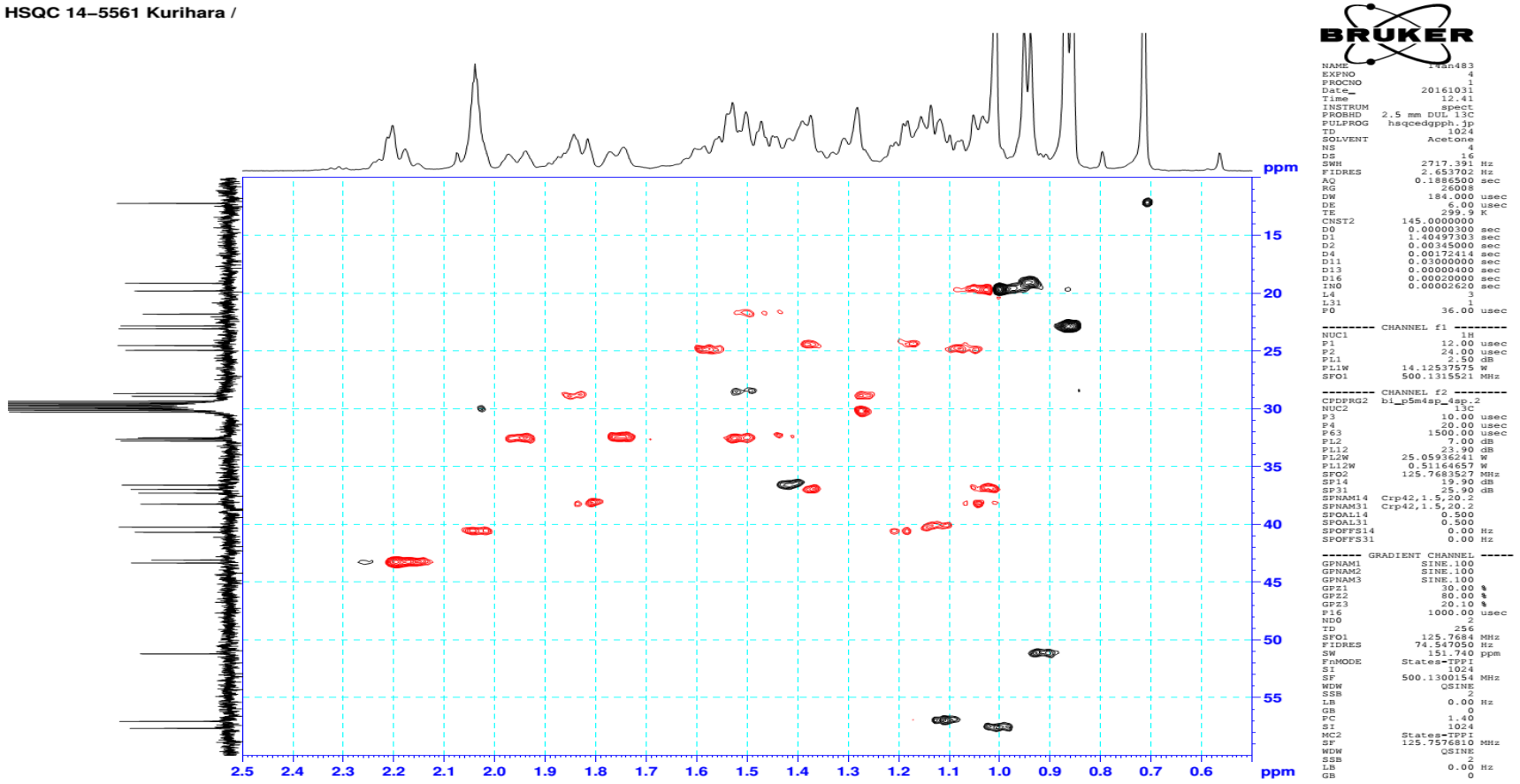


Figure 2-98. Expanded HSQC spectrum (1) of compound **A4**.

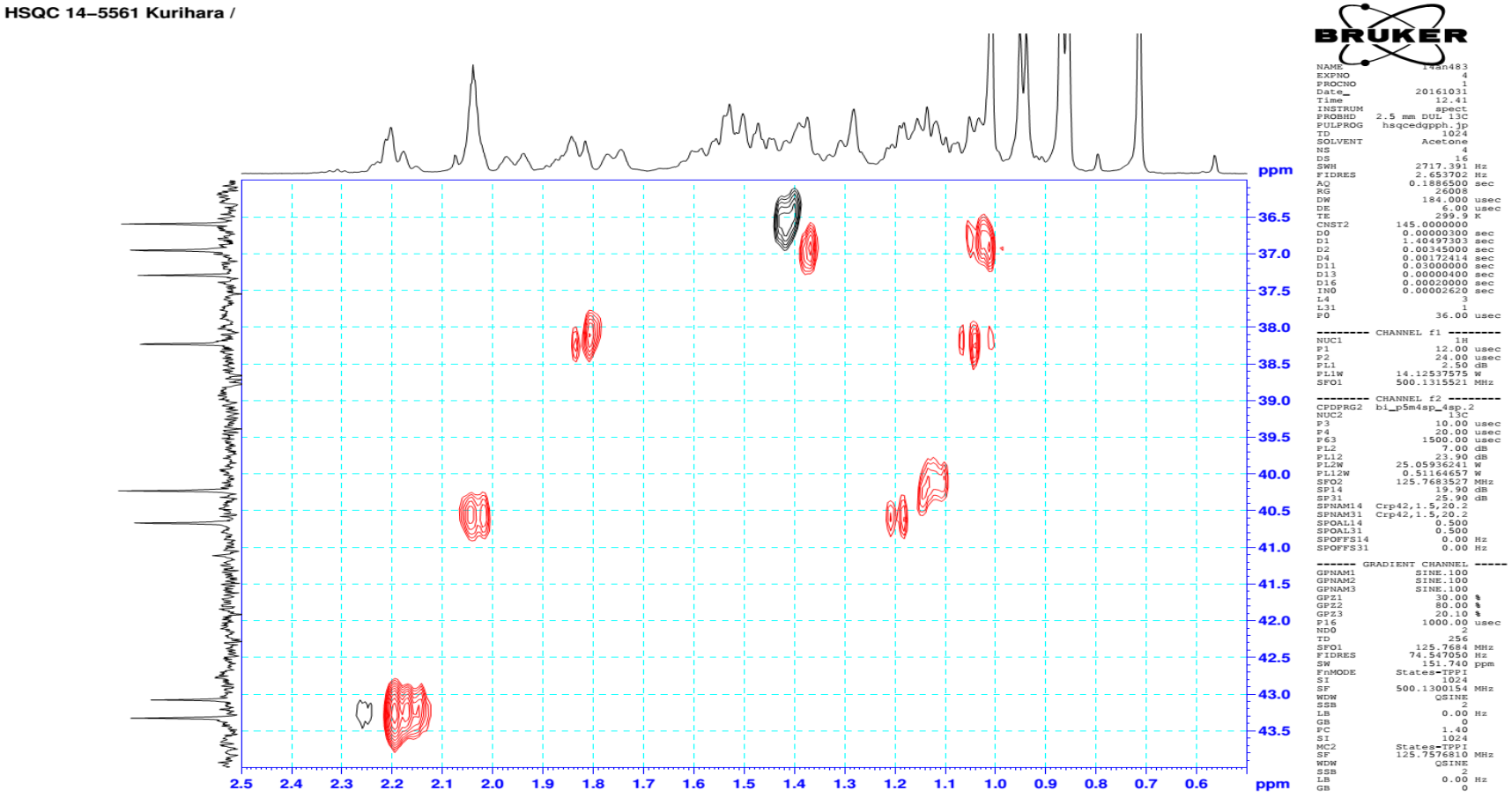


Figure 2-99. Expanded HSQC spectrum (2) of compound **A4**.

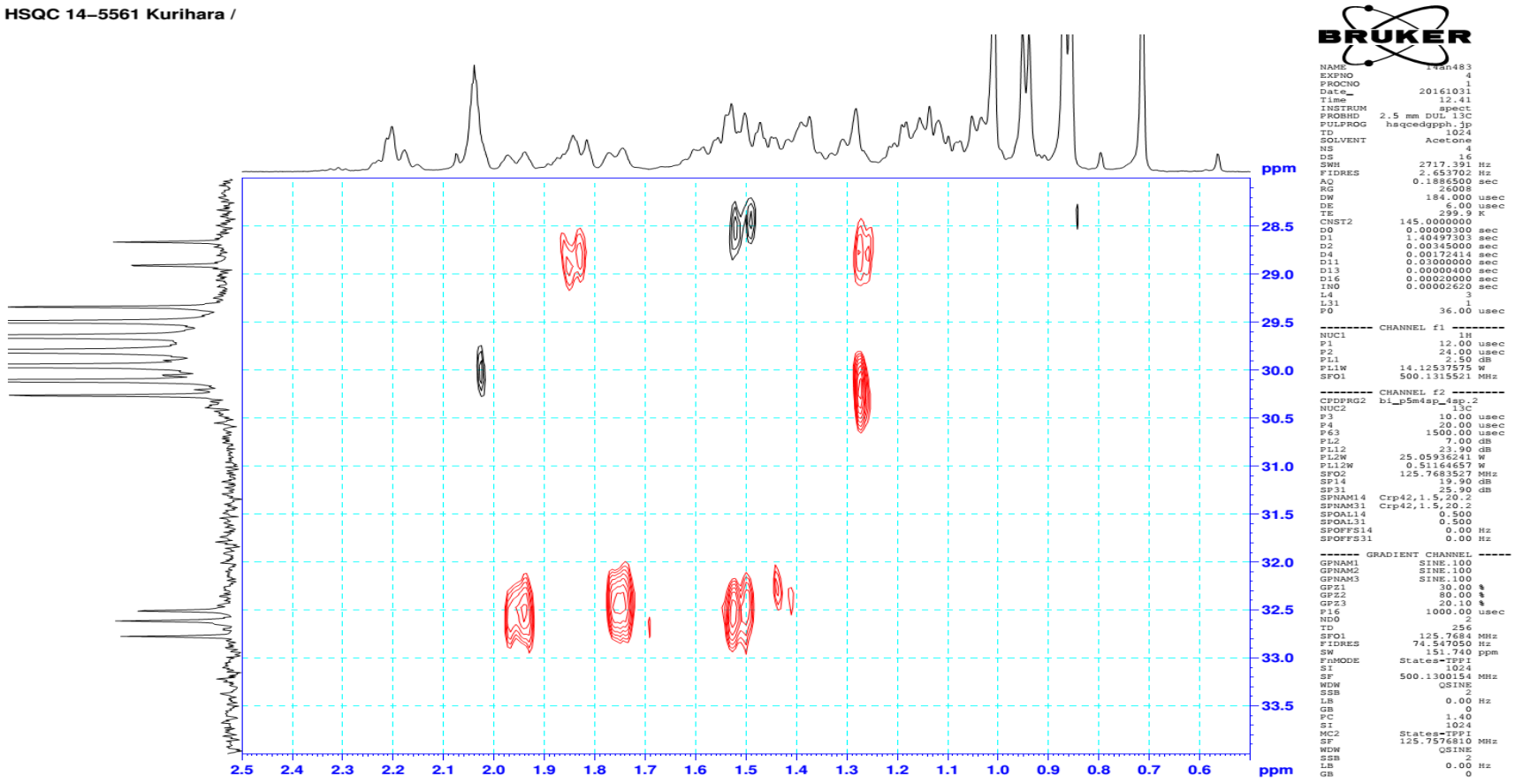


Figure 2-100. Expanded HSQC spectrum (3) of compound **A4**.

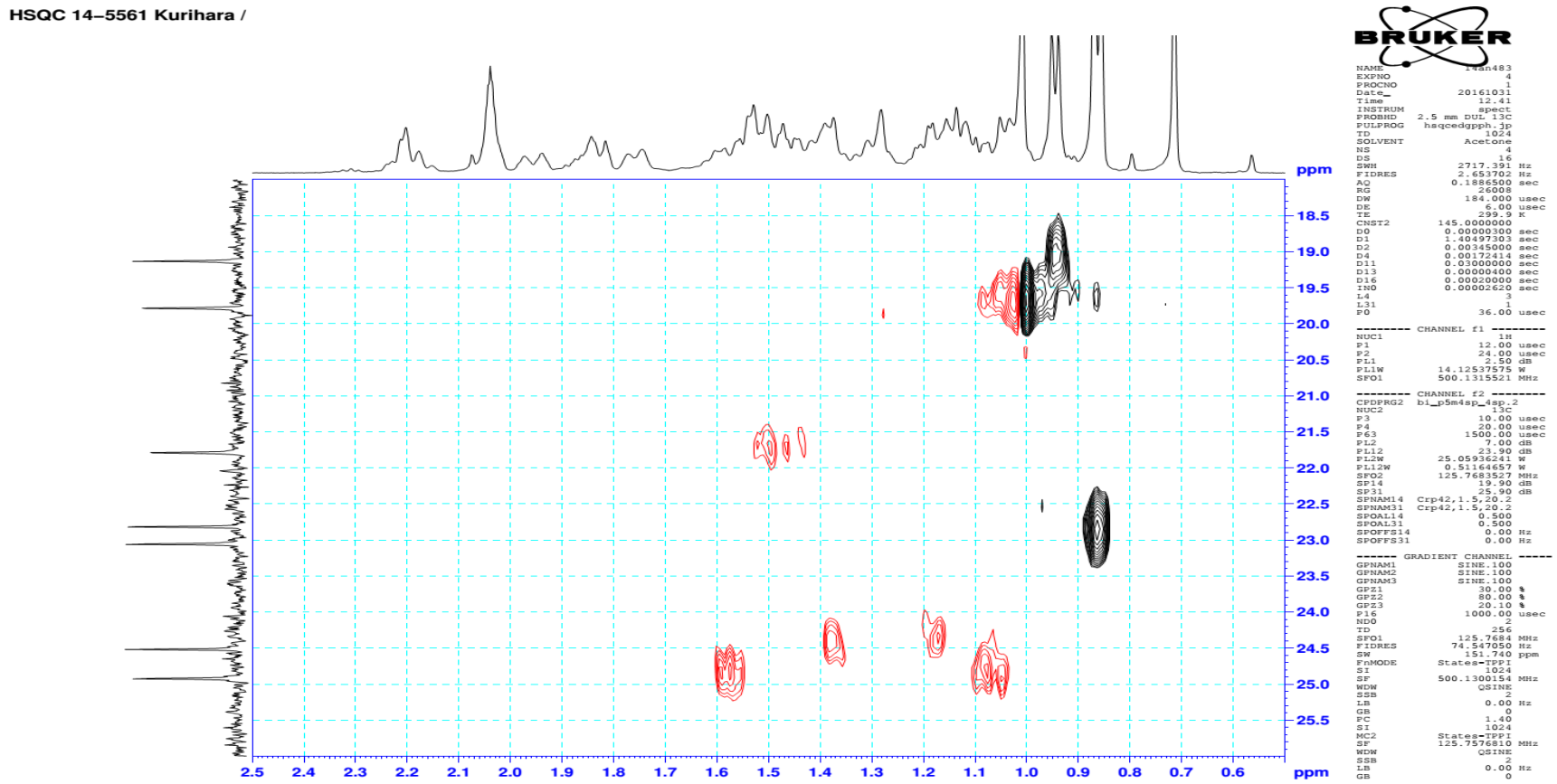


Figure 2-101. Expanded HSQC spectrum (4) of compound **A4**.

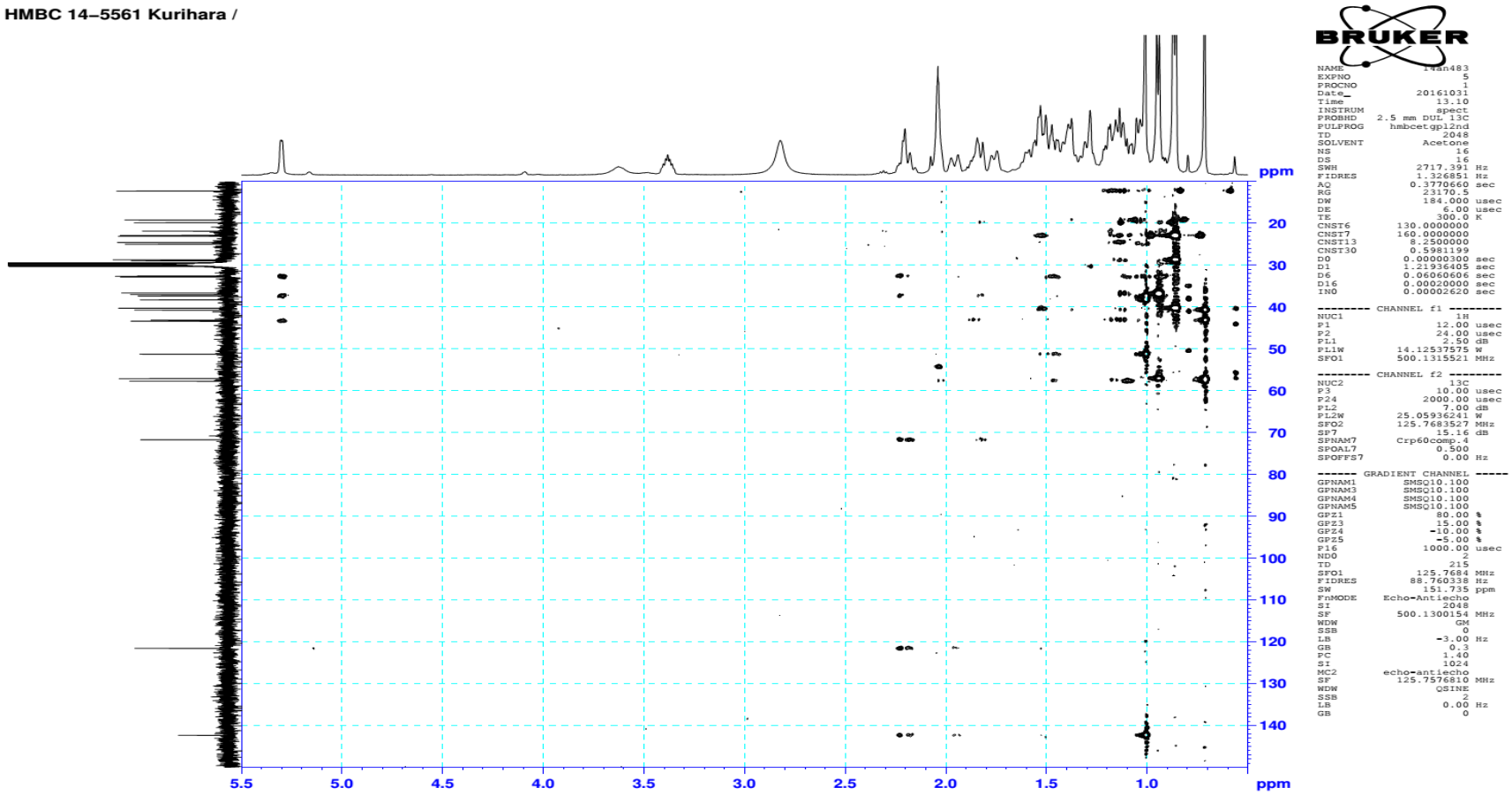


Figure 2-102. HMBC spectrum of compound **A4**.

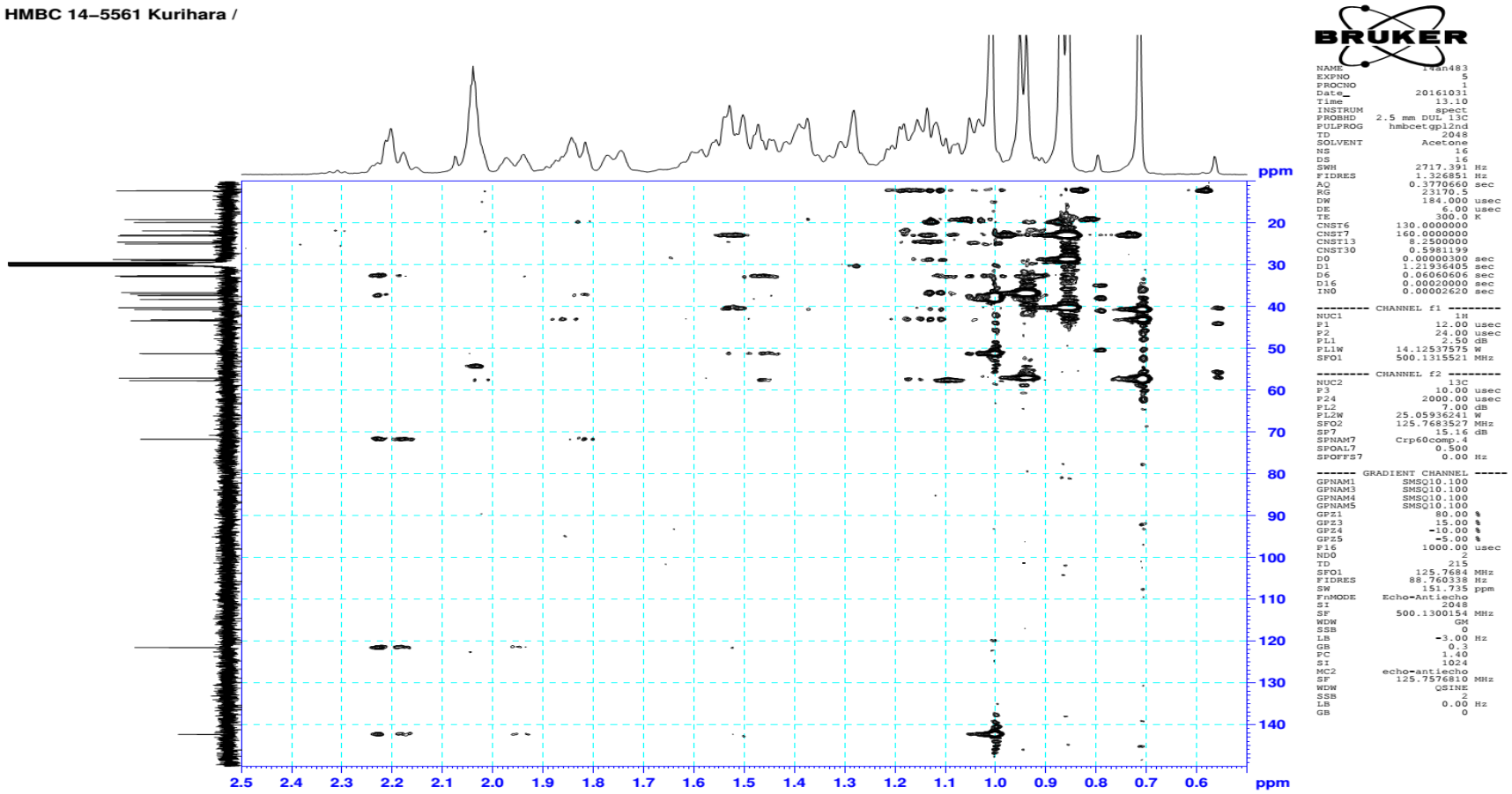


Figure 2-103. Expanded HMBC spectrum (1) of compound **A4**.

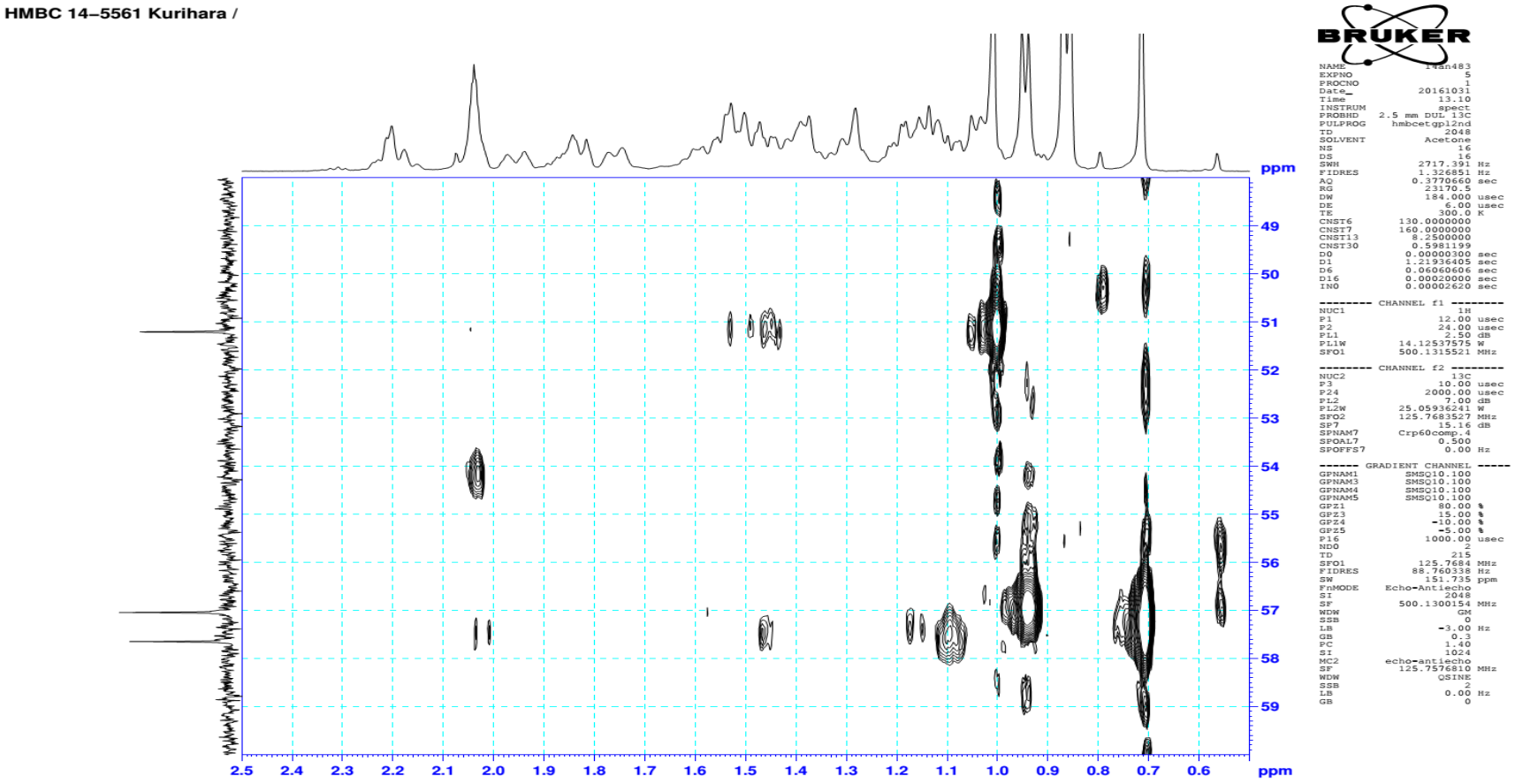


Figure 2-104. Expanded HMBC spectrum (2) of compound **A4**.

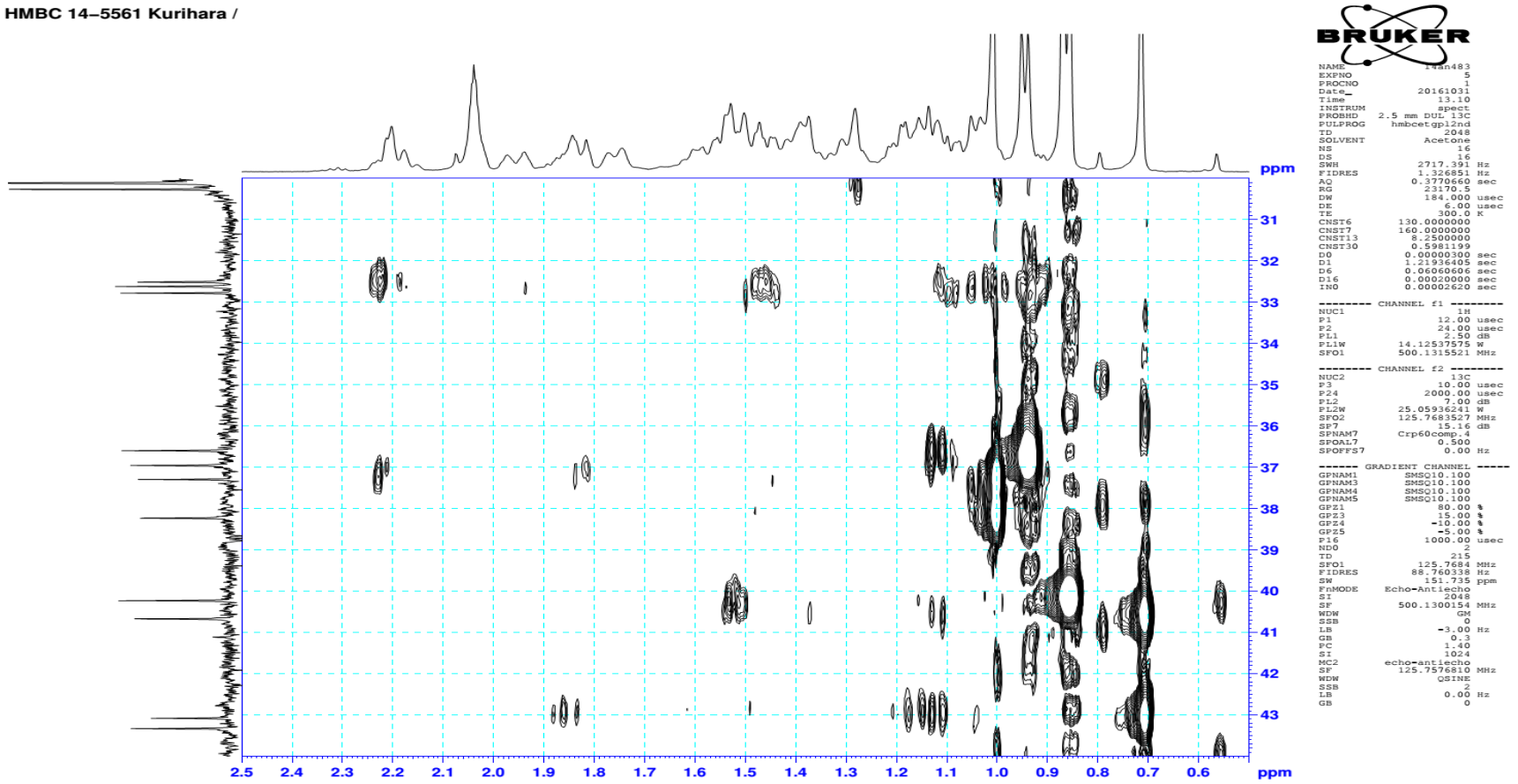


Figure 2-105. Expanded HMBC spectrum (3) of compound **A4**.

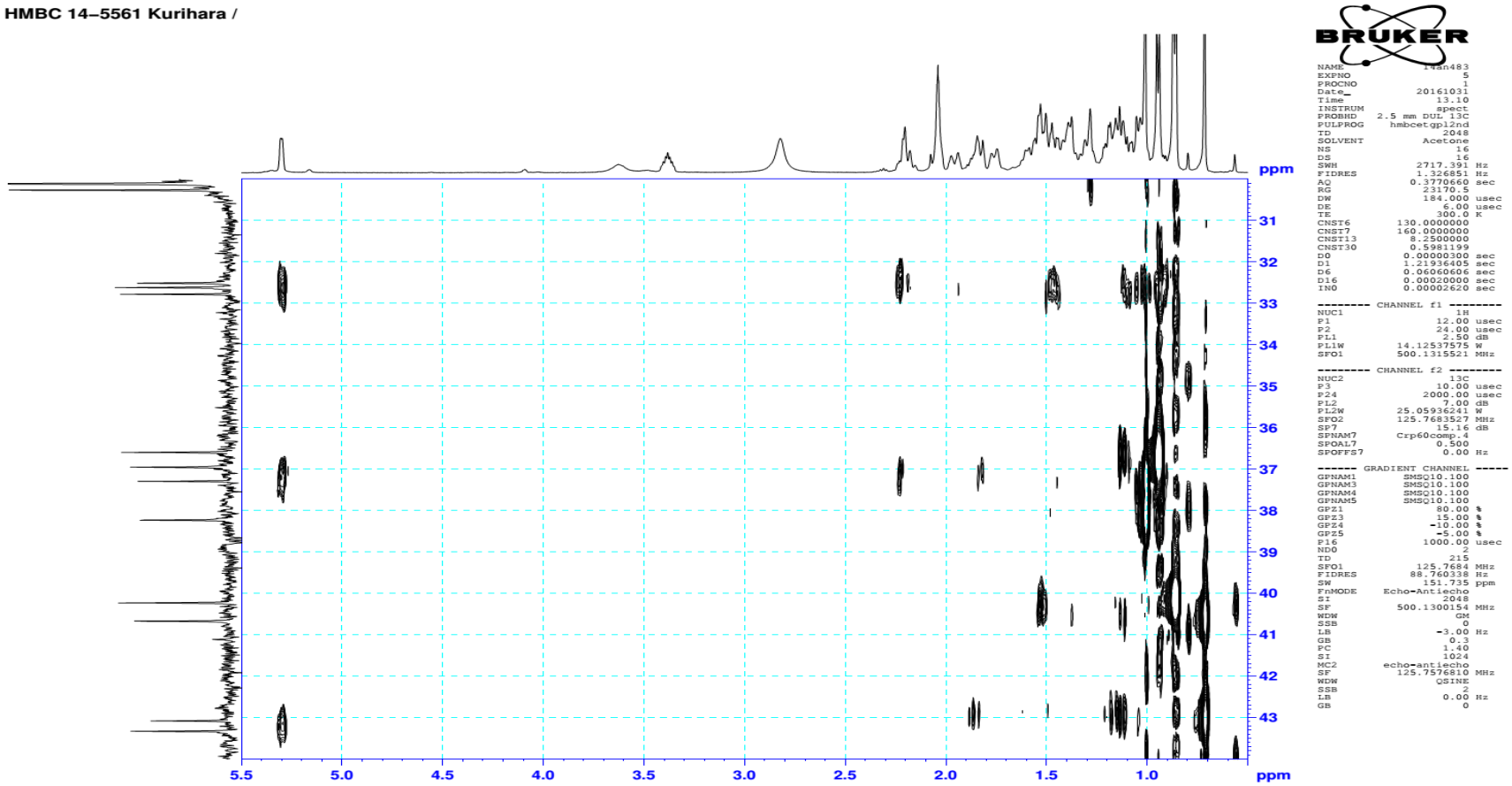


Figure 2-106. Expanded HMBC spectrum (4) of compound **A4**.

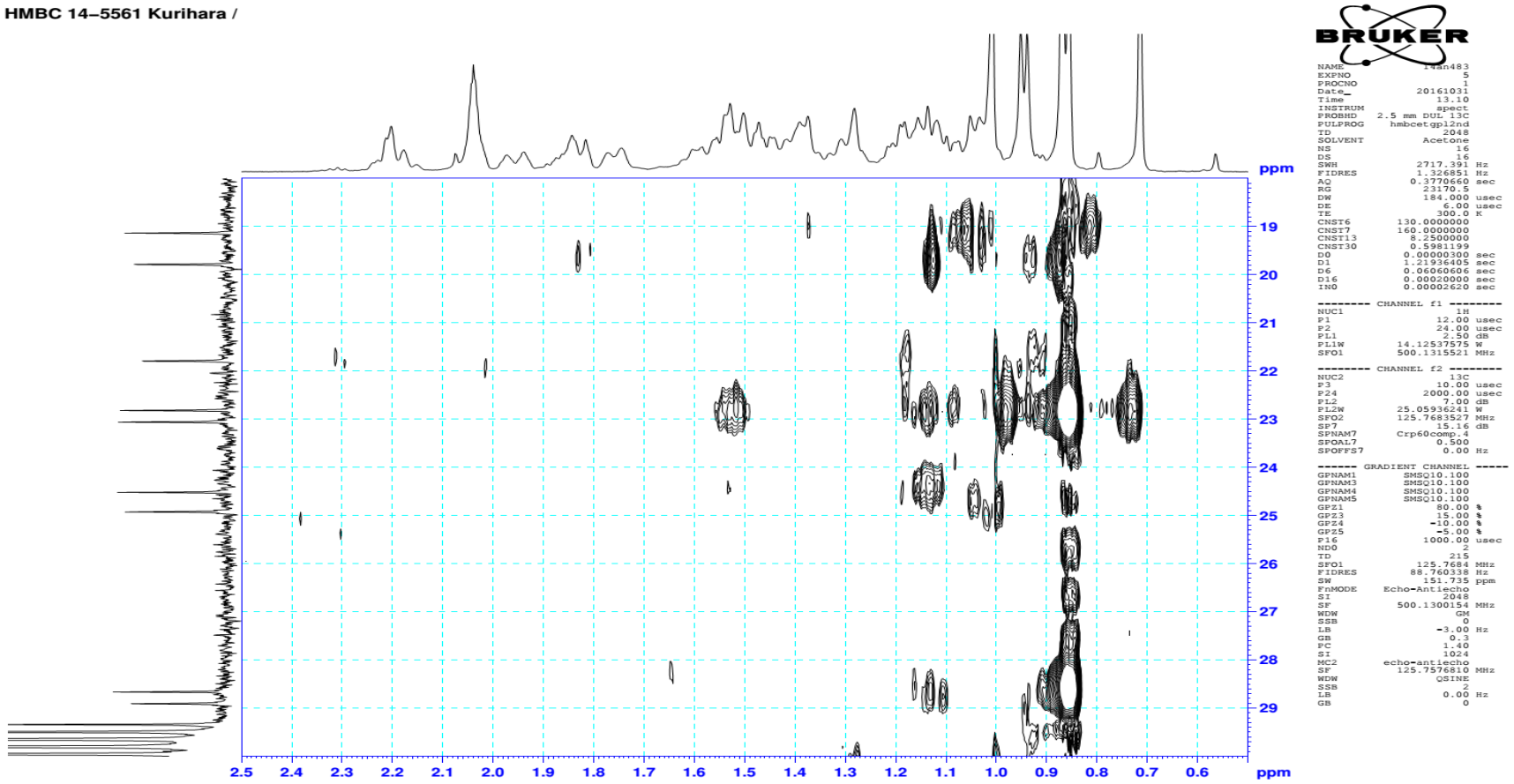


Figure 2-107. Expanded HMBC spectrum (5) of compound **A4**.

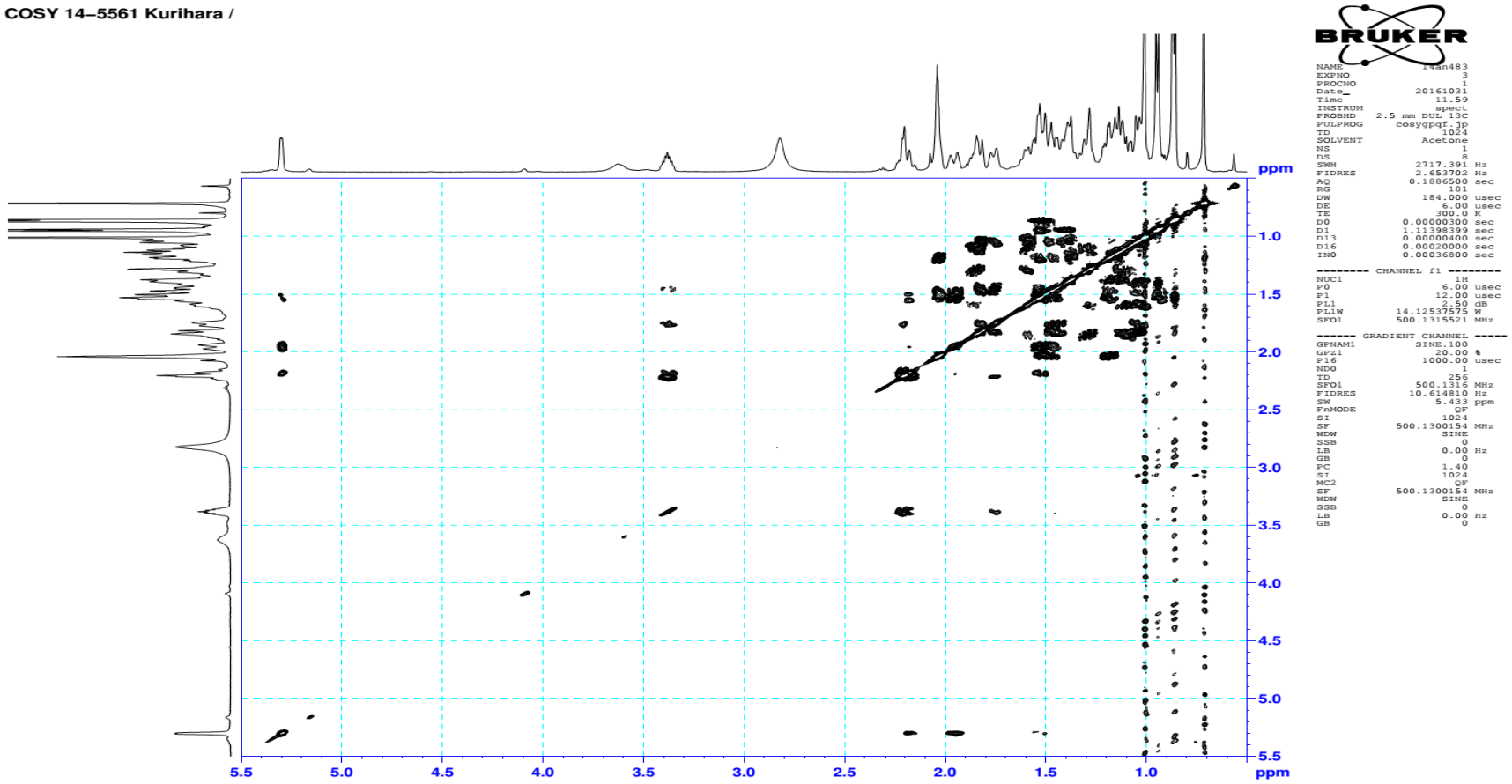


Figure 2-108. COSY spectrum of compound **A4**.

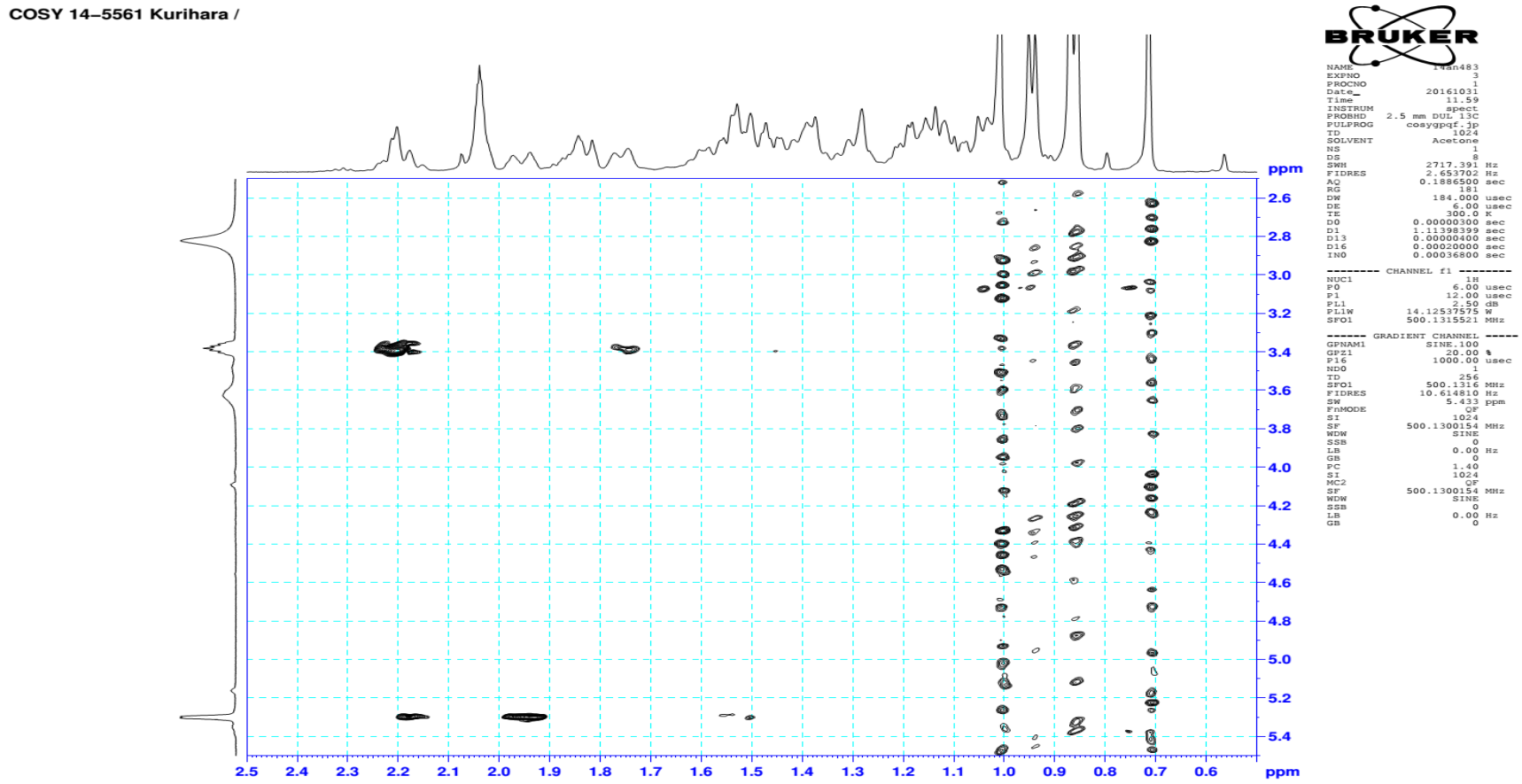


Figure 2-109.Expanded COSY spectrum (1) of compound **A4**.

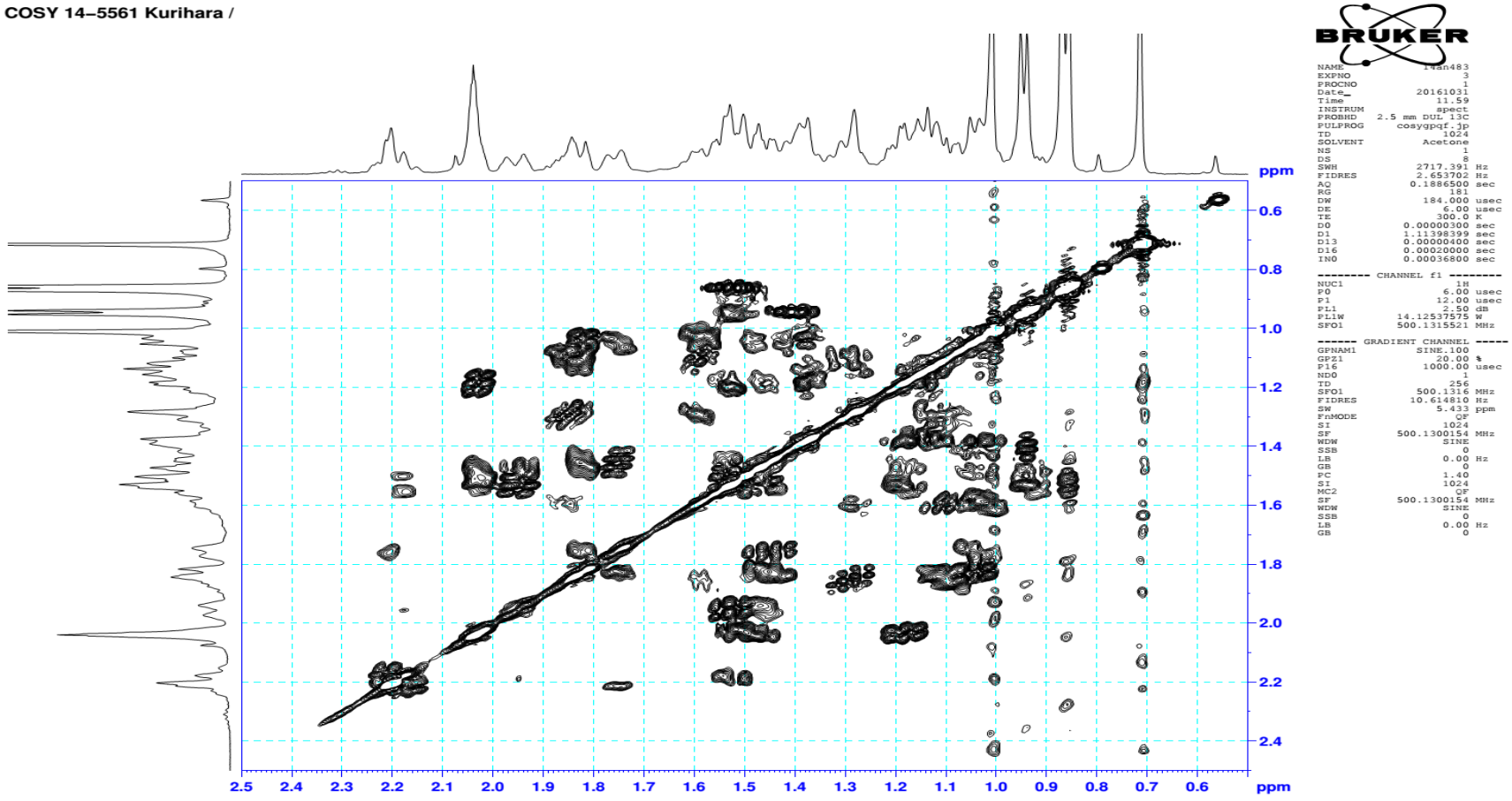


Figure 2-110. Expanded COSY spectrum (2) of compound **A4**.

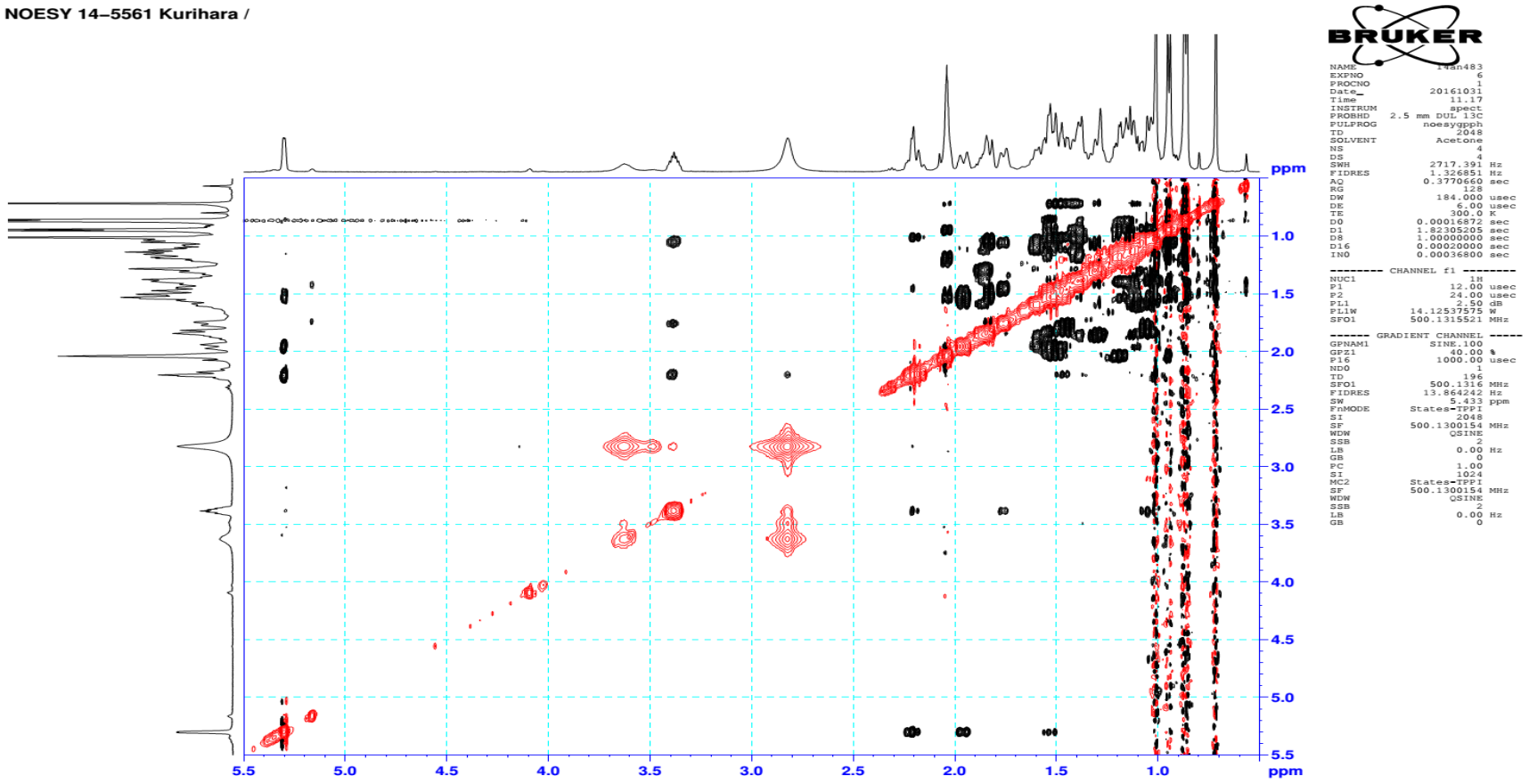


Figure 2-111. NOESY spectrum of compound **A4**.

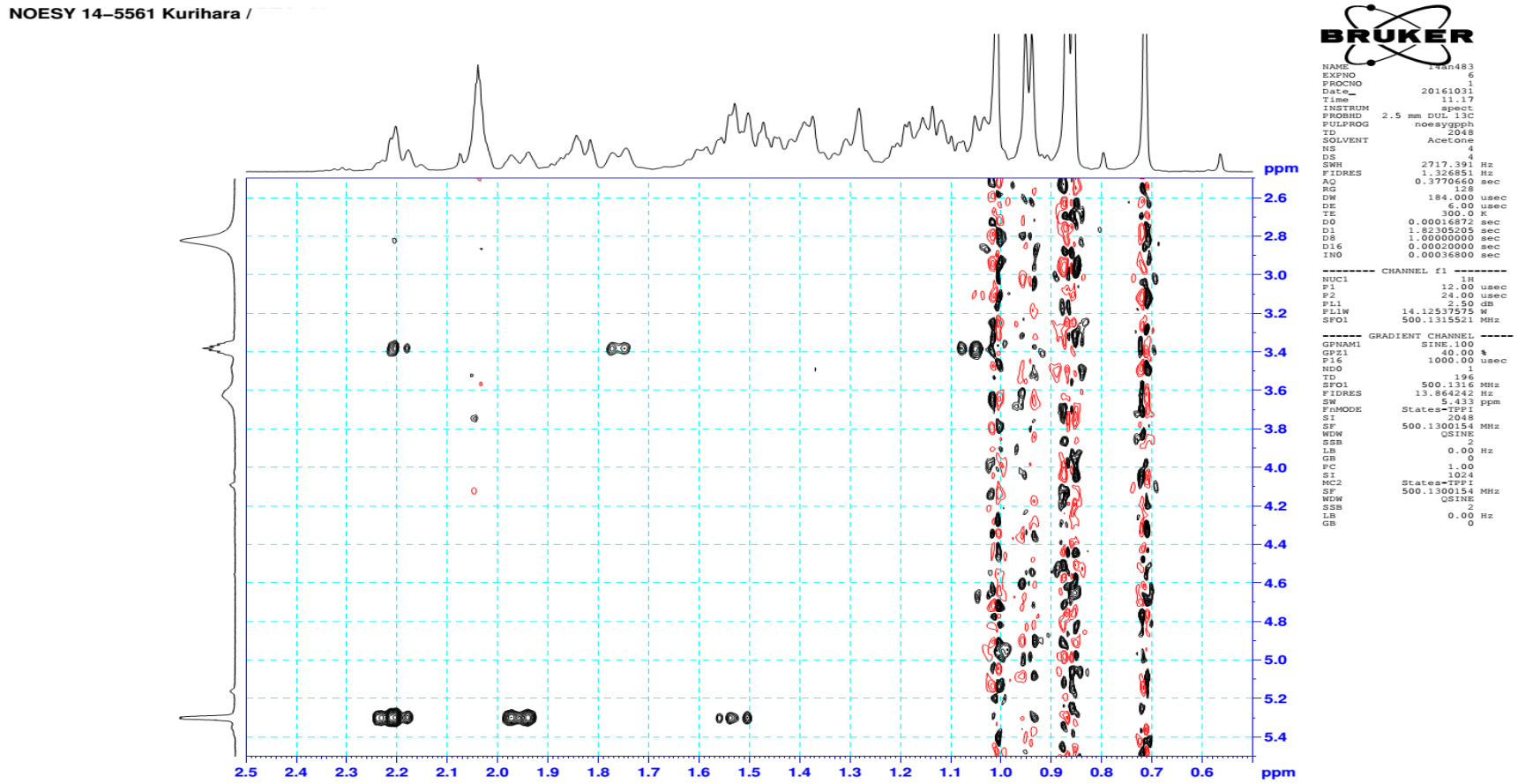


Figure 2-112. Expanded NOESY spectrum (1) of compound **A4**.

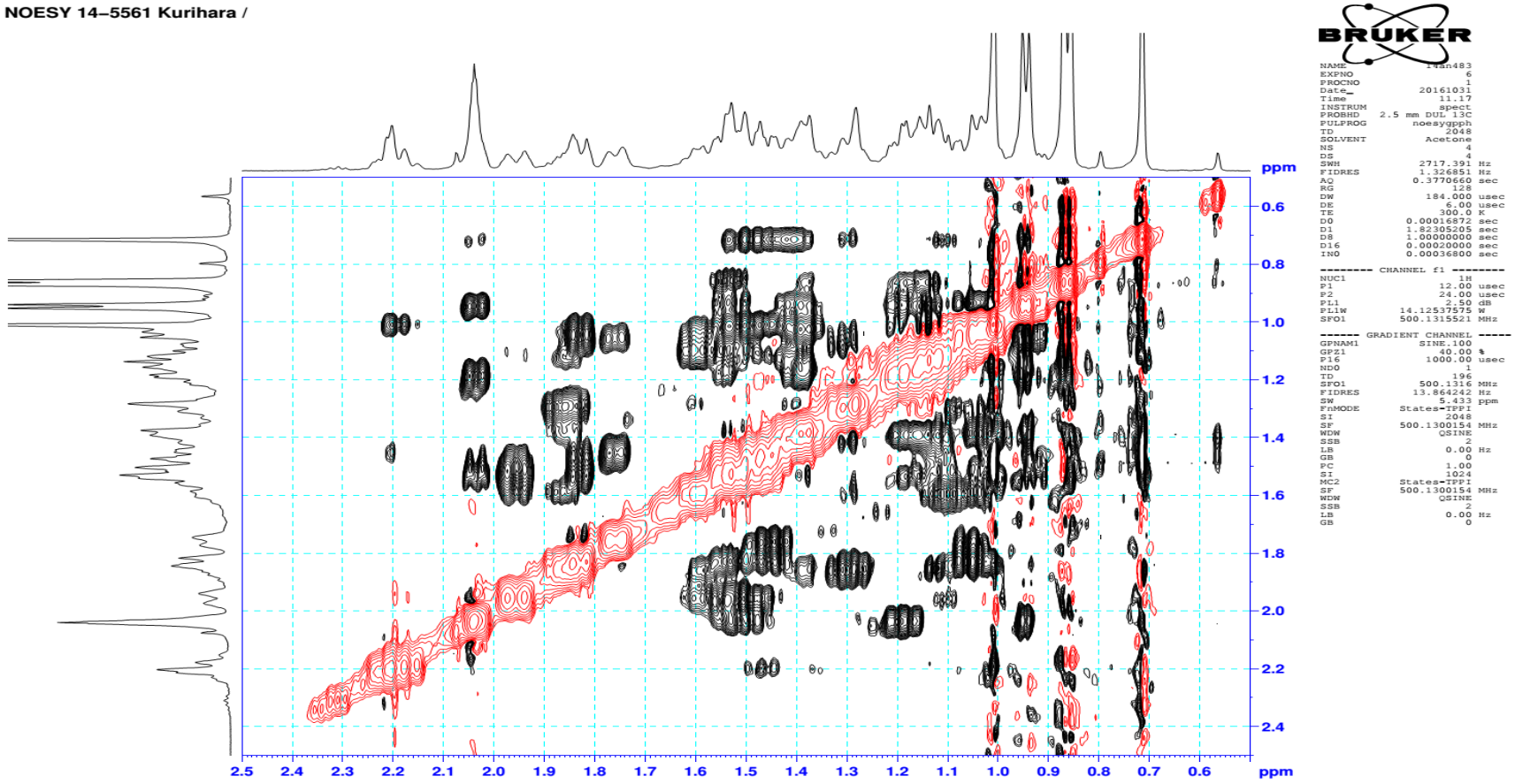


Figure 2-113. Expanded NOESY spectrum (2) of compound **A4**.

Table 2-33. Comparison of NMR data between compound **A4**[a] and literature[b]

	^{1}H NMR	^{13}C NMR	
Position	**A4**	**A4**	Literature data
1	1.82 (m, 1H); 1.04 (m, 1H)	38.2	37.2
2	1.43 (m, 1H); 1.75 (m, 1H)	32.5	31.6
3	3.38 (m, 1H)	71.7	71.8
4	2.17 (m, 2H)	43.3	42.2
5		142.3	140.8
6	5.30 (d, 6.8, 1H)	121.5	121.7
7	1.94 (m, 1H); 1.52 (m, 1H)	32.6	31.9
8	1.51 (m, 1H)	32.8	31.9
9	0.92 (m, 1H)	51.2	50.2
10		37.3	36.4
11	1.47 (m, 1H); 1.50 (m, 1H)	21.8	21.1
12	1.84 (m, 1H); 1.27 (m, 1H)	28.9	28.2
13		43.1	42.3
14	1.01 (m, 1H)	57.7	56.8
15	1.58 (m, 1H); 1.06 (m, 1H)	25.0	24.2
16	2.04 (m, 1H); 1.06 (m, 1H)	40.7	39.8
17	1.11 (m, 1H)	57.0	56.1
18	0.71 (s, 3H)	12.2	12.0
19	1.00 (s, 3H)	19.8	19.3
20	1.42 (m, 1H)	36.6	35.8

(To be continued)

(Continued)

	^{1}H NMR	^{13}C NMR	
Position	**A4**	**A4**	Literature data
21	0.94 (d, 6.4, 3H)	19.1	18.7
22	1.37 (m, 1H); 1.01 (m, 1H)	37.0	36.2
23	1.38 (m, 1H); 1.18 (m, 1H)	24.5	23.8
24	1.12 (m, 2H)	40.2	39.5
25	1.51 (m, 1H)	28.7	28.0
26	0.86 (d, 6.5, 3H)	22.8	22.7
27	0.86 (d, 6.5, 3H)	23.1	22.6

[a]The NMR data were measured in acetone-d_6 (δ_H 2.03 ppm; δ_C CO 206.1, CH_3 30.0 ppm) at 500 MHz for ^{1}H and at 125 MHz for ^{13}C.

[b]Nasir et al., 2011.

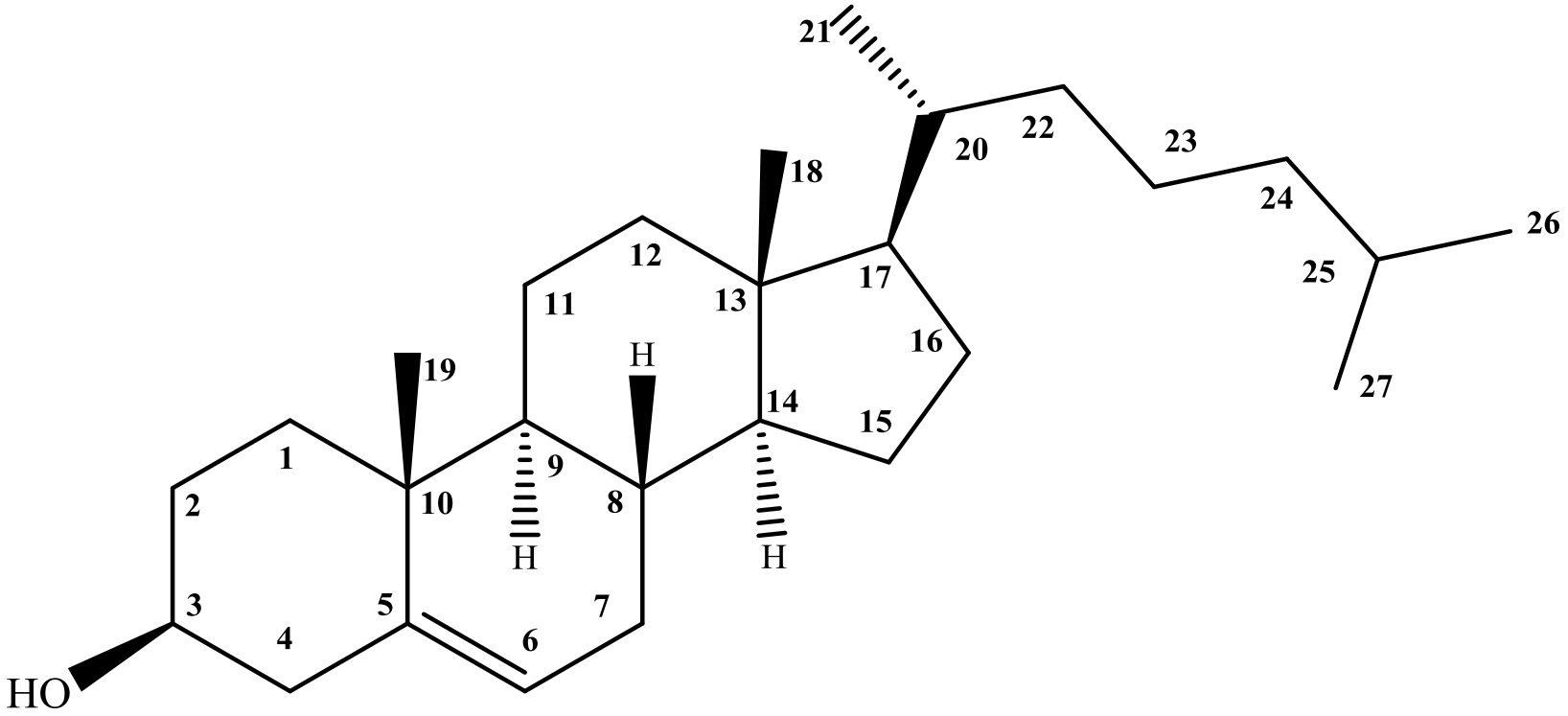


Figure 2-114. Structure of compound **A4**.

2.3.2.4 Structural elucidation of β-glucuronidase inhibitor A5

FD-MS spectrum of compound **A5** showed a molecular ion peak at *m/z* 384 (Figure 2-115). Molecular formula was determined by FD-HR-MS for $C_{27}H_{44}O$ at *m/z* 384.33948 (calculated 384.33921) which is less of 2 mass units compared with cholesterol (**A4**). ^{1}H and ^{13}C NMR spectra were close to those of cholesterol (**A4**) except for appearance of one additional double bond and disappearance of two methylenes in the side chain (Figures 2-116 and 2-117). Thus, compound **A5** was identified as 22-dehydrocholesterol (Table 2-34, Figure 2-132) with assistance of 2D NMR (Figures 2-118 to 2-131) results and the comparison with literature data (Nasir et al., 2011).

Optical rotation of compound **A5** was measured as $[\alpha]_D^{27} = -41.5°$ (*c*1.32, $CHCl_3$) which displayed the same stereochemistry as the naturally occurring one (Tsuda, Sakai, Tanabe, & Kishida, 1960).

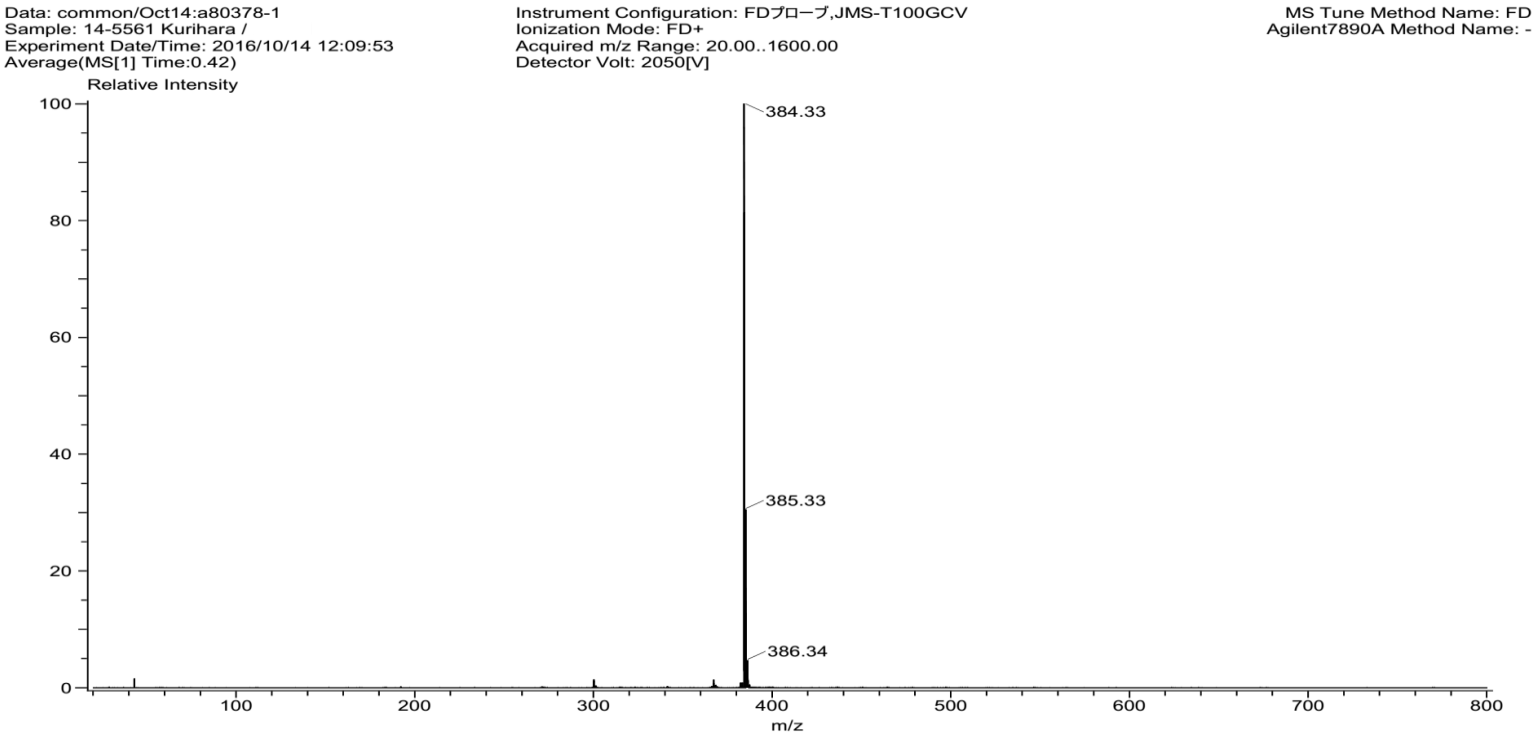


Figure 2-115. FD-MS spectrum of compound **A5**.

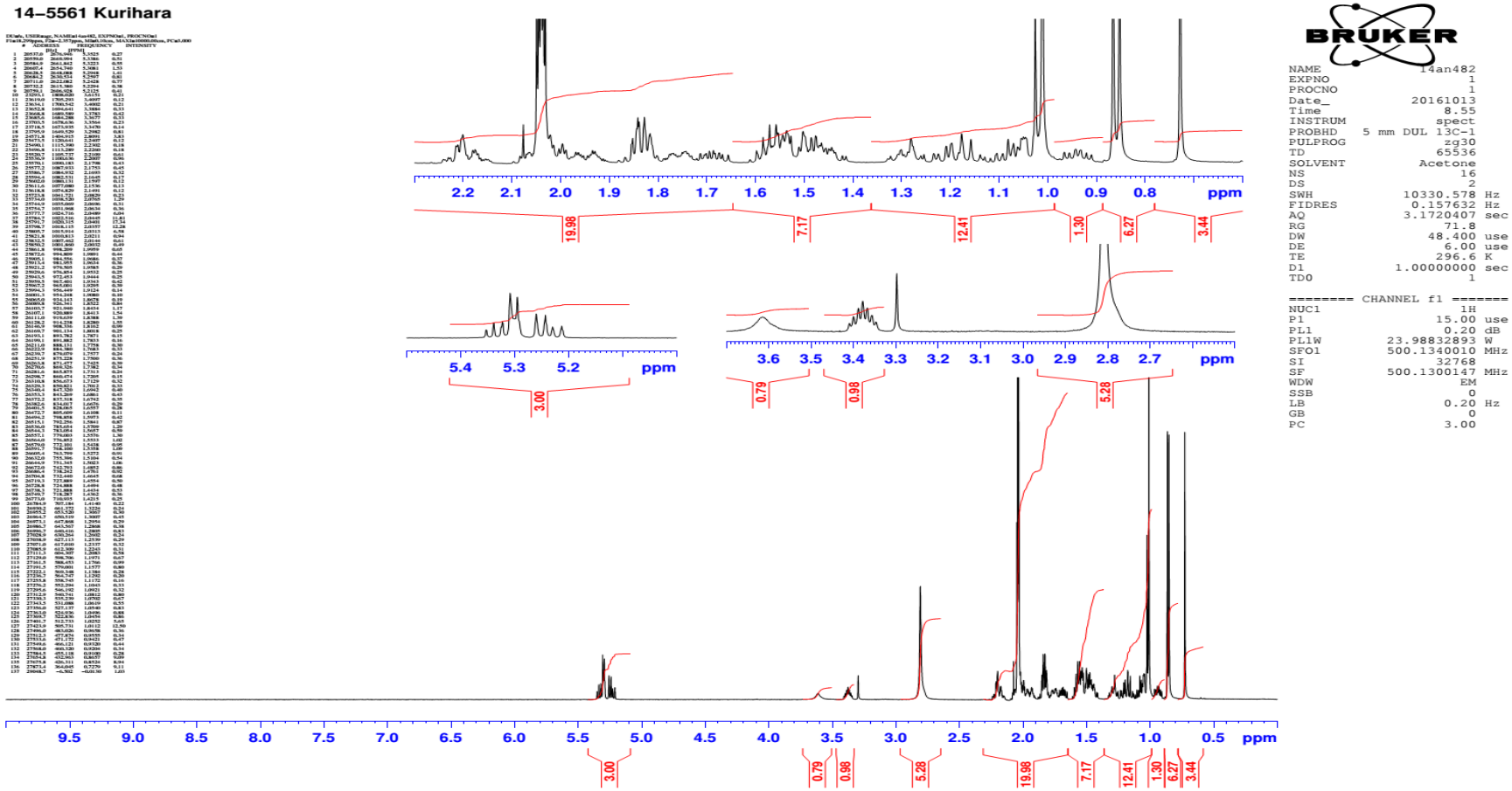


Figure 2-116. ^{1}H-NMR spectrum of compound **A5**.

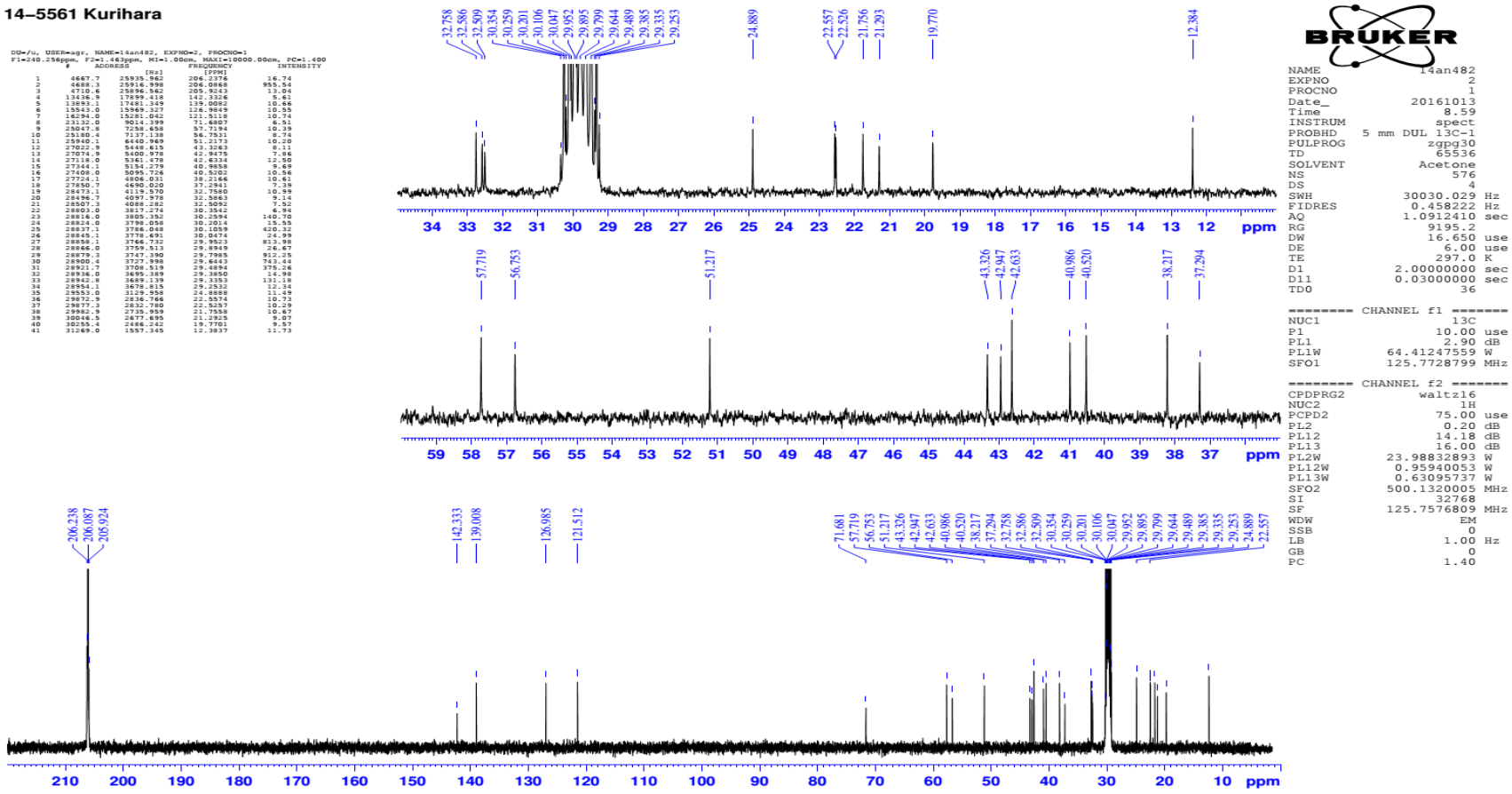


Figure 2-117. ^{13}C-NMR spectrum of compound **A5**.

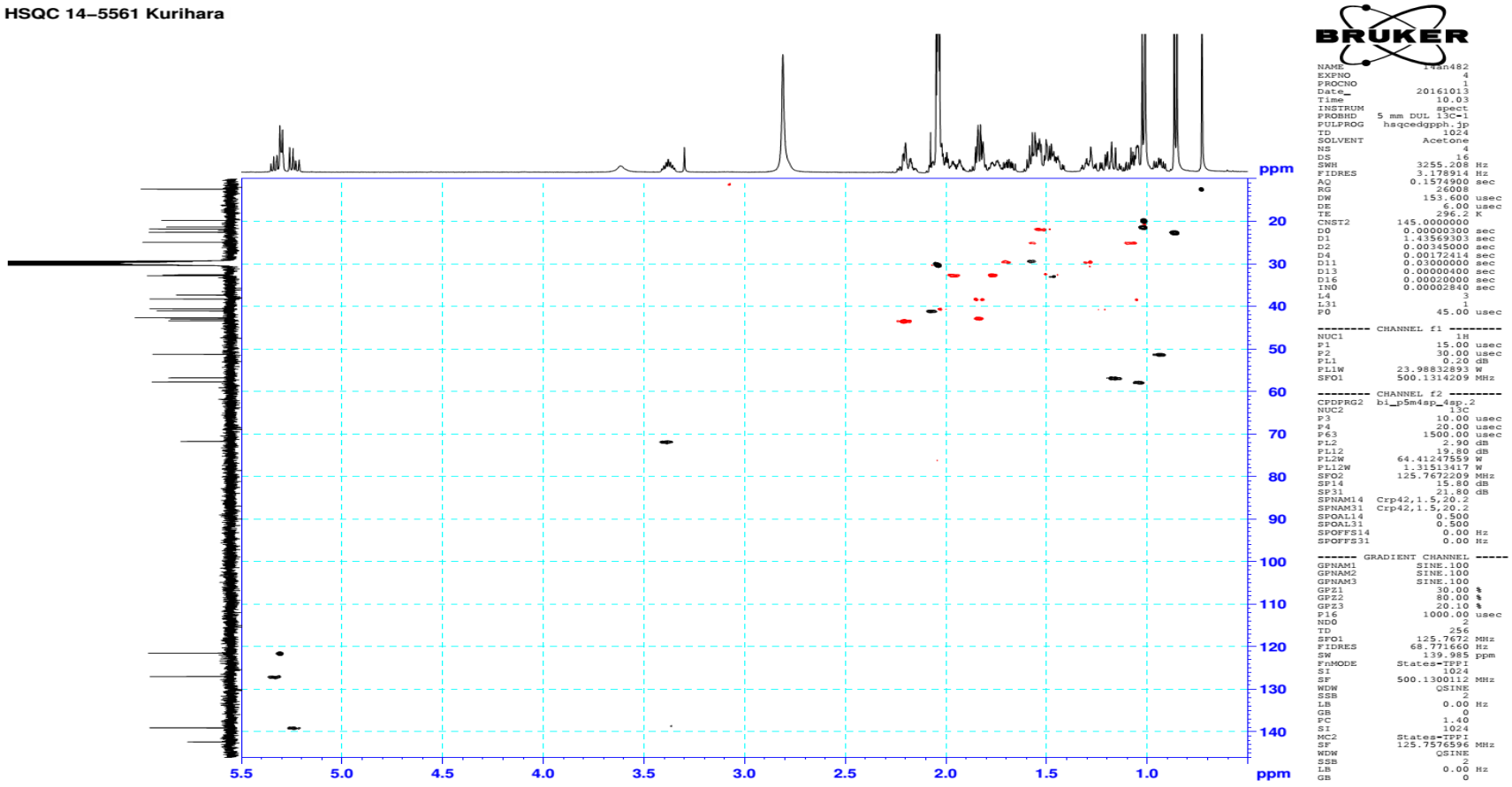


Figure 2-118. HSQC spectrum of compound **A5**.

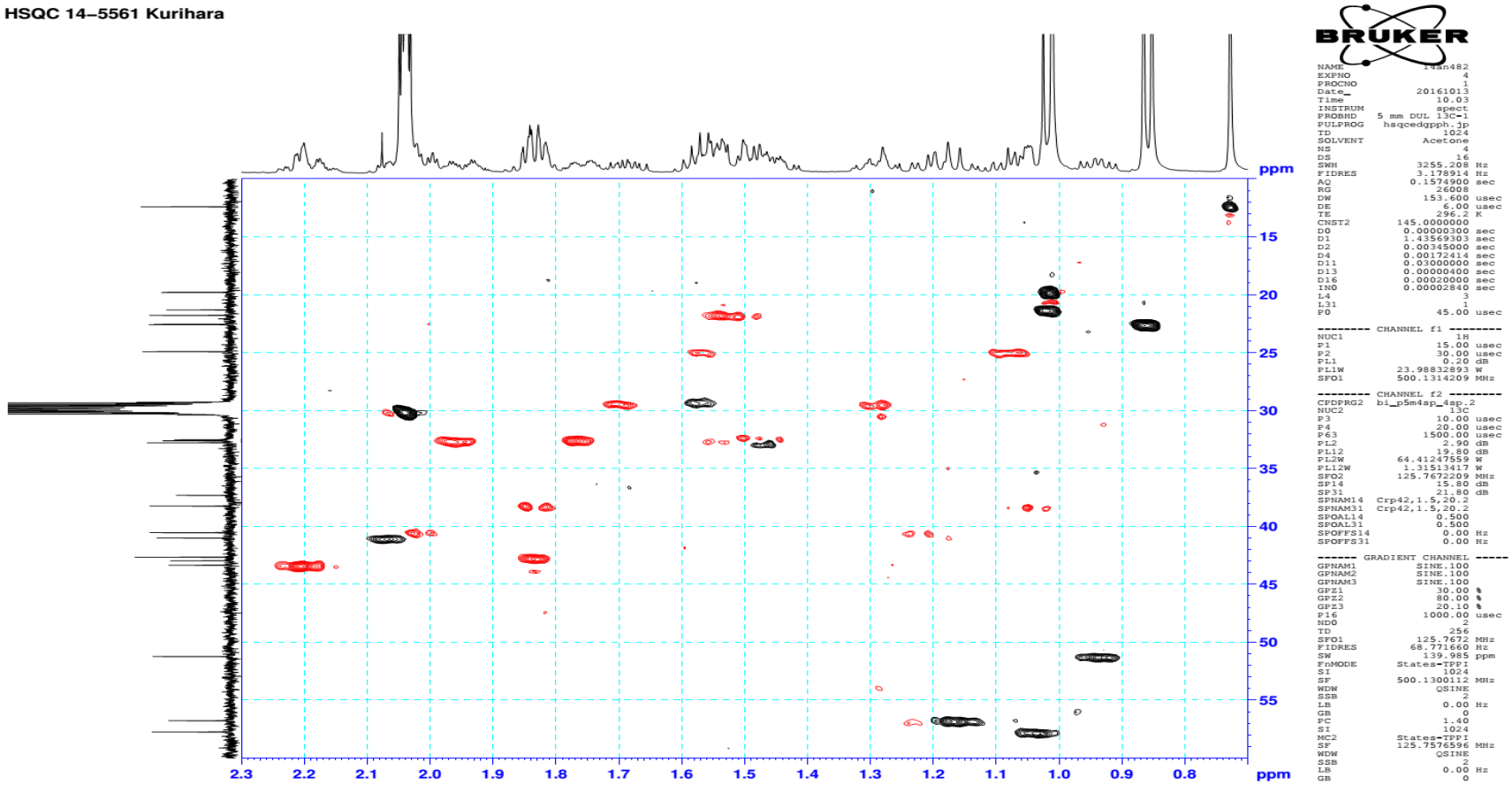


Figure 2-119. Expanded HSQC spectrum (1) of compound **A5**.

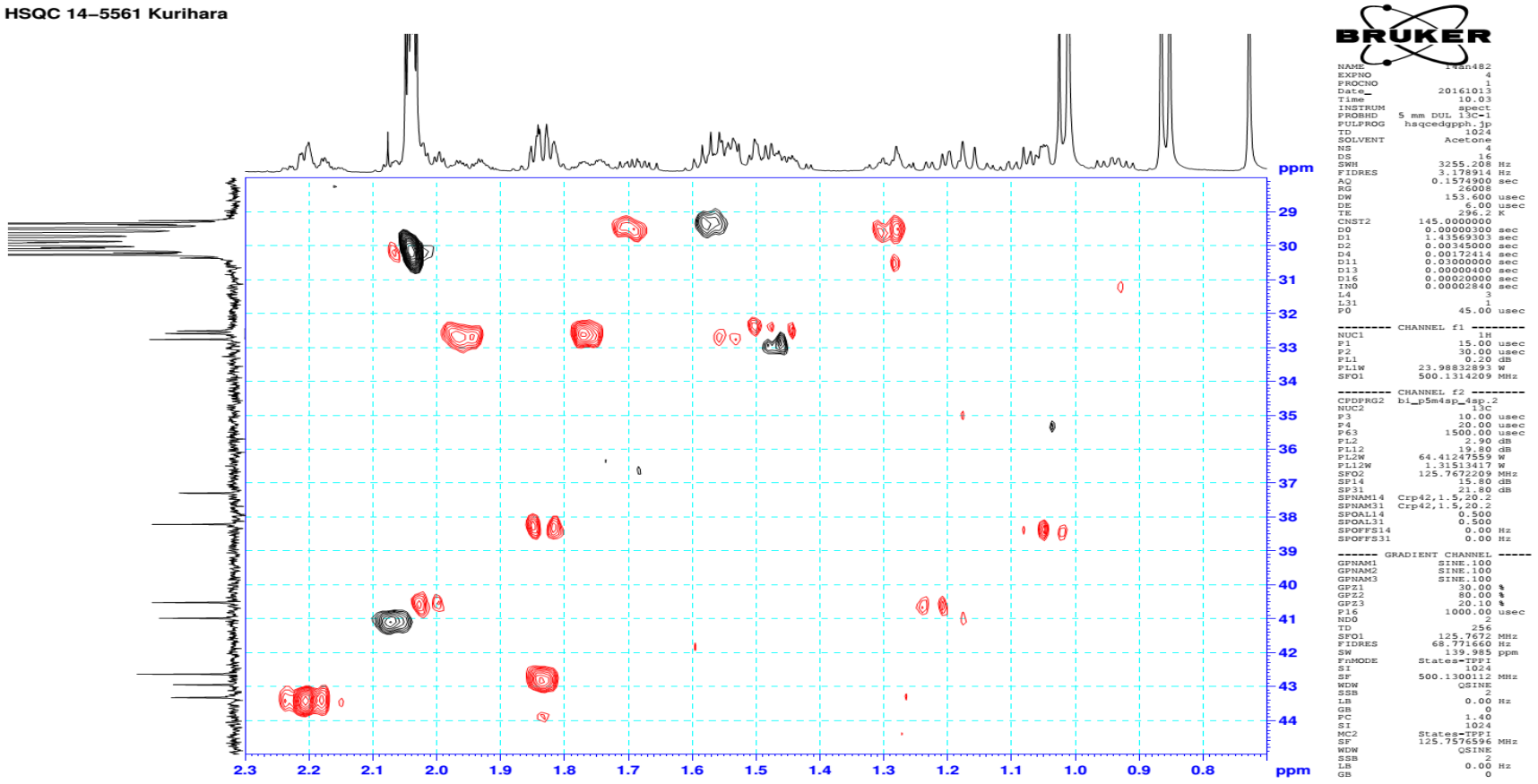


Figure 2-120. Expanded HSQC spectrum (2) of compound **A5**.

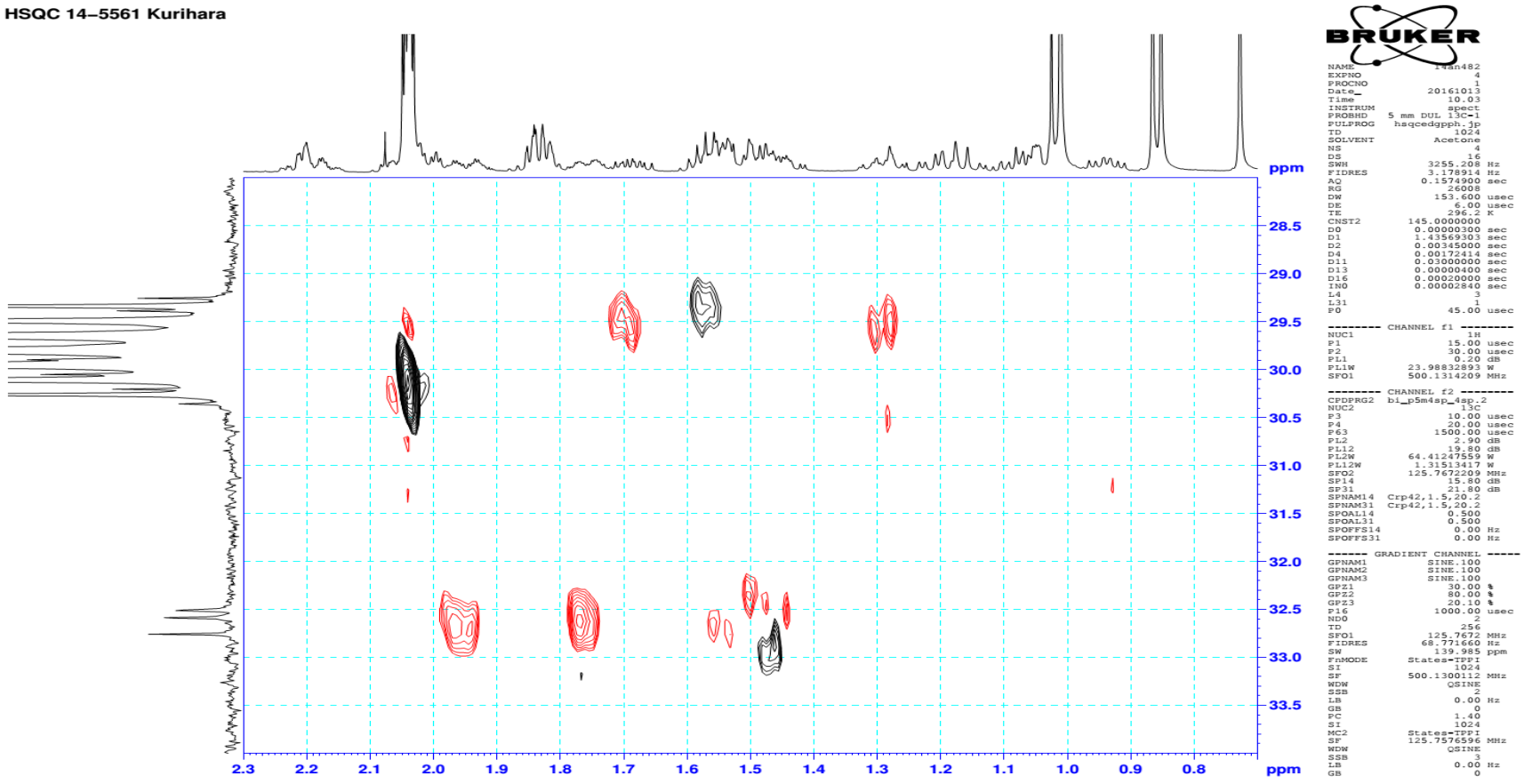


Figure 2-121. Expanded HSQC spectrum (3) of compound **A5**.

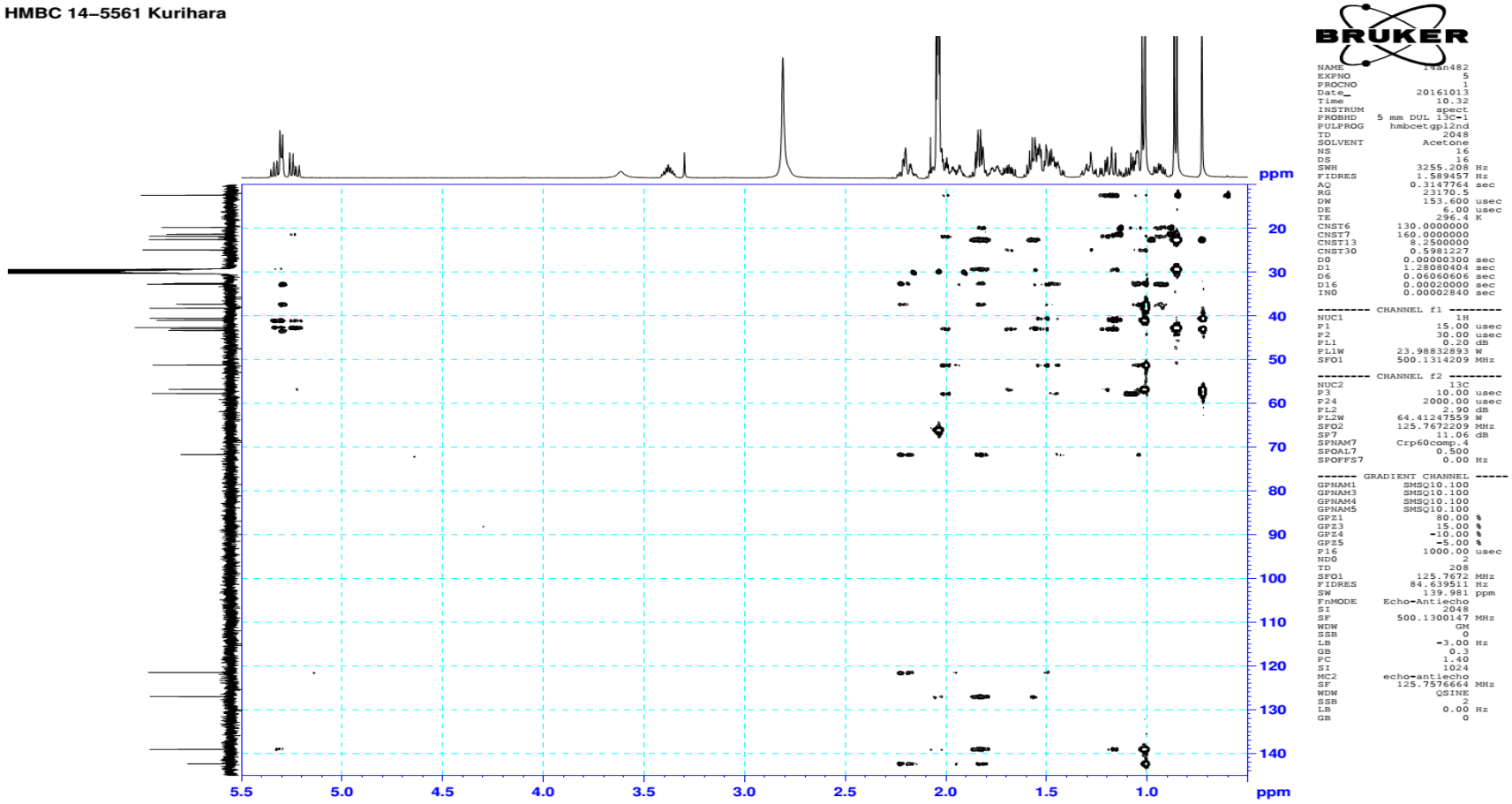


Figure 2-122. HMBC spectrum of compound **A5**.

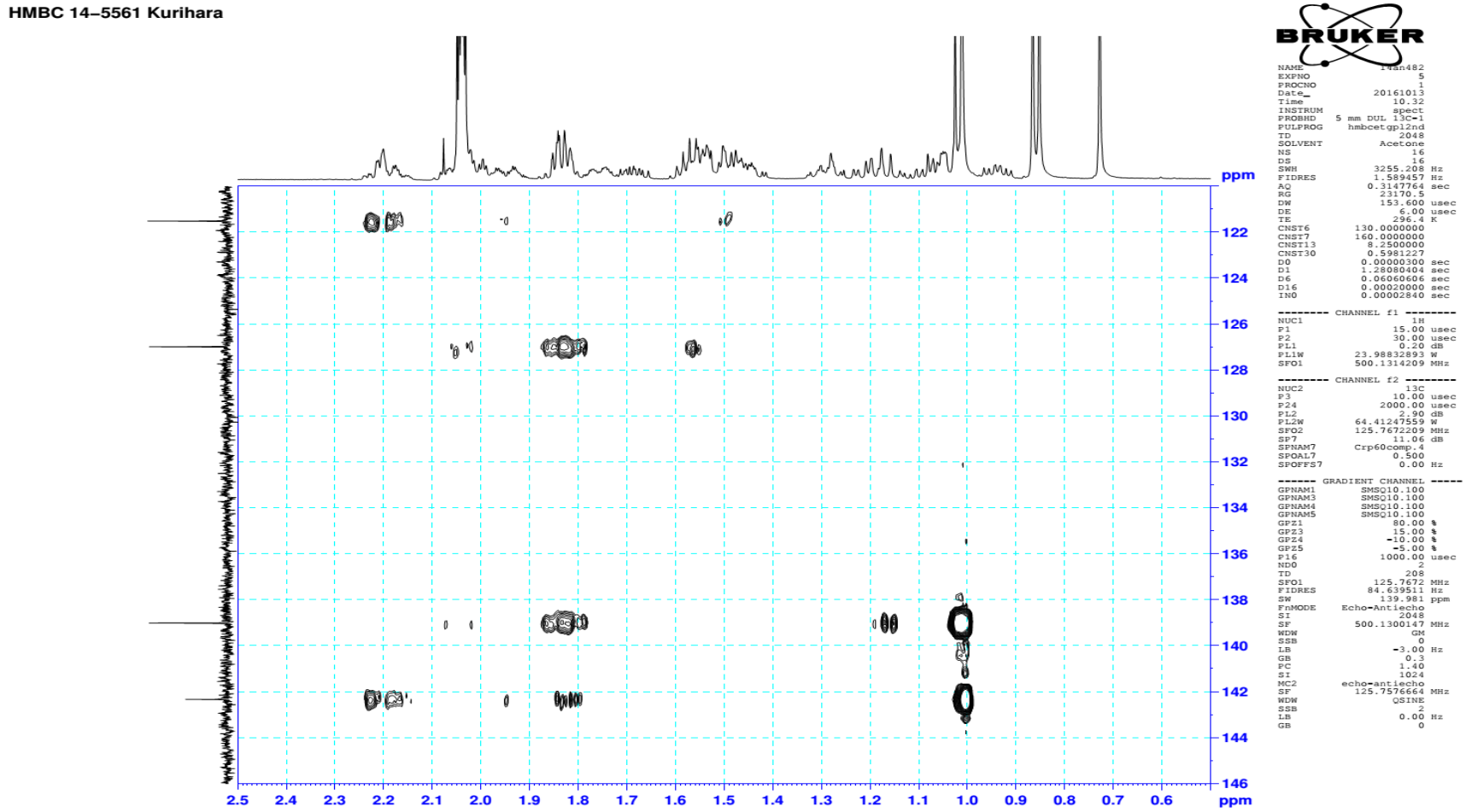


Figure 2-123. Expanded HMBC spectrum (1) of compound **A5**.

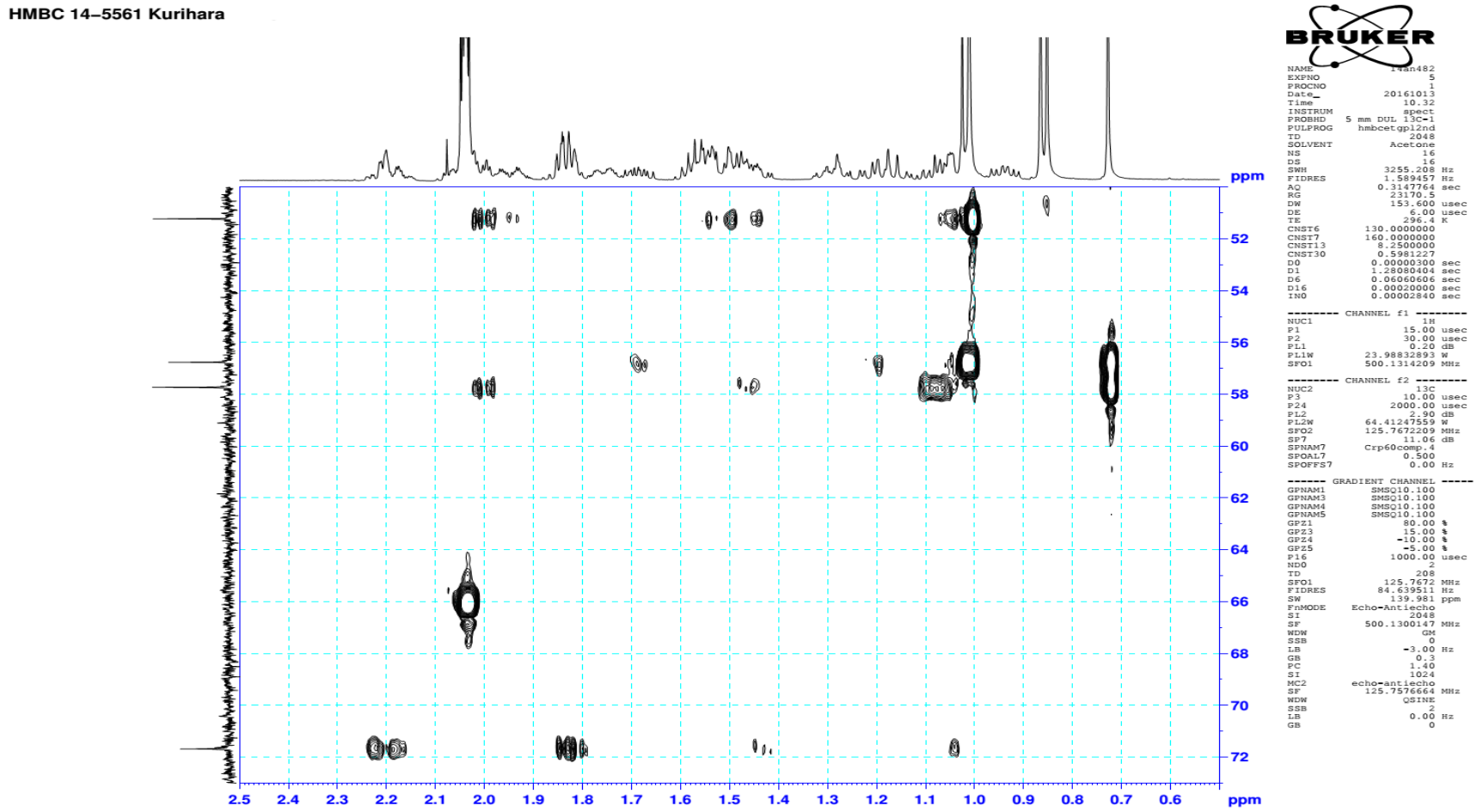


Figure 2-124. Expanded HMBC spectrum (2) of compound **A5**.

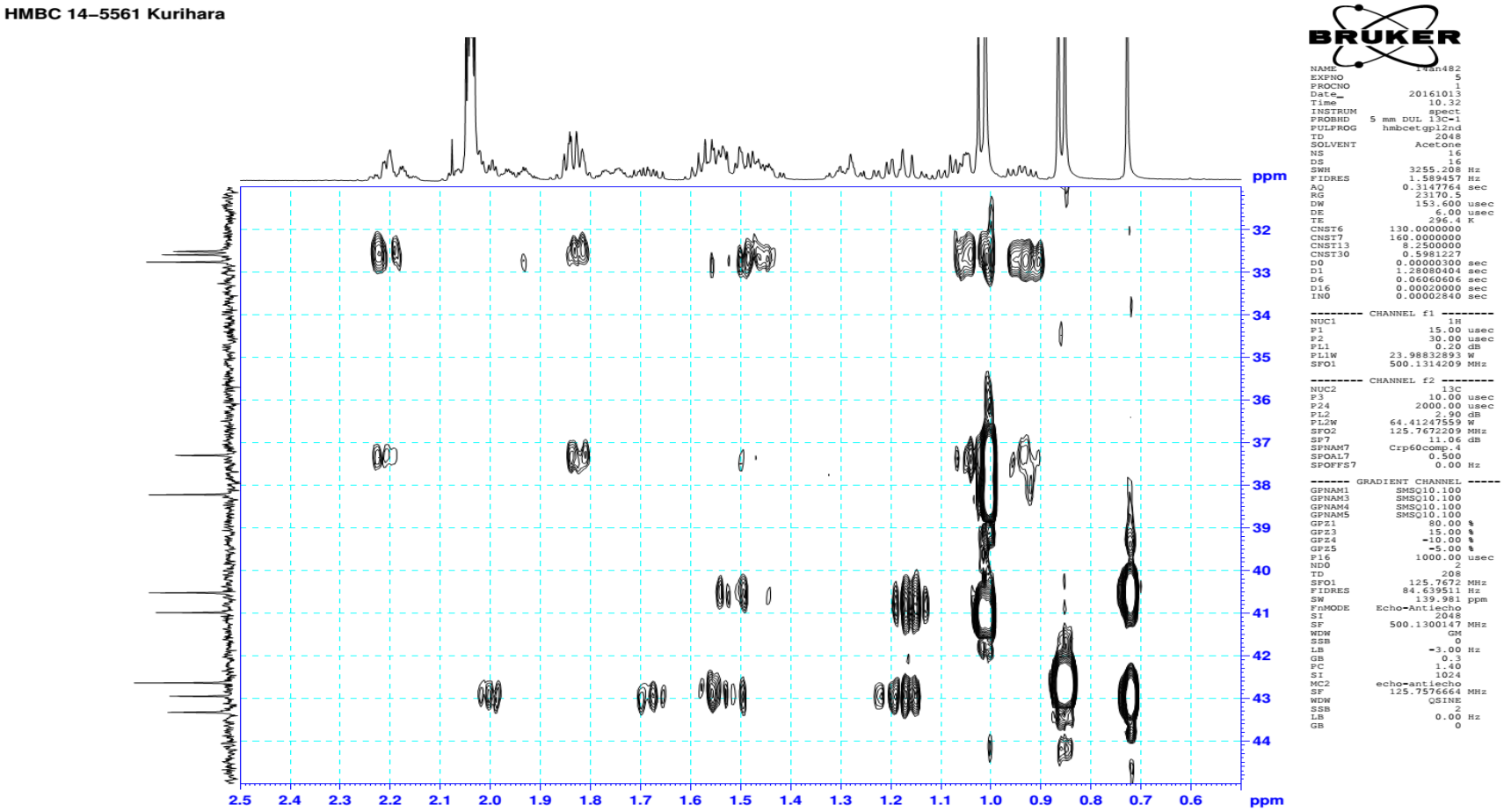


Figure 2-125. Expanded HMBC spectrum (3) of compound **A5**.

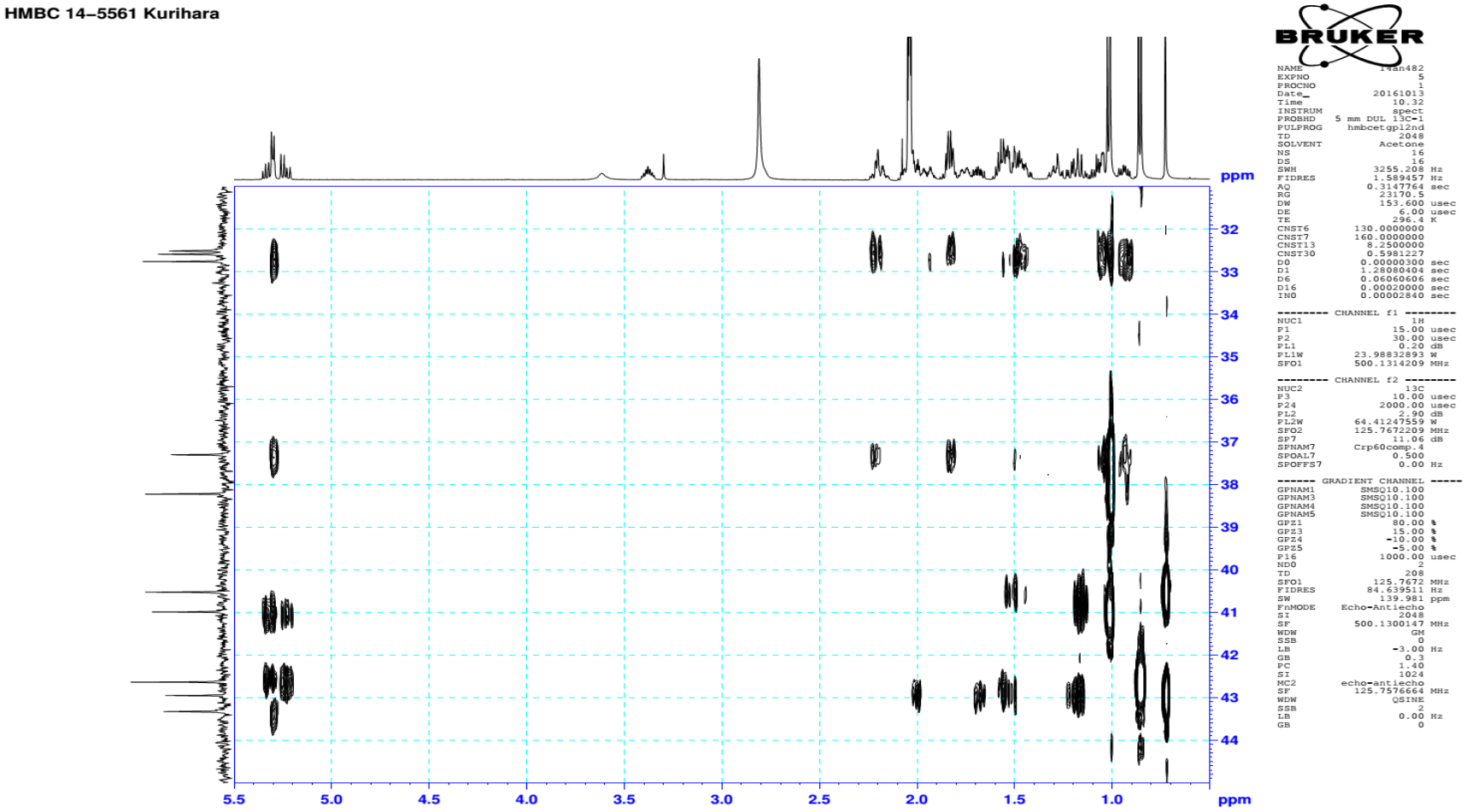


Figure 2-126. Expanded HMBC spectrum (4) of compound **A5**.

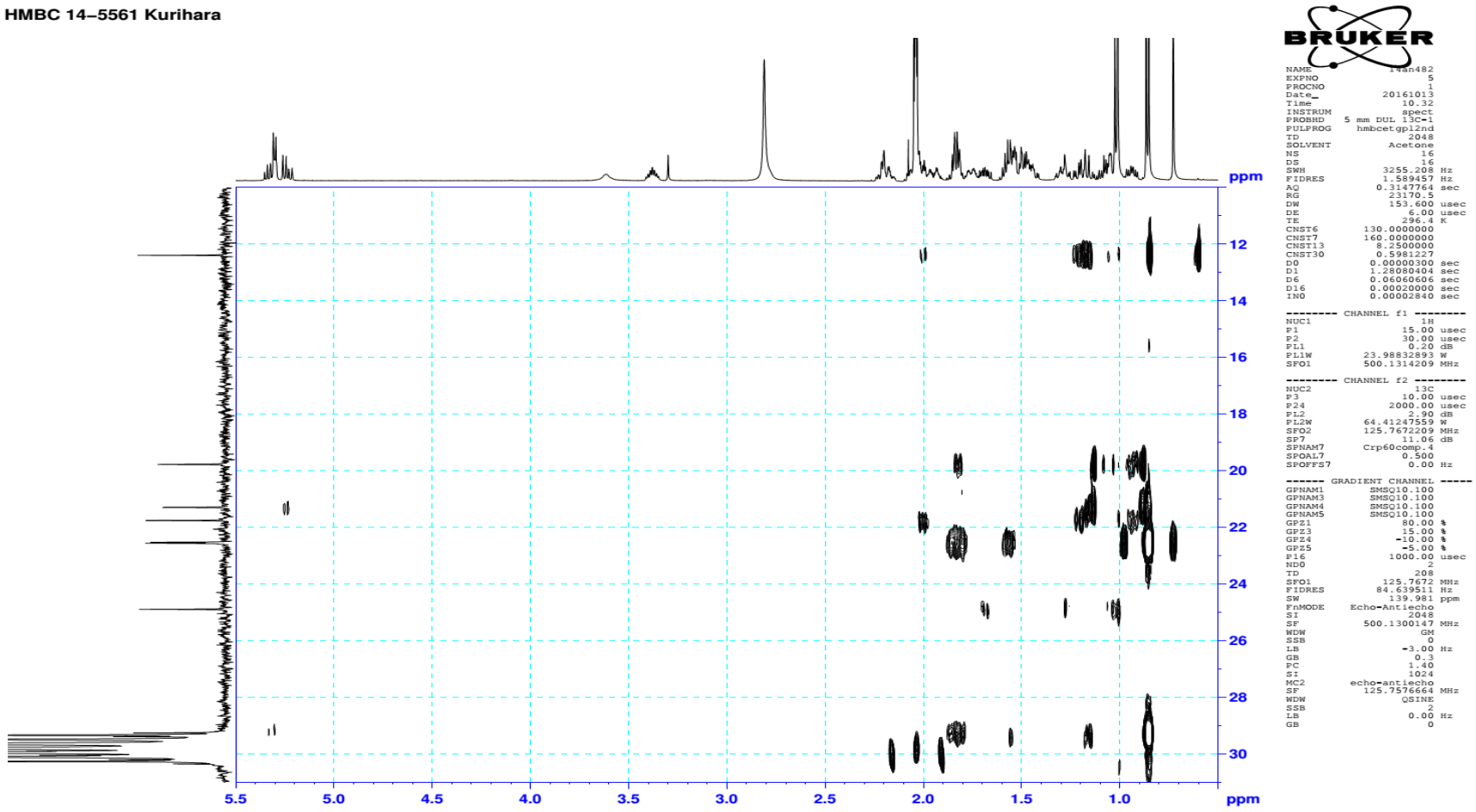


Figure 2-127. Expanded HMBC spectrum (5) of compound **A5**.

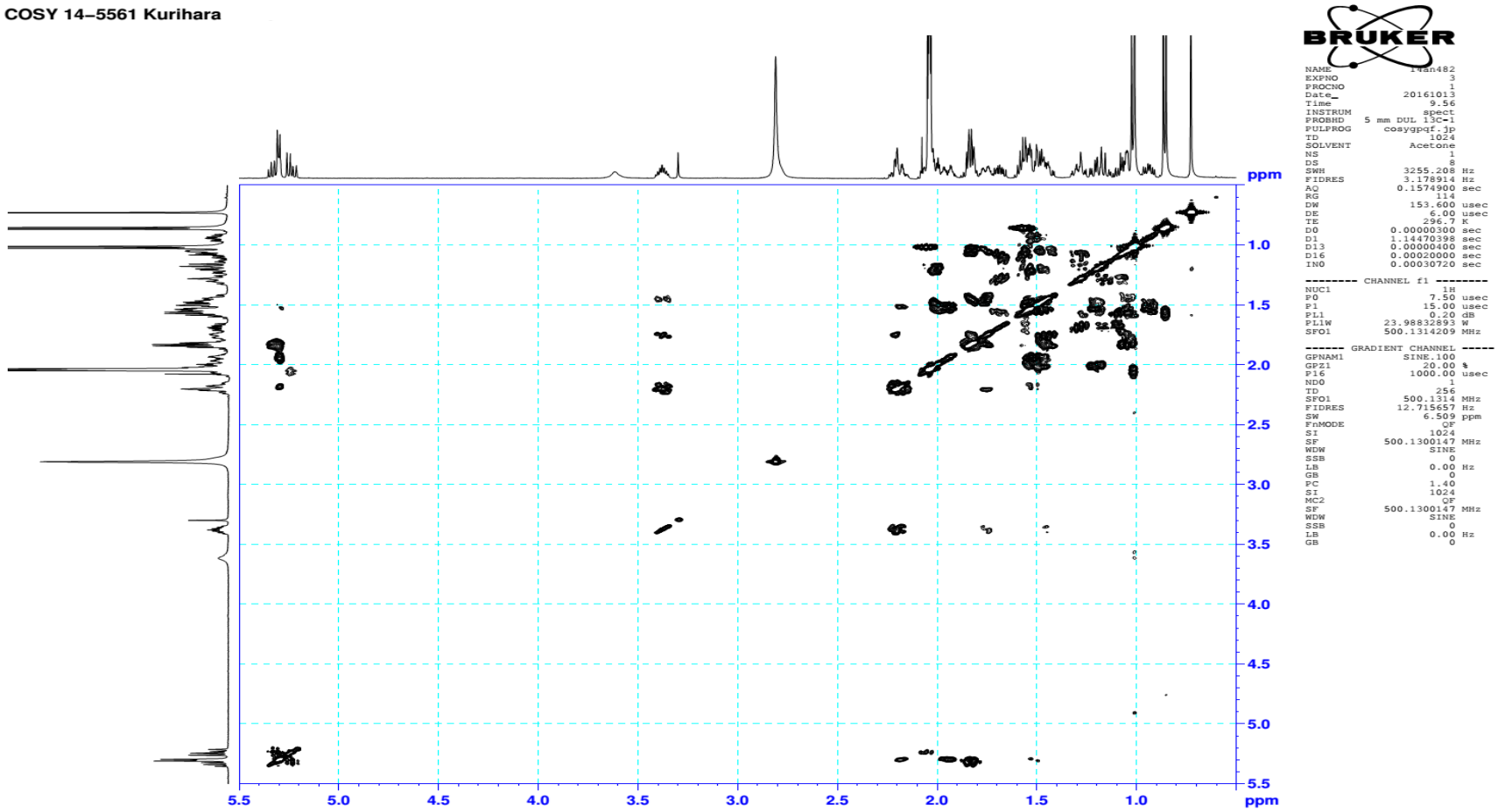


Figure 2-128. COSY spectrum of compound **A5**.

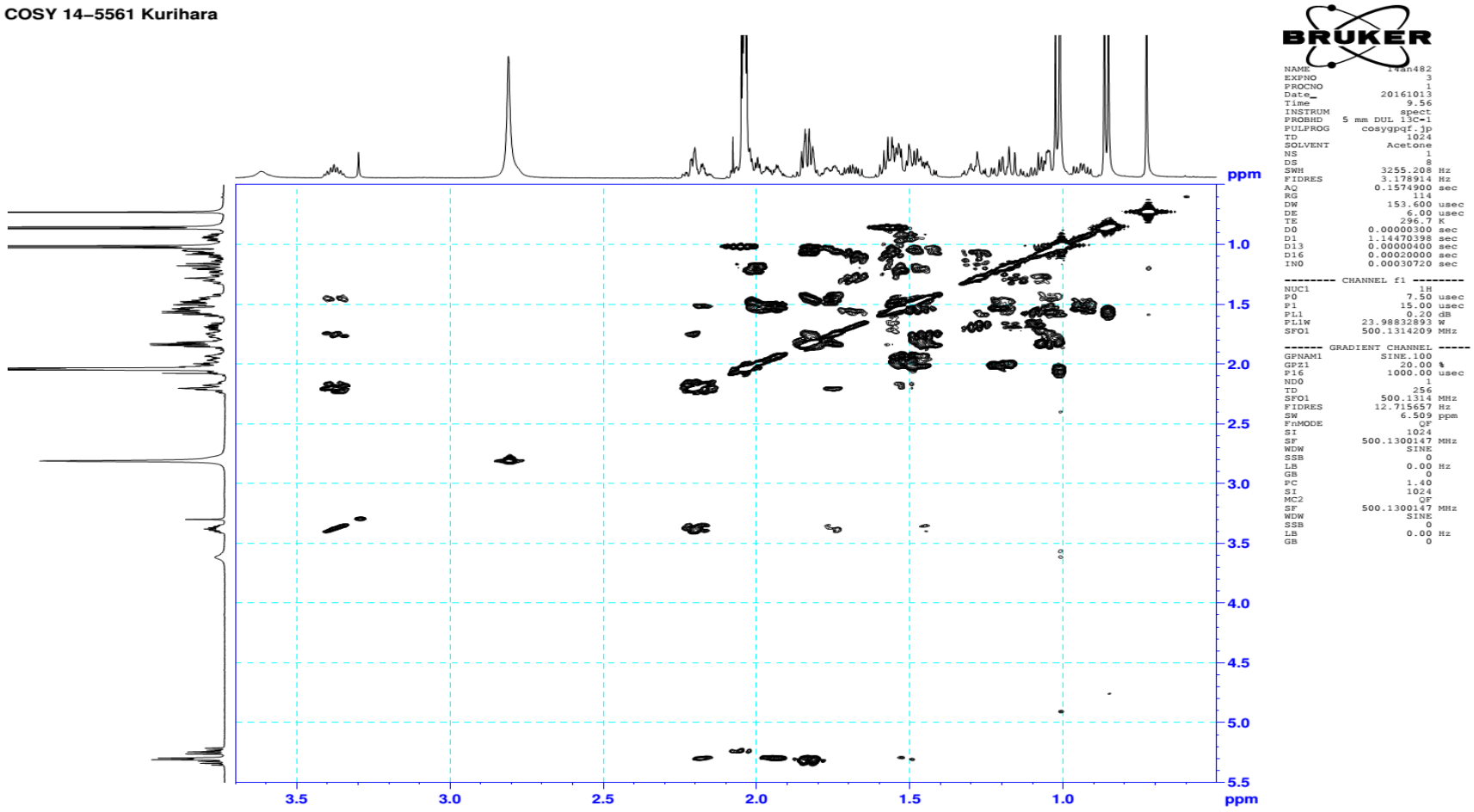


Figure 2-129. Expanded COSY spectrum (1) of compound **A5**.

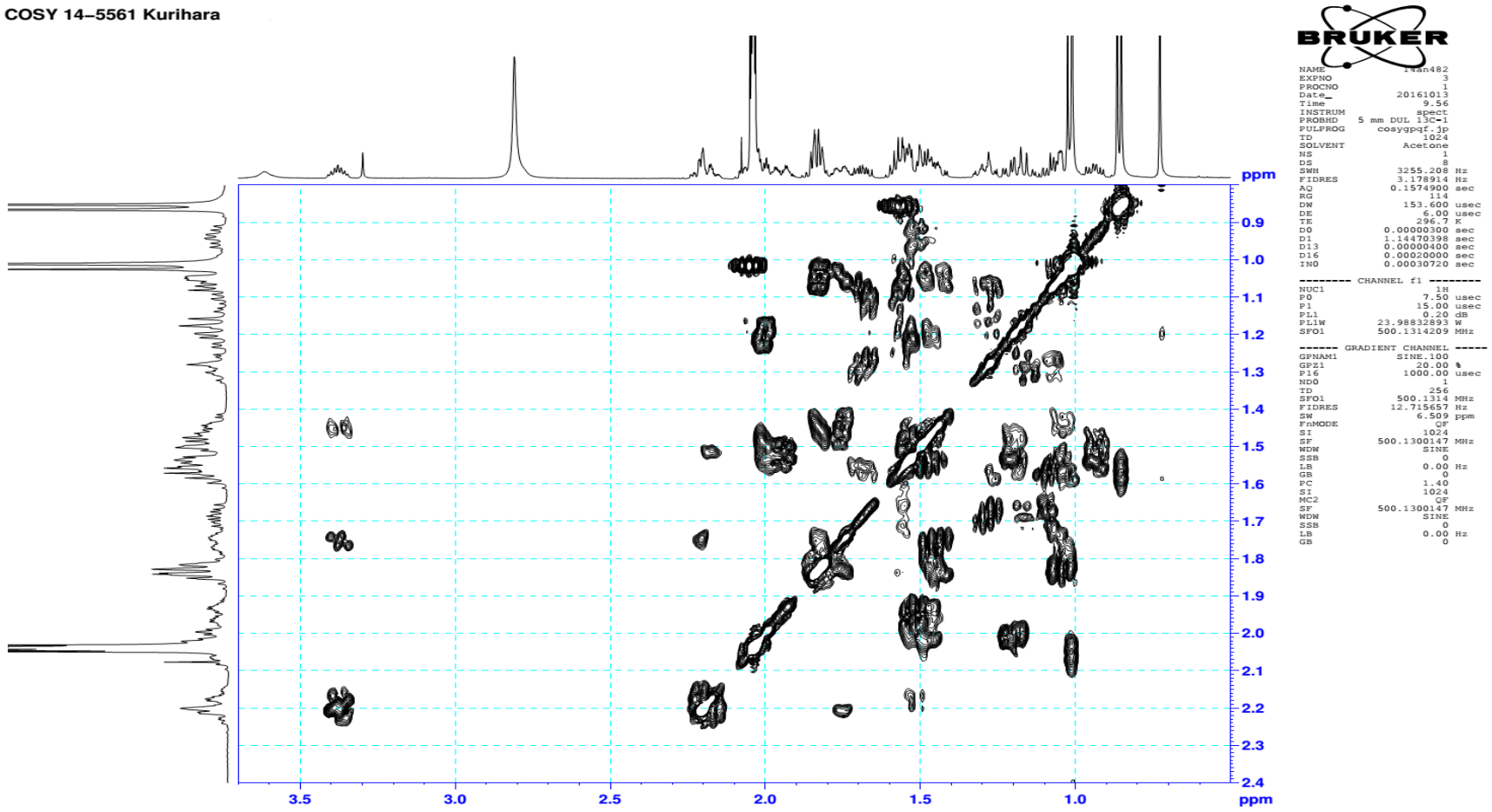


Figure 2-130. Expanded COSY spectrum (2) of compound **A5**.

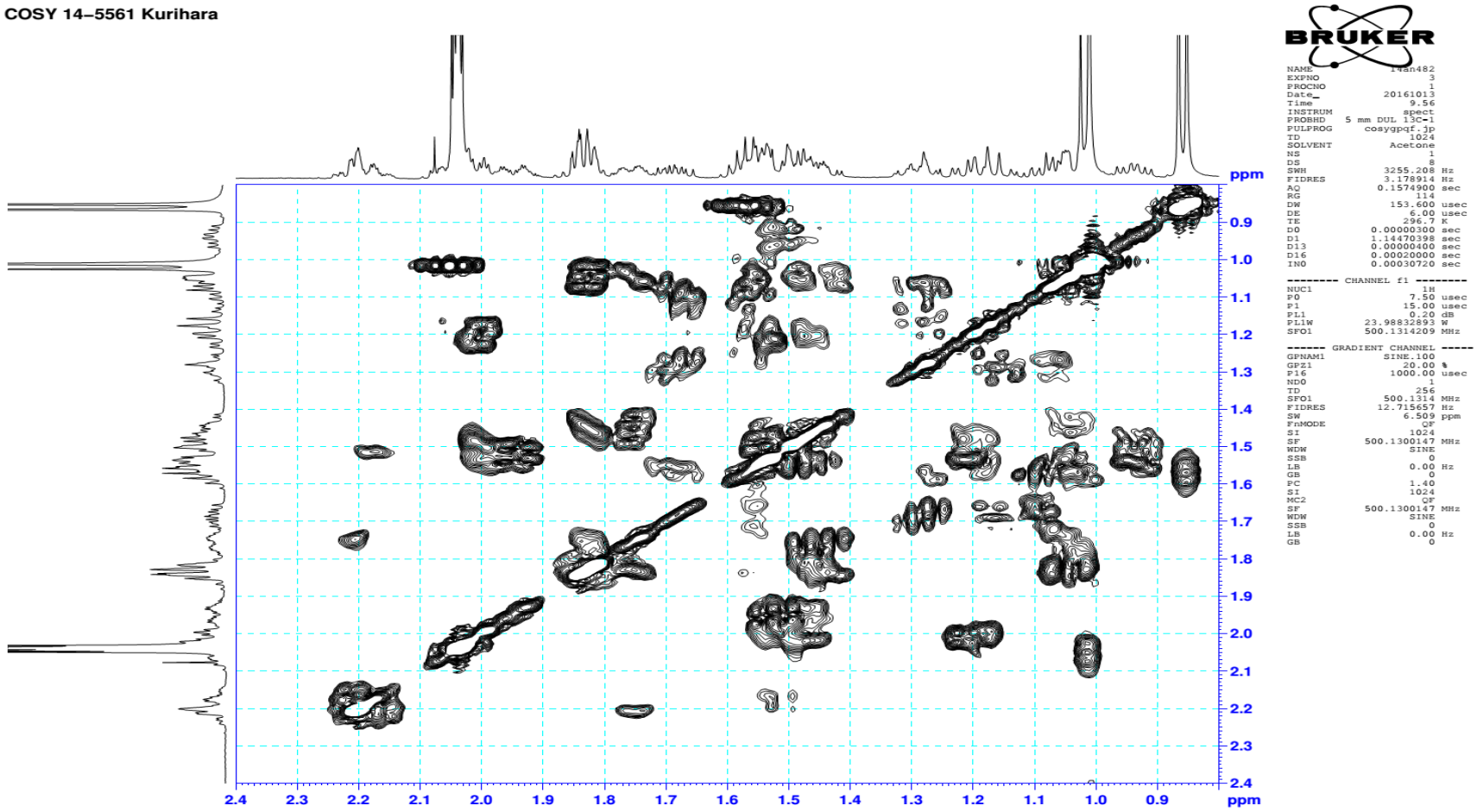


Figure 2-131. Expanded COSY spectrum (3) of compound **A5**.

Table 2-34. Comparison of NMR data between compound **A5**[a] and literature[b]

	^{1}H NMR	^{13}C NMR	
Position	**A5**	**A5**	Literature data
1	1.82 (m, 1H); 1.05 (m, 1H)	38.2	37.2
2	1.49 (m, 1H); 1.76 (m, 1H)	32.5	31.6
3	3.38 (m, 1H)	71.7	71.8
4	2.21 (m, 2H)	43.3	42.2
5		142.3	140.8
6	5.30 (t, 1H)	121.5	121.7
7	1.96 (m, 1H); 1.55 (m, 1H)	32.6	31.9
8	1.48 (m, 1H)	32.7	31.9
9	0.94 (m, 1H)	51.2	50.2
10		37.3	36.4
11	1.54 (m, 1H); 1.51 (m, 1H)	21.8	21.1
12	1.69 (m, 1H); 1.29 (m, 1H)	29.5	28.2
13		43.0	42.2
14	1.04 (m, 1H)	57.7	56.8
15	1.57 (m, 1H); 1.09 (m, 1H)	24.9	24.2
16	2.02 (m, 1H); 1.22 (m, 1H)	40.5	39.7
17	1.16 (m, 1H)	56.8	55.9
18	0.73 (s, 3H)	12.4	11.8
19	1.01 (s, 3H)	19.8	19.3
20	2.07 (m, 1H)	41.0	40.1

(To be continued)

(Continued)

	^{1}H NMR	^{13}C NMR	
Position	**A5**	**A5**	Literature data
21	1.03 (d, 6.0, 3H)	21.3	20.8
22	5.24 (t, 8.5, 1H)	139.0	128.1
23	5.33 (m, 1H)	127.0	126.2
24	1.84 (m, 2H)	42.6	41.9
25	1.57 (m, 1H)	29.3	28.6
26	0.86 (d, 6.6, 3H)	22.6	22.3
27	0.86 (d, 6.6, 3H)	22.5	22.2

[a]The NMR data were measured in acetone-d_6 (δ_H 2.04 ppm; δ_C CO 206.3, CH_3 30.2 ppm) at 500 MHz for ^{1}H and at 125 MHz for ^{13}C.

[b]Nasir et al., 2011.

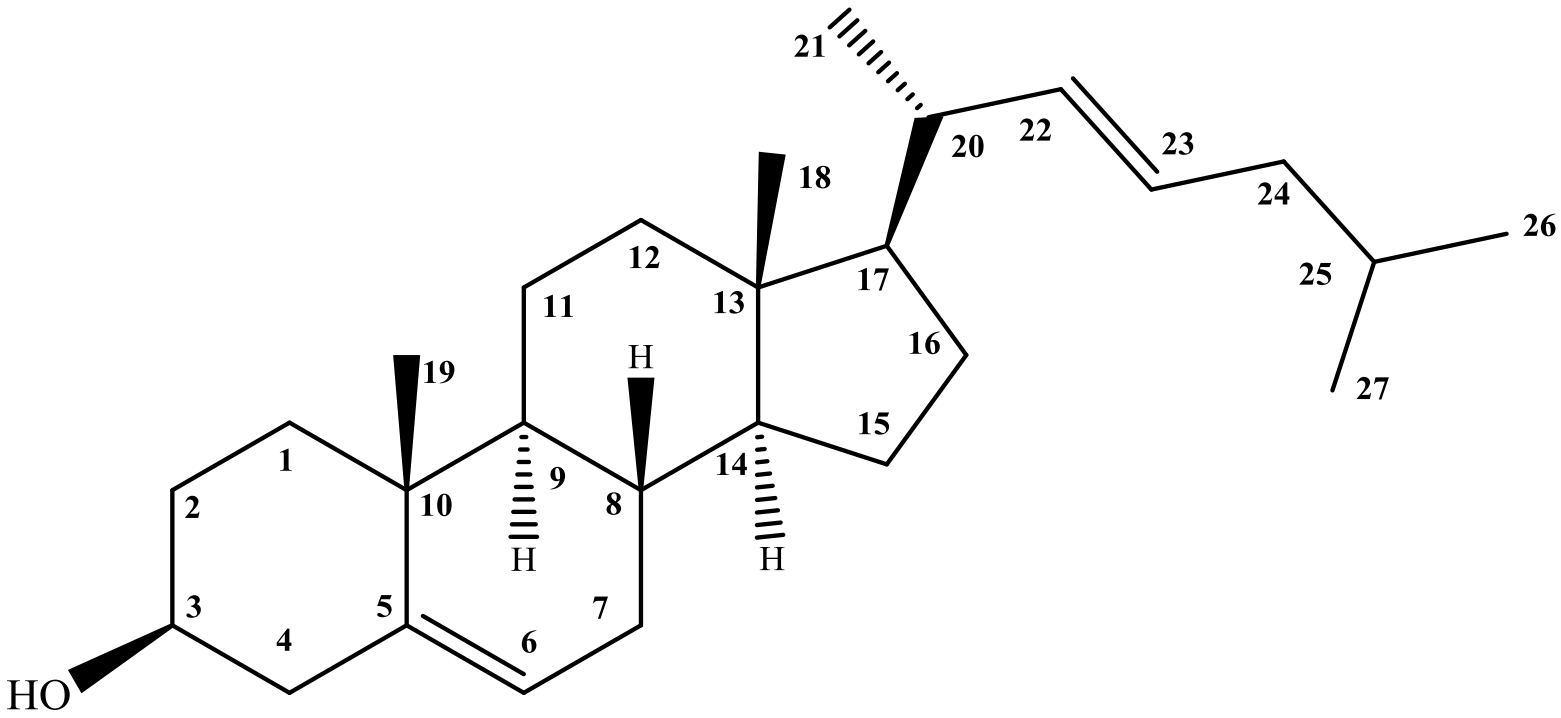


Figure 2-132. Structure of compound **A5**.

2.3.2.5 Structural elucidation of β-glucuronidase inhibitor A6

Compound **A6** was obtained as colorless oil. UV spectrum gave absorption maximum (λ_{max}) at 206 nm (log ε 2.60) in methanol (Figure 2-133). FT IR spectrum showed absorption peaks (ν_{max}) at 1769 and 1081 cm^{-1}, C=O and C-O vibration peaks in chloroform, respectively. FI-MS spectrum displayed the molecular ion peak at *m*/*z* 146 (Figure 2-134). Molecular formula was determined by FI-HR-MS at *m*/*z* 146.05861 for $C_6H_{10}O_4$ (calculated 146.05791) with 2 unsaturation index.

In the ^1H NMR spectrum, proton signals were detected as a nonequivalent oxygenated methylene at δ_H 4.33 and 4.27 (H-5), one slightly broad triplet at δ_H 3.87, an oxygenated methylene at δ_H 3.62 (H-6), a singlet methoxy at δ_H 3.12 (s, 3H, H-7) and an multiplet methylene at δ_H 2.55 (H-4) (Figure 2-135). The ^{13}C NMR spectrum presented six carbons including a ketonic carbon at δc 211.7 (C-3), a quaternary carbon at δc 101.9 (C-2), three methylenes at δc 64.2 (C-5), 63.1 (C-6) and 36.3 (C-4), a methoxy carbon at δc 50.6 (C-7) (Figure 2-136). The slightly broad triplet at δ_H 3.87 showed no correlation with any carbon signals in the HSQC spectrum (Figures 2-137), but showed correlation with the oxygenated methylene at δ_H 3.62 in the DQF COSY spectrum (Figure 2-140). Thus, the triplet signal at δ_H 3.87 was assigned to low exchangeable hydroxy proton in a hydroxymethyl moiety. All the proton and carbon signals of compound **A6** were assigned according to the HMBC cross-peaks of C-2 with H-5, H-6, H-7; C-3 with H-4, H-5, H-6; C-4 with H-5; C-5 with H-4; and C-6 with the hydroxy proton (δ_H 3.87) (Figure 2-141). Consequently, compound **A6** was elucidated as an novel acetal named isogloiosiphone B (Table 2-35, Figure 2-142), an isomer of the known compound gloiosiphone B isolated from the red alga *Gloiosiphonia verticillaris*

(Gloiosiophoniaceae, Gigartinales) (Chen, Moghaddam, & Gerwick, 1993). Compared to the signals of gloiosiphone B, ^{13}C NMR signals at C-2 and C-6 of **A6** were shifted to down-field and up-field, respectively. Compound **A6** possessed an asymmetric center in its structure, but **A6** might be a racemic mixture as the specific rotation was optically inactive ($[\alpha]_D^{27}$= 0° (*c*1.32, $CHCl_3$)).

Furthermore, with the consideration that compound **A6** might be an artefact during methanol extraction from its simple acetal structure, the alga *N*. *yendoana* was extracted by methanol, ethanol and acetone respectively following the same purification procedure as described in section 2.3.1.3. Amount and the yield coefficient were shown in Table 2-36. The purified acetal by different solvent extraction provided the same ^{1}H NMR spectra (Table 2-37, Figure 2-143) which were identical with that of compound **A6** (Figure 2-135). Therefore, isogloiosiphone B (**A6**) was confirmed as a naturally occurring compound, not an artefact. Plausible precursor of isogloiosiphone B (**A6**) and gloiosiphone B would be 1,5-dihydroxypentane-2,3-dione. After cyclization of the precursor to corresponding hemiacetal, both compounds may be derived by methylation at different positions.

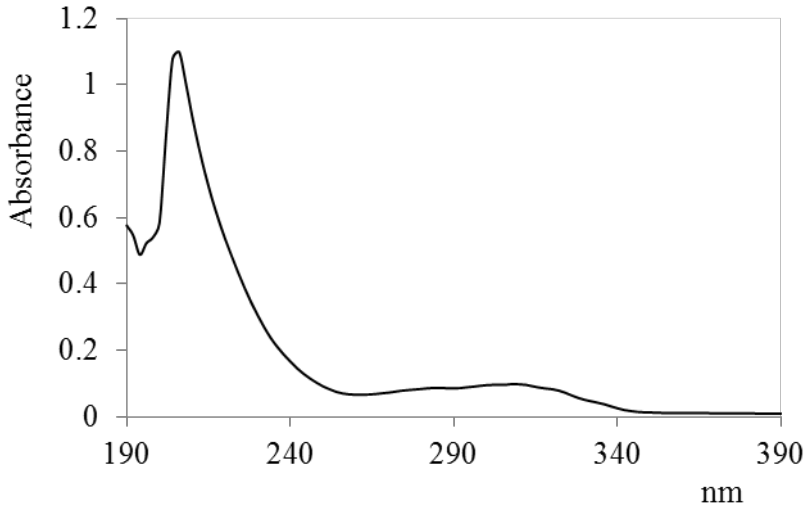


Figure 2-133. UV-Vis spectrum of compound **A6**.

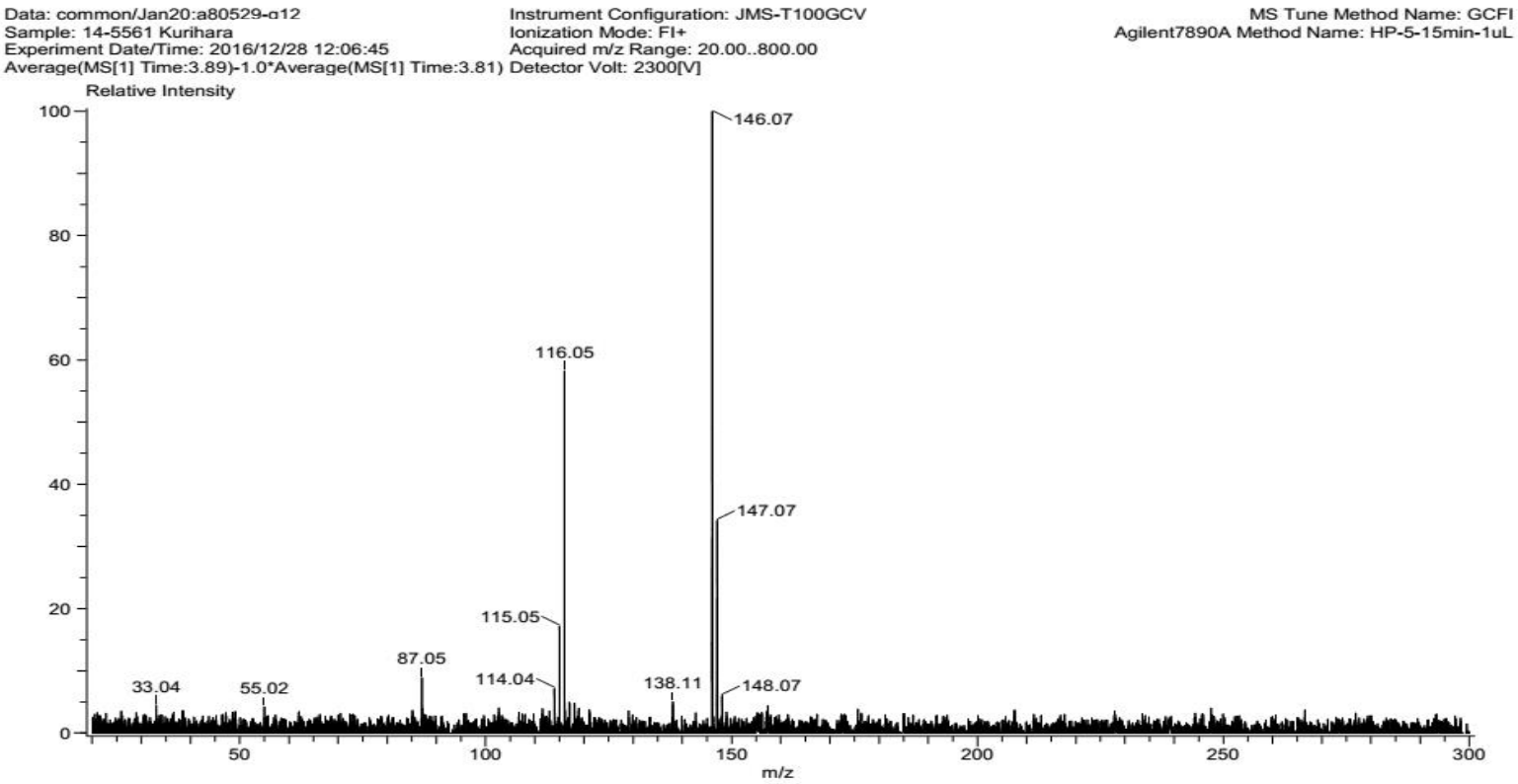


Figure 2-134. FD-MS spectrum of compound **A6**.

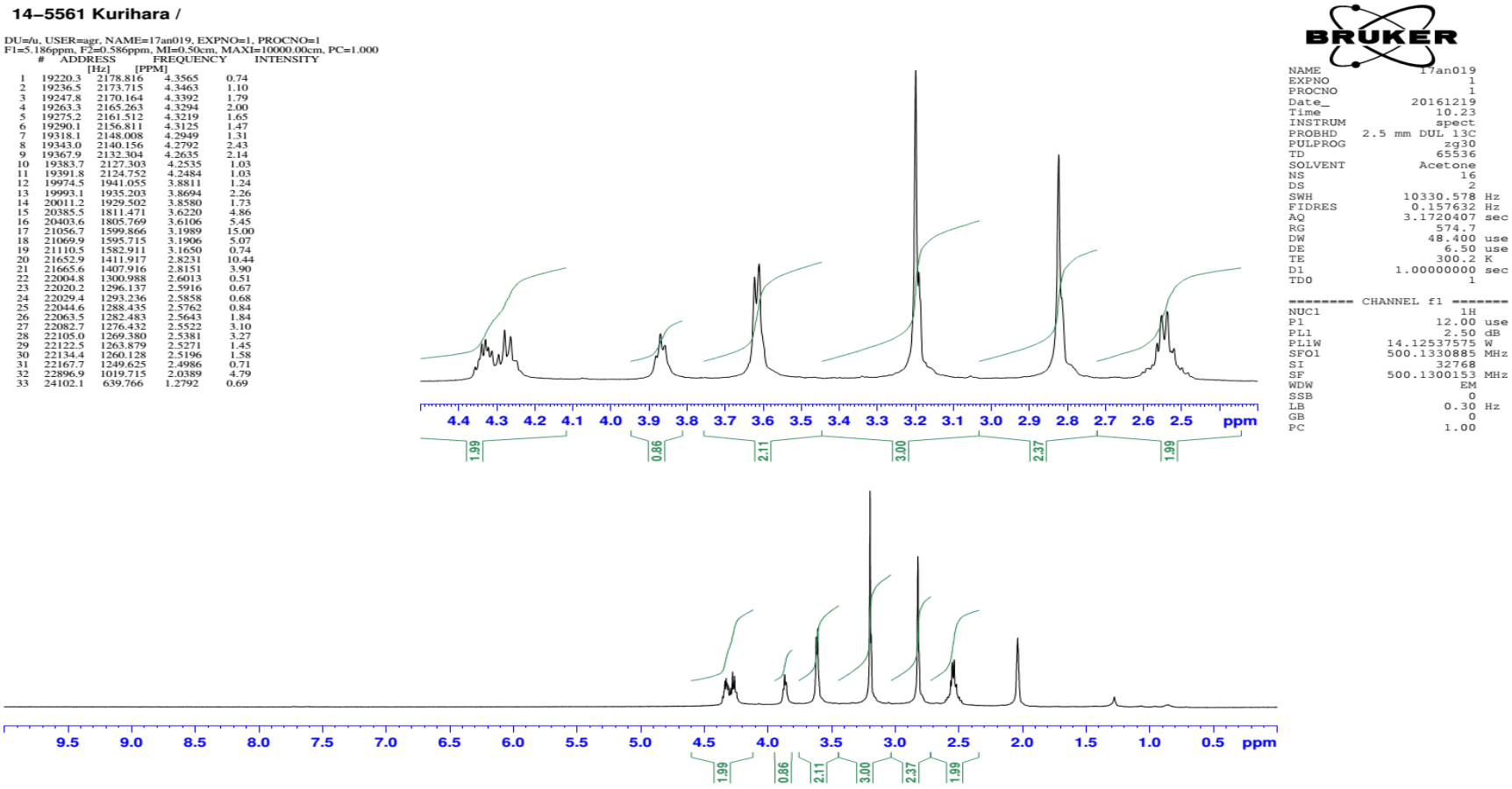


Figure 2-135. ^{1}H-NMR spectrum of compound **A6**.

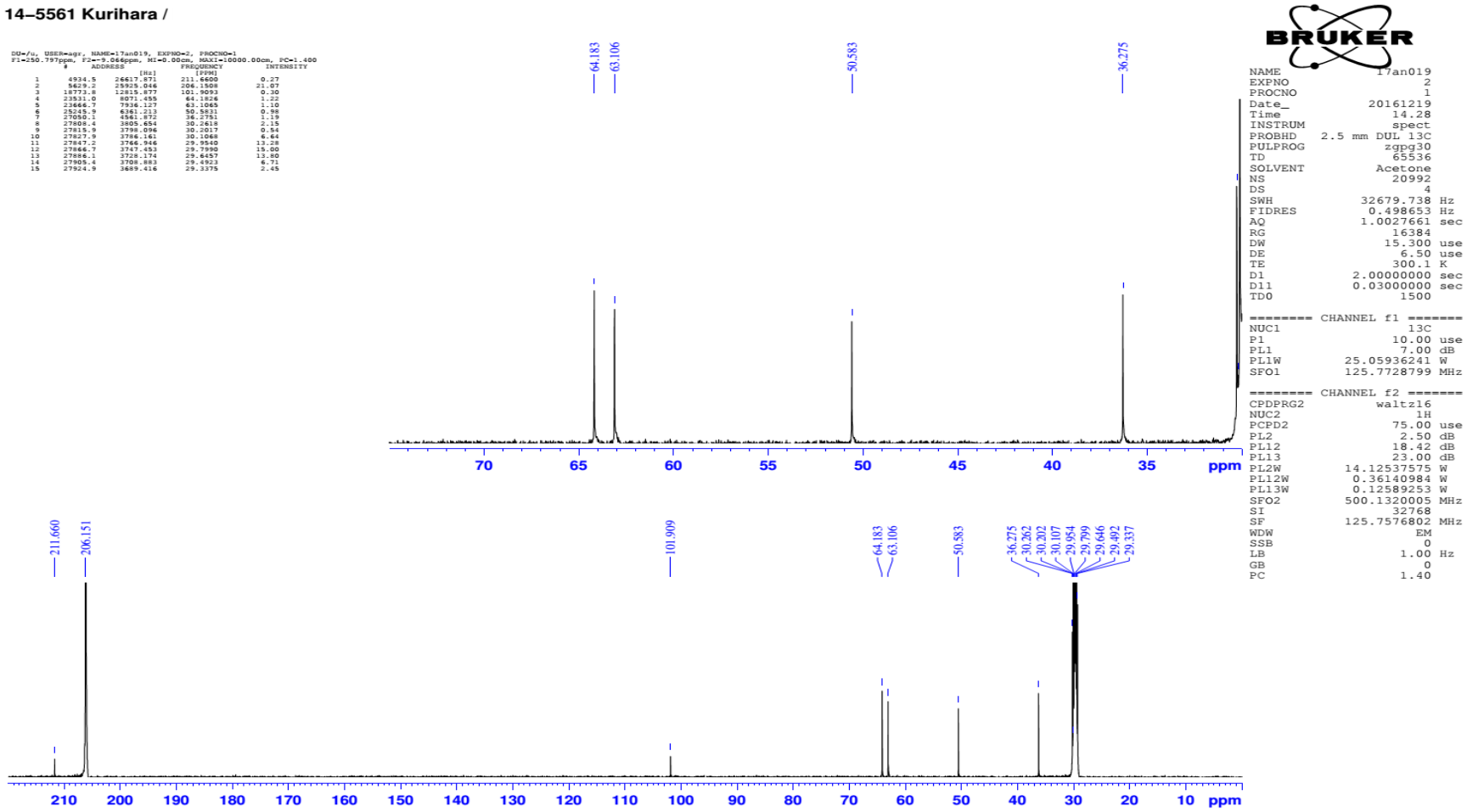


Figure 2-136. ^{13}C-NMR spectrum of compound **A6**.

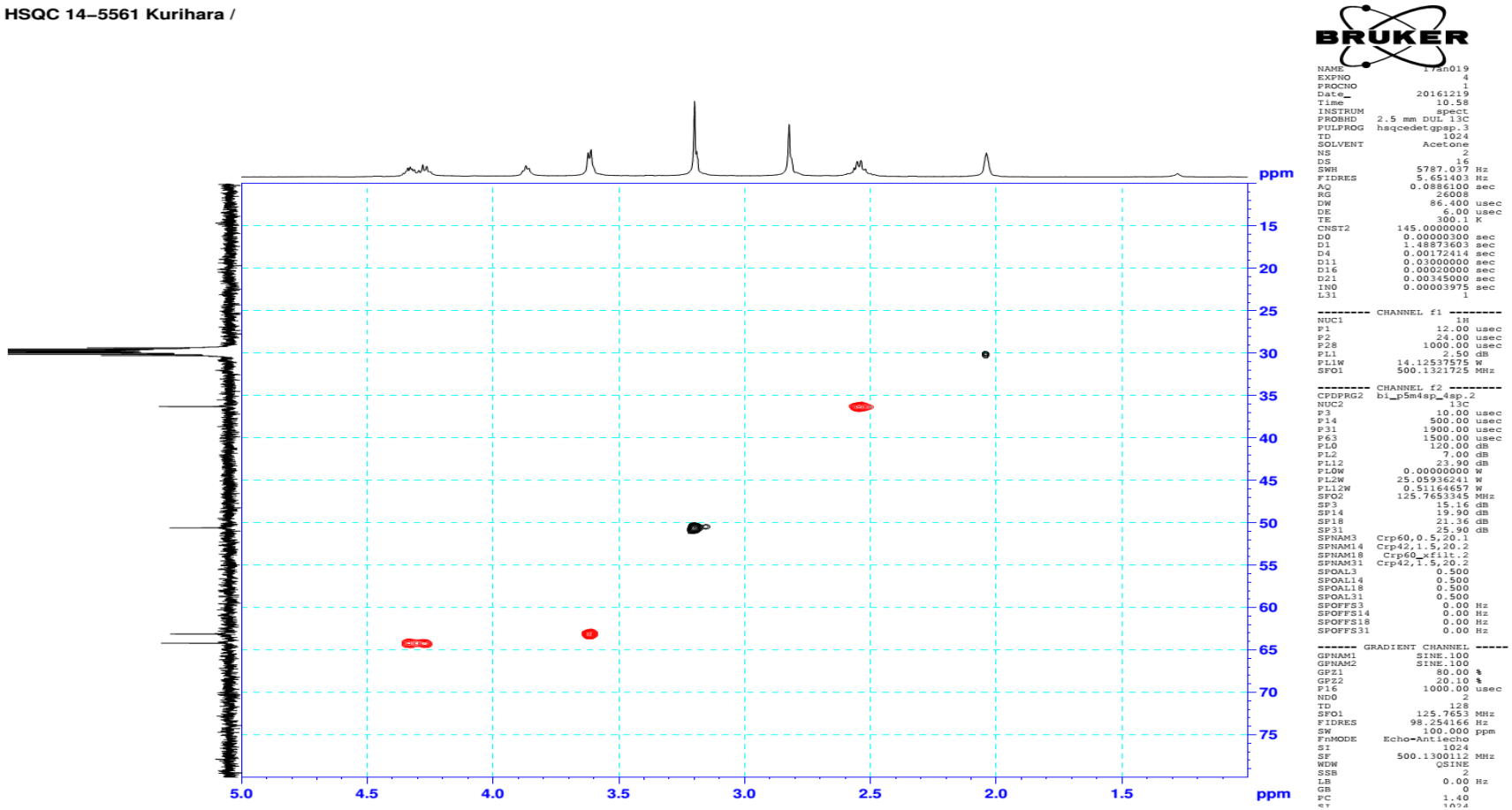


Figure 2-137. HSQC spectrum of compound **A6**.

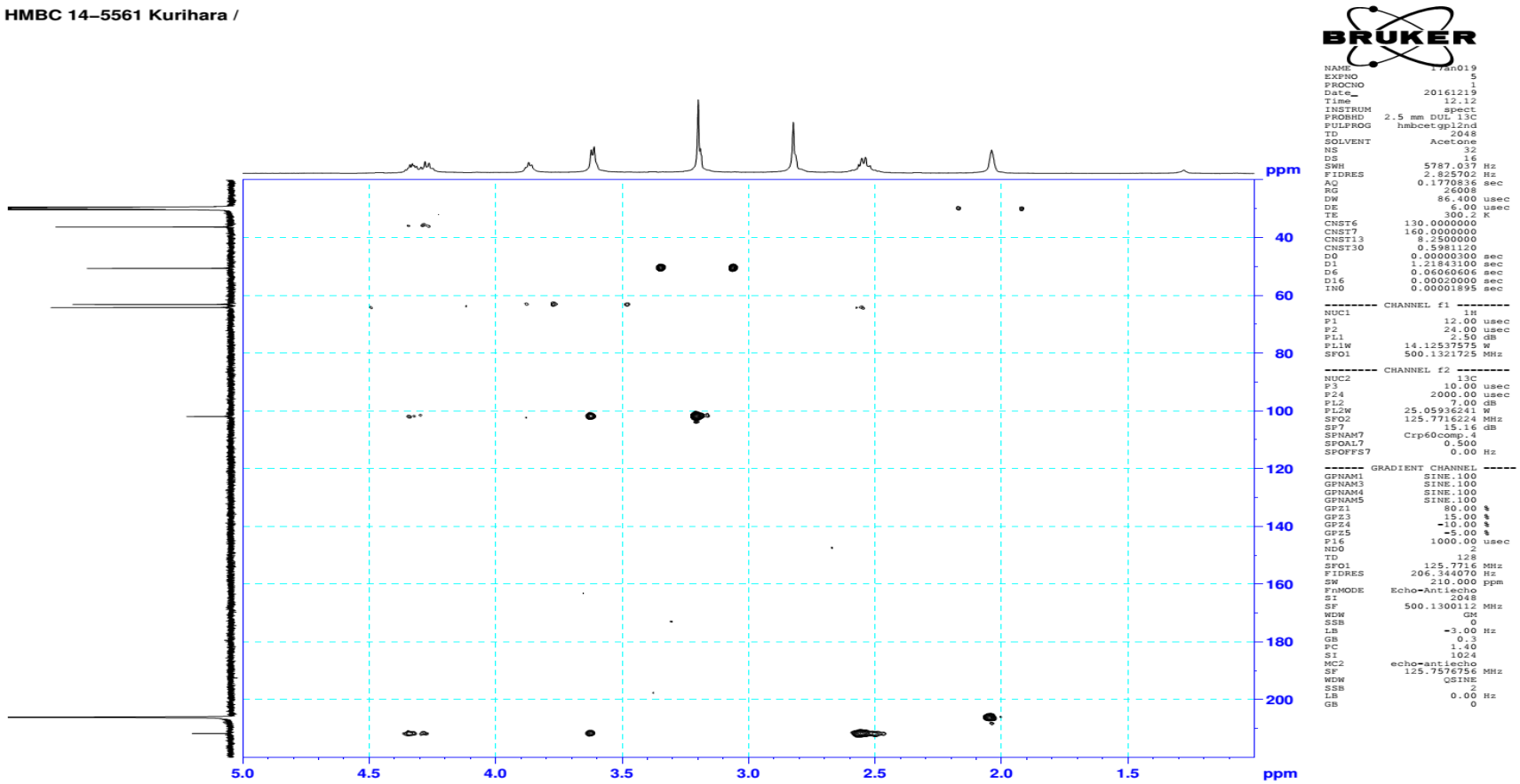


Figure 2-138. HMBC spectrum of compound **A6**.

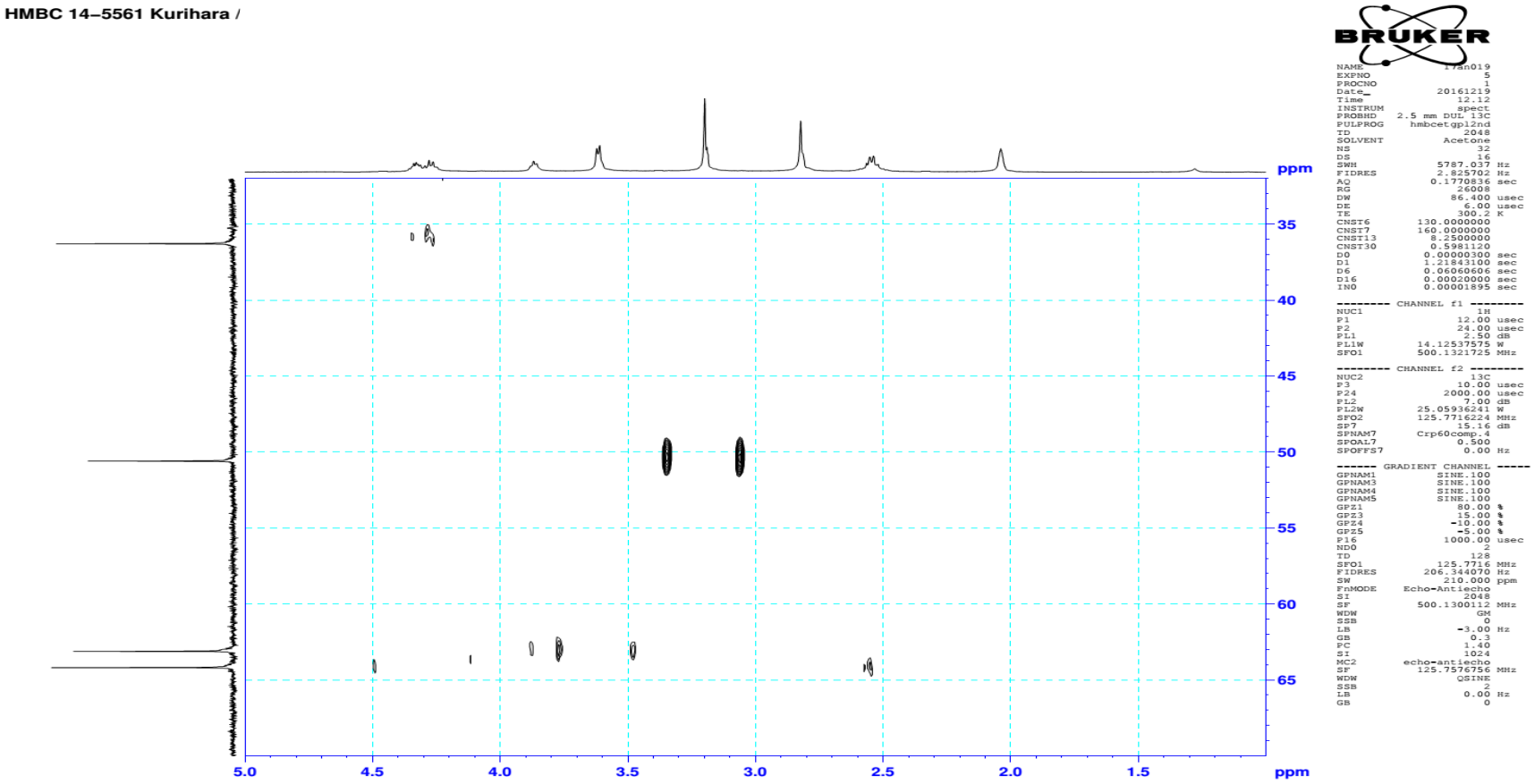


Figure 2-139. Expanded HMBC spectrum of compound **A6**.

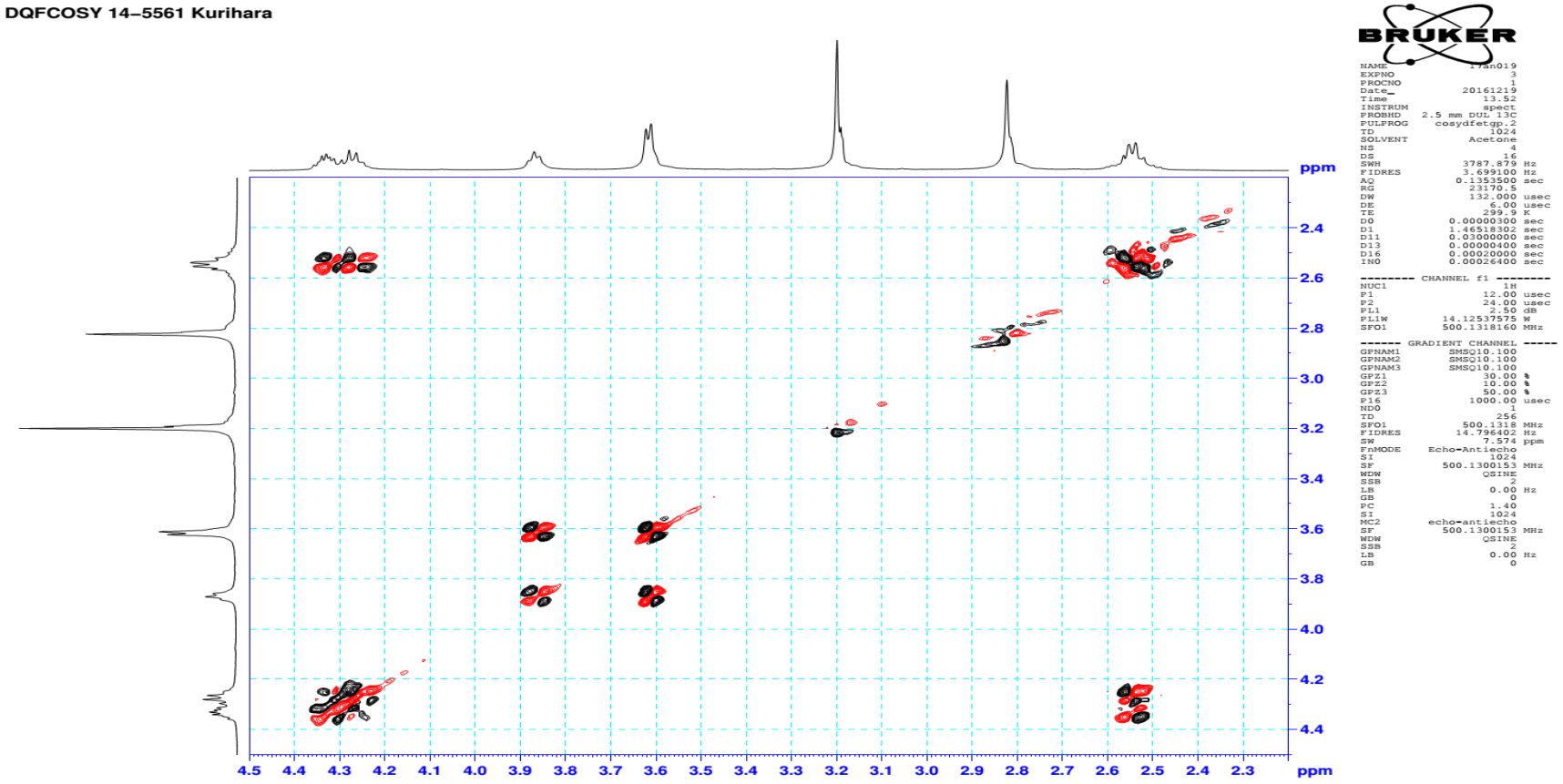


Figure 2-140. DQF-COSY spectrum of compound **A6**.

Table 2-35. Comparison of NMR data between compound **A6**[a] and gloiosiphone B[b]

	^{1}H NMR		^{13}C NMR	
Position	**A6**	Gloiosiphone B	**A6**	Gloiosiphone B
1				
2			101.9	96.0
3			211.7	208.8
4	2.55 (m, 2H)	2.88 (m, 2H)	36.3	34.2
5	4.33 (m, 1H); 4.27 (m, 1H)	4.32 (m, 1H); 4.33 (m, 1H)	64.2	62.5
6	3.62 (d, 5.7, 2H)	3.62 (d, 10.2, 2H)	63.1	72.8
-OCH_3	3.12 (s, 3H)	3.45 (s, 3H)	50.6	59.9
-OH	3.87 (t, 5.7, 1H)			

[a]The NMR data were measured in acetone-d_6 (δ_H 2.04 ppm; δ_C CO 206.2, CH_3 30.3 ppm) at 500 MHz for ^{1}H and at 125 MHz for ^{13}C.

[b]Chen et al., 1993.

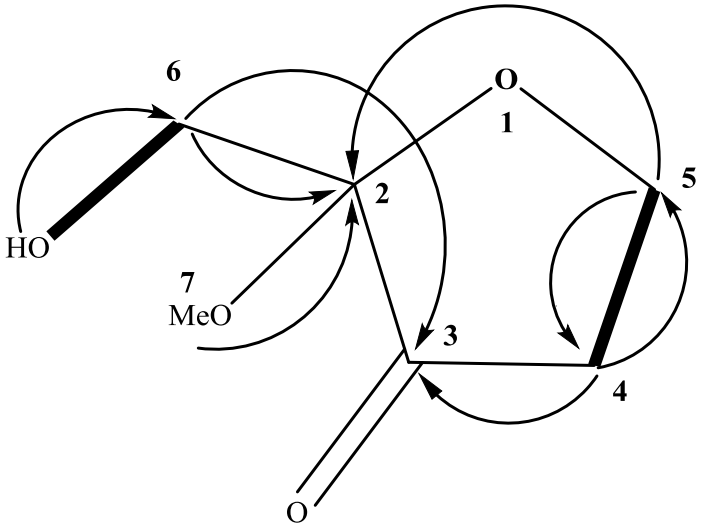
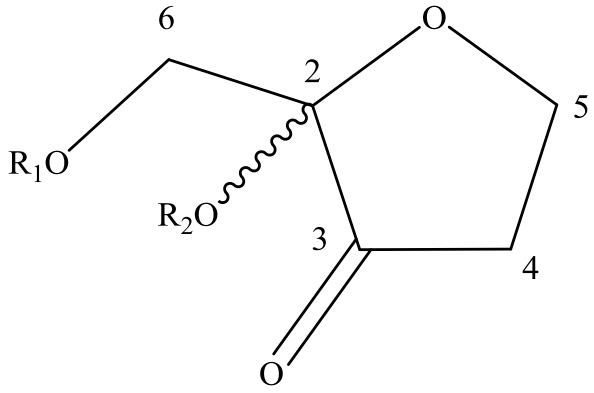


Figure 2-141. Key HMBC correlations (arrows) and ^{1}H-^{1}H COSY correlations (bold lines) of compound **A6**.



R_1=H, R_2=Me Isogloiosiphone B (**A6**)
R_1=Me, R_2=H Gloiosiphone B

Figure 2-142. Structure of compound **A6** and gloiosiphone B.

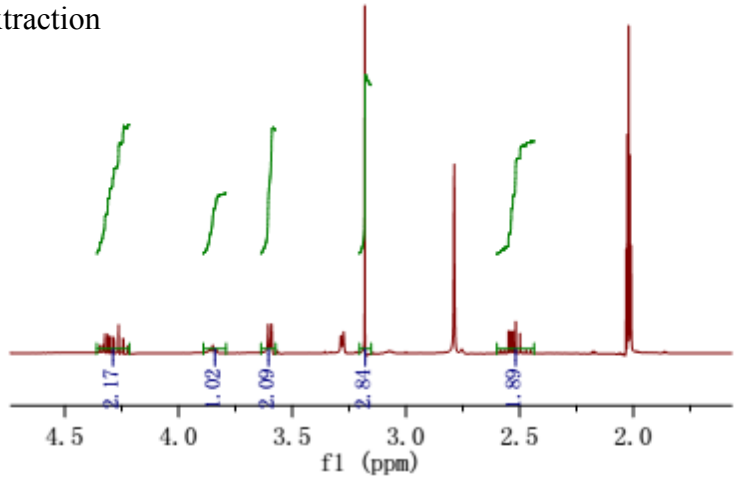
Table 2-36. Amount and yield of purified acetal by different solvent extractions

Extraction solvent	Dried amount of alga(g)	Primary extract (g)	Secondary extract (g)	*n*-Hexane soluble fraction (mg)	Ethyl acetate soluble fraction (mg)	Amount (mg)	Yield (ppm)
Methanol	338.82	10.895	1.957	341.0	785.7	1.68	5.0
Ethanol	303.19	9.592	0.916	230.6	778.8	3.46	11.4
Acetone	313.17	6.124	0.155	181.1	890.1	11.62	37.1

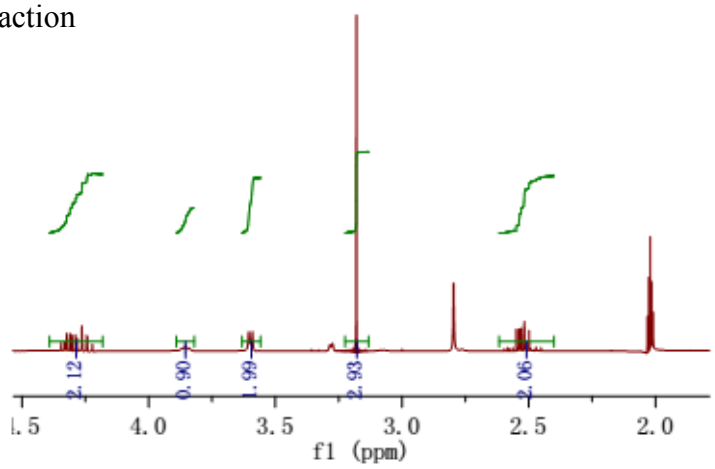
Table 2-37. ^{1}H-NMR data of purified acetal by different solvent extractions

	^{1}H NMR data for purified acetal		
Position	Methanol extraction	(Ethanol extraction)	Acetone extraction
4	2.55 (m, 2H)	2.53 (m, 2H)	2.52 (m, 2H)
5	4.27 (m, 1H); 4.33 (m, 1H)	4.23 (m, 1H); 4.31 (m, 1H)	4.28 (m, 1H); 4.32 (m, 1H)
6	3.60 (d, 6.1, 2H)	3.60 (d, 5.7, 2H)	3.60 (d, 6.2, 2H)
-OCH_3	3.12 (s, 3H)	3.19 (s, 3H)	3.18 (s, 3H)
-OH	3.86 (t, 6.3, 1H)	3.85 (t, 6.2, 1H)	3.85 (t, 6.3, 1H)

Methanol extraction



Ethanol extraction



Acetone extraction

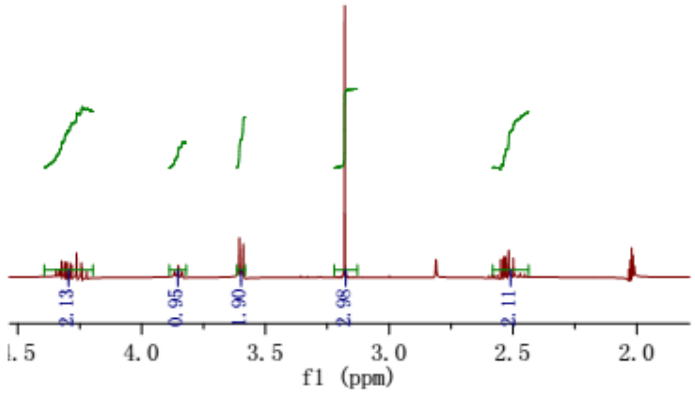


Figure 2-143. ^{1}H-NMR spectra of compounds **A6** by different solvent extractions.

2.4 Discussion

Compared to marine green and brown algae, red algae contain chemically rich bioactive compounds in terms of both abundance and diversity (Shih et al., 2017). Nearly all chemical classes of natural products have been found in red algae. Among them isoprenoids and halogenated secondary metabolites account for a large part (Leal et al., 2013). In Chapter 2, the two red marine algae *Neorhodomela aculeata* (Rhodomelaceae, Ceramiales) collected from Usujiri, Hakodate, 2015 and *Neodilsea yendoana* (Dumontiaceae, Gigartinales) collected from Usujiri, Hakodate, 2016 were used for the purification and isolation of β-glucuronidase inhibitory compounds.

Marine algae of family Rhodomelaceae are well known to be rich sources of bromophenols. In the last decades, several structure types of bromophenols have been isolated from this family (Zhao et al., 2004) and exhibited a wide spectrum of biological and pharmacological activities, such as α-glucuronidase inhibition (Kurihara, Mitani, Kawabata, & Takahashi, 1999) (K. Y. Kim, Nguyen, Kurihara, & Kim, 2010), protein tyrosine phosphatase 1B inhibition (Shi et al., 2012), glucose 6-phosphate dehydrogenase (Mikami, Kurihara, Ono, Kim, & Takahashi, 2016), carbonic anhydrase (Akbaba et al., 2013), anti-cancer (Wang et al., 2015), anti-diabetic (Shi et al., 2013), anti-inflammatory (Wiemer, Idler, & Fenical, 1991), and anti-oxidation activity (Öztaşkın, Çetinkaya, Taslimi, Göksu, & Gülçin, 2015). Most reports showed that diaryl structural types of bromophenols exhibited much higher bioactivities compared with the monoaryl structural ones. Also, numbers of bromine atoms and hydroxy or methyl groups also might impact the bioactivities (Kurihara et al., 1999).

N. *yendoana* is one of the most abundantly distributed marine red algae in the

intertidal zone along the coast of North Japan. This alga was used as a kind of architectural stucco because of the high content of polysaccharide. So far, several studies have suggested that *N*. *yendoana* comprises high concentration of amino acids (Santoso, 2013) as well as a certain number of bioactive compounds including rhodoic acid (Murakoshi & Hatanaka, 1977), polyunsaturated fatty acid (M. Suzuki, Wakana, Denboh, & Tatewaki, 1996), yendolipin (Matsuo, Ishida, Matsumoto, Tatewaki, & Suzuki, 1997) which provides potent anti-morphogenesis, allelopathic and algicidal activities.

From the ethyl acetate-soluble fraction of *N*. *aculeata*, one monoaryl bromophenol, 2,3-dibromo-4,5-dihydroxybenzyl ether (**F1**) and two diaryl bromophenols, 3-bromo-2-(2,3-dibromo-4,5-dihydroxy-benzyl)-4,5-dihydroxybenzyl methyl ether (**F2**) and bromo-2-(2,3-dibromo-4.5-dihydroxybenzyl)-4,5-dihyroxybenzyl alcohol (**F3**) were purified as β-glucuronidase inhibitors. The purified two diaryl structural bromophenols **F2** and **F3** exhibited over 3-fold more effective rather than compound **F1**.

Phytal (**A1**), mixture of phytol (**A2**) and cholesta-4,22-diene-3,6-dione (**A3**), cholesterol (**A4**), 22-dehydrocholesterol (**A5**) and a novel acetal named isogloiosiphone B (**A6**) were isolated. from the ethyl acetate-soluble fraction of *N*. *yendoana*. The novel compound **A6** showed relatively higher inhibition than other purified compounds. Compounds **A1** and **A5** showed weak inhibitory activity, while compound **A4**, similar structure of **A5**, was inactive for β-glucuronidase inhibition. β-Glucuronidase inhibitors in this study are listed in Figure 2-144.

Isoprenoids such as terpenes, steroids, carotenoids, prenylated quinones and hydroquinones are derived from the branched C5 carbon skeleton of isoprene (Zwenger & Basu, 2008). The number of repetitions, cyclization reaction, rearrangements and

further oxidation of isoprene motifs contribute for the enormous diversity of structures and biological activities of isoprenoids, such as anti-oxidation (Duan, Zhang, Li, & Wang, 2006), anti-tumor (Awad, 2004) and anti-retroviral activity (Cirne-Santos et al., 2008). Phytal, widely found as one of the pheromones in some insects (Fürstenau et al., 2013) was first purified in this alga. Phytol, an analogue of phytal exists abundantly in plants as an alcohol part of the ester side chain of chlorophyll. And it is an important precursor for the syntheses of isoprenoids such as α-tocopherol (vitamin E) and phylloquinone (vitamin K1) through the mevalonate-independent pathway (Rohmer, 1999) (Burrell, Garwood, Jackman, Oskay, & Weedon, 1966). Saikia et al. reported phytol and phytal showed potent antitubercular activity against *Mycobacterium tuberculosis* H37Rv strain (Saikia et al., 2010). Moreover, steroids (sterols) are also one kind of dominant component in marine algae, which are the major and essential lipid components of cell membrane acting as membrane stabilizers (Rohmer, 1999) (Benesch & McElhaney, 2014). Cholesterol along with 22-dehydrocholesterol are kinds of dominant sterols occurred in almost all the marine red algae (Al Easa, Kornprobst, & Rizk, 1995) (Tsuda et al., 1960) (Saeidnia, Permeh, Gohari, & Mashinchian-Moradi, 2012) (Jassbi, Mohabati, Eslami, Sohrabipour, & Miri, 2013).

In summary, three bromophenols were purified from *N*. *aculeata*, and two diterpenes, three steroids and one novel acetal, were isolated form *N*. *aculeata* as β-glucuronidase inhibitors. Among them, compounds **F2** and **F3** derived from *N*. *aculeate* exhibited extremely excellent inhibitory activity and the novel compound **A6** purified from *N*. *yendoana* exposed moderate inhibitory activity against β-glucuronidase

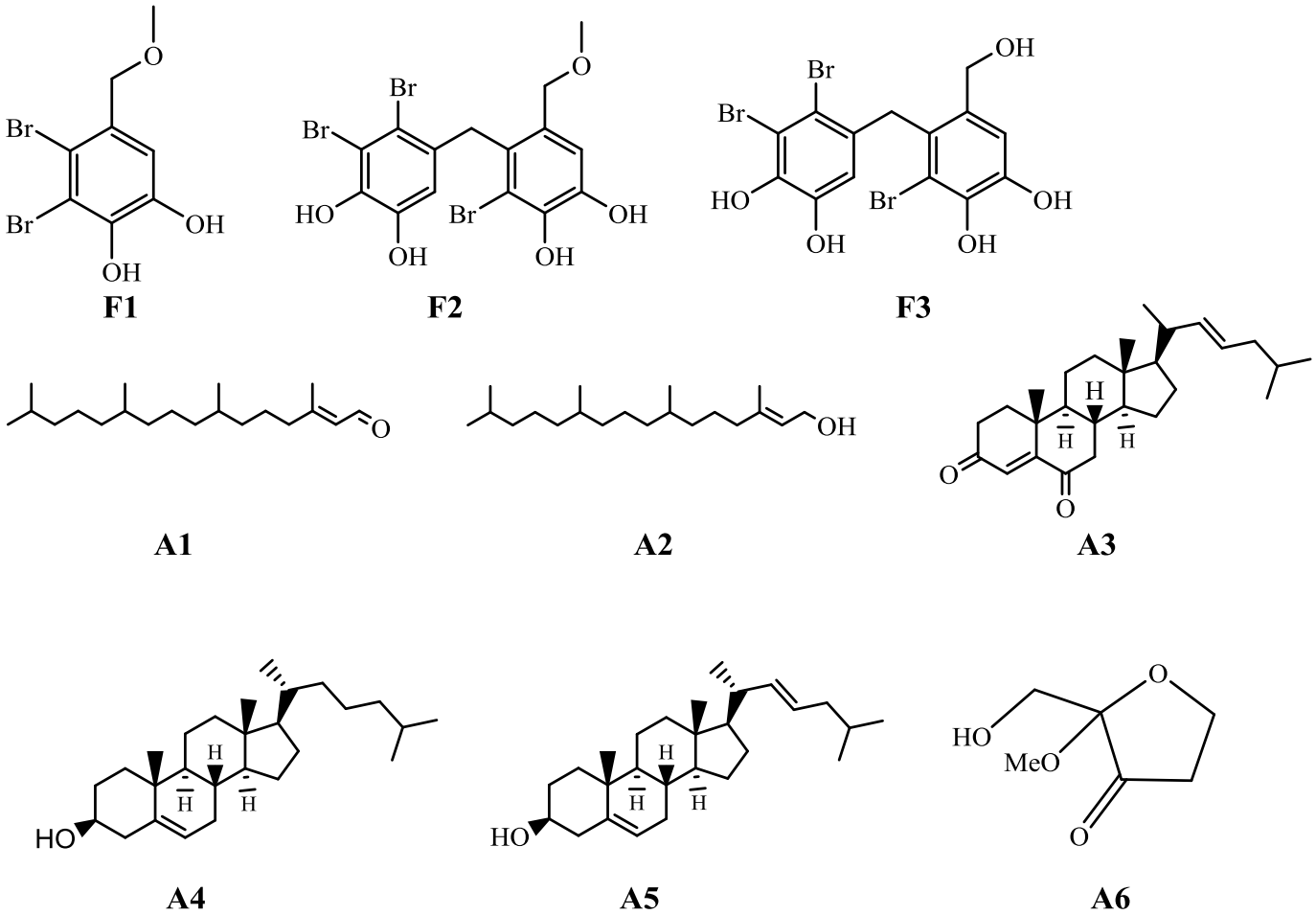


Figure 2-144. β-Glucuronidase inhibitors derived from the red algae *N*. *aculeate* and *N*. *yendoana*.

Chapter 3

β-Glucuronidase Inhibitors Derived from Marine Brown Algae

In this chapter, the three brown algae *Sargassum confusum*, *S*. *thunbergii* (Sargassaceae, Fucales) and *Agarum clathratum* (Agaraceae, Laminariales) were used for the isolation and purification of β-glucuronidase inhibitory compounds.

3.1 Chromatography and chemical analysis instruments

Chromatography and chemical analysis instruments were same as in Section 2.1. The additional items were as follow:

- High performance liquid chromatography (HPLC)

  Column:

  Intersil ODS-4 column 250 × 7.6 (5 μm) GL Sciences Inc. (Tokyo, Japan)

3.2 β-Glucuronidase inhibitors derived from the marine brown alga *Sargassum confusum*

In this section, *S*. *confusum* (Sargassaceae, Fucales) collected from Usujiri, Hakodate on June 3rd, 2015 was used to perform the isolation and purification of β-glucuronidase inhibitors (Figure 3-1).

3.2.1 Isolation of β-glucuronidase inhibitor J1 from *S*. *confusum*

Mixture of primary and secondary extracts of *S*. *confusum* was partitioned by organic solvent to obtain *n*-hexane-soluble fraction (13.32 g), ethyl acetate-soluble fraction (5.68 g) and *n*-butanol-soluble (4.61 g) fraction (Table 3-1, Figure 3-2). An aliquot (3.10 g) of the *n*-hexane-soluble fraction was chromatographed on Wakogel C-100 silica gel and eluted with *n*-hexane/ethyl acetate/methanol to give ten fractions (Table 3-2). Among them, fraction FH3 (13.9 mg) which showed the highest inhibitory

activity among the obtained fractions was developed with 100% *n*-hexane on the preparative TLC plate to obtain fractions FH3-1 to FH3-3 (Figure 3-4). The pure fraction FH3-2 (5.0 mg, 10 ppm on the basis of air-dried alga) which exhibited high inhibitory activity (Table 3-3, Figure 3-5) was named as compound **J1**.

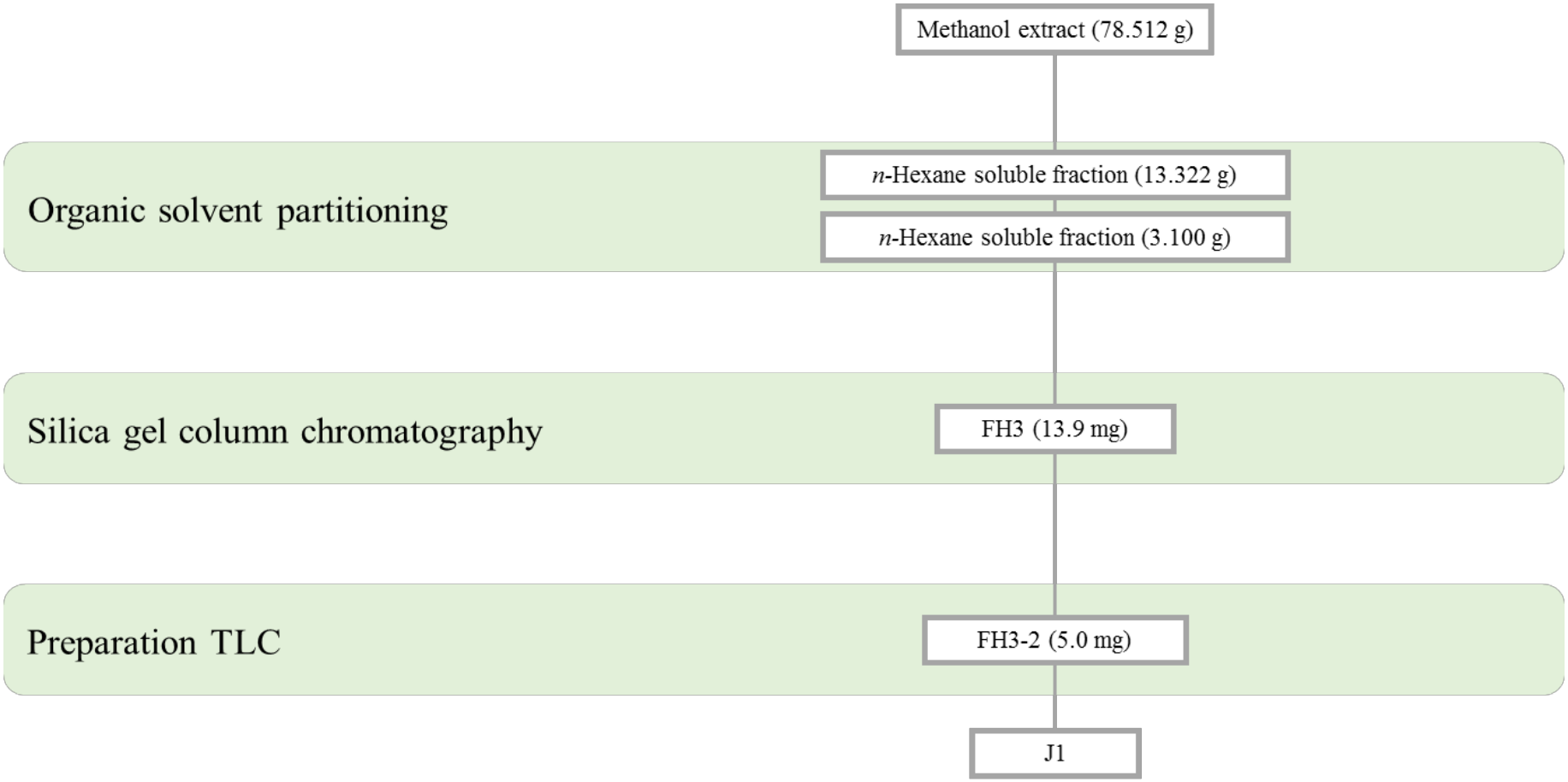


Figure 3-1. Separation scheme of the extract of *S*. *confusum* collected from Usujiri, Hakodate.

Table 3-1. Amount and β-glucuronidase inhibitory activity of the fractions[a] obtained by organic solvent partitioning

Fraction	Amount (g)	Inhibition[b] (%)
n-Hexane	13.322	19.09 ± 0.62
Ethyl acetate	5.675	9.27 ± 0.61
n-Butanol	4.609	9.27 ± 1.83

[a]Sample, 78.512 g methanol extracts of *S*. *confusum*

[b]Assay concentration was 10 μg/mL. Data represent means ± SE (n=3).

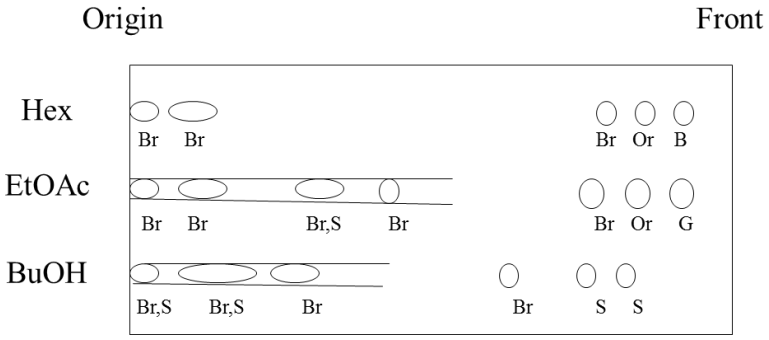


Figure 3-2. Silica gel thin layer chromatogram of the organic solvent extracts of *S*. *confusum*.

Developing solvent, chloroform: methanol = 4: 1 (v/v).

⬭, Visualized with 5% sulfuric acid reagent.

Abbreviations designate color of the spots: Br, brown; Or, orange; B, blue; G, green; S, quenching spot under short wave UV lamp.

Table 3-2. Amount and β-glucuronidase inhibitory activity of the fractions obtained from *n*-hexane-soluble fraction[a] separated by silica gel column chromatography

Fraction	Eluent (v/v)	Amount (mg)	Inhibition[b] (%)
FH1	*n*-Hexane	294.6	NI[c]
FH2	*n*-Hexane	0.7	NI
FH3	*n*-Hexane : ethyl acetate = 4 : 1	13.9	28.86 ± 9.46
FH4	*n*-Hexane : ethyl acetate = 4 : 1	1088.5	NI
FH5	*n*-Hexane : ethyl acetate = 2 : 1	758.7	6.43 ± 2.68
FH6	*n*-Hexane : ethyl acetate = 2 : 1	125.4	1.61 ± 6.21
FH7	Ethyl acetate	70.1	1.06 ± 2.49
FH8	Ethyl acetate	15.1	9.86 ± 6.59
FH9	Methanol	644.1	18.68 ± 0.57
FH10	Methanol	57.4	5.32 ± 7.42

[a]Sample, *n*-hexane-soluble fraction, 3.100 g; stationary phase, Wakogel C-100; elution volume, 460 mL/fraction.

[b]Assay concentration was 10 μg/mL. Data represent means ± SE (n=3).

[c]NI, no inhibition.

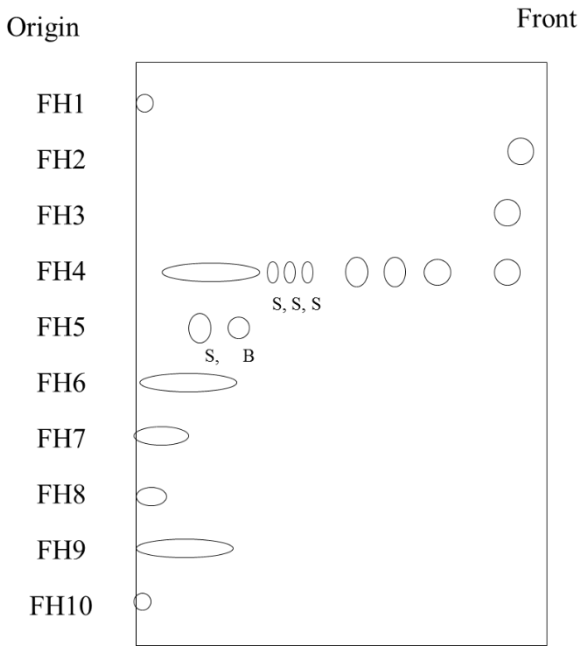


Figure 3-3. Silica gel thin layer chromatogram of fractions obtained from *n*-hexane-soluble fraction separated by silica gel column chromatography.

Developing solvent, *n*-hexane: ethyl acetate = 4: 1 (v/v).

⬭, Visualized with 5% sulfuric acid reagent.

Abbreviations designate color of the spots: B, blue; S, quenching spot under short wave.

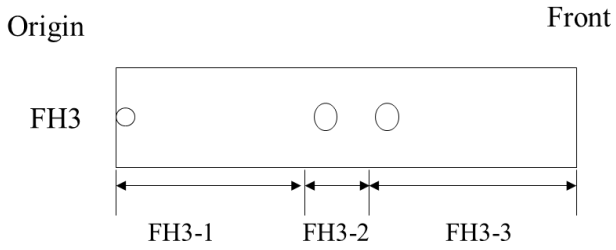


Figure 3-4. Profile of the preparative TLC of fraction FH3.

Developing solvent, *n*-hexane.

⬭, Visualized with 5% sulfuric acid reagent.

Table 3-3. Amount and β-glucuronidase inhibitory activity of the fractions obtained from fraction FH3[a] by preparative thin layer chromatography

Fraction	Amount (mg)	Inhibition[b] (%)
FH3-1	2.9	NI[c]
FH3-2	5.0	64.44 ± 1.23
FH3-3	1.7	2.70 ± 1.04

[a]Sample, fraction FH3, 13.9 mg.

[b]Assay concentration was 10 μg/mL. Data represent means ± SE (n=3).

[c]NI, no inhibition.

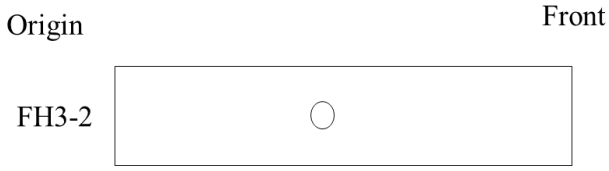


Figure 3-5. High performance silica gel thin layer chromatogram of compound FH3-2. Developing solvent, *n*-hexane.

⬭, Visualized with 5% sulfuric acid reagent.

3.2.2 Structural elucidation of β-glucuronidase inhibitor J1

Compound **J1** was obtained as colorless oil and exhibited a molecular ion peak at *m/z* 286 in its FI-MS spectrum (Figure 3-6). Molecular formula of compound **J1** was also confirmed as $C_{21}H_{34}$ by FI-HR-MS at m/z 286.26660 (calculated 286.26605). The ^{1}H NMR spectrum of compound **J1** displayed three typical *exo*-olefinic protons at δ_H 5.81 (m, 1H), 4.98 (dd, 1.4, 17.1, 1H) and 4.93 (dd, 1.4, 10.0, 1H), eight *endo*-olefinic protons at δ_H 5.35, six bisallylic methylene protons at δ_H 2.81, six allylic methylene protons at δ_H 2.04, alkyl methylene and methyl protons at δ_H 0.86-1.45 (Figure 3-7). ^{13}C NMR spectrum displayed ten sp2 and eleven sp3 carbons (Figure 3-8). Compound **J1** was identified as (6*Z*,9*Z*,12*Z*,15*Z*)-1,6,9,12,15-henicosapentaene (Table 3-4, Figure 3-13) with the assistance of HSQC (Figure 3-9 to Figure 3-11) and COSY (Figure 3-12) spectra as well as the comparison of literature data (Kurihara et al., 2014).

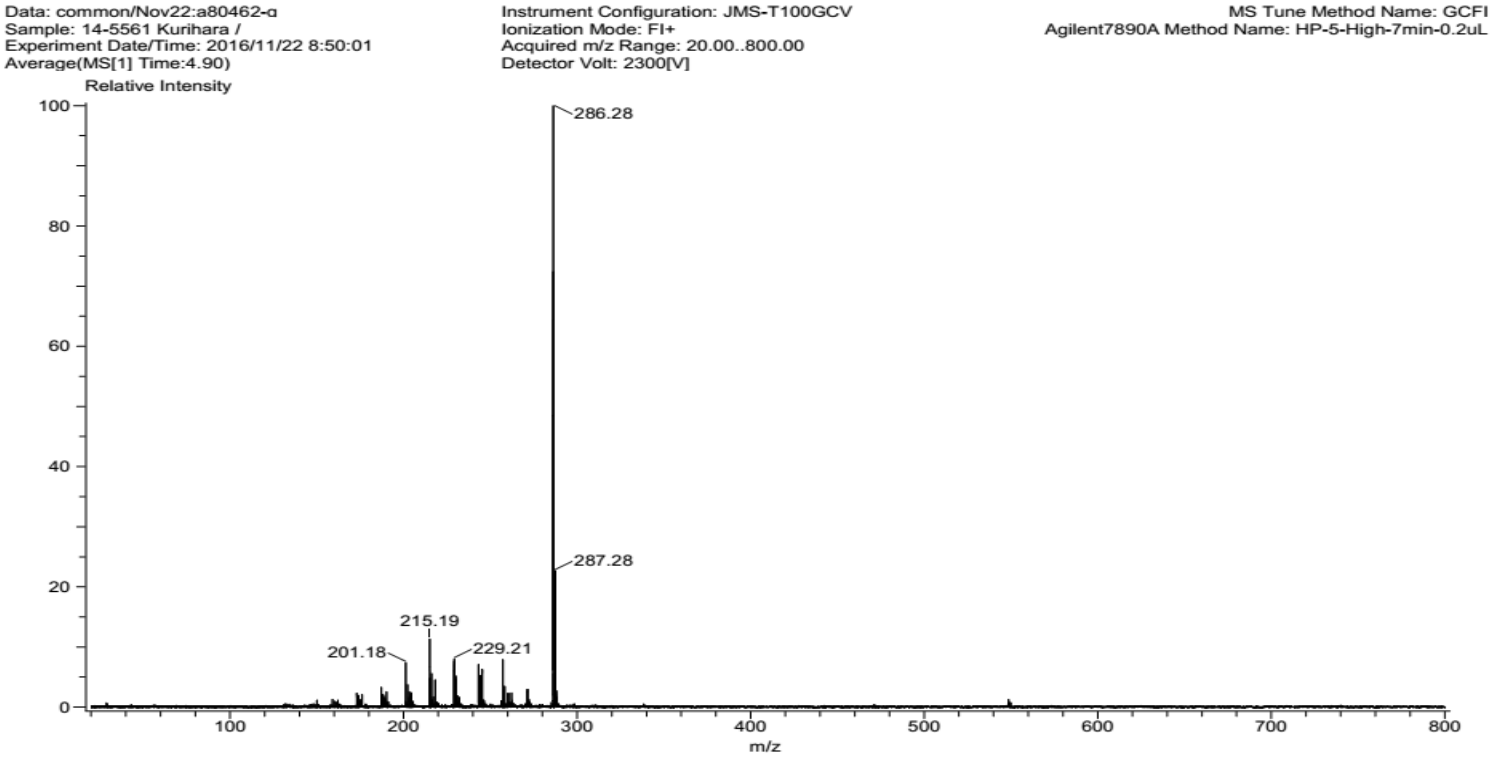


Figure 3-6. FI-MS spectrum of compound **J1**.

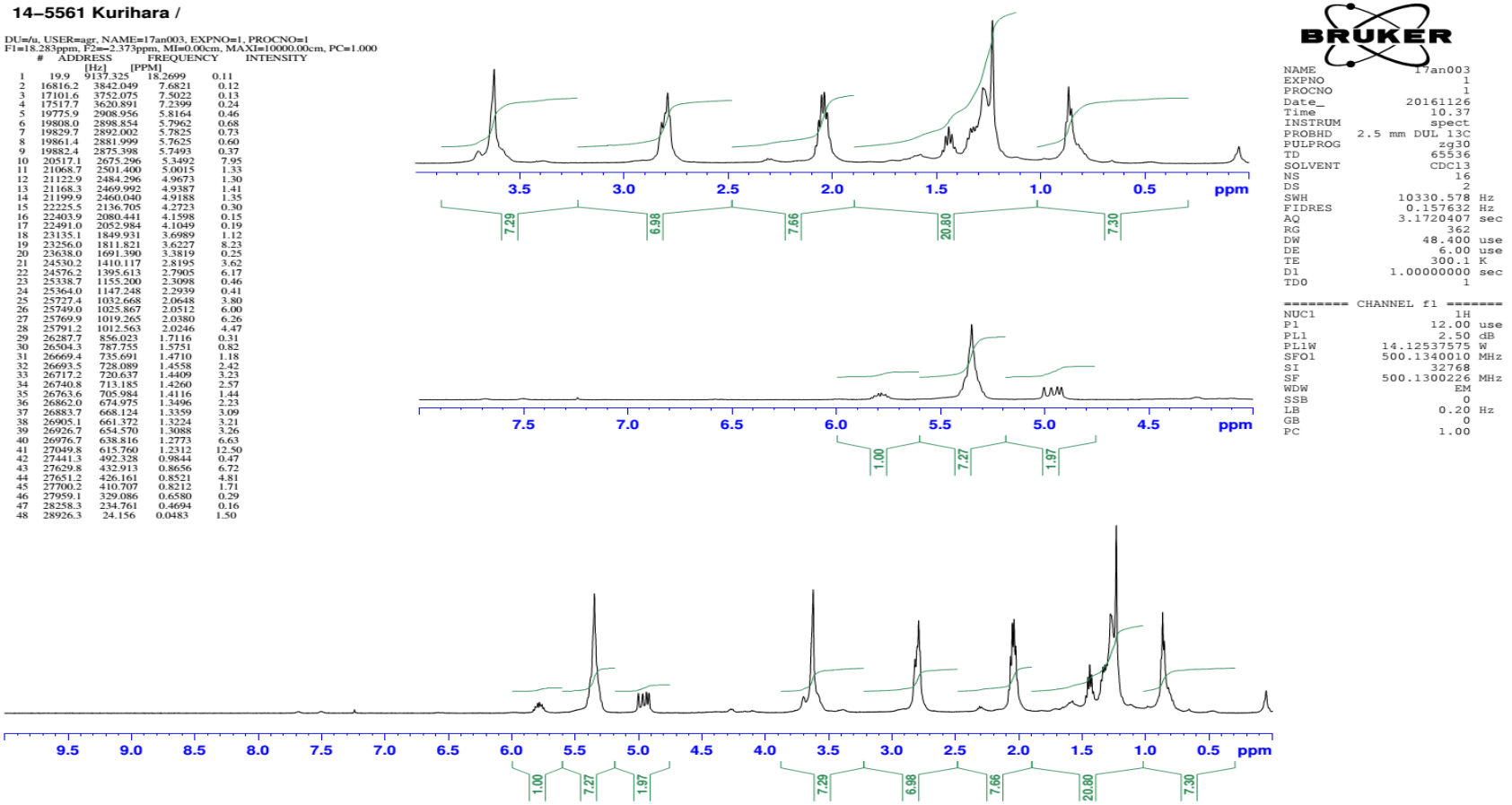


Figure 3-7. ^{1}H-NMR spectrum of compound **J1**.

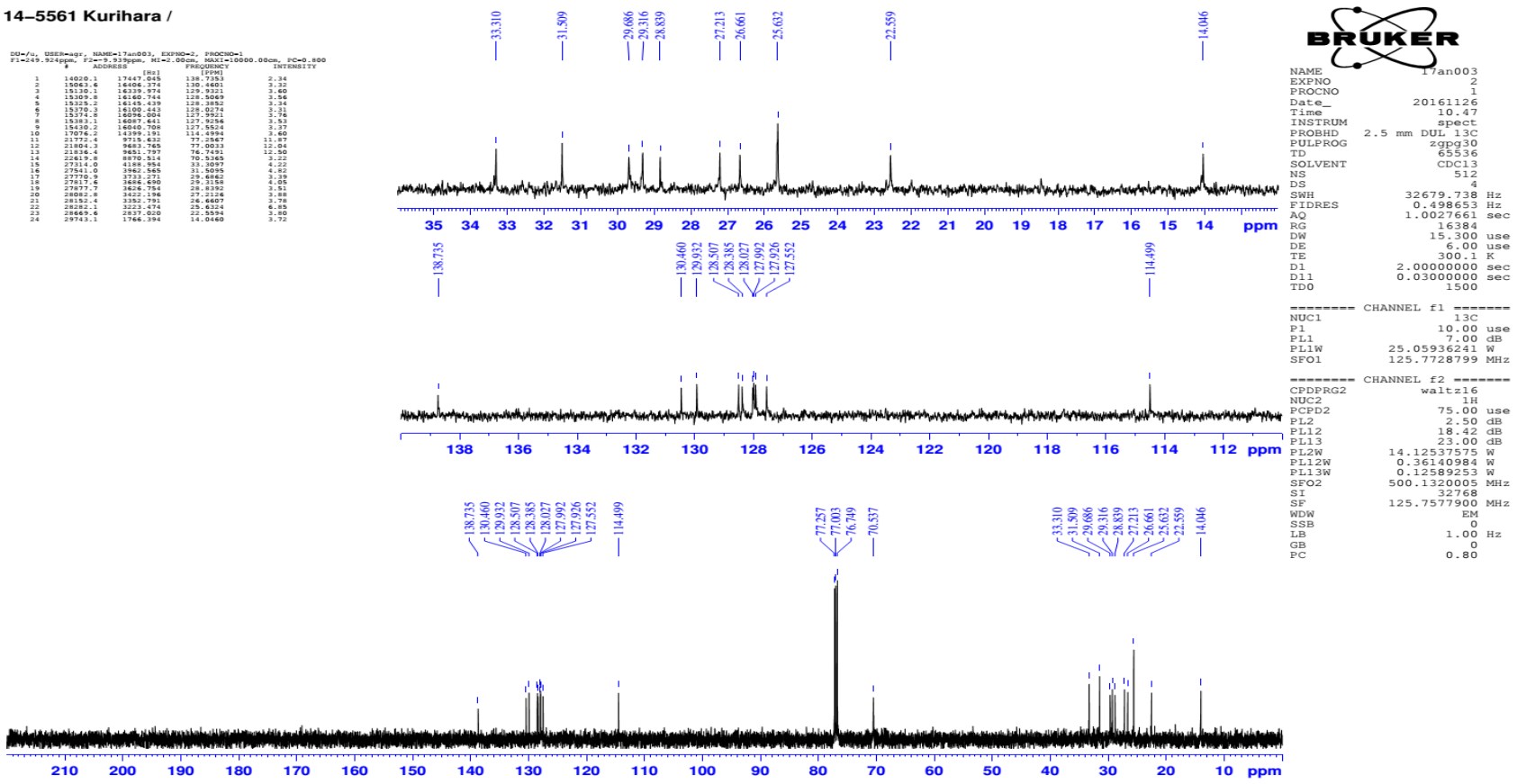


Figure 3-8. ^{13}C-NMR spectrum of compound **J1**.

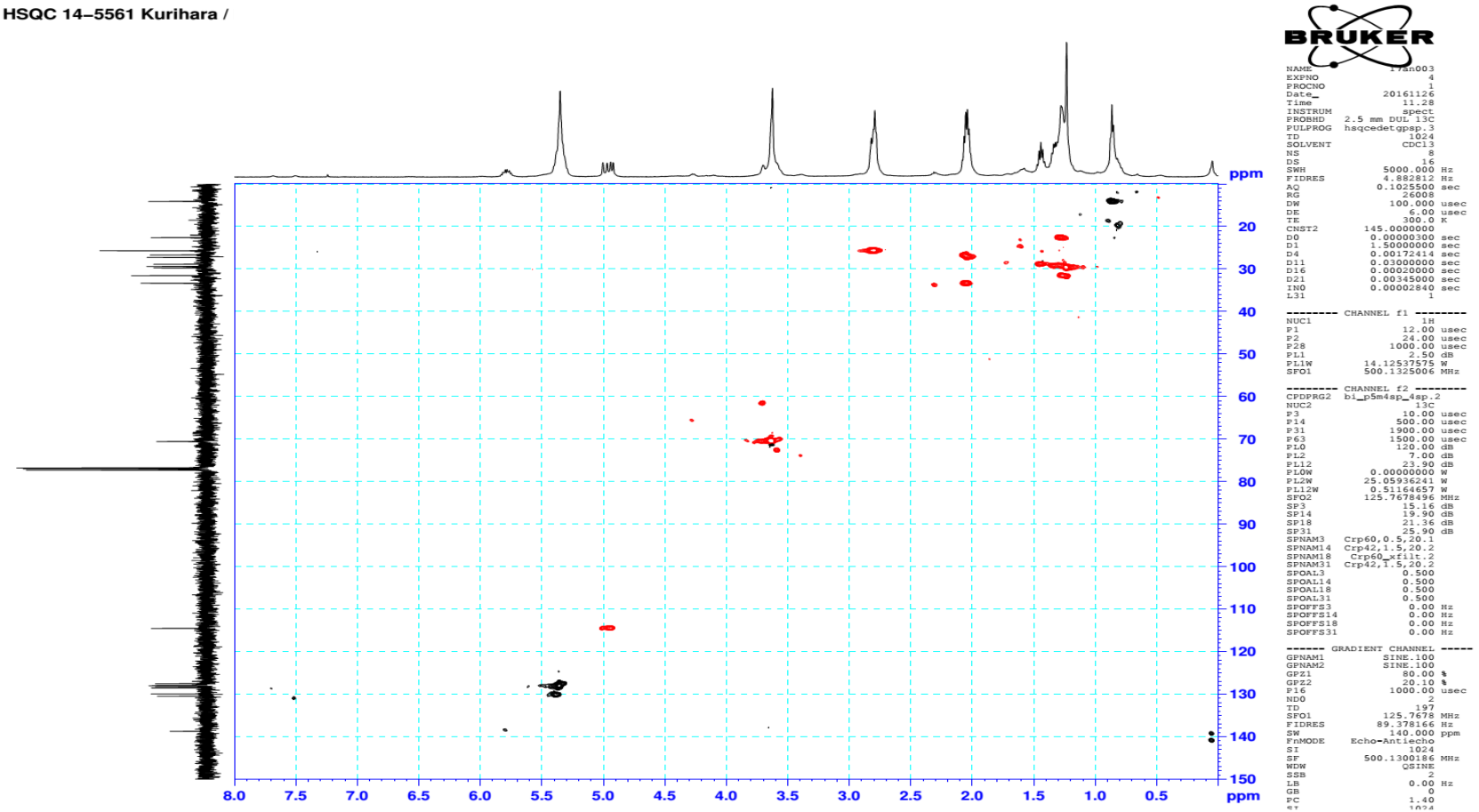


Figure 3-9. HSQC spectrum of compound **J1**.

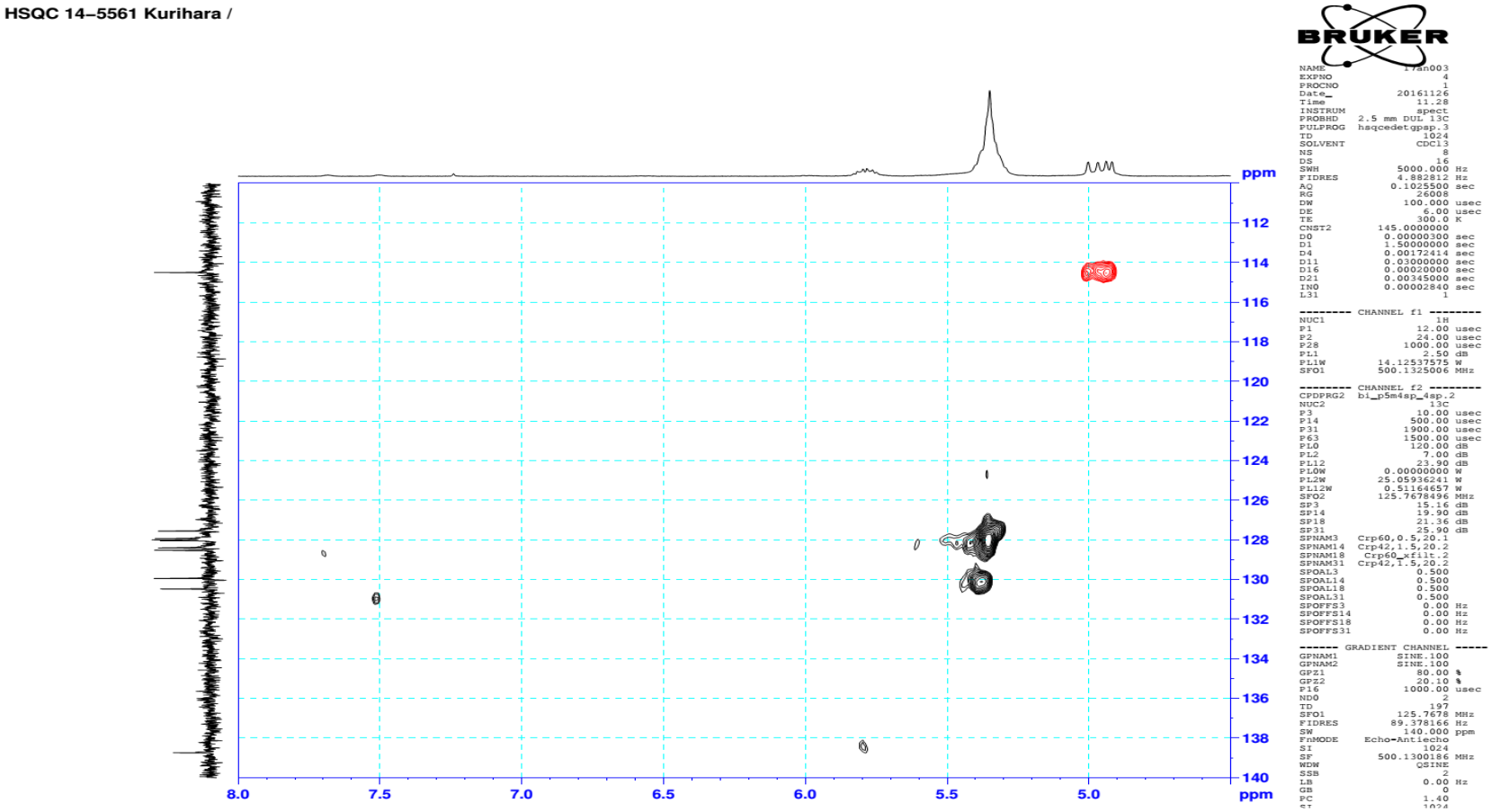


Figure 3-10. Expanded HSQC spectrum (1) of compound **J1**.

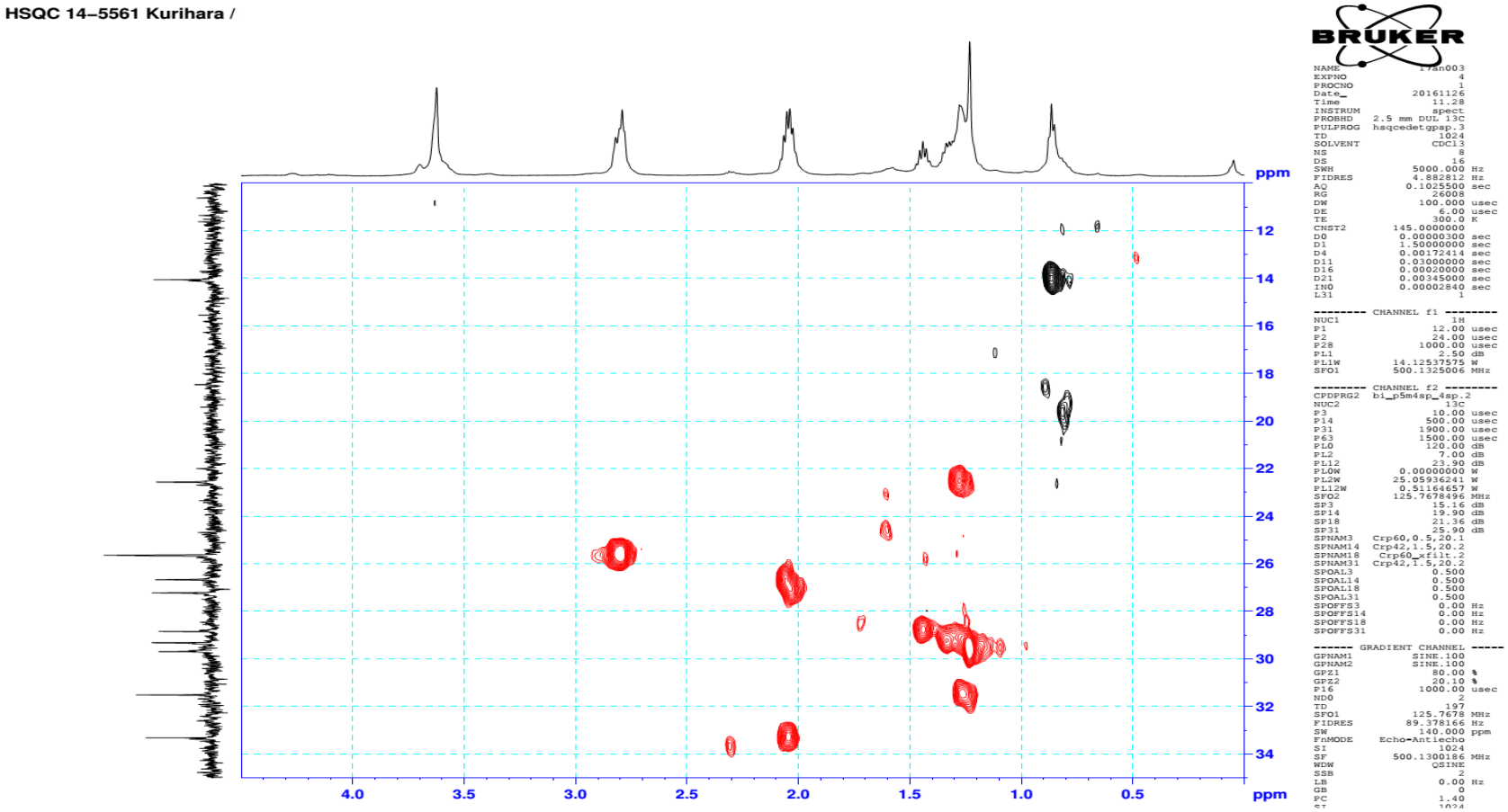


Figure 3-11. Expanded HSQC spectrum (2) of compound **J1**.

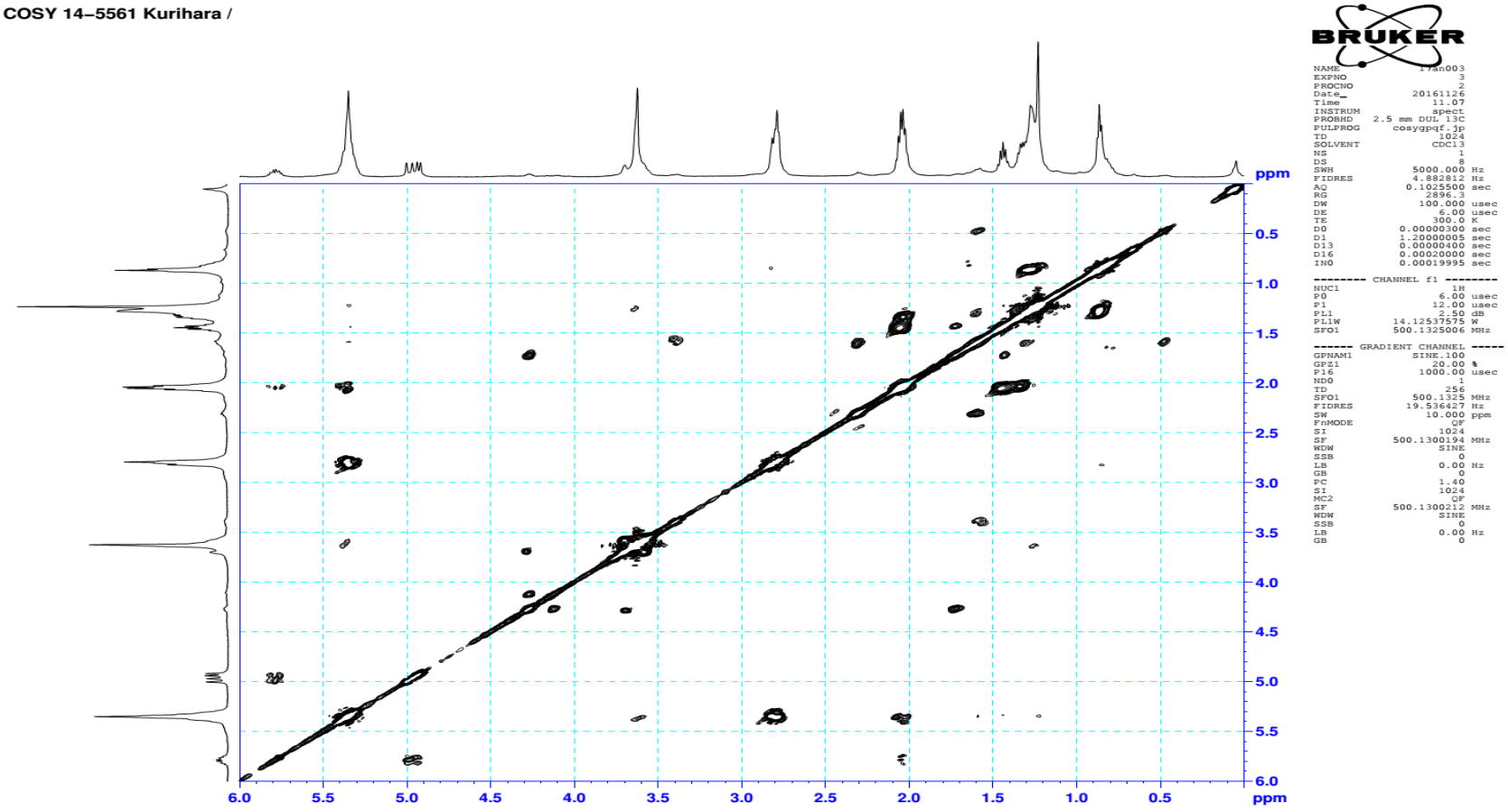


Figure 3-12. COSY spectrum of compound **J1**.

Table 3-4. Comparison of NMR data between compound **J1**[a] and literature data[b]

	^{1}H NMR		^{13}C NMR	
Position	**J1**	Literature data	**J1**	Literature data
1	4.98 (dd, 1.4, 17.1, 1H) 4.93 (dd, 1.4, 10.0, 1H)	5.00 (dd, 1.4, 17.1, 1H) 4.90 (dd, 1.4, 10.0, 1H)	114.5	114.5
2	5.81 (m, 1H)	5.80 (m, 1H)	138.7	138.7
3	2.04 (m, 2H)	2.05 (m, 2H)	33.3	33.3
4	1.45 (m, 2H)	1.45 (m, 2H)	29.3	28.8
5	2.04 (m, 2H)	2.05 (m, 2H)	26.7	26.7
6	5.35 (m, 1H)	5.35 (m, 1H)	130.5	130.5
7	5.35 (m, 1H)	5.35 (m, 1H)	129.9	129.9
8	2.81 (m, 2H)	2.80 (m, 2H)	25.6	25.6
9	5.35 (m, 1H)	5.35 (m, 1H)	128.5	128.5
10	5.35 (m, 1H)	5.35 (m, 1H)	128.4	128.4
11	2.81 (m, 2H)	2.80 (m, 2H)	26.7	25.6
12	5.35 (m, 1H)	5.35 (m, 1H)	128.0	128.0
13	5.35 (m, 1H)	5.35 (m, 1H)	128.0	128.0
14	2.81 (m, 2H)	2.80 (m, 2H)	25.6	25.6
15	5.35 (m, 1H)	5.35 (m, 1H)	127.9	127.9
16	5.35 (m, 1H)	5.35 (m, 1H)	127.6	127.6
17	2.04 (m, 2H)	2.05 (m, 2H)	27.2	27.2
18	1.28 (m, 2H)	1.28 (m, 2H)	29.7	29.3
19	1.28 (m, 2H)	1.28 (m, 2H)	31.5	31.5
20	1.28 (m, 2H)	1.28 (m, 2H)	22.6	22.6
21	0.86 (t, 6.7, 3H)	0.87 (t, 6.8, 3H)	14.0	14.0

[a]The NMR data were measured in chloroform-*d* (δ_H 7.24 ppm; δ_C 77.3 ppm) at 500 MHz for ^{1}H and at 125 MHz for ^{13}C.

[b]Kurihara et al., 2014.

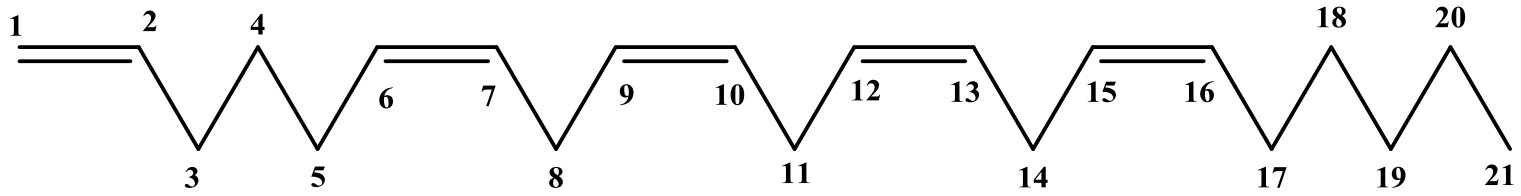


Figure 3-13. Structure of compound **J1**.

3.3 β-Glucuronidase inhibitors derived from the marine brown alga *Sargassum thunbergii*

In this section, *S. thunbergii* (Sargassaceae, Fucales), collected from Usujiri, Hakodate on May 25th, 2016 (Table 1-6) and collected from Usujiri, Hakodate on April 27th, 2017 (Table 1-9) were combined to carried out the isolation and purification of β-glucuronidase inhibitors (Figure 3-14).

3.3.1 Isolation and purification of β-glucuronidase inhibitors from *S. thunbergii*

The combined methanol extracts (55.372 g) of *S. thunbergii* were separated successively by solvent partitioning to obtain *n*-hexane-soluble fraction (6.19 g), chloroform-soluble fraction (7.41 g), ethyl acetate-soluble fraction (2.52 g) and *n*-butanol-soluble fraction (3.64 g) (Table 3-5). All of the fractions showed high inhibitory activity and the analysis of silica gel TLC was developed by chloroform/methanol (9/1, v/v) with the detection by 5% sulfuric acid, 0.2% ninhydrin and DMBA reagents. Mainly, high polar part of the *n*-hexane- and chloroform-soluble fractions showed strong ninhydrin positive responses; ethyl acetate- and *n*-butanol-soluble fractions showed strong positive responses for the DMBA reagent (Figure 3-15).

3.3.1.1 Silica gel column chromatography of *n*-hexane-soluble fraction

The *n*-hexane-soluble fraction was loaded on Wakogel C-100 silica gel column

chromatography and eluted by *n*-hexane/ethyl acetate/methanol to afford 13 fractions (Fraction H-1~H-13) (Table 3-6, Figure 3-16). Among them, fraction H-3 (22.6 mg, 19.2 ppm on the basis of air-dried alga) was determined as pure compound depended on the high performance silica gel TLC profile (Figure 3-17). MS and NMR spectra (Figures 3-19 to 3-21) were identical to those of compound **J1** purified from *S. confusum*.

Besides, fraction H-4 (1334.0 mg) which showed similar TLC profile as fraction H-3 (Figure 3-17) was determined to perform the further separation.

3.3.1.2 Silica gel column chromatography of fraction H-4

Fraction H-4 (1334.0 mg) was rechromatographed over Wakogel C-100 silica gel and eluted with a gradient increasing ethyl acetate (0-100%) in *n*-hexane to obtain fractions H4-1~H4-11 (Table 3-7). Among them, fraction H4-4 (53.8 mg, 45.7 ppm on the basis of air-dried alga) showed one single spot on high performance silica gel TLC (Figure 3-18) and named as compound **U2**.

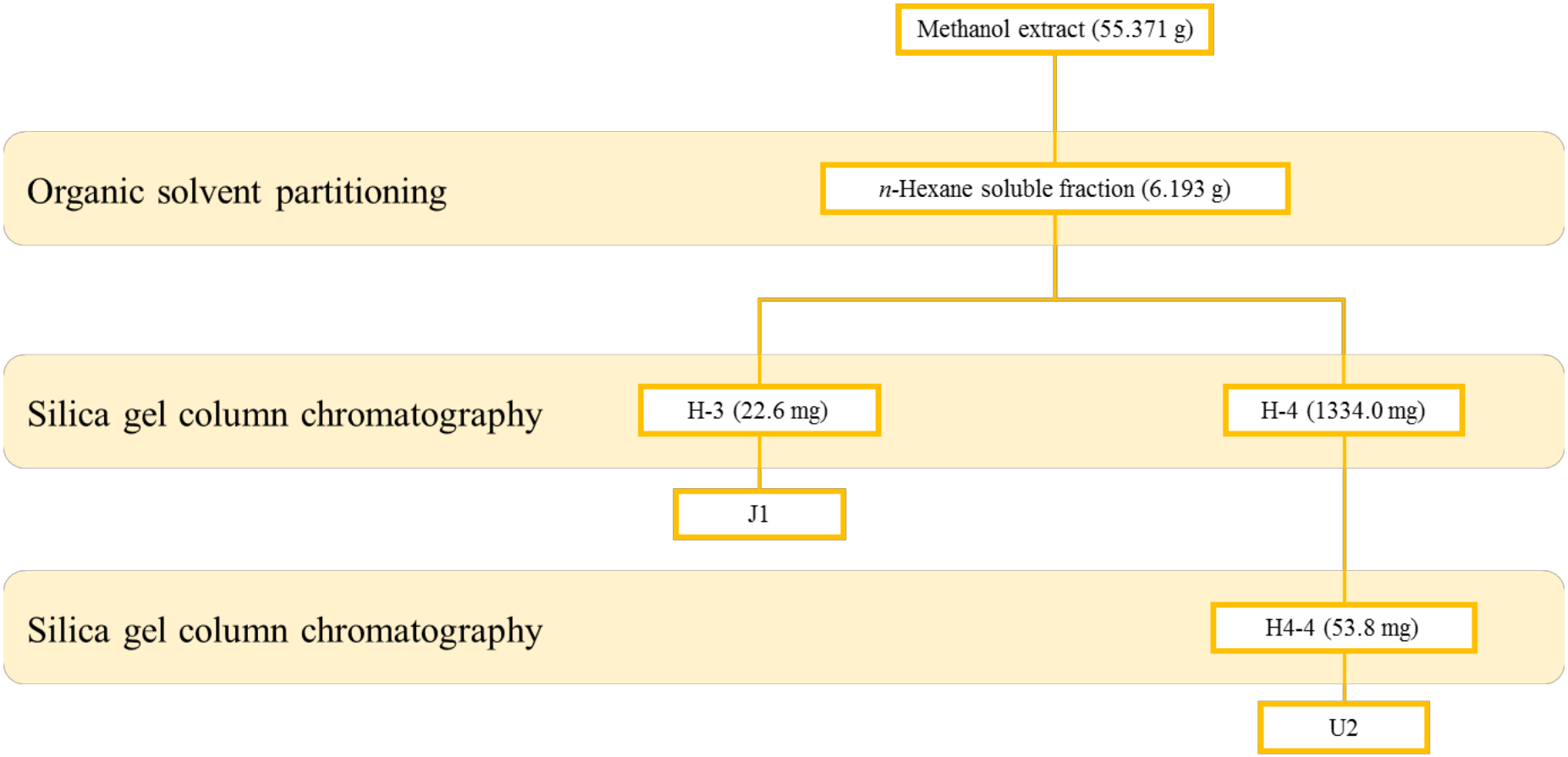


Figure 3-14. Separation scheme for the extract of *S. thunbergii* collected at Usujiri.

Table 3-5. Amount and β-glucuronidase inhibitory activity of the fractions[a] obtained by organic solvent partitioning

Fraction	Amount (g)	Inhibition[b] (%)
n-Hexane	6.193	38.60 ±3.23
$CHCl_3$	7.406	90.85 ±3.15
Ethyl acetate	2.520	97.90±0.50
n-Butanol	3.636	88.93 ± 0.80

[a]Sample, 55.371 g methanol extracts of *S*. *thunbergii*.

[b]Assay concentration was 10 μg/mL. Data represent means ± SE (n=3).

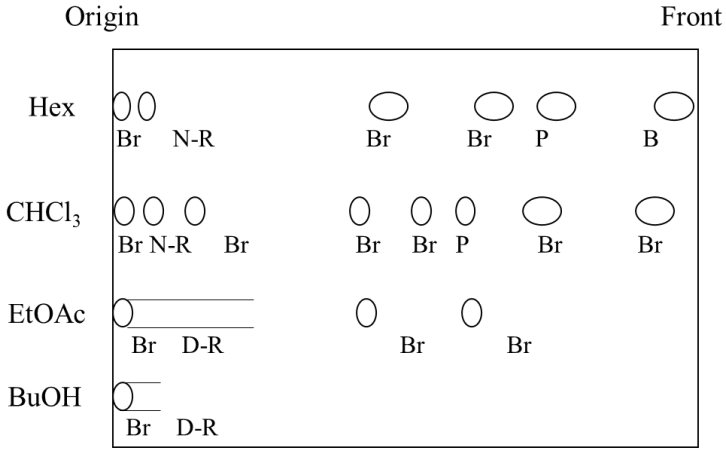


Figure 3-15. Silica gel thin layer chromatogram of the organic solvent extracts of *S*. *thunbergii*.

Developing solvent, chloroform: methanol = 9:1 (v/v).

⬭, Visualized with 5% sulfuric acid reagent; 0.2% ninhydrin reagent; DMBA reagent.

Abbreviations designate color of spots: Br, Brown; P, purple; B, blue; N-R, red color by ninhydrin reagent; D-R, red color by DMBA reagent.

Table 3-6. Amount and β-glucuronidase inhibitory activity of the fractions obtained from *n*-hexane-soluble fraction[a] separated by silica gel column chromatography

Fraction	Eluent (v/v)	Amount (mg)	Inhibition[b] (%)
H-1	*n*-Hexane	888.3	2.86 ± 2.46
H-2	*n*-Hexane	1.9	NI[c]
H-3	*n*-Hexane : ethyl acetate = 4 : 1	22.6	64.44 ± 1.23
H-4	*n*-Hexane : ethyl acetate = 4 : 1	1334.0	36.64 ± 1.17
H-5	*n*-Hexane : ethyl acetate = 2 : 1	2331.2	3.30 ± 1.71
H-6	*n*-Hexane : ethyl acetate = 2 : 1	125.7	39.20 ± 1.33
H-7	*n*-Hexane : ethyl acetate = 1 : 2	89.4	35.28 ± 1.40
H-8	*n*-Hexane : ethyl acetate = 1 : 2	37.4	25.12 ± 2.13
H-9	Ethyl acetate	15.0	18.33 ± 1.84
H-10	Ethyl acetate	37.8	24.33 ± 5.35
H-11	Ethyl acetate : Methanol = 1 : 1	896.3	6.73 ± 1.00
H-12	Ethyl acetate : Methanol = 1 : 1	169.7	9.99 ± 0.00
H-13	Methanol	104.1	NI

[a]Sample, *n*-hexane soluble fraction, 6.193 g; stationary phase, Wakogel C-100; elution volume, 694 mL/fraction.

[b]Assay concentration was 10 μg/mL. Data represent means ± SE (n=3).

[c]NI, no inhibition.

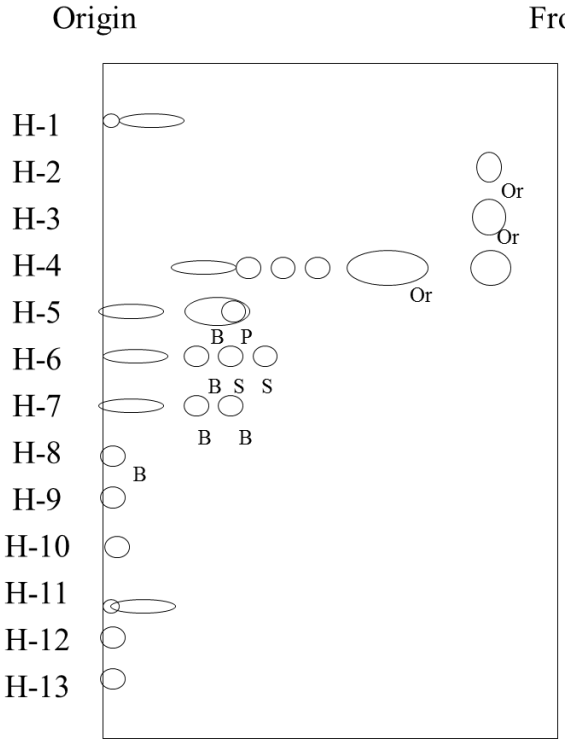


Figure 3-16. Silica gel thin layer chromatogram of fractions obtained from *n*-hexane-soluble fraction separated by silica gel column chromatography.

Developing solvent, *n*-hexane: ethyl acetate = 3: 1 (v/v).

⬭, Visualized with 5% sulfuric acid reagent.

Abbreviations designate color of the spots: B, blue; Or, orange; P, purple; S, quenching spot under short wave UV lamp.

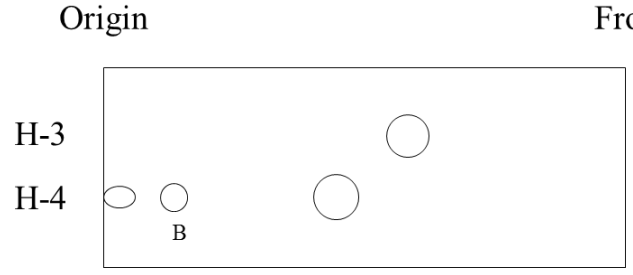


Figure 3-17. High performance silica gel thin layer chromatogram of fractions H-3 and H-4.

Developing solvent, *n*-hexane.

⬭, Visualized with 5% sulfuric acid reagent.

Abbreviation designates color of the spot: B, blue.

Table 3-7. Amount and β-glucuronidase inhibitory activity of the fractions obtained from fraction H-4[a] separated by silica gel column chromatography

Fraction	Eluent (v/v)	Amount (mg)	Inhibition[b] (%)
H4-1	*n*-Hexane	1.26	NI[c]
H4-2	*n*-Hexane	1.4	NI
H4-3	*n*-Hexane : ethyl acetate = 19 : 1	3.7	2.34 ± 0.32
H4-4	*n*-Hexane : ethyl acetate = 19 : 1	53.8	66.73 ± 0.44
H4-5	*n*-Hexane : ethyl acetate = 9 : 1	747.8	30.50 ± 1.88
H4-6	*n*-Hexane : ethyl acetate = 9 : 1	163.8	12.47 ± 1.34
H4-7	*n*-Hexane : ethyl acetate = 4 : 1	184.0	19.68 ± 1.49
H4-8	*n*-Hexane : ethyl acetate = 4 : 1	195.6	26.39 ± 1.06
H4-9	*n*-Hexane : ethyl acetate = 1 : 1	12.3	31.27 ± 0.83
H4-10	*n*-Hexane : ethyl acetate = 1 : 1	3.2	29.42 ± 0.57
H4-11	Ethyl acetate	3.1	17.85 ± 0.85

[a]Sample, fraction H-4, 1334.0 g; stationary phase, Wakogel C-100; elution volume, 245 mL/fraction.

[b]Assay concentration was 10 μg/mL. Data represent means ± SE (n=3).

[c]NI, no inhibition.

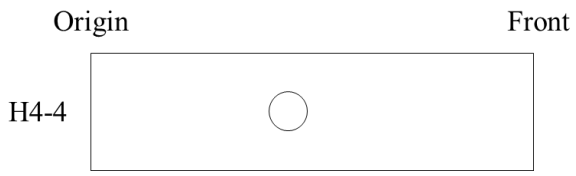


Figure 3-18. High performance silica gel thin layer chromatogram of fraction H4-4. Developing solvent, *n*-hexane.

⬭, Visualized with 5% sulfuric acid reagent.

3.3.1.3 MS and NMR data of compound J1 obtained from *S. thunbergii*

Physicochemical data for compound **J1** obtained from *S. thunbergii* were identical with compound **J1** obtained from *S. confusum* as follow: FI-MS: *m/z* 286.27$[M]^+$; FI-HR-MS: *m/z* 286.26726 (calculated 286.26605 for $C_{21}H_{34}$); ^{1}H NMR (500 MHz, $CDCl_3$) ppm: 5.80 (m, 8H, H-6, 7, 9, 10, 12, 13, 15, 16), 5.00 (dd, *J* = 1.4, 17.0 Hz, 1H, H-1), 4.90 (dd, *J* = 1.4, 10.0 Hz, 1H, H-1), 2.80 (m, 6H, H-8, 11, 14), 2.05 (m, 6H, H-3, 5, 17), 1.45 (m, 2H, H-4), 1.28 (m, 6H, H-18, 19, 20), 0.87 (t, *J* = 6.8 Hz, 3H, H-21); ^{13}C NMR (125 MHz, $CDCl_3$) ppm: 138.8 (C-2), 130.6, 130.0, 128.6, 128.5, 128.1, 128.1, 128.0, 127.6, 114.6 (C-6, 7, 9, 10, 12, 13, 15, 16), 33.4 (C-3), 31.6 (C-19), 29.4 (C-18), 28.9 (C-4), 27.3 (C-17), 26.8 (C-5), 25.7, 25.7, 25.7 (C-8, 11, 14), 22.7 (C-20), 14.1 (C-21) (Figures 3-19 to 3-21).

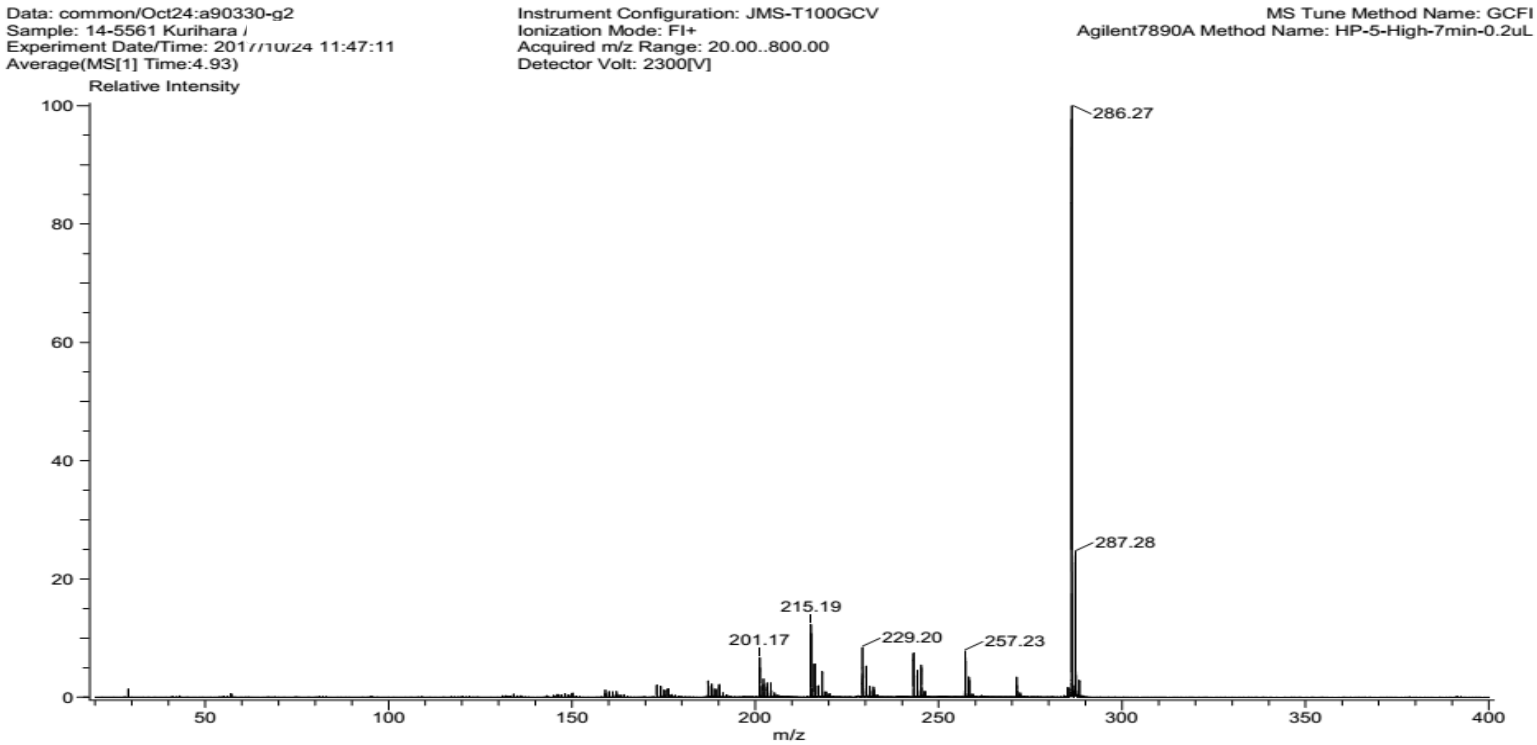


Figure 3-19. FI-MS spectrum of compound **J1** obtained from *S*. *thunbergii*.

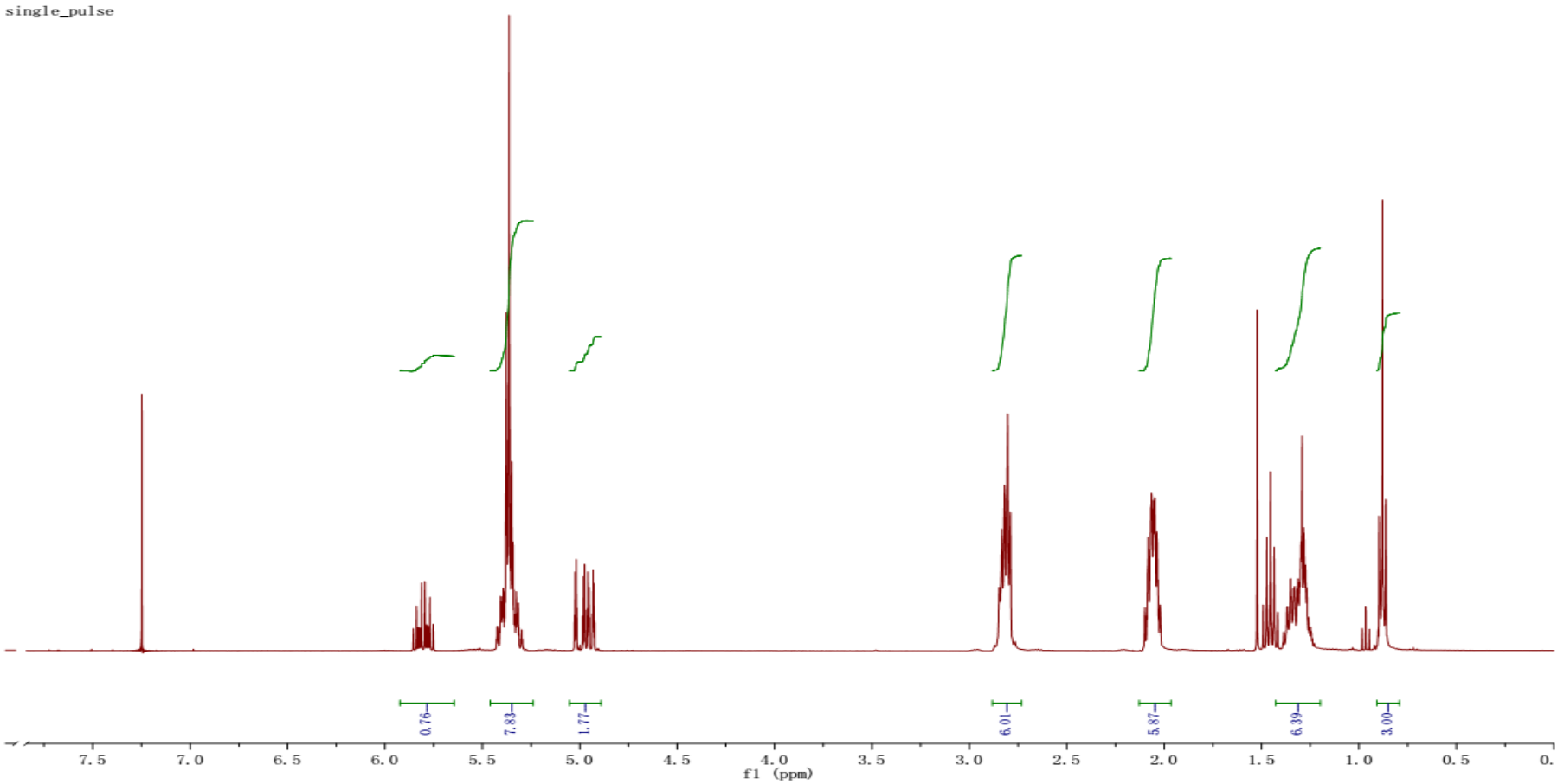


Figure 3-20. ^{1}H-NMR spectrum of compound **J1** obtained from *S. thunbergii*.

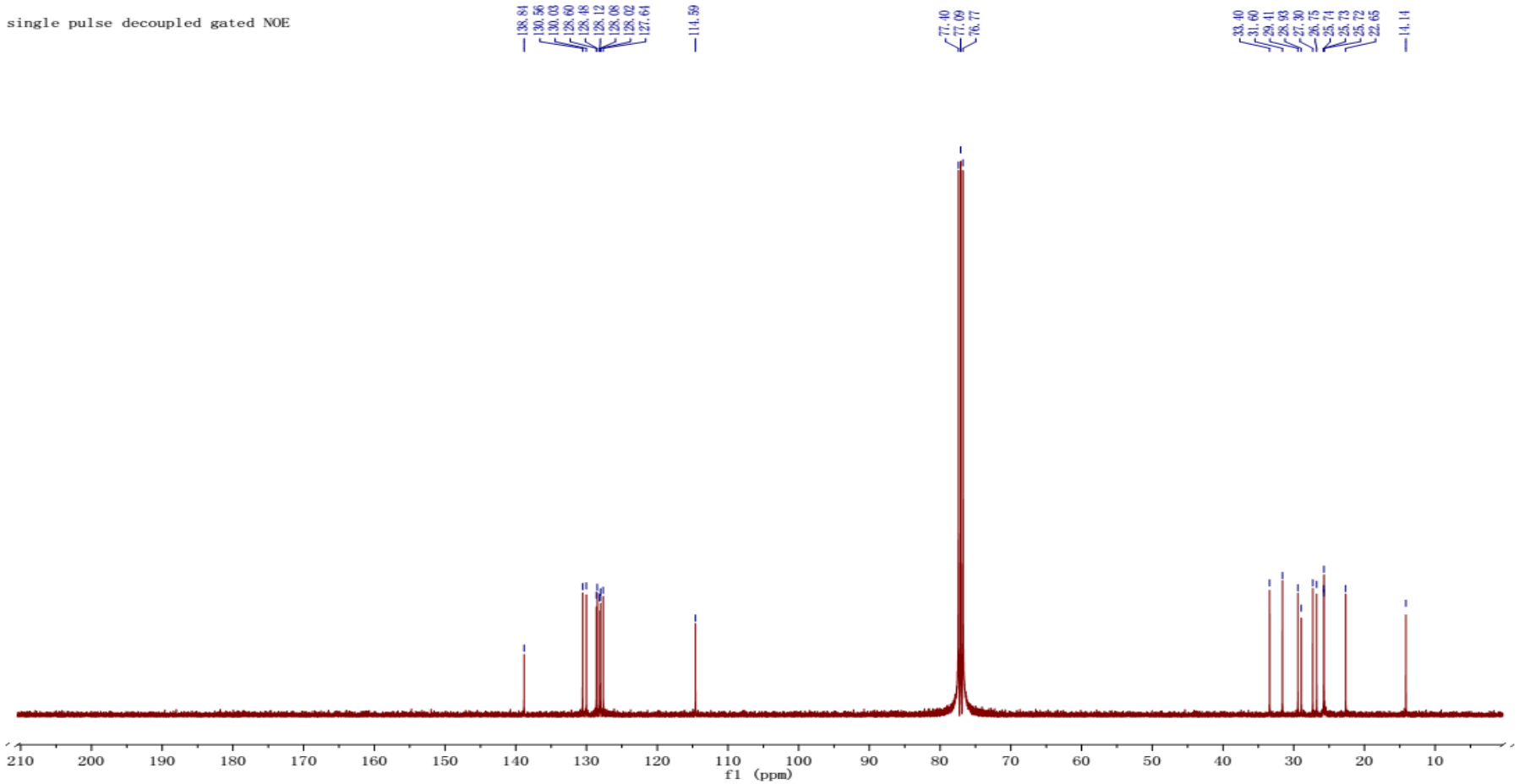


Figure 3-21. ^{13}C-NMR spectrum of compound **J1** obtained from *S. thunbergii*.

3.3.1.4 Structural elucidation of β-glucuronidase inhibitor U2

Compound **U2** was obtained as colorless oil. The FI-MS spectrum of compound **U2** revealed a molecular ion peak at m/z 284 (Figure 3-22). Molecular formula was determined by FI-HR-MS at *m/z* 284.25115 for $C_{21}H_{32}$ (calculated 284.25040), which showed 2 mass units decrease compared to compound **J1**. ^{1}H and ^{13}C NMR spectra were similar to those of compound **J1** except for the appearance of one additional double bond and disappearance of two methylenes in the side chain (Figures 3-23 and 3-24). Thus, compound **U2** was identified as (6*Z*,9*Z*,12*Z*,15*Z*,18*Z*)-1,6,9,12,15,18-henicosahexanene (Table 3-8, Figure 3-25) with comparison with literature data (Kurihara et al., 2014).

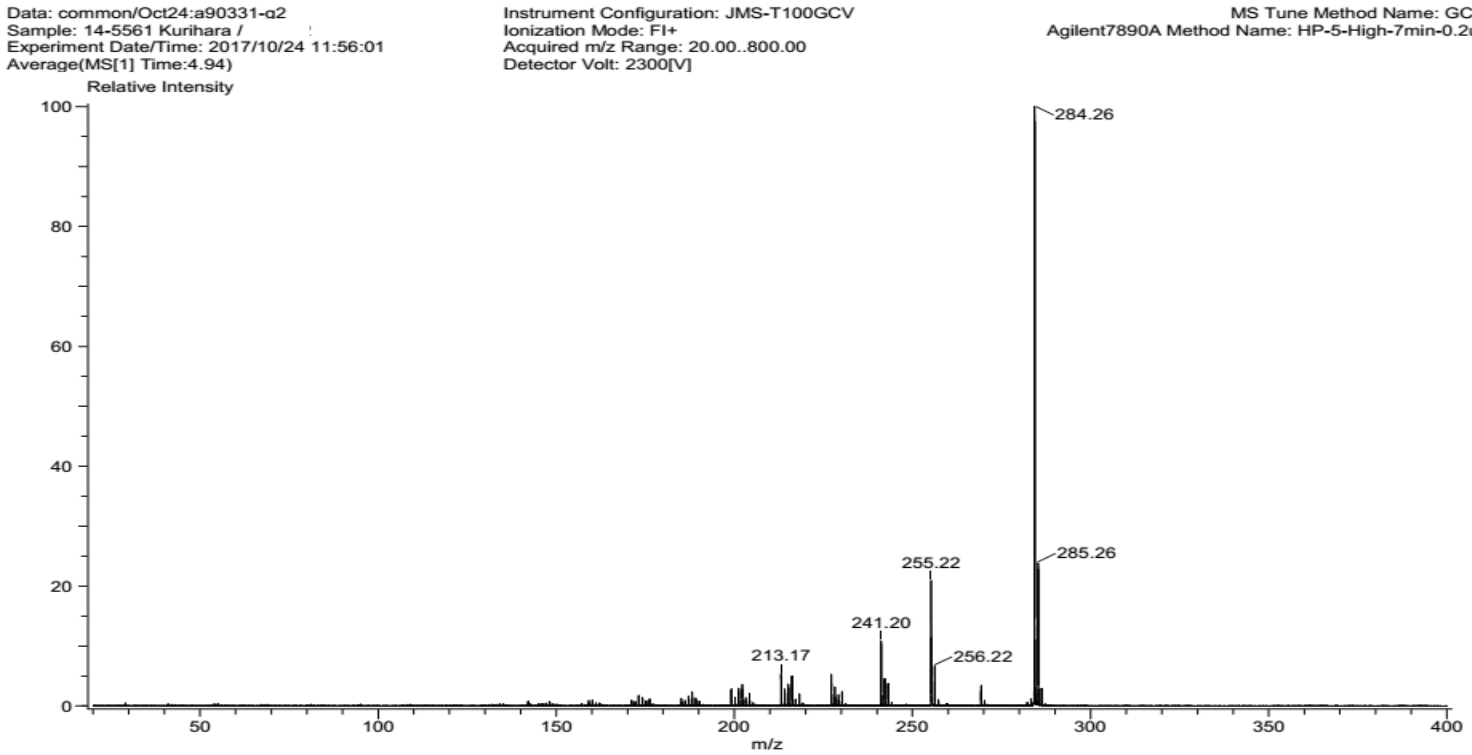


Figure 3-22. FI-MS spectrum of compound **U2**.

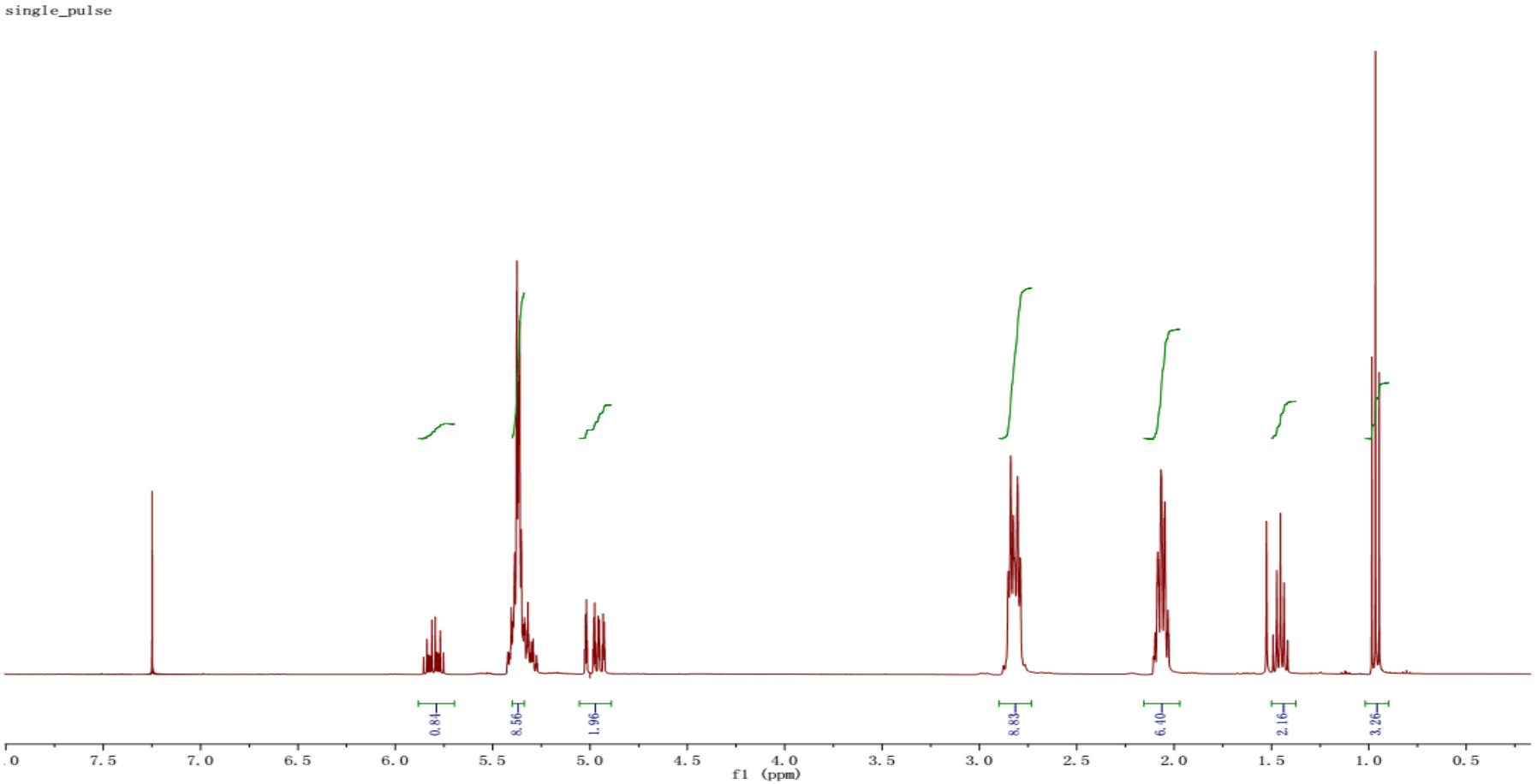


Figure 3-23. ^{1}H-NMR spectrum of compound **U2**.

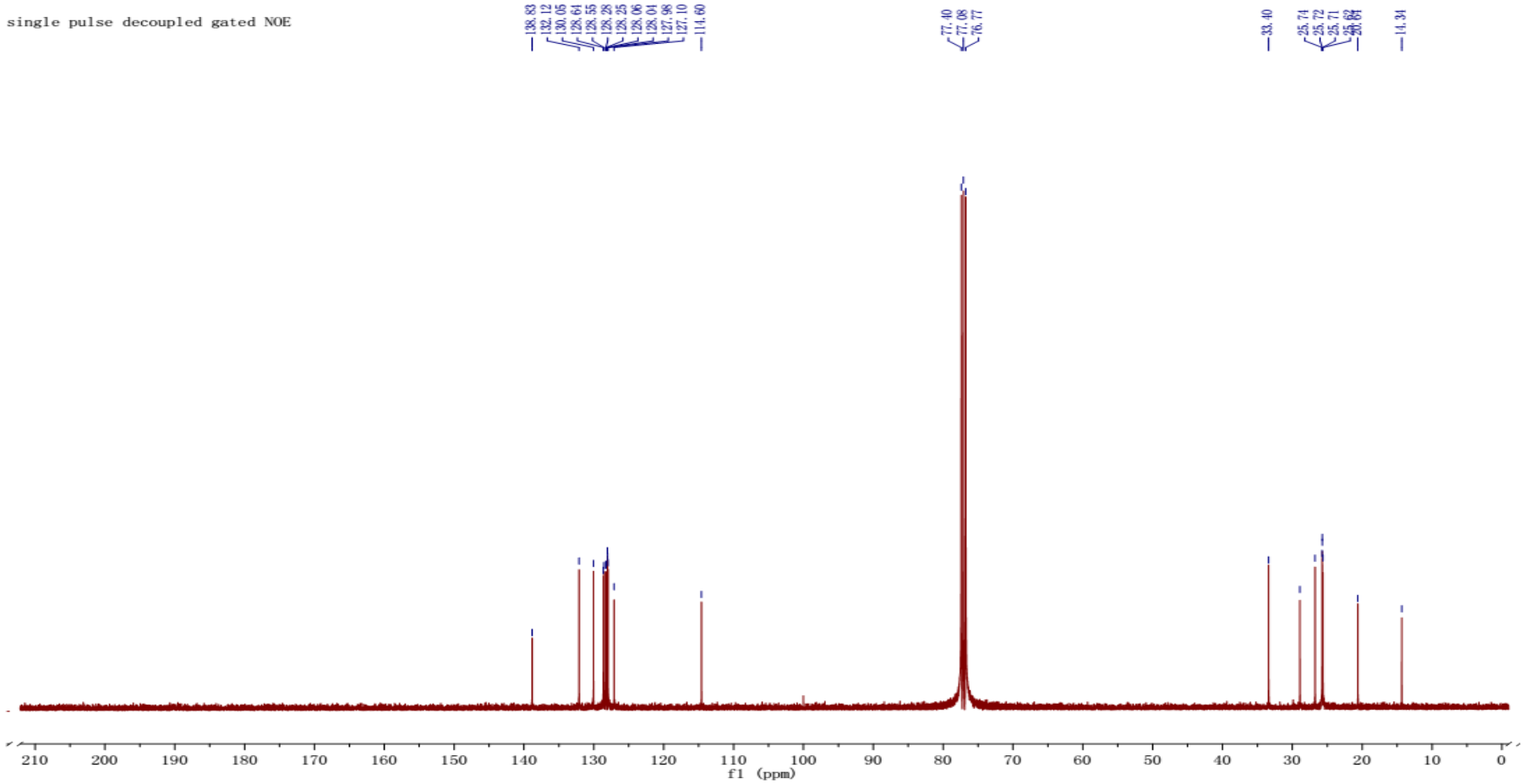


Figure 3-24. ^{13}C-NMR spectrum of compound **U2**.

Table 3-8. Comparison of NMR data between compound **U2**[a] and literature[b]

	^{1}H NMR		^{13}C NMR	
Position	**U2**	Literature data	**U2**	Literature data
1	5.00 (dd, 1.8 17.1, 1H) 4.95 (dd, 1.2, 10.2, 1H)	5.00 (dd, 1.0, 17.1, 1H) 4.94 (dd, 1.4, 10.1, 1H)	114.6	114.5
2	5.80 (m, 1H)	5.80 (m, 1H)	138.8	138.7
3	2.05 (m, 2H)	2.06 (m, 2H)	33.4	33.3
4	1.44 (m, 2H)	1.44 (m, 2H)	28.9	28.8
5	2.05 (m, 2H)	2.06 (m, 2H)	26.8	26.7
6	5.36 (m, 1H)	5.35 (m, 1H)	132.1	132.0
7	5.36 (m, 1H)	5.35 (m, 1H)	130.5	130.0
8	2.82 (m, 2H)	2.81 (m, 2H)	25.7	25.6
9	5.36 (m, 1H)	5.35 (m, 1H)	128.6	128.6
10	5.36 (m, 1H)	5.35 (m, 1H)	128.5	128.5
11	2.82 (m, 2H)	2.81 (m, 2H)	25.7	25.6
12	5.36 (m, 1H)	5.35 (m, 1H)	128.3	128.2
13	5.36 (m, 1H)	5.35 (m, 1H)	128.3	128.2
14	2.82 (m, 2H)	2.81 (m, 2H)	25.7	25.6
15	5.36 (m, 1H)	5.35 (m, 1H)	128.0	128.0
16	5.36 (m, 1H)	5.35 (m, 1H)	128.0	128.0
17	2.82 (m, 2H)	2.81 (m, 2H)	25.6	25.5
18	5.36 (m, 1H)	5.35 (m, 1H)	128.0	127.9
19	5.36 (m, 1H)	5.35 (m, 1H)	127.1	127.0
20	2.05 (m, 2H)	2.06 (m, 2H)	20.6	20.5
21	0.96 (t, 7.5, 3H)	0.96 (t, 7.5, 3H)	14.3	14.2

[a]The NMR data were measured in chloroform-*d* (δ_H 7.25 ppm; δ_C 77.4 ppm) at 400 MHz for ^{1}H and at 100 MHz for ^{13}C.

[b]Kurihara et al., 2014.

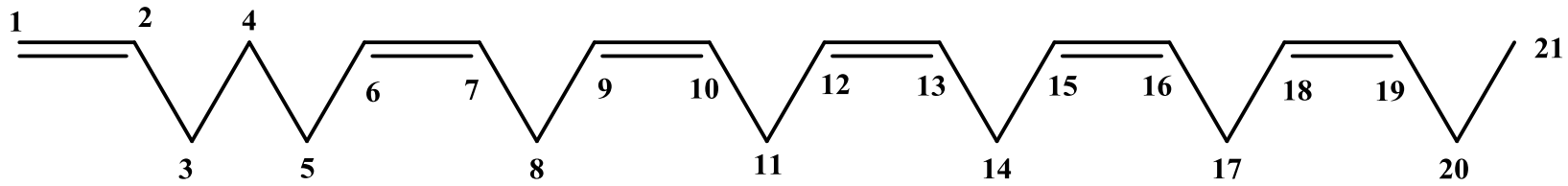


Figure 3-25. Structure of compound **U2**.

3.4 β-Glucuronidase inhibitors derived from the marine brown alga *Agarum clathratum*

In this section, *A*. *clathratum* (Agaraceae, Laminariales), collected from Habomai, Nemuro on May 26th, 2017 (Table 1-10) was used for the isolation and purification of β-glucuronidase inhibitors (Figure 3-26).

3.4.1 Isolation and purification of β-glucuronidase inhibitors from *A. clathratum*

Methanol extract (20.74 g) of *A*. *clathratum* was conducted for the successive organic solvent partitioning to afford *n*-hexane-soluble fraction (7.56 g), chloroform-soluble fraction (3.77 g), ethyl acetate-soluble fraction (2.22 g) and *n*-butanol-soluble fraction (8.41 g) (Table 3-9).

All the fractions showed high inhibitory activity, and the analysis of TLC was detected by 5% sulfuric acid and DMBA reagent. Positive response for DMBA reagent appeared at ethyl acetate soluble fraction which demonstrated the presence of phloroglucinol or its oligomers (phlorotannins) (Figure 3-27). In this part, *n*-hexane-soluble fraction and ethyl acetate-soluble fraction were selected for the further purification of β-glucuronidase inhibitory compounds

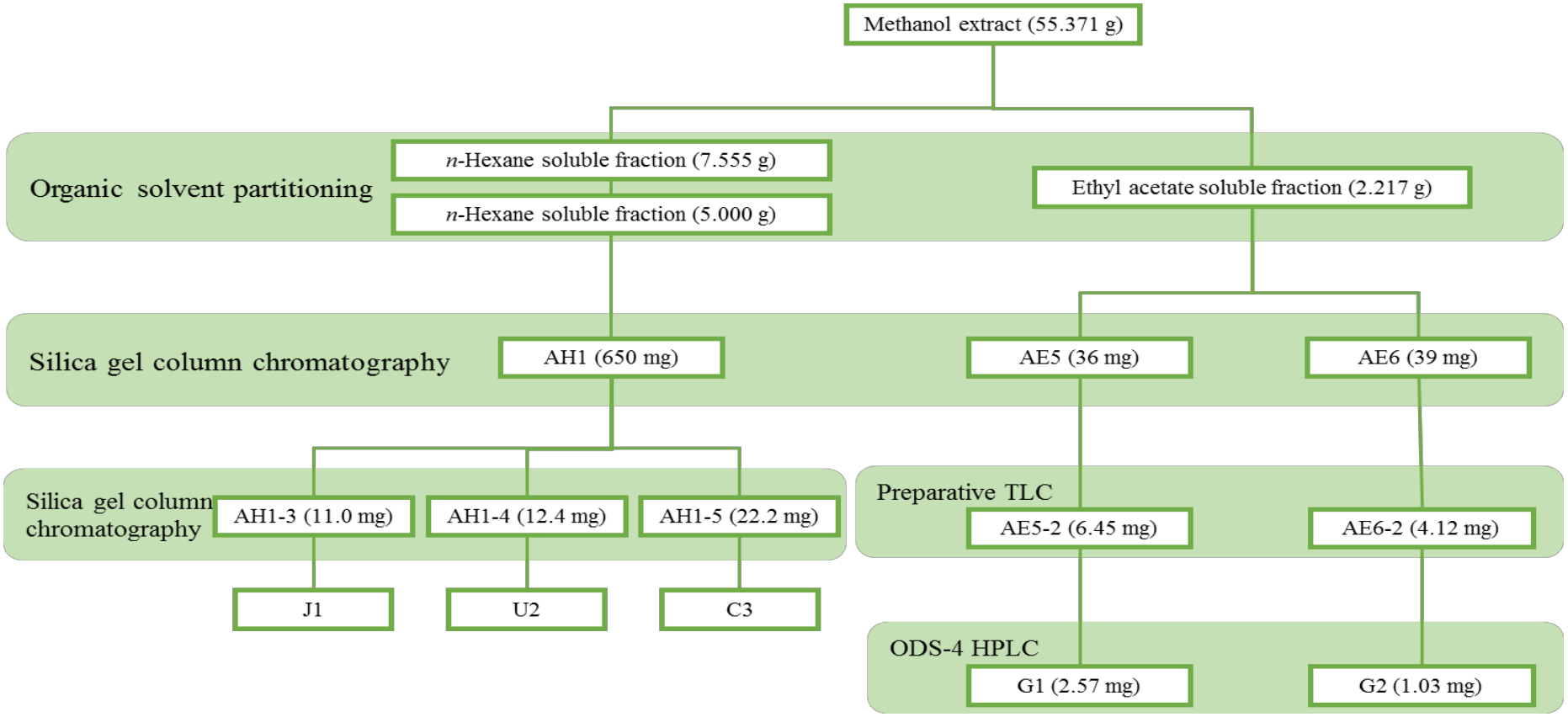


Figure 3-26. Separation scheme for the extract of *A. clathratum* collected at Habomai, Nemuro.

Table 3-9 Amount and β-glucuronidase inhibitory activity of the fractions[a] obtained by organic solvent partitioning

Fraction	Amount (g)	Inhibition[b] (%)
n-Hexane	7.555	53.75 ± 0.57
Chloroform	3.768	98.59 ± 1.11
Ethyl acetate	2.217	99.56 ± 0.59
n-Butanol	8.405	98.52 ± 0.53

[a]Sample, 20.742 g methanol extracts of *A*. *clathratum*

[b]Assay concentration was 10 μg/mL. Data represent means ± SE (n=3).

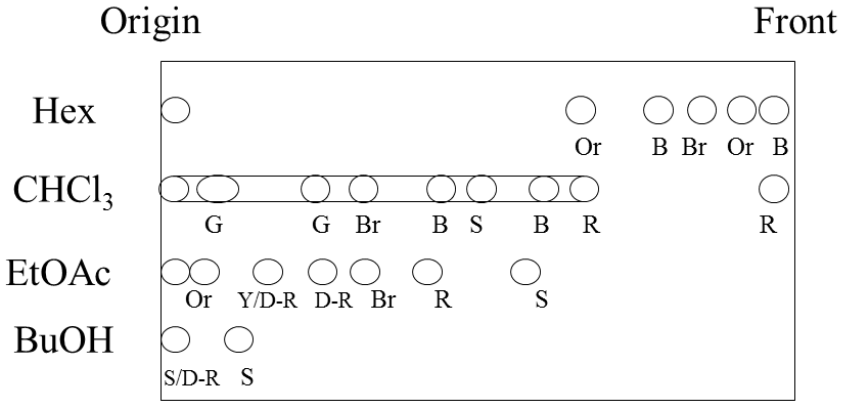


Figure 3-27. Silica gel thin layer chromatogram of the organic solvent extracts of *A*. *clathratum*.

Developing solvent, chloroform: methanol = 9: 1 (v/v).

⬭, Visualized with 5% sulfuric acid reagent and DMBA reagent.

Abbreviations designate color of spots: Br, Brown; Or, orange; B, blue; G, green; S, quenching spot under short wave UV lamp; R, red color under long wave UV lamp; D-R, red color by DMBA reagent.

3.4.1.1 β-Glucuronidase inhibitors isolated from *n*-hexane-soluble fraction of *A. clathratum*

An aliquot (5.10 g) of the *n*-hexane-soluble fraction was chromatographed on Wakogel C-100 silica gel column chromatography eluted by *n*-hexane/ethyl acetate/methanol to give fractions AH1 to AH13 (Table 3-10, Figure 3-28). Fraction AH1, the second highest inhibitory activity, showed similar spots to compounds **J1** and **U2** (Figure 3-29). Therefore, fraction AH1 was loaded on Wakogel C-100 silica gel column chromatography to do the further separation.

Fraction AH1 (650 mg) was re-chromatographed on Wakogel C-100 silica gel eluted with a gradient increasing ethyl acetate (0-100%) in *n*-hexane. Obtained fractions were combined by the analysis of TLC profiles to give six fractions AH1-1 to AH1-6 (Table 3-11). Among them, fractions AH1-3 (11.0 mg), AH1-4 (12.4 mg) and AH1-5 (22.2 mg) showed one single spot on high performance silica gel TLC (Figure 3-30). According to the TLC analysis, fractions AH1-3 and AH1-4 were confirmed as compound **J1**, (6*Z*,9*Z*,12*Z*,15*Z*)-1,6,9,12,15-henicosapentaene (**J1**, yield 10.4 ppm on the basis of air-dried alga), and (6*Z*,9*Z*,12*Z*,15*Z*,18*Z*)-1,6,9,12,15,18-henicosahexanene (**U2**, yield 11.7 ppm), respectively (Figure 3-31). Meanwhile, fraction AH1-5 (22.2 mg, yield 21.0 ppm), named compound **C3**, was conducted for the MS and NMR spectrometry experiments to determine its structure.

Table 3-10. Amount and β-glucuronidase inhibitory activity of the fractions obtained from *n*-hexane-soluble fraction[a] separated by silica gel column chromatography

Fraction	Eluent (v/v)	Amount (mg)	Inhibition[b] (%)
AH1	*n*-Hexane : ethyl acetate = 9 : 1	650	59.64 ± 2.99
AH2	*n*-Hexane : ethyl acetate = 9 : 1	366	NI[c]
AH3	*n*-Hexane : ethyl acetate = 4 : 1	592	NI
AH4	*n*-Hexane : ethyl acetate = 4 : 1	599	15.87 ± 1.28
AH5	*n*-Hexane : ethyl acetate = 2 : 1	1538	15.66 ± 1.72
AH6	*n*-Hexane : ethyl acetate = 2 : 1	69	5.34 ± 0.75
AH7	*n*-Hexane : ethyl acetate = 1 : 2	33	4.88 ± 3.31
AH8	*n*-Hexane : ethyl acetate = 1 : 2	43	68.11 ± 5.50
AH9	Ethyl acetate	9	30.68 ± 0.27
AH10	Ethyl acetate	12	29.32 ± 1.49
AH11	Ethyl acetate : Methanol = 1 : 1	758	81.00 ± 3.37
AH12	Ethyl acetate : Methanol = 1 : 1	112	55.94 ± 1.66
AH13	Methanol	78	37.39 ± 2.71

[a]Sample, *n*-hexane-soluble fraction, 5.000 g; stationary phase, Wakogel C-100; elution volume, 800 mL/fraction.

[b]Assay concentration was 10 μg/mL. Data represent means ± SE (n=3).

[c]NI, no inhibition.

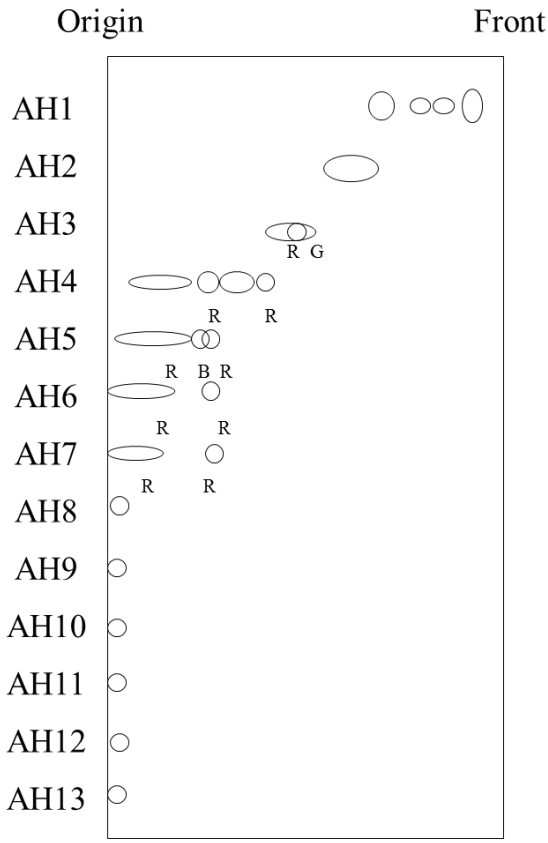


Figure 3-28. Silica gel thin layer chromatogram of fractions obtained from *n*-hexane-soluble fraction separated by silica gel column chromatography.

Developing solvent, *n*-hexane: ethyl acetate = 4:1 (v/v).

⬭, Visualized with 5% sulfuric acid reagent.

Abbreviations designate color of the spots: B, blue; G, green; R, red color under long wave UV lamp.

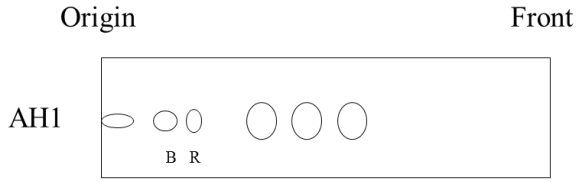


Figure 3-29. Silica gel thin layer chromatogram of fraction AH1.

Developing solvent, *n*-hexane.

⬭, Visualized with 5% sulfuric acid reagent.

Abbreviations designate color of the spots: B, blue; R, red color under long wave UV lamp.

Table 3-11. Amount and β-glucuronidase inhibitory activity of the fractions obtained from fraction AH1[a] separated by silica gel column chromatography

Fraction	Amount (mg)	Inhibition[b] (%)
AH1-1	4.5	9.39 ± 3.03
AH1-2	27.1	23.72 ± 2.02
AH1-3	11.0	64.44 ± 1.23
AH1-4	12.4	66.73 ± 0.44
AH1-5	22.2	88.23 ± 1.64
AH1-6	563.5	23.31 ± 0.39

[a]Sample, fraction AH1, 650 mg; stationary phase, Wakogel C-100; column size, H, 36.5 cm, R, 1 cm; elution, *n*-hexane/ethyl acetate.

[b]Assay concentration was 10 μg/mL. Data represent means ± SE (n=3).

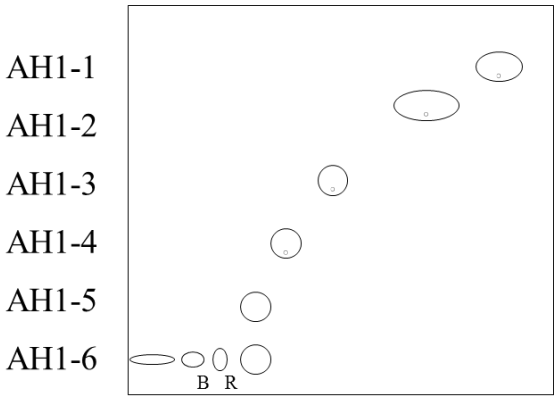


Figure 3-30. Silica gel thin layer chromatogram of fractions obtained from fraction AH1 separated by silica gel column chromatography.

Developing solvent, *n*-hexane.

⬭, Visualized with 5% sulfuric acid reagent.

Abbreviations designate color of the spots: B, blue; R, red color under long wave UV lamp.

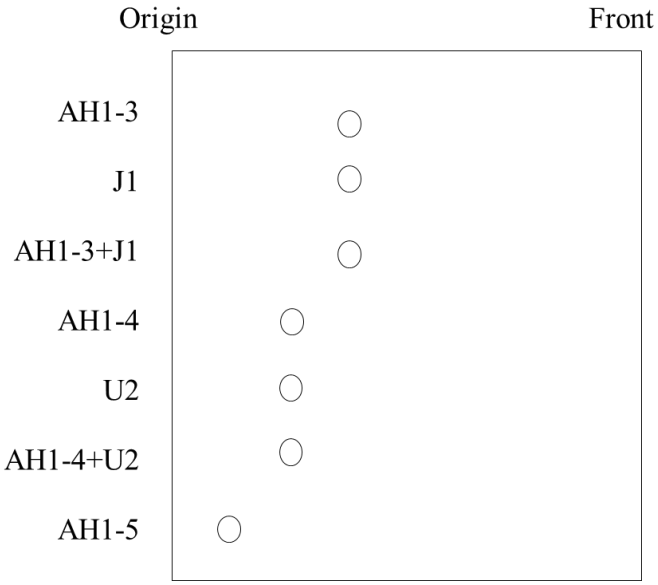


Figure 3-31. High performance silica gel thin layer chromatogram of fractions AH1-3~AH1-5 and compounds **J1**, **U2** obtained previously from *S*. *thunbergii*.

Developing solvent, *n*-hexane.

⬭, Visualized with 5% sulfuric acid reagent.

3.4.1.2 β-Glucuronidase inhibitors isolated from ethyl acetate-soluble fraction of *A. clathratum*

Ethyl acetate-soluble fraction of *A. clathratum* was charged on Wakogel C-100 silica gel column chromatography and eluted with increasing gradient methanol in chloroform to obtain fractions AE1 to AE14 (Table 3-12). Among them fractions AE5 (36 mg) and AE6 (39 mg), which showed unambiguous positive response for the DMBA reagent were chosen for the further purification (Figure 3-32).

Fraction AE5 (36 mg) was charged on preparative TLC using chloroform/methanol (6/1, v/v) as developing solvent which was divided into three fractions AE5-1 to AE5-3 (Figure 3-33). Fraction AE5-2 (6.45 mg) which showed positive response for DMBA reagent was performed for the HPLC purification (Table 3-14, Figure 3-34) to yield compound **G1** (2.57 mg, 2.44 ppm based on air-dried alga) (Table 3-15, Figure 3-35). But structure elucidation of compound **G1** was failed as its unstable properties.

Fraction AE6 (39 mg) was loaded on preparative TLC using chloroform/methanol (4/1, v/v) as developing solvent (Figure 3-36). After separation, fraction AE6-2 (4.12 mg) was purified by HPLC (Table 3-17, Figure 3-37) to give compound **G2** (1.03 mg, 0.98 ppm based on air-dried alga) (Table 3-18, Figure 3-38).

Table 3-12. Amount and β-glucuronidase inhibitory activity of the fractions obtained from ethyl acetate-soluble fraction[a] separated by silica gel column chromatography

Fraction	Eluent (v/v)	Amount (mg)	Inhibition[b] (%)
AE1	Chloroform : methanol = 39 : 1	149	38.62 ± 0.74
AE2	Chloroform : methanol = 39 : 1	160	47.83 ± 1.33
AE3	Chloroform : methanol = 9 : 1	93	62.02 ± 2.59
AE4	Chloroform : methanol = 9 : 1	212	61.13 ± 3.18
AE5	Chloroform : methanol = 5 : 1	36	94.27 ± 1.55
AE6	Chloroform : methanol = 5 : 1	39	59.72 ± 1.85
AE7	Chloroform : methanol = 2 : 1	199	64.02 ± 1.77
AE8	Chloroform : methanol = 2 : 1	68	86.03 ± 0.48
AE9	Chloroform : methanol = 1 : 2	397	99.85 ± 0.31
AE10	Chloroform : methanol = 1 : 2	128	98.52 ±0.88
AE13	Methanol	125	98.77 ± 0.45
AE14	Methanol	95	82.33 ± 2.43

[a]Sample, ethyl acetate-soluble fraction, 2.217 g; stationary phase, Wakogel C-100; elution volume, 444 mL/fraction.

[b]Assay concentration was 10 μg/mL. Data represent means ± SE (n=3).

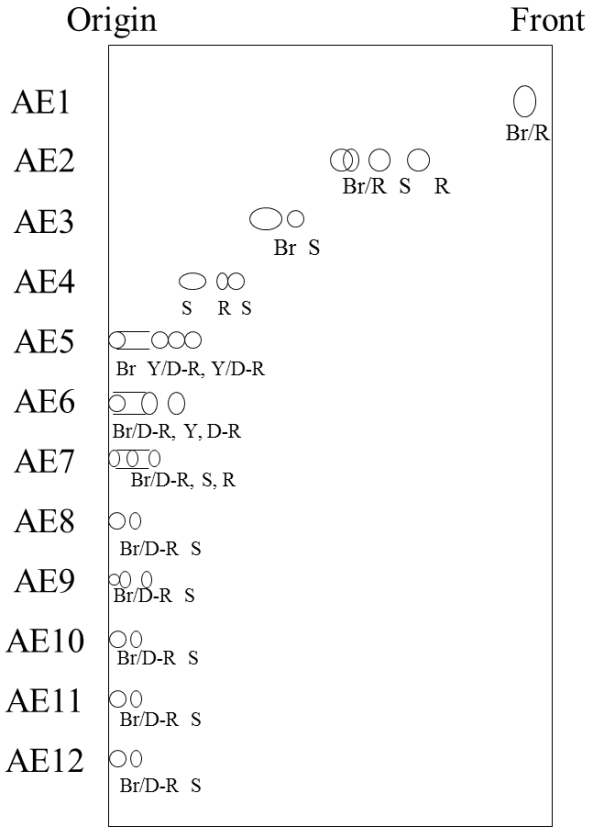


Figure 3-32. Silica gel thin layer chromatogram of fractions obtained from ethyl acetate-soluble fraction separated by silica gel column chromatography.

Developing solvent, chloroform: methanol = 9: 1 (v/v).

⬭, Visualized with 5% sulfuric acid reagent and DMBA reagent.

Abbreviations designate color of the spots: Br, brown; Y, yellow; S, quenching spot under short wave UV lamp; R, red under long wave UV lamp.

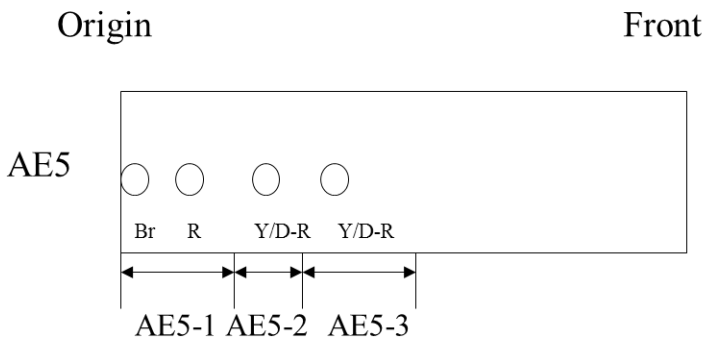


Figure 3-33. Profile of the preparative TLC of fraction AE5.

Developing solvent, chloroform: methanol = 6: 1 (v/v).

⬭, Visualized with 5% sulfuric acid reagent and DMBA reagent.

Abbreviations designate color of the spots: Br, brown; Y, yellow; R, red under long wave UV lamp; D-R, positive response for DMBA reagent.

Table 3-13. Amount of the fractions obtained from fraction AE5[a] by preparative thin layer chromatography

Fraction	Amount (mg)
AE5-1	14.09
AE5-2	6.45
AE5-3	12.31

[a]Sample, fraction AE5, 36 mg.

Table 3-14. HPLC condition for separating fraction AE5-2

Sample:	AE5-2 6.45 mg
Column:	Inertsil ODS-4 (5 μm; 250 × 7.6 mm) (GL Sciences Inc.)
Eluting solvent:	Acetonitrile : water = 1 : 4
Flow rate:	0.7 mL/min
Detection:	UV (210 nm)

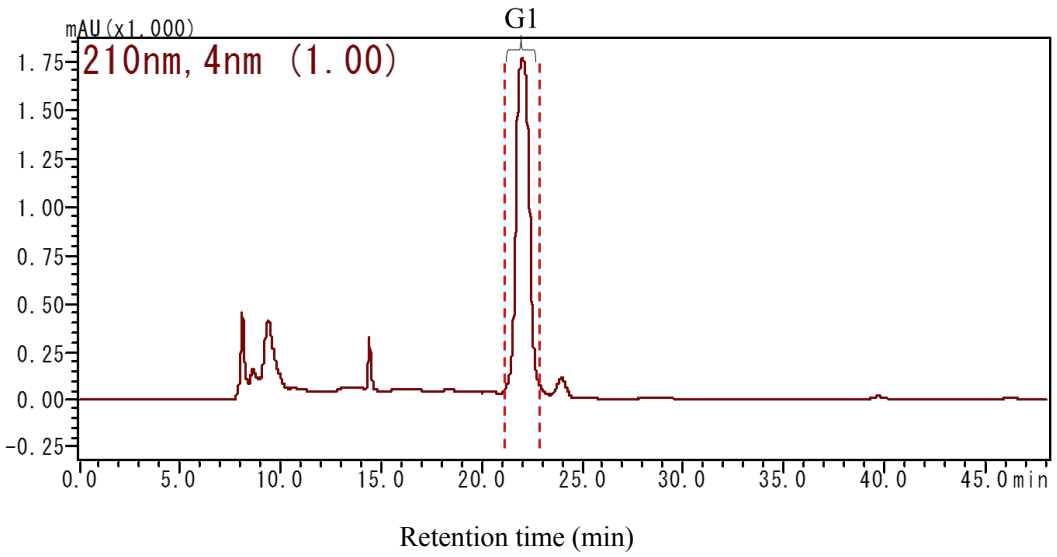


Figure 3-34. HPLC chromatogram of AE5 monitored at 210 nm.

Table 3-15. Amount and β-glucuronidase inhibitory activity of compound **G1** obtained by HPLC

Fraction	Amount (mg)	Inhibition[a] (%)
G1	2.57	89.42 ± 2.04

[a]Assay concentration was 10 μg/mL. Data represent means ± SE (n=3).

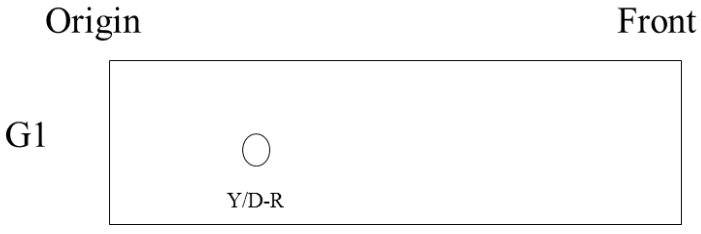


Figure 3-35. High performance thin layer chromatogram of compound **G1**.

Developing solvent, chloroform: methanol = 6: 1 (v/v).

⬭, Visualized with 5% sulfuric acid reagent and DMBA reagent.

Abbreviations designate color of the spots: Y, yellow; D-R, positive response for DMBA reagent.

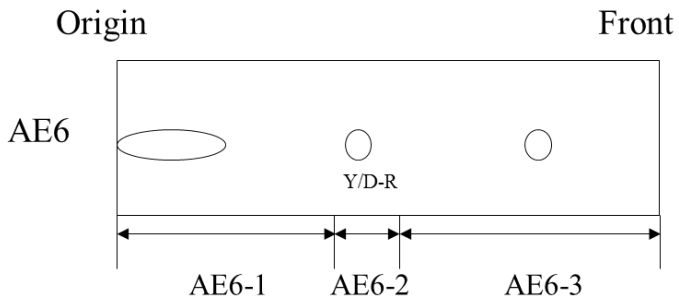


Figure 3-36. Profile of the preparative TLC of fraction AE6.

Developing solvent, chloroform: methanol = 4: 1 (v/v).

⬭, Visualized with 5% sulfuric acid reagent and DMBA reagent.

Abbreviations designate color of the spots: Y, yellow; D-R, positive response for DMBA reagent.

Table 3-16. Amount of the fractions obtained from fraction AE6[a] by preparative thin layer chromatography

Fraction	Amount (mg)
AE6-1	14.02
AE6-2	4.12
AE6-3	13.73

[a]Sample, fraction AE6, 39 mg.

Table 3-17. HPLC condition for separating fraction AE6-2

Sample:	AE6-2 4.12 mg
Column:	Inertsil ODS-4 (5 μm; 250 × 7.6 mm) (GL Sciences Inc.)
Eluting solvent:	Acetonitrile : water = 15 : 85
Flow rate:	0.7 mL/min
Detection:	UV (210 nm)

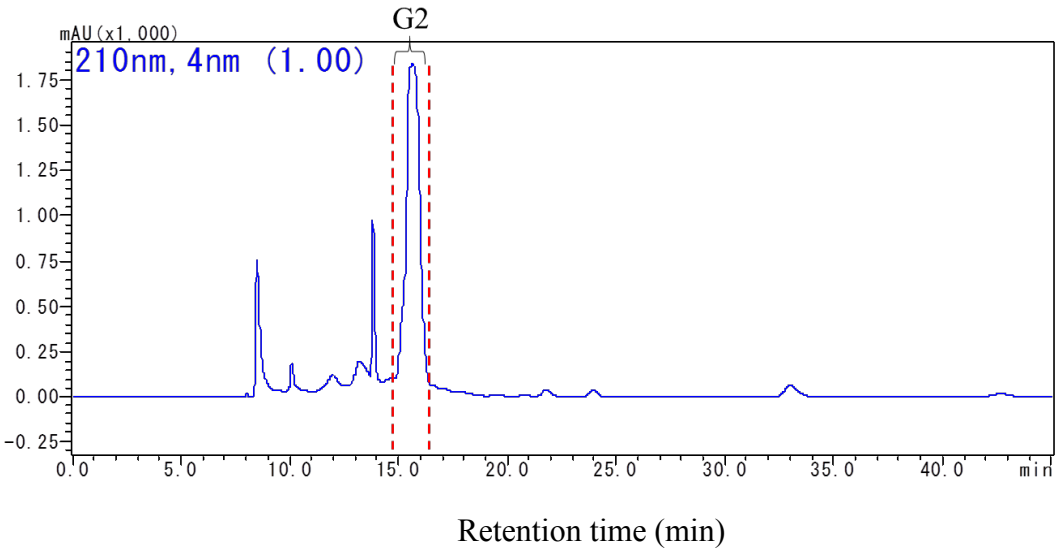


Figure 3-37. HPLC chromatogram of fraction AE6 monitored at 210 nm.

Table 3-18. Amount and β-glucuronidase inhibitory activity of compound **G2** obtained by HPLC

Fraction	Amount (mg)	Inhibition[a] (%)
G2	1.03	57.24 ± 0.68

[a]Assay concentration was 10 μg/mL. Data represent means ± SE (n=3).

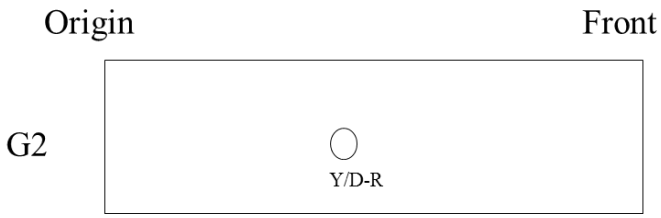


Figure 3-38. High performance thin layer chromatogram of compound **G2**.

Developing solvent, chloroform: methanol = 4: 1 (v/v).

⬭, Visualized with 5% sulfuric acid reagent and DMBA reagent.

Abbreviations designate color of the spots: Y, yellow; D-R, positive response for DMBA reagent.

3.4.2 Structural elucidation of β-glucuronidase inhibitors from *A. clathratum*

3.4.2.1 Structural elucidation of β-glucuronidase inhibitor C3

Compound **C3** was obtained as colorless oil. The FD-MS spectrum of compound **C3** displayed a molecular peak at *m/z* 410 (Figure 3-39). Molecular formula of compound **C3** was determined $C_{30}H_{50}$ from at *m/z* 410.39121 (calculated 410.39125) by FD-HR-MS. ^{1}H NMR spectrum showed the appearance of olefinic, allylic methylene and methyl protons (Figure 3-40). ^{13}C NMR and DEPT (Figure 3-35) spectra showed fifteen sp^2 and sp^3 carbons, including six olefinic, five methylene and four methyl carbons (Figure 3-41). With the consideration of its molecular formula, compound **C3** was supposed to be a symmetric structure. Therefore, according to the 2D NMR (Figure 3-42 to Figure 3-44) spectra and literature data (H. J. Kim, Su, Jung, & Koo, 2011), compound **C3** was identified as squalene (Table 3-19, Figure 3-45).

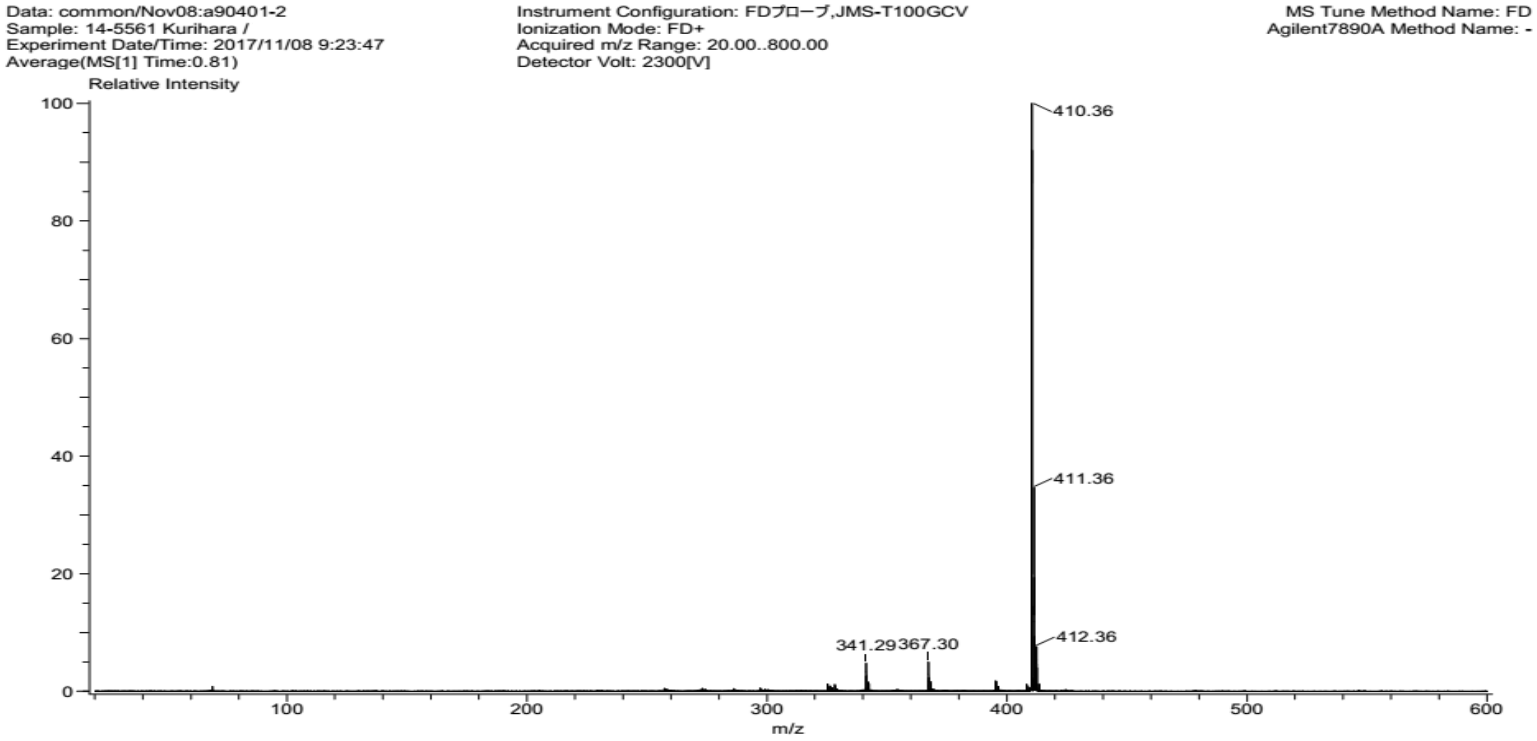


Figure 3-39. FD-MS spectrum of compound **C3**.

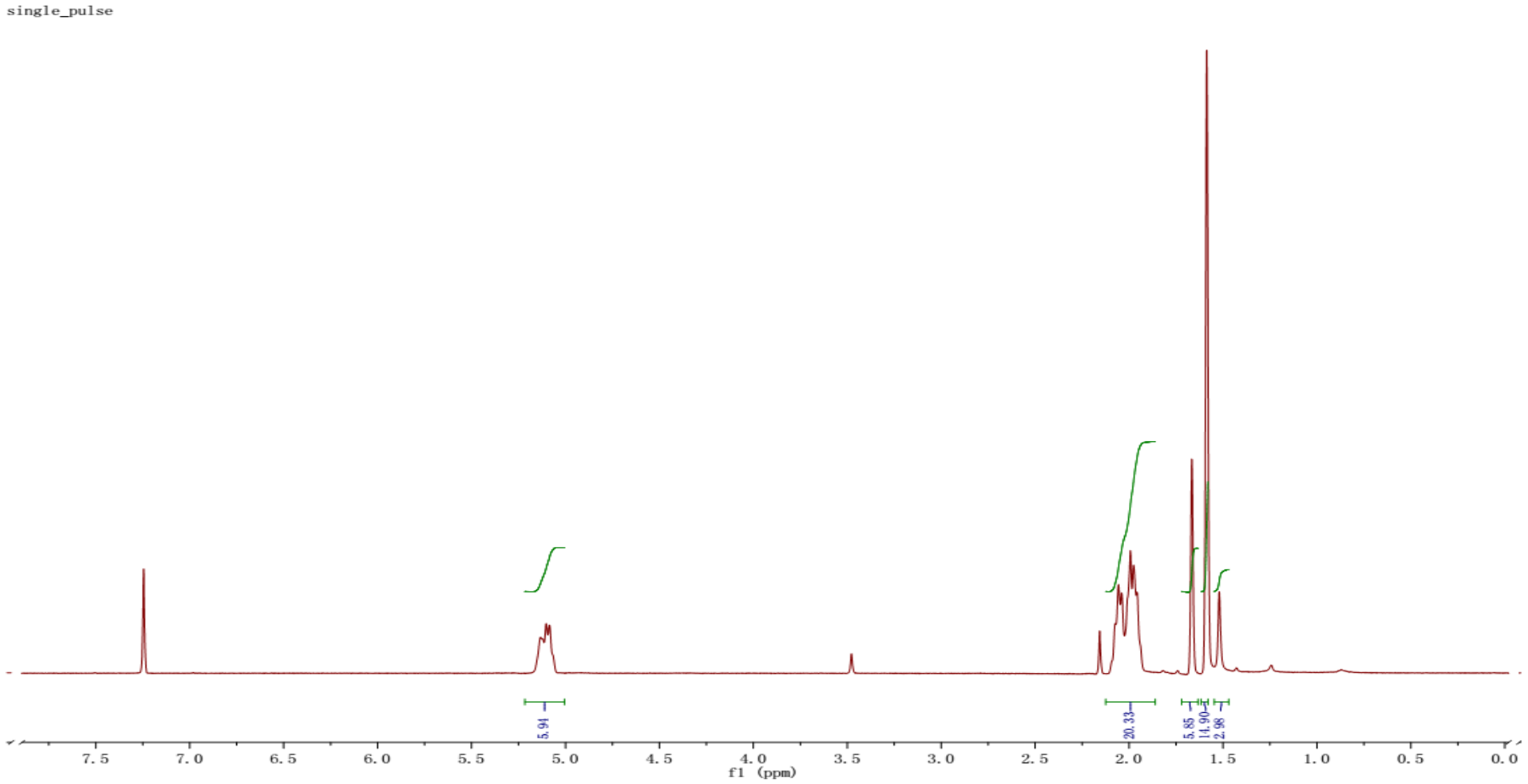


Figure 3-40. ^{1}H-NMR spectrum of compound **C3**.

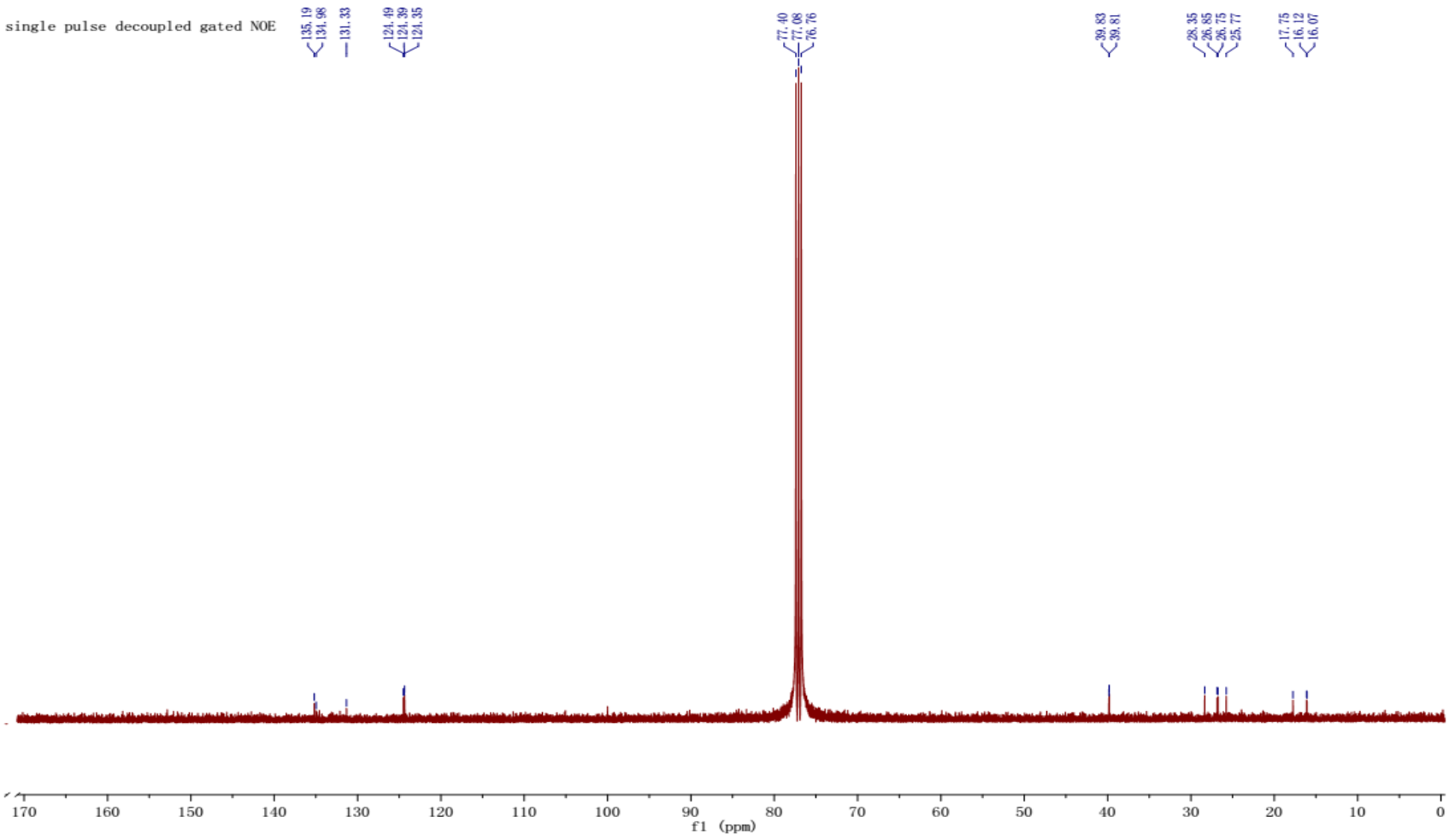


Figure 3-41. ^{13}C-NMR spectrum of compound **C3**.

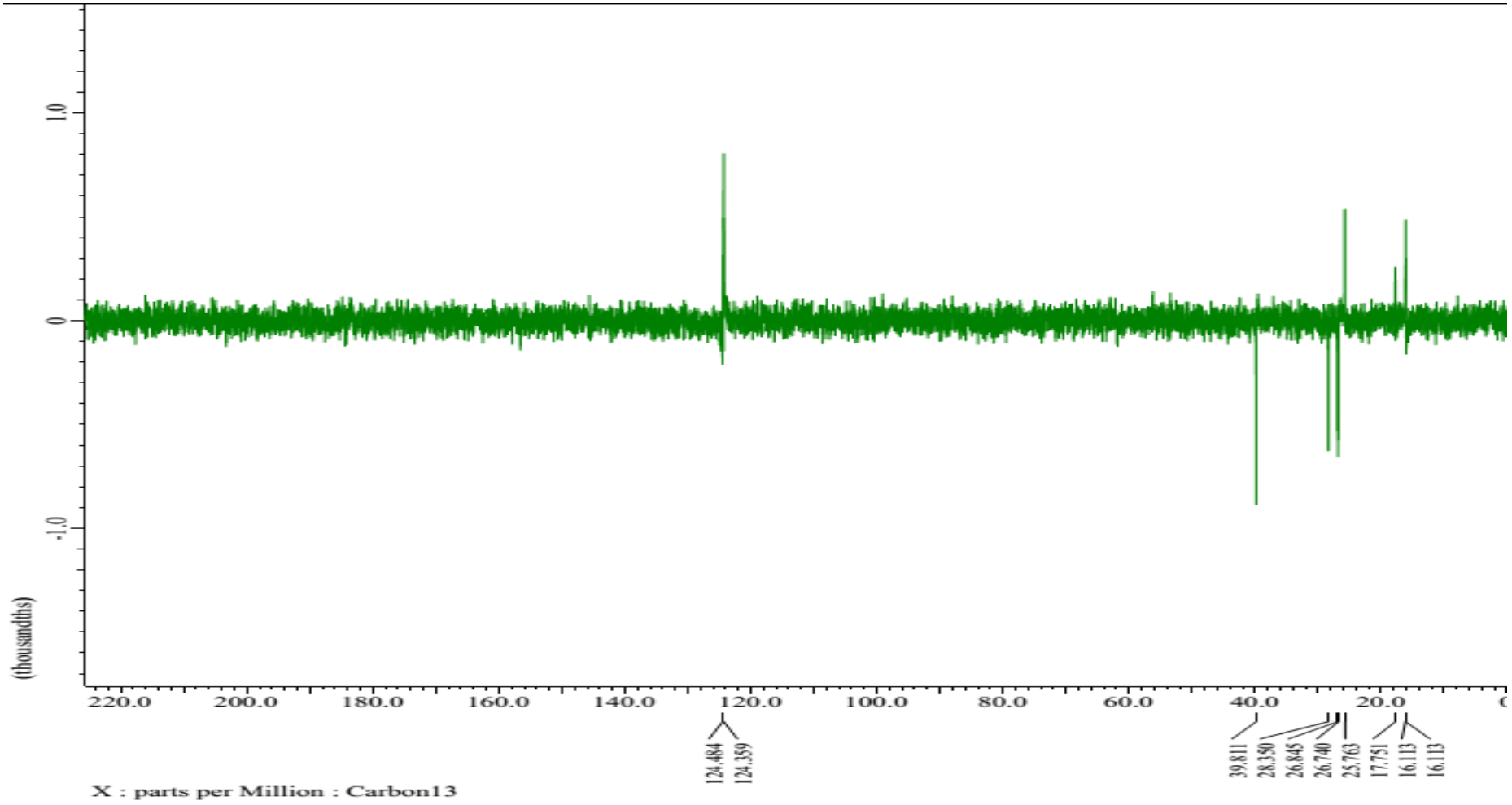


Figure 3-42. ^{13}C/DEPT (135) NMR spectrum of compound **C3**.

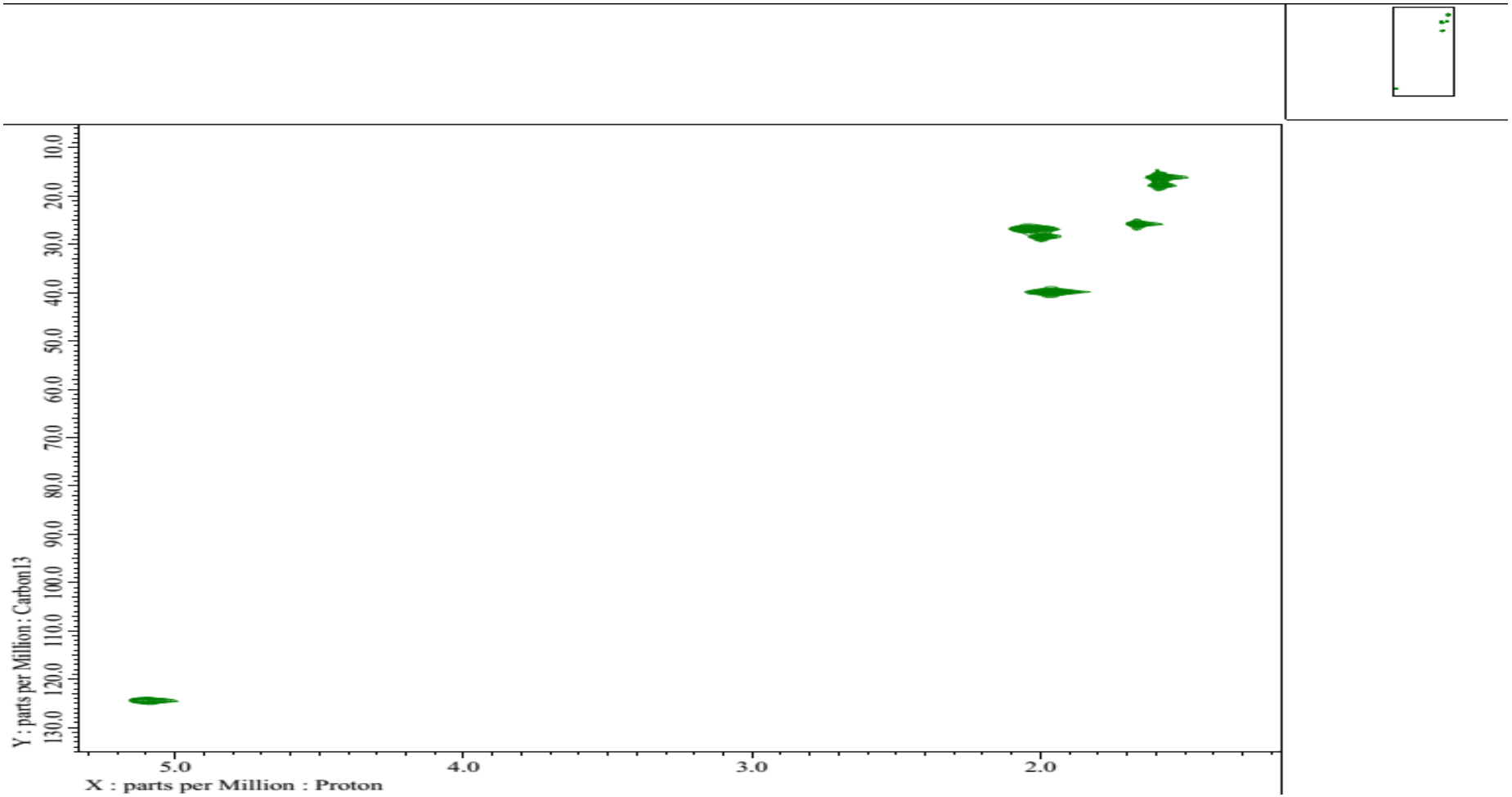


Figure 3-43. HSQC spectrum of compound **C3**.

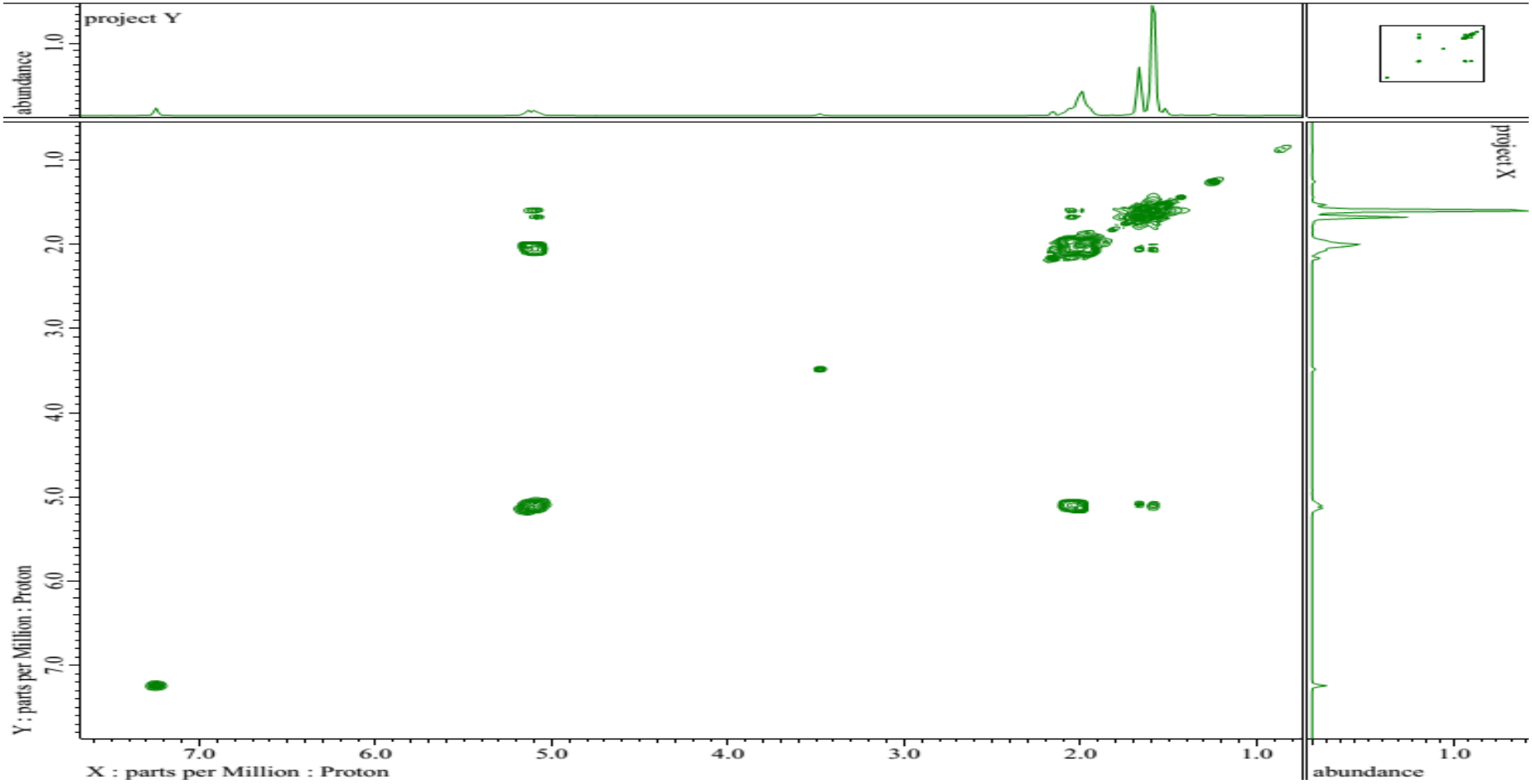


Figure 3-44. COSY spectrum of compound **C3**.

Table 3-19 Comparison of NMR data between compound **C3**[a] and literature[b]

	^{1}H NMR		^{13}C NMR	
Position	**C3**	Literature data	**C3**	Literature data
1	1.67 (s, 3H)	1.68 (s, 3H)	25.8	25.7
2			131.3	131.3
3	5.10 (m, 1H)	5.22 (t, 6.8 Hz, 1H)	124.5	124.2
4	1.98 (m, 2H)	2.02–2.12 (m, 10 H)	26.9 or 26.8	26.6
5	2.02 (m, 1H)	1.94–2.02 (m, 10H)	39.8	39.7
6			135.2 or 135.0	135.8
7	5.10 (m, 1H)	5.20 (t, 6.8 Hz, 1H)	124.4	124.3
8	1.98 (m, 2H)	2.02–2.12 (m, 10 H)	26.8 or 26.9	26.6
9	2.02 (m, 1H)	1.94–2.02 (m, 10H)	39.8	39.7
10			135.0 or 135.2	135.8
11	5.10 (m, 1H)	5.11 (t, 6.4 Hz, 2H)	124.4	124.3
12	1.98 (m, 2H)	2.02–2.12 (m, 10 H)	28.4	26.7
13	1.52 (s, 3H)	1.58 (s, 3H)	17.8	17.7
14	1.59 (s, 3H)	1.60 (s, 3H)	16.1	15.6
15	1.59 (s, 3H)	1.60 (s, 3H)	16.1	15.6

[a]The NMR data were measured in chloroform-*d* (δ_H 7.25 ppm; δ_C 77.4 ppm) at 400 MHz for ^{1}H and at 100 MHz for ^{13}C.

[b]Kim et al., 2011.

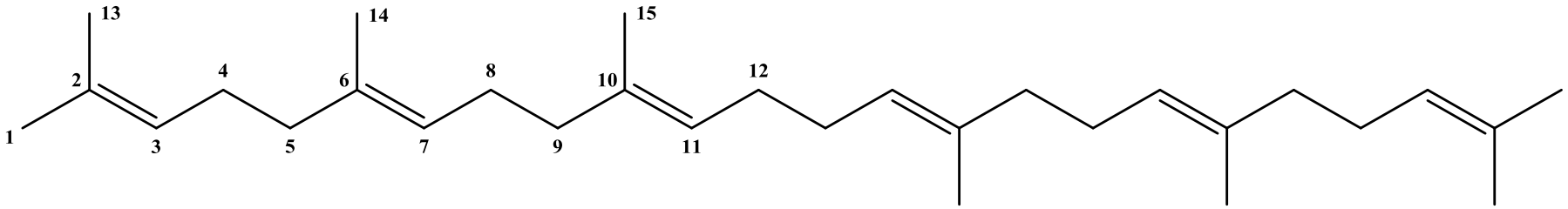


Figure 3-45. Structure of compound **C3**

3.4.2.2 Structure elucidation of inhibitor G2

Compound **G2** was obtained as gray solid. Its FD-MS spectrum exhibited a molecular ion peak at *m/z* 126 (Figure 3-46). Molecular formula of compound **G2** was determined as $C_6H_6O_3$ at *m/z* 126.03161 (calculated 126.03169) by FD-HR-MS. In the ^{1}H NMR spectrum of compound **G2**, two singlets were revealed at δ_H 8.96 (s, 3H) assignable to the hydroxy protons at 1, 3, 5-OH and 5.65 (s, 3H) assignable to the aromatic protons at H-2, 4, 6 (Figure 3-47). In the ^{13}C NMR spectrum, two signals were displayed at δc 159.4 assigned to oxygenated aromatic carbons at C-1, 3, 5 and 94.6 which was assigned to the aromatic carbons at C-2, 4, 6 (Figure 3-48).

The structure of compound **G2** was determined as phloroglucinol (Table 3-20, Figure 3-49) (Li et al., 2009). Meanwhile, analysis of high performance TLC of the standard phloroglucinol (Wako Pure Chemical Industries, Ltd.) and compound **G2** (developing solvent: chloroform/methanol, 6/1, v/v) showed same R_f value on the TLC plate (Figure 3-50) which helped to identify compound **G2** as phloroglucinol.

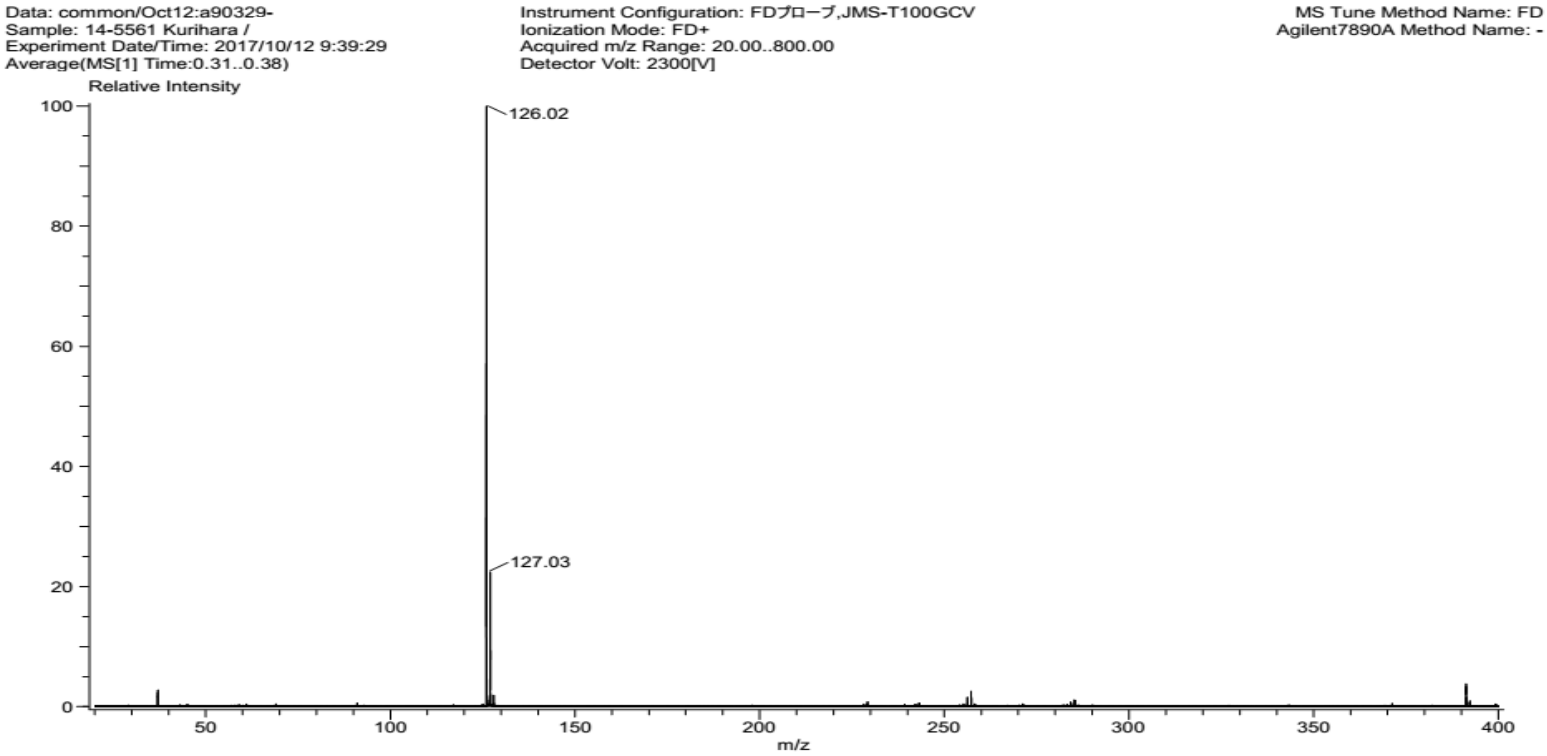


Figure 3-46. FD-MS spectrum of compound **G2**.

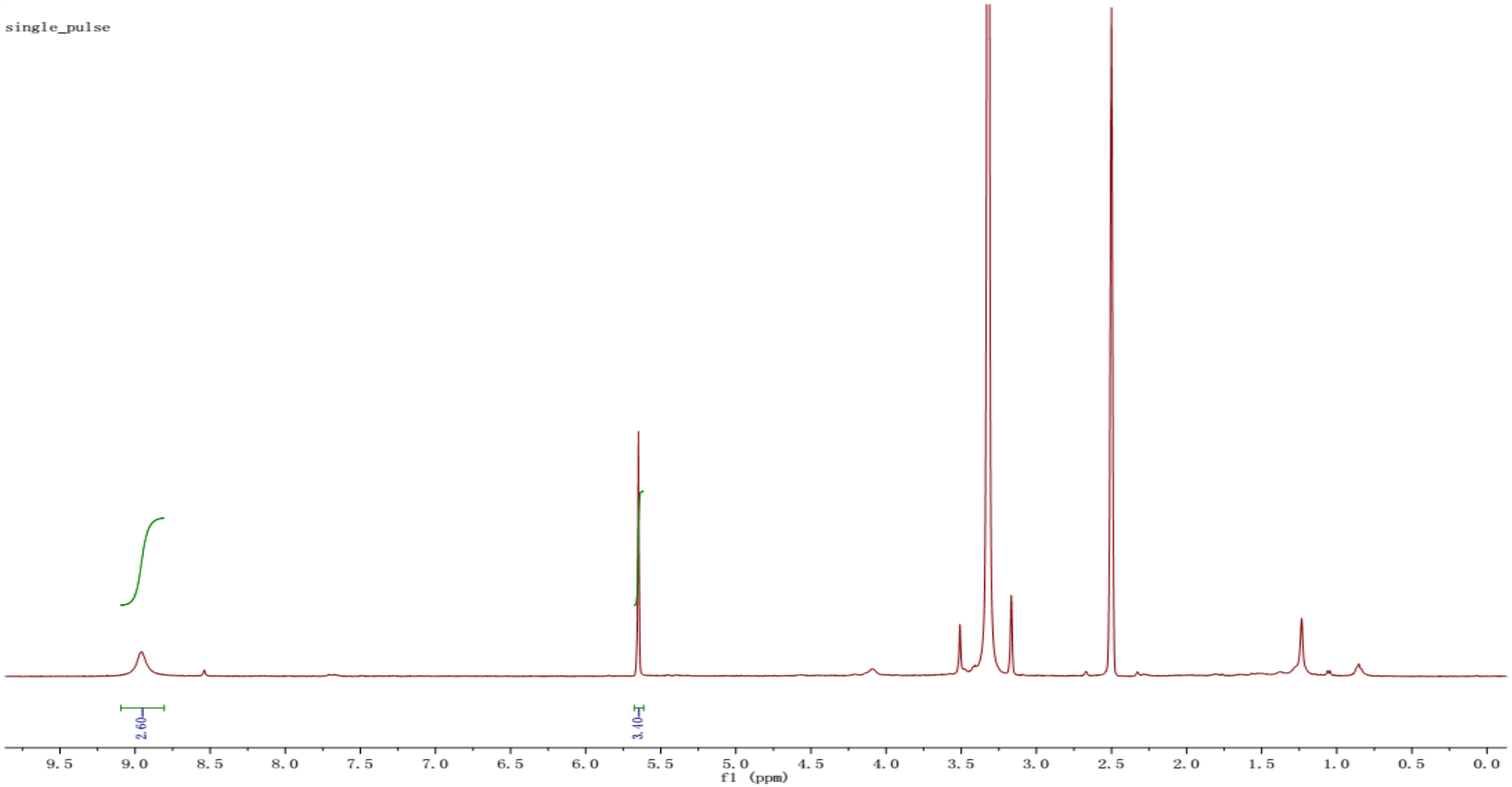


Figure 3-47. ^{1}H-NMR spectrum of compound **G2**.

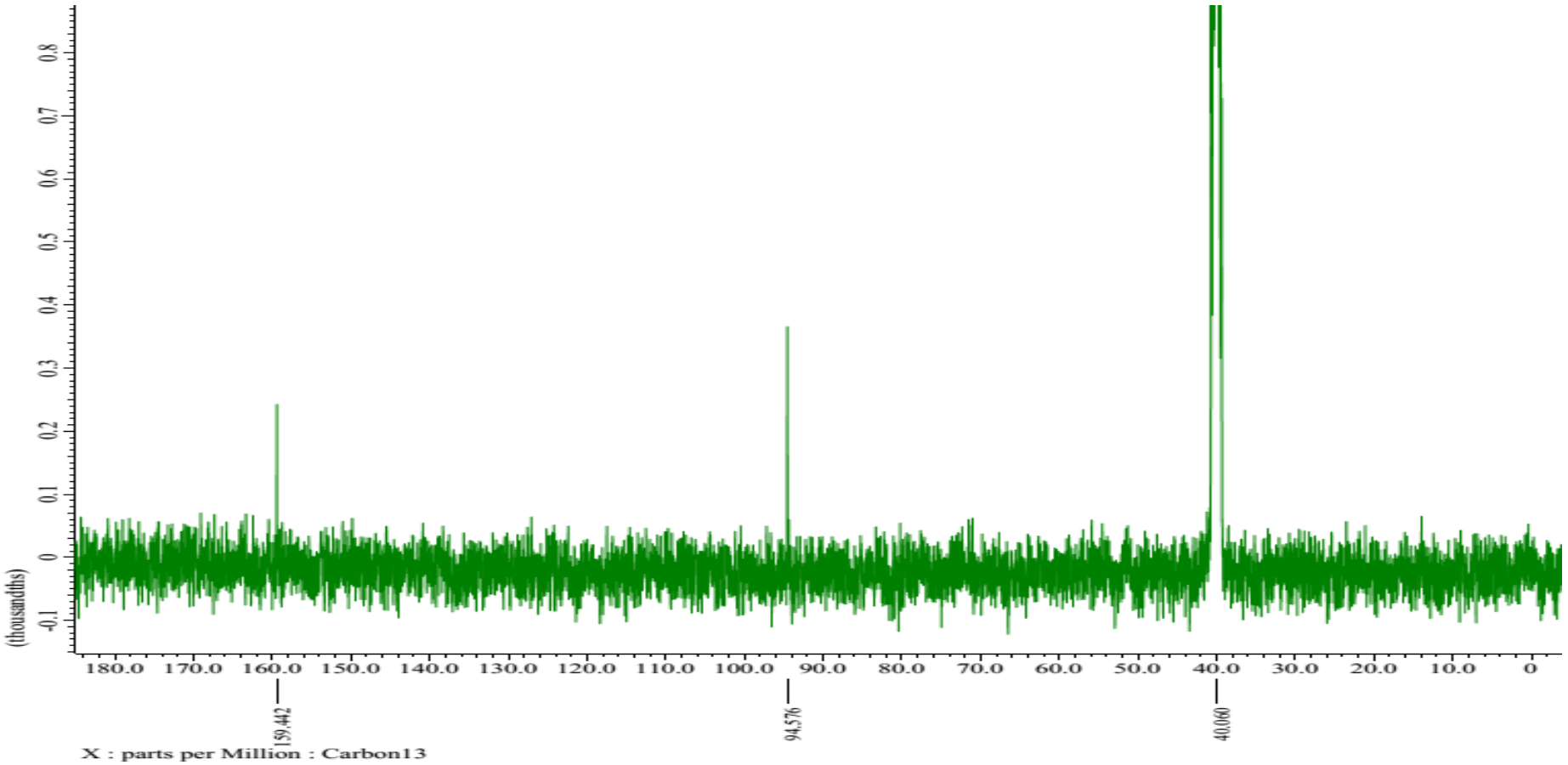


Figure 3-48. ^{13}C-NMR spectrum of compound **G2**.

Table 3-20. Comparison of NMR data between compound **G2**[a] and literature[b]

	^{1}H NMR		^{13}C NMR	
Position	**G2**	Literature data	**G2**	Literature data
1,3,5-OH	8.96 (s, 1H)	8.97 (s, 1H)	159.4	158.9
2,4,6	5.65 (s, 1H)	5.66 (s, 1H)	94.6	94.1

[a]The NMR data were measured in DMSO-d_6 (δ_H 2.50 ppm; δ_C 40.1 ppm) at 400 MHz for ^{1}H and at 100 MHz for ^{13}C.

[b]Li et al., 2009.

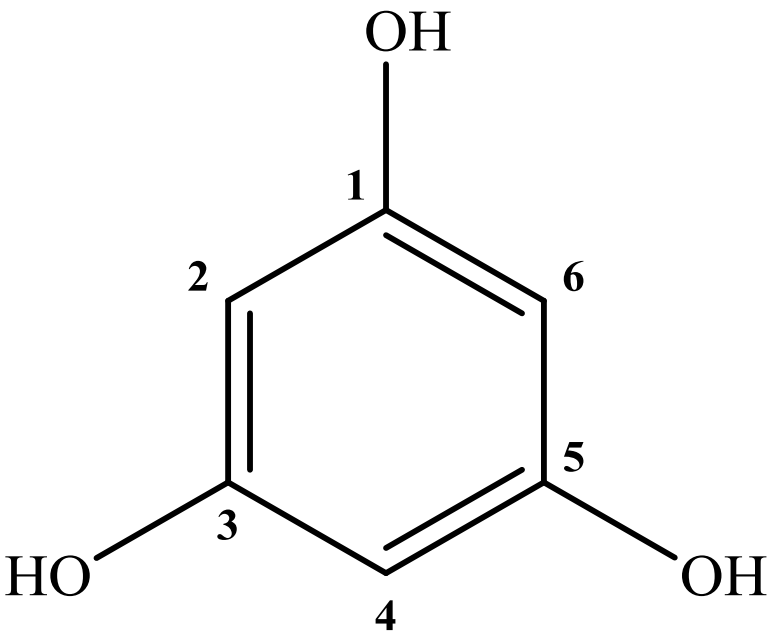


Figure 3-49. Structure of compound **G2**.

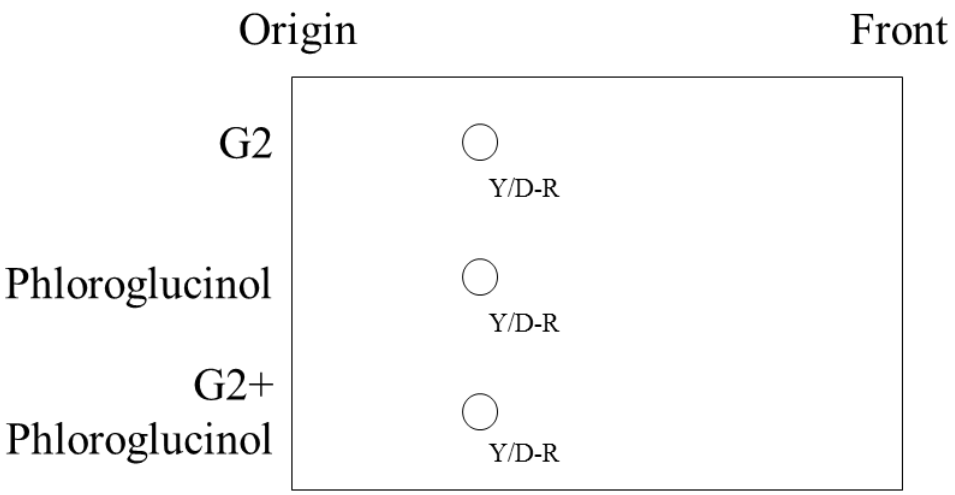


Figure 3-50. High performance thin layer chromatogram of compound **G2** and phloroglucinol.

Developing solvent, chloroform: methanol= 6: 1 (v/v).

⬭, Visualized with 5% sulfuric acid reagent and DMBA reagent.

Abbreviations designate color of the spots: Y, yellow; D-R, positive response for DMBA reagent.

3.5 Discussion

Brown algae have been well consumed as traditional food and folk herb in Asia (Jung et al., 2017). Various biologically active compounds have been identified from brown algae including phlorotannins, diterpenes, polysaccharides, phytosterols, and phytopigments (El Gamal, 2010).

In Chapter 3, the three brown algae *Sargassum confusum* (Sargassaceae, Fucales), *S. thunbergii* (Sargassaceae, Fucales) and *Agarum clathratum* (Agaraceae, Laminariales) were used for the isolation and purification of β-glucuronidase inhibitory compounds.

Brown algae of family Sargassaceae account for nearly 500 species which are distributed in the temperate zone of the Indian Ocean, the west coast of the Pacific Ocean and the coast of Australia (Yoshida, 1989). This family produced almost 45% of marine natural products among brown algae (Leal et al., 2013), including terpenoids, alkaloids, phlorotannins and polysaccharides which displayed a wide range of biological activities, such as antioxidant (J. A. Kim, Kong, & Kim, 2010), anti-pyretic, analgesic and anti-inflammation activity (J. Y. Kang et al., 2008), antitumor effect (S. Fan et al., 2017), antidiabetic activity (M. C. Kang et al., 2017) and antiviral activity (Iwashima et al., 2005).

A. clathratum belongs to the order of Laminariales, which is commonly found in the sub-tidal zone in northeastern Asian countries, the coast of Kuril Island and Bering Sea. Many studies have showed that algae of this order are excellent sources of polysaccharides and phlorotannins. They were noteworthy for broad therapeutic perspectives such as anti-inflammation (Jung, Jin, Ahn, Lee, & Choi, 2013), anticancer (Usoltseva, Anastyuk, Shevchenko, Zvyagintseva, & Ermakova, 2016), antidiabetic (M.

C. Kang et al., 2013), antioxidation (Ferreres et al., 2012), radiation protection (Swanson & Fox, 2007), anti-allergic (Sugiura et al., 2006) and other properties. Various components were characterized in *A*. *clathratum*, including carbohydrates, proteins, lipids and polyphenolic compounds (M. S. Park, Lee, & Lim, 2017). Kim et al. reported the ethyl acetate- and *n*-butanol-soluble fractions derived from ethanol extracts of *A*. *clathratum* showed strong neuroprotective activity against the transient ischemic damage (I. H. Kim et al., 2014).

In this chapter, two alkapolyenes—henicosapentaene (**J1**), henicosahexanene (**U2**), and one isoprenoid—squalene (**C3**) were isolated from the genus of *S*. *confusum*, *S*. *thunbergii* and *A*. *clathratum* in this study. And from *A*. *clathratum*, two DMBA positive response compounds **G1** and **G2** were also isolated. Compound **G1** exhibited strong β-glucuronidase inhibitory activity, but since the instability of this compound, structure of compound **G1** was failed to be elucidated. While compound **G2** was confirmed as phloroglucinol, a renowned basic unit of phlorotannins. The β-Glucuronidase inhibitors obtained in this study are listed in Figure 3-51.

Henicosapentaene (HEP) (**J1**), henicosahexanene (HEH) (**U2**) and squalene (**C3**) were polyprenyl compounds which are widely distributed in bacteria, fungi, algae, plants and animals (Ghimire, Thuan, Koirala, & Sohng, 2016). Previous studies have showed that HEP (**J1**) and HEH (**U2**) were excellent candidates of lipoxygenase inhibitors (Kurihara et al., 2014). And squalene, the precursor of steroids, hormones and vitamins have been well studied as its diversity in biological activities, involving cardioprotective (Lou-Bonafonte, Arnal, Navarro, & Osada, 2012), antioxidant (Kabuto, Yamanushi, Janjua, Takayama, & Mankura, 2013), chemopreventive (Scolastici, Ong, & Moreno, 2004), anticancer (Alwhibi, Khalil, Ibrahim, El-Gaaly, & Sultan, 2017),

anti-inflammatory, antibacterial (Sharma, Kishore, Hussein, & Lall, 2013), anti-tumor (N. Suzuki, Ito, Matsui, & Takizawa, 2016), and immune system improvement (Ohkuma, Otagiri, Tanaka, & Ikekawa, 1983).

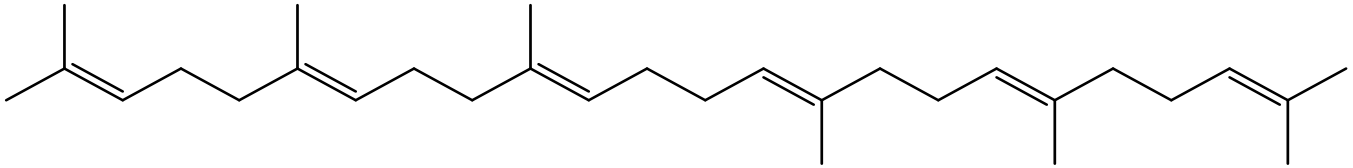
In summary, henicosapentaene (**J1**), henicosahexanene (**U2**) and squalene (**C3**) were successfully isolated from *S*. *confusum*, *S*. *thunbergii* and *A*. *clathratum* as potent β-glucuronidase inhibitory compounds. Phloroglucinol (**G2**), a basic unit of phlorotannins was purified from genus *A*. *clathratum* which showed moderate inhibitory activity. Meanwhile, ethyl acetate and *n*-butanol-soluble fractions of *A*. *clathratum* exposed strong positive response for DMBA reagent, which indicated this genus might be a promise candidate for the isolation and purification of phlorotannins.



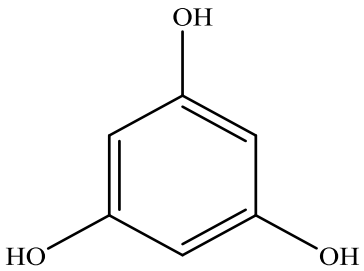
J1



U2



C3



G2

Figure 3-51. β-Glucuronidase inhibitors derived from the brown algae *S*. *confusum*, *S*. *thunbergii* and *A*. *clathratum*.

Chapter 4

Molecular Modeling Base SAR Analysis of the Purified β-Glucuronidase Inhibitors

In this chapter, *in vitro* and *in silico* analysis were performed to demonstrate the relationship between purified β-glucuronidase inhibitors and *E. coli* β-glucuronidase

4.1 *In vitro* β-glucuronidase inhibitory activities

4.1.1 Chemicals and instruments

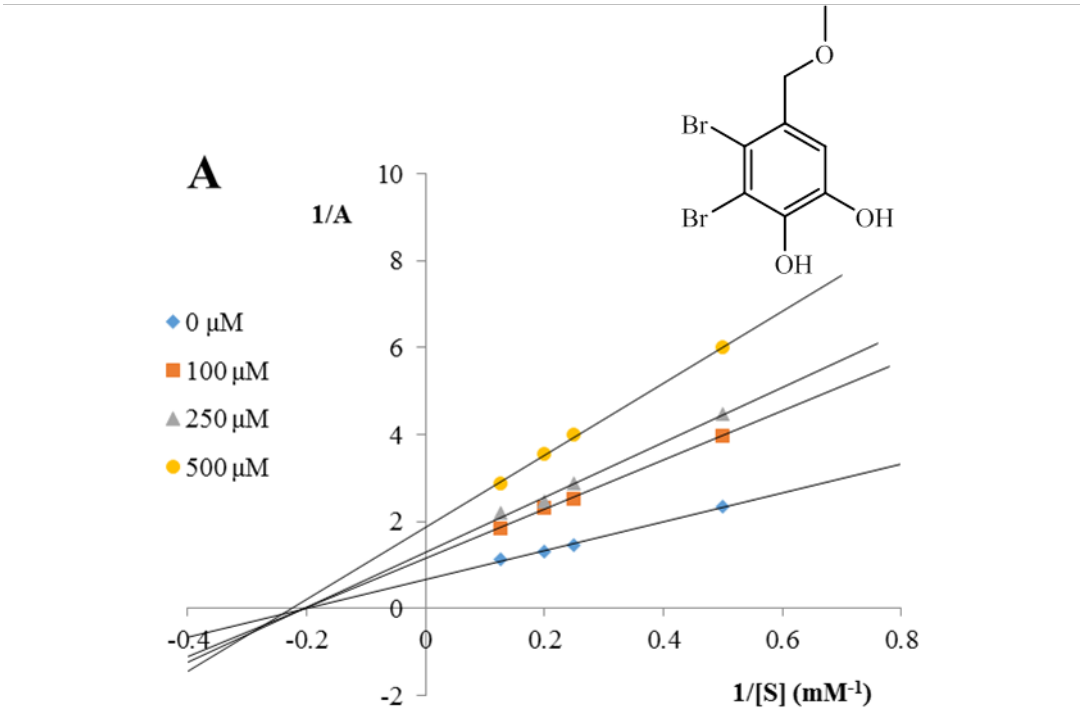
Chemicals and analysis instruments were same as 1.1.1.

4.1.2 Kinetic study of the purified β-glucuronidase inhibitors

β-Glucuronidase activity was determined by absorptiometric method using *p*-nitrophenyl β-D-glucuronide as described in Section 1.2. Reaction mixture contained 10 mM phosphate buffer (pH 7.0, 440 mL), 2 to 8 mM substance [S] in methanol (final concentration of 0 to 500 mM, 20 μL [I]). Inhibition modes and K_i values of the inhibitors, bromophenol monomer (**F1**), bromophenol dimers (**F2** and **F3**), phytal (**A1**), cholesterol (**A4**), 22-dehydrocholesterol (**A5**), isogloiosiphone B (**A6**), henicosapentaene (**J1**), henicosahexaene (**U2**), squalene (**C3**) and phloroglucinol (**G2**), were determined from Lineweaver-Burk and Dixon plots, respectively. Reciprocals of absorbance values (1/A) were employed instead of reciprocals of velocity as all the experiments under the same temperature and time condition.

Lineweaver-Burk and Dixon plots of the inhibitors obtained were presented in Figures 4-1 to 4-11. IC_{50} and *Ki* values and inhibition modes of all the purified inhibitors were shown in Table 4-1. Except cholesterol (**A4**), which exhibited as a non-competitive inhibitor, all the other compounds showed competitive inhibition mode. Compared to the positive control, D-Glucaro-1,4-lactone (IC_{50} = 77.9 ± 1.40 μM), two bromophenol dimers **F2** and **F3**, henicosahexaene (**U2**) and squalene (**C3**) showed potent β-glucuronidase inhibitory activity with IC_{50} values of 5.1 ± 0.0 μM and 2.6 ±

0.1 μM, 4.4 ± 0.0 μM and 2.2 ± 0.2 μM, respectively. Henicosapentaene (**J1**), and isogloiosiphone B (**A6**) showed moderate inhibitory activity with IC_{50} values of 20.9 ± 0.2 μM and 57.0 ± 0.6 μM, respectively. Other purified compounds showed weak inhibitor activity against β-glucuronidase. Even though compound **G1** showed 88.23% inhibitory activity at final concentration of 10 μg/mL, IC_{50} value of compound **G1** was failed to be obtained.



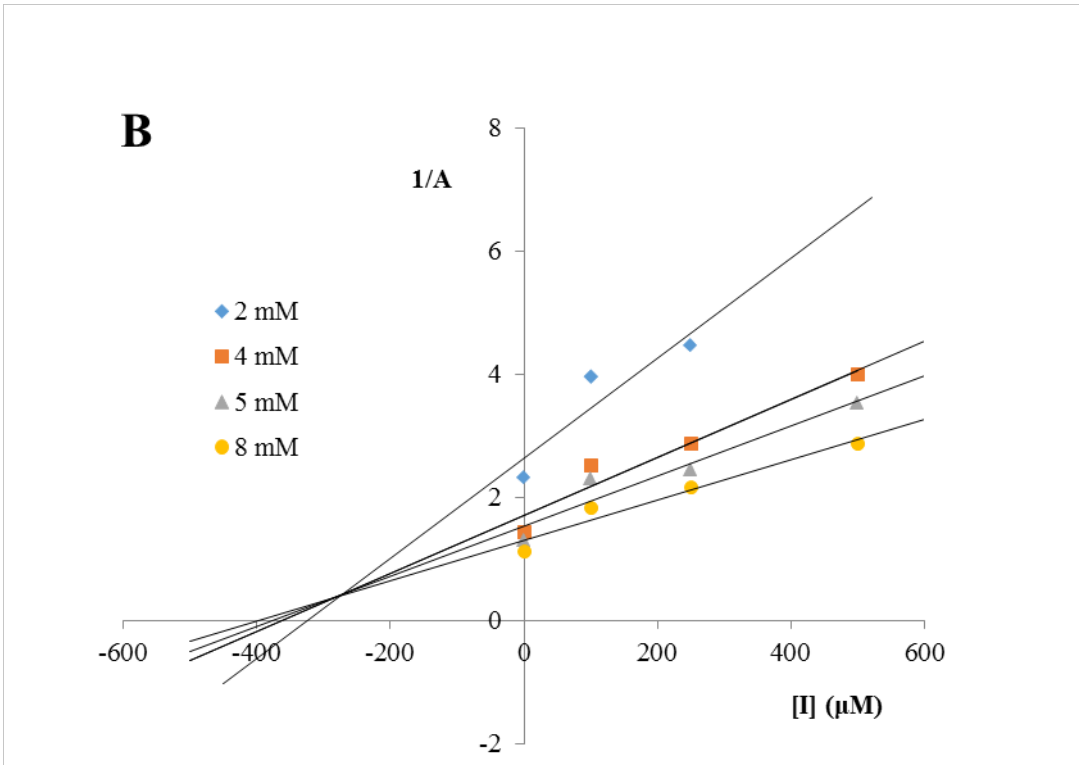


Figure 4-1. Lineweaver-Burk plot (A) and Dixon plot (B) of bromophenol monomer **F1**.

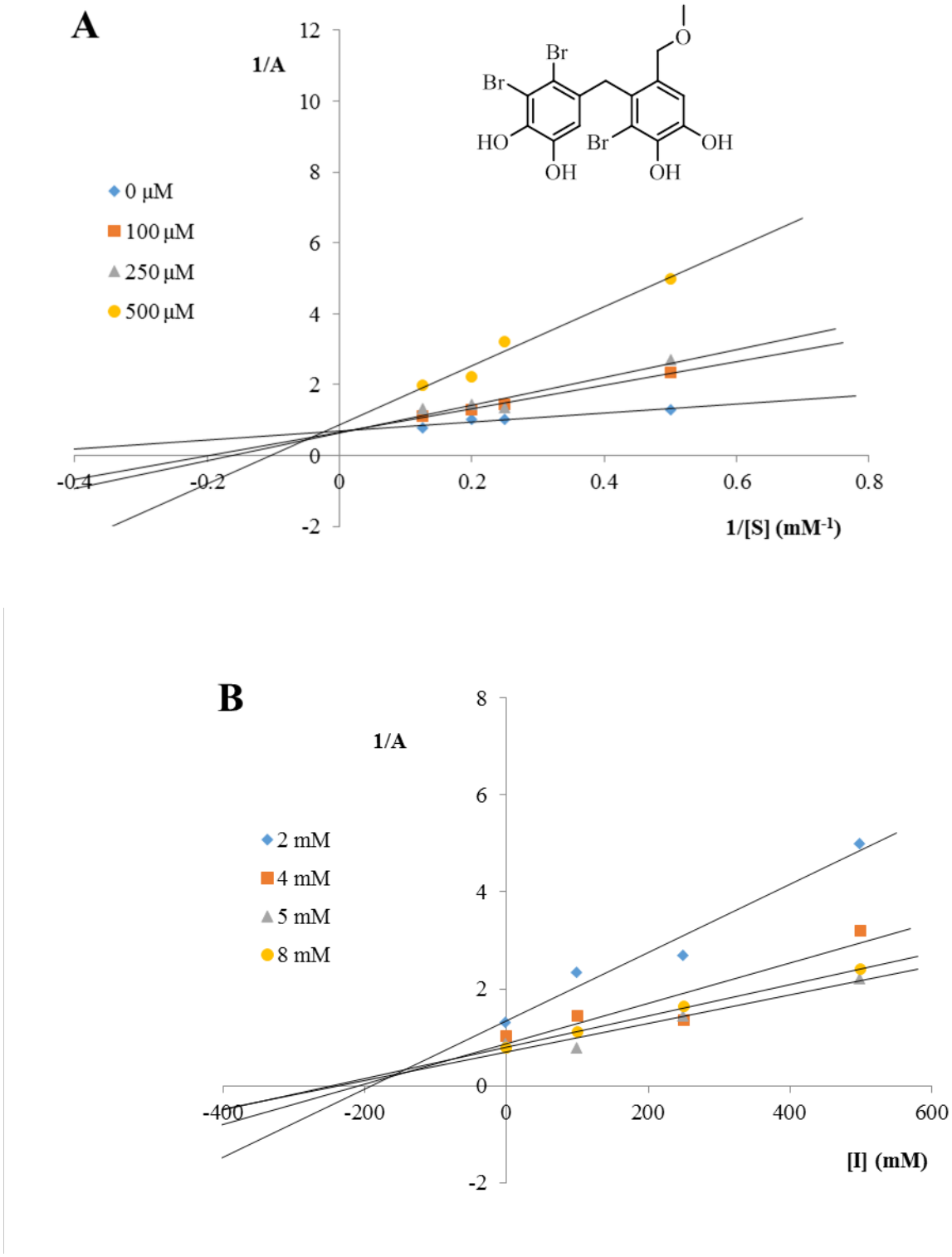


Figure 4-2. Lineweaver-Burk plot (A) and Dixon plot (B) of bromophenol dimer **F2**.

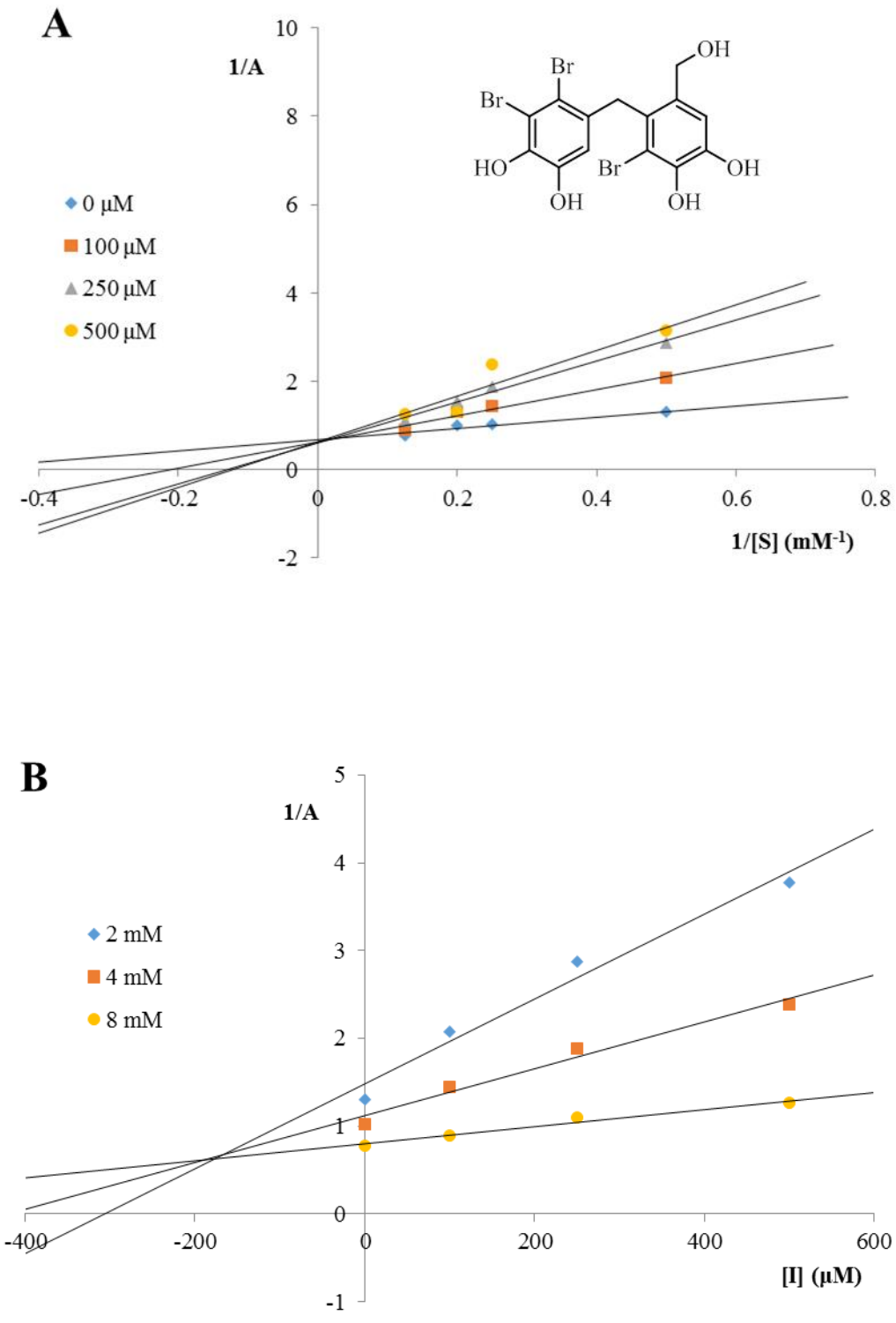


Figure 4-3. Lineweaver-Burk plot (A) and Dixon plot (B) of bromophenol dimer **F3**.

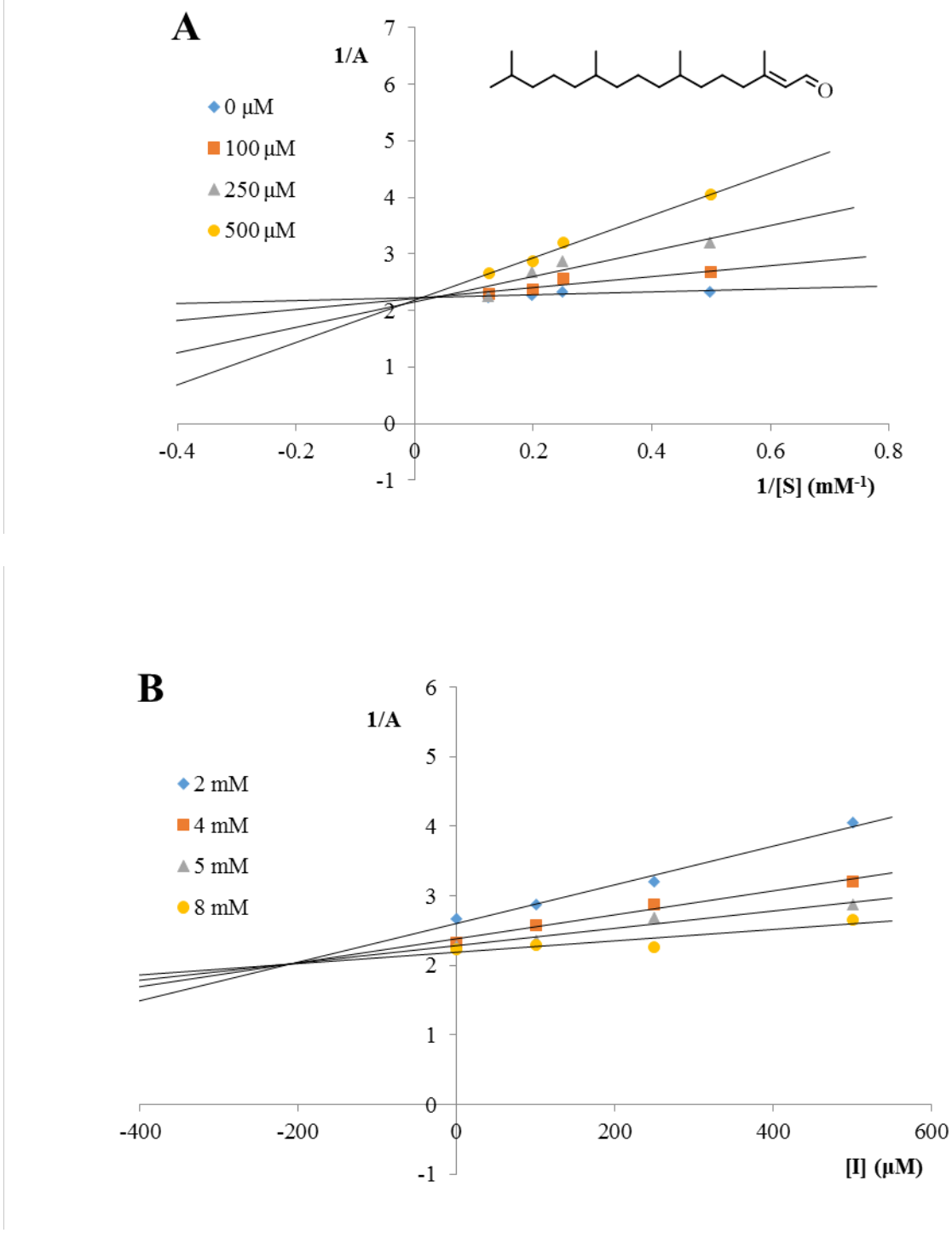


Figure 4-4. Lineweaver-Burk plot (A) and Dixon plot (B) of phytal (**A1**).

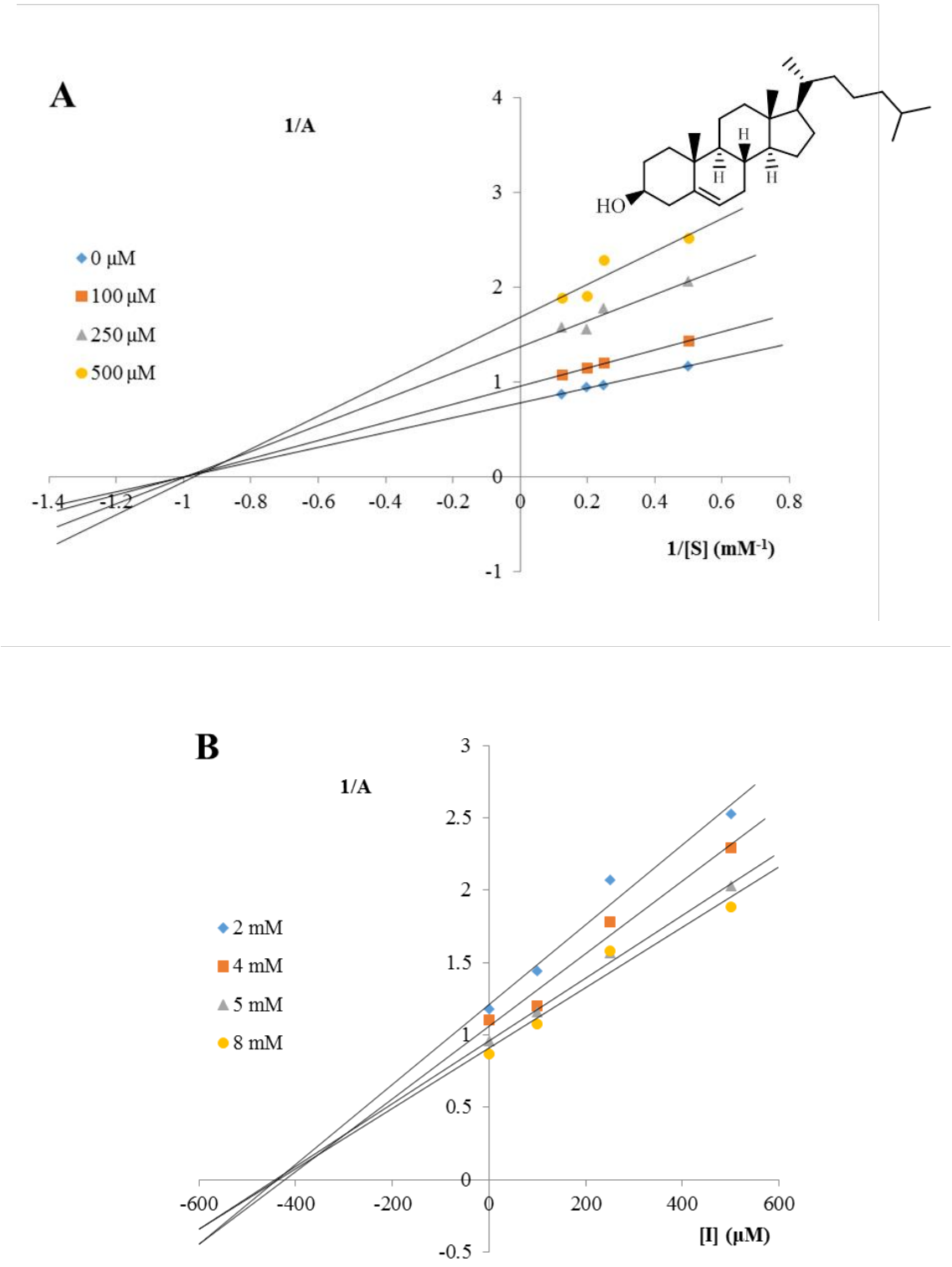


Figure 4-5. Lineweaver-Burk plot (A) and Dixon plot (B) of cholesterol (**A4**).

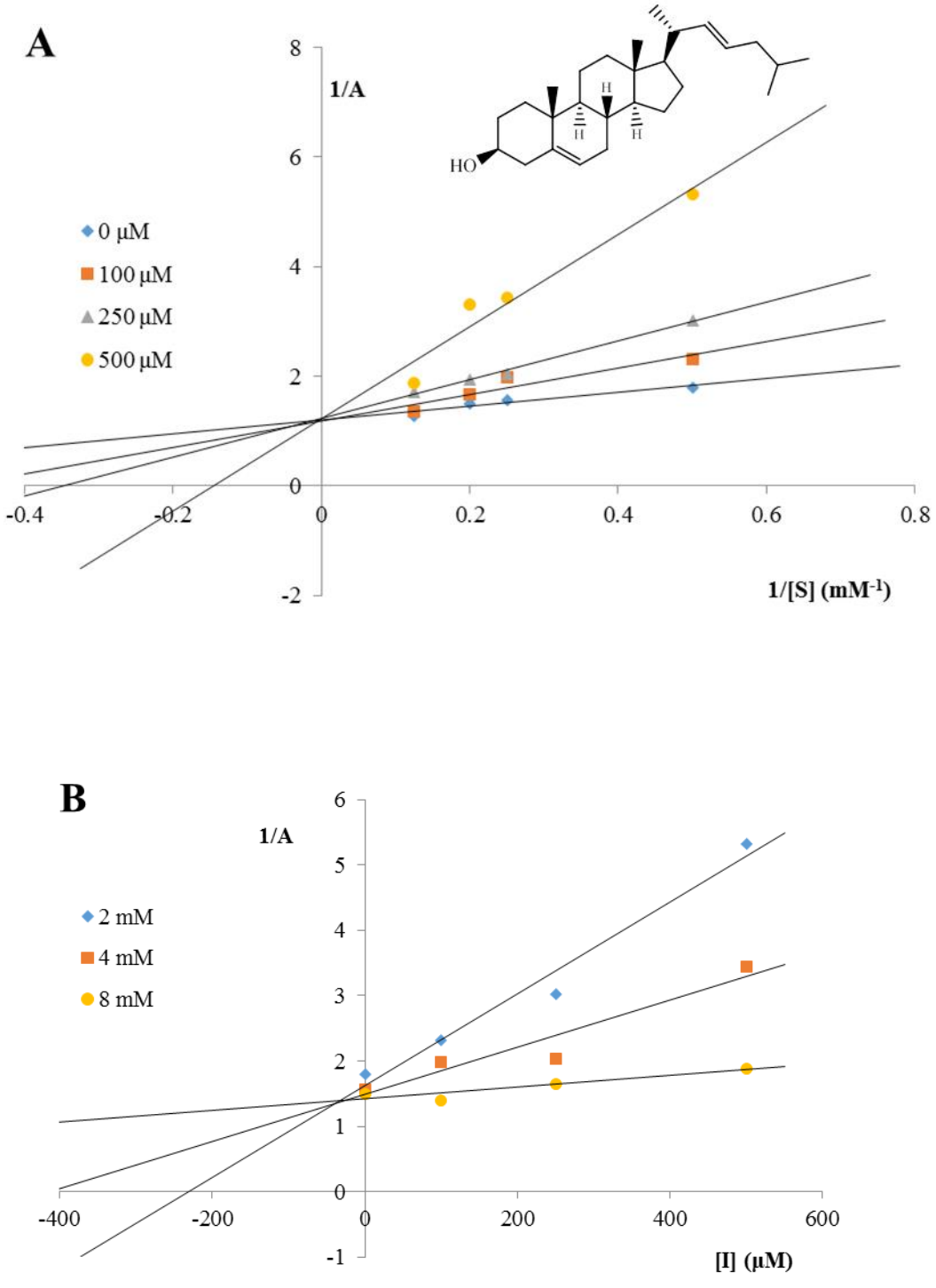


Figure 4-6. Lineweaver-Burk plot (A) and Dixon plot (B) of 22-dehydrocholesterol (**A5**).

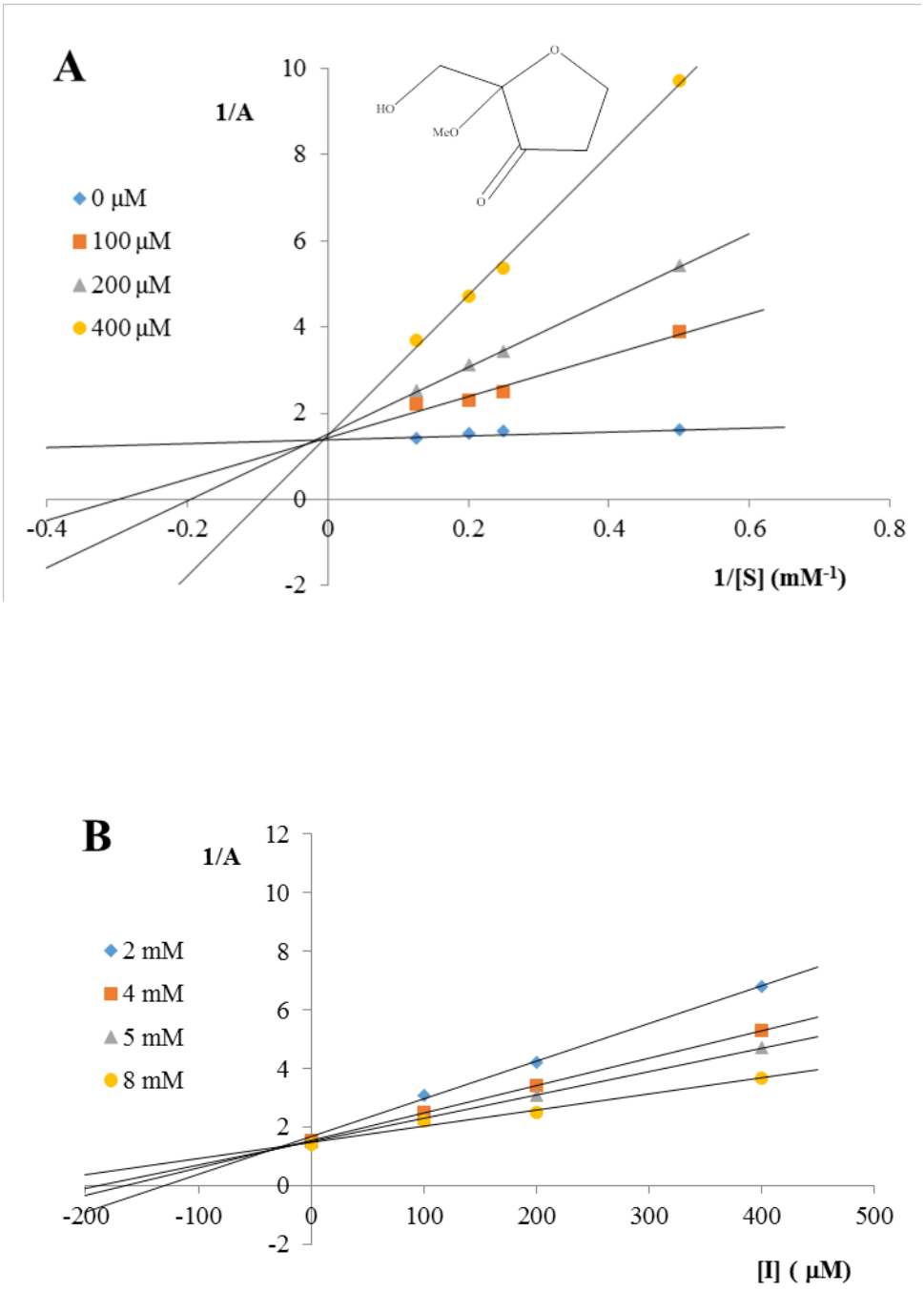
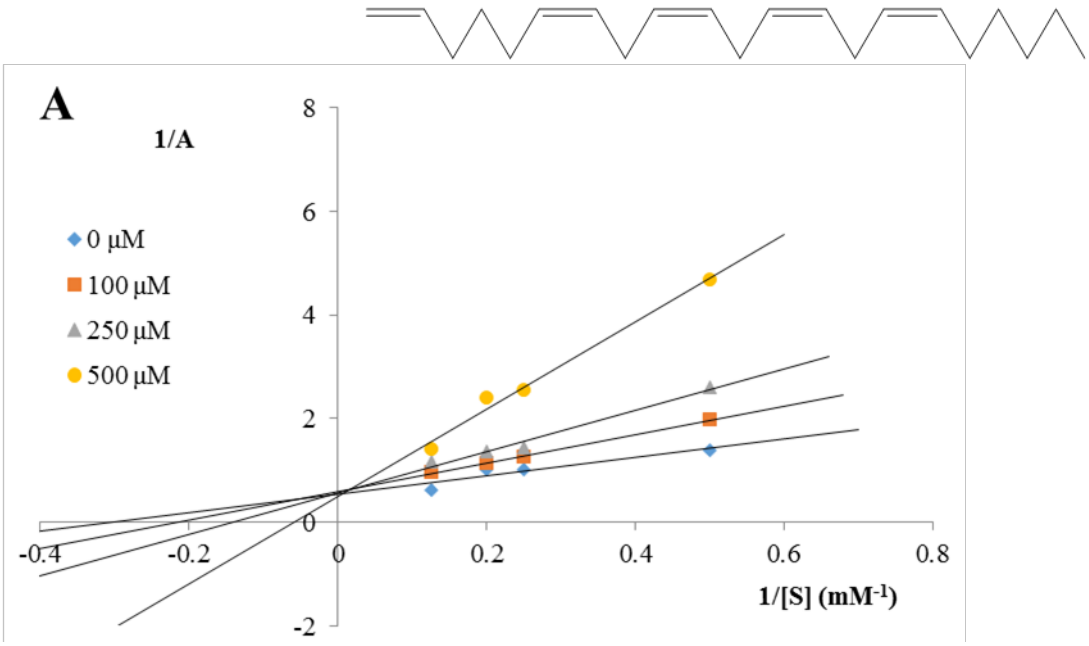


Figure 4-7. Lineweaver-Burk plot (A) and Dixon plot (B) of isogloiosiphone B (**A6**).



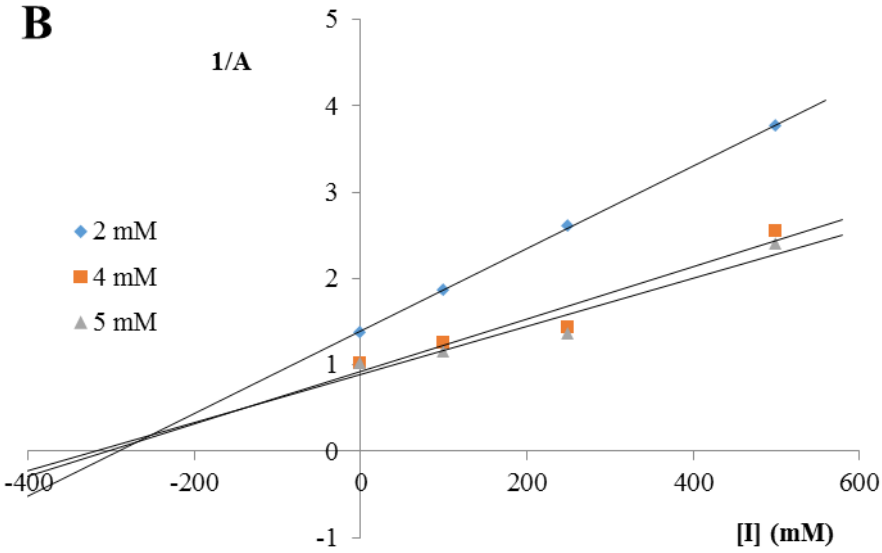


Figure 4-8. Lineweaver-Burk plot (A) and Dixon plot (B) of henicosapentaene (**J1**).

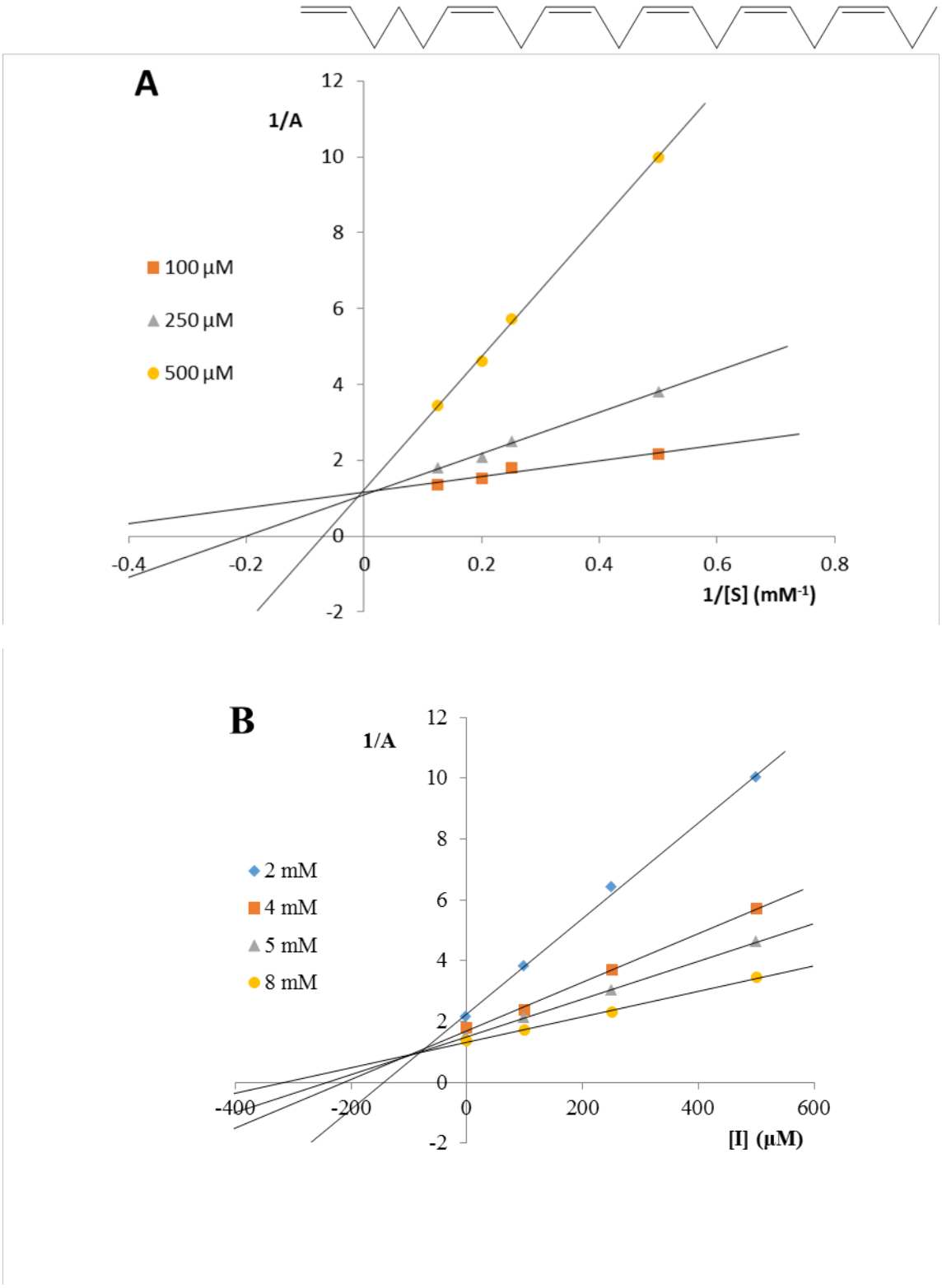


Figure 4-9. Lineweaver-Burk plot (A) and Dixon plot (B) of henicosahexaene (**U2**).

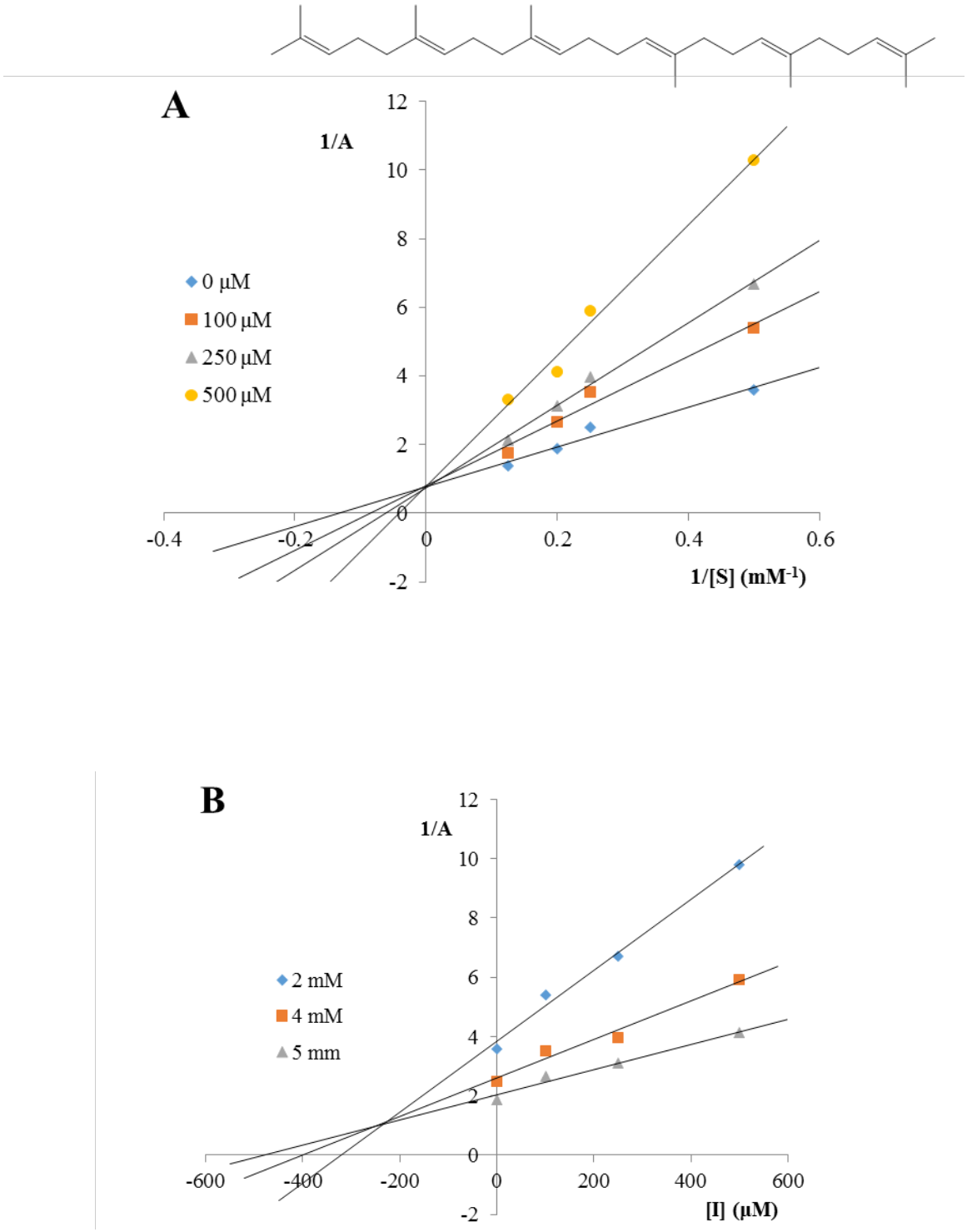
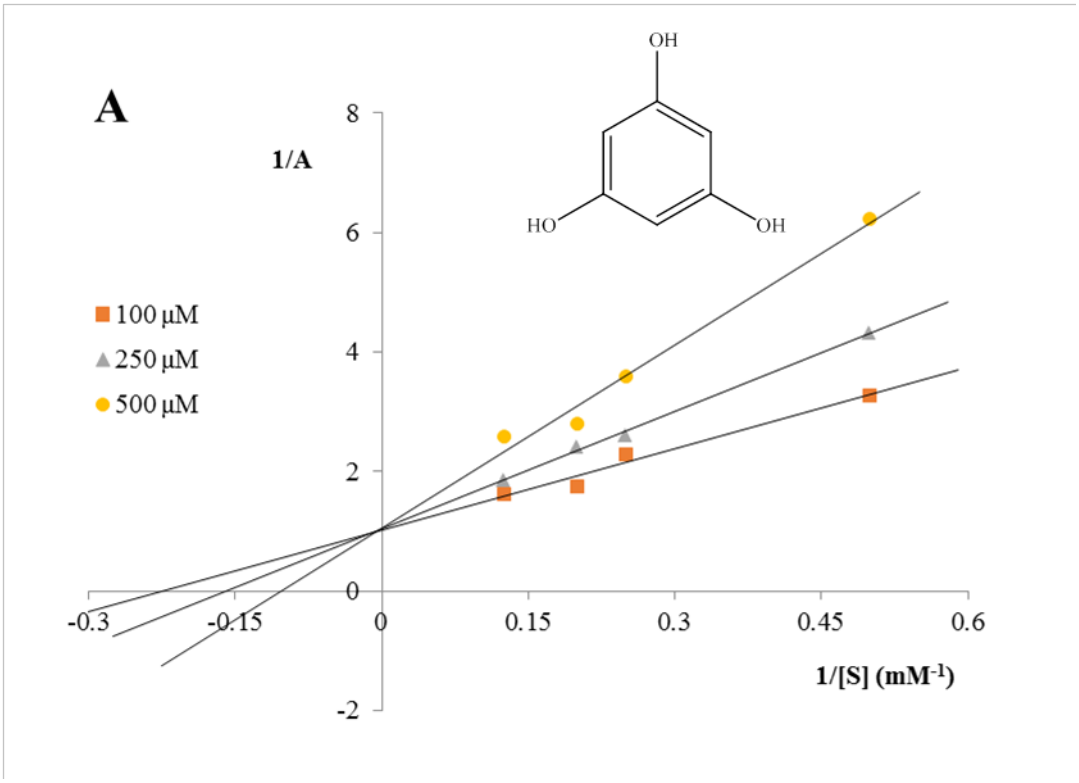


Figure 4-10. Lineweaver-Burk plot (A) and Dixon plot (B) of squalene (**C3**).



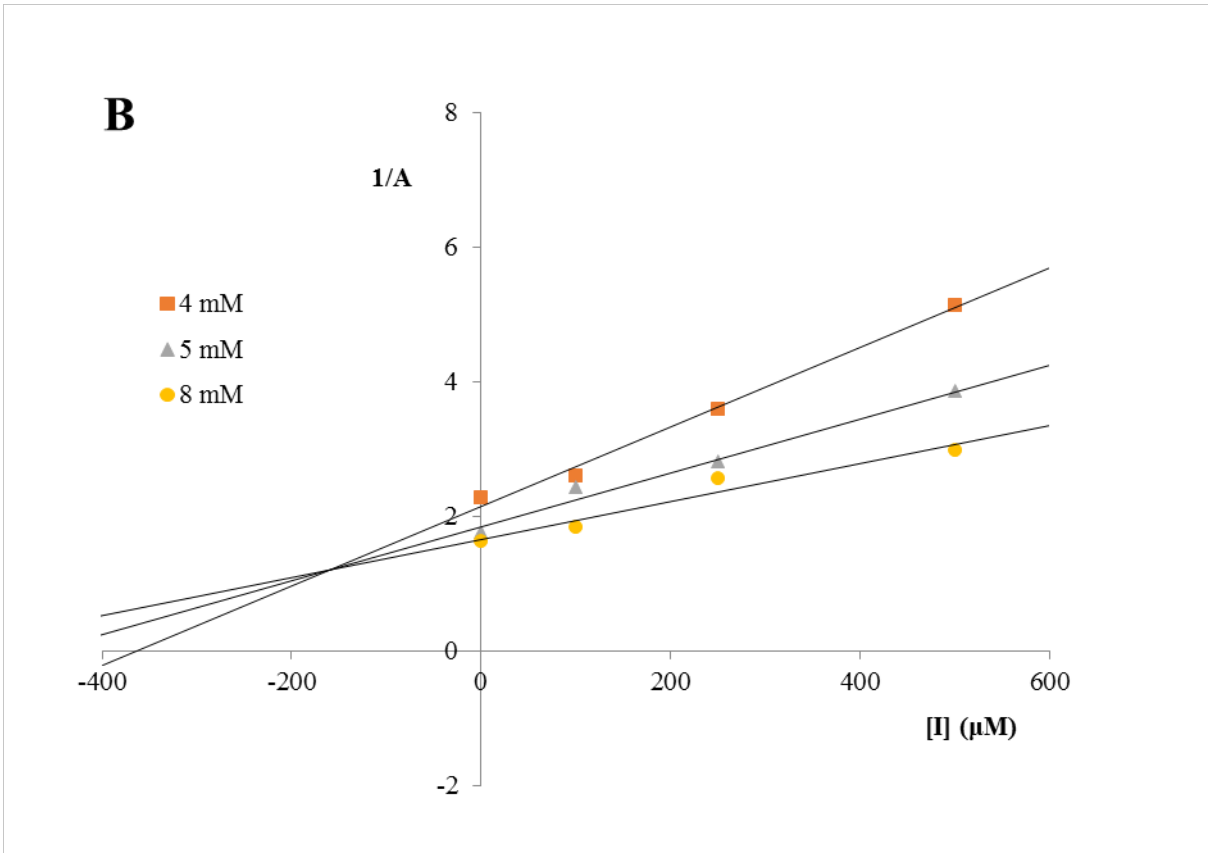


Figure 4-11. Lineweaver-Burk plot (A) and Dixon plot (B) of phloroglucinol (**G2**).

Table 4-1. β-Glucuronidase inhibitory activities of the purified compounds

Compound	IC_{50} (μM) [a]	*Ki* (μM)	Inhibition mode
F1	103.2 ± 0.3	283.2 ± 8.1	Non-competitive
F2	5.1 ± 0.0	155.7 ± 12.5	Competitive
F3	2.6 ± 0.1	180.0 ± 5.9	Competitive
A1	103.7 ± 1.0	210.7 ± 13.0	Competitive
A4	>250	421.2 ± 7.1	Non-competitive
A5	89.5 ± 0.4	32.7 ± 5.5	Competitive
A6	57.0 ± 0.6	8.3 ± 1.3	Competitive
J1	20.9 ± 0.2	236.4 ± 5.3	Competitive
U2	4.4 ± 0.0	81.1 ± 1. 5	Competitive
C3	2.2 ± 0.2	240.1 ± 12.4	Competitive
G2	194.4 ± 0.2	159.7 ± 1.3	Competitive
D-Glucaro-1,4-lactone	77.9 ± 1.4	2.5 ± 2.1	Competitive

[a] Substrate concentration of IC_{50}, 10 mM.

4.2 *In silico* β-glucuronidase inhibitory activities analysis

4.2.1 Molecular docking protocols

The three dimensional (3D) structures of all the purified β-glucuronidase inhibitors were generated by using ChemBioDraw Ultra 14.0 software (PerkinElmer Inc.). All compounds were energy minimized by MM2 and saved in separate database .pdb files and used for molecular docking.

The 3D crystal structure of *E.coli* β-glucuronidase (PDB code 3LPG) was retrieved from the Protein Data Bank at https://www.rcsb.org. From the original protein data bank file, further optimization of the crystal structure was done by AutoDockTools 4.2 (The Scripps Research Institute). Ligands bound to the enzyme as well as water molecules and heteroatoms were removed from the original .pdb file. After merging the nonpolar hydrogens and the assignment of Gastaiger charges, .pdbqt file was saved.

Docking simulations were performed with AutoDock 4.2 to assess the appropriate binding orientations and conformations of the ligand molecule with the 3LPG. The docking grid for the ligand-binding site was set as dimensions 40×40×40 Å with the center coordinates x = -11.516, y= 2.107, z = 22.866. The traditional genetic algorithm was preceded with 100 runs and 150 population size. Graphics and analysis of intermolecular interactions in the receptor were predicted by using PyMol Molecular Graphics System (Version 1.8) (Slashdot Media) and Ligplot+ (Version v.1.4.5) (European Bioinformatics Institute).

All the calculations were performed on Intel(R) Core(TM) i5-4210U CPU 2.40 GHz running Microsoft Windows 7 Professional, version 2009, service pack 1.

4.2.2 The structures of β-glucuronidase from *E. coli* (PDB code: 3LPG)

β-Glucuronidase from *E. coli* (3LPG) exists as a homotetramer composing of the protomers about 600 amino acid residues per subunit (Wallace et al., 2010) and a totol molecular weight of 272 kDa (Burchett, Folsom, & Lane, 2015). Structually, there are three motifs in each subunit: a jelly-roll β-barrel (aa22-223), an immunoglobulin-like fold (a distorted β-barrel) (aa224-342), and a TIM barrel (from N- to C-terminus) (aa343-632) (Hassan et al., 2013), which makes the asymmetric tetramar structure can be considered as a complex of two dimers each composed of two monomers arranged in head-to-head association (Safarov & Gasanov, 2015) (Figure 4-12).

The active residues of the binding pocket of 3LPG within 5 Å were found out by docking with the substrate pNPG. The active binding site included 14 kinds of amino acid residues consisting of 29 amino acids located in A chain and 27 amino acids located in B chain (Figure 4-13).

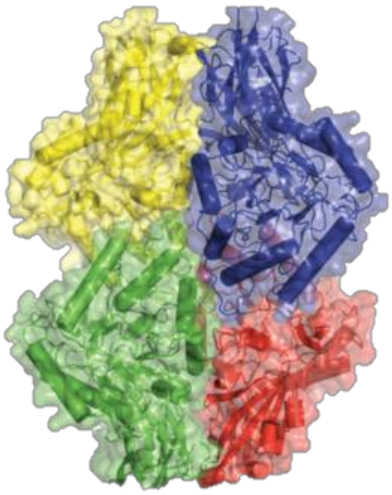


Figure 4-12. Crystal structure of the *E. coli* β-glucuronidase tetramer at 2.5 Å resolution (Wallace et al., 2010).

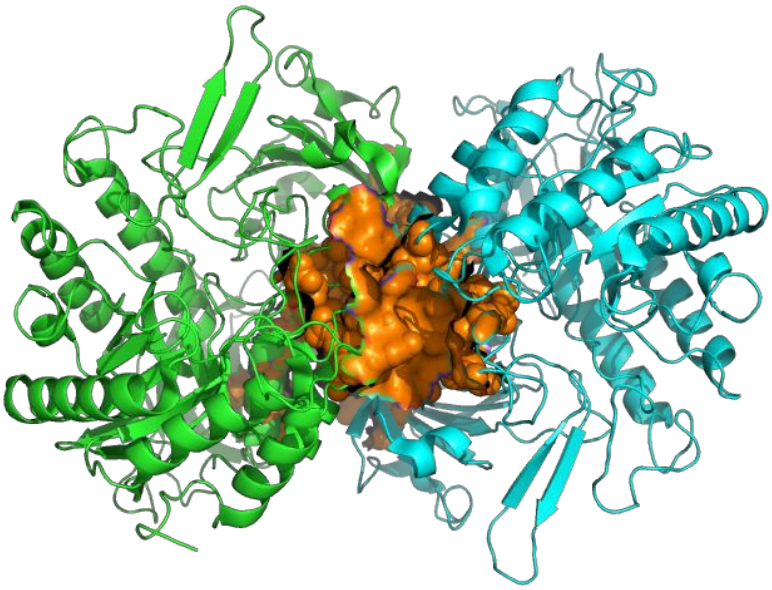


Figure 4-13. Substrate binding site of 3LPG (shown as brown surfaces and spheres).

4.2.3 Molecular modeling based SAR analysis of inhibitory compounds purified from the red algae *N. accurate* and *N. yendoana*

4.2.3.1 Molecular modeling based SAR analysis of bromophenol monomer (F1)

In vitro analysis of bromophenol monomer (**F1**) revealed compound **F1** might be a non-competitive inhibitor, while from the molecular binding simulations, compound **F1** docked into the substrate pocket of the receptor 3LPG posing the binding affinity -5.64 kcal/mol (IC_{50} of 103.2 ± 0.3 μM) (Figure 4-14(A)). Hydrogen bonds, van der Waals forces, electrostatic forces and hydrophobic interactions contributed to the stability of this conformation. Ligplot+ showed the intermolecular interactions of compound **F1** and 3LPG (Figure 4-14(B)). Three hydrogen bonds formed with the hydroxy groups of compound **F1**: two of them were with the oxygen atom of Pro48 (chain A) at distances of 2.81 Å and 2.89 Å and the other one was formed with the carbonyl oxygen atom of Phe306 (chain A) at distance of 2.63 Å. Also some hydrophobic interactions were observed at residues of Arg302, Asp307 in chain A and Phe306, Asp307, Asn308, Val309 in chain B. Additionally, presence of Br atoms further affixed the electrostatic forces, which contributed the inhibitory activity of compound **F1**.

4.2.3.2 Molecular modeling based SAR analysis of bromophenol dimer (F2)

After docking process of bromophenol dimer (**F2**), receptor-ligand complex model was analyzed and visualized by PyMol and Ligplot+ (Figure 4-15). The lowest energy orientation of compound **F2** fitted deeply into the active cavity of 3LPG with excellent docking score -8.63 kcal/mol (IC_{50} of 5.09 ± 0.0 μM) (Figure 4-15(A)). Docking mode analysis showed seven hydrogen bonds formed with the residues of

Pro48 (chain A) (2.49 Å), Arg302 (chain A) (2.59 Å and 3.28 Å), Phe306 (chain A) (2.44 Å), Asn308 (chain A) (3.01 Å) and Pro48 (chain B) (2.74 Å and 3.18 Å). Hydrophobic interactions were observed at residues of Gly17, Ala46, Asp307, Val309 of chain A and Ala46, Arg302, Phe306, Asp307, Asn308, Val309 of chain B (Figure 4-15(B)). The strong hydrogen bonding and hydrophobic interactions might be the predominant reasons for the good inhibitory activity of compound **F2** against β-glucuronidase enzyme.

4.2.3.3 Molecular modeling based SAR analysis of bromophenol dimer (F3)

Bromophenol dimer (**F3**) exhibited excellent inhibitory activity against the β-glucuronidase enzyme with IC_{50} of 2.60 ± 0.1 μM. From the molecular docking studies, compound **F3** was well fitted in the binding cave of the 3LPG enzyme (Figure 4-16(A)) with excellent docking score -8.74 kcal/mol. For the most stable orientation of compound **F3**, seven hydrogen bonds generated with the residues of Pro48 (chain A) (2.51 Å), Arg302 (chain A) (3.21 Å and 2.53 Å), Phe306 (chain A) (2.47 Å), Asn308 (chain A) (2.71 Å), Pro48 (chain B) (2.74 Å) and Phe306 (chain B) (2.61 Å). Meanwhile, some hydrophobic interactions were observed at the residues Gly17, Ala46, Asp307, Val309 of chain A and Ala46, Arg302, Asp307, Asn308, Val309 of chain B (Figure 4-16(B)). The intense interface of hydrogen bonding and hydrophobic connections reinforced interactions between ligand **F3** and receptor 3LPG. Also, the presence of Br atoms of compound **F3** increased the electron withdrawing effect to 3LPG.

4.2.3.4 Molecular modeling based SAR analysis of compound phytal (A1)

Molecular docking analysis showed phytal (**A1**) bound into the active cavity of 3LPG (Figure 4-17(A)) with the docking affinity -5.89 kcal/mol (IC_{50} of 103.7 ± 1.0 μM). Hydrogen bonding and hydrophobic interactions were observed at the ligand-receptor complex by Ligplot+. One single hydrogen bond formed at position of carbonyl oxygen of compound **A1** with the $-NH_2$ moiety of Arg302 (Chain B) at a distance of 2.76 Å. The hydrophobic interactions were observed at the amino acids Leu15, Pro48, Arg302, Phe306, Asp307, Asn308 of Chain A and Leu15, Gly17, Pro48, Phe306, Asp307, Asn308 of Chain B (Figure 4-17(B)).

4.2.3.5 Molecular modeling based SAR analysis of phytol (A2) and cholesta-4,22-diene-3,6-dione (A3)

The mixture of compounds **A2** and **A3** which was failed for the final purification exhibited 36.21% inhibitory activity at concentration of 10 μg/mL. Docking affinity of compound **A2** and **A3** were -6.72 kcal/mol and -5.77 kcal/mol, respectively. Both of the two compounds fitted into the active binding cavity of 3LPG (Figure 4-18(A)). For compound **A2**, one single hydrogen bond was observed between the hydroxy group of compound **A2** and oxygen atom of Pro48 (chain B) with distance of 2.76 Å. And hydrophobic interactions were observed at the residues of Leu15, Pro48, Arg302, Phe306, Asp307, Asn308, Val309 of chain A and Ala46, Arg302, Phe306, Asp307, Asn308, Val309 of chain B (Figure 4-18(B)). For compound **A3**, hydrophobic interactions were found at the residues of Leu15, Gly17, Pro48, Phe306, Asp307, Asn308 of chain A and Asp307, Asn308 of chain B (Figure 4-18(C)).

4.2.3.6 Molecular modeling based SAR analysis of compound cholesterol (A4)

Cholesterol (**A4**) showed quite weak inhibitory activity against β-glucuronidase *in vitro* (IC_{50} >250 μM). Molecular docking analysis showed compound **A4** fell out of the active substrate binding site with the docking score -5.85 kcal/mol (Figure 4-19(A)), which was in corresponding with the *in vitro* assay showing compound **A4** should be a non-competitive inhibitor. None of hydrogen bonds was observed and hydrophobic interactions were just found at the residues of chain A including Arg268, Asn308, Val312, Glu336, Asp339, Trp340 and Glu343 (Figure 4-19(B)).

4.2.3.7 Molecular modeling based SAR analysis of 22-dehydrocholesterol (A5)

22-Dehydrocholesterol (**A5**) showed moderate inhibitory activity against β-glucuronidase *in vitro* (IC_{50} of 89.5 ± 0.4 μM). The molecular docking analysis showed compound **A5** fitted into the active substrate cavity of 3LPG (Figure 4-20(A)) with -4.72 kcal/mol docking score. No hydrogen bonds formed and hydrophobic interactions played important roles in the docking simulations. Related hydrophobic interacting amino acid included Leu15, Arg302, Phe306, Asp307, Asn308 of chain A and Asn308 of chain B.

4.2.3.8 Molecular modeling based SAR analysis of isogloiosiphone B (A6)

Novel isogloiosiphone B (**A6**) showed higher inhibitory activity (IC_{50} of 57.0 ± 0.5 μM) against β-glucuronidase than the positive control *in vitro*. Molecular docking analysis showed compound **A6** fitted into the substrate active sites of 3LPG and hydrogen bonding interactions showed main role for the binding affinity (Figure

4-21(A)). Binding score of compound **A6** was -5.28 kcal/mol. Two hydrogen bonds were generated after molecular docking stimulations with Lys304 dominated in chain A at a distance of 2.87 Å and Gly305 situated in chain B at a distance of 2.56 Å. Hydrophobic interactions were observed at residues of His296, Glu297, Asp298, Phe307, Asp307 and Leu310 of chain A(Figure 4-21(B)).

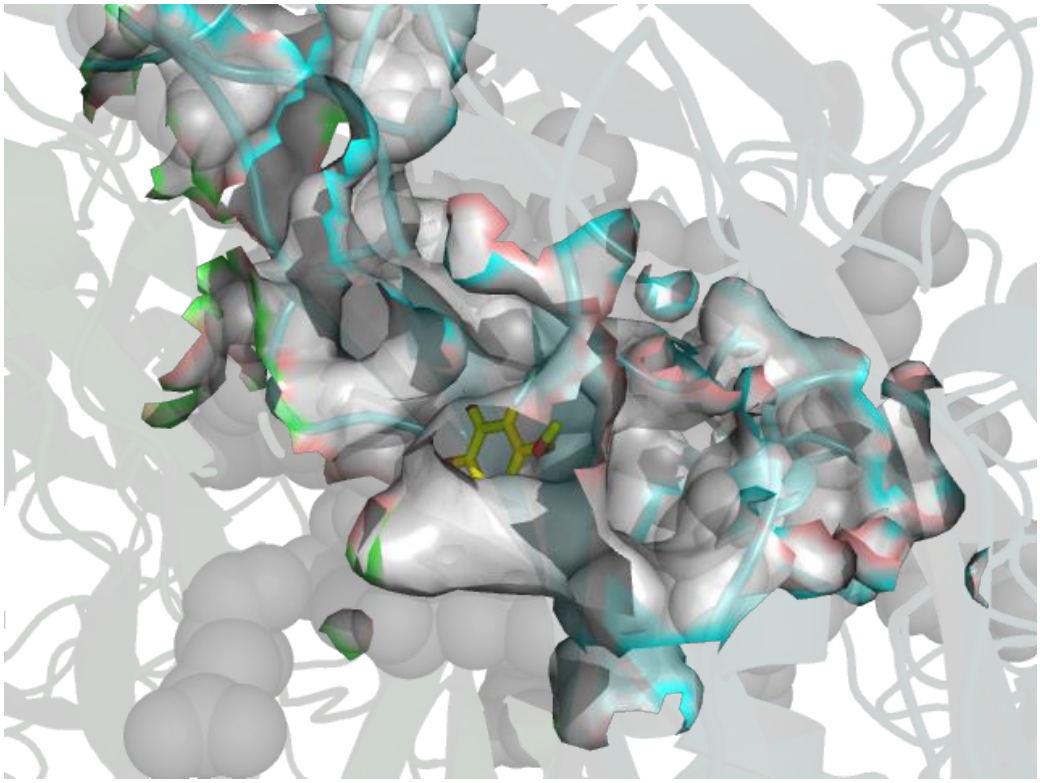


Figure 4-14 (A). Binding mode between bromophenol monomer (**F1**) and substrate active site of 3LPG. Interacting residues of 3LPG are displayed in gray surface mode. Compound **F1** is presented in balls and sticks. Atoms of **F1** are color-coded as follows: C, yellow; H, white; O, red; Br, brown.

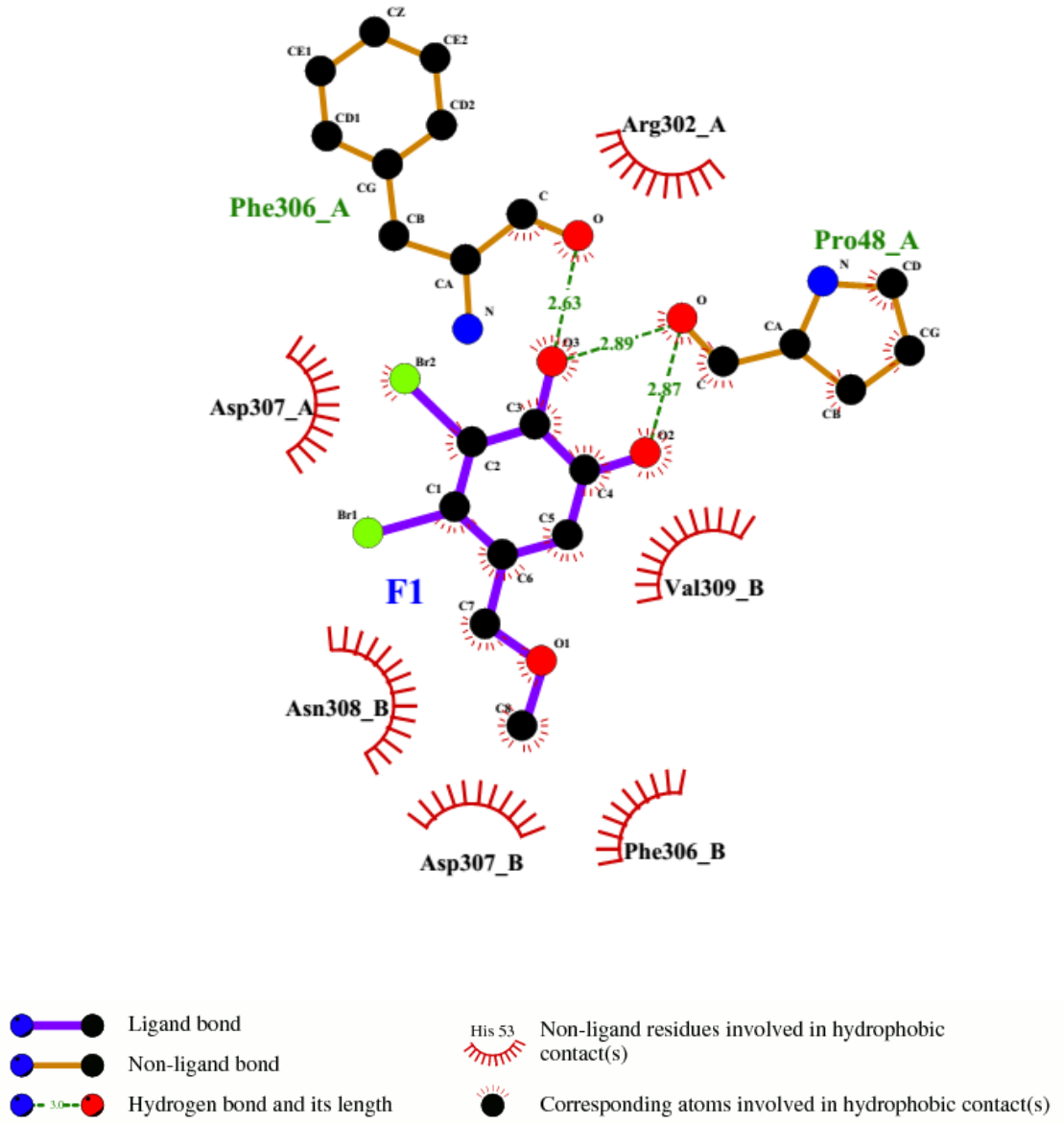


Figure 4-14 (B). Intermolecular interactions of bromophenol monomer (**F1**) with 3LPG showing by Ligplot+ (schematic 2D plot).

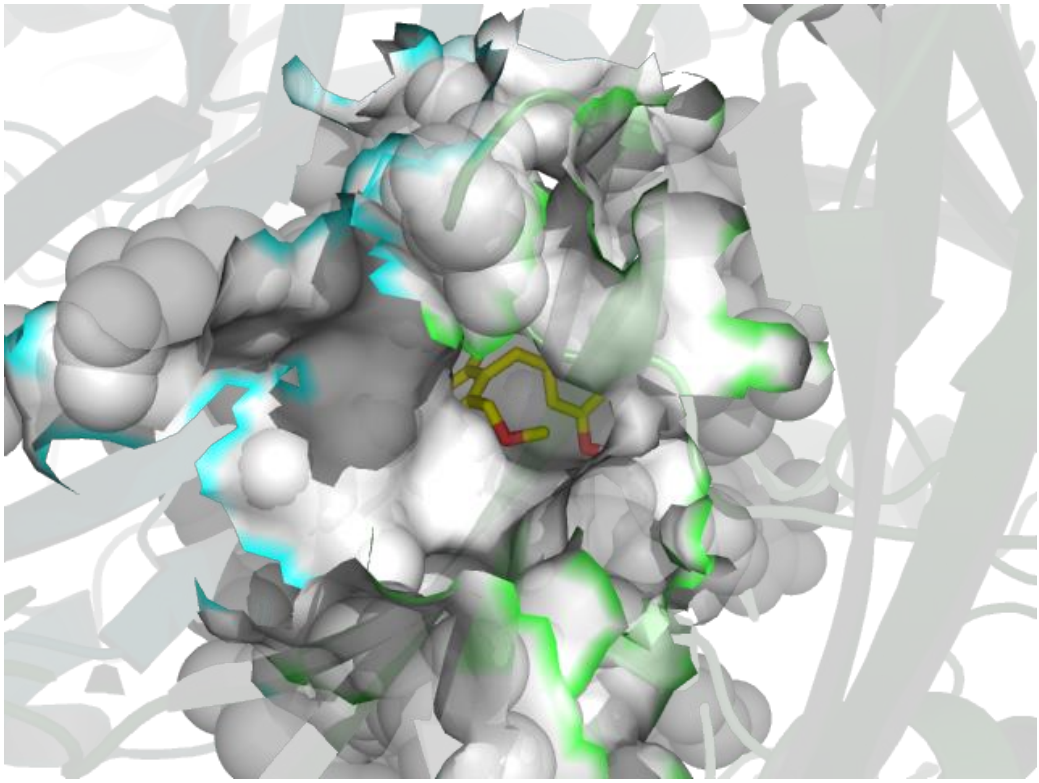


Figure 4-15 (A). Binding mode between bromophenol dimer (**F2**) and substrate active site of 3LPG. Interacting residues of 3LPG are displayed in gray surface mode. Compound **F2** is presented in balls and sticks. Atoms of **F2** are color-coded as follows: C, yellow; H, white; O, red; Br, brown.

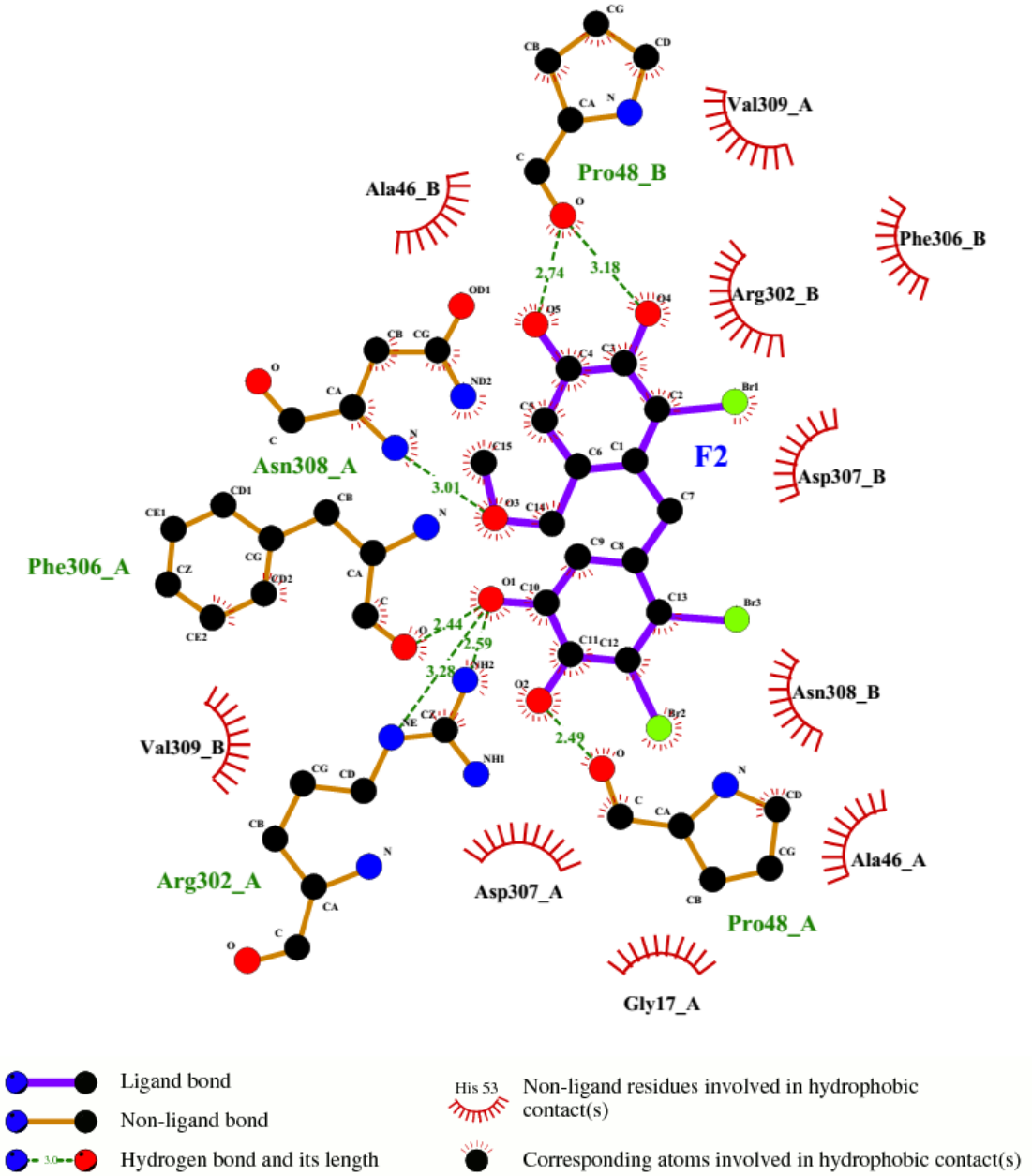


Figure 4-15 (B). Intermolecular interactions of bromophenol dimer (**F2**) with 3LPG showing by Ligplot+ (schematic 2D plot).

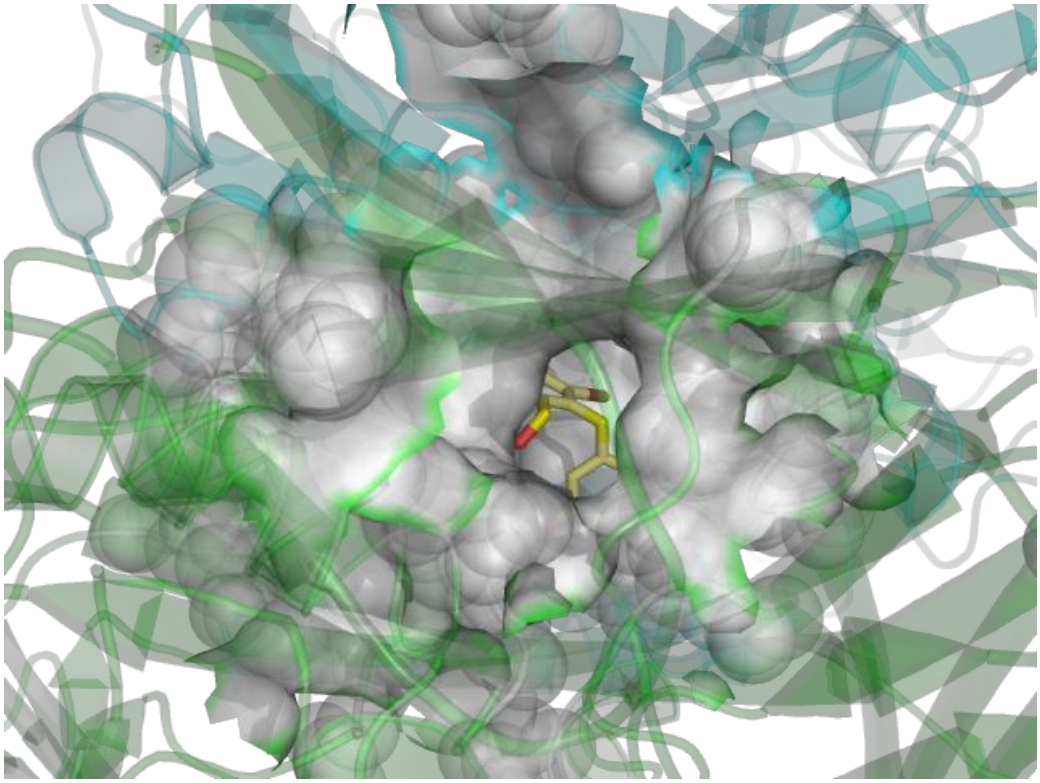
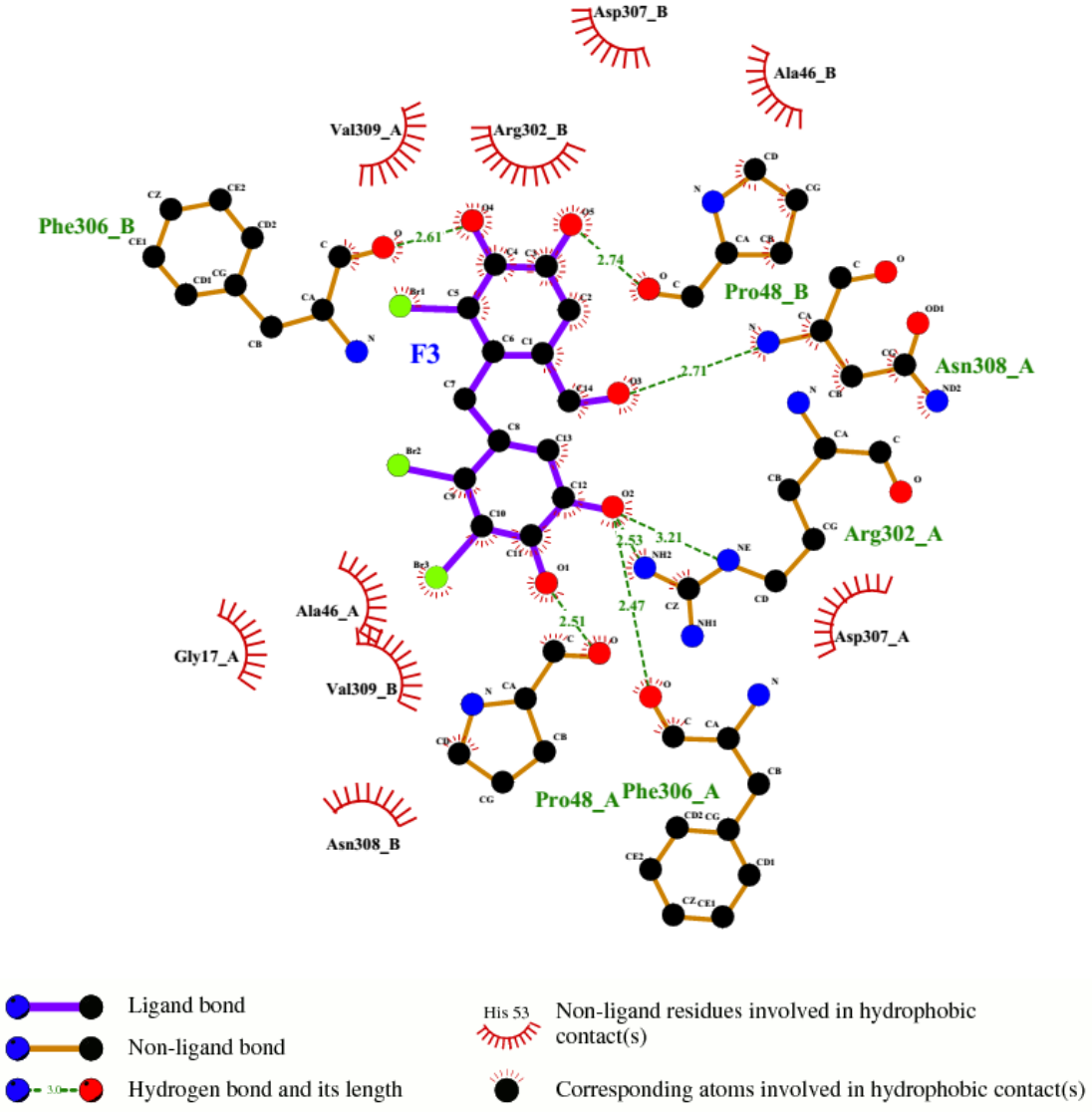


Figure 4-16 (A). Binding mode between bromophenol dimer (**F3**) and substrate active site of 3LPG. Interacting residues of 3LPG are displayed in gray surface mode. Compound **F3** is presented in balls and sticks. Atoms of **F3** are color-coded as follows: C, yellow; H, white; O, red; Br, brown.



(B)

Figure 4-16 (B). Intermolecular interactions of bromophenol dimer (**F3**) with 3LPG showing by Ligplot+ (schematic 2D plot).

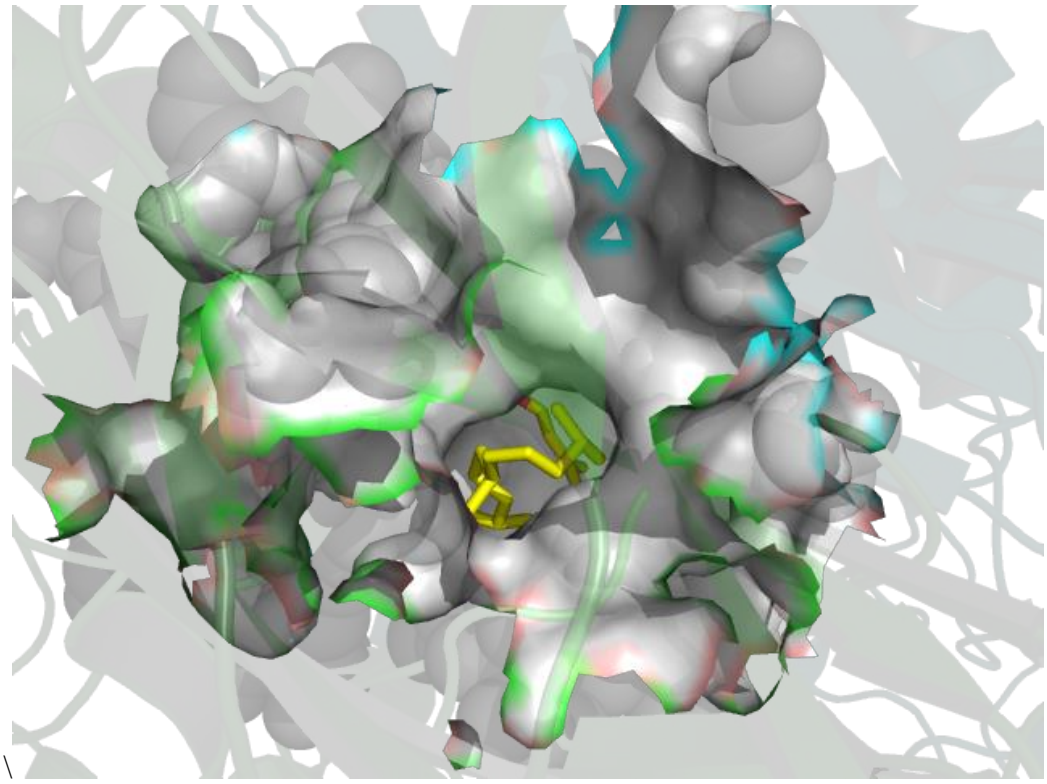


Figure 4-17 (A). Binding mode between phytal (**A1**) and substrate active site of 3LPG. Interacting residues of 3LPG are displayed in gray surface mode. Compound **A1** is presented in balls and sticks. Atoms of **A1** are color-coded as follows: C, yellow; O, red.

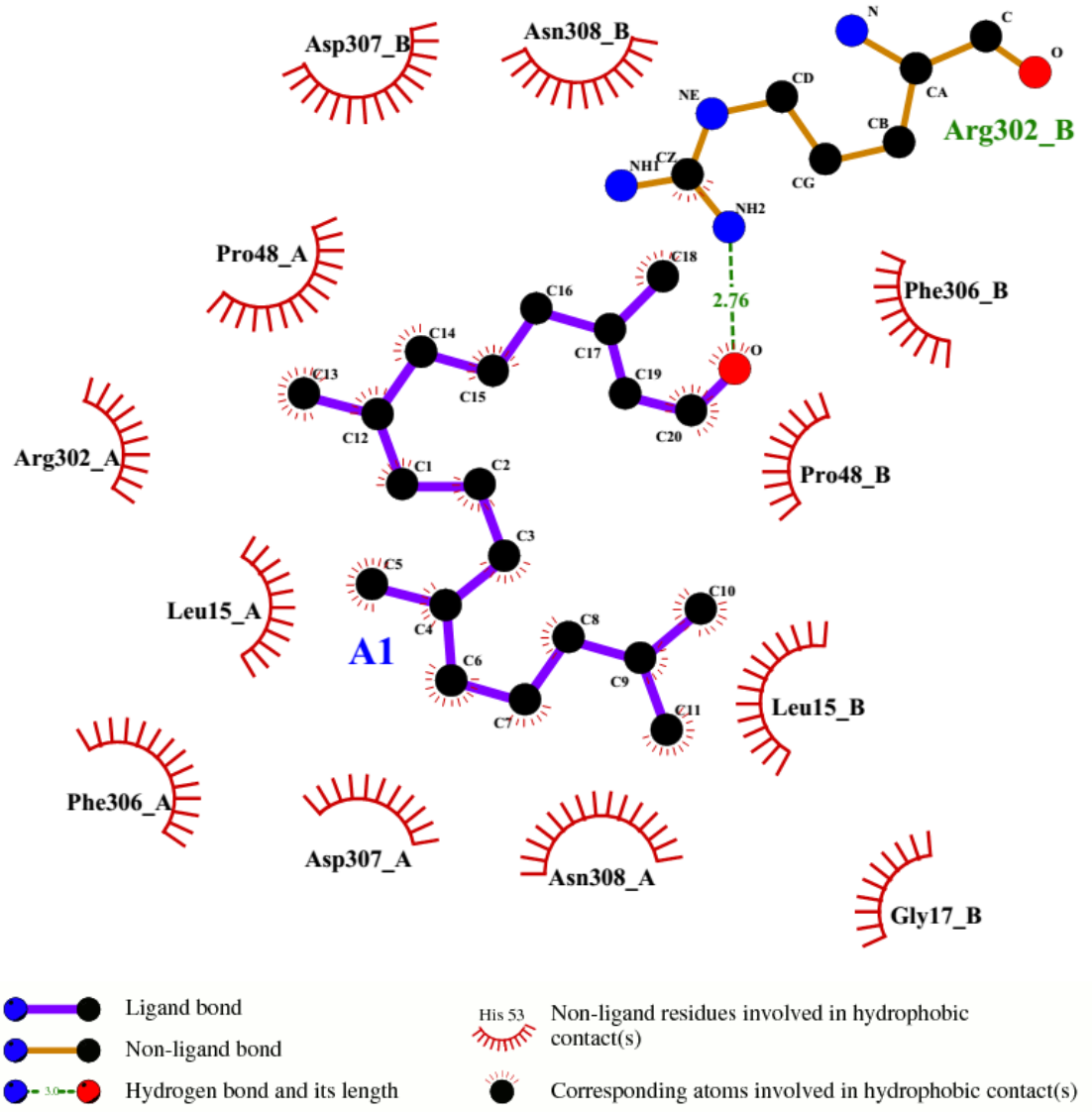


Figure 4-17 (B). Intermolecular interactions of phytal (**A1**) with 3LPG showing by Ligplot+ (schematic 2D plot).

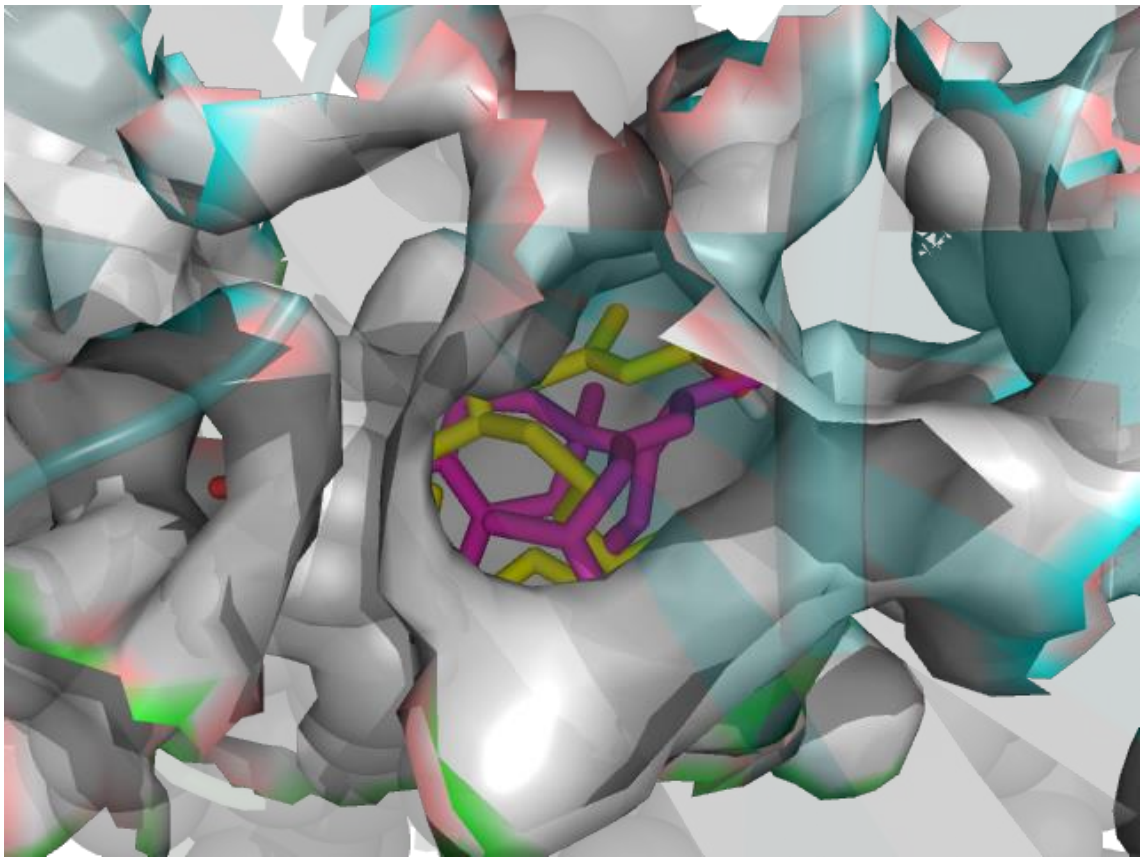


Figure 4-18 (A). Binding mode between phytol (**A2**), cholesta-4,22-diene-3,6-dione (**A3**) and substrate active site of 3LPG. Interacting residues of 3LPG are displayed in gray surface mode. Compounds **A2** and **A3** are presented in balls and sticks. Atoms of **A2** are color-coded as follows: C, yellow; O, red. Atoms of A3 are color-coded as follows: C, magenta; O, red.

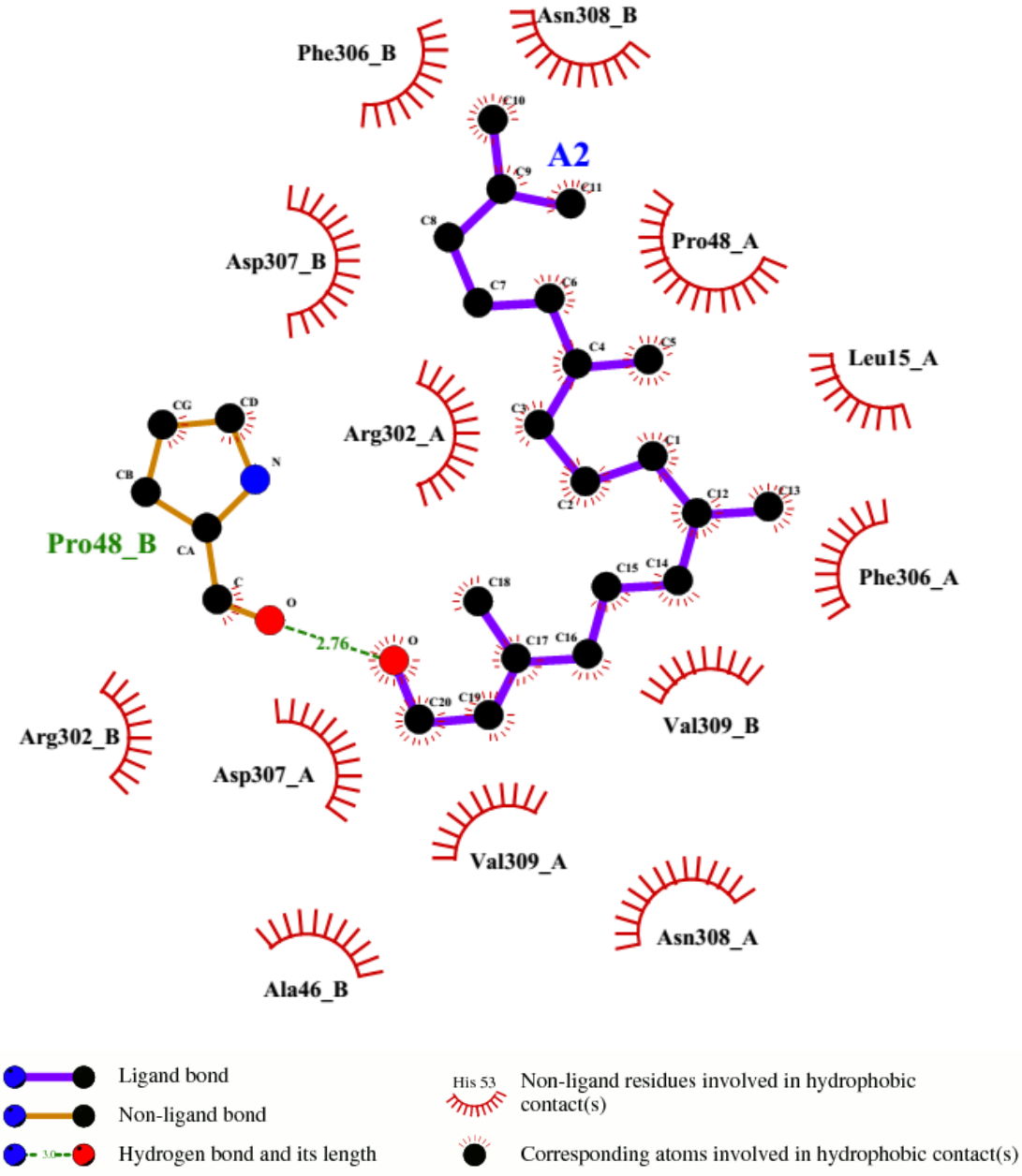


Figure 4-18 (B). Intermolecular interactions of phytol (**A2**) with 3LPG showing by Ligplot+ (schematic 2D plot).

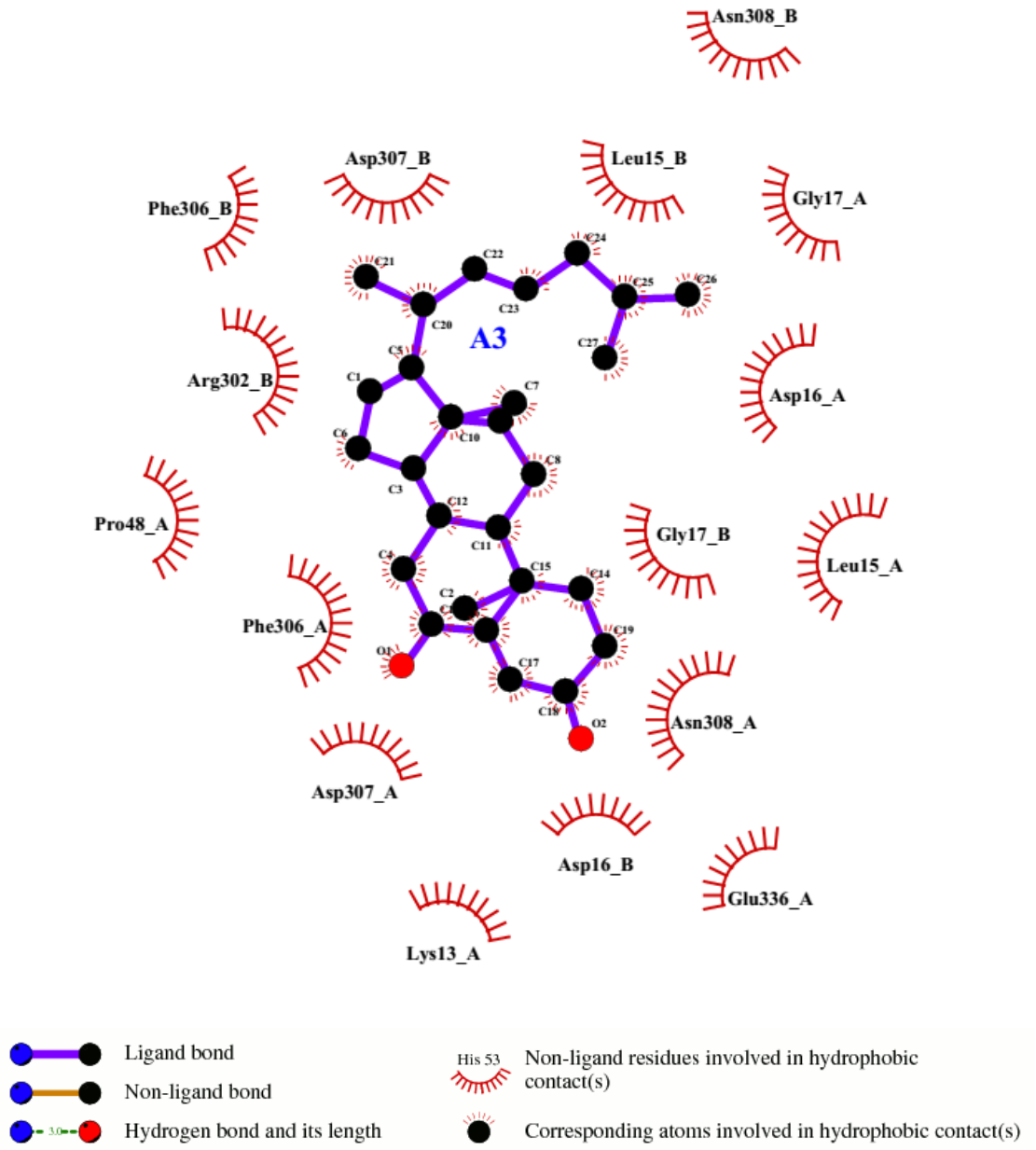


Figure 4-18 (C). Intermolecular interactions of cholesta-4,22-diene-3,6-dione (**A3**) with 3LPG showing by Ligplot+ (schematic 2D plot).

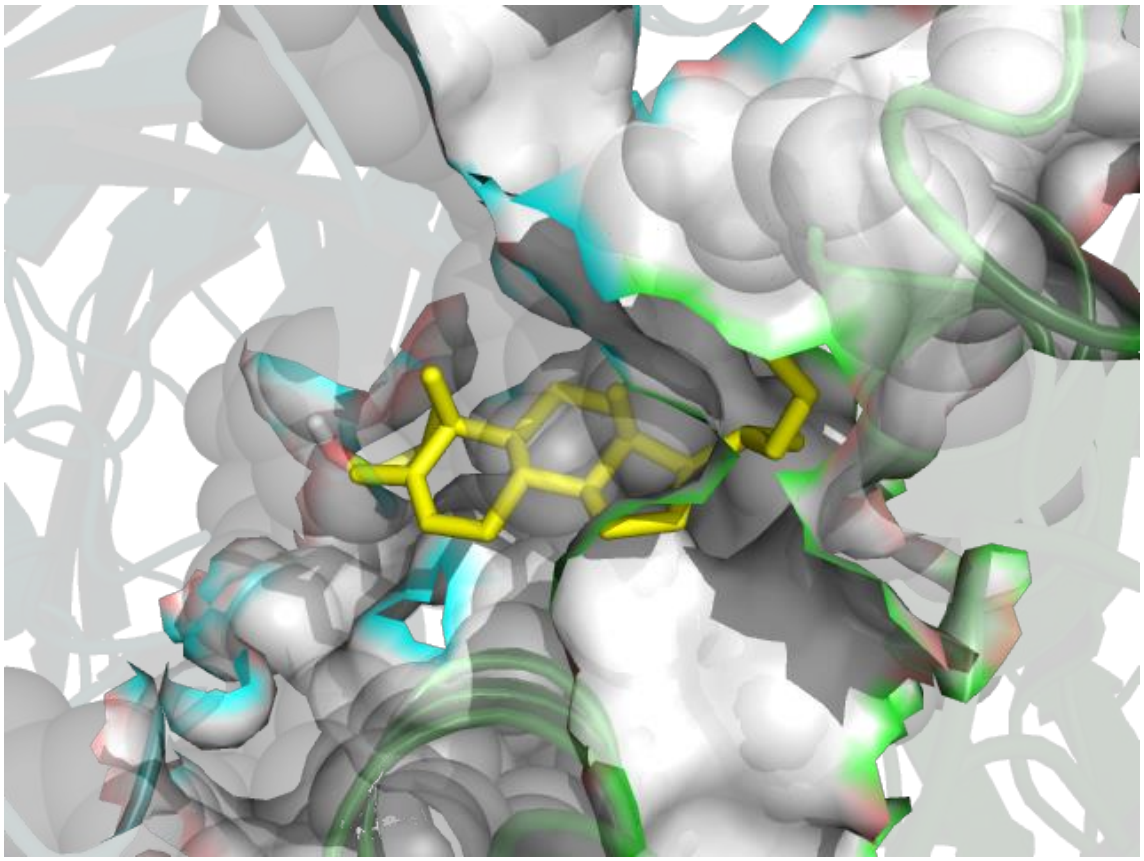


Figure 4-19 (A). Binding mode between cholesterol (**A4**) and substrate active site of 3LPG. Interacting residues of 3LPG are displayed in gray surface mode. Compound **A4** is presented in balls and sticks. Atoms of **A4** are color-coded as follows: C, yellow; H, white; O, red.

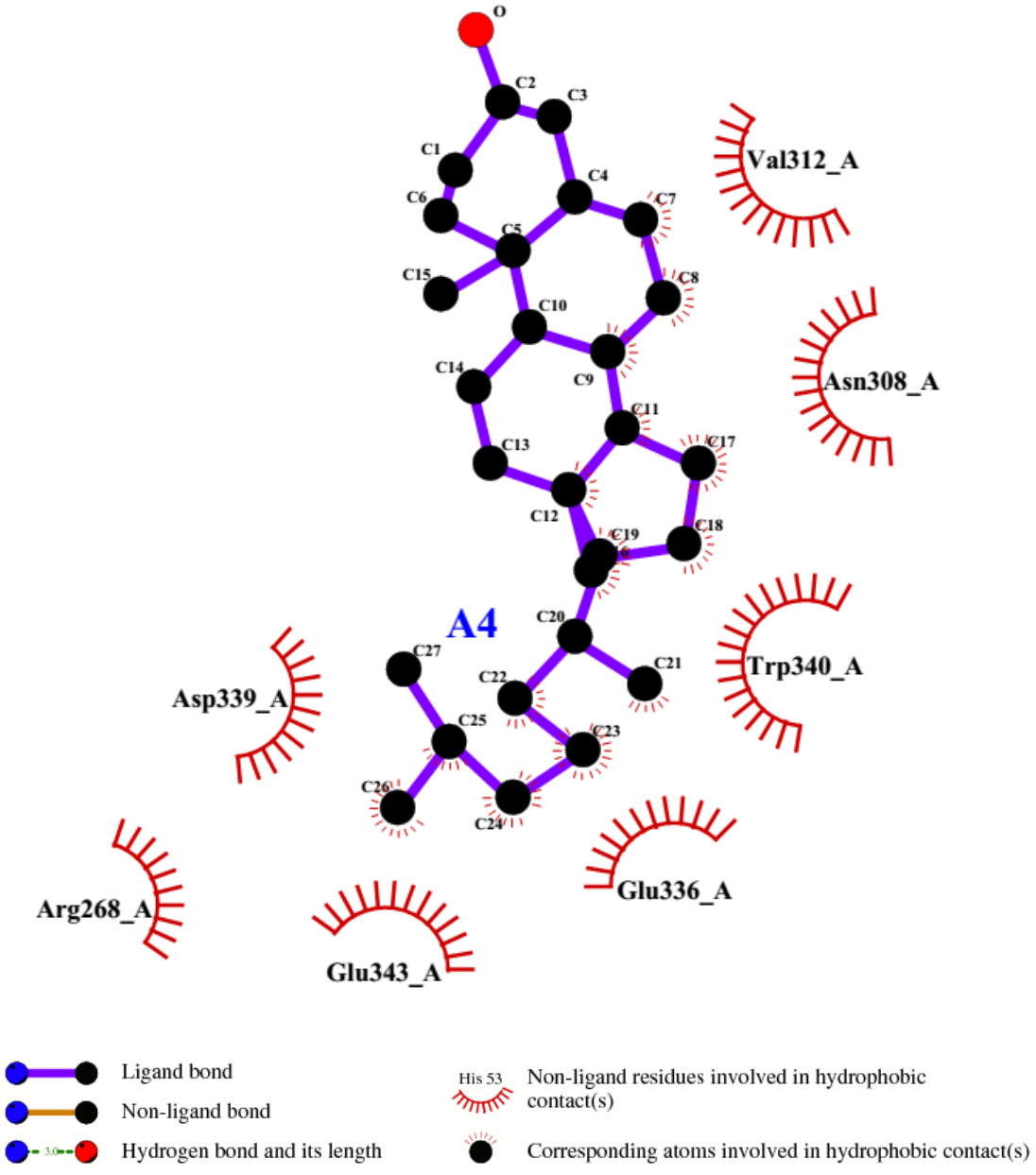


Figure 4-19 (B). Intermolecular interactions of compound cholesterol (**A4**) with 3LPG showing by Ligplot+ (schematic 2D plot).

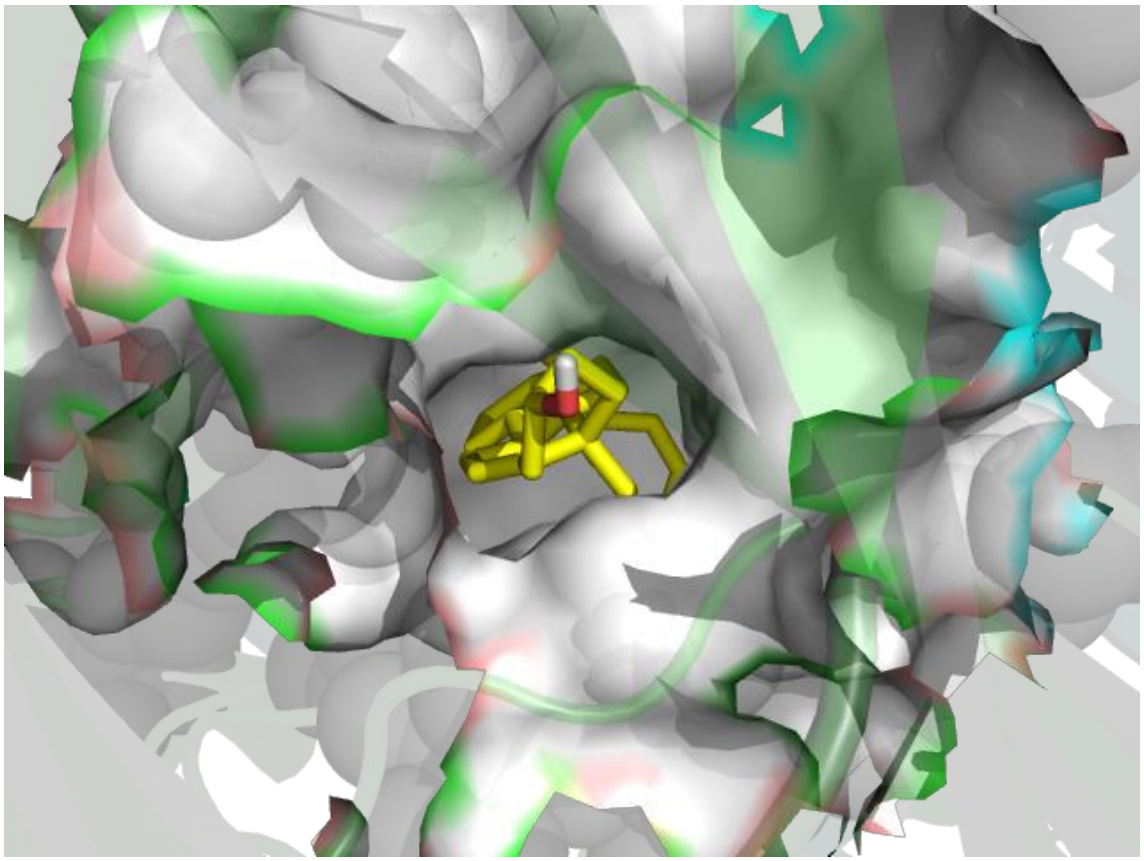


Figure 4-20 (A). Binding mode between 22-dehydrocholesterol (**A5**) and substrate active site of 3LPG. Interacting residues of 3LPG are displayed in gray surface mode. Compound **A5** is presented in balls and sticks. Atoms of **A5** are color-coded as follows: C, yellow; H, white; O, red.

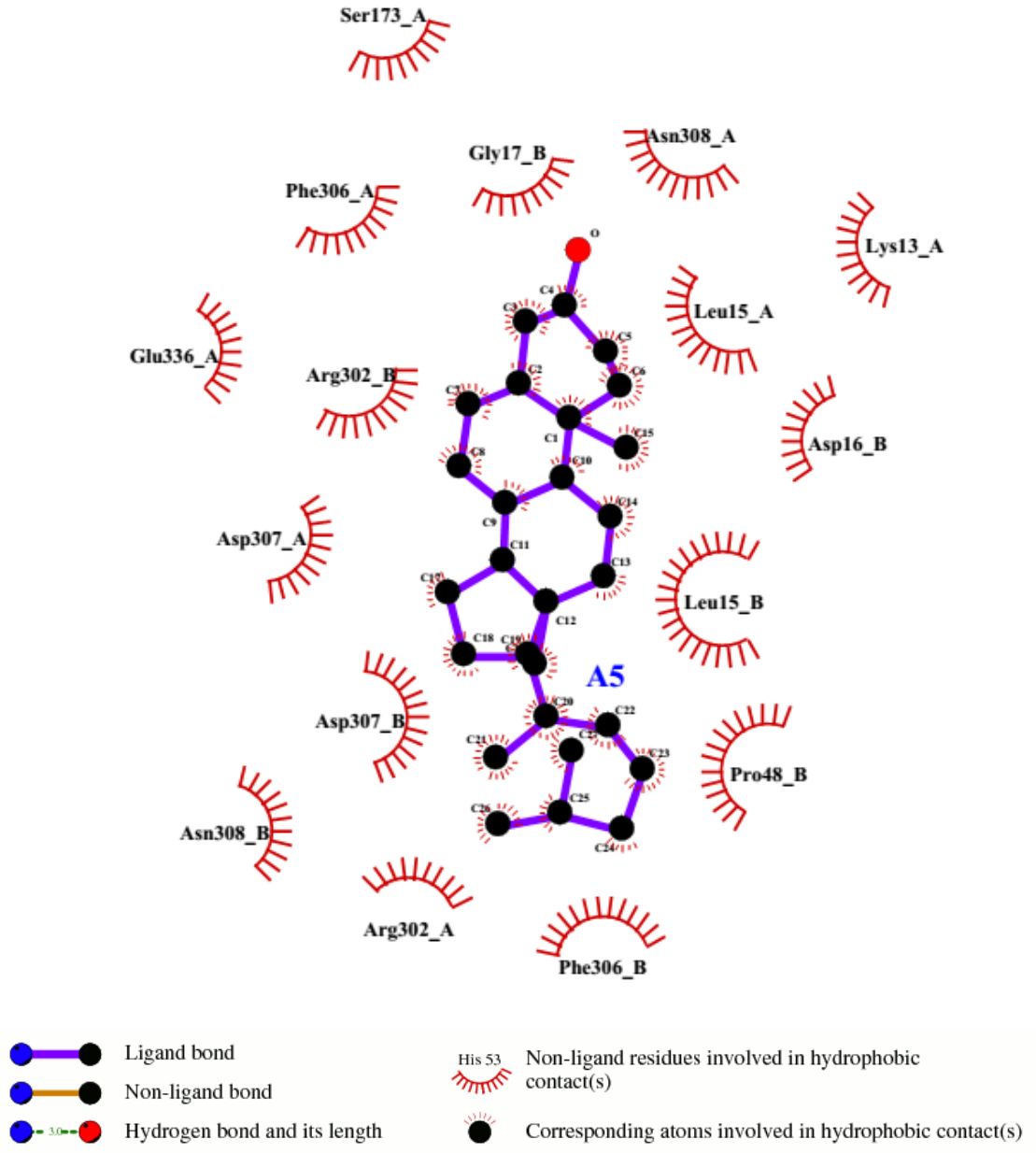


Figure 4-20 (B). Intermolecular interactions of compound **A5** with 3LPG showing by Ligplot+ (schematic 2D plot).

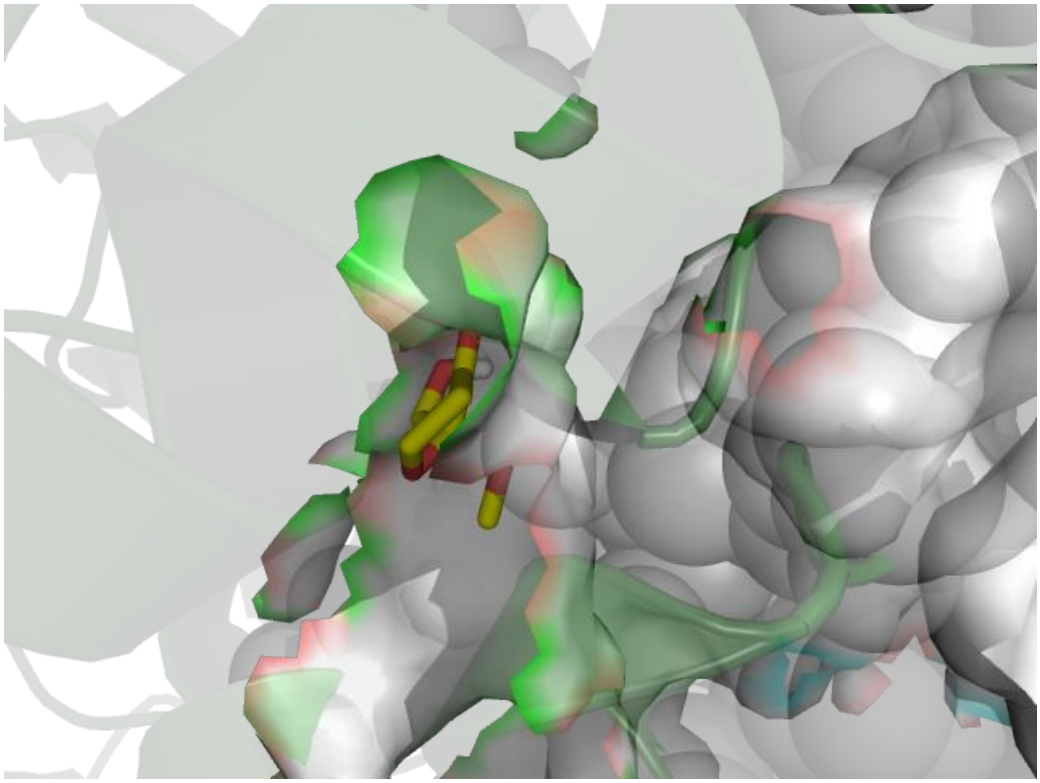


Figure 4-21 (A). Binding mode between isogloiosiphone B (**A6**) and substrate active site of 3LPG. Interacting residues of 3LPG are displayed in gray surface mode. Compound **A6** is presented in balls and sticks. Atoms of **A6** are color-coded as follows: C, yellow; H, white; O, red.

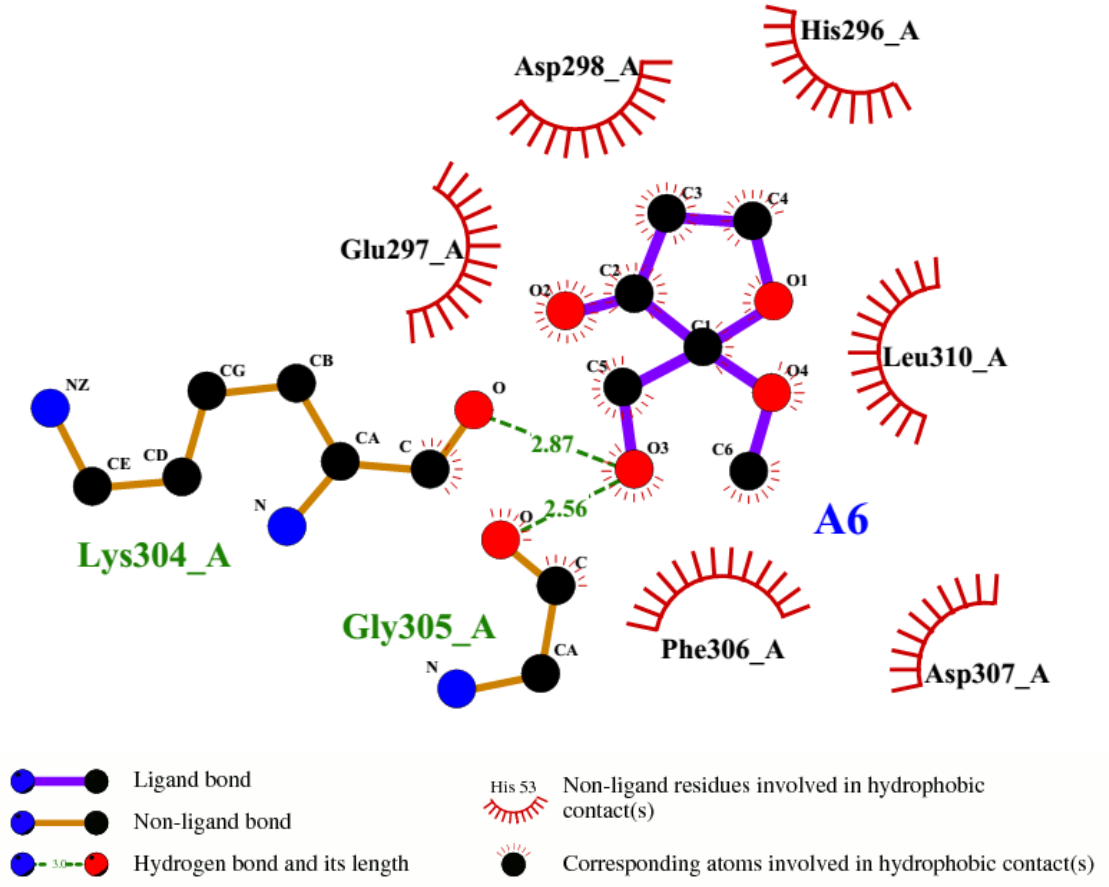


Figure 4-21 (B). Intermolecular interactions of isogloiosiphone B (**A6**) with 3LPG showing by Ligplot+ (schematic 2D plot).

4.2.4 Molecular modeling based SAR analysis of inhibitors purified from brown algae *S. confusum*, *S. thunbergii* and *A. clathratum*

4.2.4.1 Molecular modeling based SAR analysis of henicosapentaene (J1)

Henicosaphentaene (**J1**) exhibited strong inhibitory activity against β-glucuronidase *in vitro* with IC_{50} of 20.9 ± 0.2 μM. Molecular docking analysis showed compound **J1** fitted into the active substrate site of 3LPG completely (Figure 4-22(A)). Docking score was calculated as -7.2 kcal/mol by AutoDockTools 4.2. Hydrophobic interactions contributed to the high docking affinity, including amino acids Gly17, Pro48, Arg302, Phe306 Asp307, Asn308, Val309 of chain A and Leu15, Gly17, Pro48, Arg302, Phe306, Asp307, Asn308, Val309 of Chain B (Figure 4-22(B)).

4.2.4.2 Molecular modeling based SAR analysis of henicosahexaene (U2)

Molecular docking analysis showed henicosahexaene (**U2**) (IC_{50} of 4.4 ± 0.0 μM) dropped deep into the active substrate cavity of 3LPG (Figure 4-23(A)) and exhibited good docking affinity with -7.75 kcal/mol. The excellent docking affinity should be due to the hydrophobic interactions with amino acid residues Leu15, Pro48, Arg302, Phe306, Asp307, Asn308, Val309 of chain A and Leu15, Gly17, Ala46, Pro48, Arg302, Phe306, Asp307, Asn308, Val309 of Chain B (Figure 4-23(B)). The intense hydrophobic network contributed to the high inhibitory activity of compound **U2**.

4.2.4.3 Molecular modeling based SAR analysis of squalene (C3)

Squalene (**C3**) (IC_{50} of 2.2 ± 0.2 μM) showed the highest inhibitory activity against β-glucuronidase *in vitro* among all of the purified compounds. Meanwhile the

in silico analysis also revealed compound **C3** was hidden thoroughly into the active site of 3LPG (Figure 4-24(A)) with the highest docking score -8.9 kcal/mol. Hydrophobic interactions donated to the excellent docking affinity. Lys13, Leu15, Pro48, Phe306, Asp307, Asn308, Val309, Glu336 of chain A and Leu15, Gly17, Pho48, Arg302, Phe306, Asp307, Asn308, Val309 of chain B made the forceful docking grid of compound **C3** (green and cyan dots shown in Figure 4-24(B)) which should be the reason for the prominent inhibitory activity.

4.2.4.4 Molecular modeling based SAR analysis of phloroglucinol (G2)

Molecular docking analysis showed phloroglucinol (**G2**) (IC_{50} of 194.4 ± 0.2 μM) fitted into the active substrate site of 3LPG (Figure 4-25(A)) with docking score -4.64 kcal/mol. For the most stable conformation of the ligand-receptor complex, four hydrogen bonds formed at the three hydroxy groups of compound **G2** with Asp300 (chain A) (2.79 Å), Asp307 (chain A) (2.82 Å), Leu310 (chain A) (2.91 Å) and Asp300 (chain B) (2.66 Å). Hydrophobic interactions were observed at residues of Ala299, Arg302, Val309 of chain A and Leu301, Arg302 of chain B (Figure 4-25(B)).

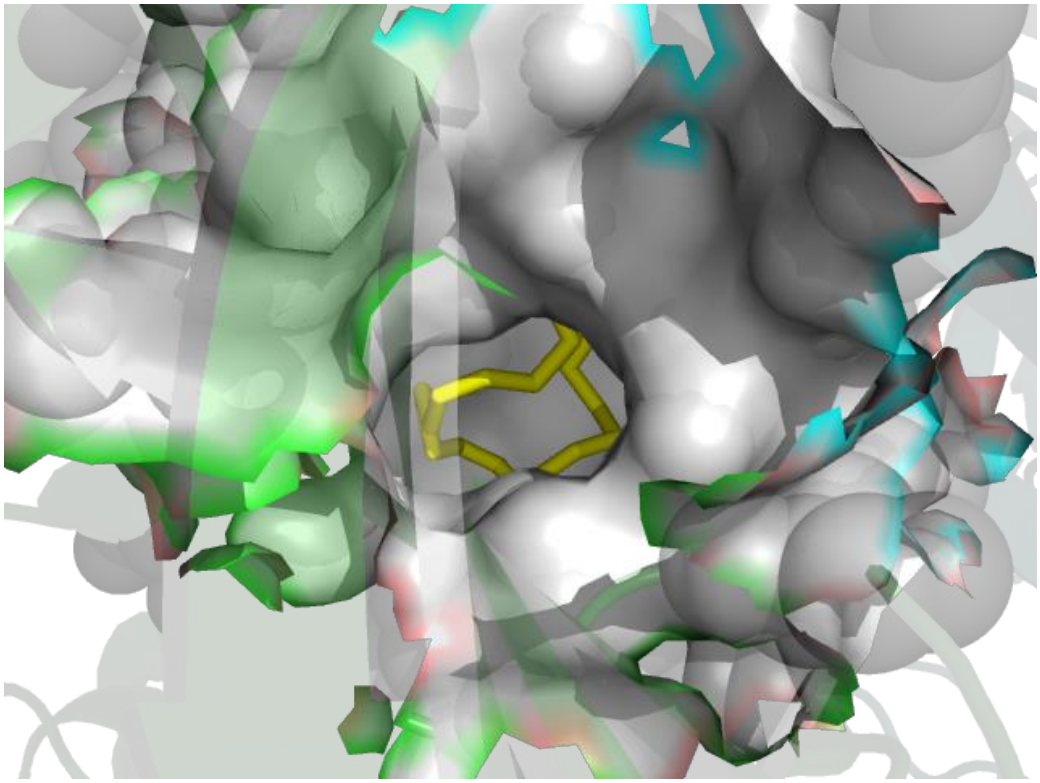


Figure 4-22 (A). Binding mode between henicosapentaene (**J1**) and substrate active site of 3LPG. Interacting residues of 3LPG are displayed in gray surface mode. Compound **J1** is presented in balls and sticks. Atoms of **J1** are color-coded as follow: C, yellow.

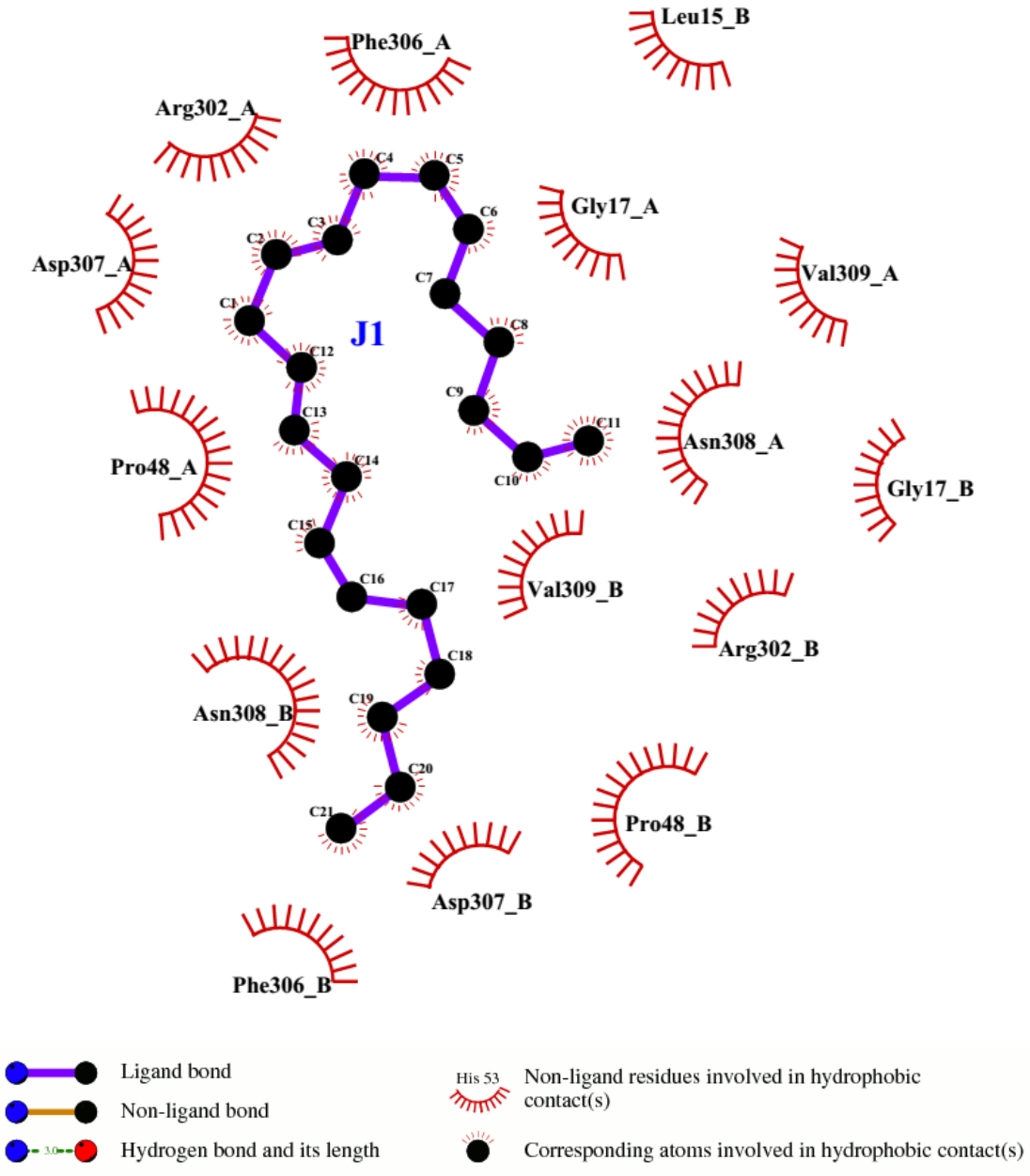


Figure 4-22 (B). Intermolecular interactions of henicosapentaene (**J1**) with 3LPG showing by Ligplot+ (schematic 2D plot).

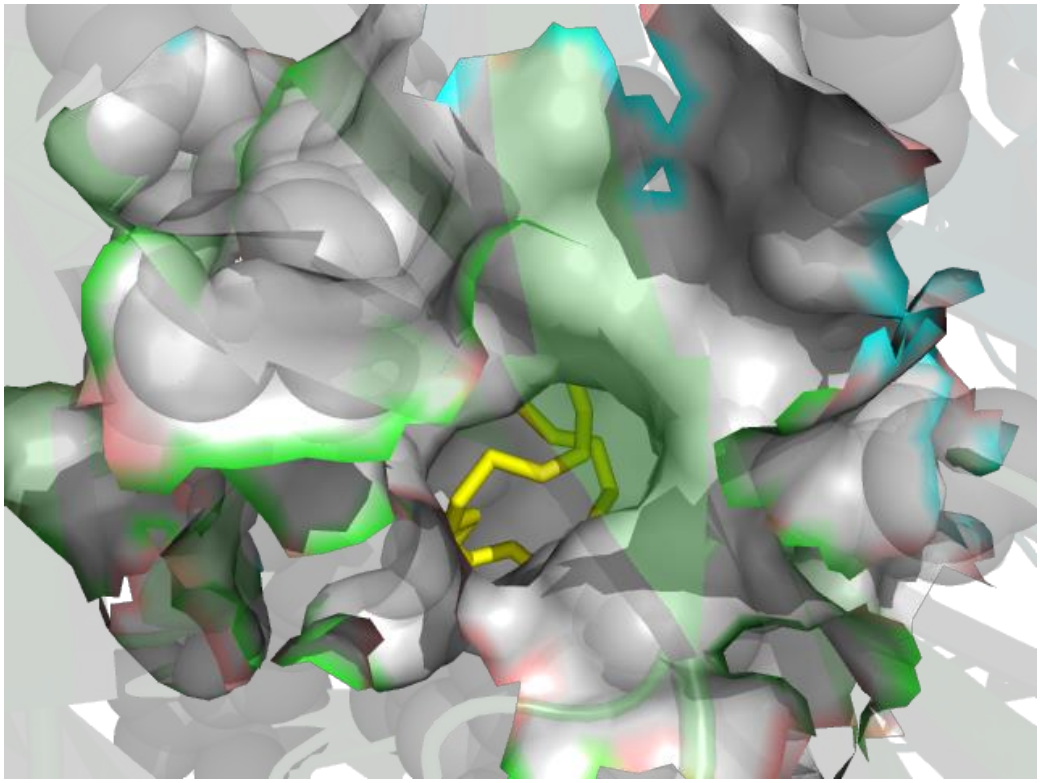


Figure 4-23 (A). Binding mode between henicosahexaene (**U2**) and substrate active site of 3LPG. Interacting residues of 3LPG are displayed in gray surface mode. Compound **U2** is presented in balls and sticks. Atoms of **U2** are color-coded as follow: C, yellow.

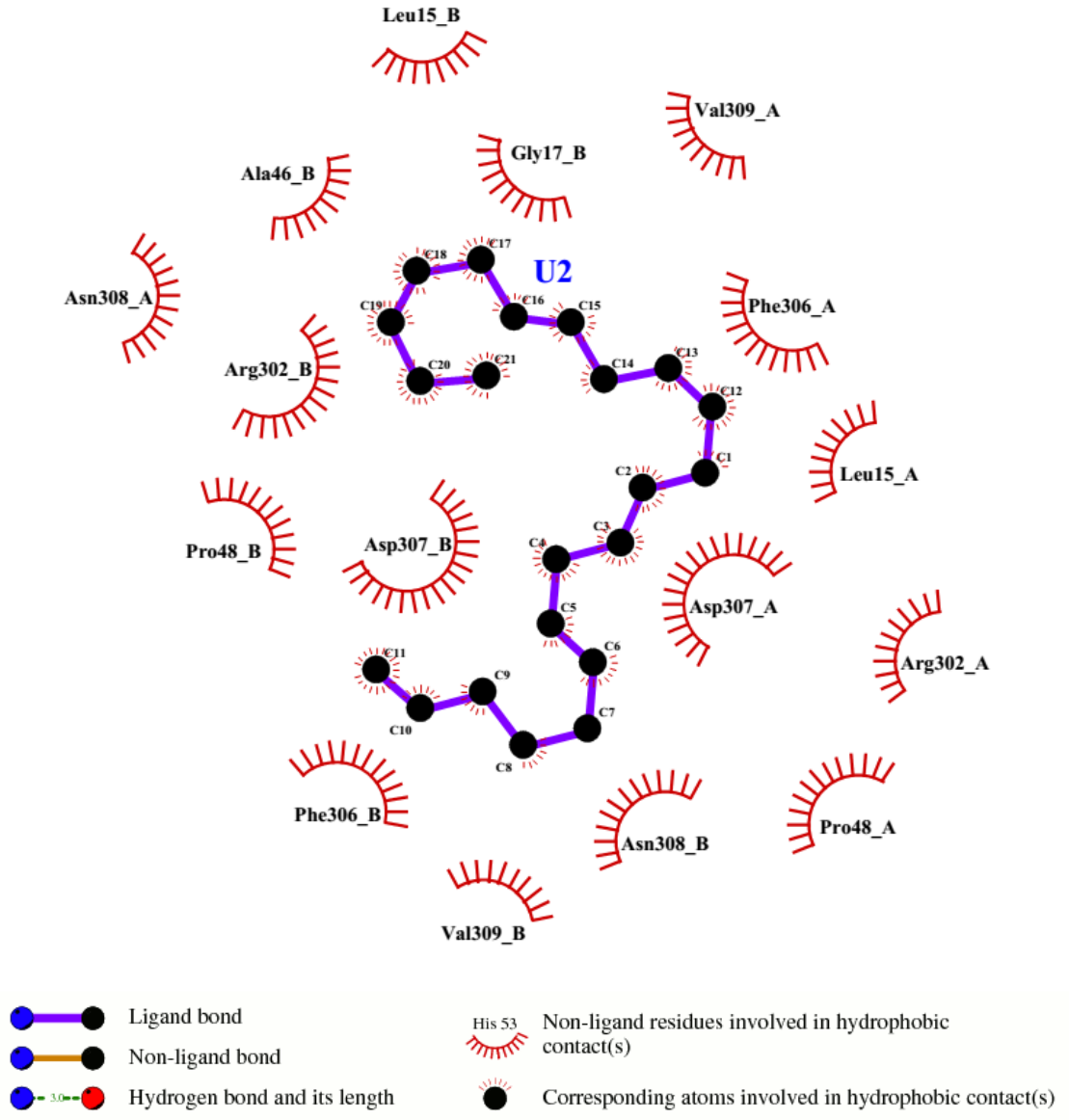


Figure 4-23 (B). Intermolecular interactions of henicosahexaene (**U2**) with 3LPG showing by Ligplot+ (schematic 2D plot).

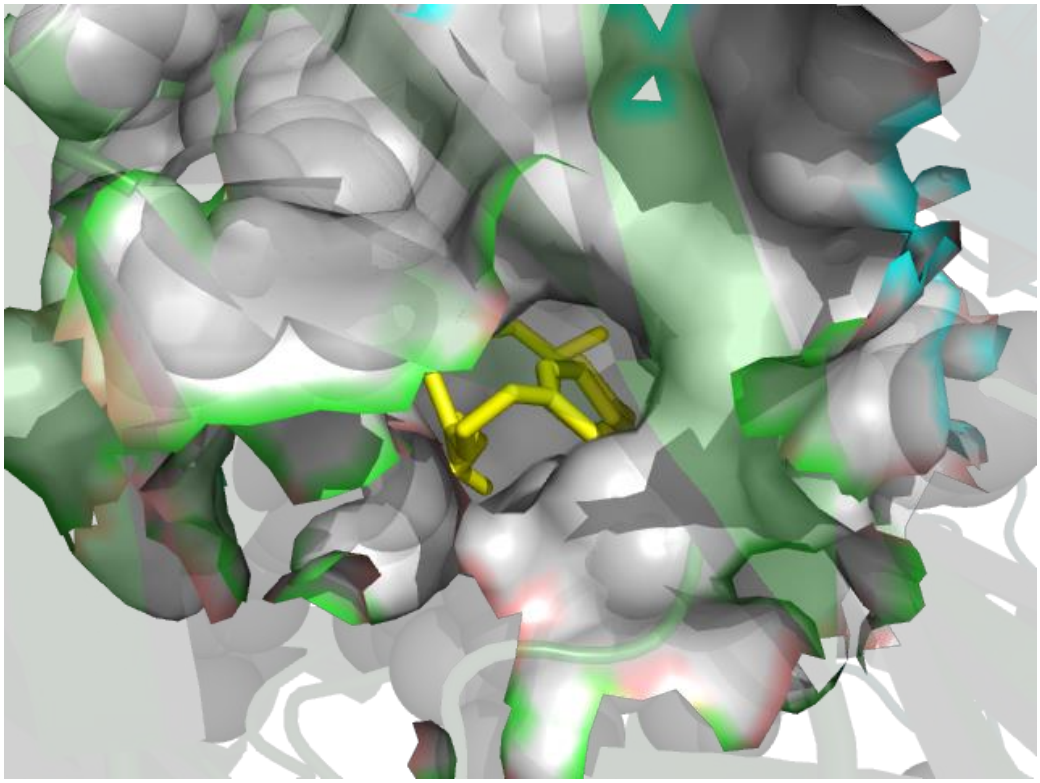


Figure 4-24 (A). Binding mode between squalene (**C3**) and substrate active site of 3LPG. Interacting residues of 3LPG are displayed in gray surface mode. Compound **C3** is presented in balls and sticks. Atoms of **C3** are color-coded as follows: C, yellow.

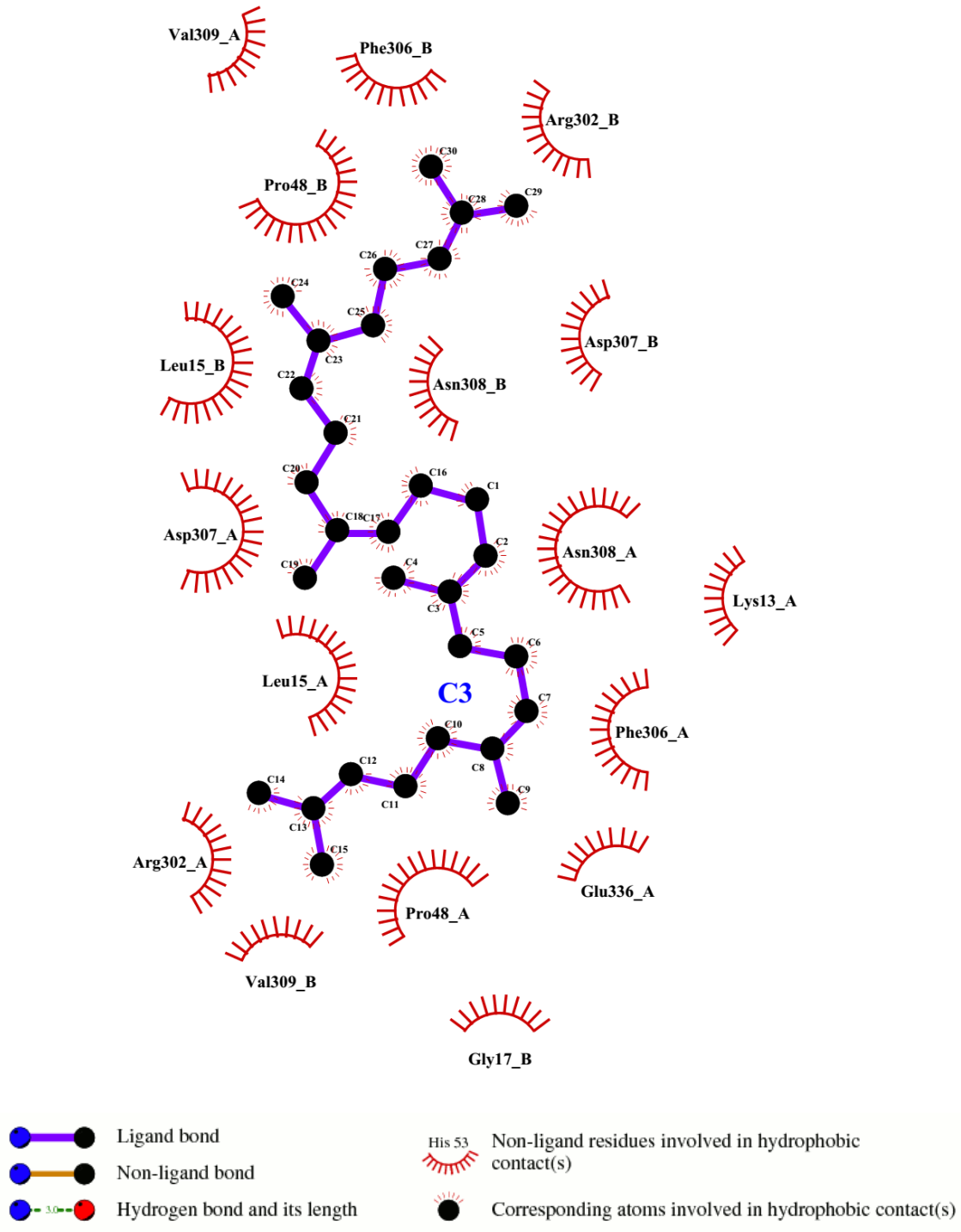


Figure 4-24 (B). Intermolecular interactions of squalene (**C3**) in the active cavity of 3LPG showing by Ligplot+ (schematic 2D plot).

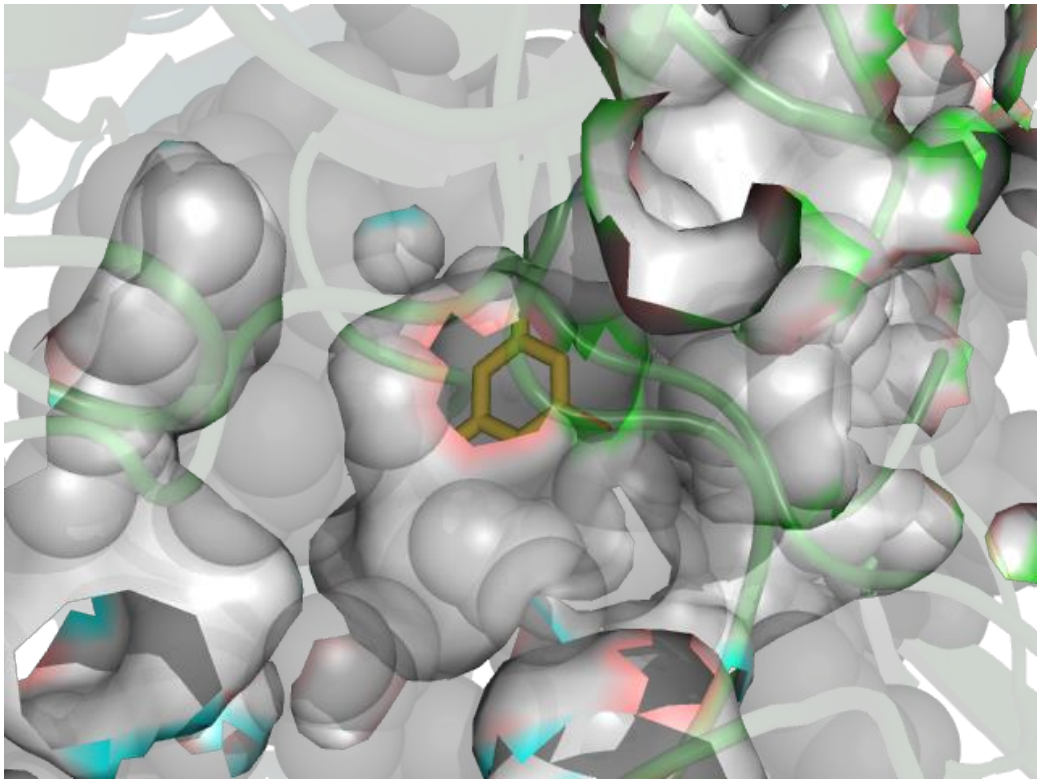


Figure 4-25 (A). Binding mode between phloroglucinol (**G2**) and substrate active site of 3LPG. Interacting residues of 3LPG are displayed in gray surface mode. Compound **G2** is presented in balls and sticks. Atoms of **G2** are color-coded as follows: C, yellow; H, white; O, red.

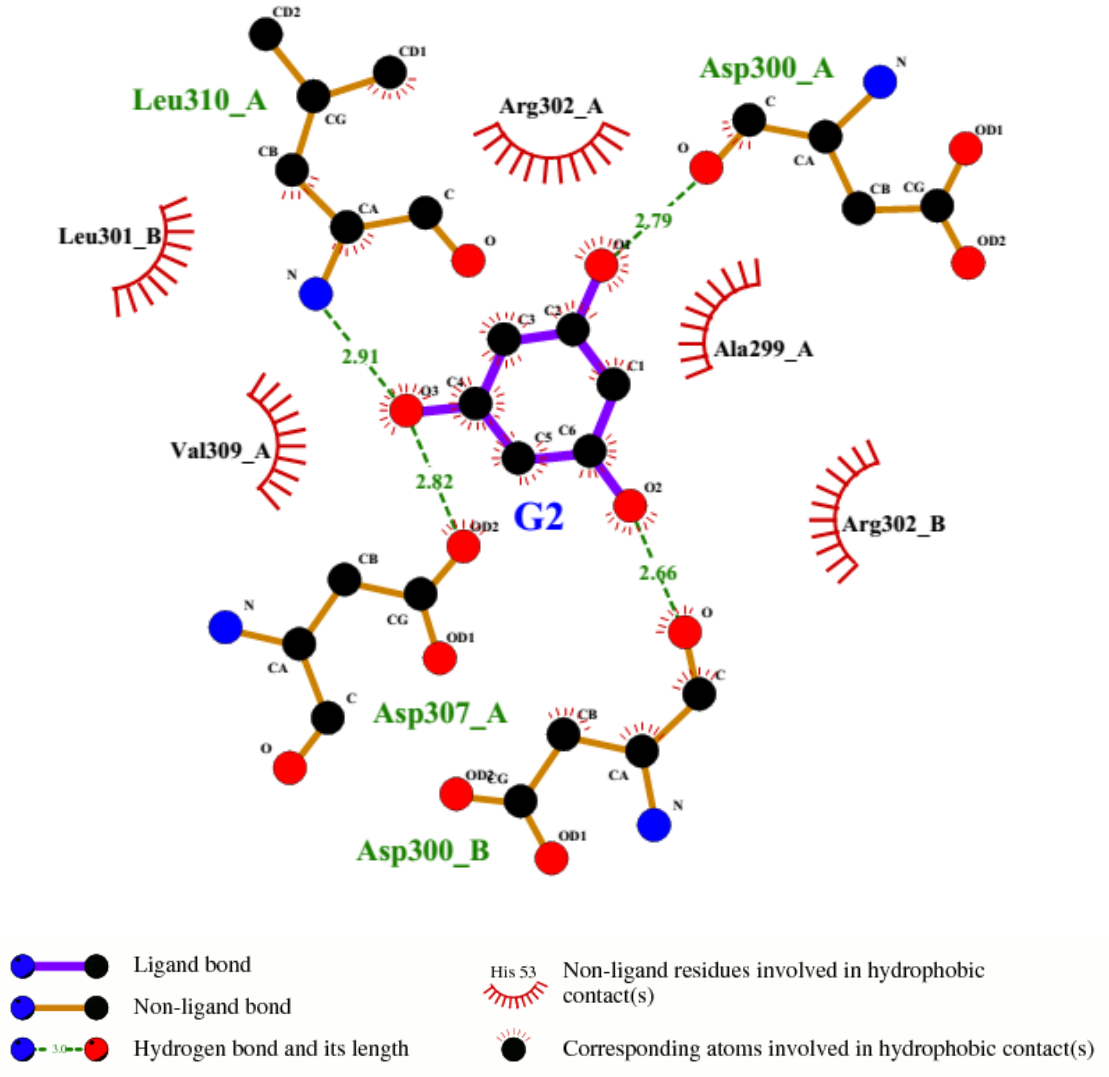


Figure 4-25 (B). Intermolecular interactions of phloroglucinol (**G2**) with 3LPG showing by Ligplot+ (schematic 2D plot).

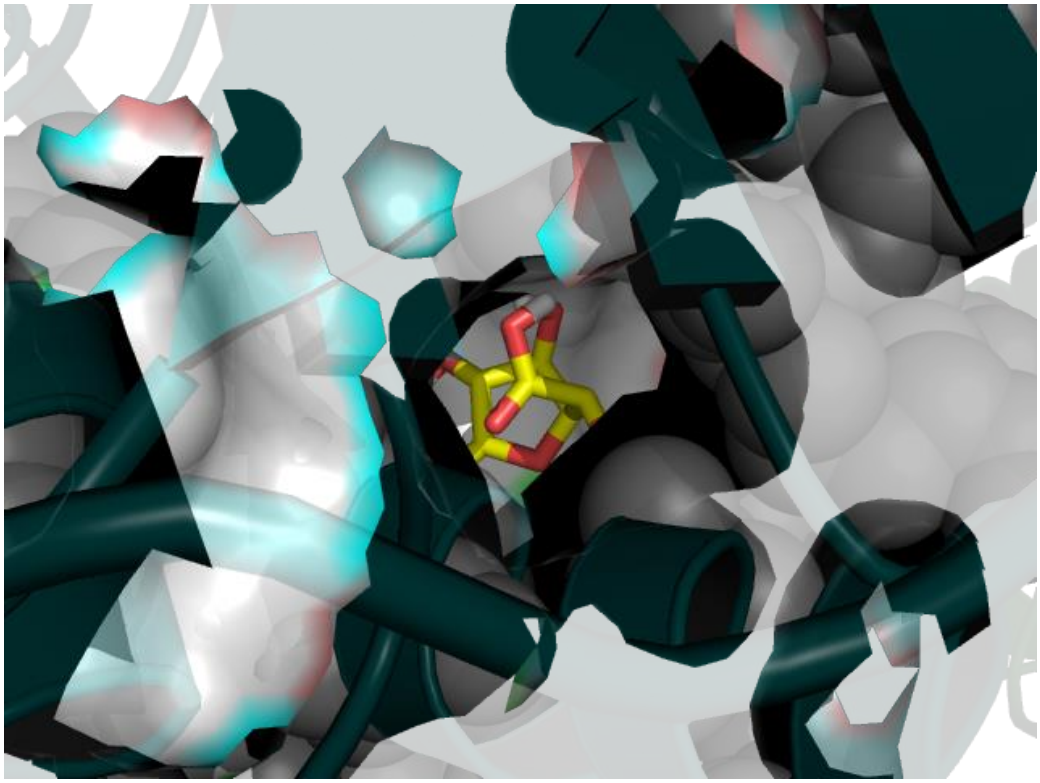


Figure 4-26 (A). Binding mode between D-glucaro-1,4-lactone and substrate active site of 3LPG. Interacting residues of 3LPG are displayed in gray surface mode. D-Glucaro-1,4-lactone is presented in balls and sticks. Atoms are color-coded as follows: C, yellow; H, white; O, red.

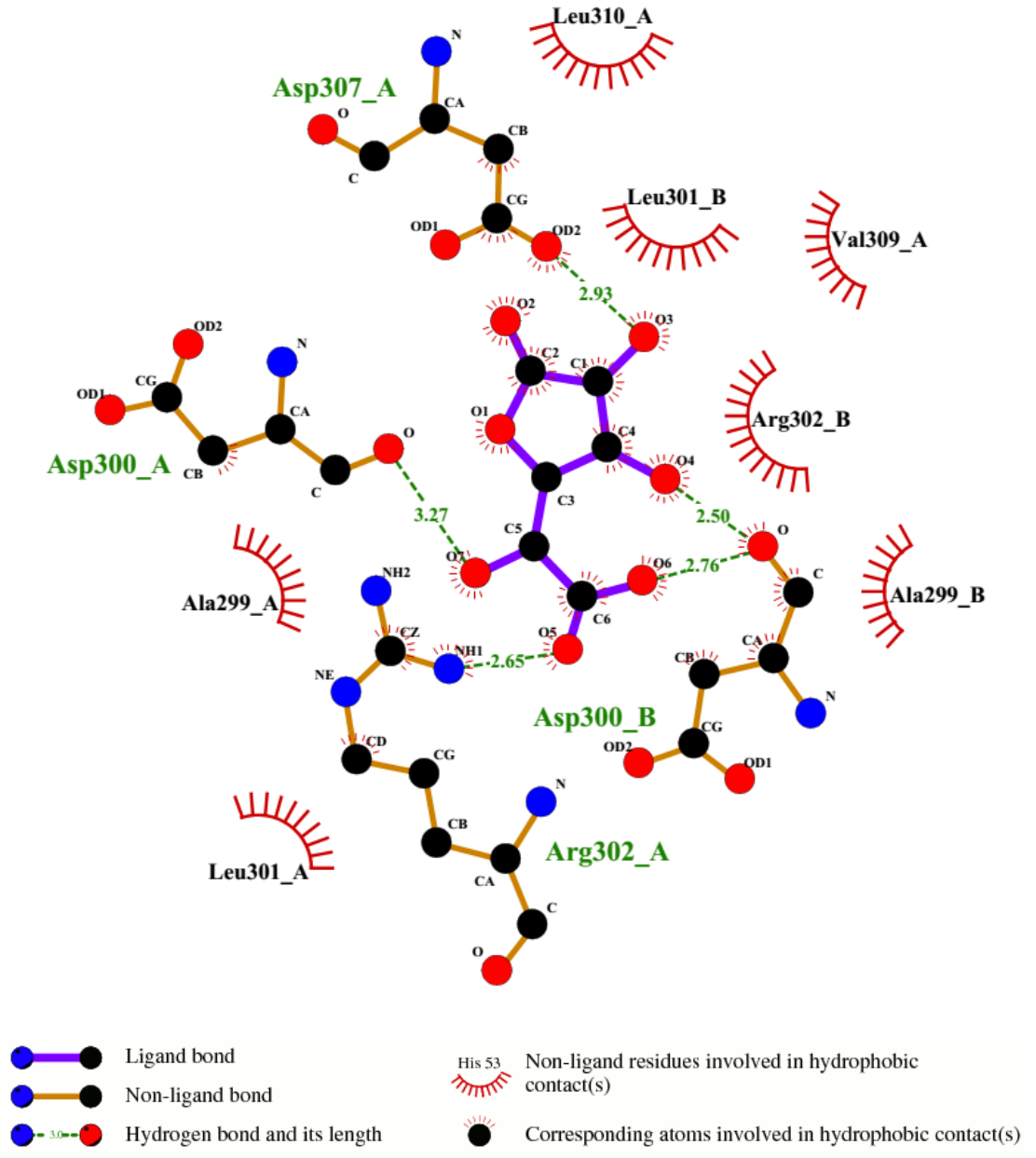


Figure 4-26 (B). Intermolecular interactions of D-glucaro-1,4-lactone with 3LPG showing by Ligplot+ (schematic 2D plot).

Table 4-2. *In vitro* β-glucuronidase inhibitory activity and docking scores of the purified compounds

Compound	IC_{50} (μM)	Docking score (kcal/mol)	Hbond + vdW energy (kcal/mol)[a]	Electrostatic energy (kcal/mol)
F1	103.2±0.3	-5.64	-6.67	-0.17
F2	5.1±0.0	-8.63	-10.86	-0.15
F3	2.6±0.2	-8.74	-10.88	-0.25
A1	103.7±1.0	-5.89	-9.75	-0.02
A2		-6.72	-10.83	-0.17
A3		-7.39	-8.67	0.08
A4	>250	-5.85	-7.38	0.00
A5	89.5±0.4	-4.72	-6.08	-0.13
A6	57.0±0.6	-5.28	-4.64	-0.04
J1	20.91±0.2	-7.20	-11.40	0.03
U2	4.4±0.0	-7.75	-11.60	-0.03
C3	2.2±0.2	-8.90	-13.39	0.02
G2	194.4±0.2	-4.64	-5.23	-0.31
D-Glucaro-1,4-lactone	77.9±1.4	-2.45	-4.60	0.43

[a] HBond + vdW energy indicates hydrogen bond energy and van der Waals energy.

4.3 Discussion

Enzymatic inhibition kinetics is one of the most important areas in medicinal chemistry and it can reveal enzyme mechanism which is directly relevant to drug discovery. In this chapter, inhibitory activities of all the purified β-glucuronidase inhibitory compounds in Chapter 2 and Chapter 3 were investigated spectrophotometrically. Furthermore, molecular docking simulations were performed to clarify the structure-activity relationship between each inhibitory compound with the active site of enzyme β-glucuronidase.

Among the purified inhibitors, compounds **F2** and **F3**, the two bromophenol dimers derived from the marine red alga *N*. *aculeata*, showed potent β-glucuronidase inhibitory activity. Meanwhile, hydrophobic compounds **J1**, **U2** and **C3**, purified from marine brown algae also exhibited predominant β-glucuronidase inhibitory activity. Novel compound **A6**, isogloiosiphone B derived from the red alga *N*. *yendoana*, showed moderate inhibitory activity.

Molecular docking studies were carried out by AutoDockTools 4.2, PyMol Molecular Graphics System and Ligplot+ software to estimate the binding energies, interacting amino acid residues, intermolecular distance between the atoms of ligands and the interacting residues of *E*. *coli* β-glucuronidase 3LPG. Active sites of enzyme 3LPG were confirmed by docking with the substrate *p*-nitrophenyl β-D-glucuronide prior to docking with the purified compounds. Substrate demonstrated that the active site residues involving 14 kinds of *E*. *coli* β-glucuronidase family conserved amino acid residues (29 residues in A chain and 27 residues in B chain). Generated active binding cavity was shown in Figure 4-13. The molecular docking studies predicted that except cholesterol (**A4**), all of the other compounds were well fitted in the active

binding pocket. Four types of non-covalent interactions act essentially between the binding of ligand to the receptor enzyme macromolecule, including hydrogen bonds, van der Waals forces, electrostatic forces and the hydrophobic interactions (Lin, Zeng, Zhang, Liao, & Gong, 2017). For the presented binding complex of purified compounds and 3LPG, hydrogen bonds and the van der Waals forces played significant roles. The overall β-glucuronidase inhibition activity and docking scores of the purified compounds were listed in Table 4-2.

The most active compound, squalene **C3** (IC_{50} = 2.2 ± 0.2 μM), derived from the brown alga *A*. *clathratum* exhibited the best docking score -8.9 kcal/mol. Van der Waals forces and the hydrophobic interactions contributed for the excellent docking affinity. No hydrogen bonds formed, whereas the intense hydrophobic interacting network formed around the conformation of compound **C3**. Hydrophobic interacting residues involved Lys13, Leu15, Pro48, Phe306, Asp307, Asn308, Val309, Glu336 of chain A and Leu15, Gly17, Pho48, Arg302, Phe306, Asp307, Asn308, Val309 of chain B. Same interaction binding mode was observed for henicosapentaene **J1** (IC_{50} = 20.9 ± 0.2 μM) and henicosahexaene **U2** (IC_{50} = 4.4 ± 0.0 μM) with binding scores of -7.2 kcal/mol and -7.75 kcal/mol, respectively. The relevant hydrophobic interacting residues of compound **J1** comprised Gly17, Pro48, Arg302, Phe306 Asp307, Asn308, Val309 (chain A) and Leu15, Gly17, Pro48, Arg302, Phe306, Asp307, Asn308, Val309 (Chain B), whereas compound **U2** generated some hydrophobic interactions with Leu15, Pro48, Arg302, Phe306, Asp307, Asn308, Val309 (chain A) and Leu15, Gly17, Ala46, Pro48, Arg302, Phe306, Asp307, Asn308, Val309 (Chain B).

Bromophenol dimer **F3** (IC_{50} = 2.6 ± 0.13 μM) derived from *N*. *aculeata* was a diaryl structural bromophenol substituted with three bromine atoms, four phenolic hydroxy and one alcoholic hydroxy groups showed second active inhibitory activity. Correspondingly, docking score ranked in the second with -8.74 kcal/mol. For this

conformation, hydrogen bonds, van der Waals forces, hydrophobic interactions and electrostatic forces contributed to the excellent binding complex. It was observed that this compound formed seven hydrogen bonds with Pro48 (2.51 Å), Arg302 (3.21 Å and 2.53 Å), Phe306 (2.47 Å), Asn308 (2.71 Å) of chain A and Pro48 (2.74 Å) and Phe306 (2.61 Å) of chain B. Compared with compound **F3**, the other bromophenol dimer **F2** (IC_{50} = 5.1 ± 0.0 μM) substituted with the same numbers of bromine atoms and four phenolic hydroxy groups but a methoxy group exhibited the third best docking score with -8.63 kcal/mol. For this binding conformation, same numbers of hydrogen bonds formed with Pro48 (2.49 Å), Arg302 (2.59 Å and 3.28 Å), Phe306 (2.44 Å), Asn308 (3.01 Å) of chain A and Pro48 (2.74 Å and 3.18 Å) of chain B. Hydrophobic interacting residues involved Leu15, Gly17, Ala46, Pro48, Arg302, Phe306, Asp307, Val309 (Chain A) and Ala46, Pro48, Asn308, Val309 (Chain B). It might be assumed that hydroxy group at the side chain might be the reason for the enhancement of inhibitory activity, as it could cause more polar interactions to the accessibility to the active site of β-glucuronidase. Such difference was also observed at synthesized dihydropyrimidones against bovine liver source β-glucuronidase (Ali et al., 2016).

Even though IC_{50} values of phytol (**A2**) and cholesta-4,22-diene-3,6-dione (**A3**) derived from *N*. *yendoana* was failed to be obtained, molecular docking simulations displayed both of the two molecules were fitted into the active cavity of 3LPG with docking scores were -6.72 kcal/mol and -7.39 kcal/mol, respectively. Alternatively, cholesterol (**A4**) (IC_{50} > 250 μM), was detected inactive against β-glucuronidase *in vitro*. The molecular docking simulations showed all the conformations of compound **A4** dropped outside of the active substrate binding pocket with a docking score of -5.85 kcal/mol. The novel isogloiosiphone B (**A6**) (IC_{50} = 57.0 ± 0.6 μM) showed moderate inhibitory activity *in vitro* analysis. Molecular docking analysis predicted

that hydrogen bond interaction provided for the docking affinity of -5.28 kcal/mol.

Besides, the weak purified inhibitors, bromophenol monomer **F1**, phytal (**A1**), 22-dehydrocholesterol (**A5**) and phloroglucinol (**G2**) exhibited docking scores of -5.64 kcal/mol, -5.89 kcal/mol, -4.72 kcal/mol and -4.64 kcal/mol respectively *in silico* analysis, which might be due to the weak hydrogen bonding interactions.

In summary, a good correlation between inhibitory activity and molecular docking study was observed among the purified inhibitory compounds. Limited structure-activity relationship indicated that the formed hydrogen bond number and distances as well as the hydrophobic interacting residues played important role in played vital roles *E. coli* β-glucuronidase inhibitory activity. Hydrogen interactions with Pro48, Arg302, Phe306, Asp307 and Asn308 and hydrophobic interactions with Leu15, Gly17, Ala46, Pro48, Arg302, Phe306, Asp307, Asn308 and Val309 in the active pocket always provided for the better binding affinity.

Conclusion

In the course of search for β-glucuronidase inhibitors, 151 algal samples (7 species of green algae, 22 species of brown algae, and 30 species of red algae) were screened in order to isolate the potential β-glucuronidase inhibitors. Based on the assay data, most of the collected red and brown algae showed strong inhibitory activity against *E. coli* β-glucuronidase while, especially genus from orders Ceramiales, Gigartinales of red algae and Fucales, Laminariales of brown algae. In this study, two species of marine red algae, *Neorhodomela aculeata* (Rhodomelaceae, Ceramiales) and *Neodilsea yendoana* (Dumontiaceae, Gigartinales), and three species of brown algae, *Sargassum confusum* (Sargassaceae, Fucales), *S. thunbergii* and *Agarum clathratum* (Agaraceae, Laminariales) were selected for the isolation of β-glucuronidase inhibitors.

From *N. aculeata*, three bromophenols were obtained as 2,3-dibromo-4,5-dihydroxybenzyl ether (**F1**), 3-bromo-2-(2,3- dibromo-4,5-dihydroxy-benzyl)-4,5-dihydroxy-benzyl methyl ether (**F2**) and 3-bromo-2-(2,3-dibromo-4.5-di-hydroxybenzyl)-4,5-dihyroxybenzyl alcohol (**F3**). From *N. yendoana*, one novel compound, 2-hydroxymethyl-2-methoxyoxolan-3-one named as isogloiosiphone B (**A6**) were purified with moderate inhibitory activity. Besides, from the same alga, phytal (**A1**), cholesterol (**A4**) and 22-dehydrocholesterol (**A5**) were isolated as moderate inhibitors. Compounds **A2** and **A3** were failed for the final purification while the mixture showed moderate inhibitory activity. They were identified as phytol (**A2**) and cholesta-4,22-diene-3,6-dione (**A3**).

From *S. confusum*, *S. thunbergii* and *A. clathratum*, three hydrophobic compounds, (6*Z*,9*Z*,12*Z*,15*Z*)-1,6,9,12,15-henicosapentaene (**J1**), (6*Z*,9*Z*,12*Z*,15*Z*,

18*Z*)-1,6,9,12,15,18-henicosahexanene (**U2**) and squalene (**C3**) were purified as β-glucuronidase inhibitors. Meanwhile, phloroglucinol (**G2**) were also isolated from *A. clathratum*.

With the comparison of inhibitory activity of all the purified compounds against *E. coli* β-glucuronidase (3LPG) were investigated by inhibition kinetic study and molecular docking simulations. A good correlation was observed between IC_{50} values and the molecular binding modes. Hydrogen bonds, van der Waals forces, electrostatic forces and the hydrophobic interactions showed important roles in the binding affinity. Potent bromophenol inhibitors **F2** and **F3** might access to the active site of *E. coli* β-glucuronidase through hydrogen bonding and hydrophobic interactions with the residues Pro48, Arg302, Phe306, Asp 307, Asn308 and Leu15, Gly17, Ala46, Pro48, Arg302, Phe306, Asp307, Asn308, Val309, respectively. The potent hydrophobic inhibitors **J1**, **U2** and **C3** might approach to the active site of *E. coli* β-glucuronidase via the hydrophobic interactions with residues Leu15, Gly17, Ala46, Pro48, Arg302, Phe306, Asp307, Asn308 and Val309.

In conclusion, marine red and brown algae may be the exceptional sources for the isolation of *E. coli* β-glucuronidase inhibitory compounds. Although further investigation is also warranted, the encouraging correlation between *in vitro* inhibition analysis and *in silico* molecular docking simulations may provide the guidance for the exploration of effective *E. coli* β-glucuronidase inhibitors.

References

Ahmad, S., Hughes, M. A., Lane, K. T., Redinbo, M. R., Yeh, L. A., & Scott, J. E. (2011). A high throughput assay for discovery of bacterial β-glucuronidase inhibitors. *Current Chemical Genomics*, *5*, 13–20.

Akbaba, Y., Balaydın, H. T., Menzek, A., Göksu, S., Şahin, E., & Ekinci, D. (2013). Synthesis and biological evaluation of novel bromophenol derivatives as carbonic anhydrase inhibitors. *Archiv Der Pharmazie*, *346*(6), 447–454.

Al Easa, H. S., Kornprobst, J. M., & Rizk, A. M. (1995). Major sterol composition of some algae from Qatar. *Phytochemistry*, *39*(2), 373–374.

Ali, F., Khan, K. M., Salar, U., Iqbal, S., Taha, M., Ismail, N. H., … Ali, B. (2016). Dihydropyrimidones: as novel class of β-glucuronidase inhibitors. *Bioorganic & Medicinal Chemistry*, *24*(16), 3624–3635.

Alwhibi, M. S., Khalil, M. I. M., Ibrahim, M. M., El-Gaaly, G. A., & Sultan, A. S. (2017). Potential antitumor activity and apoptosis induction of Glossostemon bruguieri root extract against hepatocellular carcinoma cells. *Evidence-Based Complementary and Alternative Medicine*, *2017*, 1–14.

Awad, N. E. (2004). Bioactive brominated diterpenes from the marine red algaJania rubens(L.) Lamx. *Phytotherapy Research*, *18*(4), 275–279.

Baharudin, M. S., Taha, M., Imran, S., Ismail, N. H., Rahim, F., Javid, M. T., … Ali, M. (2017). Synthesis of indole analogs as potent β-glucuronidase inhibitors. *Bioorganic Chemistry*, *72*, 323–332.

Bank, N., & Bailine, S. H. (1965). Urinary beta-glucuronidase activity in patients with urinary-tract infection. *New England Journal of Medicine*, *272*(2), 70–75.

Bar, S., Kumar, J. N., Amar, M., Toledo, H., Batrice, R. J., & Szpilman, A. M. (2015). Catalytic aerobic oxidation of alcohols using recoverable IAPNO α-hydrogen

nitroxyl radicals. *ChemCatChem*, *7*(7), 1129–1134.

Barakat, A., Islam, M. S., Al-Majid, A. M., Ghabbour, H. A., Yousuf, S., Ashraf, M., … Ul-Haq, Z. (2016). Synthesis of pyrimidine-2,4,6-trione derivatives: anti-oxidant, anti-cancer, α-glucosidase, β-glucuronidase inhibition and their molecular docking studies. *Bioorganic Chemistry*, *68*, 72–79.

Bello, I. C. di, Dorling, P., Fellows, L., & Winchester, B. (1984). Specific inhibition of human β-D-glucuronidase and α-L-iduronidase by a trihydroxy pipecolic acid of plant origin. *Federation of European Biochemical Societies*, *176*(1), 61–64.

Benesch, M. G. K., & McElhaney, R. N. (2014). A comparative calorimetric study of the effects of cholesterol and the plant sterols campesterol and brassicasterol on the thermotropic phase behavior of dipalmitoylphosphatidylcholine bilayer membranes. *Biochimica et Biophysica Acta*, *1838*(7), 1941–1949.

Bissantz, C., Kuhn, B., & Stahl, M. (2010). A medicinal chemist's guide to molecular interactions. *Journal of Medicinal Chemistry*, *53*(14), 5061–5084.

Blunt, J. W., Copp, B. R., Keyzers, R. A., Munro, M. H. G., & Prinsep, M. R. (2017). Marine natural products. *Natural Product Reports*, *34*, 235–294.

Blunt, J. W., Copp, B. R., Munro, M. H. G., Northcote, P. T., & Prinsep, M. R. (2006). Marine natural products. *Natural Product Reports*, *23*, 26–78.

Burchett, G. G., Folsom, C. G., & Lane, K. T. (2015). Native electrophoresis-coupled activity assays reveal catalytically-active protein aggregates of Escherichia coli β-glucuronidase. *PLoS ONE*, *10*(6), e0130269.

Burrell, J. W. K., Garwood, R. F., Jackman, L. M., Oskay, E., & Weedon, B. C. L. (1966). Carotenoids and related compounds. Part XIV. Stereochemistry and synthesis of geraniol, nerol, farnesol, and phytol. *Journal of the Chemical Society C: Organic*, 2144–2154.

Caldwell, J., Gardner, I., & Swales, N. (1995). An introduction to drug disposition: the

basic principles of absorption, distribution, metabolism, and excretion. *Toxicologic Pathology*, *23*(2), 102–114.

Chen, J. lu, Moghaddam, M. F., & Gerwick, W. H. (1993). Gloiosiphones A and B, novel metabolites from the red marine alga Gloiosiphonia verticillaris. *Journal of Natural Products*, *56*(8), 1205–1210.

Chihara, M. (2002). Seaweeds of Japan <Field best encyclopedia (vol.11)>. *Tokyo: Gakken Plus Co., Ltd*, 1-271. (In Japanese)

Cirne-Santos, C. C., Souza, T. M. L., Teixeira, V. L., Fontes, C. F. L., Rebello, M. A., Castello-Branco, L. R. R., … Bou-Habib, D. C. (2008). The dolabellane diterpene Dolabelladienetriol is a typical noncompetitive inhibitor of HIV-1 reverse transcriptase enzyme. *Antiviral Research*, *77*(1), 64–71.

Croom, E. (2012). Metabolism of xenobiotics of human environments. *Progress in Molecular Biology and Translational Science*, *112*, 31–88.

Diez, T., & Cabezas, J. A. (1979). Properties of two molecular forms of β-glucuronidase from the mollusc Littorina littorea L. *European Journal of Biochemistry*, *93*(2), 301–311.

Duan, X. J., Zhang, W. W., Li, X. M., & Wang, B. G. (2006). Evaluation of antioxidant property of extract and fractions obtained from a red alga, Polysiphonia urceolata. *Food Chemistry*, *95*(1), 37–43.

El Gamal, A. A. (2010). Biological importance of marine algae. *Saudi Pharmaceutical Journal*, *18*(1), 1–25.

Fan, S., Zhang, J., Nie, W., Zhou, W., Jin, L., Chen, X., & Lu, J. (2017). Antitumor effects of polysaccharide from Sargassum fusiforme against human hepatocellular carcinoma HepG2 cells. *Food and Chemical Toxicology*, *102*, 53–62.

Fan, X., Xu, N. J., & Shi, J. G. (2003). Bromophenols from the red alga Rhodomela confervoides. *Journal of Natural Products*, *66*(3), 455–458.

Ferreres, F., Lopes, G., Gil-Izquierdo, A., Andrade, P. B., Sousa, C., Mouga, T., & Valentão, P. (2012). Phlorotannin extracts from fucales characterized by HPLC-DAD-ESI-MSn: approaches to hyaluronidase inhibitory capacity and antioxidant properties. *Marine Drugs*, *10*(12), 2766–2781.

Fujii, M. T., Cassano, V., Stein, É. M., & Carvalho, L. R. (2011). Overview of the taxonomy and of the major secondary metabolites and their biological activities related to human health of the Laurencia complex (Ceramiales, rhodophyta) from Brazil. *Brazilian Journal of Pharmacognosy*, *21*(2), 268–282.

Fürstenau, B., Muñoz, L., Coca-Abia, M., Rosell, G., Guerrero, A., & Quero, C. (2013). Phytal: a candidate sex pheromone component of the moroccan locust Dociostaurus maroccanus. *ChemBioChem*, *14*(12), 1450–1459.

Gambato, G., Baroni, É. D. G., Garcia, C. S. C., Frassini, R., Frozza, C. O. S., Moura, S., … Roesch-Ely, M. (2014). Brown algae Himantothallus grandifolius (Desmerestiales, Phaeophyceae) suppresses proliferation and promotes apoptosis-mediated cell death in tumor cells. *Advances in Biological Chemistry*, *4*(2), 98–108.

Ghimire, G. P., Thuan, N. H., Koirala, N., & Sohng, J. K. (2016). Advances in biochemistry and microbial production of squalene and its derivatives. *Journal of Microbiology and Biotechnology*, *26*(3), 441–451.

Graaf, M. de, Boven, E., Scheeren, H. W., Haisma, H. J., & Pinedo, H. M. (2002). Beta-glucuronidase-mediated drug release. *Current Pharmaceutical Design*, *8*(15), 1391–1403.

Guido, R. V. C., Oliva, G., & Andricopulo, A. D. (2008). Virtual screening and its integration with modern drug design technologies. *Current Medicinal Chemistry*, *15*(1), 37–46.

Han, M. J., Bae, E. A., & Kim, D. H. (2001). Effect of Lentinus edodes water extract on

some enzymes of mouse intestinal becteria. *Korean Journal of Food Science and Technology*, *33*(1), 142–145.

Han, M. J., & Kim, N. Y. (1999). The preference and inhibitory effect of root vegetables on β-glucuronidase and tryptophanase of human intestinal bacteria. *Korean Journal of Food and Cookery Science*, *15*(6), 555–564.

Hassan, M. I., Waheed, A., Grubb, J. H., Klei, H. E., Korolev, S., & Sly, W. S. (2013). High resolution crystal structure of human β-glucuronidase reveals structural basis of lysosome targeting. *PLoS One*, *8*(11), e79687.

Hayashi, T., Kawasaki, M., Okamura, K., Tamada, Y., Morita, N., Tezuka, Y., … Taga, T. (1992). Scoparic acid A, a β-glucuronidase inhibitor from Scoparia dulcis. *Journal of Natural Products*, *55*(12), 1748–1755.

Iorizzi, M., Minale, L., Riccio, R., Debray, M., & Menou, J. L. (1986). Starfish saponins, part 23. Steroidal glycosides from the starfish Halityle regularis. *Journal of Natural Products*, *49*(1), 67–78.

Iwashima, M., Mori, J., Ting, X., Matsunaga, T., Hayashi, K., Shinoda, D., … Hayashi, T. (2005). Antioxidant and antiviral activities of plastoquinones from the brown alga Sargassum micracanthum, and a new chromene derivative converted from the plastoquinones. *Biological & Pharmaceutical Bulletin*, *28*(2), 374–377.

Jacox, R. F., & Feldmahn, A. (1955). Variations of beta glucuronidase concentration in abnormal human synovial fluid. *Journal of Clinical Investigation*, *34*(2), 263–267.

Jassbi, A. R., Mohabati, M., Eslami, S., Sohrabipour, J., & Miri, R. (2013). Biological activity and chemical constituents of red and brown algae from the Persian gulf. *Iranian Journal of Pharmaceutical Research*, *12*(3), 339–348.

Jung, H. A., Jin, S. E., Ahn, B. R., Lee, C. M., & Choi, J. S. (2013). Anti-inflammatory activity of edible brown alga Eisenia bicyclis and its constituents fucosterol and phlorotannins in LPS-stimulated RAW264.7 macrophages. *Food and Chemical*

Toxicology, *59*, 199–206.

Jung, H. A., Roy, A., Jung, J. H., & Choi, J. S. (2017). Evaluation of the inhibitory effects of eckol and dieckol isolated from edible brown alga Eisenia bicyclis on human monoamine oxidases A and B. *Archives of Pharmacal Research*, *40*(4), 480–491.

Kabuto, H., Yamanushi, T. T., Janjua, N., Takayama, F., & Mankura, M. (2013). Effects of squalene/squalane on dopamine levels, antioxidant enzyme activity, and fatty acid composition in the striatum of Parkinson's disease mouse model. *Journal of Oleo Science*, *62*(1), 21–28.

Kang, J. Y., Khan, M. N. A., Park, N. H., Cho, J. Y., Lee, M. C., Fujii, H., & Hong, Y. K. (2008). Antipyretic, analgesic, and anti-inflammatory activities of the seaweed Sargassum fulvellum and Sargassum thunbergii in mice. *Journal of Ethnopharmacology*, *116*(1), 187–190.

Kang, M. C., Ding, Y., Kim, E. A., Choi, Y. K., Araujo, T. De, Heo, S. J., & Lee, S. H. (2017). Indole derivatives isolated from brown alga Sargassum thunbergii inhibit adipogenesis through AMPK activation in 3T3-L1 preadipocytes. *Marine Drugs*, *15*(4), 119–129.

Kang, M. C., Wijesinghe, W. A. J. P., Lee, S. H., Kang, S. M., Ko, S. C., Yang, X., … Jeon, Y. J. (2013). Dieckol isolated from brown seaweed Ecklonia cava attenuates type II diabetes in db/db mouse model. *Food and Chemical Toxicology*, *53*, 294–298.

Kawasaki, M., Hayashi, T., Arisawa, M., Morita, N., & Berganza, L. H. (1988). 8-Hydroxytricetin 7-glucuronide, a β-glucuronidase inhibitor from Scoparia dulcis. *Phytochemistry*, *27*(11), 3709–3711.

Khan, K. M., Ambreen, N., Taha, M., Halim, S. A., Zaheer-Ul-Haq, Naureen, S., … Choudhary, M. I. (2014a). Structure-based design, synthesis and biological

evaluation of β-glucuronidase inhibitors. *Journal of Computer-Aided Molecular Design*, *28*(5), 577–585.

Khan, K. M., Rahim, F., Halim, S. A., Taha, M., Khan, M., Perveen, S., … Choudhary. (2011). Synthesis of novel inhibitors of β-glucuronidase based on benzothiazole skeleton and study of their binding affinity by molecular docking. *Bioorganic & Medicinal Chemistry*, *19*(14), 4286–4294.

Khan, K. M., Rahim, F., Wadood, A., Taha, M., Khan, M., Naureen, S., … Choudhary, M. I. (2014b). Evaluation of bisindole as potent β-glucuronidase inhibitors: synthesis and in silico based studies. *Bioorganic & Medicinal Chemistry Letters*, *24*(7), 1825–1829.

Khan, K. M., Saad, S. M., Shaikh, N. N., Hussain, S., Fakhri, M. I., Perveen, S., … Choudhary, M. I. (2014c). Synthesis and β-glucuronidase inhibitory activity of 2-arylquinazolin-4(3H)-ones. *Bioorganic & Medicinal Chemistry*, *22*(13), 3449–3454.

Khan, K. M., Shujaat, S., Rahat, S., Hayat, S., Rahman, A., & Choudhary, M. I. (2002). β-N-Cyanoethyl acyl hydrazide derivatives : a new class of beta-glucuronidase inhibitors. *Chemical and Pharmaceutical Bulletin*, *50*(11), 1443–1446.

Kim, D. H., Shim, S. B., Kim, N. J., & Jang, I. S. (1999). β-Glucuronidase-inhibitory activity and hepatoprotective effect of Ganoderma lucidum. *Biological & Pharmaceutical Bulletin*, *22*(2), 162–164.

Kim, H. J., Su, L., Jung, H., & Koo, S. (2011). Selective deoxygenation of allylic alcohol: stereocontrolled synthesis of lavandulol. *Organic Letters*, *13*(10), 2682–2685.

Kim, I. H., Yoo, K. Y., Park, J. H., Yan, B. C., Ahn, J. H., Lee, J. C., … Won, M. H. (2014). Comparison of neuroprotective effects of extract and fractions from Agarum clathratum against experimentally induced transient cerebral ischemic

damage. *Pharmaceutical Biology*, *52*(3), 335–343.

Kim, J. A., Kong, C. S., & Kim, S. K. (2010). Effect of Sargassum thunbergii on ROS mediated oxidative damage and identification of polyunsaturated fatty acid components. *Food and Chemical Toxicology*, *48*(5), 1243–1249.

Kim, K. Y., Chi, K. S., Kurihara, H., & Kim, S. M. (2008). β-Glucuronidase inhibitory activity of bromophenols purified from Grateloupia elliptica. *Food Science and Biotechnology*, *17*(5), 1110–1114.

Kim, K. Y., Nguyen, T. H., Kurihara, H., & Kim, S. M. (2010). α-Glucosidase inhibitory activity of bromophenol purified from the red alga Polyopes lancifolia. *Journal of Food Science*, *75*(5), 145–148.

Kontiza, I., Abatis, D., Malakate, K., Vagias, C., & Roussis, V. (2006). 3-Keto steroids from the marine organisms Dendrophyllia cornigera and Cymodocea nodosa. *Steroids*, *71*(2), 177–181.

Kurihara, H., Kagawa, Y., Konno, R., Kim, S. M., & Takahashi, K. (2014). Lipoxygenase inhibitors derived from marine macroalgae. *Bioorganic & Medicinal Chemistry Letters*, *24*(5), 1383–1385.

Kurihara, H., Konno, R., & Takahashi, K. (2015). Fucophlorethol C, a phlorotannin as a lipoxygenase inhibitor. *Bioscience, Biotechnology, and Biochemistry*, *79*(12), 1954–1956.

Kurihara, H., Mitani, T., Kawabata, J., & Hatano, M. (1997). Inhibitory effect on the α-glucosidase reaction by the aggregated state of sulfoquinovosyldiacylglycerol. *Bioscience, Biotechnology, and Biochemistry*, *61*(3), 536–538.

Kurihara, H., Mitani, T., Kawabata, J., & Takahashi, K. (1999). Two new bromophenols from the red alga Odonthalia corymbifera. *Journal of Natural Products*, *62*(138), 882–884.

Leal, M. C., Munro, M. H. G., Blunt, J. W., Puga, J., Jesus, B., Calado, R., … Madeira,

C. (2013). Biogeography and biodiscovery hotspots of macroalgal marine natural products. *Natural Product Reports*, *30*(11), 1380–1390.

Levvy, G. A. (1952). The preparation and properties of β-glucuronidase. 4. Inhibition by sugar acids and their lactones. *Biochemical Journal*, *52*(3), 464–472.

Li, Y., Qian, Z. J., Ryu, B. M., Lee, S. H., Kim, M. M., & Kim, S. K. (2009). Chemical components and its antioxidant properties in vitro: An edible marine brown alga, Ecklonia cava. *Bioorganic & Medicinal Chemistry*, *17*(5), 1963–1973.

Li, Y. X., Li, Y., Je, J. Y., & Kim, S. K. (2015). Dieckol as a novel anti-proliferative and anti-angiogenic agent and computational anti-angiogenic activity evaluation. *Environmental Toxicology and Pharmacology*, *39*(1), 259–270.

Lin, S., Zeng, L., Zhang, G., Liao, Y., & Gong, D. (2017). Synthesis, characterization and xanthine oxidase inhibition of Cu(II)–chrysin complex. *Spectrochimica Acta Part A: Molecular and Biomolecular Spectroscopy*, *178*, 71–78.

Lou-Bonafonte, J. M., Arnal, C., Navarro, M. A., & Osada, J. (2012). Efficacy of bioactive compounds from extra virgin olive oil to modulate atherosclerosis development. *Molecular Nutrition and Food Research*, *56*(7), 1043–1057.

Mabkhot, Y. N., Barakat, A., Yousuf, S., Choudhary, M. I., Frey, W., Ben Hadda, T., & Mubarak, M. S. (2014). Substituted thieno[2,3-b]thiophenes and related congeners: synthesis, β-glucuronidase inhibition activity, crystal structure, and POM analyses. *Bioorganic & Medicinal Chemistry*, *22*(23), 6715–6725.

Mansoor, T. A., Lee, Y. M., Hong, J., Lee, C. O., Im, K. S., & Jung, J. H. (2006). 5,6:8,9-Diepoxy and other cytotoxic sterols from the marine sponge Homaxinella sp. *Journal of Natural Products*, *69*(1), 131–134.

Matsuo, Y., Ishida, R., Matsumoto, T., Tatewaki, M., & Suzuki, M. (1997). Yendolipin, a novel lipobecaine with an inhibitory activity toward morphogenesis in a foliaceous green alga Monostroma oxyspermum. *Tetrahedron*, *53*(3), 869–876.

Mikami, D., Kurihara, H., Kim, S. M., & Takahashi, K. (2013). Red algal bromophenols as glucose 6-phosphate dehydrogenase inhibitors. *Marine Drugs*, *11*(10), 4050–4057.

Mikami, D., Kurihara, H., Ono, M., Kim, S. M., & Takahashi, K. (2016). Inhibition of algal bromophenols and their related phenols against glucose 6-phosphate dehydrogenase. *Fitoterapia*, *108*, 20–25.

Monaco, R. R., & Quinlan, R. F. (2014). Novel natural product discovery from marine sponges and their obligate symbiotic organisms. *bioRxiv*, *5454*.

Mori, K., Ooi, T., Hiraoka, M., Oka, N., Hamada, H., Tamura, M., & Kusumi, T. (2004). Fucoxanthin and its metabolites in edible brown algae cultivated in deep seawater. *Marine Drugs*, *2*(2), 63–72.

Morimoto, C. (2016). Lipoxygenase inhibitors derived from marine algae (master dissertation), 1-147. (In Japanese)

Murakoshi, I., & Hatanaka, S. I. (1977). Sulfur-containing amino acids in nature. *Bulletin of the Japanese Society of Scientific Fisheries*, *5*(35), 343–353.

Narita, M., Nagai, E., Hagiwara, H., Aburada, M., Yokoi, T., & Kamataki, T. (1993). Inhibition of β-glucuronidase by natural glucuronides of Kampo, medicines using glucuronide of SN-38 (7-ethyl-10-hydroxycamptothecin) as a substrate. *Xenobiotica*, *23*(1), 5–10.

Nasir, M., Saeidnia, S., Mashinchian-moradi, A., & Gohari, A. R. (2011). Sterols from the red algae, Gracilaria salicornia and Hypnea flagelliformis, from Persian Gulf. *Pharmacognosy Magazine*, *7*(26), 97–100.

Nautiyal, O. H. (2013). Natural products from plant, microbial and marine species. *International Journal of Science and Technology*, *10*(1), 611–646.

Nawaz, H. R., Malik, A., Khan, P. M., Shujaat, S., & Rahman, A. (2000). A novel β-glucuronidase inhibiting triterpenoid from Paeonia emodi. *Chemical and*

Pharmaceutical Bulletin, *48*(11), 1771–1773.

Nylund, G. M., & Pavia, H. (2005). Chemical versus mechanical inhibition of fouling in the red alga Dilsea carnosa. *Marine Ecology Progress Series*, *299*, 111–121.

Ohkuma, T., Otagiri, K., Tanaka, S., & Ikekawa, T. (1983). Intensification of host's immunity by squalene in sarcoma 180 bearing ICR mice. *Journal of Pharmacobio-Dynamics*, *6*, 148–151.

Ohta, H., Ono, M., Sekiya, C., & Namiki, M. (1992). Serum immunoreactive β-glucuronidase determined by an enzyme-linked immunosorbent assay in patients with hepatic diseases. *Clinica Chimica Acta*, *208*, 9–21.

Oleson, L., & Court, M. H. (2008). Effect of the β-glucuronidase inhibitor saccharolactone on glucuronidation by human tissue microsomes and recombinant UDP-glucuronosyltransferases (UGTs). *Journal of Pharmacy and Pharmacology*, *60*(9), 1175–1182.

Öztaşkın, N., Çetinkaya, Y., Taslimi, P., Göksu, S., & Gülçin, I. (2015). Antioxidant and acetylcholinesterase inhibition properties of novel bromophenol derivatives. *Bioorganic Chemistry*, *60*, 49–57.

Parish, R. W. (1977). Inhibition of Dictyostelium discoideum β-glucosidase by purines. *Journal of Bacteriology*, *129*(3), 1642–1644.

Park, M. S., Lee, S., & Lim, Y. W. (2017). A new record of four Penicillium species isolated from Agarum clathratum in Korea. *Journal of Microbiology*, *55*(4), 237–246.

Park, S. H., Song, J. H., Kim, T., Shin, W. S., Park, G. M., Lee, S., … Ham, J. (2012). Anti-human rhinoviral activity of polybromocatechol compounds isolated from the rhodophyta, Neorhodomela aculeate. *Marine Drugs*, *10*(10), 2222–2233.

Raddatz, S., Guy-Haim, T., Rilov, G., & Wahl, M. (2017). Future warming and acidification effects on anti-fouling and anti-herbivory traits of the brown alga

Fucus vesiculosus (Phaeophyceae). *Journal of Phycology*, *53*(1), 44–58.

Rhee, Y. K., Kim, D. H., & Han, M. J. (1998). Inhibitory effect of Zizyphi fructus on β-glucuronidase and tryptophanase of human intestinal bacteria. *Korean Journal of Food Science and Technology*, *30*(1), 199–205.

Roberts, A. B., Wallace, B. D., Venkatesh, M. K., Mani, S., & Redinbo, M. R. (2013). Molecular insights into microbial β-glucuronidase inhibition to abrogate CPT-11 toxicity. *Molecular Pharmacology*, *84*, 208–217.

Rohmer, M. (1999). The discovery of a mevalonate-independent pathway for isoprenoid biosynthesis in bacteria, algae and higher plants. *Natural Product Reports*, *16*(5), 565–574.

Rowland, A., Miners, J. O., & Mackenzie, P. I. (2013). The UDP-glucuronosyltransferases: their role in drug metabolism and detoxification. *International Journal of Biochemistry & Cell Biology*, *45*(6), 1121–1132.

Saeidnia, S., Permeh, P., Gohari, A. R., & Mashinchian-Moradi, A. (2012). Gracilariopsis persica from Persian gulf contains bioactive sterols. *Iranian Journal of Pharmaceutical Research*, *11*(3), 845–849.

Safarov, N., & Gasanov, R. (2015). Structure insights into β-glucuronidase inhibition to mitigate camptothecin chemoterapeutics side effect. *International Journal of Pharmaceutical Chemistry*, *5*(11), 365–380.

Saikia, D., Parihar, S., Chanda, D., Ojha, S., Kumar, J. K., Chanotiya, C. S., … Negi, A. S. (2010). Antitubercular potential of some semisynthetic analogues of phytol. *Bioorganic & Medicinal Chemistry Letters*, *20*(2), 508–512.

Salar, U., Taha, M., Ismail, N. H., Khan, K. M., Imran, S., Perveen, S., … Riaz, M. (2016). Thiadiazole derivatives as new class of β-glucuronidase inhibitors. *Bioorganic & Medicinal Chemistry*, *24*(8), 1909–1918.

Santoso, J. (2013). Free amino acids, catechins and flavonoids contents in some

Indonesian seaweeds. *Jurnal Ilmu Dan Teknologi Pangan*, *2*(2), 9–20.

Schumacher, U., Adam, E., Zangemeister-Wittkel, U., & Gossrau, R. (1996). Histochemistry of therapeutically relevant enzymes in human tumours transplanted into severe combined immunodeficient (SCID) mice: nitric oxide synthase — associated diaphorase, β-D-glucuronidase and nonspecific alkaline phosphatase. *Acta Histochemica*, *98*(4), 381–387.

Scolastici, C., Ong, T. P., & Moreno, F. S. (2004). Squalene does not exhibit a chemopreventive activity and increases plasma cholesterol in a Wistar rat hepatocarcinogenesis model. *Nutrition and Cancer*, *50*(1), 101–109.

Sharma, R., Kishore, N., Hussein, A., & Lall, N. (2013). Antibacterial and anti-inflammatory effects of Syzygium jambos L. (Alston) and isolated compounds on acne vulgaris. *BMC Complementary and Alternative Medicine*, *13*(1), 292–302.

Shi, D., Guo, S., Jiang, B., Guo, C., Wang, T., Zhang, L., & Li, J. (2013). HPN, a synthetic analogue of bromophenol from red alga Rhodomela confervoides: synthesis and anti-diabetic effects in C57BL/KsJ-db/db mice. *Marine Drugs*, *11*(2), 350–362.

Shi, D., Li, J., Jiang, B., Guo, S., Su, H., & Wang, T. (2012). Bromophenols as inhibitors of protein tyrosine phosphatase 1B with antidiabetic properties. *Bioorganic & Medicinal Chemistry Letters*, *22*(8), 2827–2832.

Shih, C. C., Hwang, H. R., Chang, C. I., Su, H. M., Chen, P. C., Kuo, H. M., … Wen, Z. H. (2017). Anti-inflammatory and antinociceptive effects of ethyl acetate fraction of an edible red macroalgae Sarcodia ceylanica. *International Journal of Molecular Sciences*, *18*(11), 2437–2452.

Shim, S. B., Kim, N. J., & Kim, D. H. (2000). β-Glucuronidase inhibitory activity and hepatoprotective effect of 18β-glycyrrhetinic acid from the rhizomes of Glycyrrhiza uralensis. *Planta Medica*, *66*(1), 40–43.

Song, M. C., Kim, D. H., Hong, Y. H., Kim, D. K., Chung, I. S., Kim, S. H., … Baek, N. I. (2003). Terpenes from the aerial parts of Chrysanthemum coronarium L. *Agricultural Chemistry & Biotechnology*, *46*(3), 118–121.

Spanogiannopoulos, P., Bess, E. N., Carmody, R. N., & Turnbaugh, P. J. (2016). The microbial pharmacists within us: a metagenomic view of xenobiotic metabolism. *Nature Reviews Microbiology*, *14*(5), 273–287.

Sperker, B., Backman, J. T., & Kroemer, H. K. (1997). The role of β-glucuronidase in drug disposition and drug targeting in humans. *Clinical Pharmacokinetics*, *33*(1), 18–31.

Sugiura, Y., Matsuda, K., Yamada, Y., Nishikawa, M., Shioya, K., Katsuzaki, H., … Amano, H. (2006). Isolation of a new anti-allergic phlorotannin , phlorofucofuroeckol-B , from an edible brown alga , Eisenia arborea. *Bioscience, Biotechnology, and Biochemistry*, *70*(11), 2807–2811.

Suzuki, M., Wakana, I., Denboh, T., & Tatewaki, M. (1996). An allelopathic polyunsaturated fatty acid from red algae. *Phytochemistry*, *43*(1), 63–65.

Suzuki, N., Ito, T., Matsui, H., & Takizawa, M. (2016). Anti-inflammatory and cytoprotective effects of a squalene synthase inhibitor, TAK-475 active metabolite-I, in immune cells simulating mevalonate kinase deficiency (MKD)-like condition. *SpringerPlus*, *5*(1), 1429–1443.

Swanson, A. K., & Fox, C. H. (2007). Altered kelp (Laminariales) phlorotannins and growth under elevated carbon dioxide and ultraviolet-B treatments can influence associated intertidal food webs. *Global Change Biology*, *13*(8), 1696–1709.

Taha, M., Ismail, N. H., Imran, S., Anouar, E. H., Ali, M., Jamil, W., … Kashif, S. M. (2016). Identification of bisindolylmethane–hydrazone hybrids as novel inhibitors of β-glucuronidase, DFT, and in silico SAR intimations. *Royal Society of Chemistry*, *6*, 3276–3289.

Taha, M., Ismail, N. H., Imran, S., Selvajar, M., & Rhim, F. (2016a). Synthesis of novel inhibitors of β-glucuronidase based on the benzothiazole skeleton and their molecular docking studies. *Royal Society of Chemistry*, *23*(22), 3303–3012.

Taha, M., Ismail, N. H., Imran, S., Selvaraj, M., Rahim, A., Ali, M., … Khan, K. M. (2015). Synthesis of novel benzohydrazone-oxadiazole hybrids as β-glucuronidase inhibitors and molecular modeling studies. *Bioorganic & Medicinal Chemistry*, *23*, 7394–7404.

Taha, M., Ismail, N. H., Imran, S., Selvaraj, M., Rashwan, H., Farhanah, F. U., … Ali, M. (2015a). Synthesis of benzimidazole derivatives as potent β-glucuronidase inhibitors. *Bioorganic Chemistry*, *61*, 36–44.

Taha, M., Ismail, N. H., Imran, S., Wadood, A., Rahim, F., Muqarrabin, L. M. R., … Khan, F. (2016b). Synthesis of novel disulfide and sulfone hybrid scaffolds as potent β-glucuronidase inhibitor. *Bioorganic Chemistry*, *68*, 15–22.

Taha, M., Shah, S. A. A., Khan, A., Arshad, F., Ismail, N. H., Afifi, M., … Choudhary, M. I. (2015b). Synthesis of 3,4,5-trihydroxybenzohydrazone and evaluation of their urease inhibition potential. *Arabian Journal of Chemistry*.In press.

Taha, M., Sultan, S., Nuzar, H. A., Rahim, F., Imran, S., Ismail, N. H., … Ullah, H. (2016c). Synthesis and biological evaluation of novel N-arylidenequinoline-3-carbohydrazides as potent β-glucuronidase inhibitors. *Bioorganic & Medicinal Chemistry*, *24*(16), 3696–3704.

Tohda, H., Kurihara, H., Hosokawa, M., & Takahashi, K. (1999). Inhibition of β-glucuronidase by purine nucleotides. *Fisheries Science*, *65*(4), 667–668.

Tsuda, K., Sakai, K., Tanabe, K., & Kishida, Y. (1960). Steroid studies. XVI. Isolation of 22-dehydrocholesterol from Hypnea japonica. *Journal of the American Chemical Society*, *82*(6), 1442–1443.

Tukey, R. H., & Strassburg, C. P. (2000). Human UDP-glucuronosyltransferases:

metabolism, expression, and disease. *Annual Review of Pharmacology and Toxicology*, *40*, 581–616.

Uemoto, S. (2011). Xanthine oxidase inhibitors derived from marine algae of the genus Odonthalia (master thesis), 1-141. (In Japanese)

Usoltseva, R. V., Anastyuk, S. D., Shevchenko, N. M., Zvyagintseva, T. N., & Ermakova, S. P. (2016). The comparison of structure and anticancer activity in vitro of polysaccharides from brown algae Alaria marginata and A. angusta. *Carbohydrate Polymers*, *153*, 258–265.

Wallace, B. D., Wang, H., Lane, K. T., Scott, J. E., Orans, J., Koo, S. J., … Redinbo, M. R. (2010). Alleviating cancer drug toxicity by inhibiting a bacterial enzyme. *Science*, *330*(6005), 831–835.

Wang, L. J., Wang, S. Y., Jiang, B., Wu, N., Li, X. Q., Wang, B. C., … Shi, D. Y. (2015). Design, synthesis and biological evaluation of novel bromophenol derivatives incorporating indolin-2-one moiety as potential anticancer agents. *Marine Drugs*, *13*(2), 806–823.

Wiemer, D. F., Idler, D. D., & Fenical, W. (1991). Vidalols A and B, new anti-inflammatory bromophenols from the Caribbean marine red alga Vidalia obtusaloba. *Experientia*, *47*(8), 851–853.

Xu, C., Li, C. Y.-T., & Kong, A.-N. T. (2005). Induction of phase I, II and III drug metabolism/transport by xenobiotics. *Archives of Pharmacal Research*, *28*(3), 249–268.

Yokoya, N. S., Ávila, M., Piel, M. I., Villanueva, F., & Alcapan, A. (2014). Effects of plant growth regulators on growth and morphogenesis in tissue culture of Chondracanthus chamissoi (Gigartinales, Rhodophyta). *Journal of Applied Phycology*, *26*(2), 819–823.

Yoshida, T. (1989). Taxonomy of Sargassum. *The Korean Jounal of Phycology*, *4*(2),

107–110.

Zhao, J., Fan, X., Wang, S., Li, S., Shang, S., Yang, Y., … Shi, J. (2004). Bromophenol derivatives from the red alga Rhodomela confervoides. *Journal of Natural Products*, *67*(6), 1032–1035.

Zwenger, S., & Basu, C. (2008). Plant terpenoids: applications and future potentials. *Biotechnology and Molecular Biology Reviews*, *3*(1), 1–7.

Acknowledgements

I would like to give my deepest gratitude to my academic supervisor *Dr. Hideyuki Kurihara* for his scholastic guidance, advice and support for this study. And I really appreciated his great efforts and helpful comments in scrutinizing reviewing this thesis.

I do my great pleasure to express my special thanks and gratitude to *Prof*. *Hideki Kishimura* and *Prof*. *Ryuichi Sakai* for their valuable advices and constructive criticism to improve this thesis. In addition, I would like to extend sincere appreciation to Dr. *Eri Fukushi* and Mr. *Yusuke Takata* for MS and NMR analysis.

I also wish to express the deepest gratitude and profound regards to the former lab Prof. *Koretaro Takahashi*; *Prof*. *Beiwei Zhu* and *Prof*. *Shuhong Ye* of School of Food Science and Technology, Dalian Polytechnic University for their invaluable encouragement and inspiration throughout all my PhD life.

I also want show my special appreciation to my precious friends *Wen Xin*, *Dr. Aokai Zhang*, *Zongyuan Lu*, *Dr. Liang Qu*, *Yannan Ji*, *Haruka Tsurumi*, *Yoshika Hasebe* and all of my "*Shokuichi*" brothers and sisters for their constant spiritual and technical support throughout my whole PhD study.

I sincerely acknowledge the China Scholarship Council (CSC) for providing me the scholarship.

Finally, I want to extend my deepest sense of gratitude to my beloved parents, my elder sister, my brother-in-law and my nephew for their absolute love, continuous support, encouragement and inspiration and I dedicate this work to all my families.

Duo Zhang

Hakodate, January 2018